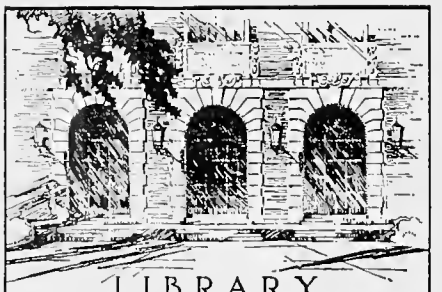

UNIVERSITY OF ILLINOIS
URBANA

AERONOMY REPORT NO. 1

DIRECT AERONOMIC MEASUREMENTS IN THE LOWER IONOSPHERE—AN INFORMAL CONFERENCE RECORD

edited by
S. A. Bowhill

December 1, 1963

Final Report
Contract DA-11-022-AMC-890(R)
Ballistics Research Laboratories
Aberdeen Proving Ground, Maryland

Department of Electrical Engineering
Engineering Experiment Station
University of Illinois
Urbana, Illinois

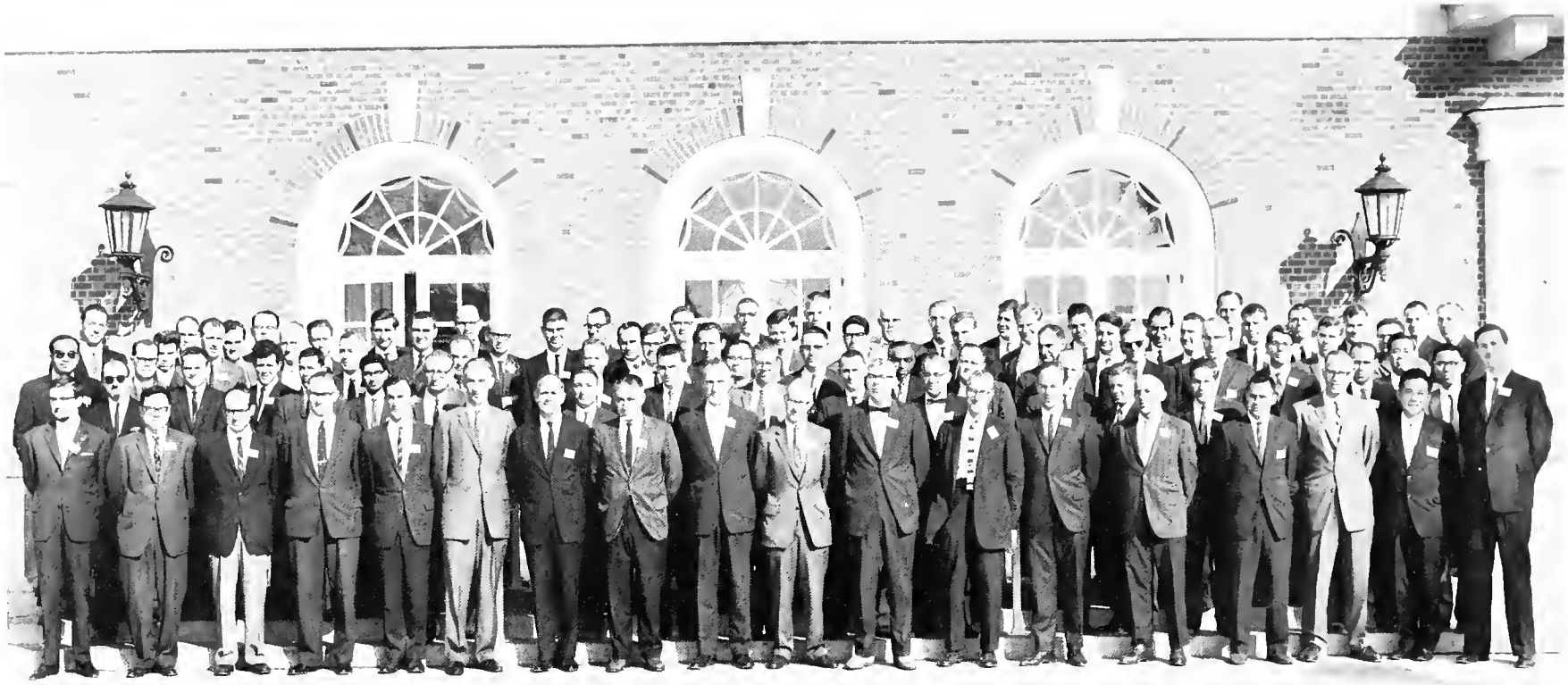

Conference Photograph. South steps of the Illini Union Building. October 22, 1963.

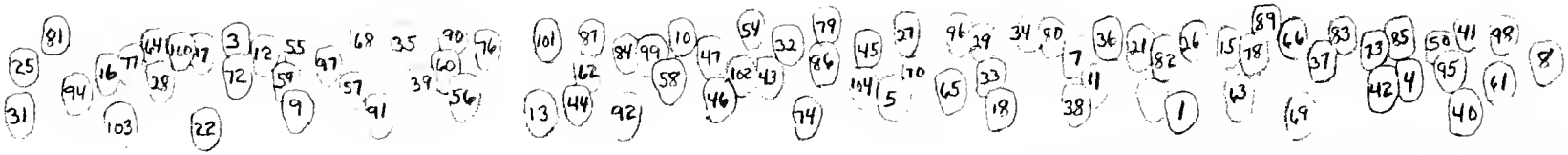

Key to Photograph. Numbers refer to sequence number in list of attendees, pp. 225 to 228.

AERONOMY REPORT NO. 1

DIRECT AERONOMIC MEASUREMENTS IN THE LOWER IONOSPHERE -- AN INFORMAL CONFERENCE RECORD

edited by

S. A. Bowhill

Conference held October 21, 22 and 23, 1963
Illini Union, University of Illinois, Urbana, Illinois

Papers in this report are not to be cited
without the permission of the respective authors.
The citations will then be "private communications."

December 1, 1963

Final Report
Contract DA-11-022-AMC-890 (R)
Ballistics Research Laboratories
Aberdeen Proving Ground, Maryland

Department of Electrical Engineering
Engineering Experiment Station
University of Illinois
Urbana, Illinois

CONFERENCE PLANNING AND UNIVERSITY OF ILLINOIS FACULTY AND STAFF

CONFERENCE GENERAL CHAIRMAN

S. A. Bowhill, Professor of Electrical Engineering, University of Illinois

TECHNICAL PROGRAM COMMITTEE

D. Alpert, Coordinated Science Laboratory, University of Illinois, Urbana, Illinois
W. W. Berning, Ballistics Research Laboratories, Aberdeen Proving Grounds, Aberdeen, Maryland
R. E. Bourdeau, Goddard Space Flight Center, NASA, Greenbelt, Maryland
L. H. Brace, Goddard Space Flight Center, NASA, Greenbelt, Maryland
C. Y. Johnson, Naval Research Laboratory, Washington 25, D. C.
W. Pfister, Geophysics Research Directorate, Air Force Cambridge Research Laboratories, Bedford, Massachusetts
S. F. Singer, Department of Physics, University of Maryland, College Park, Maryland

UNIVERSITY OF ILLINOIS FACULTY

D. D. Henry, President
W. L. Everitt, Dean, College of Engineering
R. J. Martin, Director of the Engineering Experiment Station
E. C. Jordan, Department Head, Department of Electrical Engineering

CONFERENCE SERVICES

K. G. Balmain, Chief Reporter
Miss R. Cornell, Secretarial Assistance
Mrs. J. Gschwendtner, Secretarial Assistance
J. C. Hofer, Local Arrangements

CONFERENCE REPORTERS

A. B. Bhattacharya
B. E. Cherrington
D. G. Detert
G. L. Duff
J. E. Geisler
A. B. Gschwendtner
O. B. Kesler
G. G. Kleiman
N. Mathur
P. Paramasivaiah
T. R. Pound
P. E. Sticha

FOREWORD

The lower ionosphere, consisting of the D-region and part of the E-region below 120 km height, is perhaps the most imperfectly understood part of the ionosphere at the present time. Pulsed radio wave sounding, at the low frequencies needed for reflection in this height range, yields results which are difficult to interpret despite an abundance of experimental data; and the relatively high gas pressures make environmental measurements with sounding rockets hard to carry out.

In setting up this conference, we were guided by the concept that its prime purpose should be the dissemination of viewpoints, technical information and scientific results among a relatively small number of active researchers. From this premise it followed that the meeting could not be open to all who might desire to attend; however, an honest attempt was made to include all individuals who would have a useful contribution to make to the discussions. To those whom we were unable to invite, we offer our apologies, and the hope that this volume will be of some value to them.

When soliciting papers for the conference, we made it clear that presentation of a paper would not constitute publication, and that the regular aeronomic journals were the proper place for the scientific work to appear in final form. Several advantages accrued from this. Firstly, many scientists were prepared to describe very new results and invite comments on them before publication; secondly, work already published could be described, where appropriate; and thirdly, the delays associated with formal review and publishing procedures were very much reduced.

A logical consequence of this approach was the slightly unusual form taken by the present volume, which is not a "Conference Proceedings" in the usual sense. It is an informal record, only one degree more permanent than the spoken word. Its purpose is to alert researchers to the identities of other scientists working in this subject, and to give some flavor of their thoughts, attitudes, and scientific achievements. If it encourages others to delve into the published work of the participants, to correspond with them, and to stimulate constructive thought and discussion, it will have amply justified itself.

It has been necessary to specify, on the title page and on every text page, that the papers contained in this volume are "not citable" except (with the explicit permission of the authors) as private communications. We have wielded a heavy and sometimes arbitrary editorial hand in preparing the papers, and the discussion, in a coherent form for printing. Accordingly, we take full responsibility for any misquotation or misrepresentation of a participant's remarks which may appear by mischance. This, unfortunately, is the price to be paid for the reasonably prompt appearance of this document.

We would like to acknowledge the help freely given by many individuals in the running of the conference and the production of this volume; first to Mr. John C. Hofer, for his most professional organization of the conference, and technical production of this record; next to Dr. Keith G. Balmain, chief reporter, and his able and dedicated staff of assistants; but most of all to program committee, opening speakers, session chairmen and participants for the excellent quality of the science which they brought with them to Urbana.

S. A. Bowhill
General Chairman

TABLE OF CONTENTS

Conference Photograph — Frontispiece

Conference Planning and Conference Staff — iv

Preface — v

MEASUREMENT TECHNIQUES

0900 - 1200, Monday, October 21, 1963 Chairman: W. W. Berning

Electron and Ion Density and Electron Temperature

1.A Smith, L. G. -- "Measurement of Electron Density in the Lower Ionosphere" — 1

1.B Boyd, R. L. F. -- "Direct Measurement of Electron and Ion Temperature" — 7

1.1 Brace, L. H. -- "A Cylindrical Electrostatic Probe for Measurement of Electron Temperature in the Ionosphere" — 12

1.2 Hirao, K., Miyazaki, S. -- "Ion Probe Used in the Japanese Sounding Rocket" — 14

1.3 Hirao, K., Miyazaki, S., Muraoka, T. -- "Resonance Probe Available for the IQSY" — 17

1.4 McNamara, A. G. -- "A Multiple Langmuir Probe System for D- and E-Region Ionization Experiments" — 21

1.5 Sagalyn, R. C., Smiddy, M. -- "Theory of Electrostatic Probes for the Study of D-Region Ionization" — 22

1.6 Takayama, K. -- "New Discharge Tube and Spherical Mesh Probe" — 26

1300 - 1700, Monday, October 21, 1963 Chairman: C. G. Little

Impedance

2.A Pfister, W. -- "Survey of RF Impedance Probes" — 31

2.1 Adey, A. W. -- "The Operation of RF Probes for the Measurement of Electron Density and Collision Frequency in the Ionosphere" — 37

2.2 Grard, R. J. L. -- "The Sheath Capacitance at Very Low Frequency of a Metallic Body Moving in the Ionosphere" — 41

2.3 Heikkila, W. J. -- "A Radio Frequency Probe for Electron Density Measurements" — 45

2.4 Sayers, J. -- "A Radio-Frequency Electron Density Probe for a Wide Range of Ionospheric Measurements" — 52

Conductivity

3.A Whipple, E. C. Jr. -- "Direct Measurements of the Electrical Conductivity of the Atmosphere" 57

3.1 Dolezalek, H., Oster, A. L. -- "Ion-Spectrometer for the Upper Stratosphere and Mesosphere" 59

3.2 Pedersen, A. -- "A Gerdian Condensor Rocket Probe For Measurement of Ion and Electron Concentrations in the D-Region"

Neutral and Ion Composition

4.A Johnson, C. Y. -- "Measurement of Neutral and Ion Composition" 63

4.1 Herzog, R. F. K. -- "The Monopole Mass Spectrometer and Its Advantages for Upper Atmosphere Research" 66

4.2 Spencer, N. W. -- "A Technique for Thermosphere Structure Measurement" 69

1900 - 2100, Monday, October 21, 1963 Chairman: D. Alpert

Magnetic Field

5.A. Cahill, L. J. -- "Measurement of Electrical Currents in the Ionosphere" 73

Pressure, Density and Wind

6.A Spencer, N. W. -- "Techniques for the Pressure, Temperature, Density and Wind Determination in the Mesosphere and Lower Thermosphere 76

6.1 Grossi, M. D. -- "A Technique for Wind Measurements in the Lower Ionosphere by Collection and Processing of Doppler Information Contained in VHF Radar Returns From Meteor Trails" 82

6.2 Rosenberg, N. W. --"Ionospheric Wind Patterns Through the Night" 88

Airglow

7.A Dubin, M. --"Airglow Measurement" 95

0900 - 1200, Tuesday, October 22, 1963 Chairman: N. W. Spencer

Solar Radiation

8.A Chubb, T. A. -- "Solar Radiation Measurements" 101

Supersonic Flow

9.A Yen, S. M. -- "In-Flight Measurement of Supersonic Flow" 106

RESULTS

Results of Measurements of Composition

10.1 Holmes, J. C , Young, J.M. -- "Positive Ion Composition Above White Sands, New Mexico" 114

10.2 Nier, A. O., Hoffman, J. H., Johnson, C. Y., Holmes, J. C. -- "The Neutral Composition of the Atmosphere in the 100-200 km Range" 120

10.3 Schaefer, E. J., Nichols, M. H. -- "Recent Results Obtained from a Rocket-Borne Mass Spectrometer" 126

10.4 Taylor, H. A. -- "Some Results of Positive Ion Composition Measurements Above Wallops Island" 130

1300 - 1700, Tuesday, October 22, 1963 Chairman: C. Y. Johnson

Results of Measurements of Electron and Ion Density and Temperature

11.1 Buchau, J., Jacobs, K. G., Kaiser, P., Rawer, K. -- "Simultaneous Measurement of Plasma Density by Three Different Methods" 135

11.2 Heikkila, W. J. -- "Radio Frequency Probe Measurements of D-Region Electron Density" 137

11.3 Hirao, K. -- "Electron Temperature Profile Depending on the Geomagnetic Latitude" 139

11.4 Hodges, R. R., Jr. -- "Rocket-Borne Gyro-Interaction Experiments in the Lower Ionosphere" 142

11.5 Israel, G. -- "Direct Measurement of Atmospheric Pressure in the Mesosphere at Hammaguir" 147

11.6 Kavadas, A. -- "Microstructure in Auroral Displays and the Ionosphere" 151

11.7 Knudsen, W. C., Sharp, G. W. -- "Ion Concentration and Thermal Analysis of Data Obtained from an Ion Trap Carried in a Low-Altitude Rocket" 154

11.8 McNamara, A. G. -- "Rocket-Borne Langmuir Probe Measurements in Aurora" 157

11.9 Nisbet, J. S. -- "Rocket Measurements of Electron Density in the D-Region During and After a Solar Eclipse" 159

11.10 Ortner, J. -- "Electron Energy Spectrum Measurements During Auroral Absorption" 162

11.11 Pedersen, A. -- "Some Preliminary Results of a Gerdian Condensor Measurement" 164

11.12 Sagalyn, R. C. -- "Positive and Negative Ion Density Measurements in the D- and E-Regions" 167

11.13 Smith, L. G. -- "Lower Ionosphere Profiles with a Rocket-Borne Probe" 169

11.14 Ulwick, J. C., Pfister, W., Haycock, O. C. -- RF Probe Measurements From a Recent Churchill Firing Into an Auroral Absorption" 173

0900 - 1200, Wednesday, October 23, 1963 Chairman: W. J. Heikkela

Results of Radio Propagation Measurements

12.1 Belrose, J. S. -- "Electron Content at the D-Region by the Method of Partial Reflection" 177

12.2 Hall, J. E. -- "Rocket Measurements of Low Frequency Wavefields for the Determination of D-Region Electron Densities" 182

12.3 Landmark, B., Peterson, O -- "Electron Density Observations in the D-Region During Auroral Absorption" 185

12.4 Moler, W. F. -- "An Examination of D-Region Aeronomy with a VLF Ionospheric Sounding System" 190

12.5 Little, C. G., Lesfald, G. M., Parthasarathy, R. -- D-Region Electron Density Profiles During Aurora Using the Cosmic Noise Technique" 195

INTERPRETATION OF LOWER IONOSPHERIC MEASUREMENTS

13.1 Poppoff, I. G., Whitten, R. C. -- "Ionization by Auroral Electrons" 197

13.2 Reid, G. C. -- "On the Negative Ion Composition of the D-Region" 202

13.3 Whitten, R. C., Poppoff, R. C. -- "Ion Kinetics in the Lower Ionosphere" 205

CONCLUDING STATEMENTS

1300 - 1500, Wednesday, October 23, 1963 Chairman: S. A. Bowhill

14.1 Smith, L. G. -- "Concluding Statement on Electron and Ion Density" 211

14.2 Boyd, R. L. F. -- "Concluding Statement on Electron Temperature" 213

14.3 Pfister, W. -- "Concluding Statement on Impedance" 216

14.4 Whipple, E. C. Jr. -- "Concluding Statement on Conductivity" 217

14.5 Johnson, C. Y. -- "Concluding Statement on Neutral and Ion Composition" 219

14.6 Spencer, N. W. -- "Concluding Statement on Pressure, Density and Wind" 221

14.7 Dubin, M. -- "Concluding Statement of Airglow" 222

14.8 Chubb, T. A. -- "Concluding Statement on Solar Radiation" 223

List of Attendees 225

Index of Authors Cited 229

Index of Authors and Conference Speakers 233

1.A MEASUREMENT OF ELECTRON AND ION DENSITY IN THE LOWER IONOSPHERE

L. G. SMITH
Geophysics Corporation of America
Bedford, Massachusetts

1. Introduction

The principal feature distinguishing the lower ionosphere from the adjacent regions is the ratio of negative ion density to electron density, usually denoted by λ. In the higher ionosphere the negative ion density is negligible, while below the region, in the domain of atmospheric electricity, the electron density is negligible. Thus in the region a great dynamic range is encountered. Another, not unrelated, property of the region is electron collision frequency which has a profound effect on the propagation of radio waves through the region, particularly with respect to absorption.

Before taking up the question of techniques, we consider very briefly what values of electron and ion density we can expect to measure in the D-region. The present information on electron density is based almost entirely on RF experiments, using ground-based equipment. The most important of these are:

(a) Propagation of very low frequency and low frequency waves, i.e., frequencies below 300 kc/s, which is the plasma frequency for an electron density of 10^3 cm^{-3}.
(b) Low frequency vertical sounders (or radar).
(c) Partial reflection sounders, i.e., a vertical sounder in which the frequency (fixed) exceeds the plasma frequency anywhere in the region (for example, 2 Mc/s).
(d) Wave interaction (cross-modulation).
(e) Cosmic noise absorption (riometer).

Each of these techniques has its limitations and a complete and unambiguous profile of electron density is not obtained. However, such data does give an idea of the magnitude of the electron density and its variation with height and serves as a guide to the design of experiments. Figure 1 illustrates this variation for a quiet day, a quiet night and a disturbed day. Superimposed on these general variations with height, are important structural features, the exact nature of which cannot be determined from ground based experiments. However, it is known, for example, from partial reflection sounders, that certain heights are preferred while others are observed irregularly. Another important feature which shows up in measurements of D-region absorption in temperate latitudes, is that only when the quietest days are selected is a marked dependence on solar zenith angle. It also points up the importance of simultaneous measurements by the different techniques to be discussed in this conference.

The situation with respect to negative ion density is somewhat worse than for electron density. The only guide at present, to numbers to be expected, comes from theoretical treatments such as those of Nicolet and Aikin, who predict for a very quiet sun a value of 10^2 cm^{-3} at about 75 km increasing to 10^3 cm^{-3} at about 55 km. These are daytime values. Measurements from balloons show values of 3 x 10^3 to 4 x 10^3 cm^{-3} in the height range from 10 to 30 km.

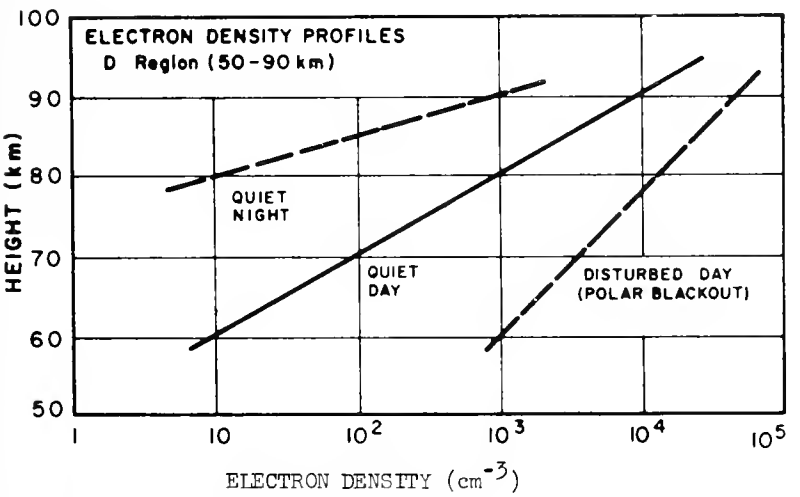

Figure 1. Electron density profiles in the D-region

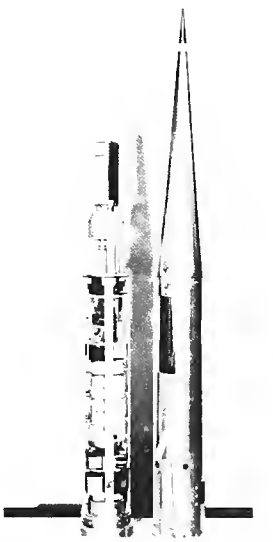

Figure 2. Nike-Apache payload showing nose tip electrode

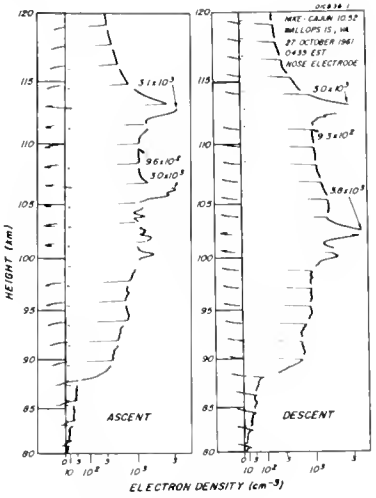

Figure 3. Electron density profiles in the nighttime E-region.

2. RF Propagation Techniques

We now turn to those techniques which involve instrumentation at the location being measured. This is direct measurement in its broadest sense. The first groups of experiments, and the only ones which are unique to the D-region, are those which involve the measurement of the attenuation of an RF wave traversing the medium. The energy is lost by collisions of the oscillating electrons with neutral gas particles and actually results in heating of the region. The attenuation due to absorption is, in the simplest case, proportional to

$$\frac{N\nu}{\nu^2 + (\omega \pm \omega_H)^2}$$

where N is the electron density, ν the electron collision frequency, ω ($=2\pi f$) is the wave angular frequency and ω_H ($=2\pi f_H$) is the angular gyro-frequency, f_H being of the order of 1.5 Mc/s. The plus sign indicates the ordinary component and the minus sign the extraordinary component.

This technique has been used in several variations. The simplest is to have a fixed frequency transmitter on the ground and a receiver on the rocket, the signal strength being telemetered back to the ground. No distinction is made between the components so that, in effect, the ordinary component alone is measured and an independent measurement of collision frequency is required. Rawer and Argence [1] made use of terrestrial broadcast receivers and used a swept-frequency receiver on the rocket. They have obtained a daytime profile of electron density from 70 to 87 km by this technique. Bowhill and Mechtly [2] used a 512 kc/s transmitter in nighttime shots and showed the very sharp lower boundary of the D-layer at about 75 km. They were able to measure electron density down to about 100 cm^{-3} but they estimate that in daytime it should be possible to measure down to 10 cm^{-3} by this technique.

The more sophisticated version of the technique distinguishes the two components and, by measuring them separately, obtain the electron collision frequency as well as the electron density, as has been described by Seddon [3]. The technique has the additional advantage that the height range of the measurement is increased; for a given transmitter frequency the extraordinary component is attenuated lower in the region than is the ordinary component.

There are experimental difficulties associated with the absorption techniques, such as the disturbance caused by signals reflected from the E-layer, but this, at present, appears to be one of the best methods for this region of the ionosphere.

The other propagation technqiues which will be considered briefly here were, originally developed for the higher regions of the ionosphere (E and above) and have been used to as low altitude as possible. The Seddon [4] CW propagation technique (also known by the more descriptive name of dispersive Doppler) is still unchallenged for accurate values of electron density in the E-region and is useful in the D-region down to an electron density of about 10^3 cm^{-3}. The measurement actually gives refractive index for the ordinary and extraordinary wave and, as Kane [5] has shown, the calculation of electron density must properly include electron collision frequency.

Faraday rotation, the rotation of the plane of polarization of a plane polarized wave tra-

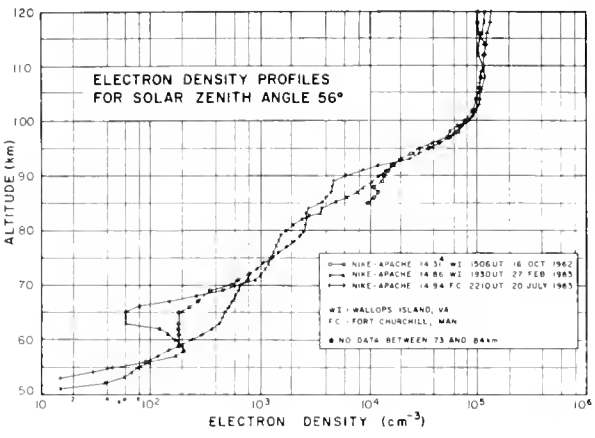

Figure 4. Electron density profiles measured for solar zenith angle 56 deg, assuming probe current proportional to electron density.

velling through the ionosphere has also been used in the D-region. This technique though, like the dispersive Doppler technique, seems to have limited usefulness in the D-region. They both depend on measuring a beat frequency and it does not appear feasible to measure electron densities much below 10^3 cm^{-3}.

3. RF Probes

Again we find we are dealing with experiments designed primarily for the E-region. The plasma resonance probes such as those used by Hirao sweep the frequency of an electrode in the plasma and determine the point of resonance, in this case by the maximum in the DC current into the probe. In the heavily damped conditions of the D-region it may be difficult to detect the resonance point but it will be interesting to hear more about the technique. In the instrument which Hirao uses the plasma resonance technique is combined with an ingenious variation of the Langmuir probe technique, the latter being used to measure electron temperature.

Another group of techniques may be called capacitance probes. The capacity of an electrode system in the plasma is measured and compared with the capacity in free space. This gives the dielectric constant and immediately leads to a value for electron density. The measurement is made at a frequency well above the plasma frequency and which should also be greater than the collision frequency to avoid heavy damping in the D-region. The actual change in capacity is consequently very small and presents formidable experimental problems.

4. DC Probes

The ionospheric techniques in this category are largely derived from the Langmuir probe and may be better termed retarding potential analysers. They can be the simplest type where an electrode is inserted in the plasma and a current having both positive and negative components measured; or it may be one of the more elaborate types where one or more grids are used to separate these components. The instruments are then known as ion traps.

The theory of the Langmuir probe is an extension of the kinetic theory of gases to a plasma. The current density to an electrode at the potential of the plasma due to the random thermal motion of the electrons is

$$j_e = ne\,\bar{v}/4$$

where $\bar{v}$, the mean velocity of the electrons is given by

$$\bar{v} = (8kT/\pi m)^{1/2}.$$

The positive ion random current density is given by the same expressions and, because of the greater mass of the positive ion, is about two orders of magnitude smaller than the electron random current density. As the electrode is made negative with respect to the plasma electrons are retarded and the current reduced according to the relation

$$j = j_e \exp\,[eV/kT]$$

where V is the retarding potential of the electrode. This variation which is the basis of the techniques for measuring electron temperature is independent of the shape of the electrode. We have found it convenient to use the nose tip of the rocket as seen in Figure 2. For accelerating potentials the variation of current with voltage does depend on the electrode shape and size and the plasma properties but in any case lies between two limits: one is saturation at the random current density j_e and the other is a linear increase of the form

$$j = j_e\,(1 + \frac{eV}{kT}).$$

The standard procedure is to prepare a semi-log plot of electron current versus voltage; then to obtain the electron temperature from the retarding potential region. The point at plasma potential is identified and the random current density read off. The mean velocity is computed from the temperature and the electron density obtained. This is a tedious procedure and various techniques have been devised for easing the data handling problem. Those for electron temperature I shall leave for Professor Boyd. For electron density we have adopted what might be called an interpolation technique. Each sweep of probe potential gives only one value of electron density: however, by holding the probe potential constant at a small positive (i.e., accelerating) potential we are able to see fine structure in the elec-

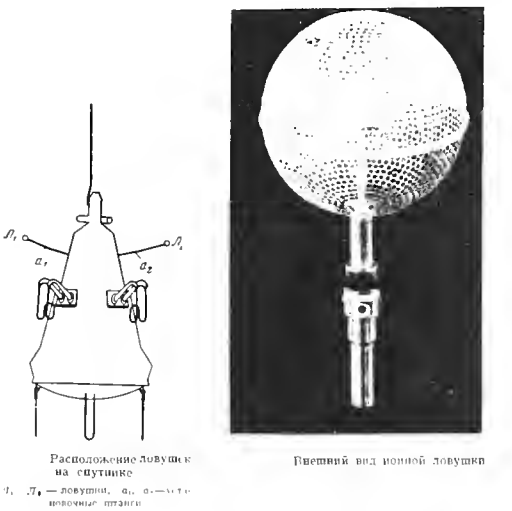

Figure 5. Ion trap on Sputnik III.

tron density profile. An example of this in the nighttime E-region is shown in Figure 3. Surprisingly the proportionality of probe current with electron density is found to hold over a rather wide range of electron density in the E region, and in fact, when we compare profiles of probe current taken in the daytime, at sunset and at night we are led to believe that the proportionality holds true throughout the D-region. Figure 4 shows profiles from three flights made with the same solar zenith angle of 56°. Data is missing on one flight between 73 and 84 km. The three profiles agree closely in the E-layer from 110 km down to 93 km but in the D-region a much greater variability shows up. Let me repeat that there is as yet no theoretical basis for using the probe in this way (i.e., at constant potential) below about 85 km and, in fact, a better case can be made for interpretation in terms of conductivity but this appears to give a good indication of structure and should be used with caution pending further investigation.

The addition of a grid allows the separation of the two components of current. This has two advantages over the simple probe, first the electron current can be measured to larger retarding potentials and second the positive ion current can be measured and analysed separately. The grid may be either spherical, as were these on Sputnik III, Figure 5, and those used by Mrs. Sagalyn [6], or may be planar as have been used by Bourdeau [7], by McKibbin [8] and by Hinteregger [9]. The spherical geometry has the advantage of symmetry and hence no aspect correction while the planar types are generally easier to construct. Again, the ion traps are sometimes mounted on booms while others are mounted directly on the rocket (or satellite). Boom mounting appears preferable: the instrument is not influenced by the space charge sheath of the vehicle and the outer grid can be swept through space potential. Also the use of a boom minimizes the time the instrument spends in the rarefied wake of the vehicle.

5. Atmospheric Electricity Techniques

There are two methods of measuring ion density in the lower atmosphere. In the one the quantity measured is conductivity σ; this is related to ion density n by

$$\sigma = nek$$

where k is the mobility and is itself related to ion collision frequency ν by

$$k = \frac{1}{2}\frac{e}{m\nu}$$

The conductivity is measured by applying a small voltage across a suitable electrode system, which is usually the Gerdien arrangement of concentric cylinders. A basic assumption of atmospheric electricity techniques is that currents are so small that no space charge problems arise.

It is instructive to compare the current flow to a small sphere, radius a, by Langmuir probe theory (no collisions) and by conductivity theory (collision-controlled motion). For the probe and slope of the current-voltage curve in the accelerating region is

$$\frac{di}{dV} = \frac{A\, j_e}{kT/e}$$

Putting $A = 4\pi a^2$

$$j_e = nev/4$$

and $$kT/e = \frac{1}{2} mv^2$$

we have

$$\frac{di}{dV} = 2\pi a^2 \left(\frac{ne}{mv}\right)$$

For the conduction of current to the probe, on the other hand,

$$\frac{di}{dV} = 4\pi\sigma C$$

where C is the capacity of the probe.

Putting $$\sigma = \frac{1}{2}\frac{ne^2}{m\nu}$$

$$\nu = v/\ell \quad (\ell \text{ is mean free path})$$

$$C = a$$

we have $$\frac{di}{dV} = 2\pi a\ell \left(\frac{ne}{mv}\right).$$

This differs from the Langmuir probe equation in having $a\ell$ where the other equation had a^2. Thus both treatments give the same result at the height at which $\ell = a$. This confirms what might be otherwise felt to be obvious, that the two regimes are divided at the point at which the mean free path (ion or electron) equals the probe radius. For probes of the order of 1 cm this places the boundary at about 85 km for ions and at about 80 km for electrons. It should be possible to derive an expression valid in the transition region of the upper D-region.

The other atmospheric electricity technique is the ion counter. This is really the same as an ion trap in which all ions of one sign entering the device (usually consisting of concentric cylinders) are collected. The current is given by

$$i = nevA$$

where v is the velocity of the gas into the instrument and A is the area of the aperture.

The DC techniques of ionospheric physics and atmospheric electricity are now developed to a point where it should be possible to measure ion and electron density throughout the D-region. Vehicles are available for carrying instruments through the region and modern techniques of instrumentation have facilitated the measurement of very small currents. Several problems must be recognized and eliminated but there is no obvious fundamental limitation. Important problems are:

1. Presence of free electrons. It is necessary to use biassed grids and magnets if negative ions are to be measured in the presence of electrons.

2. Return current. Design of the instrument must take account of electrically floating system which is regarded as a bi-polar system.

3. High velocity. Theoretical treatments relate only to low velocity, laminar flow. Theories must be developed for supersonic flight. For example a rocket which just reaches 90 km has a velocity at 50 km of at least 0.9 km/sec which is exactly twice the mean ion velocity at that height. A trajectory with an apogee of 200 km gives velocities of 1.7 and 1.5 km/sec at 50 and 90 km. These are about four times the mean ion velocity in the region.

There are other practical problems in applying these techniques to rocket measurement but on the whole they can be solved. For example, RF breakdown at antennas can change the vehicle potential and bias off a Langmuir probe. Similarly contamination of the environment by gas escaping from the payload can be avoided by proper venting. Another problem area is interference between probes on the same vehicle. These are not considered fundamental limitations on the use of probes and can be eliminated by proper design.

6. Conclusions

The differential absorption experiment is probably the best developed technique for electron density measurement in the D-region. The Faraday rotation experiment is useful but appears to be rather limited in accuracy.

Probes, both RF and DC, have advantages under rapidly changing conditions. It is likely that the DC probe will be the more useful for the lowest part of the D-region.

The measurement of ion density is more difficult, and successful methods will probably be adapted from the atmospheric electricity techniques with due regard to the presence of free electrons and the very high velocity of rockets.

References

[1] Rawer, K. and E. Argence, "Information Obtained by Passive Radio Frequency Spectrometers in Rockets," in Space Research II, ed. van de Hulst et al., 1220-1237, (1961).

[2] Bowhill, S.A. and E.A. Mechtly, "An Ionosphere Electron Density Experiment Particularly Suited for Small Rockets," in Space Research II, ed. van de Hulst, et al., 1208-1214, (1961).

[3] Seddon, J.C., "Differential Absorption in the D and Lower E Regions," J. Geophys. Res. 63, 209-216, (1958).

[4] Seddon, J.C., "Propagation Measurements in the Ionosphere with the Aid of Rockets," J. Geophys. Res., 58, 323-335, (1958).

[5] Kane, J.A., "Re-evaluation of Ionosphere Electron Densities and Collision Frequencies Derived from Rocket Measurements of Refraction Index and Attenuation," JATP, 23, 338-347, (1962).

[6] Sagalyn, R.C., M. Smiddy and J. Wisnia, "Measurement and Interpretation of Ion Density Distributions in the Daytime F Regions," J. Geophys, Rev., 68, 199-211, (1963).

[7] Bourdeau, R.E. and J.L. Donley, "Explorer VIII Satellite Measurements in the Upper Atmosphere," NASA X-615-63-165, August 1963. (To be published in Proc. Roy. Soc.)

[8] McKibbin, D.D., "A Direct Measurement of Charge Density in the F2 Region," IRE Transactions on Instrumentation, 96-99, December 1962.

[9] Hinteregger, H.E., "Combined Retarding Potential Analysis of Photoelectrons and Environmental Charge Particles up to 234 km." Space Research, ed. Bijl, North-Holland Publishing Co., Amsterdam, 1960, pp. 304-327.

DISCUSSION

B. Landmark: In Figure 6, results obtained by a DC probe of the type described by L. G. Smith are compared with results from electron density observations obtained simultaneously from propagation experiments. These included the inverse Seddon technique at 2.5 Mc/s, and Faraday rotation at 4.9 and 15 Mc/s.

This rocket was launched into a weak auroral absorption event (riometer absorption of

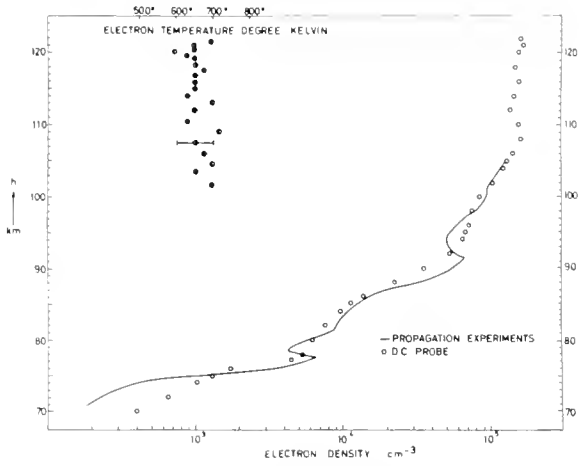

Figure 6. Comparison of electron densities measured simultaneously by DC probe and radio propagation techniques.

0.5 db at 27.6 Mc/s). It was one of a joint Danish-Norwegian NASA programme and the DC probe was included by Dr. J.A. Kane of Goddard Space Flight Center.

The results from the DC probe are normalized to those of the propagation experiment by making the observed electron densities equal with a height of 100 km.

It should be noted that the detailed structure observed in the profiles measured by the propagation techniques are believed to be due to time changes, and the agreement therefore is quite good. It appears that the electron density may be obtained down to 75 km by the DC probe technique.

R.L.F. Boyd: Is not the temperature rather higher than might be expected?

B. Landmark: Yes, but one must remember that this was an auroral absorption event, not a quiet ionosphere.

L.G. Smith: The electron density curve was deduced from a constant-voltage made of probe operation, while each temperature was deduced from a full sweep of the probe curve, and does not depend on the normalization.

1.B DIRECT MEASUREMENT OF ELECTRON AND ION TEMPERATURE

R. L. F. BOYD
University College of London
London, England

1. Introduction

This paper will consider only the measurement of electron temperature at altitudes great enough for neutral particle collisions of the electrons to be neglected in interpretation of Langmuir type probes. Since it is very difficult to see how electrons could fail to be in thermal equilibrium with the neutral gas at altitudes where the mean free path is less than a centimeter or so, this restriction is probably unimportant. At heights where disequilibrium may be expected, Langmuir probe theory should be applicable. The measurement problems therefore concern techniques rather than the basic physics of probe action.

Measurements of electron temperature by studies of collision frequency will not be considered, but this should be interpreted as a challenge to development of adequate means of interpreting such measurements in terms of electron temperature.

It is to be noted that the use of the term temperature implies the assumption of a Maxwellian velocity distribution for the particles. This may not always be valid; indeed it cannot be exactly true where disequilibrium exists between some charged species and the other particles. Some reference will be made to methods of studying energy distributions.

2. Use of Boltzmann's Relation

Practical methods of finding the electron temperature, T_e, make use of Boltzmann's relation for the concentration $N_e(V)$ of electrons in a region of potential V (a negative quantity in practice) to the concentration $N_e(0)$ where the potential is zero.

$$N_e(V) = N_e(0) \exp(eV/kT_e)$$

We note that $(kT_e/e) \sim 20$ mvolt at 100 km if there is thermal equilibrium. This fact points up the experimental problem that must be faced in view of the absence of a firmly established fixed potential datum.

In principle any method of local measurement of N_e may be used to find T_e providing the potential of the locality can be accurately varied. The following brief notes concern several possible ways of varying V and measuring N_e to obtain T_e.

3. Variants of the Langmuir Probe

3.1 The Langmuir Analysis[1] The positive ion component i_+ and the photo-emission component i_{phot} are removed by linear extrapolation from high negative values of probe potential. T_e is found from

$$\frac{d(\ln i_e)}{dV} = \frac{e}{kT_e}$$

The major problem arises from the variation of vehicle equilibrium potential with time due to --

a) changing aspect, velocity and ambient ionization resulting in changing ion flux to the vehicle

b) changing photoemission from the vehicle due to changing aspect and altitude

c) RF fields from antennae varying electron fluxes

d) changing vehicle potential due to the need to return current collected by probes to the plasma (current dumping)

e) changing surface conditions with outgassing, uv radiation, ion bombardment, etc.

Garscadden and Emeleus[2] have shown that for changes in reference potential less than about $(kT_e/2e)$ the value of $\frac{d(\ln i_e)}{dV}$ is unaffected provided we average currents over times long compared with the periods of the potential "noise"

It follows that if the fluctuations in vehicle potential are fast and less than about 10 mvolt a slow voltage sweep may be used, otherwise the i-V curve must be obtained in a time short compared with the time over which the vehicle potential changes by a few mvolt. The latter approach has been used by most workers.

3.2 Gridded Probes[3] The use of a grid has some value in providing an instrumental method of removing i_e and i_{phot} (which may well by varying with aspect so as to complicate the extrapolation method of removing them). It is important, however, to recognize that the effect of sheath field penetration on the energy distribution of the particles may lead to anomalous results if the mean energy of the attracted particles is much less than that of the repelled species. This could occur, for example, if a positive grid were used to reject hypersonic positive ions so as to enable a retardation analysis to be carried out by a collector behind it. For this reason it is safer to separate the

charged species by a suitable bias on the collector and to perform the retardation analysis by means of the grid.

It must not be overlooked that a grid is not the idealized equipotential surface we might like it to be.

3.3 Druyvesteyn Analysis[4] Druyvesteyn has shown that the important quantity in determining the energy distribution of charged particles by a retardation analysis is the second derivative of the i-V characteristic:

$$f(E.dE) = \frac{2}{A.e} \left(\frac{2m}{e}\right)^{\frac{1}{2}} V^{\frac{1}{2}}. \frac{d^2i}{dV^2} dE$$

where A is the area of the probe and the other symbols have their customary significance. This result is true for an isotropic distribution with any non-entrant probe shape or an anisotropic distribution with a spherical probe. For supersonic ions, therefore, a spherical geometry is to be preferred. (A plane geometry can be used if the angle between the vehicle velocity vector and the plane normal is known and is not changing too rapidly.)

The system used on the Ariel satellite determines the first derivative i' and the ratio of the second to first derivatives i''/i' by using the i-V characteristic to mix two small audio frequency voltages. Some such automatic method of finding i' would seem to be necessary as taking the second difference of telemetered quantities would normally introduce an unacceptable amount of inaccuracy.

For a Maxwellian distribution.

$$i = i_{eo} \exp \frac{eV}{kT_e} + i_+ + i_{phot}$$

$$i' = i_{eo} \left(\frac{e}{kT_e}\right) \exp \frac{eV}{kT_e}$$

$$i'' = i_{eo} \left(\frac{e}{kT_e}\right)^2 \exp \frac{eV}{kT_e}$$

so $\frac{i''}{i'} = \frac{e}{kT_e}$

i_+ and i_{phot} are almost constant so that i'_+ and i'_{phot} can be neglected.

3.4 Resonance Rectification Probe Used Off Resonance

The difference in current drawn by a resonance rectification probe at frequencies well above and well below resonance is a measure of the rectification produced by the probe, that is of the second derivative of the characteristic. Providing alternative means are available for finding the operating point on the curve (such as plotting the whole i-V curve) this can be used to obtain T_e. Alternatively since the effect of the Nth derivative of the characteristic on the magnitude of the rectified current depends on the nth power of the AC amplitude, the use of two different amplitudes can be used to obtain T_e.

4. Resonance Rectification Probe Used at Resonance

This system gives the plasma frequency. In principle the region studied could be enclosed in a suitable open mesh gridded structure so as to enable N_e to be varied according to Boltzmann's relation.

It may also be worth noting that, since the resonance probe gives the collision frequency and the electron concentration from the resonance curve, T_e should also be obtainable.

5. Impedance Probes

Impedance probes, especially of the almost closed configuration used by Sayers can, in principle, at any rate, be used to give Te by an application of Boltzmann's relation to the value of N_e found for varying potentials of the system.

6. Illustrative Material

Figure 1 shows how gases from a rocket motor can seriously affect the experiments. These are measurements of electron density made with Langmuir probes in a Black Knight liquid fueled rocket; the density measured drops zero when the vehicle rolls so as to bring the motor ahead of the probe. These are high altitude measurements, but the same phenomena occur

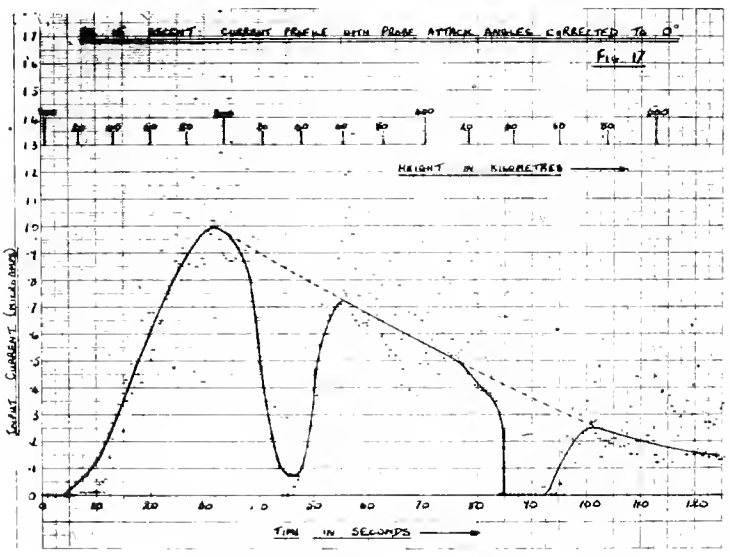

Figure 1. Langmuir probe current in a tumbling rocket

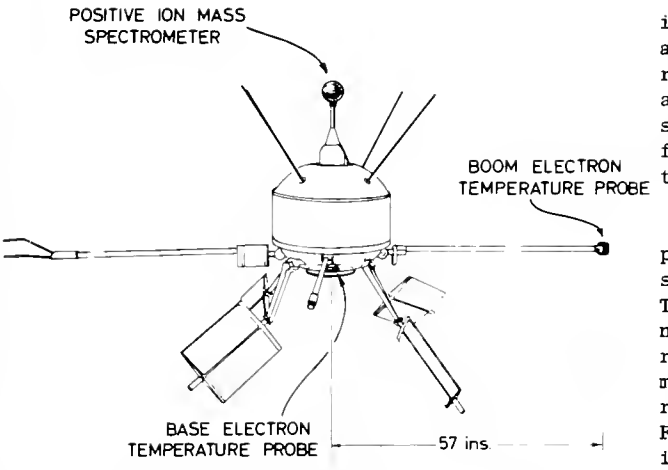

Figure 2. Probe arrangement on the Ariel satellite

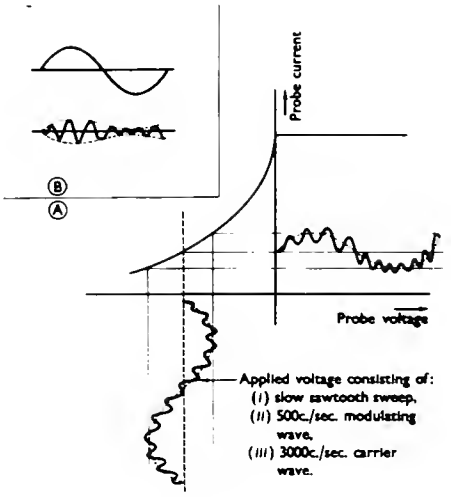

Figure 3. Principle of the Druyvesteyn analysis

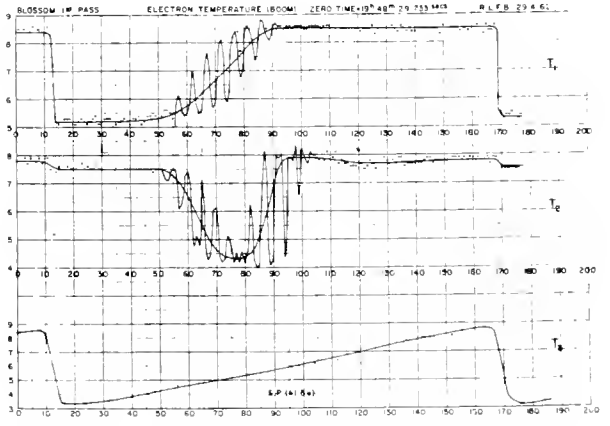

Figure 4. Telemetry record showing effect of induced voltages

in the lower ionosphere. The F-layer peak is at about 35 sec, and subsequent parts of the record correspond to altitudes above the peak, and up to about 520 km. At the time of the sudden drop at 85 sec, we ejected some nitrogen from the vehicle, which completely destroyed the instrument response.

Figure 2 illustrates the configuration of probes on the satellite Ariel. A spherically symmetrical ion probe is used on the roll axis. The two electron probes have their surfaces normal to the roll axis so as not to receive rapidly varying insolation. The vehicle is made as symmetrical as practicable so as to reduce roll modulation of vehicle potential. For the same reason the solar "paddles" are insulated from the main structure.

Figure 3 shows the method by which we obtain the ratio of the first to the second derivative of the probe curve. Two different audio frequencies are added to the probe voltage; then because the lower frequency moves the higher up and down the characteristic, it is amplified to different degrees, and the output can be resolved into two components, one sinusoidal and one modulated. It can be shown that the fractional depth of modulation is a measure of the ratio of the first to the second derivative, i''/i', of the probe curve; it is, therefore, a direct measure of the reciprocal

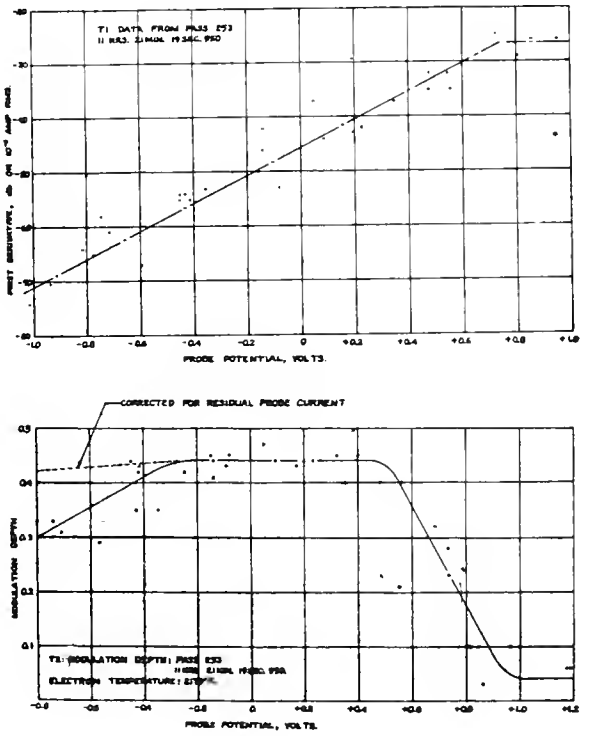

Figure 5. Curves for i' and i''/i' corrected for induced voltages

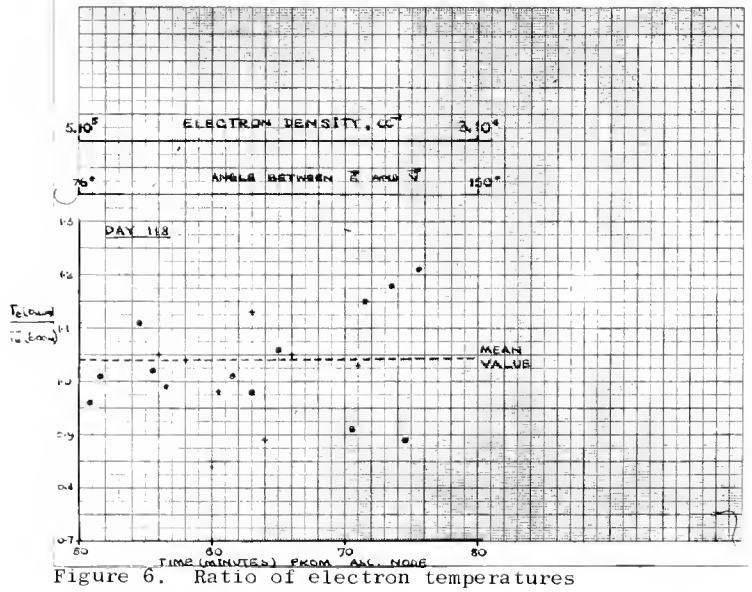

Figure 6. Ratio of electron temperatures deduced from two independent probes

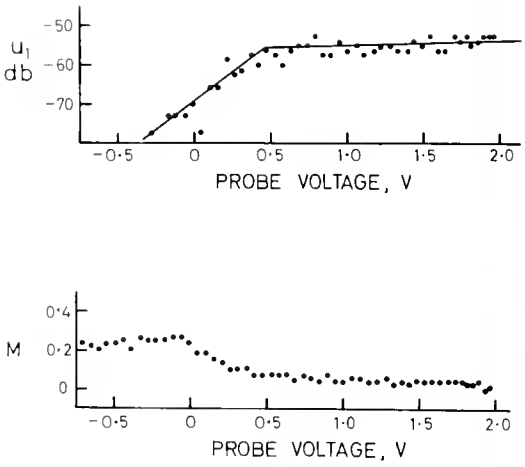

Figure 8. Base probe curve: probe near edge of wake

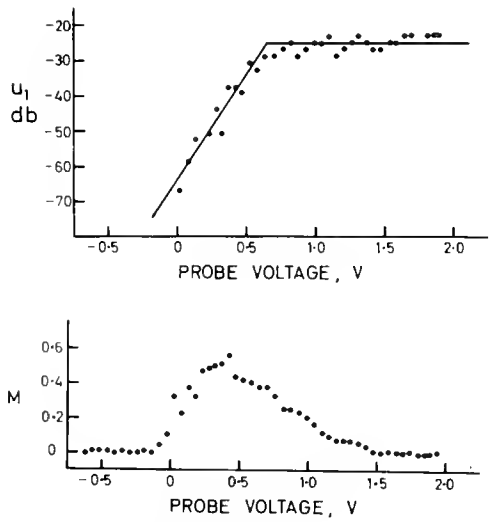

Figure 7. Base probe curve: probe looking forward

of the electron temperature. This system has an accuracy of about 4%, and has been in operation for some 18 months on the satellite Ariel.

Figure 4 shows a telemetry record from the electron temperature probe mounted on the boom of the Ariel satellite, the ordinate being the reciprocal of the electron temperature. The record shows a modulation in i' due to an e.m.f. induced by the earth's magnetic field in the boom carrying the probe. This effect was absent from the probe mounted on the roll axis. This effect could well be important in the lower ionosphere if the vehicle precesses.

Figure 5 illustrates the constancy of i''/i' after correcting for the induced e.m.f. effect over most of the characteristic. It is this fact that makes the cross modulation technique relatively insensitive to variations in vehicle potential and most economical of telemetry band width. Incidentally, it also illustrates that the departure of the electron energy distribution from Maxwellian form in the top side ionosphere is less than about 1%.

Figure 6 shows the ratio of the electron temperature measured by a probe on the boom, to that measured in the base of the vehicle. The mean value of the ratio is 1.04; this is almost certainly a systematic error in setting up the instrumentation, and gives a measure of the precision of the electron temperature determination. The scatter of the ratio is real and is attributable to irregularities in the temperature field and the fact that the measurements by the two instruments were not simultaneous.

Figures 7 and 8 taken together illustrate in the latter case an anomalous set of values of M = i''/i' obtained as the base probe passed into the wake. Analysis of this behaviour shows that it must be attributed to variations in the plasma properties at frequencies near those used in the cross modulation system. That is to say the curves show evidence for turbulence or plasma oscillation in the wake. It may be that similar effects could cause errors (which might go undetected) in measurements of electron temperature by conventional analysis of probe curves taken in the lower ionosphere.

7. Positive Ion Energy and Spectrum

It is interesting to note that if the energy distribution of ions is measured from a

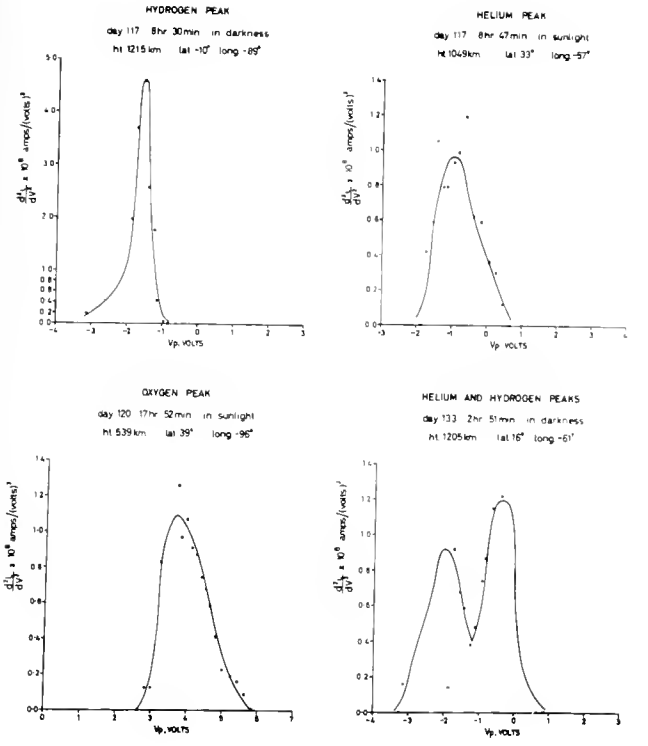

Figure 9. Positive ion spectrum peaks

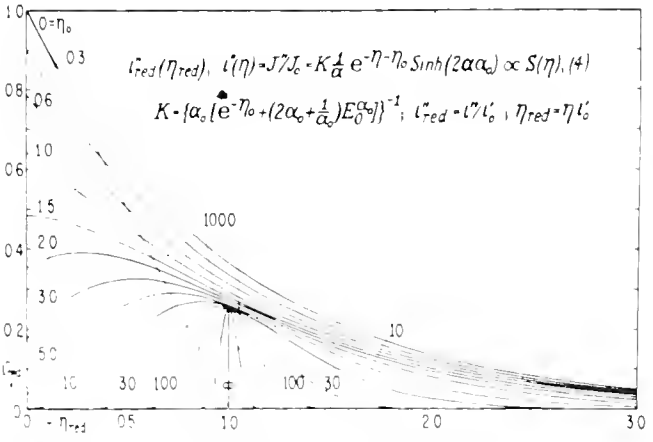

Figure 10. Idealized positive ion spectra for various vehicle velocities (after Medicus [5])

hypersonic vehicle the energy spectrum line is broadened in such a way that for very high Mach numbers, such as are found using satellites, the peak width is given by $4(kT_+ + \frac{1}{2}m_+v^2)^{\frac{1}{2}}$ where v is the vehicle velocity. Such measurements are thus less sensitive to variation in vehicle potential than are the electron temperature measurements. Figure 9 shows some spectrum peaks observed on the satellite Ariel for various ions; hydrogen, helium and oxygen. The width can be used to estimate the ion temperature; though not with the same accuracy as electron temperature, due to instrumental broadening.

At lower Mach numbers the energy spectrum peak is greatly distorted from the gaussian form. However, the theory has been given by Medicus[5] so there is no reason why ion temperatures should not be obtained at quite low Mach numbers or at subsonic velocities. Figure 10, by Medicus, gives the value of i'' as a function of energy for various vehicle velocities, showing the transition from a spectrum of the type of Figure 9, for a hypersonic vehicle, to a Langmuir probe curve for a stationary vehicle.

8. References

[1] General Electric Rev. 27, 449 (1924)

[2] Proc. Roy. Soc. 79, 535 (1962)

[3] Proc. Roy. Soc. A201, 329 (1950)

[4] Z. Phys. 64, 790 (1930)

[5] J. Appl. Phys. 32, 2512 (1961)

DISCUSSION

N. W. Spencer: Over what distance was it necessary to average in determining the temperature?

R. L. F. Boyd: We determine temperature once per sweep; because of the very small bandwidth, this is once per minute.

N. W. Spencer: You drew attention to the scatter of the ratio in your Figure 6. Did each point refer to one measurement?

R. L. F. Boyd: Yes; while the measurements are separated by a considerable distance, this is above 400 km, where horizontal distances are less important than in the lower ionosphere. In the rocket launches we used a much faster sweep, because of better telemetry.

N. W. Spencer: We have observed changes over relatively small distances.

K. W. Champion: On Figure 9, how do you obtain a hydrogen peak and a helium peak at the same altitude and almost the same time?

R. L. F. Boyd: The ratio depends critically on geomagnetic latitude and local time. We have a complete distribution of the altitude for equal quantities of H and He over the earth as a function of nearly everything. These are just two selected examples. At other times one may find equal amounts of H and He at 1200 km.

1.1 A CYLINDRICAL ELECTROSTATIC PROBE FOR THE MEASUREMENT OF ELECTRON TEMPERATURE IN THE IONOSPHERE

L. H. BRACE
Goddard Space Flight Center
NASA
Greenbelt, Maryland

The electrostatic probe used on the Explorer 17 satellite and on several rocket flights (including a rocket-borne ejectable instrument called the Thermosphere Probe, Figure 1) is a spring-loaded Langmuir probe modified by the addition of a guard electrode which permits the plasma measurement to be made outside the disturbing ion sheath which surrounds the instrument. A 5 c/s sawtooth voltage is applied to the collector and guard and the resulting collector current characteristic is detected in two ranges of sensitivity. There is also a hemispherical collector; the two collectors are developments of the dumbbell experiment recently reported in JGR, and are here combined with a neutral particle experiment for the measurement of gas temperature.

The main emphasis in the cylindrical probe has been on electron temperature; it is ejected at an altitude of about 100 km, rises to 300 or 400 km and falls back, telemetering its data.

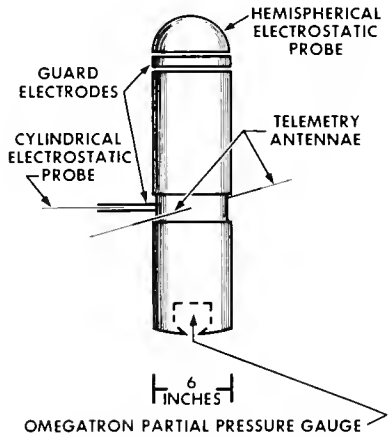

Figure 1. General arrangement of the thermosphere probe

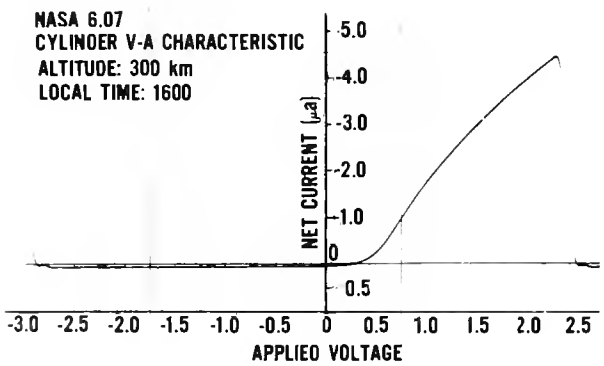

Figure 2. Telemetered i-V curve; coarse mode

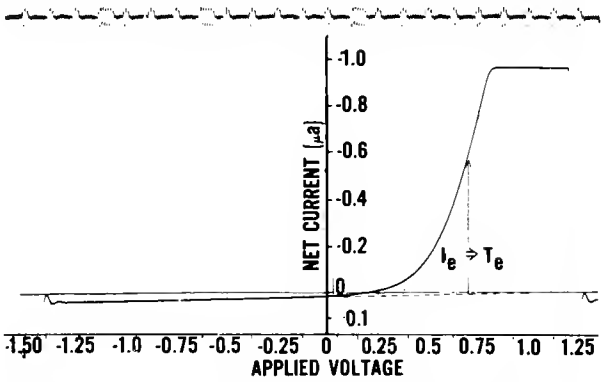

Figure 3. Telemetered i-V curve: fine mode

Figures 2 and 3 show typical i-V characteristics recorded in the high voltage-high current mode (coarse mode) and the low voltage-low current mode (high resolution). Note that the electron current versus voltage characteristic is obtained by subtracting the extrapolated ion current (shown dashed) from the measured (total) current. The electron temperature is then derived from the slope of the plot of $\ln i_e$ against v, as shown in Figure 4, for the curve of Figure 3. The plot is essentially linear over two decades of current; this is used to calculate the electron temperature, the plasma potential being the point where the characteristic deviates from linear. There is, however, some question as to whether that is the exact location of the plasma potential. We use the characteristic in both the ion mode, the

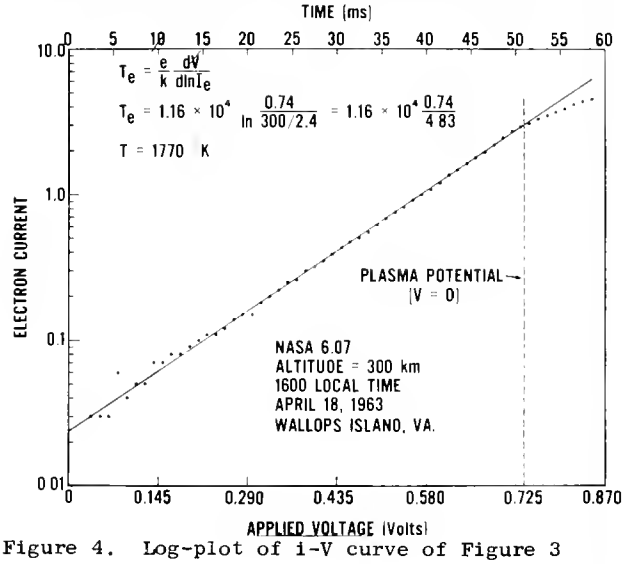

Figure 4. Log-plot of i-V curve of Figure 3

small ion current being resolved by more sensitive detectors, and in the electron saturation region.

The electron temperature data from this flight will be discussed in a later section by N. W. Spencer in his paper concerning the neutral N_2 experiment carried aboard the Thermosphere Probe instrument.

DISCUSSION

R. L. F. Boyd: What is the time period of the sweep?

L. H. Brace: 200 msec for the full six volt sweep. We went through the exponential in about 20 msec.

N. W. Spencer: A key factor in orientation and photoemission effects is the area ratio of the electrodes of the probe system. If the electrode which is primarily responsible for establishing a potential, the vehicle itself, has a ratio sufficiently large with respect to the probe, then the change of the probe potential has no effect upon the vehicle potential, and it will remain constant provided that one performs the sweep rapidly enough. The fact that one can is demonstrated by Figure 4 that Dr. Brace showed, which was in fact a very good straight line over a considerable portion of the sweep.

If the electrode pair have areas that are somewhat comparable, as in the dumbbell probe, the potential of the body varies with the probe potential; this means that you must either know how the potential varies as a function of orientation, which has been solved theoretically, or you again can sweep fast. In satellites you have in addition to the orientation change the effect of magnetic field, as Dr. Boyd noted. Once again if you sweep fast enough this too can be totally ignored. In techniques that measure the total current, as opposed to selecting components of the current, the values of photoemission that we find (which are in accord with those measured by Hinteregger) at altitudes up to about 1000 km provides no problem. At lower altitudes it is completely overwhelmed by the other currents, and in those cases where we have made measurements near 100 km we have been able to measure the photocurrent and either consider or ignore it, but in any case one can avoid these problems by sweeping fast.

1.2 ION PROBE USED IN THE JAPANESE SOUNDING ROCKET

K. HIRAO and S. MIYAZAKI
Radio Research Laboratories
Kokubunji, Tokyo, Japan

1. Introduction

The Japanese rocket sounding of the ionosphere started at 1960 by using Langmuir ion probe. A remarkable feature of this ion probe was a meshed spherical probe. A meshed spherical probe can reduce the effect of photoelectron emission by solar radiation due to its small surface area, but it is equivalent to solid spherical probe in catching ions from surrounding atmosphere by supplying adequate high negative voltage to it. In the first three experiments, swept voltages from +10 to -20 volts and stepping voltages of each 10 volts from -30 to -100 volts were supplied to a probe and obtained was the ion density by analyzing the observed Langmuir characteristic curbe. Since the fourth experiment, the same type probe has been used, but the supplied voltage was not variable but constant in about -22 volts. In the analysis of ion probe measurement, it is the most important problem to distinguish a characteristic height to make a different analysis according to many collision region, one collision region and orbital motion region. The fundamental equations are the Mott-Smith-Langmuir equation for one collision and orbital motion regions and the equation of space charge conduction for many collision regions. In this paper, an example of the accurate reduction of obtained data will be shown.

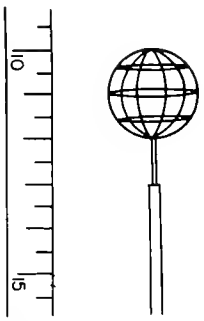

Figure 1. Meshed spherical probe

The second problem treated in this paper is the effect of solar radiation on a probe. Both the meshed spherical probe and the solid spherical probe were simultaneously installed on a rocket, and the difference between these two probes was estimated as the effect of photoelectron emission.

2. Instrument

The ion probe is a part of the Direct Ionosphere Sounding instrument type II, which contains an ion probe, resonance probe and Langmuir probe for electron measurement. Figure 1 shows a meshed spherical probe. A meshed spherical probe is made of gold-plated molybdenum or nickel wire of 0.2 mm in diameter. A wire is bent in circle and spot welded into spherical cage of 2 cm in diameter. Solid spherical probes also have their diameters of 2 cm and made of gold-plated copper plate of 0.3 mm thickness. The circuit diagram of ion probe is shown in Figure 2. Internal calibrater is used in the input of amplifier and send out a calibration signal cyclicly in every six seconds. Probe voltage supply is made by mercury cells and the actual supplied voltage is corrected by the observed ion current.

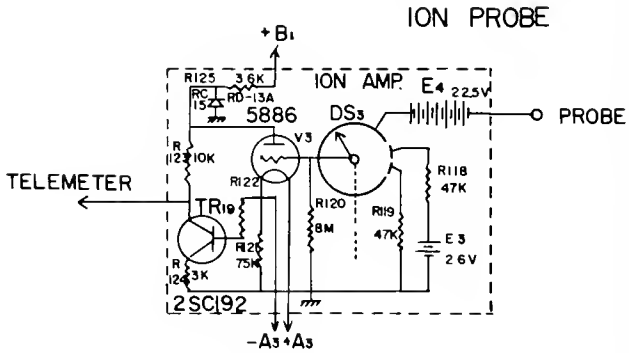

Figure 2. Circuit of ion probe

3. Discussion about the ion sheath and photoemission

The equations for the calculation of ion density from the observed current in orbital motion and one collision region are

$$i = \frac{16}{9}\pi\varepsilon_0\left(\frac{2e}{M}\right)^{1/2}\frac{V_p^{3/2}}{\alpha^2} \qquad \alpha = f\left(\frac{a}{r_p}\right)$$

$$i = 4\pi r_p^2\,\frac{a^2}{r_p^2}\,J\left\{1-\frac{a^2-r_p^2}{a^2}\exp\left(-\frac{r_p^2}{a^2-r_p^2}\frac{eV_p}{KT_+}\right)\right\}$$

where

- i : positive ion current to the spherical probe
- r_p : radius of the spherical probe
- a : radius of the ion sheath
- J : ion current density flowing from plasma to the ion sheath
- K : Boltzmann's constant
- T_+ : ion temperature
- e : unit charge of electron
- V_p : probe to plasma voltage
- M : mass of ion

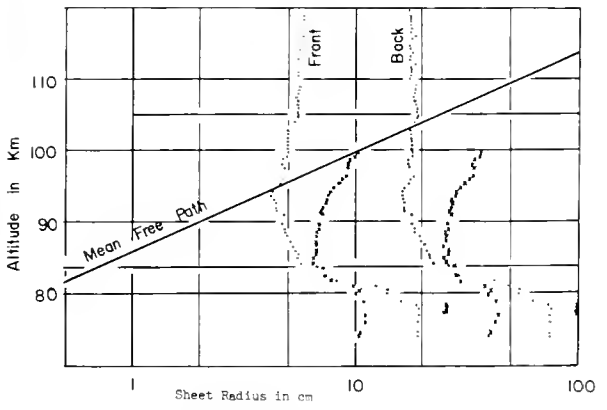

Figure 3. Dimensions of ion sheath

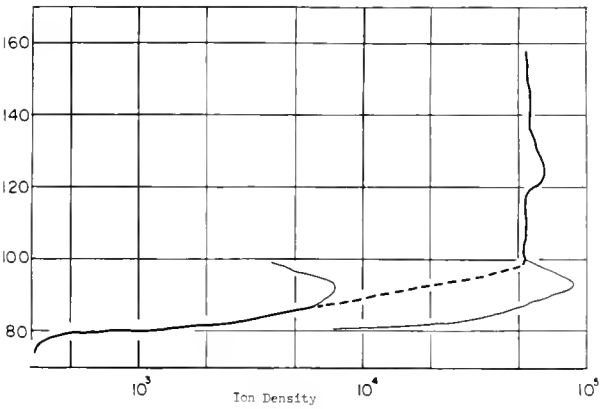

Figure 4. Ion density distribution obtained by meshed spherical probe

ε_0 : dielectric constant

α : the transendental function of a/r_p

ε : base of natural logarithm.

α is the solution of the following equation

$$3\alpha\frac{d^2\alpha}{d\gamma^2} + \frac{d\alpha}{d\gamma} + 3\alpha\frac{d\alpha}{d\gamma} - 1 = 0$$

where

$$\gamma = \log\left(\frac{a}{r_p}\right)$$

The effect of a meshed spherical probe is, of course, very complicated problem, but is approximately treated by considering the transparency of meshed probe for the motion of charged particle inside the sheath.

While the equations for the calculation of ion density in the many collision region are

$$i = 4\pi r_p^2\left(\frac{a^2}{r_p^2}\right)J$$

$$i = \frac{4}{3}K_0'\frac{1}{(p_0 r_p)^{1/2}}\frac{V_p^{3/2}}{(\phi_{sb})^{2/3}}$$

$$\phi_{sb} = \left(\frac{a}{r_p}\right)^{\frac{1}{3}}\int_1^{\frac{a}{r_p}}\left(1 - x^{-2}\right)^{2/3}dx$$

where K'o is obtained experimentally from the following relation

$$v_+ = K_0'\left(\frac{E}{p_0}\right)^{\frac{1}{2}}$$

and p_0: gas pressure in 0^oC

v_+: velocity of ion

E: electric field.

Figure 3 shows the calculated dimension of the ion sheath around the probe in the actual rocket sounding data. In this figure, the dimension of both the front and backward ion sheath towards the direction of movement of rocket are shown with the mean free path of ion.

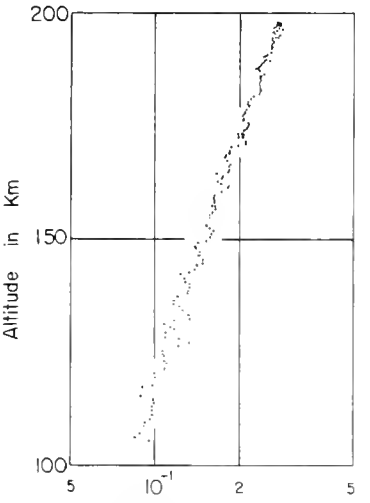

Figure 5. Photoemission current density in $\mu A/cm^2$

Dots in Figure 3 are the sheath dimension calculated under the condition of orbital motion and crosses are that of many collisions. From this figure, it is considered that the altitude region lower than about 85 km is the many collision region and that higher than 105 km is the orbital motion region.

Figure 4 shows the ion density distribution, where the thick solid line shows the most reasonable distribution of ion density.

Two thin lines show the apparent value of ion density calculated under the condition of many collision and orbital motion, respectively. The final determination of ion density distribution is thus carried out.

Next, the effect of photoemission will be discussed. The difference between the ion current of solid sphere probe and the product of the reciprocal of transparency of meshed spherical probe and its current, is calculated. Roughly speaking, it is caused by the photoemission by the solar radiation from the probe

surface. This calculation is made from the data obtained at the altitude higher than 105 km. The calculated current density is about 10^{-1} $\mu A/cm^2$ and is shown in Figure 5. This current corresponds to the photo electron flow of 6.25×10^{11} number / cm^2 sec and is considered to be reasonable value. There remains many problems to be discussed in the observed results, but the observed materials are not yet enough to make the analysis completely.

The final determination of ion density distribution is thus carried out.

References

[1] T. Ichimiya, K. Takayama and Y. Aono: A probe for measuring ion density in the ionosphere. Space Research 1 (1960).

[2] T. Ichimiya, K. Takayama and Y. Aono: Measurement of positive ion density in the ionosphere. Re. Ionos. Space Res. in Japan XIII (1959) No. 3.

[3] T. Dote, T. Ichimiya and F. Tamaki: Some experiment on probe characteristics drifting plasma. Jour. Phy. Soc. Japan 18 (1963) No. 2.

[4] Y. Aono, K. Hirao and S. Miyazaki: Rocket observation of ion density electron density and electron temperature in the ionosphere. Jour. Rad. Res. Labs. 9 (1963) No. 46.

DISCUSSION

N. W. Spencer: You mentioned photocurrent densities of about 10^{-7} ampere; Hinteregger's measurements, and our own, show much lower densities.

R. L. F. Boyd: I agree, but none of us have used gold.

N. W. Spencer: Perhaps that is the answer, but values we see for stainless steel or tungsten are about 1 or 2 times 10^{-9} ampere/cm^2, or a factor of 100 less.

1.3 RESONANCE PROBE AVAILABLE FOR THE IQSY

K. HIRAO and S. MIYAZAKI
Radio Research Laboratories, Kokubunji, Tokyo, Japan

and

T. MURAOKA
Yokokawa Electric Works, Musashino-shi, Tokyo, Japan

1. Introduction

The resonance probe is one of the RF plasma probes, which was discovered in Japan. When a Langmuir probe is supplied by constant RF voltage as well as a DC voltage, a characteristic curve deforms. If a frequency of supplied voltage is fairly lower than plasma frequency, the deviation is almost constant in such a frequency range and expressed theoretically as a function of electron temperature of an environmental plasma as follows.

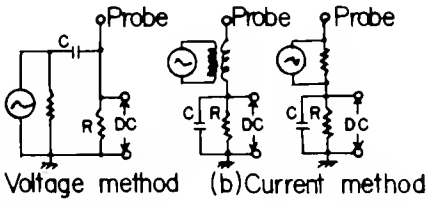

Figure 1. Fundamental circuit of resonance probe

$$\Delta V = \frac{k\,l e}{e} \log_{\varepsilon} I_0\left(\frac{ea}{kT_e}\right)$$

where k: Boltzmann's constant
T_e: Electron temperature
e: Electronic charge
a: Supplied RF voltage
ΔV: Voltage shift of probe wall potential

When the frequency of supplied RF voltage approaches to the plasma frequency of the environmental plasma, the deviation becomes large. If the supplied frequency just fits to the plasma frequency, the deviation becomes maximum and then decreases as the increase of supplied frequency to the original characteristic curve, i. e., the level of no RF supply. This is a brief description of the resonance probe phenomenon. Therefore, both the electron temperature and electron density can be obtained simultanously by getting the resonance probe characteristic of plasma. This phenomenon, however, appears when the electron collision frequency is fairly smaller than the plasma frequency. Therefore, if the resonance probe is used in the direct sounding of the ionosphere, it is valid in the altitude higher than 95 or 100 km. In Japan, seven resonance probes were already flown with good results and also three resonance

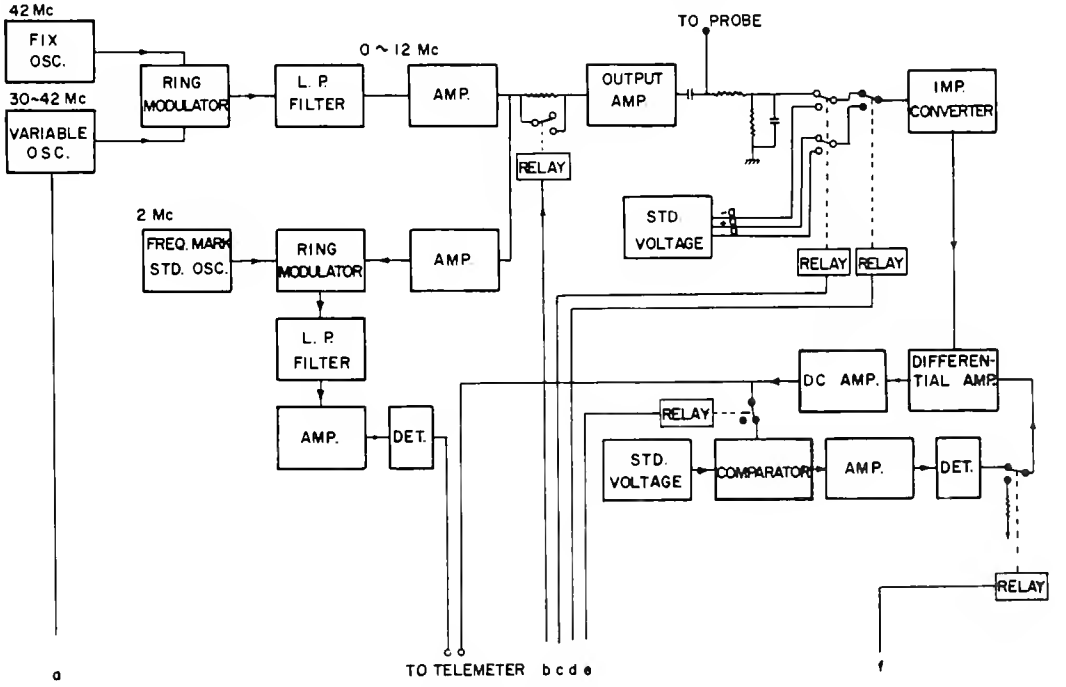

Figure 2. Measuring circuit and frequency marker circuit

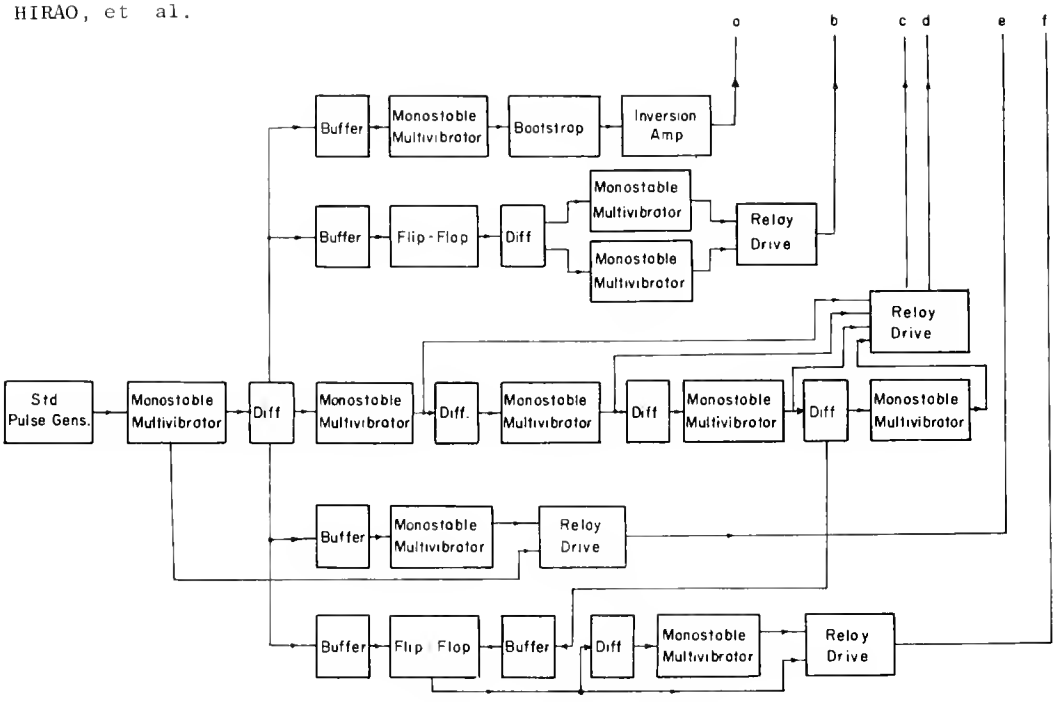

Figure 3. Timing circuit

Figure 3. Timing circuit

probes were used in Nike-Cajun rocket as the joint Japanese-U.S. experiment at Wallops Island also with sufficient success. In this paper, new type of resonance probe which will be available in many kinds of rockets for ionosphere sounding, is described briefly.

2. Circuit of Resonance Probe

The fundamental circuits of resonance probe in laboratory experiment are shown in Figure 1 A and B. Circuit A is "a voltage method" which detects the voltage deviation of characteristic curve, while Circuit B is "a current method" which detects the current deviation. From each of these two methods, both the electron temperature and density can be determined. In laboratory experiment, a current method is frequently used, but in rocket experiment a voltage method is very convenient to use as a rocket-borne circuit. The actual block diagram of the newly designed resonance probe is shown in Figures 2 and 3. The sweeping range of frequency is set to be from 0 to 12 Mc/s. This range is considered to be satisfactory to measure the whole region of ionosphere. As is seen in Figure 2, the level of swept frequency voltage becomes half cyclically, because the electron temperature is more accurately obtained if the temperature is calculated from the ratio of two deviations. This switching as well as the others are made by relays which are derived by signals from timing circuit.

In the probe measurement, the change of floating potential is always inevitable. In this probe, the circuit for automatic compensation of the change of floating potential is used. The internal calibration system is also used in this probe to check the DC electronic circuit.

3. Mechanical Construction of Resonance Probe

Whole these electronic parts are mounted on the seven circular boards of diameter of about 120 mm and connected by printed circuits. These boards are contained in a can of which diameter is 140 mm and height is also 140 mm and connected mutually through microconnectors on each board. This can is shown in Figures 4 and 5. This size of can is selected as it is available in a small sounding rockets as Kappa-8L and Nike-Cajun, etc. In IQSY, the synoptic rocket sounding of the ionosphere has been recommended by COSPAR. Therefore, such a small size of instrument is useful in any rocket, even if there remains a small space in bigger sounding rocket for the other items. As for the power supply for this instrument, a can of same size will be used with Nickel-Cadmium batteries inside. However, any other power supply will be available if it can supply +28V and -8V less than 300 mA and 10 mA, respectively.

As the probe electrode for resonance probe, solid spherical probe has been used in Japanese rocket sounding. However, the shape of electrode does not affect so much to the results of resonance probe. Tip probe on the top of nose cone of rocket as well as a plane probe on the side wall of rocket will be also available for the resonance probe. As the electrode of resonance probe is in almost the same potential as the floating potential, the ion sheath around the probe is not so big that the distance

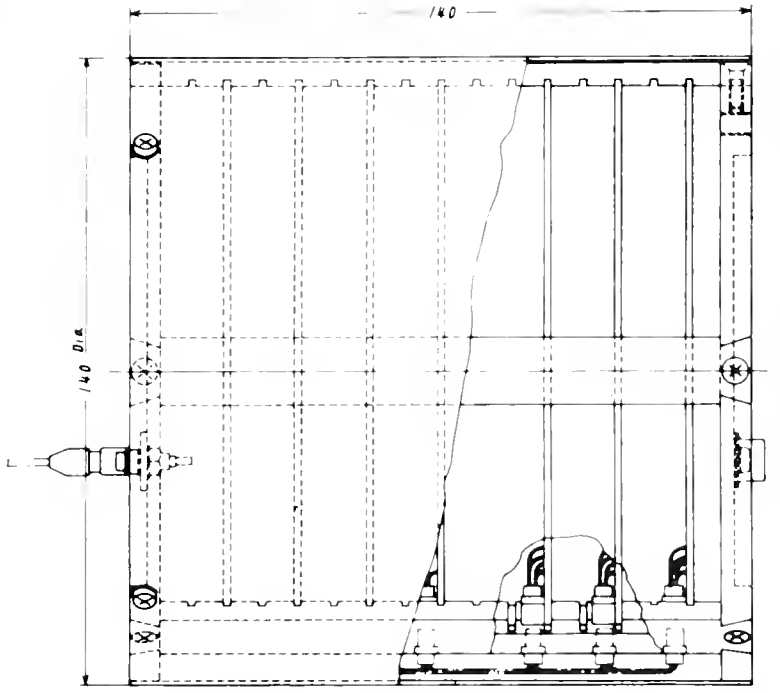

Figure 4. Measuring section front view

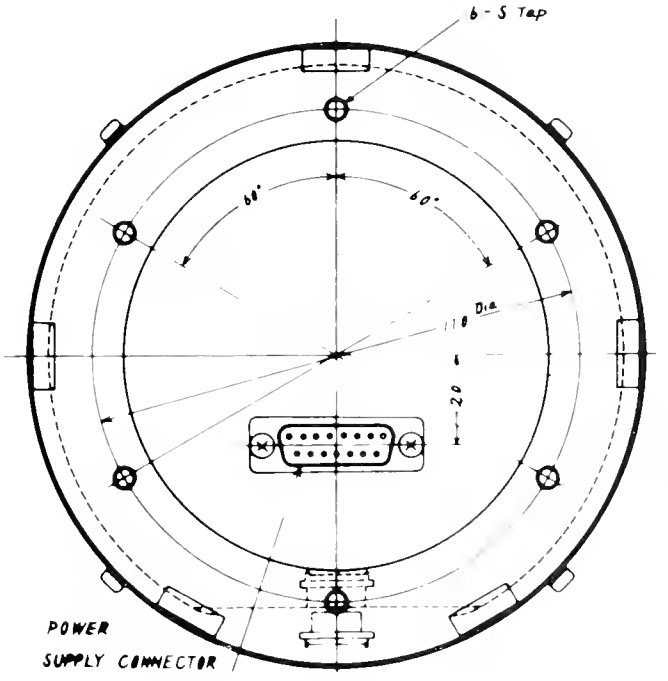

Figure 5. Measuring section bottom side view

between probe and rocket body is not necessary so large. Therefore, the design of probe itself is considered to be rather easy. The weight of the electronic part is about 1.5 kg, power supply part 2.5 kg and the probe section is 0.3 kg. Therefore, the total weight is about 4.3 kg.

Many resonance probes have been already used in the Japanese and joint Japanese-U.S. experiments with many successes in the measurements of electron density and temperature. Those probes had a mechanical slide resistor to generate a variable voltage which should be used in a variable oscillator. Moreover, they had mechanical commutators to change the calibrating voltages or so. Those slide resistors and commutators were so delicate that they could not work completely in so long duration. The present new type resonance probe had been improved in these points. This new one will be fired at December 1963 in Kagoshima rocket range with Lambda-2 rocket.

References

1. S. Miyazaki et al: Resonance probe - A new probe method for measuring electron density and electron temperature in the ionosphere. Rep. Ionos. Space Res. in Japan XIV (1960) No. 2.

2. K. Takayama H. Ikegami and S. Miyazaki: Plasma resonance in a radio frequency probe. Phys. Rev. 5(1960) No. 6.

3. K. Maeda and K. Hirao: A review of upper atmosphere rocket research in Japan. Jour. Planet. Space Sci. 9(1962) July.

4. K. Hirao and T. Muraoka: Technical instruction of resonance probe. not yet published.

5. Y. Ichikawa and H. Ikegami: Theory of resonance probe. Progress of Theoretical Physics 28(1962) No. 2.

DISCUSSION

L. C. Hale: In this paper, and the preceding one [1.2], you seem to have neglected the current due to the vehicle sweeping up ions. Could this be the source of much of the very large positive current you attribute to photoemmision?

K. Hirao: The ion current is not important for the resonance probe. It is important for the ion probe, but in the analysis we are not concerned with the change in vehicle potential.

R. L. F. Boyd: Could you explain how your cyclic halving of the RF voltage assists you in determining the electron temperature?

K. Hirao: We essentially measure the potential difference between two floating potentials, taking some small current from the circuit; it is almost impossible to measure the floating potential itself.

R. L. F. Boyd: The change in floating potential is determined by both i' and i; since $i = i_+ + i_{phot}$, it is necessary to make a correction. Dr. Hall may have some technique to do this.

L. G. Smith: I am interested in the application of your technique in the D-region. How low in altitude and electron density can you make appreciable measurements?

K. Hirao: The lowest height at which I can get a resonance peak is 95 km, with a peak frequency of 1.6 - 1.7 Mc/s; under that height I could not find any resonance peak, I think due to damping.

A. Nagy: The highest pressure at which you made laboratory measurements was 10^{-3} mm. Did you try to go higher?

K. Hirao: No, above that pressure there was no peak.

1.4 A MULTIPLE LANGMUIR PROBE SYSTEM FOR D-AND E-REGION IONIZATION EXPERIMENTS

A. G. MCNAMARA
National Research Council
Ottawa, Canada

To make measurements in the D- and E-regions from rockets, the measurements must be made with extreme rapidity to resolve the fine spatial structure which may exist. However, in going to sufficiently high sweep rates on the probes, the ability to measure very small currents and the accuracy of temperature determination is adversely affected. In addition, extreme ranges of particle density, collision frequency, mean free path, and sheath dimensions are encountered through these regions.

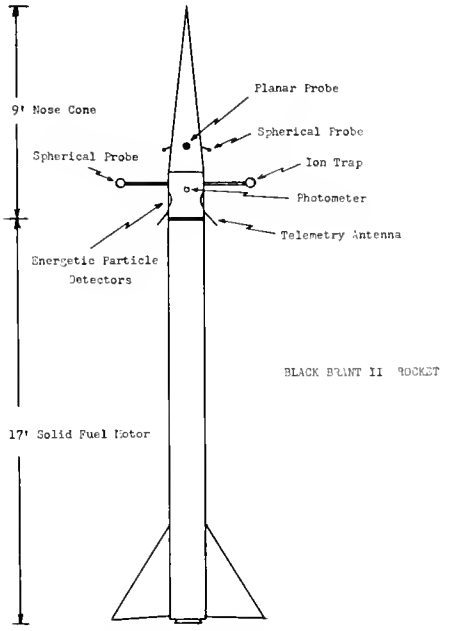

Figure 1. Payload configuration on Black Brant II rocket.

A solution to the problem has been attempted by a multiple probe installation on the rocket with all probes performing various functions simultaneously. A typical rocket probe arrangement is shown in Figure 1. Probes are mounted in pairs having several spherical and planar geometries. The general mode of operation is to hold one probe of a pair at a fixed potential and telemeter the probe current signal to give a continuous high resolution record of the ionization spatial structure. The other probe of each pair is programmed with a sweep voltage to trace out the complete voltage-current characteristic from which to derive the electron temperature and the absolute value of the charged particle density.

The planar and the small spherical probes are in operation continuously from launch, and permit measurements to be made from very low altitudes corresponding to charged particle densities of about 100 particles per cc. The probe construction is sufficiently rugged to withstand the large aerodynamic stresses which are encountered. The larger spherical probes are extended a distance of 60 cm from the rocket surface after the rocket has risen to approximately 60 km. In-flight calibration is performed repeatedly from all probes. The metallic surface of the rocket body is used as the reference electrode to return the currents to the ionosphere. Hence the entire surface of the nose cone is thoroughly cleaned prior to launch.

A bonus results from the multiple installation of probes of various geometries, sizes, and extensions. The system allows investigation of probe operation as a function of these parameters, and study of the rocket sheath and wake effects.

1.5 THEORY OF ELECTROSTATIC PROBES FOR STUDY OF D-REGION IONIZATION

R.C.SAGALYN and M. SMIDDY
Geophysics Research Directorate
Air Force Cambridge Research Labs.
Bedford, Massachusetts

This paper briefly outlines the methods used at AFCRL to measure the properties of negative ions, positive ions, and electrons in the D- and E-regions; particularly, the densities and temperatures of electrons above about 90 km; the energy distribution of positive ions in regions where the mean free path is very large compared with the dimensions of our sensors; and the mobilities, densities, and the conductivities of the positive and negative ions, in the region below about 80 km where the ions reach a terminal velocity proportional to their mobility times the electric field strength. Also discussed will be some of the experimental problems involved in making measurements on charged particles with a long spin-stabilized vehicle, moving with greatly varying velocity with respect to the charged particles and the gas. Finally, a few examples will be given of the results obtained, and their interpretation.

For the past 3 1/2 years the authors have been developing experimental and theoretical aspects of spherical electrostatic analyzers, using from one to three concentric electrodes of radii depending on the altitude range to be investigated, the vehicle velocity, and the local time of day.

For the study of electrons, we have used spherical one- and two-electrode analyzers. The Langmuir probe theory is used, together with the Druyvesteyn method for electron temperature, involving the second derivative of the voltage curve in the retarding potential region.

In the study of positive ions or negative ions, we always use at least two electrodes and on daytime measurements, we have been using three, with an intermediate grid as a photoelectron suppressor. This is maintained at about 20 volts negative with respect to the innermost electrode, the collector, because according to laboratory measurements the average energy of the secondary electrons emitted by the solar photons is about 15 ev.

Boyd was the first to report the use of two-electrode analyzers in the study of gaseous discharges in 1950, and Gringauz and Zelickman first described a method for measuring positive ions on a satellite vehicle in 1957. They considered the case of a satellite moving much faster than the random thermal velocities of the gas, so they could make many simplifying assumptions in the interpretation of the densities which they measured.

For various rockets, from the Arcas or Nike-Cajun, to deep space probes such as the EGO, the ratios of the velocity of the vehicle to the most probable velocity of the ions in the gas, vary between about .2 to about 18, so that one can no longer make the simplifying assumption that the velocity for the vehicle is much larger than the most probable velocity of the ions in the gas.

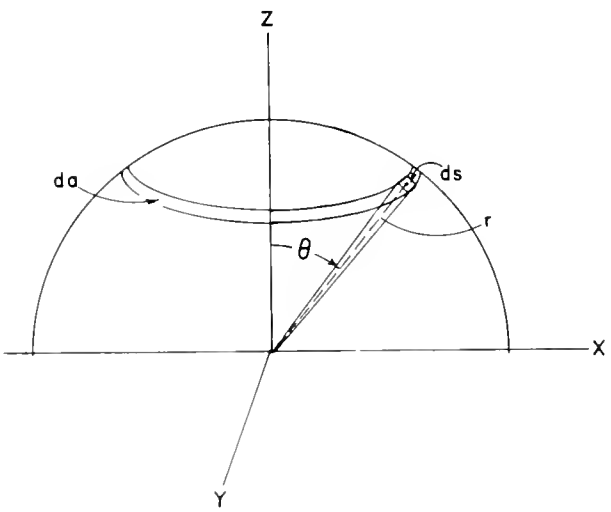

Figure 1. Sphere of integration for moving probe.

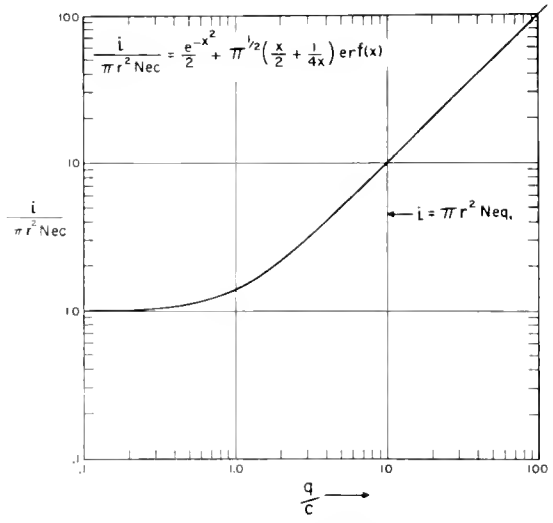

Figure 2. Current to moving probe as a function of velocity.

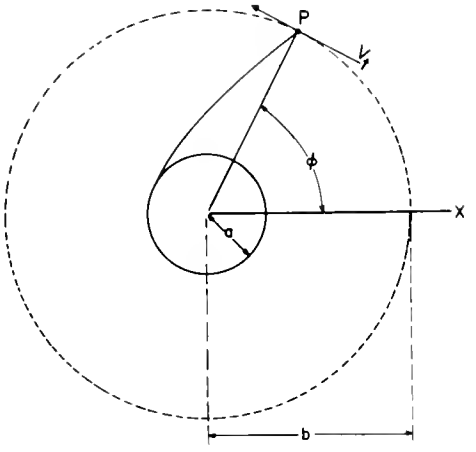

Figure 3. Particle motion in a central force field.

The practice in our experiments has been to place a spherical electrostatic analyzer on a boom about three to six feet in length, depending upon the space available in the vehicle, and to operate in three modes.

In the first mode a fixed voltage is applied between the collector and the outermost electrode. The appropriate voltage is found by solving the equations of motion of charged particles within this electrode system. In the case of altitudes above 80 - 90 km, we consider charged particles in a central force field where collisions can be neglected; and below this altitude, the effect of collisions has also been solved. In this mode we obtain the charge density of the appropriate polarity along the vehicle trajectory, and also look at the small-scale fluctuations of charge density.

In the second mode we sweep the voltage on the outer electrode with respect to the vehicle surface in varying amounts--in the case of electrons, about plus or minus 2.5 volts, positive or negative with respect to the vehicle surface. It is operated for electrons as a Langmuir probe; for positive ions, as Prof. Boyd pointed out, one must be very careful in the retarding potential region because of the dumping problem. We have solved this problem exactly for positive ions in the accelerating potential region, and, by looking simultaneously at the electron sensor as the positive sensor is swept, one can determine when the vehicle potential is affected. In this case, we have solved the equations exactly including vehicle motion, and can find the ratio of the mass of the ions to their temperature.

In the third mode of operation, the voltage between the inner collector and the outermost electrode is stepped for both electrons and positive ions.

Consider the current to a sphere in a Maxwellian gas which is moving at variable velocity, when the probe is near space potential. In the case of electron collection, this is part of the solution of the mode one operation. In this case, a slight accelerating potential is applied to the outer electrode, because we have observed that even a small rocket has a potential varying from about -0.1 to -1.4 volt. A fixed voltage of 1 - 1.5 volt is therefore applied to ensure measurement of the electrons independent of the vehicle potential.

In the E-region and above, where there are few negative ions, the electron current is simply proportional to $\pi r^2 NEq$, where q is the vehicle velocity, corrected for a transmission loss, which is determined experimentally in the laboratory, and a correction for the vehicle potential which we determine from mode 2 operation.

In the first case we solved for the current to a sphere, moving with a velocity q in a Maxwellian gas in the direction of the z axis, as shown in Figure 1. We integrate over the surface of the sphere by considering the current to an element of area dA where the current density is uniform since the velocity distribution is uniform over that surface. The tangential and radial components of the velocity are not, of course, uniform over the total surface of the sphere. The solution, when one carries out the integration, gives the current in the form shown in Figure 2. It is a function of x, the ratio of the vehicle velocity q to the most probable ion velocity c. It is for values of less than about .3 or greater than about 3, which is a region which most rockets go through in a normal flight, that the form of the curve is important.

For two electrode system in mode 3, we solve the equations of motion assuming a central force field, as shown in Figure 3.

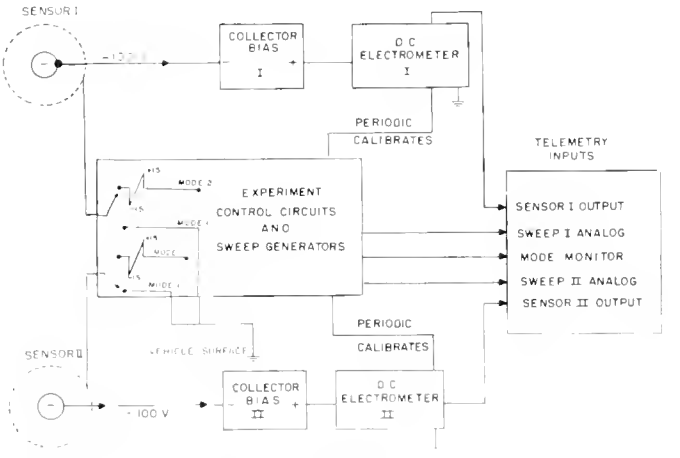

Figure 4. Block diagram of the probe instrumentation.

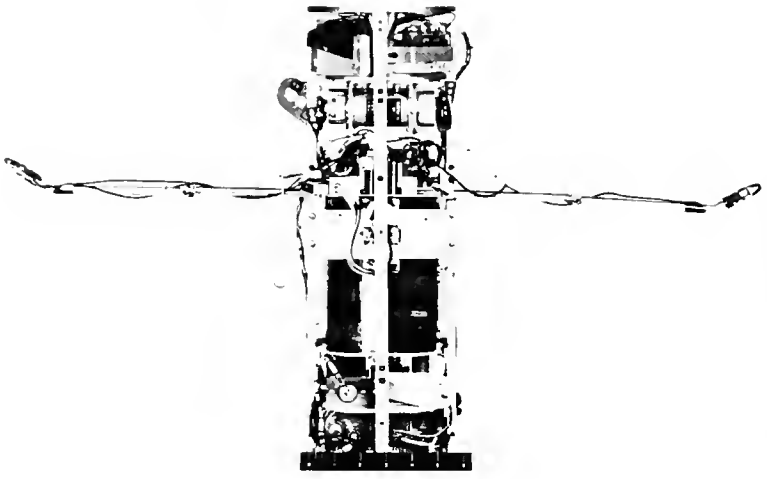

Figure 5. Package for daytime flight.

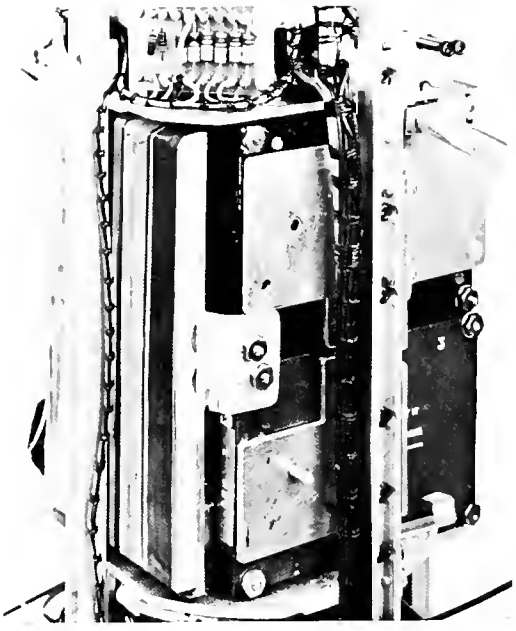

Figure 6. Electronics package.

In the mobility controlled region, the saturation voltage is proportional to q/K, where K is the ion mobility. We are therefore going from an ion counter, in a region where there are no collisions within the sensors, to an ion counter of the type which has been tradiationally used in the lower atmosphere; where the current to a charged conductor is $4\pi Q\sigma$, where σ is the conductivity of the medium and Q the charge on the conductor.

In the lower atmosphere, the current is given for positive ions, as long as one applies the appropriate potential; but in the case of negative charged particles, the negative current will equal the electron current plus the negative ion current. The latter current has the same form as that for positive ions, and the electron current will be simply $\pi r^2 N_e q$. One can see immediately in the experimental data the transition from the region where the positive ion and electron densities are equal, to the region where the negative ions begin to become important. The ratio of the currents is about 100 to 150 above 100 km in the daytime. At lower heights this ratio decreases until it is about unity at 50 km.

The time sequence of events for any vehicle depends upon the telemetry available and the velocity profile of the vehicle. In general for vertical soundings the sweep period for mode 2 operations is about 1 - 1.5 sec, with sampling rates of the order of a hundred to a thousand samples/sec. The stepping sequence for mode 3, to get the differential energy distribution of the ions, is about 2 sec duration.

Figure 4 shows a block diagram of the system. For a two-electrode analyzer, for positive ion collection, we first apply a collector voltage of 50 - 100 volts. In more recent versions of the instrument, the collector bias and the electrometer are interchanged to avoid leakage problems.

Figure 5 is a photograph of two sensors which will be flown next week with Dr.Narcisi's ion composition package and the electronics for the experiment is contained in volume 6 by 4 1/4 by 4 1/3, and contains all the electronic components except for the battery pack which is on the top deck. On the left is the three-electrode analyzer, which is a fine mesh with an open surface area of about 80% . At the right is the negative ion and electron sensor.

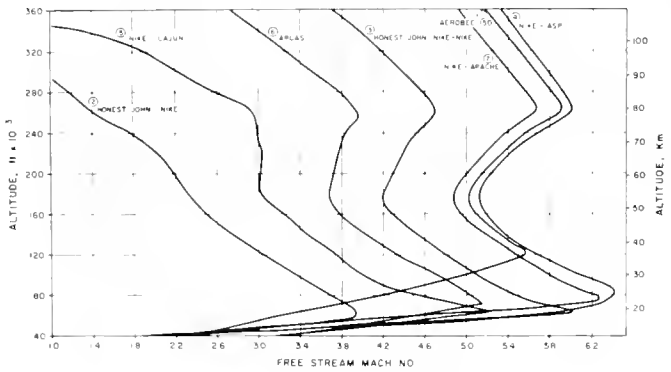

Figure 7. Free stream Mach numbers for various vehicles.

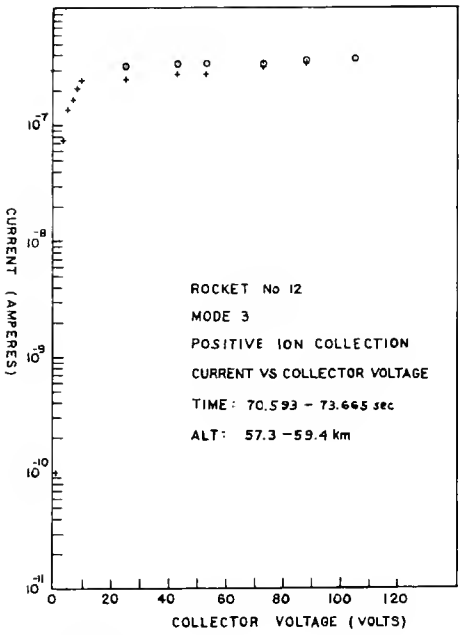

Figure 8. Mode 3 i-V curve showing saturation.

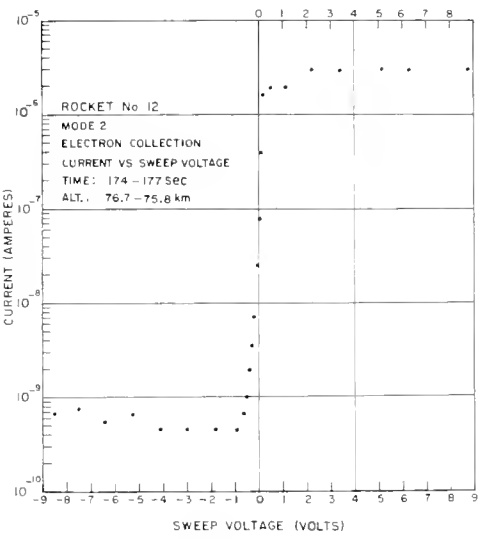

Figure 9. Electron collection i-V curve.

The inner collector is about 1 cm diameter, and the outer grid is about 1 3/4 inch. A close-up of the electronics package is shown in Figure 6.

One of the problems which we have been loo looking at recently is the effect of the high Mach number of a vehicle in looking at D-region ionization. Figure 7 shows the altitude versus free stream Mach number for a variety of common vehicles; in the region 40 to 70 km, the Mach number varies between about 3 and 5. Because of thise, we've been carrying out studies with the MIT wind tunnel. We are interested in investigating the shock around the sensors, and have found from these experiments (which are still being carried out), that the Schlieren photographs do not show a shock on the grid itself, it is so open, but do show a shock on the small collector. However, Mach numbers of 3 to 5 give small Mach angles and give a very small contribution to the total integration over the sphere.

Figure 8 is a current-voltage mode 3 curve in the D-region where we see a saturation potential as predicted. Figure 9 is the corresponding curve for electron collection just above 75 km.

DISCUSSION

R.L.F. Boyd: What is the point of using a small inner collector and solving the equations for the orbital motion analysis when it could be done equally well without complicating the mathematics by making the inner collector nearly the same diameter as the outer collector?

R. Sagalyn: The main purpose was to keep the photoelectron emission and secondary emission to a minimum. We solved the equations of motion so it was no particular problem. They agree with our experimental results, but this was certainly our original purpose (minimizing photoemission and secondary emission).

1.6 NEW DISCHARGE TUBE AND SPHERICAL MESH PROBE

K. TAKAYAMA
Institute of Plasma Physics,
Nagoya University
Nagoya, Japan

PART I. DISCHARGE TUBE

1. Introduction

In the laboratory, the preliminary requirement is to produce a test plasma similar to the ionosphere. That is, the very low density, homogeneous, quiet and electric fieldless plasma is required in a large tube.

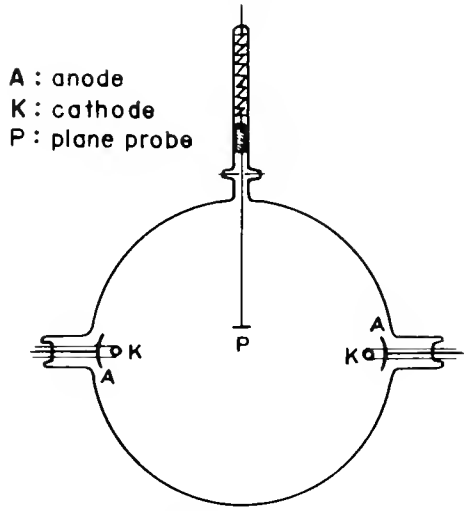

Figure 1. Configuration of early discharge tube

An early discharge tube [1], [2] used is shown in Figure 1. The mercury discharge tube is constructed with a sphere of Pyrex glass, 30 cm in diameter, two pairs of anodes and hot cathodes near the tube wall as a plasma source. When the discharge current exceeds 30mA, all parts in the tube are the glows, the ion density is more than 10^8 ions per cm^3 and the electron temperature exceeds 7000°K. In a region of discharge current from 10 mA to 25 mA, the electron temperature increases with the discharge current. Below 10 mA of discharge current, the electron temperature takes a constant value of 2000°K. The tube is then for the most part occupied by dark plasma, the electric field does not exist and the plasma is formed by diffusion from the plasma sources. When the discharge current exceeds 10 mA, the uniformity of the plasma is sufficient for measurements; its variation across the tube is then within 3%. Below 0.5 mA it becomes about 40%.

Thus it seems that the plasma produced in this discharge tube has many good properties; such as the much rarefied density, the excellent uniformity, a considerable quiescence, the low electron temperature and no electric field in it. However, this tube has the following unsatisfactory facts resulted from the configuration of the electrodes.

(a) When the gas pressure is lowered below 10^{-3} mm Hg, the discharge becomes unstable and the life of hot cathode is shortened by the ion bombardment.

(b) The space potential and the quiescent state of dark plasma are influenced on an unstable state of the boundary between the dark and the glow plasma near anode.

These defects have been almost eliminated by the following improved construction of the electrodes which will give a useful plasma source in a space chamber.

2. New Discharge Tube

The new discharge tube is the same one as the early tubes except for the part of electrode. The electrode configuration is shown in Figure 2. The special merits are to insert the grid No. 1 (G1) and the grid No. 2 (G2) into the space between the cathode and anode, and to separate the space ranging from the G1 to the

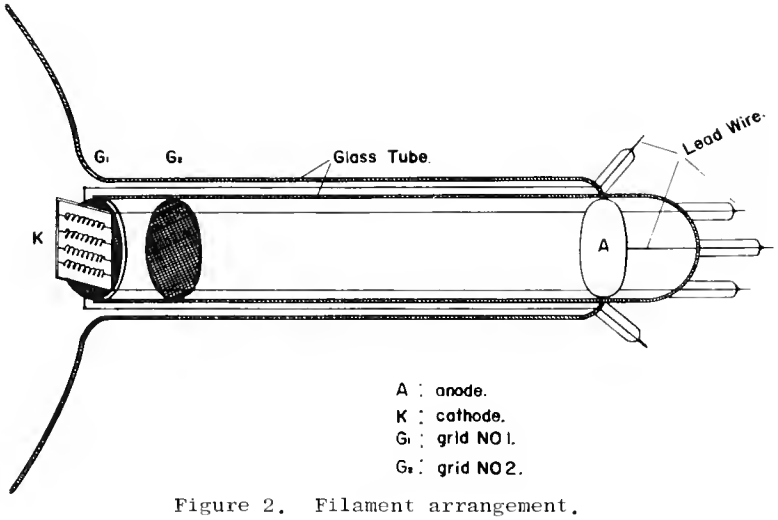

Figure 2. Filament arrangement.

In Naiseless States.	OLD TYPE	TP-NO.1
Pressure of Hg Vapor.	$2\times10^{-4}\sim10^{-3}$mmHg	$2\times10^{-4}\sim10^{-3}$mmHg
Total Dischrage Current.	unstable $40\mu A-2.5$ mA	$20\mu A-12$mA
Range of Electron Density.	$10^{7}-10^{9}$/cc	$10^{4}-10^{5}$/cc
Electron Temperature.	0.5−1.5eV	0.3−0.7eV
Space Potentiol in regard to Cathode.	30V	2−10V
Fine Adjustment of Electron Density.	difficult	easy

anode from the other space by an inner cylindrical glass tube. Several coated filaments used in a fluorescent lamp are arranged as seen from Figure 2.

The cathode is grounded and the voltage of the G1 is set below about 10 volts, but the voltage of the G2 and the anode are changeable independently upon the gas pressure and plasma density. Thus, the space from the G1 to anode is used as a positive column or a space of the B. K. oscillations where ions are produced by energetic electrons. The ions created in this space spread over the whole of tube through the G1 and the cathode. The dark plasma produced in this tube is very quiet and large noises or oscillations are not observed with a high gain oscilloscope. The G1 separates the glow plasma from the dark plasma and sets the space potential of the dark plasma in low values; this is an important function suppressing noises or oscillations.

Several results obtained in two tubes are shown in Table 1; one is the new discharge tube called TP. No. 1, the other is an old type - discharge tube where a positive column is produced in the center part and each tube has the same dimension. From Table 1, it is obviously seen that the new discharge tube produces a much better plasma.

PART II. SPHERICAL MESH PROBE

1. Introduction

It has been proposed[1] that a spherical mesh probe is convenient for measurement of positive ion density in the height range below 100 km.

In Japan, a first telemetry record taken by the rocket-borne spherical mesh probe (KAPPA III-3 sounding rocket flown on Sept. 22, 1960) was used for calculations of the ion density in the region ranging from 80 km to 180 km [2,3]. However, the measurements with this probe were not performed under favourable conditions, because the KAPPA III-3 rocket was flown higher than the height range which was suitable for the spherical mesh probe. Since then, this probe has not been used under better conditions.

2. Spherical Mesh Probe

The spherical mesh probe is made of thin wires as shown in Figure 3. Previously, it has been verified that, when the plasma density is very low, the spherical mesh probe behaves as if it were a spherical probe; the lower the density, the more exact it is.

From the geometrical construction, it is clear that the spherical mesh probe is nearly transparent to solar radiation, and the photo-electron current from the spherical mesh probe is not larger than 10% of that from the spherical probe. Moreover, the spherical mesh probe disperses the photo-electron current symmetrically.

A shock wave in front of the spherical probe is less pronounced than that in front of the the spherical probe. The ion density is calculated from the voltage-current curve in the ion current collected by the spherical mesh probe. It is well known that the voltage-current curves in the region of ion current collected by a negative charged probe are separated into three classes according to behaviour of ions in the sheath. That is, these classes are a region of one collision, a region of many collisions and a region of orbital motion. In the first two regions, the ion density calculations from the voltage current curves obtained with the spherical mesh probe are the same as that from the voltage current curves obtained with the spherical probe, because the ions entering into the ion sheath are trapped ultimately on the spherical mesh probe. In the region of orbital motion, the trapping mechanism of ions in the spherical mesh probe is highly complex and differs from that on the spherical probe. Therefore, the mechanism has not been analysed exactly; but

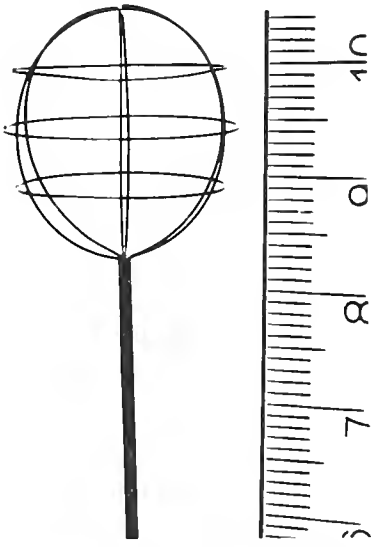

Figure 3. The spherical mesh probe.

Table II

Comparison between the spherical probe and the spherical mesh probe

	The spherical probe	The spherical mesh probe
The electron collection by a positively charged probe	orbital motion	not same
	one collision	same
	many collisions	same
The electron and ion collection	electron temperature	not same
	space potential	?
The ion collection by negatively charged probe	orbital motion	not same
	one collision	same
	many collisions	same
	photo-electron current	not same reduced to below 10% more symmetrical
	shock wave	not same smaller than
	plasma density	not same only very thin
	effect of electron negative ions	same
	effect of probe-drift	same

the demerits of the spherical mesh probe do not appear in measurement in the height range below 100 km, because the behavior of the ions belongs to the regime of many collisions or one collision. The influences of negative ions [4] and probe-drift [5] on the ion currents entering into probe have been examined in the laboratory, and these results can be applied to the spherical mesh probe. In Table II, the spherical mesh probe is compared with the spherical probe.

It is concluded that the spherical mesh probe is the most convenient probe for measurement of the positive ion density in the D-layer or in the lower part of the E-layer of the ionosphere.

References

[1] I. Ichimiya, K. Takayama, and Y. Aono: Proceeding of the Cospar Space Symposium (North Holland Publishing Company, Amsterdam, 1960).

[2] K. Takayama, H. Ikegami and S. Miyazaki: Phys. Rev. Letters 5, 238 (1960).

[3] T. Dote, K. Takayama and T. Ichimiya: J. Phys. Soc. (Japan) 17, 174 (1962).

[4] R. L. F. Boyd and J. B. Thompson: Pro. Roy. Soc. A, 252, 102 (1962).

[5] T. Dote, T. Ichimiya and F. Tamaki: J. Phys. Soc. (Japan) 18, 260 (1963).

DISCUSSION

R. L. F. Boyd: It is often not realized how important and how difficult it is to do laboratory experiments. There is an interesting alternative method of getting a low density and cool plasma and that is by expanding a plasma. We have experimented with a low-density wind tunnel in which we expand the mercury vapor and then recondense it; this gives the advantage that of supersonic flow which simulates the conditions in the E-region when a rocket is going through. If you produce the plasma in the throat of the expansion nozzle it has cooled significantly by the time you get to the point of making experiments in it, and it is also reduced in density, so you can run your plasma at a reasonable density where you can keep a discharge going and expand it before you study it. We use tungsten cathodes which get us over the problem of destruction by positive ion bombardment. Of course, they are hot

and bright but they are very easy to replace. Also, we allow a much larger space between the cathode and the anode and this enables one to work down to lower pressures because the cathode dark space can be so much larger.

I might also mention the value of RF cathodes. When you are working in oxygen it is easy to poison your cathode and you can use a system very much as that described but instead of running a discharge with a hot cathode you can run a RF discharge in a carefully screened system and allow the electrons to diffuse out of a grid at the end. It is very difficult in an ordinary discharge to get a flux comparable to that which you have in the ionosphere; on the other hand it is very common to have a random flux of metastable particles, particularly with the inert gases, very very much larger. Curious effects in a discharge in argon, for example may well be due to a large number of metastable particles in the discharge.

2.A SURVEY OF RF IMPEDANCE PROBES

W. PFISTER
Geophysics Research Directorate
Air Force Cambridge Research
Laboratories
Bedford, Massachusetts

1. Introduction

The RF impedance probe technique for the measurement of electron densities was first used by Jackson in 1957. He used the transmitting antenna of the familiar Seddon CW propagation experiment at 7.75 Mc/s and measured the antenna impedance during the rocket flight by using the voltages on both sides of the matching network between the antenna and the transmitter. The electron density deduced was too low by a factor of three which was attributed to the ion sheath formed around the antenna.

2. Standing Wave Impedance Probe

In order to avoid such complications and to allow an easy interpretation of the impedance measurements we at AFCRL designed an experiment with the following features: an antenna as long as feasible; a frequency well above the gyrofrequency; an RF voltage on the antenna below 1 volt, and finally, a DC voltage on the antenna sweeping between 0 and 5 volts for removal of the ion sheath. The engineering part of the experiment was given to the University of Utah which proposed an impedance measurement with a sampling of the standing wave pattern on the transmission line feeding the antenna. The instrument designed according to these features is now called the standing wave impedance probe. It has been described in the literature and has been flown with considerable success in rocket and satellite flights. A representative block diagram is shown in Figure 1. It shows two artificial transmission lines, one for each half of the antenna; the voltage sampling is done on one of them. A sawtooth generator varies the voltage on the antenna.

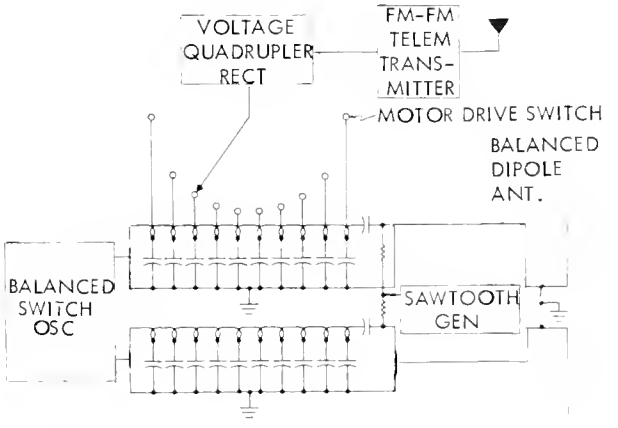

Figure 1. Block diagram of impedance probe.

3. Interpretation of Impedance Data

The interpretation of the impedance data in terms of electron density is straight-forward at least in a first degree approximation. The antenna used is electrically short and its capacity is proportional to the dielectric constant of the medium.

The circuit diagram of the impedance probe is as shown in Figure 2:

L_i is the series inductance introduced to provide a rough matching of the antenna to the transmission line.

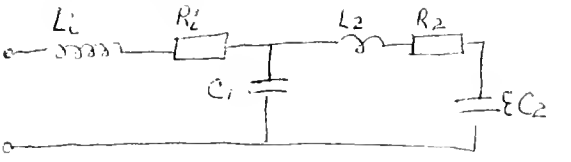

Figure 2. Circuit diagram of impedance probe.

R_i is the series resistance usually in the order of 100 Ω. This resistance increases the sensitivity range of the instrument, however, it decreases the sensitivity if only a limited range is of interest.

C_1 is the shunt capacity of the antenna mounting which should be held as small as possible.

L_2 is the inductance of the antenna itself which usually is small and in this case can be lumped together with L_i.

R_2 is the ohmic resistance together with the the radiation resistance of the antenna. Since it is small it can as a first order approximation be lumped together with R_i.

C_2 is the free space capacity of the antenna itself. ϵ finally is the dielectric constant of the medium. If the earth's magnetic field can be neglected it can be written as

$$\epsilon = 1 - \frac{x}{1 - jz}$$

where $x = \frac{\omega_N^2}{\omega^2}$ and $z = \nu/\omega$

2.A PFISTER

What we measure is the difference of the impedance against the free space impedance

$$\Delta = \Delta R - j\Delta X$$

Introducing

$$C_o = C_1 + C_2 \text{ and } \bar{x} = \frac{C_2}{C_o} x$$

and using the approximations indicated above we obtain for the real part of the impedance change

$$\Delta R = \frac{\bar{x}\, z}{\omega C_o \left[(1 - \bar{x})^2 + z^2\right]}$$

and for the reactance change

$$\Delta X = \frac{\bar{x}\,(1 - \bar{x})}{\omega C_o \left[(1 - \bar{x})^2 + z^2\right]}$$

The final solution of these equations is

$$\bar{x} = \frac{\omega C_o \left(\Delta X + (\Delta R)^2/\Delta X\right)}{1 + \omega C_o \left(\Delta X + (\Delta R)^2/\Delta X\right)}$$

and

$$z = \frac{\Delta R/\Delta X}{1 + \omega C_o \left(\Delta X + (\Delta R)^2/\Delta X\right)}$$

For negligible collisions the equation for the electron density reduces to

$$N = \frac{f^2}{80.6} \frac{C_o}{C_2} \frac{\Delta X}{\Delta X + 1/\omega C_o}$$

where f is the frequency in Mc/s.

4. Importance of Free Space Impedance

One weak point of the standing wave imped-

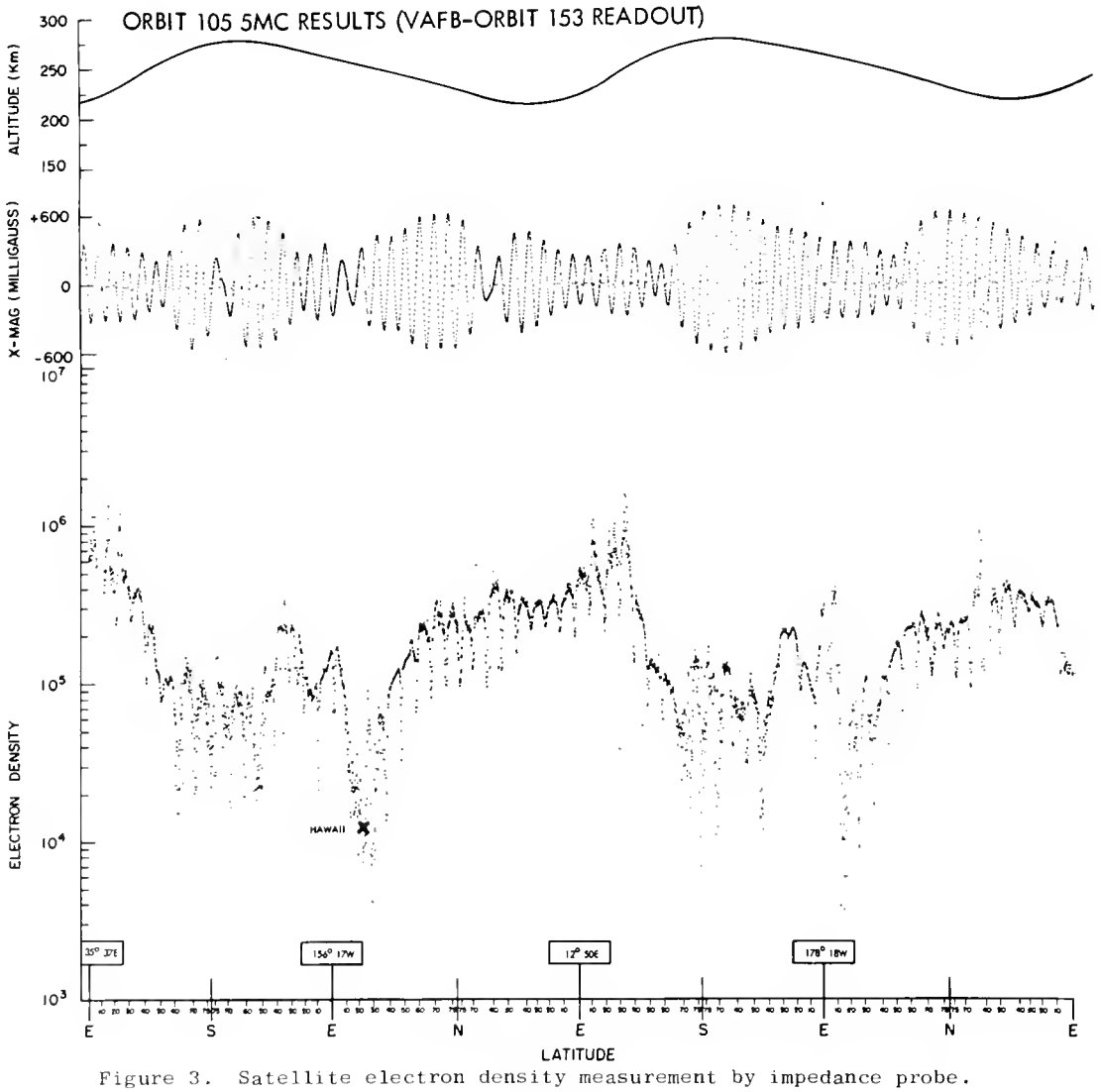

Figure 3. Satellite electron density measurement by impedance probe.

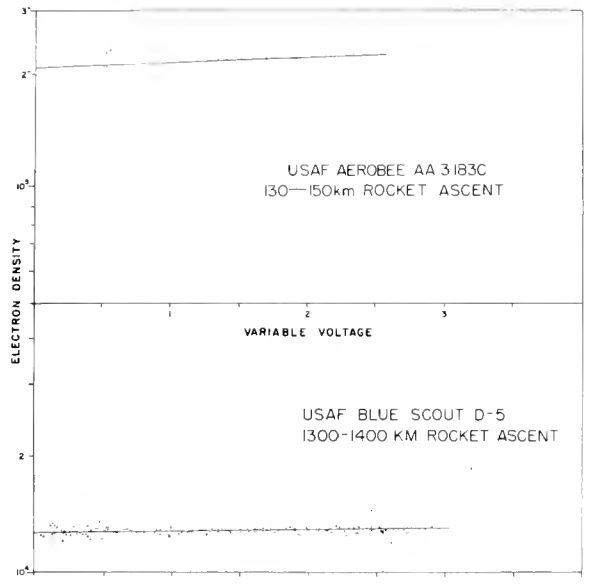

Figure 4. Effect of DC probe voltage on apparent electron density.

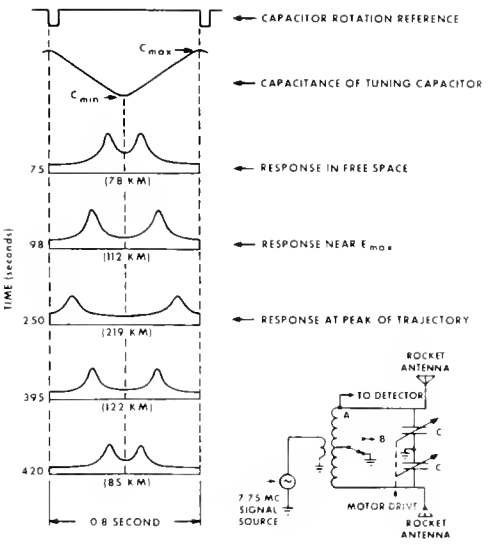

Figure 5. NASA impedance probe circuit and typical responses.

ance probe is the need of an accurate knowledge of the free space impedance, which cannot easily by recalibrated during the flight. Usually a careful calibration is made before the flight in the laboratory and with the help of a mock-up vehicle in the field. In addition we have found it useful to switch the oscillator successively between two frequencies like 7 and 12 Mc/s. This enables an extension of the range of the instrument and a check on the calibration in flight and if necessary correction of the calibration in flight.

We have flown the instrument on rockets and satellites with measurements between 70 and 1800 km. In comparing our results with ionosonde data or positive ion measurements we believe that the instrument measures electron densities with an accuracy of about 5% or better.

5. Effects of Earth's Magnetic Field

In principle it is no problem to include the effect of the earth's magnetic field in the interpretation of the impedance measurements, provided the theory for the antenna configuration at hand had been worked out. Formulas for the short dipole at an arbitrary direction with the magnetic field are published by Kayser. Balmain has treated the longitudinal and transverse antenna in a lossy medium. A more general treatment of an antenna of any length has been given by Katzin. For a frequency above the gyrofrequency the effect of the magnetic field diminishes rapidly according to the ratio ω_H^2/ω^2. The lowest frequency we used so far was 3 Mc/s. At this frequency the magnetic field should produce a measurable effect. An antenna rotating in the magnetic field is expected to lead to a higher electron density the closer it is oriented in a longitudinal direction. We have at the present time no definite proof of the effect, because of its obscuration by the wake effect.

6. Wake Effect

The presence of the rocket or satellite vehicle disturbes the ambient medium. Especially a moving vehicle creates a deficiency of ions in the rear which in turn, by action of the electrostatic force, causes a reduction in electron density. Since we measure the impedance only on one-half of the antenna we notice a reduction of electron density when this half is passing totally or partly through the wake. A convincing example of this effect is seen on a record obtained from satellite measurements (Figure 3).

7. Outgassing

Another effect of disturbance by the vehicle encountered by us is outgassing of fuel. It acts as an effective agent for electron attachment and reduces the electron density on ascent above about 150 km when the diffusion velocity exceeds the vehicle velocity. We have observed the effect on Aerobee rockets where the fuel valves have been left open after burnout. We also have observed the effect to a lesser degree on the solid fuel Astrobee 200 the propellant of which still smolders after burnout.

8. Ion Sheath

Still another disturbing effect is the ion sheath around the antenna. We may distinguish

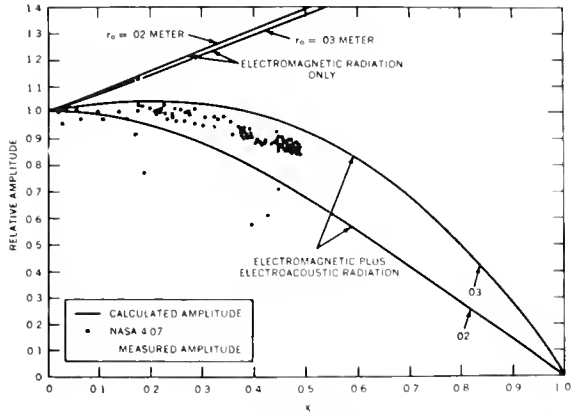

Figure 6. Effect of electroacoustic radiation.

two kinds of sheath: the normal ion sheath and the enhanced ion sheath caused by RF voltages on the antenna.

The normal ion sheath is produced by the difference of thermal electron and ion velocities which results in the formation of a negative potential on the antenna and the vehicle with respect to the environment. The potential is in the order of 1 volt and the sheath thickness is in the order of the Debye length. The ion sheath reduces the value of the measured electron density unless correction in the analysis is applied. It is obvious that the errors or corrections are greater for antennas of smaller length.

According to our experience with antennas of 8 or 10 feet length the ion sheath effect is negligible. We came to this conclusion on account of two observations. Firstly we varied the DC voltage between the antenna and the vehicle from 0 to 5 volts in order to change the ion sheath. The current measured behaves as expected in a Langmuir probe. However, the computed electron density shows only a small variation which can hardly be picked out of the noise (Figure 4).

Additionally, whenever we had a chance to compare the densities from the standing wave impedance probe with those from other DC type probes or from ionosonde or other propagation data we found no significant deviations.

9. NASA Impedance Probe

These experiences are at variance with the conclusions reached by the experimenters at NASA. The impedance probe flown by Jackson, Kane and Whale is very similar to ours. The antenna has about the same length and configuration and the frequency is about the same. The technique of measuring the impedance is different, however, as shown in Figure 5. A tuning capacitor is rotated by a motor drive and the voltage across the tuning circuit is telemetered. The distance between the peaks is a measure of the capacitance, and the height of the peaks is a measure of the resistance.

By comparing the measurements with those of the Seddon type propagation experiment flown in the same rocket Kane, Jackson and Whale found a difference of 20 to 30% in electron density. They made reasonable assumptions about the thickness of the ion sheath and found that in fact the formation of the ion sheath can account for the difference. I have no arguments against the way they came to their conclusion; the only suggestion I can give to reconcile the different observations is the insertion of a relatively high resistor between the antenna and the vehicle body, which might achieve more or less floating potential on the antenna.

10. Effect of RF Voltage

As mentioned earlier an RF voltage on the antenna will increase the size of the ion sheath. A quantitative estimate of this effect has been given by Kane, Jackson and Whale as well as by Getmantsev and Denisov. Although both approaches

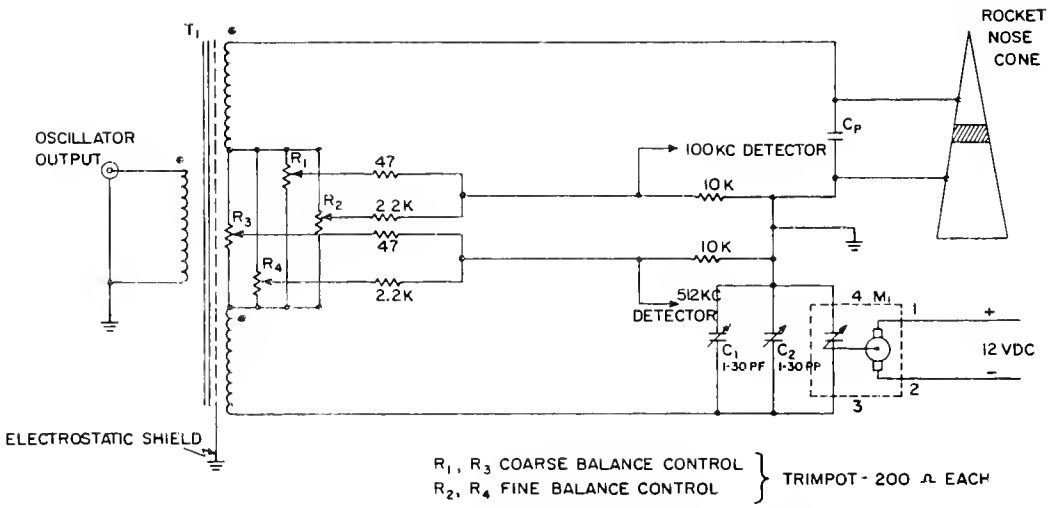

Figure 7. RF conductivity probe circuit.

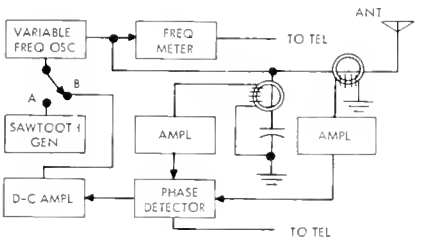

Figure 8. Plasma frequency probe block diagram.

are different the results are pretty much the same and agree roughly with the observations. An RF voltage of 200 volt at 7 Mc/s reduces the measured electron density by a factor of 3 or 4 in the F-layer. The error decreases with increasing frequency and has a maximum at plasma resonance. On the other hand, the effect of the RF voltage is negligible at 0.5 volt for all practical purposes.

11. Electroacoustic Waves

Another interesting effect has been detected and studied by Whale. Figure 6 shows the nature of the effect. In the NASA experiment the amplitude of the antenna current is measured as a function of the tuning capacity. In the tuned position the amplitude depends only on the resistive component of the load. Since the radiation resistance decreases with the plasma frequency the amplitude should increase provided collisions can be neglected. However, the measurements show a decrease in amplitude and the explanation found by Whale is the excitation of a compressional wave in the electron gas, sometimes called an electroacoustic wave. This wave requires a gradient in the electric field as furnished by the cylindrical geometry of the antenna and stimulates further studies. Our own experiments up to date are not very suitable for observations of this wave because we have inserted a series resistance of 100 ohms in the antenna for reasons mentioned before.

12. Planar RF Probe

The electroacoustic wave phenomenon is not expected to play any role in an experiment using a planar geometry, like the one designed by Prof. Sayers at the University of Birmingham, and flown in the Ariel satellite. This experiment is described in another paper [Paper 2.4].

13. RF Conductivity Probe

In order to measure low electron densities as they occur in the lower part of the D-layer it is necessary to use frequencies below the gyro-frequency. The Pennsylvania State University has developed such an instrument known as an RF conductivity probe. The essential features are indicated in Figure 7. The sensor consists of an insulated nose cone section. Two frequencies are used simultaneously 100 kc/s and 512 kc/s. The capacitance is measured with a bridge circuit with the help of a rotating condensor similar to the NASA experiment. The separation of two adjacent nulls determines the capacitance and the conductance is determined by the voltage at the null. For the analysis of electron densities it is necessary to take into account the effect of the magnetic field and the ion sheath; the latter, by using Langmuir probe theory.

14. VLF Admittance Probe

It is worthwhile mentioning that serious studies are underway to extend the impedance probe measurements to very low frequencies. I shall mention only the studies of Mlodnosky and Garriot. They analyzed the admittance measurements made at 16 kc/s on a Nike-Cajun rocket using the rocket itself as an antenna. At these low frequencies quasi-static conditions exist and the dipole can be viewed as a symmetrical Langmuir probe. The admittance than can be analyzed in terms of electron density and temperature.

15. Antenna Resonance

A modification of the RF impedance probe uses a variable frequency for tuning of the antenna. I am aware of two such experiments. The first one was flown by the University of Birmingham in 1958. The probe is formed by insulating a forward section of the nose cone against the remainder of the rocket. The capacity of this section and the main body is used as a tuning capacity of an oscillator whose frequency is transmitted to the ground. A second experiment built by the University of Utah used a sweep frequency on a circuit including the dipole antenna. The voltage at the antenna terminal was monitored while going through a resonance. These antenna resonance probes are basically in no way different from the impedance probes.

16. Plasma Frequency Probes

The impedance of an antenna shows drastic changes when the oscillator frequency is varied across the plasma frequency of the medium. This effect lead to the development of a different type of RF probe which I might call a plasma frequency probe. Several instruments of this type have come to my attention. As an example I shall describe an instrument of the University of Utah. The block diagram is shown in Figure 8. A variable frequency oscillator feeds a signal into an antenna of reasonable length. In free space the reactance of the antenna is capacitive for the entire frequency range. Close to the plasma frequency the resistive loading of the antenna is high and the phase of the antenna current goes through zero. The output of the phase detector can be telemetered to the ground or it can be used to lock the variable frequency oscillator to

zero phase condition. In an ideal case the locked frequency would be equal to the plasma frequency. Practically, however, it is affected by the earth's magnetic field and by the collision frequency. Small corrections also have to be made for the inductance of the antenna and for the ion sheath. The probe has the advantage that it can be analyzed without a knowledge of the free space impedance. However, it cannot be used in the D-region where the collision frequency is too high.

DISCUSSION

A. Kavadas: When you say an electro-acoustic wave, do you mean one in which the electric vector is in the direction of propagation?

W. Pfister: Yes, it is a longitudinal wave.

A. Kavadas: Do you not need very stringent conditions for this?

W. Pfister: One must have a gradient of electric field; it cannot be produced in a plane wave condition. It is caused by an oscillation of the space charge. Whether it propagates or not has not been determined; it is known only that it causes a loss in the antenna.

C.G. Little: The topside sounder satellites see resonance phenomena which are interpreted in terms of a longitudinal electro-acoustic wave. The antenna is pulse excited; after the transmitter has been switched off, RF noise is picked up on the antenna in the receiving cycle, and this is attributed to an oscillation of the electrons in the vicinity of the satellite.

2.1 THE OPERATION OF RF PROBES FOR THE MEASUREMENT OF ELECTRON DENSITY AND COLLISION FREQUENCY IN THE IONOSPHERE

A. W. ADEY
Defence Research Telecommunications Establishment
Defence Research Board
Ottawa, Ontario, Canada

1. Introduction

The RF probe has had a history of over fifty years as a diagnostic tool for the study of the electrical properties of plasma. Until comparatively recently its use was confined to laboratory studies and it is only during the last decade or so that it has been adapted to upper atmosphere work. Some of the earlier laboratory instrumentation may seem by present standards somewhat unsophisticated, but it was certainly not at the time. It is interesting to note some of the aspects of the operation of an RF probe in a plasma that the early investigators concerned themselves with. In 1906 Wilson and Gold [1] introduced the concept of ion sheaths formed when RF is applied to a probe. In 1930 Appleton and Childs [2] were trying to take into account the effect of the sheaths on the capacitance of their parallel-plate condensers used in resonant circuits to determine plasma properties. Their study was inspired, in part, by the series of papers in the French literature, during the previous three years, which discussed the subject of the relative importance of purely inertial and quasi-elastic forces acting on electrons in the presence of an RF field producing resonances in a plasma. In 1932 Childs [3] was biasing his probes to effect a collapse of the ion sheaths. This is all in the best modern tradition. The geometries used were mainly open-wire transmission lines and resonant circuits, and parallel-plate and cylindrical condensers.

In this paper we are concerned with the operation of RF probes in the ionosphere. An attempt will be made to review the basic designs that have been used or proposed, the problems and limitations associated with their use and, in conclusion, to suggest some directions in which further effort might profitably be expended toward a clearer understanding of their operation, relative merits, and areas of applicability.

Spaceflight ionospheric measurements based on propagation techniques, and performed under comparatively quasi-constant ionospheric conditions, have provided much valuable data. The RF probe is especially adaptable to measurements in a patchy, disturbed ionosphere, when the propagation experiment fails. But it has associated with it problems peculiar to itself. Some of these problems, as already discussed, were realized in early laboratory studies, but others arise due to the high velocity of the vehicle, and its changing aspect with respect to the lines of the earth's magnetic field.

2. Types of RF Probe

Ionospheric studies using RF probes seem to have started with Jackson and Seddon [4] in the late 1940's, who noted the impedance changes of a dipole antenna being used in a propagation experiment to measure electron density. The concept of determining electron density by measuring the impedance of an antenna subsequently became the basis of an independent experiment [5]. Since then a number of other geometries have been introduced by other workers and various methods have been used to measure the impedance. In addition, techniques other than impedance measurement have been developed.

Figure 1 indicates some of the geometries that have been used or proposed. The insulated nose cone (Figure 1a) was pioneered by Sayers of Birmingham [6], and has subsequently been used by DRTE [7] and by the University of Pennsylvania [8]. The transmission line resonator (Figure 1c) which has been used in the laboratory is now being proposed for rocket use by the University of Toronto [9]. The dipole (Figure 1d) was used by NASA [10], by DRTE (in the Alouette satellite) [11], and by the University of Utah [12]. A monopole variation is being used by the University of Saskatchewan [13]. The Sayers probe in the Ariel satellite has the form of a parallel-plate condenser (Figure 1b) supported at the end of a boom [14]. The parallel-plate condenser or the cylindrical form (Figure 1e) were seen in many of the earlier laboratory instruments. Storey has proposed the combination dipole-loop configuration (Figure 1f) for a VLF experiment in a satellite [15]. The Japanese resonance probe uses the supported sphere geometry (Figure 1g) [16].

3. Choice of Geometry

There are a number of considerations involved in the choice of a specific geometry. Some are more amenable than others to a theoretical treatment.

Closely associated with the problem of geometry is the location of the sensor on the vehicle and the usual requirement to accommodate as many experiments as possible with a minimum of interaction, and avoidance of places where there is local contamination of the medium by propellants and experimental chemical agents. In these respects the insulated nose cone is attractive, since it makes use of an existing rocket contour. The question of mechanical feasibility has to be considered, in the case of some geometries. This involves the requirement

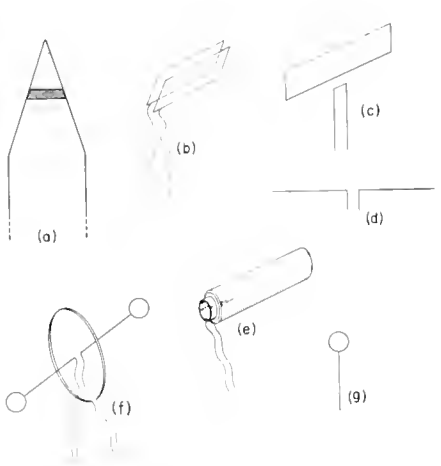

Figure 1. Possible geometries for RF probes.

to deploy the sensor or to expose it by ejecting a cover. Many of the difficulties associated with these mechanical operations are related to the minimum height at which measurements are to be made, which are aggravated in the D-region because of high aerodynamic drag which results in heating problems causing difficulties both with materials and with dimensional and component changes.

The probes have to be calibrated. The simpler geometries, such as spheres, parallel-plate condensers and dipoles (using the image principle) are attractive in this respect.

4. Measurement Techniques

Four basic measuring techniques have been utilized or proposed for upper atmosphere probes. Figure 2 illustrates these techniques.

The first method involves measuring the impedance of the sensor more-or-less directly. NRL measured the reflection coefficient with the equivalent of a Micromatch. Utah sampled the voltage from a series of probes on the feed line to the dipole to synthesize the standing wave pattern. Penn State used a bridge, while Birmingham measured the current due to an impressed RF voltage.

In the second method, the sensor is either made an element of the resonant circuit of an oscillator, whose frequency is monitored, as is done by Birmingham, DRTE, and NASA, or forms an open-wire transmission-line resonator whose frequency is monitored, as has been used in laboratory studies by Toronto and proposed for ionospheric work.

The third, or plasma frequency, method, takes several forms. The Japanese resonance probe is essentially a Langmuir probe with an RF voltage of variable frequency superimposed on the usual DC. The local plasma frequency is indicated by the marked change in the current drawn by the probe as the frequency passes through the local plasma frequency. The Saskatchewan probe utilizes a bridge whose excitation frequency is forced, by a feedback loop, to follow the local plasma frequency. This will be modified for future flights to form a sweep-frequency system, but still based on the sharp change in the sensor impedance in the vicinity of the local plasma frequency. Instrumentation on a topside sounder satellite can, in principle, determine the local plasma frequency in several ways--(a) by an indication of the onset frequency for the reception of cosmic noise, (b) by a measurement of antenna impedance and (c) by the interaction in the transmitted sounding signal with the plasma in the vicinity of the satellite, through such indications as plasma resonances and the breakthrough of the sounding signal.

The fourth method, proposed by Storey, involves measuring separately the **E** and **H** components of a VLF signal transmitted from the ground. The ratio gives information about the wave impedance of the medium in the vicinity of the satellite.

5. Requirement to Measure Independently Electron Density and Collision Frequency

As far as studies in the lower ionosphere are concerned, one is interested in the possibility of using a specific method for making two independent measurements necessary to determine both electron density and collision frequency. In the first method shown in Figure 2 one has to measure the complex impedance. In the second, or resonant circuit, method, the measurement must be made at two frequencies, or a measurement at one frequency combined with a determination of the amplitude of the resonance. In certain of the resonance (or plasma frequency) probes of the third method the sharpness or the Q of the resonance can be used as the second measurement parameter.

The choice of frequencies for either the impedance or the resonant circuit methods involve a compromise among a number of conflicting considerations. Sensitivity to both electron density and collision frequency require that

① IMPEDANCE	② FREQUENCY
UTAH	BIRMINGHAM
PENNA.	DRTE
NRL (NASA)	NASA
BIRMINGHAM	TORONTO

③ PLASMA FREQUENCY	④ WAVE IMPEDANCE
TOKYO	CNET (FRANCE)
SASKATCHEWAN	
DRTE	

Figure 2. Summary of RF probe techniques

the frequencies be made as low as possible. Reducing the frequency also tends to minimize the tendency for the sensor to radiate. However, this conflicts with two other factors. First, unless the frequency is high with respect to the electron gyrofrequency, the earth's magnetic field must be taken into account in the theory. This is difficult, except in the case of the simpler geometries, and also implies the availability of good aspect information. Second, keeping the frequency higher than the highest plasma frequency expected, in the case of oscillators whose frequency is controlled by the plasma, lessens the chance of oscillator failure. Thus the conflicting factors of sensitivity and plasma frequency determine the range of electron density and collision frequency over which measurements can be made. Wide dynamic range can be had by either inflight switching of frequencies, or by simultaneous operation at more than one frequency, but only at the expense of increased instrumentation complexity. High sensitivity and wide dynamic range are serious conflicting requirements in attempts to combine either low-altitude PCA and higher-altitude auroral, or daytime and nighttime, experiments, in a single instrument.

6. Assessment of Measurements

Assessment of RF probes for use in ionospheric studies always presents a problem. The practice has usually been to assess them in comparison with simultaneous propagation experiments, either carried on the same vehicle or performed by ground-based, vertical soundings. This is difficult for measurements with probes in the lowest layers, for which reliable propagation data may not be available, or for satellite work, where care must be taken to establish the validity of extrapolating to satellite use an assessment made at possibly much lower altitudes and under different operating and environmental conditions. The increasing availability of low-level data from absorption and partial-reflection studies may help to solve the calibration and assessment difficulties.

More effort could justifiably be devoted to establishing, by comparison measurements using several probe designs simultaneously, a proper assessment of the relative areas of validity of the various techniques. Since the RF probe is a comparatively new device, as far as operation in the upper atmosphere is concerned, unless reliable, independent calibration or comparison data, are available, the validity of results gained by single designs under different conditions is always open to question.

7. Some Directions for Further Effort

In conclusion, a discussion of problems associated with the operation of RF probes in the lower ionosphere introduces the opportunity to suggest some areas in which further exploitation of the potentialities of the device should be directed. The subject of calibration and assessment has just been mentioned. Thus, for example, the application of dispersion interferometers, Faraday rotation, and Langmuir probes is based on neglect of electron collisions and is therefore inappropriate in the lowest layers. In some cases, e.g. the Faraday rotation experiment, the effect of collisions can be taken into account, provided an independent measurement of differential absorption is made. Much of the uncertainty about the usefulness of the probe as a D-region device arises from some lack of knowledge about the nature and relative importance of the various loss processes involved in its operation. For low-power probes radiation and ohmic circuit losses are usually considered negligible relative to dielectric dissipation. However, electroacoustic, or pressure, waves in the electron gas have been suggested as an important source of loss [17], but again, the calculations have been based on a neglect of collision effects and only for a dipole geometry [18]. The loss factor is important when both high collision frequency and low electron density are to be measured.

The sampling volume of the sensor is relevant for at least four reasons, and is certainly geometry-sensitive. It determines the extent of the interaction between the sensor and other instruments (through sheath effects), it is a factor in the flexibility of the geometry as far as positioning on the vehicle is concerned, it is an important factor in attempts at calibration on the ground, and for those who contemplate using the RF probe to study the inhomogeneity of the ionosphere, it is a parameter determining the spatial resolution possible. Any geometry involves a compromise between reduced sampling volume and sensitivity to sheath effects.

It was suggested earlier, in discussing the choice of frequencies for a resonant circuit probe, that magnetic field effects should be minimized or taken into account in the theory. An indication of the magnitude of these effects could be obtained by locating and orienting the sensor so as to take advantage of any indication of modulating effects due to changes of orientation with respect to the field lines.

A number of agencies have incorporated a variable DC bias into their probes in an attempt to neutralize the perturbing effects of ion sheaths. The value of this technique has not really been established, since the only results are those of Utah from two daytime flights [19], and these were inconclusive. Recent flights by DRTE have given a positive result, but the technique should be exploited further.

Until recently the relaxation time of the ion sheaths around a sensor did not attract serious attention, since it was always considered short in terms of instrumentation parameter such

as DC sweep periods and periods of antenna voltage cycling such as had been practiced by NASA in theor RF probe-dispersion interferometer comparison tests. However, an increasing interest is being shown in the possibility of having rocket- and satellite-borne pulsed, sweep-frequency sounders serve the double function of ionosonic and RF probe. In addition, there might be a requirement to operate an RF probe in the vicinity of the field of such an ionospheric sounder. High-power, pulsed operation presents a new set of challenging problems, which include such factors as the time constant of the ion sheath, the sensitivity of the probe, as a function of both geometry and orientation, to plasma perturbations by the RF field, and the nature of the perturbation during a pulse period. For sweep-frequency systems the question of the nature of the variation of this perturbation as the frequency passes through the local plasma frequency is vital to any attempt to interpret sounding records in terms of the parameters of the plasma in the vicinity of the vehicle.

References

[1] H. A. Wilson and E. Gold, Phil. Mag., 11, 484 (Jan-June, 1906).

[2] E. V. Appleton and E. C. Childs, Phil. Mag., 10, 969 (Dec., 1930).

[3] E. C. Childs, Phil. Mag., 13, 873 (May, 1932).

[4] J. E. Jackson and A. D. Pickar, NRL Rpt. 4940 (May, 1957).

[5] J. E. Jackson and J. A. Kane, J. Geophys. Res., 64, 1074 (Aug., 1959).

[6] H. S. W. Massey, Fifth CSAGI Conference, Moscow (July, 1958).

[7] W. J. Heikkila, Paper at this meeting.

[8] J. R. Herman, Penn. State Univ., E. E. Dept., Iono. Res. Lab., Sci. Rep. No. 180, (Mar. 1, 1963).

[9] N. A. McDonald, H. Trieal and J. L. Yen, URSI-IRE Meeting, Ottawa (Oct. 15-17, 1962).

[10] J. A. Kane, J. E. Jackson and H. A. Whale, NASA Tech. Note No. TN D-1098 (Jan., 1962).

[11] R. C. Langille and J. C. W. Scott, J. Brit. IRE, 23, 61 (Jan., 1962).

[12] O. C. Haycock and K. D. Baker, Electronics, 88 (Jan. 13, 1961).

[13] P. A. Forsyth and A. Kavadas, Canad. Aero. Jour., 7, 105 (Mar., 1961).

[14] J. Sayers, P. Rothwell and J. H. Wager, Nature, 195, 1143 (Sept. 22, 1962).

[15] W. C. Hoffman, Report on "Symposium on the use of Space Vehicles", Fall 1958 URSI Meeting. Planet. Space Sci., 1, 238 (July, 1959).

Also L. R. O. Storey, J. Res. NBS, 63D, 325 (Nov.-Dec., 1959).

[16] Y. Aono, K. Hirao and S. Miyazaki, J. Rad. Res. Labs. Japan, 8, 453 (Nov., 1961).

[17] J. A. Kane, Provate Communication (1960).

[18] H. A. Whale, J. Geophys. Res., 68, 415, (Jan. 15, 1963).

[19] W. Pfister and J. C. Ulwick, Amer. Astronaut. Symp., Washington, D. C. (March 17, 1961).

DISCUSSION

S. A. Bowhill: Dr. Balmain of our laboratory has shown that the Debye length is approximately equal to the distance traveled by an electron in one period of the plasma frequency. The collapse time of the sheath is therefore of this order, and this gives a simple picture of the different behivior of the resonance probe above and below the plasma frequency.

T. E. Van Zandt: Regarding the plasma resonance method, Warren and Lockwood of DRTE thought there was a discrepancy between the electron densities found from the resonances seen on the Alouette vehicle, and the electron densities far from the satellite; in other words, that the satellite was perturbing the observations. I can now report that everyone, including Warren, now agrees that there is no significant perturbation; this makes the plasma resonance technique very promising, because it samples a volume much larger than the sheath. CRPL is developing a rocket payload to study this effect, and attempt to develop it into a useful probe for atmospheric studies.

J. S. Belrose: I believe they agreed that the experimental data contradict the earlier interpretation; however, there is no rigorous theory to explain what is seen.

T. E. Van Zandt: I believe there is no general agreement on this latter point.

L. C. Hale: In a rapidly moving medium the ion density in the sheath is the same as in an undisturbed medium.

2.2 THE SHEATH CAPACITANCE AT VERY LOW FREQUENCY OF A METALLIC BODY MOVING IN THE IONOSPHERE

R.J.L. GRARD
Radioscience Laboratory
Stanford University
Stanford, California

1. Introduction

Accurate knowledge of the sheath impedance of a body moving in the ionosphere is of high interest because it is a function of the density and temperature of the ions and the electrons.

We will deal here with the sheath capacitance at very low frequency of equipotential probes, assuming an isotropic medium, then, for the case of an elongated probe, we will take into account the influence of an electromotive force induced by a magnetic field.

2. Poisson's Equation in the Sheath

We assume that the probe travels through the plasma at a velocity large with respect to the ion thermovelocity and small with respect to the electron thermovelocity. Furthermore, we consider that the variation of the equilibrium potential of the probe has a small amplitude and a frequency low enough to let the electrons adjust their density instantaneously to the ambient potential, but high enough to let the ion density remain the same.

Consequently we apply Boltzmann's law to the electron density, assuming a Maxwellian velocity distribution function and considering that the ion density is unperturbed, we write Poisson's equation:

$$\nabla^2 \phi = - \frac{ne}{\epsilon_o} \left[1 - \exp \left(+ \frac{e\phi}{kT} \right) \right],$$

where ϕ is the potential in the sheath,
n is the unperturbed electron (or ion) density,
e is the charge of one electron,
ϵ_o is the dielectric constant of free space,
k is Boltzmann's constant
and T is the electron temperature.

An exact formulation would require a complete integration of Boltzmann's equation and would lead to an expression explicitly a function of the geometry and velocity of the probe.

3. Definition of the Sheath Capacitance

It has already been shown [1] that a body moving in a plasma and surrounded by a sheath is characterized by a dynamic capacitance when the equilibrium potential is allowed to have small variations at a given frequency.

The current flowing through this capacitance is the derivative of the charge Q with respect to the time:

$$i = \frac{\partial Q_o}{\partial t} = \frac{\partial Q_o}{\partial \phi_o} \frac{d\phi_o}{dt},$$

where ϕ_o is the potential of the body.

Since $i = C \frac{d\phi_o}{dt}$ the capacitance is $C = \frac{\partial Q_o}{\partial \phi_o}$ . .

We will give a common expression of the capacitance for a plane surface in rectangular coordinates, a cylinder of revolution in cylindrical coordinates, and a sphere in spherical coordinates. We assume respectively planar, cylindrical or spherical symmetry for the electric quantities on the surface of the body and within the sheath. We neglect the edge effect on the borders of the plane surface and at the tips of the cylinder.

From Gauss' theorem we can write for the charge borne by each body:

$$Q_o = A \epsilon_o E_o$$

Where E_o is the electric field at the surface and A the area.

By definition the electric field in the medium surrounding each probe is $E = - \frac{\partial \phi}{\partial r}$; because of the symmetry in each case we have $\nabla \phi = \frac{\partial \phi}{\partial r}$.

Consequently, $E_o = - \left(\frac{\partial \phi}{\partial r} \right)_o$ where $\left(\frac{\partial \phi}{\partial r} \right)_o$ is the value of $\frac{\partial \phi}{\partial r}$ on the surface.

Then the expression of the capacitance, $C = \frac{\partial Q_o}{\partial \phi_o}$ becomes $C = -A \epsilon_o \frac{\partial}{\partial \phi_o} \left(\frac{\partial \phi}{\partial r} \right)_o$.

It is practical to define a new set of variables:

$$y = \frac{e\phi}{kT}$$

and $x = \frac{r}{\lambda_D}$ where $\lambda_D = \sqrt{\frac{\epsilon_o kT}{ne^2}}$ is the Debye length.

2.2 GRARD

Using these dimensionless variables in the expression of the capacitance we write:

$$C = -A \frac{\epsilon_o}{\lambda_D} \frac{\partial}{\partial y_o} \left(\frac{\partial y}{\partial x}\right)_o, \text{ where } y_o = \frac{\epsilon \phi_o}{kT}.$$

If, furthermore, we define a third dimensionless quantity Υ such that $\Upsilon = \frac{C}{A} \frac{\lambda_D}{\epsilon_o}$, we finally obtain: $\Upsilon = - \frac{\partial}{\partial y_o} \left(\frac{\partial y}{\partial x}\right)_o$.

Expressing Poisson's equation for a sheath of a body moving in a plasma in terms of y and x, we have:

$$\frac{\partial^2 y}{\partial x^2} = e^y - 1, \text{ in rectangular coordinates,}$$

$$\frac{1}{x} \frac{\partial}{\partial x} \left(x \frac{\partial y}{\partial x}\right) = e^y - 1, \text{ in cylindrical coordinates and } \frac{1}{x^2} \frac{\partial}{\partial x} \left(x^2 \frac{\partial y}{\partial x}\right) = e^y - 1, \text{ in spherical coordinates.}$$

4. Planar Geometry

Poisson's equation, $\frac{\partial^2 y}{\partial x^2} = e^y - 1$, is integrated once to give $\frac{\partial y}{\partial x} = \pm \sqrt{2(e^y - y - K)}$. At $x = \infty$, y goes to zero and so does its derivative with respect to x, therefore the constant of integration K is evaluated to be 1 and

$$\frac{\partial y}{\partial x} = \pm \sqrt{2(e^y - y - 1)}$$

The value of $\frac{\partial y}{\partial x}$ on the surface is found by replacing y by y_o:

$$\left(\frac{\partial y}{\partial x}\right)_o = \pm \sqrt{2(e^{y_o} - y_o - 1)}$$

And finally $\Upsilon = - \frac{\partial}{\partial y_o} \left(\frac{\partial y}{\partial x}\right)_o$ or :

$$\Upsilon = \mp \frac{e^{y_o} - 1}{\sqrt{2(e^{y_o} - y_o - 1)}}.$$

When one adds to the potential ϕ_o some increment $\nabla\phi_o$, it turns out that the charge borne by the body Q_o changes by a corresponding crement ∇Q_o; the ratio $\frac{\nabla Q_o}{\nabla \phi_o}$, which is precisely the capacitance when the increments are infinitesimal, is always positive and so is Υ.

Consequently in the above expression of Υ, we choose the plus sign when y_o is positive and the minus sign when y_o is negative.

Thus we can write

$$\Upsilon = \frac{|e^{y_o} - 1|}{\sqrt{2(e^{y_o} - y_o - 1)}}$$

5. Cylindrical Geometry

In cylindrical coordinates Poisson's equation is written:

$$\frac{1}{x} \frac{\partial}{\partial x} \left(x \frac{\partial y}{\partial x}\right) = e^y - 1$$

It is not easy to obtain $\frac{\partial y}{\partial x}$ by integrating the above equation, however, the quantity Υ can be reached for two limit values of Υ, first when y goes to zero, then when y goes to minus infinity.

The small potential approximation gives

$$\Upsilon = \frac{K_1(x_o)}{K_o(x_o)},$$

where x_o is the radius of the cylinder divided by the Debye length, and K_o and K_1 are the modified Bessel functions of second kind and zero and first order respectively.

The large negative potential approximation gives the following expression involving Υ, y_o and x_o:

$$1 + \frac{4y_o}{x_o^2} = e^{\frac{2}{\Upsilon x_o}} \left(1 - 2\frac{2}{\Upsilon x_o}\right)$$

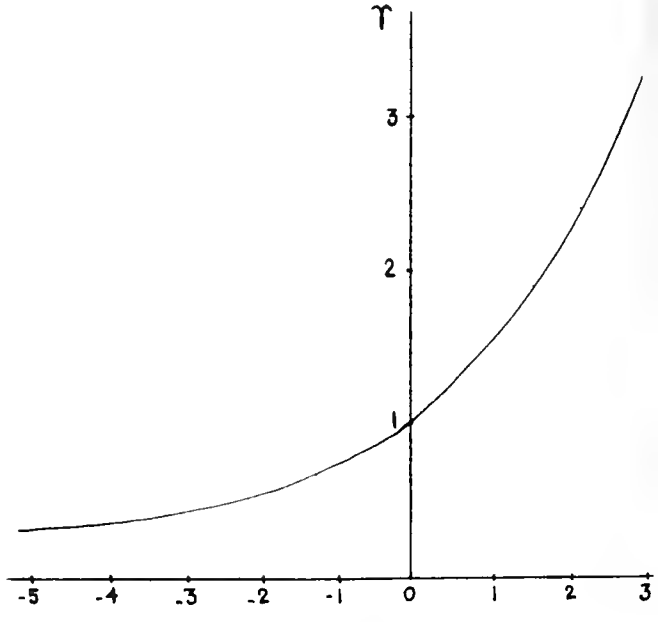

Figure 1. Curve of $\Upsilon = \frac{C}{A} \frac{\lambda_D}{\epsilon_o}$ vs. $y = \frac{e\phi_o}{kT}$.

6. Spherical Geometry

In spherical coordinates Poisson's equation,

$$\frac{1}{x^2}\frac{\partial}{\partial x}\left(x^2\frac{\partial y}{\partial x}\right) = e^y - 1,$$

is not easier to integrate than in cylindrical coordinates. But the problem can be worked out in two cases, as above, when y is very small and when y is very large and negative.

The first approximation gives

$$\gamma = 1 + \frac{1}{x_o},$$

where x_o is the radius divided by λ_D; the second approximation gives

$$1 + 6\frac{y}{x_o^2} = \frac{1 - \frac{3}{\gamma x_o}}{\left(1 - \frac{1}{\gamma x_o}\right)^3}$$

The partial results found for a cylinder and a sphere must be completed by computation, in each case we obtain a family of curve γ vs. y_o with x_o as parameter.

7. Influence of an Electromotive Force Induced in a Cylindrical Probe.

Since ϕ is varying not only in the sheath along a direction perpendicular to the surface, but also in a direction along the probe itself (Figure 2), the Laplacian of ϕ must be written

$$\nabla^2\phi = \frac{1}{r}\frac{\partial}{\partial r}\left(r\frac{\partial\phi}{\partial r}\right) + \frac{\partial^2\phi}{\partial z^2} \text{ in cylindrical}$$

coordinates.

By chance the variation of potential due to an electromotive force induced by the earth's magnetic field is a linear function of z and consequently $\frac{\partial^2\phi}{\partial z^2} = 0$. Therefore our previous results are still valid.

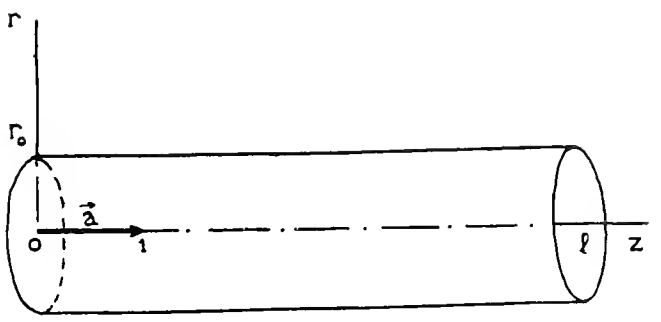

Figure 2. Cylindrical probe.

However, the distributed capacitance will be a function of z, so we will find the total capacitance by an integration.

If the radius of the cylinder is large with respect to the Debye length, we can use the planar approximation and write for an element of length dz

$$dC = 2\pi r_o dz \frac{\epsilon_o}{\lambda_D}\gamma(z)$$

$$\text{with } \gamma(z) = \frac{\left|\exp y_o(z) - 1\right|}{\sqrt{2[\exp y_o(z) - y_o(z) - 1]}}$$

The sheath capacitance of a cylinder of length ℓ is:

$$C = 2\pi r_o \frac{\epsilon_o}{\lambda_D}\int_0^{\ell}\gamma(z)dz,$$

$$\text{but } dy_o = \frac{e}{kT}d\phi_o = \frac{e}{kT}[\vec{v}, \vec{B}, \vec{a}]dz,$$

where $[\vec{v}, \vec{B}, \vec{a}]$ is the scalar triple product of the probe velocity, the magnetic field vector and the unit vector along the axis of the cylinder.

If $\xi = \frac{e}{kT}[\vec{v}, \vec{B}, \vec{a}]$, the integration becomes

$$C = 2\pi r_o \frac{\epsilon_o}{\lambda_D}\frac{1}{\xi}\int_{y_o(0)}^{y_o(\ell)}\gamma dy_o.$$

If $y_o(0)$ and $y_o(\ell)$ are for instance both negative and if ξ is positive, we obtain:

$$C = 2\pi r_o \frac{\epsilon_o}{\lambda_D}\frac{1}{\xi}\left[-\sqrt{2[\exp y_o(\ell) - y_o(\ell) - 1]} + \sqrt{2[\exp y_o(0) - y_o(0) - 1]}\right]$$

If the radius of the cylinder is not large with respect to the Debye length, we must do a graphical integration on the curve γ vs. y_o which is characterized by the parameter

$$x_o = \frac{r_o}{\lambda_D}.$$

8. Conclusion

We have found an expression of the capacitance in the case of planar geometry, and this result can still be used when the radius of curvature is large with respect to the Debye length. The solution needs to be completed in cylindrical and spherical geometries.

When the potential of the probe goes to minus infinity, the result goes to a limit which is the solution found for a sharply-bounded sheath. However, this result can still be used when the potential of the probe goes to zero or to positive values, in which case the notion of sheath thickness is meaningless. This can occur when the photoemission current is important.

Another improvement would be brought about by considering the effect of the ion wake on the sheath capacitance.

Reference

[1] R.F. Mlodnosky and O.K. Garriott, "The V.L.F. Admittance of a Dipole in the Lower Ionosphere," Proceedings of the Int'l. Conference on the Ionosphere, London, July 1962, Adlard & Son Ltd., Bartholomew Press, Dorking, England, 1963, 484-491.

2.3 A RADIO FREQUENCY PROBE FOR ELECTRON DENSITY MEASUREMENTS*

W. J. HEIKKILA
Southwest Center for Advanced Studies
P. O. Box 8478
Dallas 5, Texas

1. Introduction

A radio frequency probe for electron density measurements in the D and E-regions of the ionosphere has been developed at the Defence Research Telecommunications Establishment, Ottawa, Canada, and used successfully on two rocket flights in May and June, 1963. The sensing element of the probe consists of the capacitor formed by the 25 inch long nose tip of the rocket, which is separated from the rest of the rocket by a 5 inch fiberglass spacer. This capacitor forms a major part of the capacity in the tank circuit of a high frequency oscillator. When the tip is immersed in a plasma, the effective capacity is reduced and the oscillator frequency is raised. From the measured increase in frequency, it is possible to deduce the real part of the dielectric constant of the medium, and hence the electron density if the collision frequency is known or assumed. By the use of two slightly differing oscillator frequencies it is possible to estimate the electron collision frequency as well as the electron density.

2. Simple Circuit Theory of the Probe

Consider two conducting spheres, one of radius R_o representing the rocket or satellite vehicle in space, and the other of smaller radius R representing the probe held at a fixed distance from the vehicle (Figure 1). Let the probe be connected by an insulated wire to an inductance L inside the main vehicle. The spherical probe acts as a condenser of capacitance $C_p = 4\pi\epsilon\epsilon_o R$ farads when it is infinitely far from other bodies and embedded in a uniform medium with dielectric constant ϵ (MKS units). Neglecting for the moment the effect of other capacities, the probe capacity in series with the inductance will resonate at a frequency f given by

$$f = \frac{1}{2\pi\sqrt{LC_p}} \qquad (1)$$

$$= \frac{1}{2\pi\sqrt{LC_{po}}} \cdot \frac{1}{\sqrt{\epsilon}}$$

$$\text{or} \quad f = \frac{f_o}{\sqrt{\epsilon}} \qquad (2)$$

where ϵ is the dielectric constant and the subscript o indicates values of the capacity and resonant frequency in free space when $\epsilon = 1$. The device thus constitutes a probe for the measurement of the dielectric constant of the medium in which the probe is immersed.

In practice, the probe capacity will not be the only capacity in the circuit. The probe itself (C_p) is effectively in series with the space vehicle (C_v). Furthermore, stray capacities C_c associated with the leads, the inductance, and the oscillator are effectively in parallel with the combination as shown in Figure 1b. Resistance elements R_p and R_v have been included to show the possible presence of losses in the dielectric medium; these may affect the resonant frequency if the oscillator does not seek the zero phase shift point, but will be neglected here. Since C_v will in general be large compared to C_p, its effect in series with C_p is small. In practice, the stray-capacity, C_c, may be comparable to C_p and must be taken into account. The combined result of these other elements is to reduce the frequency dependence on the external dielectric constant; it will be assumed in the following that C_c is the only significant element in the circuit other than C_p. The relative frequency change $\frac{f - f_o}{f}$ under these assumptions is as follows:

$$f = \frac{1}{2\pi\sqrt{L(C_c+\epsilon C_p)}}$$

$$f_o = \frac{1}{2\pi\sqrt{L(C_c+C_p)}}$$

$$\frac{f - f_o}{f_o} = \sqrt{\frac{C_c + C_p}{C_c + \epsilon C_p}} - 1$$

$$= \frac{1-\epsilon}{2} \cdot \frac{C_p}{C_c+C_p} \qquad (1-\epsilon) \text{ small}$$

or

$$\frac{f - f_o}{f_o} = \frac{K}{2}(1 - \epsilon) \qquad (3)$$

This is the probe equation for small departures of ϵ from 1. The factor 1/2 arises from the square root dependence of frequency on capacity; the factor K, equal to the ratio of the probe capacity that is affected by the external medium to the total circuit capacity, represents

*This work was supported by NASA Grant NsG269-62.

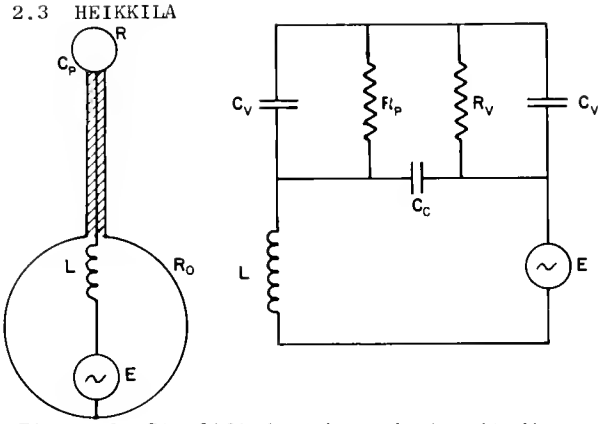

Figure 1. Simplified probe and circuit diagram.

the approach to an ideal circuit with no stray capacities for which K = 1. For the DRTE probe, K ≈ 1/2; it may be evaluated by a calibration procedure in which the frequency change for a known capacity change is measured.

3. Electron Density Measurement

In a plasma in which electron collisions and the magnetic field may be neglected, the dielectric constant ϵ at a frequency f is given in terms of the electron density N, charge e and mass m by

$$\epsilon = 1 - \frac{e^2 N}{4\pi^2 \epsilon_o m f^2} \tag{4}$$

or

$$\epsilon = 1 - \frac{81\ N}{f^2} \tag{5}$$

where N is the electron density per cubic meter, and f is in c/s. When the operating frequency f is much greater than the plasma frequency, $f_c = 81N = \frac{\omega_c}{2\pi}$, and the probe equation is

$$\frac{f - f_o}{f_o} = \frac{81KN}{2f^2} = \frac{K}{2}\frac{\omega_c^2}{\omega^2}, \quad \omega_c^2 \ll \omega^2 \tag{6}$$

For very small electron densities $f \approx f_o$, the change in operating frequency is directly proportional to the electron density in the plasma.

$$f - f_o = \text{const.} \times N \tag{7}$$

This simple linear dependence is followed closely as long as the oscillating frequency is several times the plasma frequency.

4. Electron Collision Frequency Measurement

When the electron collision frequency ν is appreciable the real part of the dielectric constant must be used in the probe equation. According to the Appleton-Hartree theory it is given by

$$E_r = 1 - \frac{\omega_c^2}{\nu^2 + \omega^2} \tag{8}$$

The probe equation then becomes

$$\frac{f - f_o}{f_o} = \frac{K}{2} \cdot \frac{\omega_c^2}{\nu^2 + \omega^2} \tag{9}$$

In this case the frequency change is reduced by an amount that depends on the operating frequency. This dependence provides the possibility of evaluating the collision frequency as well as the electron density by the use of two probes with different frequencies f_1 and f_2; then the ratio R of the relative frequency changes is given by

$$R = \left(\frac{f_1 - f_{10}}{f_{10}}\right) \Big/ \left(\frac{f_2 - f_{20}}{f_{20}}\right) = \frac{\nu^2 + \omega_2^2}{\nu^2 + \omega_1^2} \tag{10}$$

$$= \frac{\nu^2 + 4\pi^2 f_2^2}{\nu^2 + 4\pi^2 f_1^2} \tag{11}$$

It is now generally accepted that the effect of electron collisions is not satisfactorily taken into account in the Appleton-Hartree theory, in which ν is assumed to be independent of electron velocity. The generalized theory, as presented by Sen and Wyller [1] and other,

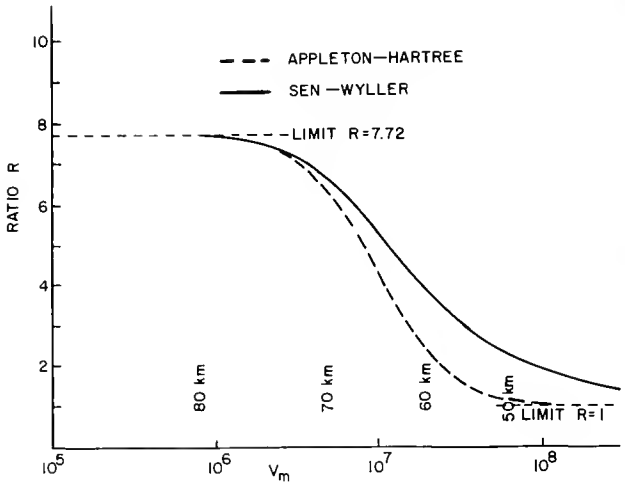

Figure 2. Ratio R of relative frequency changes at 4.5 Mc/s and 12.5 Mc/s as a function of the collision frequency.

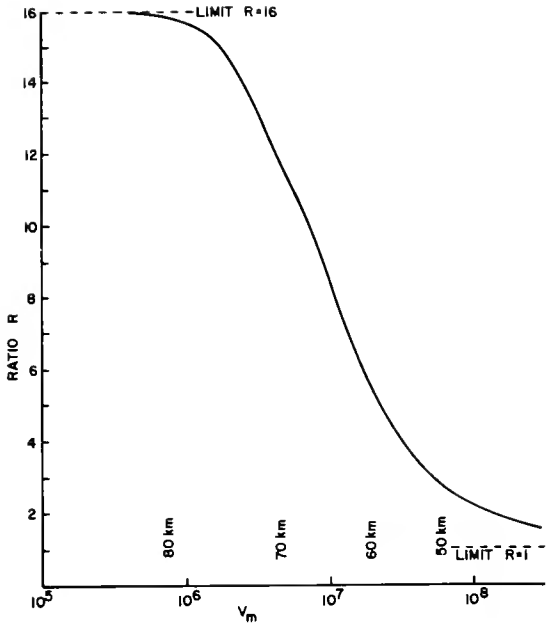

Figure 3. Ratio R of relative frequency shifts at 3.0 Mc/s and 12 Mc/s as a function of V_m the collision frequency in the generalized theory.

permits taking a velocity dependence of ν into account. Observations have indicated that ν is proportional to the electron energy in air, $\nu = \nu_m \frac{mv^2}{2kT}$. Again neglecting the effect of the steady magnetic field, equation (56) of Sen and Wyller's paper gives

$$1 - \epsilon_r = \frac{\omega_c^2}{\nu_m^2} C_{3/2}\left(\frac{\omega}{\nu_m}\right) \qquad (12)$$

where

$$C_{3/2}(x) = \frac{1}{(3/2)!}\int_0^\infty \frac{t^{3/2} e^{-t}}{t^2 + x^2} dt \qquad (13)$$

has been tabulated [2,3]. The ratio R at two frequencies is again independent of electron density;

$$R = C_{3/2}\left(\frac{\omega_1}{\nu_m}\right) \Big/ C_{3/2}\left(\frac{\omega_2}{\nu_m}\right) \qquad (14)$$

When the collision frequency is low ($\nu_m \ll \omega$) we may use the approximation

$$R \approx \frac{\omega_2^2}{\omega_1^2} \frac{\left[1 - \frac{35}{4}\frac{\nu_m^2}{\omega_1^2} + \ldots\right]}{\left[1 - \frac{35}{4}\frac{\nu_m^2}{\omega_2^2} + \ldots\right]} \qquad (15)$$

This is equivalent to the Appleton-Hartree formula, provided we take $\nu_m^2 = \frac{4\nu^2}{35}$. We can easily compute the ratio R as a function of ν_m for any ω_1 and ω_2. This has been done for the DRTE probe for which $\omega_1 = 2.83\times10^7$ and $\omega_2 = 7.87\times10^7$, $\omega_2 = 2.78\omega_1$ and the result is shown in Figure 2. The Appleton-Hartree result is also shown, and the difference can be seen to be appreciable. Heights in the ionosphere corresponding to the collision frequency profile adopted by Belrose [4] are shown on the figure. It can be seen that (provided the frequency shifts are measurable) the collision frequency in the lower D-region may be determined from the experimentally measured ratio R. With electron densities of $10^2/cm^3$ at 60 km, which are observed by Belrose, the frequency shifts are of the order of 100 cps. This small shift was not measurable with the present form of the probe, and the best that may be expected is confirmation of the order of magnitude of ν near 70 km. However, the experience gained shows the main shortcoming to be the data handling procedure used, and improvements can readily be made to permit useful measurements of both N and ν down to 55 or 60 km. A slightly lower value of f_1 would improve the performance, while still keeping the gyromagnetic influence small. Calculations for $f_1 = 3$ Mc/s and $f_2 = 12$ Mc/s are shown in Figure 3. The ratio R in this case is a strong function of ν over the range of values from 2×10^6 to 5×10^7 sec^{-1}, corresponding to ionospheric heights from 75 km down to 55 km.

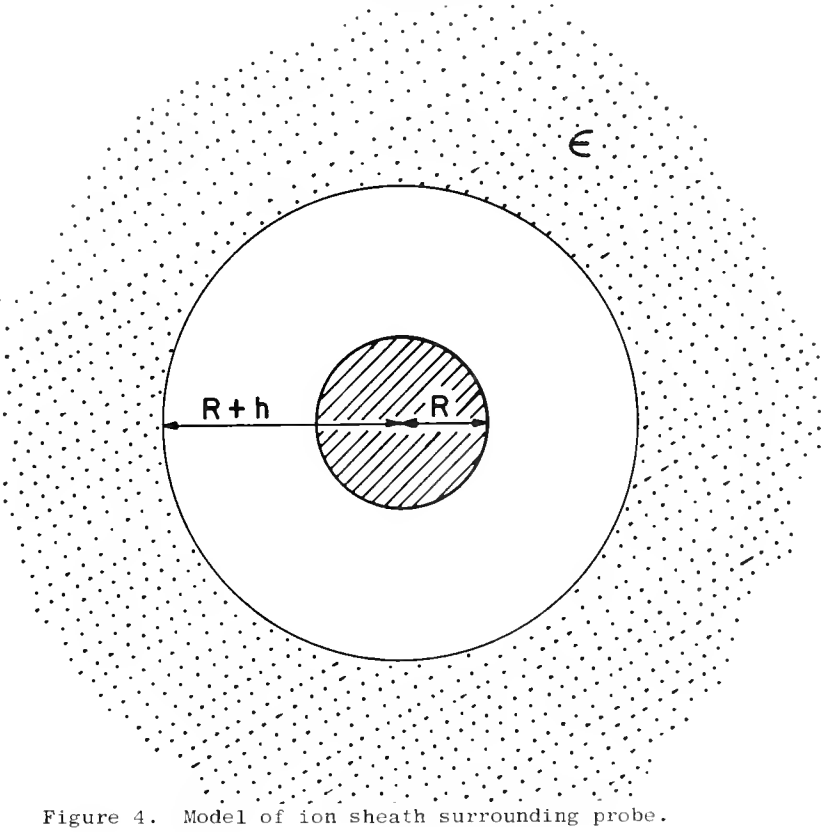

Figure 4. Model of ion sheath surrounding probe.

The neglect of the magnetic field is justified for two reasons. Firstly, even the lower operating frequency is at least two or three times the gyro frequency, and the effect of the field is therefore small, and is especially so in the presence of collisions as shown by the theory. Secondly, the probe determines some sort of average, not readily established, over the different directions of the field; this average will be closer to the zero field value than the value for either magneto-ionic mode.

5. Sampling Volume

An estimate of the sampling volume of the spherical capacitance probe may be made by considering the case in which the sphere is surrounded by an ion sheath, devoid of electrons, of thickness h (Figure 4). Inside the sheath $\epsilon = 1$, and beyond the sheath ϵ takes the value characteristic of the medium. The potential V of the sphere with a charge q on it is obtained by integrating the work done on a unit charge in bringing it from infinity to the sphere.

$$V = \frac{q}{4\pi\epsilon_o}\left[\frac{1}{\epsilon}\int_{\infty}^{R+h}\frac{dr}{r^2} + \int_{R+h}^{R}\frac{dr}{r^2}\right]$$

$$= \frac{q}{4\pi\epsilon_o}\left[\frac{1}{\epsilon(R+h)} - \frac{1}{(R+h)} + \frac{1}{R}\right] \qquad (16)$$

$$C = \frac{q}{V} = 4\pi\epsilon\epsilon_o R \cdot \left(\frac{R+h}{R+\epsilon h}\right)$$

When $\epsilon = 1$, C reduces to $4\pi\epsilon_o R$, the capacity in free space. When $h = 0$, the correct formula for the capacity of a sphere in a dielectric medium is obtained. In the presence of a sheath a correction factor must be applied which is a function of both the relative sheath thickness and the dielectric constant.

When the capacity of the sphere is taken to be a measure of ϵ, the effective values are related to the real values as follows.

$$4\pi\epsilon_{eff}\epsilon_o R = 4\pi\epsilon\epsilon_o R\left(\frac{R+h}{R+\epsilon h}\right)$$

$$\epsilon_{eff} = \epsilon\left(\frac{R+h}{R+\epsilon h}\right) \qquad (17)$$

In a weak plasma the effective electron density is then approximately related to the correct value by:

$$N_{eff} = N \cdot \frac{R}{R+h} \qquad (18)$$

This relation is plotted in Figure 5. The relative error is related simply to the sheath thickness relative to the probe dimension, and is otherwise independent of the actual electron density. When h = R the apparent electron density is one half the actual value. Throughout most of the ionosphere the Debye length is not over one centimeter, and therefore the ion sheath is not a serious problem for a probe with dimensions of ten centimeters or more, as would be the case in practice.

It may therefore be concluded that the sampling volume extends out a distance of the order of the probe dimension.

6. The DRTE Probe

The operation of the DRTE probe is indicated by the block diagram (Figure 6). Two frequencies, 4.5 and 12.0 Mc/s, are each chosen for 40 msec in turn by a relay across part of the tuning coil providing so-called low-frequency and high-frequency modes of operation. Two mixer stages lead to an output signal of near zero frequency in free space in either mode of operation when the circuitry is properly adjusted. As the probe penetrates the plasma, the tip oscillator frequency increases. A total increase of 2 Mc/s is within the bandwidth capabilities of the mixers, filters, and coder. This variation permits the measurement of electron densities up to $4 \times 10^5/cm^3$ with the 4.5 Mc/s oscillator, and over $10^6/cm^3$ with the 12.0 Mc/s oscillator. Great care was taken to achieve

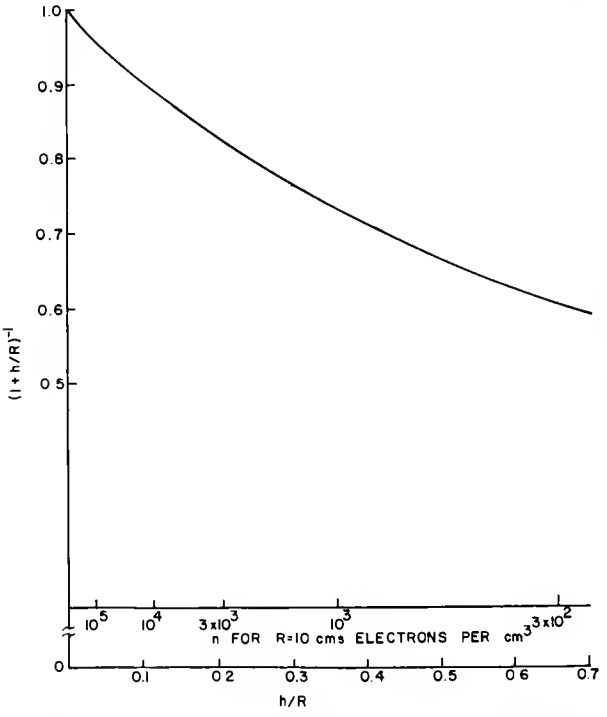

Figure 5. Ratio of apparent to actual electron density vs ion sheath thickness or electron density.

good circuit stability in order to permit measurement of low electron densities.

During the 40 msec of operation in either mode, a bias voltage on the tip is swept from -3 to +3 volts with respect to the rocket. As an additional part of the program of operation, a constant bias of about -100 volts is applied during every eighth 40 msec period in each mode of operation.

7. Operation During Rocket Flights

This probe was flown on two Black Brant rockets at the Churchill Research Range, Canada, during Spring 1963. The first rocket BBII-22 was fired at 1431 hours CST, 7 May during undisturbed ionospheric conditions; the second, at 2305 hours 10 June during an auroral radio wave absorption event. Two more flights are planned for Autumn 1963. On both of the spring flights the lower frequency mode provided good results in the D-region above 70 or 75 km, but the high frequency mode was somewhat erratic. Electron density profiles have been deduced and are discussed in a companion paper.

A perplexing feature of both flights was a large variation of the tip oscillator frequency above 100 km (in both modes) at the spin rate of the rocket; there must accordingly be some significant departure from cylindrical symmetry about the rocket spin axis, but the nature of this assymmetry has not been established.

While the results from the actual flights are still of a preliminary nature, they do verify that the present approach is satisfactory.

During each 40 msec period of operation the oscillator frequency increased with the bias voltage on the tip until the tip was slightly positive with respect to the rocket. With further increase in bias the frequency remained constant. Since the ratio of electron to ion mobility is at least 170 and the collection area ratio of the nose-cone to the tip was only 25, it may be assumed that the tip always remained slightly negative with respect to the plasma. The frequency during the time it was independent of bias was taken as the measure of electron density in the plasma; the ion sheath during this period may be assumed to be nearly equal to the Debye length $h_D = 6.9\sqrt{\frac{T}{n}}$, and a correction may then be applied as in Figure 5 to obtain the actual electron density.

The frequency shift in the low frequency mode for BBII-21 is plotted as the upper curve in Figure 7. In the D-region the shift is only a few hundred cycles per second, and in fact shifts of only a few cycles per second would need to be measured in order to determine the electron density down to 55 - 60 km. Such a small shift requires a high instrumental stability, of the order of 1 part in 10^6. Ordinarily this would not be attainable for the duration of the flight as drifts as high as 1 part in 10^2 may occur due to changes in the temperature of the circuit components, and particularly of the nose-tip itself. However, the stability requirement may be reduced to short-term effects only by the use of the high negative bias on the tip, as shown by the middle curve in Figure 7. The effect of the negative bias is to repel the electrons far from

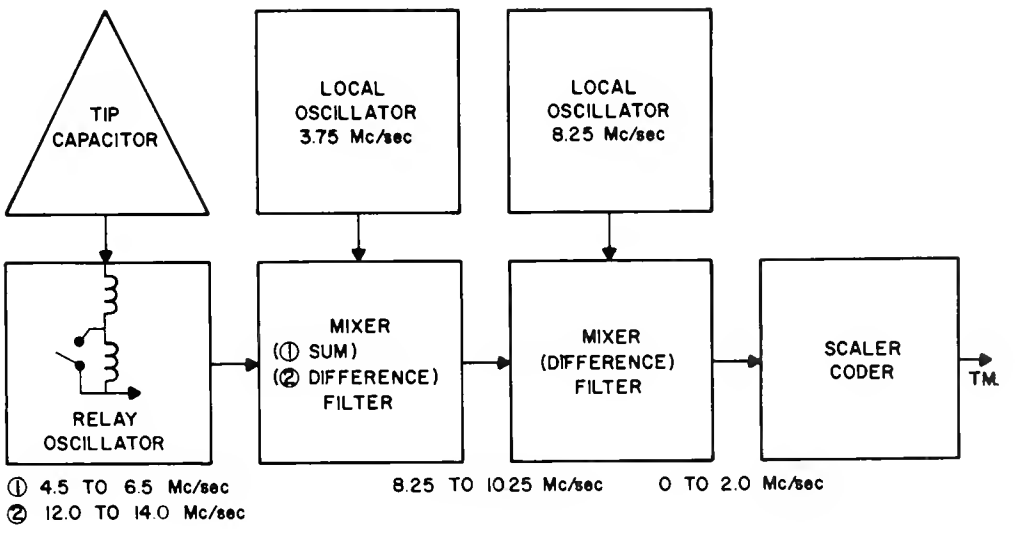

Figure 6. Block diagram showing the operation of the RF probe.

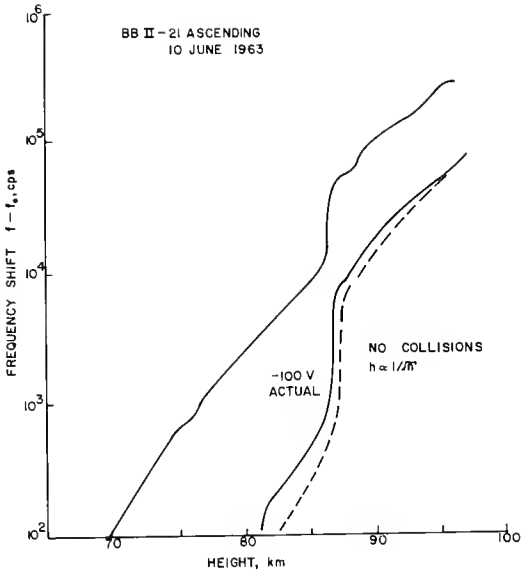

Figure 7. Frequency shift of 4.5 Mc/s oscillator due to the effect of the plasma.

the tip, and thus to bring the oscillator frequency to near the free space value. The difference between these curves, especially for low values of N, is a good measure of N, and it may be obtained experimentally in about one second or even less; for such short periods a stability of 1 part in 10^6 is attainable. In the present instrument the stability approached this value, but accuracy was lost in the data coding and telemetry adopted.

The opposing effects of ion acceleration when the high negative bias is applied and of the converging geometry might reasonably lead to an approximately constant value of ion density within the sheath. The calculation on this basis provides an order of magnitude of 50 cm for the sheath thickness near the E-region. The observed ratio of electron density with and without the -100 V bias is from Figure 7 equal to 6 at 95 km; if the radius 6 cms of the case of the tip is taken as a typical dimension of the probe, equation 18 yields a sheath thickness of 30 cm, in qualitative agreement with the calculation.

The sheath thickness might be expected to vary inversely as the square root of the electron density, as in the expression for the Debye length. This dependence is in fact verified by the results shown in Figure 7 in the height range 86 to 88 km. There the electron density changes by a factor of 4 over the short height range of 2 km (over which the collision frequency would change by only a small amount) and the sheath thickness changes by approximately a factor of 2.

While an accurate estimate of the effect of ion collisions is not easy, it may be shown qualitatively that they should increase the ion density near the probe and thereby should decrease the sheath thickness. This factor is thought to account for the difference between the actual curve obtained with the high negative bias and the dashed curve in Figure 7 which follows the $N^{-1/2}$ law from the E-region down. These results suggest that the combination of a DC bias with the RF probe may provide a convenient method for studying the properties of the ion sheath.

8. Conclusions

An RF probe operating well above the plasma and gyromagnetic frequencies has been shown to be a sensitive instrument for the measurement of D region electron density. An instrument operating at 3 Mc/s with a short term frequency stability of 1 part in 10^6 would permit measurements of electron density as low as a few electrons per cm^3 in the absence of collisions. The sensitivity is decreased by a factor of 8 at 50 km because of the effect of collisions, but densities as low as a few tens of electrons per cm^3 are still detectable.

The electron density and collision frewuency may be regarded as two independent variables, and their simultaneous determination requires two independent measurements. Two suitable measurements are the values of the dielectric constant at two different frequencies. In fact the ratio of the frequency shifts obtained using this form of probe operating at two frequencies is dependent only on the collision frequency and not on the density. With a choice of 3 Mc/s and 12 Mc/s the collision frequency can be measured accurately in the D-region between 50 and 80 km. If high accuracy in the frequency shift measurements is completely preserved in the telemetry, then collision frequencies as low as 5×10^4 sec^{-1} characteristic of the E-region at 100 km have a detectable effect.

References

[1] Sen, H.K. and A.A. Wyller, Journal of Geophysical Research 65, 3931-3950 (Dec. 1960) On the Generalization of the Appleton-Hartree Magneto-ionic Formulas.

[2] Dingle, R.B., D. Arndt, and S.K. Roy, App. Sci. Res. 6, 155-164, 1956-1957, The Integrals Cp(X) and Dp(X) and Their Tabulation.

[3] Burke, M.J. and E.H. Hara, Tables of the Semiconductor Integrals Cp(X) and Their Approximations for Use with the Generalized Appleton-Hartree Magneto-ionic Formulas, DRTE Report 1113, May, 1963.

[4] Belrose, J.S. and M.J. Burke. Study of the Lower E and D-regions Using Partial Reflections - Method of Analysis and Preliminary Results, Can. J. Phys. (to be published).

DISCUSSION

W.J. Heikkila: It is desirable to have geometric symmetry about the spin axis. However, on all these flights we received a large modulation of the apparent electron density at the spin rate, not the yaw rate. This was a factor of ten in electron density above the E-layer. Flights in daylight, twilight and at night all showed the same effect. We would like comments as to possible causes.

R.L.F. Boyd: I wonder if it might be due to gassing from the vehicle, perhaps more on one side than the other.

W.J. Heikkila: I do not believe this can be so, since the same effect on all three flights. Further, the rocket was "nose up" on both ascent and descent.

W. Pfister: Is the effect correlated with magnetic field direction?

W.J. Heikkila: No. However, some modulation occurred during the whole flight which could depend either on yaw or altitude.

R.L.F. Boyd: Perhaps the vehicle was asymmetrical with regard to its photoemissive properties.

W.J. Heikkila: Yes, but we found the effect on both shots.

2.4 A RADIO-FREQUENCY ELECTRON DENSITY PROBE FOR A WIDE RANGE OF IONOSPHERIC MEASUREMENTS

J. SAYERS
Department of Electron Physics
University of Birmingham
Edgbaston, Birmingham 15, England

1. Introduction

The local plasma electron density is determined by measuring the electric permittivity of the medium using an RF signal of 39 Mc/s and an electrode system which produces only slight radiation at this frequency. The electrodes consist of a pair of flat circular grids of fairly high transparency - approximately 80%. The diameter of the grids is 3 in. and they are supported $2\frac{1}{2}$ in. apart on the ends of two short tubes containing inner co-axial rods connected to the grids. These tubes are mounted forkwise on a small junction box which, in turn, is fixed on the end of a retractable boom of approximately 3 ft. in length. The permittivity is measured in terms of the current which flows between these two electrodes in response to a constant applied signal of 3 volts rms. This signal is supplied by a 39 Mc/s crystal controlled oscillator whose amplitude is electronically stabilized at the above value.

2. Basic Principles

The electric permittivity of a medium containing free electrons in the presence of a magnetic field and subject to collisions between the electrons and the neutral gas has been derived by Appleton [1]. In the notation adopted by Ratcliffe [2] the permittivity may be expressed:

$$= 1 - \frac{X}{1-iZ-\frac{1}{2}Y_T^2/(1-X-iZ) \pm \left[\frac{1}{4}Y_T^4(1-X-iZ)^2+Y_L^2\right]^{1/2}}$$

In this expression:

$$X = \frac{\omega_o^2}{\omega^2}$$

where

ω_o is the plasma frequency neglecting the effects of the magnetic field or of electron collisions, and

ω is the wave frequency.

$$Z = \nu/\omega$$

where

ν is the electron collision frequency with the gas, and

$$Y_L = \omega_L/\omega$$

$$Y_T = \omega_T/\omega$$

where

ω_L and ω_T are the longitudinal and transverse magneto-ionic frequencies for the electrons.

The Appleton equation shows that the medium is anisotropic and in order to relate the electric permittivity to the electron population density in the general case we must have knowledge of the geometry of the electrode system in relation to the magnetic field direction. A further difficulty in solving the problem in general terms arises from the fact that the permittivity is a complex quality and any measuring device would need to include an accurate measurement of phase as well as of amplitude. Both the above difficulties can be eliminated if we choose a probing frequency 'ω' which is an order of magnitude higher than either the electron collision frequency or the gyro-frequency. In the ionosphere this choice results in the probing frequency being also high compared with the plasma resonance frequency, and this is useful in providing a linear response in the practical equipment. With these assumptions, the Appleton formula reduces to the very simple form:

$$\epsilon = \epsilon_o \left(1 - \frac{4\pi N_e^2}{m\omega^2}\right)$$

In this expression the term in brackets is to be evaluated using CGS electrostatic units and the formula then reduces to:

$$\epsilon = \epsilon_o \left(1 - 8.06 \times 10^7 \frac{N}{f^2}\right)$$

where

ϵ_o is the permittivity of free space,

N is the electron density in the medium (cm^{-3}),

f is the probing frequency (c/sec).

With a probing frequency of 39 megacycles and $N = 10^6$ cm^{-3}

$$\epsilon = .947\ \epsilon_o$$

The dielectric constant is thus reduced by approximately 5% for an electron density of 10^6 or by 5 parts in 10^6 for an electron density of 100 cm^{-3}, the relationship being linear. The experimental requirement is thus to measure accurately very small charges in permittivity which the free electrons produce. Before considering in detail how this measurement is carried out, it is necessary to review the properties of space charge sheaths on the electrodes.

3. Space Charge Sheaths and Electron Depletion

In a number of historic papers on plasma probes Langmuir showed that when a probing electrode in an ionized gas has a potential which is more negative than the local plasma potential, the current to the electrode which results is carried by + ve ions and the effect of the applied negative potential is to displace the plasma electrons from the immediate vicinity of the electrode. The positive ions are accelerated towards the electrode in this region, but because of their inertia they move comparatively slowly and form a substantial positive space charge which has a screening effect on the applied probe potential. At a certain distance, which is calculable when the geometry and other factors are known, the screening is complete. The applied probe potential does not penetrate beyond this point which is recognized as the sheath boundary. The sheath boundary is, in fact, never quite sharp: the diffuseness of the boundary being determined by the temperature conditions in the plasma. In the geometry of the RF electron probe which has been quoted, the application of a few volts negative potential to the electrodes with respect to space potential is sufficient to establish an ion sheath which excludes all electrons from the space between the grids and from the fringe area around the grids in which the RF probing field is appreciable. Under these conditions the effective permittivity is equal to that of free space. The small changes in permittivity produced by the plasma electrons are thus measured by a circuit which subtracts the value of the RF current between the grids when the latter are at space potential from the current with the electrodes at some suitably large negative potential.

4. Electronic Circuit Functions

In principle the foregoing can be achieved by the circuit arrangement shown in Figure 1. R_1 is the viewing resistance across which a small RF voltage is developed proportional to the current flowing between the grids. Subtraction of the electron data signal at 3 kc/s from the much larger DC signal corresponding to the free space displacement current between the grids is achieved by the condenser C_1. For all electron density levels a 3 kc/s tuned amplifier gives a useful bandwidth reduction in the amplifiers, but for low electron densities it is necessary in addition to use phase sensitive detectors on the output in order to maintain an adequate signal/noise ratio.

5. Location of Space Potential

The foregoing simplified arrangement cannot be used in practice because, in general, space potential is not known relative to the vehicle. Our ability to locate space potential depends on the fact that if the potential on the grid electrodes is made more positive than plasma potential electrons are accelerated as they pass close to or between the grids. Provided they do not lose an appreciable fraction of their added energy in collisions with the gas - and a few tens of collisions will be admissible - the average population density of the electrons in the vicinity of the grids will be less than in the undisturbed plasma. A maximum electron density between the grids thus occurs only at space potential and this is representative of the true plasma population density. The actual circuit used embodies the above principles and differs from the simplified circuit already discussed in that the square bias waveform applied to the electrodes has a slow sawtooth modulation superimposed in order to scan for space potential. In this the

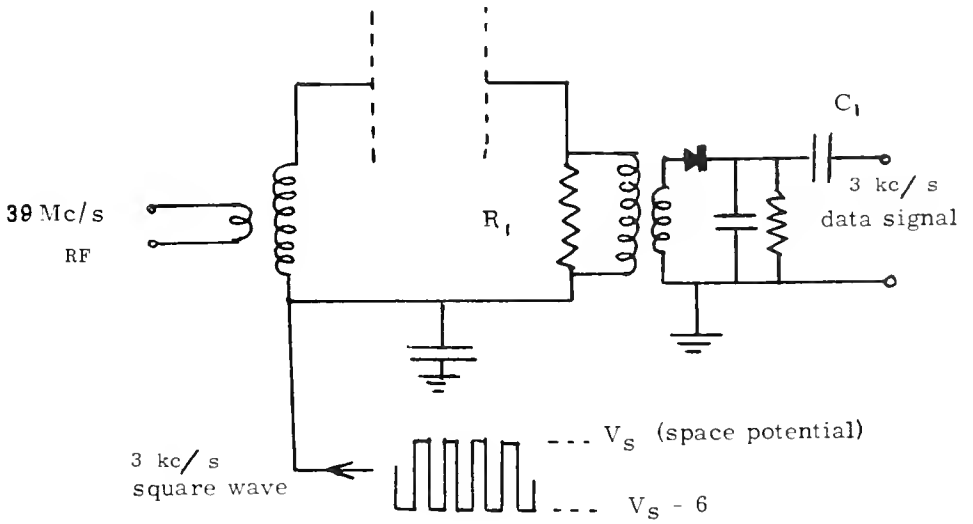

Figure 1. Circuit arrangement for impedance measurement.

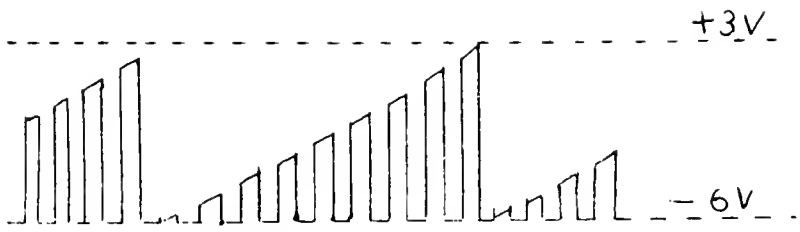

Figure 2. Modulated sawtooth voltage.

negative end of the square wave modulation is clamped at - 6 V relative to the vehicle potential and the positive end follows the sawtooth envelope from - 6 V to + 3 V, as shown in Figure 2.

The electron data signal is modulated in response to the sawtooth envelope and the signal reaches its maximum and true value when space potential is encountered somewhere between the above two limits which are suitable for ionospheric rocket probes. For exosphere or interplanetary probes the + ve limit has to be varied considerably.

6. Functional Block Diagram

The functional block diagram of the electronic equipment is shown in Figure 3. The 39 Mc/s generator is electronically regulated at a constant amplitude except during the first 10 msec of each sweep when a shallow 3 kc/s modulation is applied to the generator. This modulation appears on the data as an artificial electron signal and is used as a continuous in-flight check that the pre-flight calibration of the instrument is valid for the reduction of the data. The remainder of the circuit functions have already been explained. The battery pack is an integral part of the system and consists of re-chargeable nickel-cadmium cells so that the probe equipment is self-contained and makes no call on vehicle power supplies.

7. Pre-Flight Calibrations

The data signal, which is represented by the depth of modulation of the 39 Mc/s signal appearing across the viewing resistance R_1, is a linear function of electron density and for the conditions chosen in the experiment the constant of proportionality can be readily calculated. Completion of the calibration requires the measurement of the gain factors in the various amplifiers and detector circuits. The amplifiers are provided with very heavy negative feed-back and a design requirement of

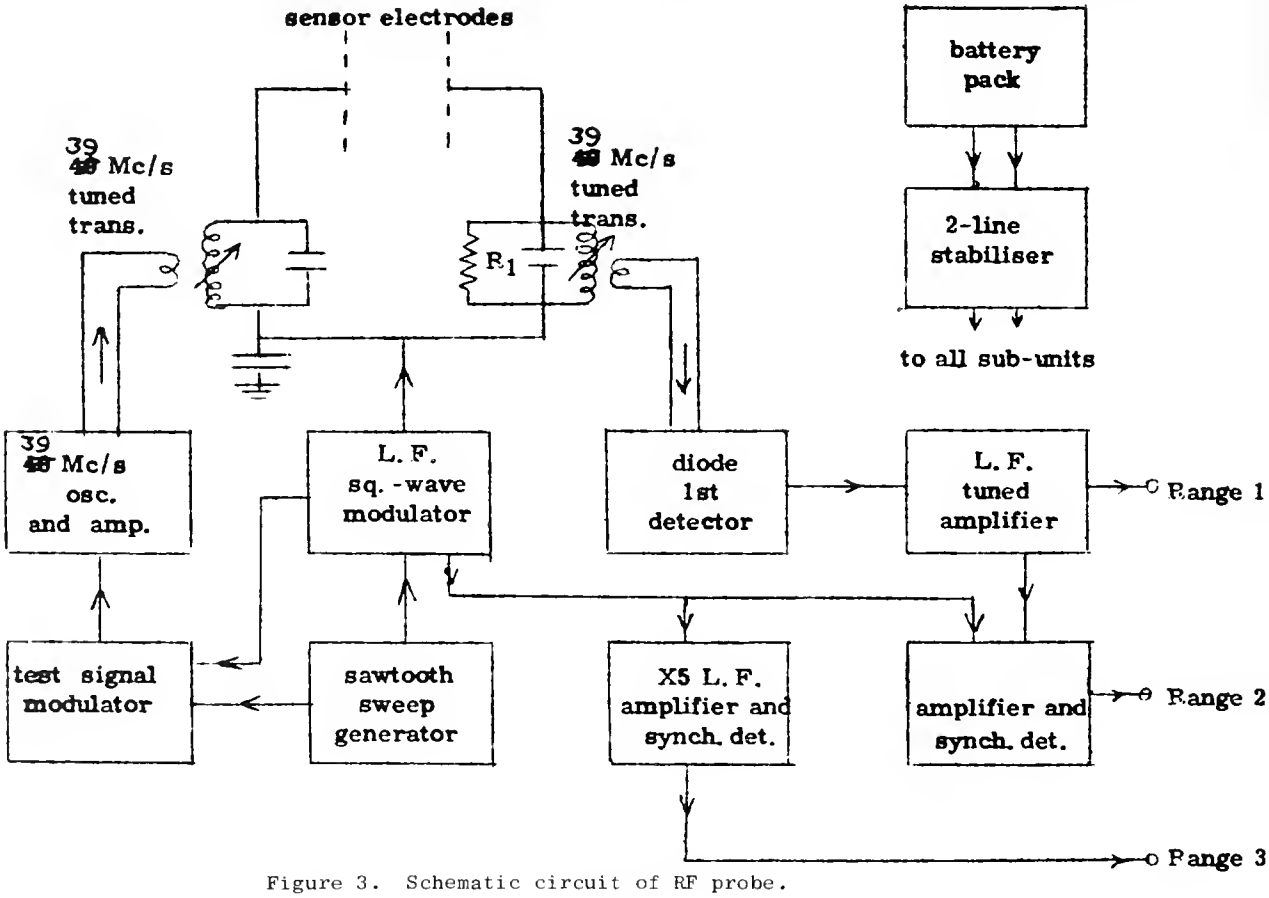

Figure 3. Schematic circuit of RF probe.

the complete system is that the calibration of each data channel in terms of electron density shall be represented by a constant multiplying factor which shall be independent of temperature in the range -15 to 70 degrees C. As already indicated the reliability of the calibration during flight is verified by noting the constancy of the artificial test signals appearing at the start of each sawtooth sweep.

8. Sensitivity Ranges Suitable for Measurements in the D- and E-Regions of the Ionosphere at Sunspot Minimum

Four sensitivity ranges are required to cover the wide range of electron density which is encountered in the lower ionosphere. These are shown in Table 1.

Channel	Electron Density Range of Measurement
1	100 to 2000 $cm.^{-3}$
2	2×10^3 - $10^4 cm.^{-3}$
3	10^4 - $5 \times 10^4 cm.^{-3}$
4	5×10^4 - $2.5 \times 10^5 cm.^{-3}$

TABLE 1.

In any vehicle where telemetry is very limited it is possible to avoid transmission of the data and sawtooth scan and present to the telemetry only the data peaks corresponding to space potential. This enables the electron density to be transmitted using a bandwidth which need not exceed that required by the rate at which the density is changing along the vehicle trajectory. In this case no further data reduction is needed after demodulation of the telemetry signals, apart from the correlation of the data with the vehicle trajectory in terms of position and time.

9. Plasma-Dynamic Effects due to the Hypersonic Velocity of the Electrodes through the Medium

Rockets and earth satellites have velocities which are small compared with the thermal velocities of the free electrons, so we are not concerned with any direct effects on the electrons. However, vehicle velocities are, in general, higher than the thermal velocities of the ions or neutral gas particles. This will result in the setting up of a shock wave front extending back from all leading edges of the sensor electrodes at an angle to the trajectory path whose cosecant is equal to the Mach number. This disturbance in ion flow past the sensor electrodes will be transmitted also to the electrons by means of the ambipolar coupling, and if not elminiated it can lead to substantial errors in measurement. The boundary at the wave front ahead of which the region is undisturbed will be diffuse to the extent of one mean free path for the gas particles, and when this mean free path is long compared with the dimensions of the sensor electrode geometry the shock wave disturbance will not be appreciable. Since these dimensions are of the order of 5 cm the above effect is only important in the lower ionosphere.

10. Effects of Shock Wave Disturbances in the Lower Ionosphere

The effects of shock waves generally present a major problem in the interpretation of local plasma experiments in these regions. It is fortunate that in the case of the RF electron probe this problem can be easily eliminated. Since the major contribution to the permittivity measurement of the plasma is that part of the local plasma which lies between the electrodes it is only necessary to ensure that the shock front lies entirely outside the space between the electrodes. This is achieved by arranging that the velocity vector of the vehicle lies in a plane of symmetry between the two sensor electrodes and by setting the electrodes in planes which make an angle with the plane of symmetry which is equal to or greater than half the included angle of the shock front. This geometry is illustrated in Figure 4.

This geometry is necessary in the D- and lower E-regions of the ionosphere.

11. Special Vehicle Requirements

In common with all other local plasma measurements the RF electron probe is sensitive

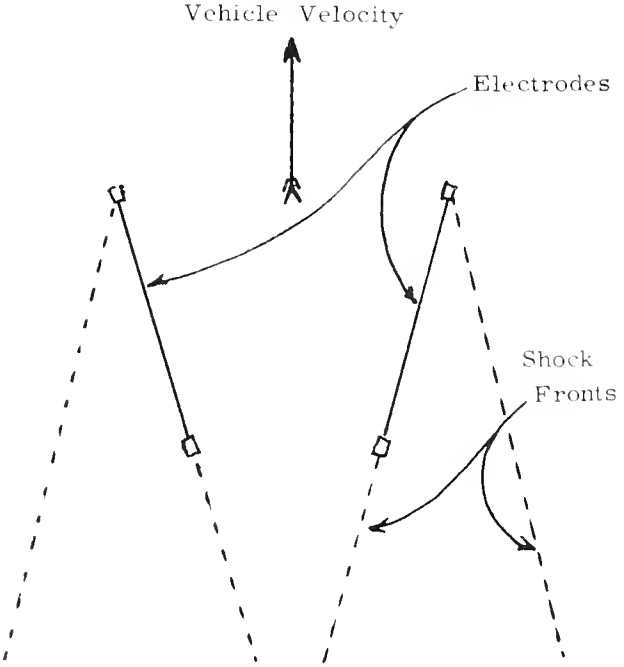

Figure 4. Electrode geometry at supersonic velocity.

to disturbance of the plasma by gas escaping from the rocket vehicle. The effect of any such escaping gas is to reduce the ionization density in the vicinity of the rocket by replacing the ionized gas with neutral gas, and it is possible to estimate the rate of gas flow for which this disturbance will be appreciable. Since the effect of gas from the rocket will depend to a great extent on the distribution of the points of emergence relative to the probe electrodes, it is not possible to carry out a precise analysis of this problem which will be applicable to any particular rocket. On the assumption that the gas escapes as from an imaginary point source at the centre of the rocket head, it is possible to estimate the maximum rate of gas escape which can be tolerated in the electron density measurements. This has been found, in the case of Skylark rockets, to agree in order of magnitude with the experimental observations. With the data available to date it appears that for accurate measurements by the RF electron probe the electrodes must be carried on the end of a boom of approximately 2 ft. in length and the escape of gas must not exceed 1 cm^{-3} sec^{-1} at NTP. This rate is higher than normal outgassing rates for metal surfaces of small rockets, and the problem only becomes serious when there is inadequate sealing of pressurized compartments.

12. The Choice of Modulation Frequency in Relation to the Rocket Velocity in the Lower Ionosphere

It should be noted that in the lower ionosphere mobility of ions and electrons sets an upper limit to the modulation frequency which can be used with full plasma response. In practice, for a vehicle Mach number in the range 2 to 5 a modulation frequency in the region 2 to 3 kc/s will be suitable. A frequency in this range is being adopted for D-region probes. For E- and F-region probes a modulation frequency of up to 20 kc/s can be used.

References

[1] Appleton, E.V., 1932, Wireless Studies of the Ionosphere, J. Inst. Elect. Eng. 71, 624.

[2] Ratcliffe, J.A., 1959, The Magneto-Ionic Theory and its Applications to the Ionosphere, Cambridge Univ. Press.

DISCUSSION

A. Nagy: How is it planned to move the plates for the lower D-region flights?

S.A. Bowhill: They will not be moved but will be prearranged to the Mach angle of the shock wave.

L.C. Hale: If you adjust to the Mach angle you may approach a situation where the wave will detach if there is a slight wobble.

R.L.F. Boyd: The Sayers probe and a Langmuir probe were both used on the satellite Ariel, so we have data to compare. At the high electron densities there is good correspondence between the two, however there is a departure at lower densities, about 10^4 cm^{-3}. Further results will be forthcoming.

W.J. Heikkila: The frequency used seems very high.

S.A. Bowhill: The reason is to enable measurement to lower altitudes and lower electron densities.

K.W. Champion: Was 40 Mc/s used on the Ariel probe?

S.A. Bowhill: No; 10 Mc/s. The choice in that case was made to get above the plasma frequency.

3.A DIRECT MEASUREMENTS OF THE ELECTRICAL CONDUCTIVITY OF THE ATMOSPHERE

E. C. WHIPPLE, JR.
NASA
Goddard Space Flight Center
Greenbelt, Maryland

1. Introduction

Since the concept of conductivity implies that collisions are important in determining the motion of ions, it is apparent that the direct measurement of conductivity is restricted to situations where ions experience a significant number of collisions in the immediate vicinity of the measurement apparatus. Hence the use of probes to measure atmospheric conductivity is limited to altitudes below about 85 km where the mean path is approximately one cm.

2. Theory of Simple Probes

Consider an isolated body of any shape in the atmosphere on which there is an electric charge Q [1]. There is an electric field surrounding the body, and also an air flow velocity pattern if the atmosphere is not at rest with respect to the body. The current density at any point due to motion of ions is the vector sum of a drift motion due to the electric field and the convective motion due to the air flow, if diffusion may be neglected. The total current to the body is obtained by integrating the current density over a closed surface with the result that

$$I = n\ e\ k\ Q/E = \sigma\ CV/\epsilon$$

where n is the ion density, e the ion charge, k the ion mobility, $\sigma = n\ e\ k$ the ion conductivity, and ϵ the permittivity of the air; and where space charge within the volume enclosed by the surface has been neglected. The charge, Q has been expressed in terms of the capacitance C and the potential V of the body with respect to the atmosphere.

The effect of diffusion may be included by adding a third term to the expression for the current density. The resulting equation [2] has been solved only for a spherical body at rest,

$$I_+ = \sigma_+[CV/\epsilon][\exp(eV/kT) - 1].$$

For other geometries one would expect the same qualitative result that diffusion is unimportant when the absolute value of the probe potential is large compared with the equivalent thermal energy of the ions. The effects of space charge are much more difficult to evaluate quantitatively. It seems reasonable to neglect space charge effects, however, if ion densities are less than $10^4/cm^3$.

In practice one never has an isolated body with which to make a measurement. The presence of a second body (e.g. the rocket body) complicates the determination of the probe to atmosphere potential. Smith [3] has shown that if C_1 and C_2 are the capacitances of the first and second bodies, then

$$I = \frac{C_1 C_2\ \sigma_+ \sigma_-\ V}{\epsilon[C_1 \sigma_+^- + C_2 \sigma_-^+]}$$

where in this case V is the potential difference between the first and second bodies, and where diffusion and space charge have again been neglected. The upper subscripts are used for $V>0$.

3. Gerdien Condensers

The Gerdien condenser, Figure 1 (a), has been used for many years to measure ion density and conductivity in the lower atmosphere. Ions entering the outer cylinder are collected by the inner cylinder at a rate proportional to the potential difference between the cylinders. The current saturates when all the ions entering the cylinder are collected. A typical current-voltage curve for air containing ions of one mobility is shown in Figure 1 (b). When many species of ions are present it is convenient to define a mobility distribution function f(k) such that

$$\sigma = e \int k\ f(k)\ dk$$

It can be shown that f(k) may be derived from the shape of the current-voltage characteristic curve obtained with a Gerdien condenser [4].

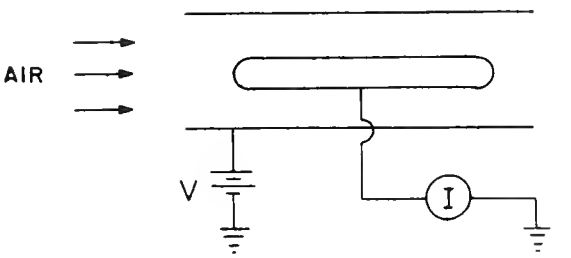

Figure 1 (a). The Gerdien condenser

3.A WHIPPLE

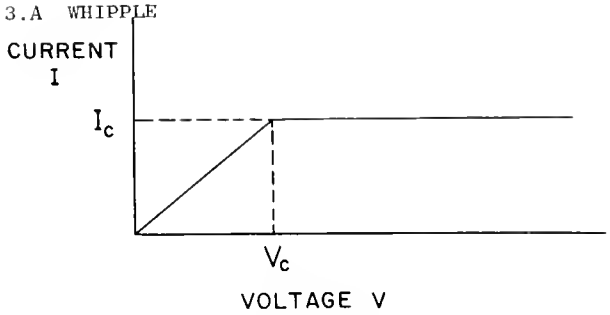

Figure 1 (b). Characteristic curve for air containing ions of one mobility

4. Practical Difficulties

In order to compute the atmospheric ion density from the measured current, it is necessary to know either the ion mobility, or, in the case of the Gerdien condenser, the volume rate of air flow through the condenser. Since the ion species in the D-region and below are unknown at present, mobilities must be either estimated or measured simultaneously. There is in addition the problem that at high field to pressure ratios (E/p > one volt/cm per mm Hg) the ion mobility is not independent of the magnitude of the electric field. For a typical experimental field of one volt/cm, the ratio $E/p > 1$ above 45 km.

At vehicle velocities greater than Mach one shock wave effects control the volume rate of air flow through the condenser. Hence it is necessary to design the condenser to take this into account, and wind tunnel tests to verify the design are desirable. Some effort at present is directed to the development of a drag device such that a payload ejected from a rocket above 80 km would reach a terminal velocity of less than Mach one by 70 km.

Other difficulties which must be taken into account either in the design of the experiment or in the data reduction process are the effects of contact potential between the collector and other surfaces which may change during a flight, and photoemission which may be effective to altitudes as low as 30 km.

References

[1] Swanu, W. F. G., Terr. Mag. and Atmos. Elec., 19, 81, 1914.

[2] Gunn, Ross, Journ. Meteor., 11, 339, 1954.

[3] Smith, L. G., personal communication.

[4] Whipple, E. C. Journ. Geophys. Res., 65, 3679, 1960.

DISCUSSION

J. O. Thomas: Does the shock wave set up near the leading edges of a Gerdien condenser moving at supersonic speeds increase or decrease the effective aperture area required in the conductivity measurement?

E. C. Whipple: If the shock waves are attached, the aperture is well defined; but if the shock wave detaches the answer is unclear.

R. L. F. Boyd: Why does one not measure the mobility in the laboratory? Also, are the first and second derivative approaches applicable and, if so, are they applied? Is it possible to use cylindrical grid structures so as to have a free flow of air to create less shock wave problems, and yet make them opaque to ions?

E. C. Whipple: On the first question, the laboratory air is different from the actual air because of impurities. The other suggestions are interesting.

3.1 ION-SPECTROMETER FOR THE UPPER STRATOSPHERE AND MESOSPHERE

HANS DOLEZALEK and A. L. OSTER
AVCO-Corporation,
Research & Advanced Development
Division
Wilmington, Massachusetts

In principle, the Gerdien Condenser may be applied up to altitudes where the mean free path becomes comparable with the geometrical dimensions of the apparatus. However, the mobility increases with altitude, and it becomes difficult to obtain a sufficient resolution without increasing air velocity and/or decreasing driving voltage beyond practicable limits. Air velocity must remain subsonic to prevent alterations of the nature or the number of ions to be measured.

In order to get a workable instrument, in spite of these facts, a new concept was introduced. A differential Gerdien Chamber of the second order is used. That means, that the ion intake occurs only at a predetermined radius, and that the receiving electrode is divided into several insulated parts. Furthermore, the driving electrode is divided into several parts, as shown in Figure 1.

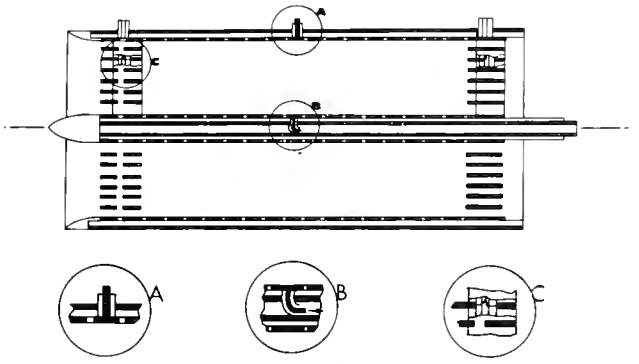

Figure 1. Cross section of modified Gerdien chamber. Air flows from left to right. First set of coaxial rings at air intake serves as ion gate. Second and third sets provide correct electric fields inside. Driving and receiving electrodes are divided in 16 parts each. All rings and electrodes are connected to highly insulated wires leading out.

If, now, an AC driving voltage, with an amplitude increasing along the axis, is applied, ions with the different mobilities marked I, II, III in Figure 2 will move as indicated. Thus, the resolution is increased.

The principle is tested, at present, in a specific low pressure wind tunnel. Air velocities between zero and almost sound can be steadily maintained and regulated with pressures between 1000 mb and 10 μb; the test section is 20 cm wide. An ageing section allows simulation

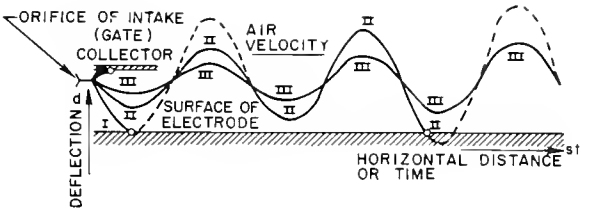

Figure 2. Effect of AC voltage on ion movement. Ions with mobilities I (high), II (medium), and III (low intercept the receiving electrode at separated points. AC voltage increasing from left to right.

of ionization and temperature, and control of velocity profile and boundary layer. A tank of 400 m^3 and a total constant air removal of 15 m^3/sec, done by eight pumps, provide the required conditions.

A number of ion-physical and technological problems are involved, such as distortions of the ion paths due to field-dependent mobilities, influence of velocity profile, diffusion, edge effects, displacement currents.

Ion intake is provided only during certain intervals. Figure 3 demonstrates, that by a short opening at t = T/4, ions of the indicated mobility will be intercepted at the point T/2, while ions of a by 10% smaller mobility will reach the receiving electrode at the point 3T/2, outside the figure.

The nature of atmospheric ions, in the range from 30 to 80 km, changes from "cluster ions" to molecular ions to atomic ions. The

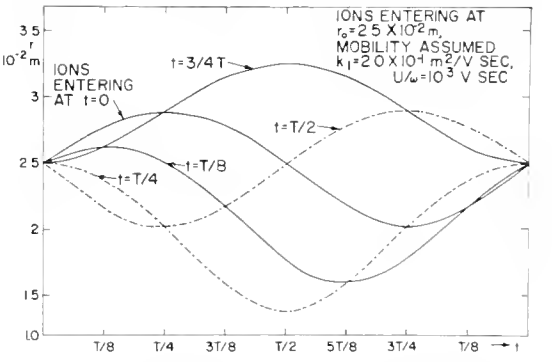

Figure 3. Paths of ions of the same mobility entering through the orifice at certain time intervals. The abscissa can be read as time axis as well as dimension along the cylinder axis

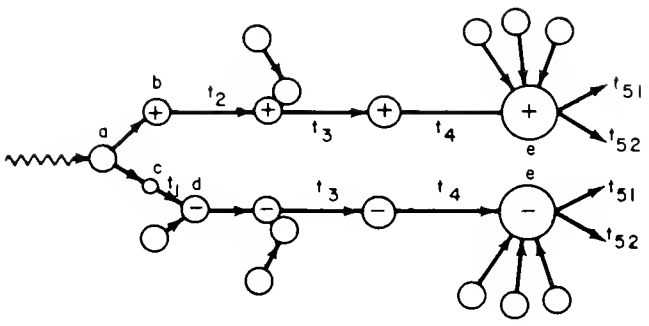

Figure 4. Formation of "mall ions" (cluster ions), schematic, after Wait.

formation of cluster ions in the troposphere, as shown schematically in Figure 4 occurs less than a microsecond. In higher altitudes, however, the periods t_1, t_2, t_3 are much longer, and t_4 is practically infinite. Furthermore, recombination between the earlier stages will occur. Those are, actually, the phenomena to be measured where the mobility spectrum is to be made. Furthermore, in the regions under consideration, the mobility constitutes the only possibility to obtain information on the ion mass, while maintaining rather closely the natural environment.

References

H. Dolezalek: "On the Measurement of Mobility and Conductivity in the Mesosphere", Zeitschrift fur Geophysik, 1962.

DISCUSSION

M. A. Biondi: Have you any data that suggest you can distinguish mobilities?

H. Dolezalek: No, we have just begun.

3.2 A GERDIEN CONDENSER ROCKET PROBE FOR MEASUREMENT OF ION AND ELECTRON CONCENTRATIONS IN THE D-REGION

A. PEDERSEN
Uppsala Ionospheric Observatory
Uppsala 10, Sweden

1. Introduction

The purpose of the experiment is to measure ion and electron concentrations at heights between 40 and 80 km. A Gerdien condenser and connected instrumentation and a parachute is separated from an Arcas rocket at 80-90 km height and measurements are done during the descent. The Gerdien condenser takes advantage of the collision between charged particles and neutral particles in measuring the effect of ions drifting in an electric field. Measurements are limited to heights below 80 km, where the mean free path is small compared with the probe dimensions.

The Gerdien condenser was first developed for measurements of ion concentrations at ground level. Air is flowing through a cylindrical condenser with a radial electric field, Figure 1a. An ion entering the probe will drift towards the collector at the same time as it follows the air stream. Figure 1b shows the electrode arrangement used in the rocket experiment. The latter offers smaller end effects and makes possible that both excitation voltage batteries and current amplifier can be referred to ground potential. From the current-voltage characteristic shown in Figure 1c information about ion conductivities and concentrations can be obtained.

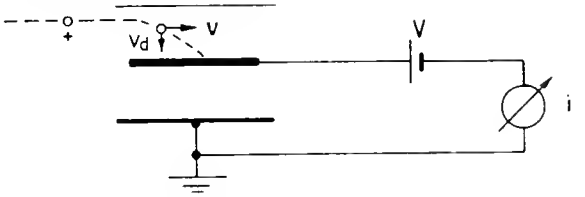

Figure 1a. Cylindrical condenser with a radial electric field

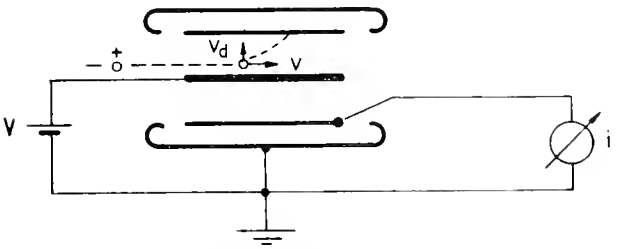

Figure 1b. Electrode arrangement used in rocket experiment

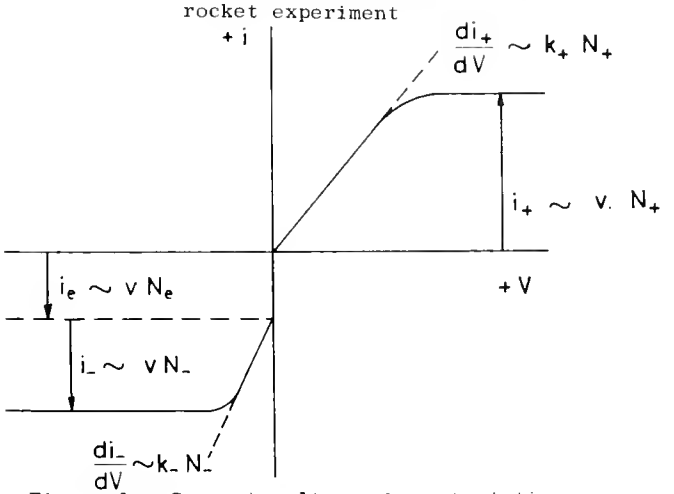

Figure 1c. Current-voltage characteristics

A measurement during descent using a parachute has several advantages, compared with a direct rocket measurement. The slower passage through the atmosphere makes possible a better height resolution of the measurements and the air flow through the probe is more well defined.

2. Rocket Payload

Figure 2 is a block diagram of the electronic instrumentation packed in the Arcas nosecone. A program unit operated with a small DC motor gives sawtooth voltages to the Gerdien condenser and at the same time changes the sensitivity of the electrometer over three different ranges from 10^{-10} A to 10^{-7} A. Information about the electrometer current during the voltage sweeps are telemetered to the ground. Antennas are made as springs coming out after payload separation. The Gerdien condenser is stored in the Arcas rocket cylinder together with a parachute made of metalized Mylar.

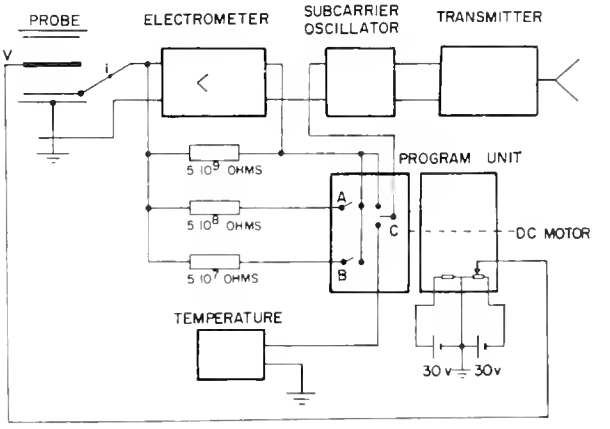

Figure 2. Block diagram of the electronic instrumentation.

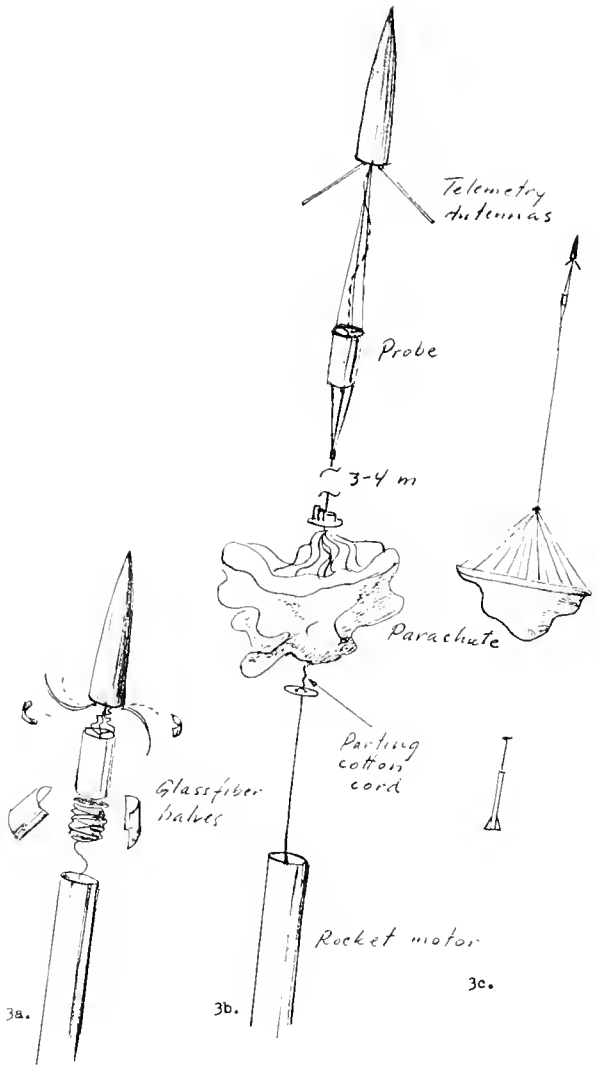

Figure 3. The separation procedure

3. The separation procedure

The separation of the payload from the Arcas rocket will take place at about 130 seconds after the start. A charge operating at a piston pushes the whole payload out of the rocket cylinder. The exit velocity being close to 8 m/s. As sketched in Figure 3, the system will be stretched out and after bursting of the parting cotton cord the payload is free from the rocket. The inflating of the parachute is helped by a torus filled with residual air at the leading edge of the parachute.

4. The Descent of the Payload

The drag forces acting on the parachute is very small close to 85 km, where the payload is expected to be separated. The payload will therefore most probably experience some tumbling and the descent will at first be almost a free fall. Drag forces will increase with increasing speed, but the system will certainly still behave in an irregular manner. In order to compensate the tumbling of the parachute and trying to give the Gerdien condenser a close to vertical direction, the connection line between parachute and probe is elongated to 25 m about 30 seconds after the separation. In order to obtain some information about the velocity during the descent some calculations have been made. For the actual payload of 4.5 kg weight and a parachute of 32 m diameter the time of descent from 80 to 40 km is approximately 4 minutes for a drag coefficient of 0.5 and 6 minutes for a drag coefficient of 1.0 assuming a regular behavior of the parachute. Maximum velocity is 300 - 400 m/s at about 70 km. The numbers quoted here are very uncertain as very little is known about the behavior of parachutes at high altitudes.

The flow through the condenser may be supersonic for part of the descent. The construction shown with the nosecone ahead of the probe has been determined by the rocket construction. Further development of the system should include a probe moving ahead of the instrumentation to secure a more defined flow through the probe.

DISCUSSION

J. O. Thomas: Have you compared the results of the subsonic Gerdien condenser with those of Whipple and others who had conducted supersonic experiments?

A. Pedersen: Though the experiments were carried out under different conditions, there was good agreement between the two types of measurements.

4.A MEASUREMENT OF NEUTRAL AND ION COMPOSITION

C. Y. JOHNSON
E. O. Hulburt Center for Space Research
Naval Research Laboratory
Washington 25, D. C.

The acquisition in 1946 of the V2 rocket opened up the field of insitu upper air research. It also permitted instrumentation to be taken above the absorbing atmosphere to measure the spectral distribution and intensity of the energetic solar radiation. Thus, the rocket vehicle became the key tool in solving the fundamental problem of the interaction of solar radiation with a planetary atmosphere. Early rocket experiments were directed along this line of endeavor: for example, Seddon and Jackson determined the electron distribution with altitude; and Tousey, Friedman and Chubb measured the solar radiation and by its attenuation through the tenuous atmosphere, the atmospheric composition and density. Direct composition measurements were made with sample bottles by the University of Michigan group.

In the early fifties mass spectrometry, for both neutral and ion composition measurements, was begun. Initial results of both neutral and ion measurements were severely contaminated by rocket gases and, in the ion measurements, by other active experiments on the vehicle. Interpretation of the initial mass spectrometric results may well be briefly stated: the eary composition experiments were developing the techniques.

At the time that the IGY started, ten years of upper atmosphere rocket exploration had passed. The model atmosphere was a good guess to actual conditions of density and composition because properly instrumented and executed experiments had not yet taken place, with the possible exception of X-ray density measurements in the D- and lower E-region at solar minimum. Two reasons exist for this poor understanding and knowledge of the upper atmosphere. First, vehicles designed for upper atmosphere experiments did not exist which would go sufficiently high into the upper atmosphere to permit the parameters to be investigated. Second, was a lack of understanding of the part that the vehicle and instrumentation play in the execution of upper air experiments. This point is still a factor in experiments today.

The IGY fostered rocket developments. This was an indirect effort but a required one. The Aerobee-Hi and Nike-boosted vehicles were produced. Experiments carried in these vehicles to measure aeronomic parameters were the best available at the time. The results were equally indicative of the state of the art and the experiments ability to interpret this data. Neutral composition measurements made with Bennett RF mass spectrometers (Figure 1), axially mounted in Aerobee rockets reported the level of gravitational diffusive separation to be 105-120 km in the arctic from the behavior of argon and molecular nitrogen, in spite of the abrupt discontinuity at the starting level. Molecular and atomic oxygen did not fare too well in this spectrometer (Figure 2). The O_2/N_2 ratio increased with altitude instead of decreasing as it should have if oxygen dissociation and diffuse separation were taking place. Similarly the O/O_2 ratio never exceeded 1; yet there was good evidence from solar studies that sufficient dissociative energy reached the upper atmosphere. In spite of these obvious errors due to the geometry of the mass spectrometer and recombination of atmoic oxygen on its inner surfaces, the RF spectrometer was used for neutral gas studies as late as 1961.

Today new approaches to the analysis of the neutral constituents have been introduced. More attention has been put on the location of the ion source and its geometry. The mass spectrometer analyzer section has been changed from the Bennett analyzer to the magnetic sector, or the massenfilter system. Emphasis has been placed on keeping the analyzer as clean as possible either by inflight vacuum pumping or by adequate venting to the ambient atmosphere. The new results to be presented later on in this conference using these new approaches have been fruitful. The techniques have been or will be described and are not difficult. Later speakers will give results from rocket-borne neutral

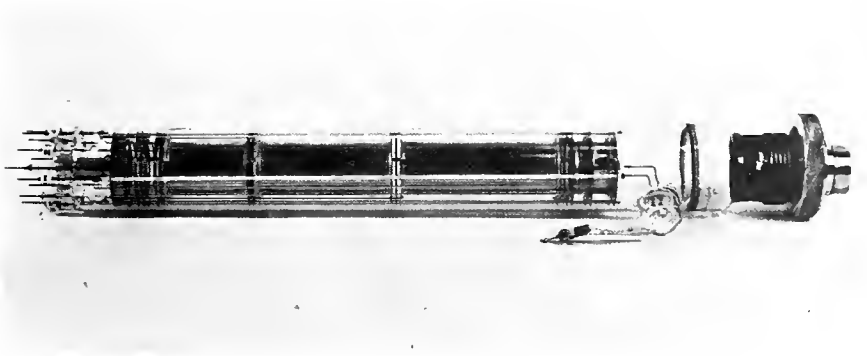

Figure 1. Bennett RF neutral mass spectrometer

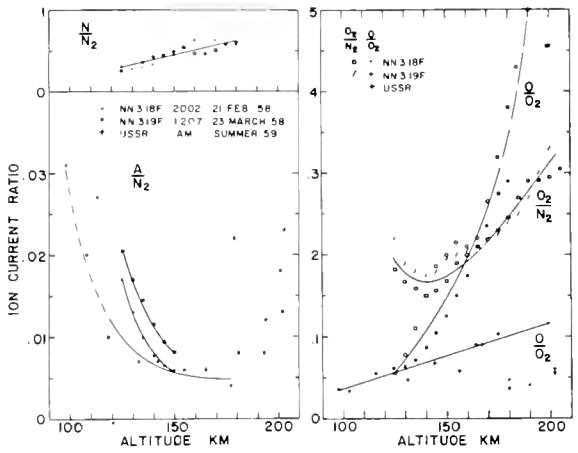

Figure 2. Early neutral composition measurements

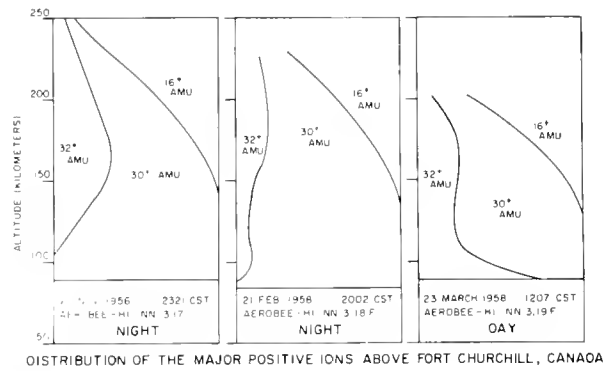

Figure 4. Distribution of ions with altitude

gass mass spectrometers which, I believe, present an accurate measurement of the fundamental aeronomic parameters above 100 km, while differentiating against contaminants carried into the region by the rocket vehicle. Extension of these measurements below 100 km, where the mean free path consideration creates serious problems, are also being solved.

Neutral gas composition measurements made by measuring the absorption of solar radiation as a function of altitude have been reported for many years. From the mass spectrometry point of view, agreement between the optical absorption and mass spectrometer results are within a factor of 3 or 4 and may readily be brought into agreement if a laboratory measurement or theoretical calculation of absorption cross sections are in error by that amount.

Application of the Bennett RF ion mass spectrometer, Figure 3, to ion composition measurements have fared much better since 1956. Consistent results have been obtained on ionosphere composition by experiments at the NRL, NASA, and in the Soviet Union. The non-magnetic feature, large entrance aperture, and simple electronics have found considerable favor with experiments for the investigation above 100 km.

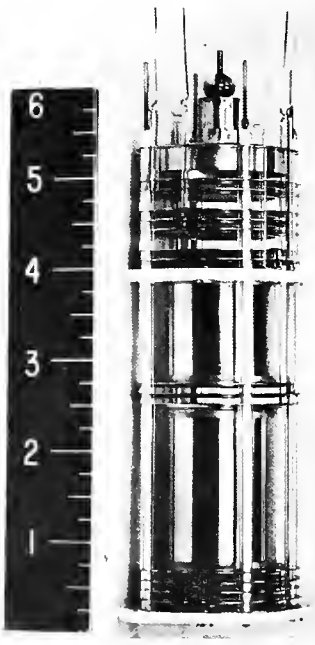

Figure 3. Bennett RF ion mass spectrometer

The main problems in ion composition studies are not with the instrumentation if the measurement is to be made above 100 km. Data collection and interpretation of the results to provide a consistent picture of the reactions occuring in and controlling the ionosphere are the problem. For instance from 1956 to 1962 four IGY flights at Fort Churchill by NRL, two flights at Wallops Island by NASA, and three or more by Russian experimenters have done little more than identify the ions and their distributions with altitude as shown in Figure 4. Interpretation of the ion results in terms of aeronomic parameters have not materialized. The reason, I believe, is quite simple - the normal behaviour of the ionosphere ion composition from day to night was not known. This year two flights at White Sands provided that information and, will permit further interpretation of the results obtained in the past. Mr. Holmes will describe these measurements.

Before closing, I would like to quote the first sentence of a Pennsylvania State University Scientific Report "The Ionospheric

Conditions" by Nicolet and Swider. It says, "The problem of the interpretation of the physics and chemistry of the ionosphere is in a state of confusion." I am confident the results of this conference, when published by the individual participants will reduce the state of confusion.

DISCUSSION

J. Ortner: Have there been any measurements below 100 km in the USA?

C. Y. Johnson: Yes, 100 km was just an approximate altitude.

R. L. F. Boyd: The energy distribution can be determined using a Langmuir probe; thereby the nature of the positive or negative ions can be determined using retardation techniques.

H. A. Taylor: Calibration was carried out in the laboratory by the use of chlorine gas ionized by an electron beam in a bell jar.

4.1 THE MONOPOLE MASS SPECTROMETER AND ITS ADVANTAGES FOR UPPER ATMOSPHERIC RESEARCH

R. F. K. HERZOG
Geophysics Corporation of America
Bedford, Massachusetts

I am going to talk about a new mass spectrometer which has not been used for aeronomic research so far, but shows a number of attractive features which are valuable for this purpose.

The monopole mass spectrometer, which has been recently invented and tested by Ulf von Zahn [1] is a modified version of Paul's [2] "massenfilter". Both instruments use the same field; however, the manner in which this field is produced is different. The quadrupole mass spectrometer uses four parallel cylindrical electrodes arranged in a square, as shown in Figure 1. Both pairs of opposite electrodes are electrically connected and the voltage applied to one pair is equal and of opposite sign to the voltage applied to the other pair. The characteristic feature of this field is the fact that the field strength is essentially proportional to the distance from the center. It is obvious that the potential on the two diagonal symmetry planes is zero and the addition of grounded metal sheets at this location would not alter the field. If the beam is confined to the space between the grounded V-shaped electrode and one rod, then the other three rods may be omitted and we face the typical field of the monopole mass spectrometer. The ion orbits are the same in both instruments and rather complicated. In the X-direction the movement is approximately a resonant oscillation with the applied AC frequency. These ions are able to pass the quadrupole instrument. However, they can pass the monopole instrument only if it is shorter than the half length of the beat. In general, all ions which cross the diagonal planes in the quadrupole instrument are removed from the beam in the monopole instrument. Therefore, some features are common for both instruments and some are different. The most important common features are: (1) In contrast to other mass spectrometers, the initial energy of the ions has essentially no effect on the mass scale and the resolution is improved if the initial energy is lowered. For this reason, both instruments are particularly well suited for upper atmospheric research where particles of rather widespread energy distribution have to be analyzed. The successful flights of Schaefer have proved the value of the quadrupole instrument. (2) The mass scale is linear and proportional to the voltage on the rod. (3) The resolution is proportional to the mass and highest for the heavy masses where high resolution is needed most. Equal peak width for all masses permits faster scanning and better utilization of the telemetry capabilities. (4) Both instruments can be operated at somewhat higher pressures than conventional mass spectrometers without loss of resolution. This feature is important for measurements in the D-region.

The difference between both instruments can be described best with the aid of the stability diagram. The ordinate is proportional to the applied DC voltage and the abscissa to the superimposed AC voltage. Since the applied DC voltage is kept proportional to the AC voltage, scanning is done along a line through the origin. Different masses are distributed along this line. Only the masses within the triangular area are capable to pass the mass filter. Higher masses, which are at the left of the stable area, are collected by the negative rods;

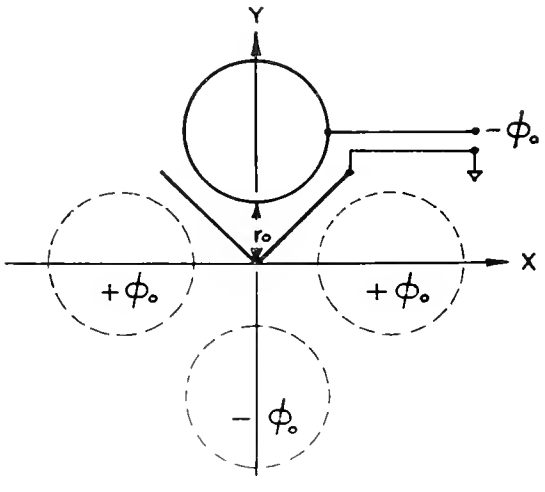

Figure 1. The relationship between the quadrupole and monopole arrangements.

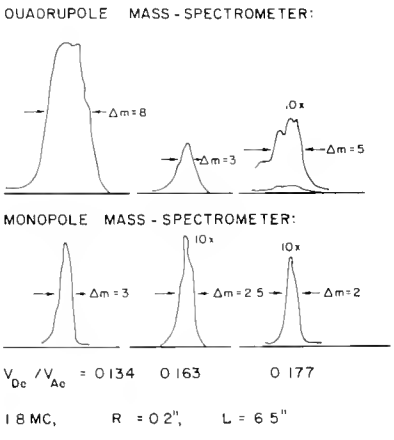

Figure 2. Typical peak shapes for sodium ions, 90 volt.

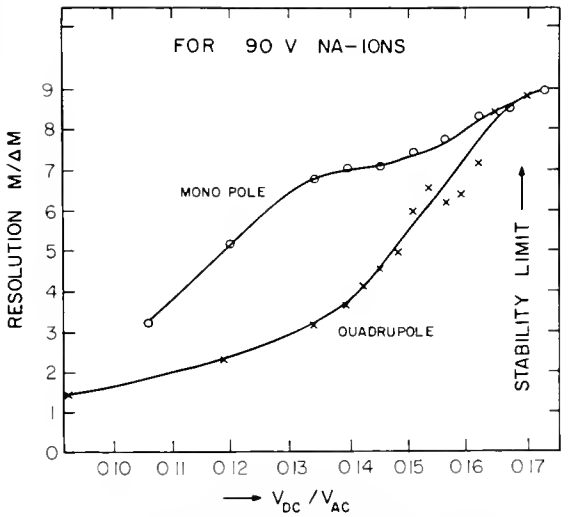

Figure 3. Comparison of resolution of quadrupole and monopole instruments.

lower masses, at the right, are collected by the positive rods. Good resolution of the quadrupole instrument requires operation in the narrow region quite near the top of the stability area. The adjustment of the DC to AC voltage ratio is therefore rather critical. In contrast to this, the stable area of the monopole instrument is a narrow stripe and far less dependent of the voltage ratio. This permits operation of the monopole instrument with smaller voltages than those required for the quadrupole instrument.

Preliminary experiments have been carried out during the last weeks to compare the performance of the two instruments under identical operating conditions; that is, the same rod dimensions, the same frequency and the same ion beam entering the instruments. The sodium peak (Figure 2) has been observed with different settings of the DC/AC voltage ratio. The peak in the middle has been obtained with a voltage ratio in the stable region quite near the top of the stability diagram. Here the monopole and quadrupole instruments have about the same resolution. The same is true for the right peaks which have been obtained with a voltage setting in the unstable area and which are therefore rather weak. The left peaks have been obtained with a smaller voltage ratio. Here the difference between the monopole and quadrupole instrument is obvious: The resolution of the quadrupole is lost whereas the one of the monopole stays essentially constant. Figure 3 shows this more clearly. The resolution of the monopole instrument is higher, especially for lower voltages. For instance, the same resolution which the quadrupole instrument shows near the top of the stability area can be achieved with the monopole instrument with 30% smaller AC voltages. This means - in connection with the fact that only one instead of four rods have to be charged - that the total power consumption of the monopole instrument is about one order of magnitude lower than that of the quadrupole instrument. This fact is of extreme importance for space applications, especially if good resolution of higher masses is required. Other features in favor of the monopole instrument are the simpler and lighter design of the rod system and particularly of the power supply. The main purpose of my present experiments is to compare the transmission of both instruments. So far I have found that with the same setting of the voltage ratio the transmission of the monopole instrument is somewhat lower than the transmission of the quadrupole instrument. However if different voltage ratios are used in order to obtain the same resolution, then the transmission is about equal.

So far these experiments have been made with the same injected beam. It is expected that both instruments can be improved if the injection conditions are individually chosen. These experiments will provide a fairer and more accurate comparison of both instruments. Although the design of a laboratory model of the monopole mass-spectrometer is quite simple, the development of a flyable model in which all parameters have to be optimized will require a considerable amount of theoretical and experimental work. However, the prospect of obtaining a superior instrument justifies the requires effort.

References

[1] Ulf von Zahn, Rev. Scient. Instr. 34, 1, 1963.

[2] Paul, Reinherd, Zahn, Zeifschrift, f. Physik, 152, 143, 1958.

DISCUSSION

C. Reber: How does the response as a function of entrance angle of the monopole compare with the quadrupole?

R. F. K. Herzog: About the same, or perhaps somewhat narrower, because the space which is available for the beam in the monopole instrument is narrower than in the quadrupole arrangement.

C. Y. Johnson: Would you recommend that this instrument be used for neutral or for ion analysis in the upper atmosphere?

R. F. K. Herzog: It could be used for both purposes.

C. Y. Johnson: If the ion is off axis it is not seen. Now this to our knowledge is not true in the Bennett system, we do not have very much modulation. Now the quadrupole instrument will accept an ion which is comiing nearly straight in, so it may have a characteristic more like a neutral instrument, in that it has a large amount of roll modulation.

is coming nearly straight in, so it may have a characteristic more like a neutral instrument, in that it has a large amount of roll modulation.

R. F. K. Herzog: I think it depends very much on the acceleration applied to the ions before they enter the system. If this is very small, the original angular distribution will still exist in the analyzer section; if the acceleration is greater, say 100 volts, then the angle will be fairly narrow, and the question whether this beam can pass depends entirely on the geometry of the rods. It needs an accurate investigation, with the purposes of the instrument specified.

N. W. Spencer: I think that focusing is possible, but the power required by the system goes up logarithmically, and this turns up as mass discrimination, eventually.

W. Brubaker: Using a collimated beam of sodium ions, incident upon the quadrupole with the same velocity as for an orbiting satellite, I have experimentally shown finite transmission for ions incident at 30 deg relative to the axis of the instrument. Of course, at lesser angles the transmission is higher.

C. Y. Johnson: What about for a monopole?

W. Brubaker: The answer appears definite for the monopole that if the ions are directed towards the square they will not get through. If the monopole is rotating, there is only one position for favored transmission, whereas this is not true for the quadrupole.

R. F. K. Herzog: It is mainly a question of the direction you inject the original beam; it doesn't have to be injected parallel to the axis. If it is injected towards the walls, it is away from the V-shape electrode, and the particles will not be lost.

The problem with both instruments, the quadrupole and the monopole, is that during the injection of the beam into the rod system the ions have to pass the relatively strong fringe field of the rods, which deflects the beam and changes the original velocity. So this has to be taken into account to find the performance of both instruments.

N. W. SPENCER
Goddard Space Flight Center
National Aeronautics and Space
Administration
Greenbelt, Maryland

The technique to be descrived is derived from the "dumbbell" experiment and thus is based upon the experimental concept of ejecting an instrument container from a rocket nosecone, at an appropriate altitude, to help optimize the experimental conditions. The dumbbell experiment provided information regarding electron temperature which indicated that thermal equilibrium should not, in general, be expected to prevail in the ionosphere.

To enable more concerted study of this problem, by making possible the simultaneous measurement of neutral particle and electron

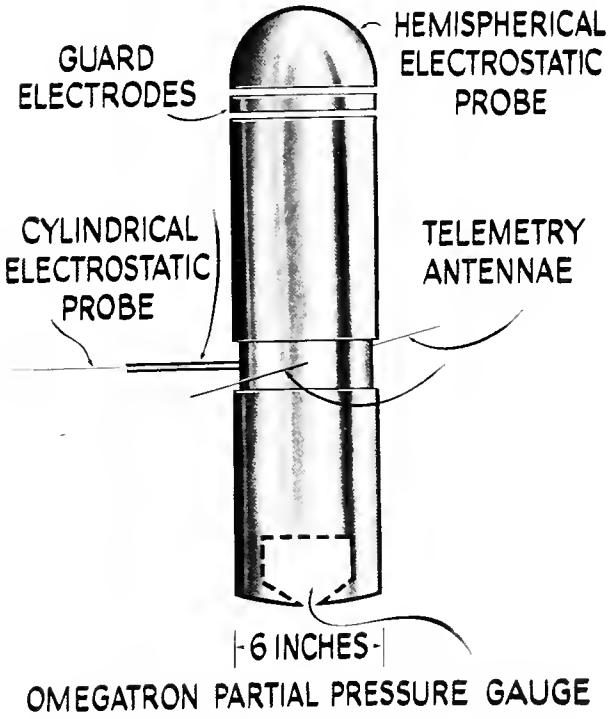

Figure 1. Schematic illustration of thermosphere probe.

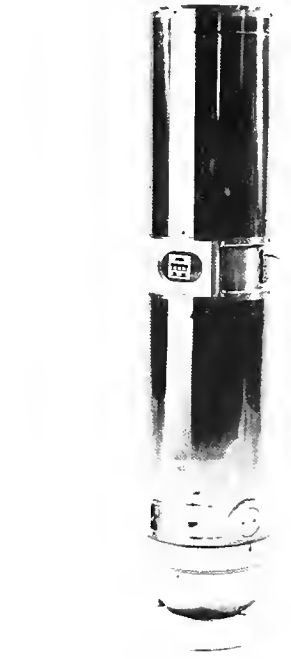

Figure 2. Photograph of typical thermosphere probe.

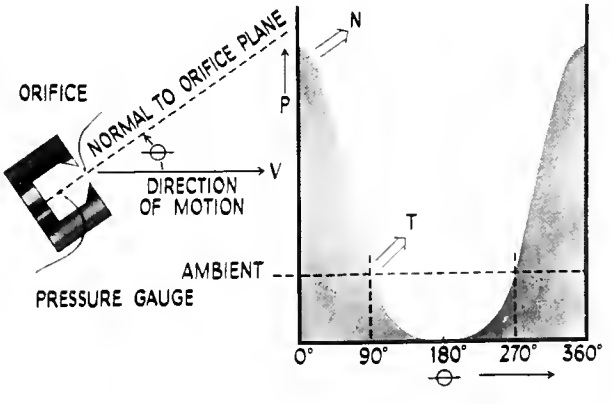

Figure 3. Chamber detail and pressure variation for a tumble cycle.

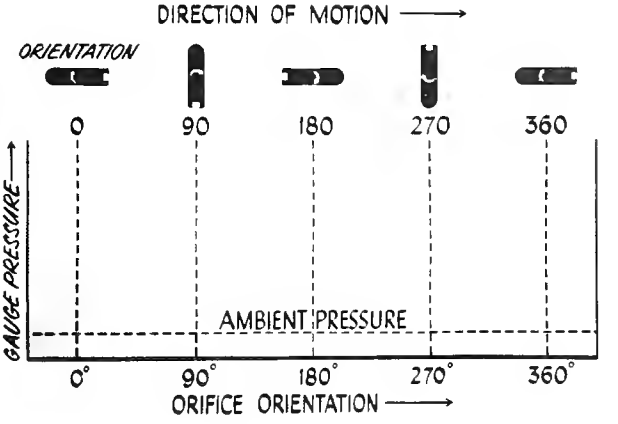

Figure 4. Illustration of scan technique.

temperature, an omegatron mass spectrometer was added to the system to permit determination of the N_2 density profile of the thermosphere. The expanded experimental setup is considered only a first step in the direction of the development of an experiment which will enable, in due course, the simultaneous determination of numerous aeronomic parameters, knowledge of which is essential for a detailed study of thermosphere physics.

Figure 1 illustrates the present device which is called a "Thermosphere Probe," "TP" for short. One end is a hemispherical electron temperature probe electrode derived from the dumbbell, and the other end contains the omegatron in an axially centered, orificed chamber, as shown. At the midsection are located a cylindrical electron temperature probe, the telemetry antennae, an optical aspect sensor, and the supporting system electronics. Figure 2 is a photograph of a recent TP.

Upon ejection from the rocket into the thermosphere, the TP is caused to tumble end-over-end by a rocket-attached lanyard. Thus the omegatron chamber orifice is oriented, cyclicly, into and out of the general direction of the free stream velocity vector, as the TP follows a trajectory differing from that of the carrier rocket by only the small additional velocity increment acquired at ejection. Figure 3 shows a typical chamber pressure variation (N_2) for a case when the tumble plane (orientation invariant in space) includes the velocity vector. Figure 4 illustrates further the tumbling, and pressure variations to be expected, and which are observed in flight.

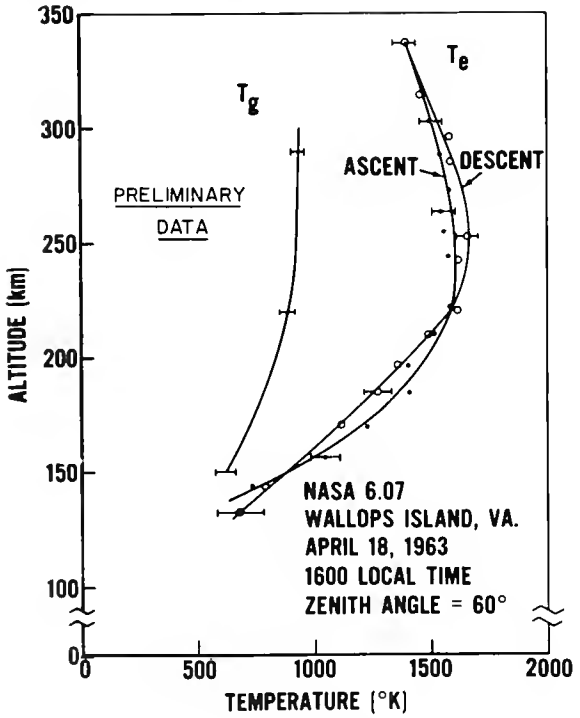

Figure 5. Typical neutral N_2 temperature data resulting from a TP flight. Electron temperature data measured simultaneously is also shown.

The pressure variation can be expressed in terms of ambient conditions by the following equation:

$$p_i = p_o \sqrt{\frac{T_i}{T_o}}\ f(s)$$

where p_i = internal N_2 pressure

p_o = ambient N_2 pressure

T_o = ambient N_2 temperature

T_i = internal N_2 temperature

and

$$f(s) = \exp(-s^2) + \sqrt{\pi}\ S[1 + \operatorname{erf}(s)]$$

where

$$s = \frac{V \cos\theta}{C_m}$$

V = velocity

θ = angle between velocity vector and axis of orifice

C_m = most probable velocity of N_2

$$= \sqrt{\frac{2kT_{N_2}}{m_{N_2}}}$$

From these considerations, specifically the maxima and minima of the N_2 variations, Figure 5 the N_2 density profile of the thermosphere is obtained. Further computation, using equation

$$T_b = \frac{n_a}{n_b} T_a + \frac{Gm}{R} \int_b^a \frac{n(h)}{n_b}\ dh$$

where

h_x = number density, altitude x

R = gas constant

m = mass of gas species (N_2)

G = gravitational constant

yields the N_2 temperature profile, as illustrated in Figure 5. Also plotted for comparison are simultaneously measured values of the electron temperature. From these data, the degree of thermal non-equilibrium is apparent, thus illustrating the mechanism whereby energy imparted to the electrons by solar UV appears

as increased temperature, and which eventually is transferred through collisions to the neutral particles.

In summary a technique is described which is believed to optimize experimental conditions, by (a) avoiding rocket-borne contaminants and other constraints through separation of an experimental package from a rocket vehicle, and (b) employing a predictable and simple motion of an idealized physical configuration for sensor transport.

By way of acknowledgment of the many contributors which make this effort possible, this experiment is a joint effort of the Goddard Space Flight Center Physics Branch, and the University of Michigan Space Physics Research Laboratory. The contributions of the many contributing individuals are sincerely acknowledged.

DISCUSSION

C.Y. Johnson: Is the minimum value of current limited by instrumentation or by the residual pressure?

N. W. Spencer: Both effects are important.

5.A MEASUREMENT OF ELECTRICAL CURRENTS IN THE IONOSPHERE

L. J. CAHILL
Department of Physics
University of New Hampshire
Durham, New Hampshire

1. Introduction

Although the first rocket measurement of electrical currents in the ionosphere took place in 1951, the study of the surface effects of these currents has been in progress for over 100 years. It was early realized that the diurnal variation in the earth's magnetic field must be produced by a global system of electrical currents, flowing above the earth's surface. When the ionosphere was discovered, it was recognized as the logical location for the current system.

An idealized view of the "Sq" current system was responsible for the diurnal variation is shown in Figure 1. Also shown is a current system centered on the north magnetic pole,

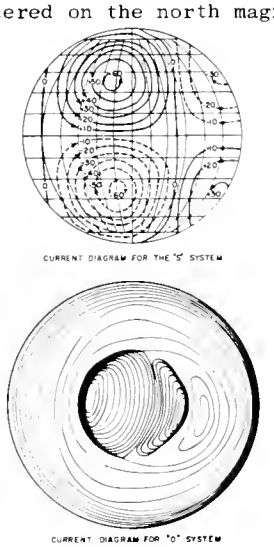

Figure 1. Sq and polar cap current systems

thought responsible for some of the variations observed in polar regions. These systems are fixed with respect to the sun and the magnetic variation at a station is produced as the station travels under the currents during the daily rotation of the earth. Not shown clearly on this figure is a region of high current density on the magnetic equator, called the equatorial electrojet.

The current density depends on the global conductivity of the ionosphere and on global tidal wind patterns thought to be caused by solar heating and by the tidal forces of the sun and moon. The wind patterns move the conductive medium perpendicular to the earth's magnetic field and generate currents - positive ions flowing one way; electrons the other. The conductivity depends in a complex way on the direction between the wind, the magnetic field and the electric fields that are induced. The conductivity is thought to limit substantial current flow to a region between 100 and 150 KM. World wide measurements of winds at these altitudes are not yet available. Electric current measurements have been made at only a few locations.

Singer in 1951 made the first rocket magnetometer measurement near the magnetic equator and detected a sizable electric current there. Cahill and Van Allen, at the University of Iowa, conducted a series of small rocket firings during the IGY and detected currents near the magnetic equator and in the polar cap region. Heppner sent a rocket magnetometer through a visible auroral arc in 1957 and apparently the

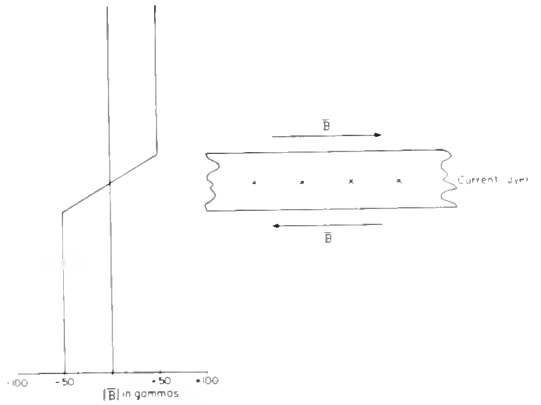

Figure 2. Magnetic field due to infinite current sheet

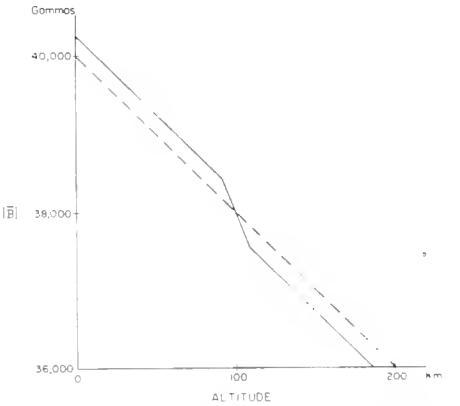

Figure 3. Magnetic field record expected on passing through current sheet

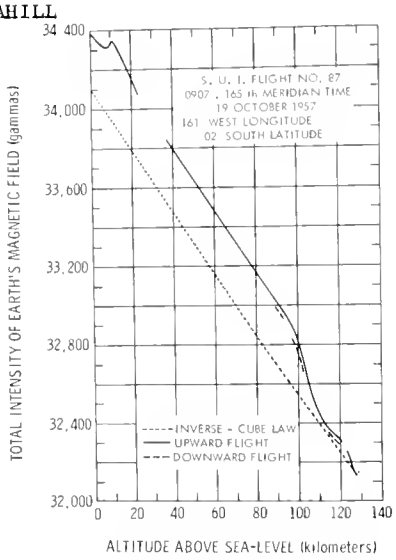

Figure 4. Record from SUI Flight 87, October 1957

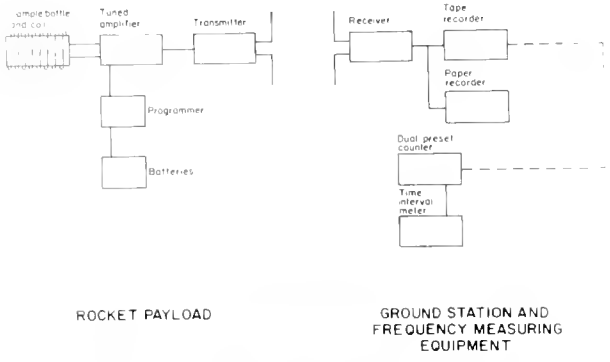

Figure 5. Block diagram of proton magnetometer, rocket payload and ground station

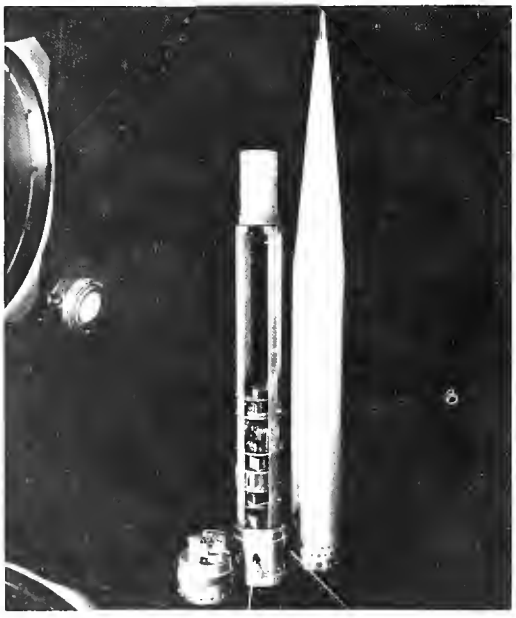

Figure 6. Photograph of proton magnetometer payload

rocket passed completely over a thin ribbon of electric current imbedded in the arc. Other flights have been conducted in an effort to detect the "Sq" current system in mid latitudes, but to date these attempts have been unsuccessful.

2. Measurement Principle

The principle of measuring ionospheric currents by rocket magnetometer is demonstrated in Figure 2. Assuming an infinite horizontal sheet with flowing east, a magnetic field pointing northward results beneath the current, a southward field above. As the rocket passes through the current sheet the field changes as $\frac{d/B/}{dh} = 0.4\pi j$, where h is the altitude in km, /B/ the field in gammas and j the current density in amperes/km^2.

As the rocket rises, the earth's main field decreases at the rate of 15-30 gammas/km. The measured field is the vector sum of the main field and the current sheet field. The expected rocket record is shown in Figure 3.

The record from a magnetometer in October 1957 near the magnetic equator is shown in Figure 4. Note the change in slope near 100 km, the resumption of the original slope between 110-120 km and a second change is slope near 120 km. This was interpreted as due to two layers of electric current. The ionospheric currents measured on two successive days were in approximate agreement with surface magnetic field measurements taken at a nearby island.

3. Measurement Technique

Since the magnetic fields due to horizontal current layers are generally horizontal and the main field has a rapidly increasing vertical component away from the equator, the total field over much of the earth is the vector sum of a large, nearly vertical, main field vector and a small, horizontal, disturbance vector. We are interested in the disturbance vector, so it would appear desirable to measure only the horizontal component and this is done at surface observatories. We would need to measure a horizontal disturbance component of perhaps 20 gammas on a main field component of 20,000 gammas (0.1% sensitivity). Component magnetometers, suitable for rocket flight such as the fluxgate magnetometer, are hard pressed to provide this sensitivity together with comparable stability. More serious is the need for a stable platform. A 1° change in the orientation of the component magnetometer could produce several hundred gammas change in the component measured. Because of the difficulty of providing a stable platform, magnetic measurements to data have been done by measuring total field magnitude.

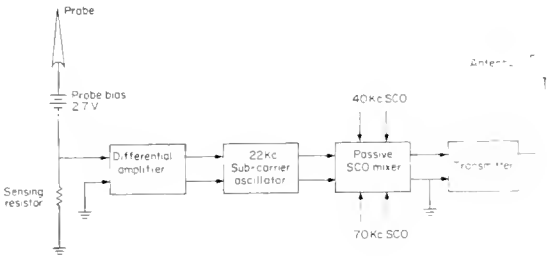

Figure 7. Schematic diagram of simple Langmuir probe

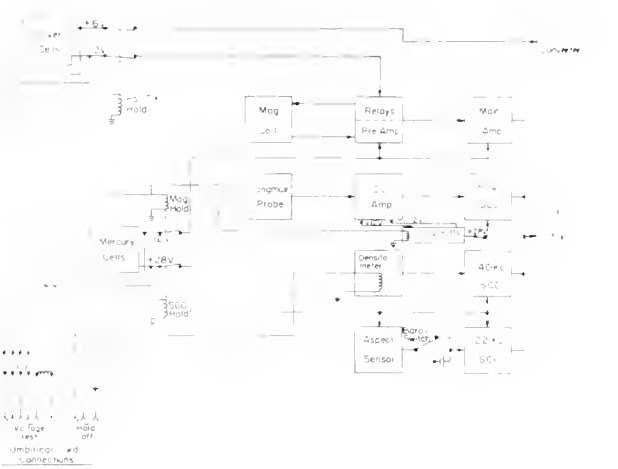

Figure 8. UNH payload block diagram

Singer's measurements were made with a three-component fluxgate magnetometer; the signals were electronically combined to give field magnitude. Instruments based on the principle of atomic or nuclear free procession have been in use since 1956. The advantages are: (1) freedom from calibration and drift problems, and (2) ease of construction in a compact, rugged, rocket instrument. Magnetometers of this type, proton, Rubidium vapor, and Helium, are available commercially from Varian Associates, Texas Instruments and companies in Canada and England.

4. Proton Magnetometer Payload

The proton procession magnetometer constructed at UNH will be described as an example. A block diagram of the apparatus is shown in Figure 5. The programmer applies a current through a coil surrounding the sample bottle. An excess of the protons in the sample acquire the direction of the applied magnetic field. A net magnetic moment of the ensemble of protons remains when the magnetic field is rapidly collapsed. This moment precesses about the earth's magnetic field, inducing a signal at the Larmor precession frequency. After amplification, and filtering to limit the noise spectrun, the signal directly modulates a transmitter. It is convenient to tape record the signal, together with a higher reference frequency, for later frequency measurement.

A payload recently flown on a Nike-Apache vehicle is shown in Figure 6. The nose cone is fiberglass, the coil and sample are at the top, as far removed from the other circuitry as possible. Also carried on this payload were a magnetic aspect sensor giving spin rate and rocket precession cone angle, a "baro" switch and a densitometer for altitude determination, and a simple Langmuir probe, to yield information about the structure of electron density in the region of electric current flow above 90 km. A schematic diagram of the probe circuit is given in Figure 7. Figure 8 is a block diagram of the entire payload.

5. Special Problems with Magnetometer Payload

Since the magnetometer has a high gain amplifier, some care is necessary to present interference from RF. The amplifiers are enclosed in copper boxes with wave traps on entering leads when necessary.

The amplitude of the precession signal depends on the angle θ, between magnetic field vector and coil axis, as $\sin^2 \theta$ so the trajectory and rocket orientation must be such that θ remains large throughout the flight.

Perhaps the most stringent requirement in building the payload is that the magnetic field at the coil location due to magnetic materials and DC current in the rest of the rocket should be less than one gamma. This requires careful placement of components, twisting of leads, and redesigning assemblies using non-magnetic materials. It also requires adequate test procedures to insure the 1 gamma restriction is met. We have found that, although most components or assemblies can be designed to be non-magnetic, items readily available are too magnetic to be used without some redesign. A more complete report on the UNH magnetometer payload described above will be available shortly as a UNH Research Report.

DISCUSSION

G.V. Groves: What is the nature of the densitometer?

L.J. Cahill: It consists of an ionization chamber with a radioactive source. The number of particles which reach a central electrode control an oscillator.

6.A TECHNIQUES FOR PRESSURE, TEMPERATURE, DENSITY AND WIND DETERMINATION IN THE MESOSPHERE AND LOWER THERMOSPHERE

N. W. SPENCER
NASA
Goddard Space Flight Center
Greenbelt, Maryland

Considerable effort has been devoted, for at least 15 years, toward the development of techniques which can be used with confidence to obtain extensive measurements of the pressure, temperature, and density of neutral particles, and the winds. As a consequence of these efforts, four techniques have emerged and are being adopted for measurements at widely spaced locations, on a global scale. The techniques are applicable at altitudes above those readily attainable by balloon, and up to nearly 200 km in one case. The experiments are providing data of interest and importance to study of mesosphere and thermosphere physics.

The grenade technique (Nordberg) which provides, possibly, the most accurate data on temperature and wind up to 90 km, employs a system involving the periodic ejection of grenades, which are detonated a small distance from the rocket by a lanyard. The times and directions of the arrival of resulting acoustic waves observed by the ground-based microphone network, with a knowledge of the rocket trajectory and the times of grenade explosions, permit computation of the temperature and wind values corresponding to the average temperature and wind for the altitude intervals between grenade explosions. Density can then be computed using the temperature values obtained.

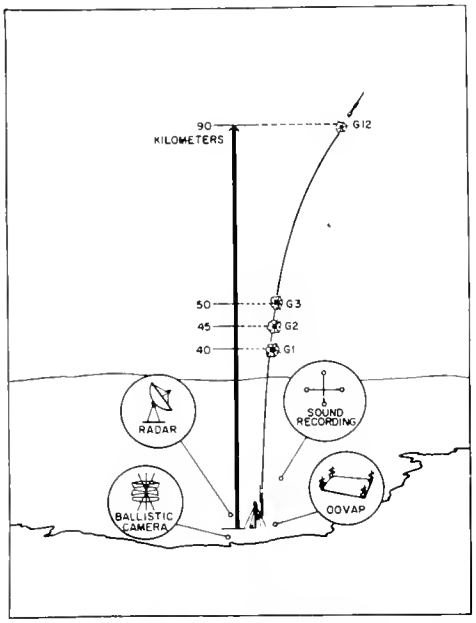

Figure 1. Schematic representation of grenade experiment.

Figure 1 is a schematic representation of the technique, and a photograph of the instrumentation is shown in Figure 2. Representative temperature data will be shown below in comparison with similar data from the other experiments to be described.

The release of sodium vapor from a rocket into the atmosphere comprises a second technique (Bedinger, Blamont), which enables a direct determination of ionosphere winds, from 60-170 km, by ground based camera triangulation of the physical movement of the visible trail resulting from resonance radiation. Figure 3 is a photograph of a typical sodium trail.

Observation of the diffusion of the trail, and the sodium line width, permit temperature determination as shown by Blamont's data, in Figure 4.

Observation of the atmospheric drag imposed upon a falling sphere permits, with knowledge of the drag coefficient, determination of atmospheric density, and, through an integration process, the ambient temperature. Jones has developed a small solid sphere containing an omnidirectional accelerometer, a technique useful for measurements to altitudes of 70-100 km. Other

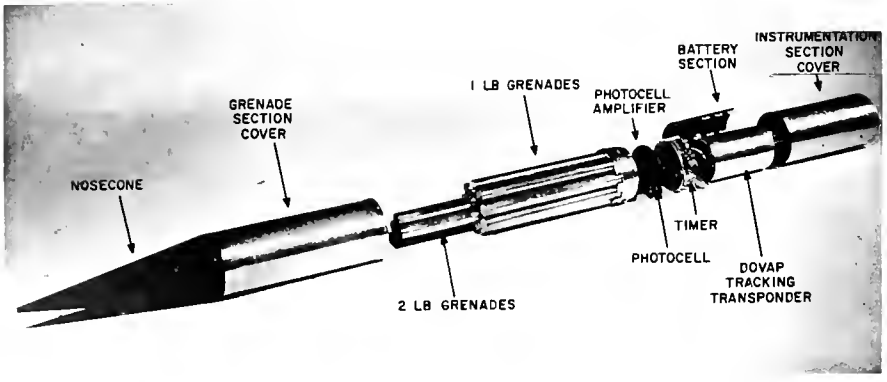

Figure 2. Photograph of grenade instrumentation.

Figure 3. Photograph of sodium vapor trail.

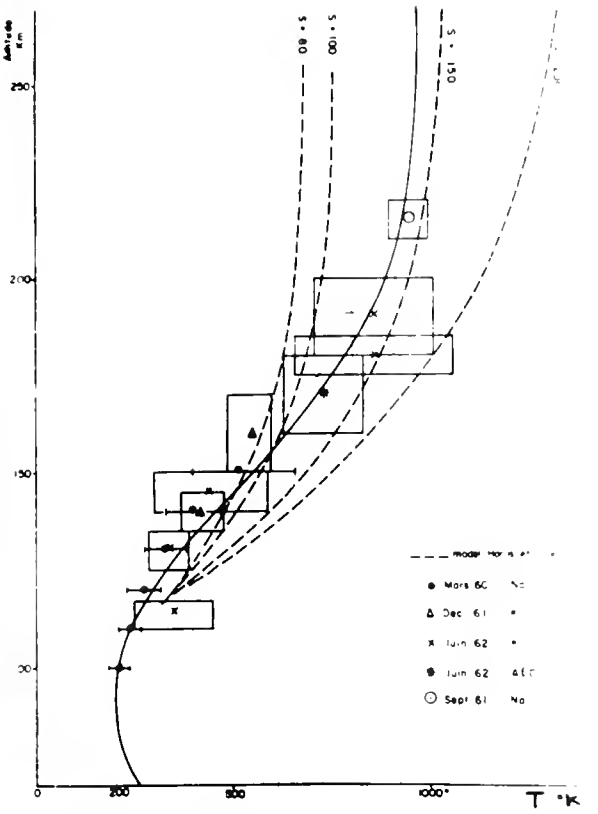

Figure 4. Representation of sodium trail temperature values (Blamont).

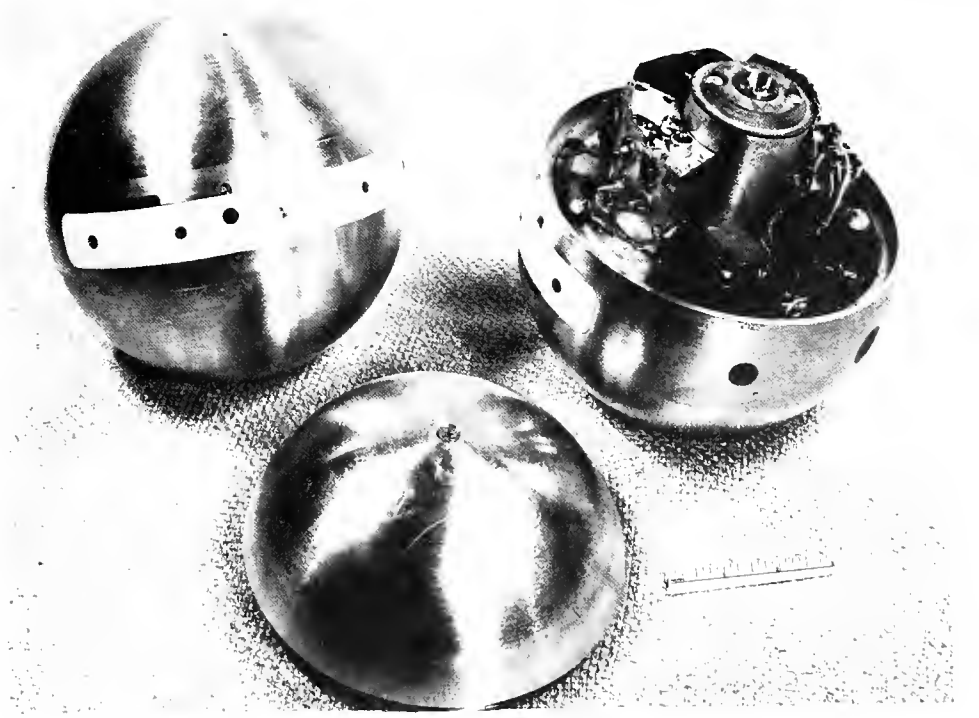

Figure 5. Photograph of seven inch "falling sphere".

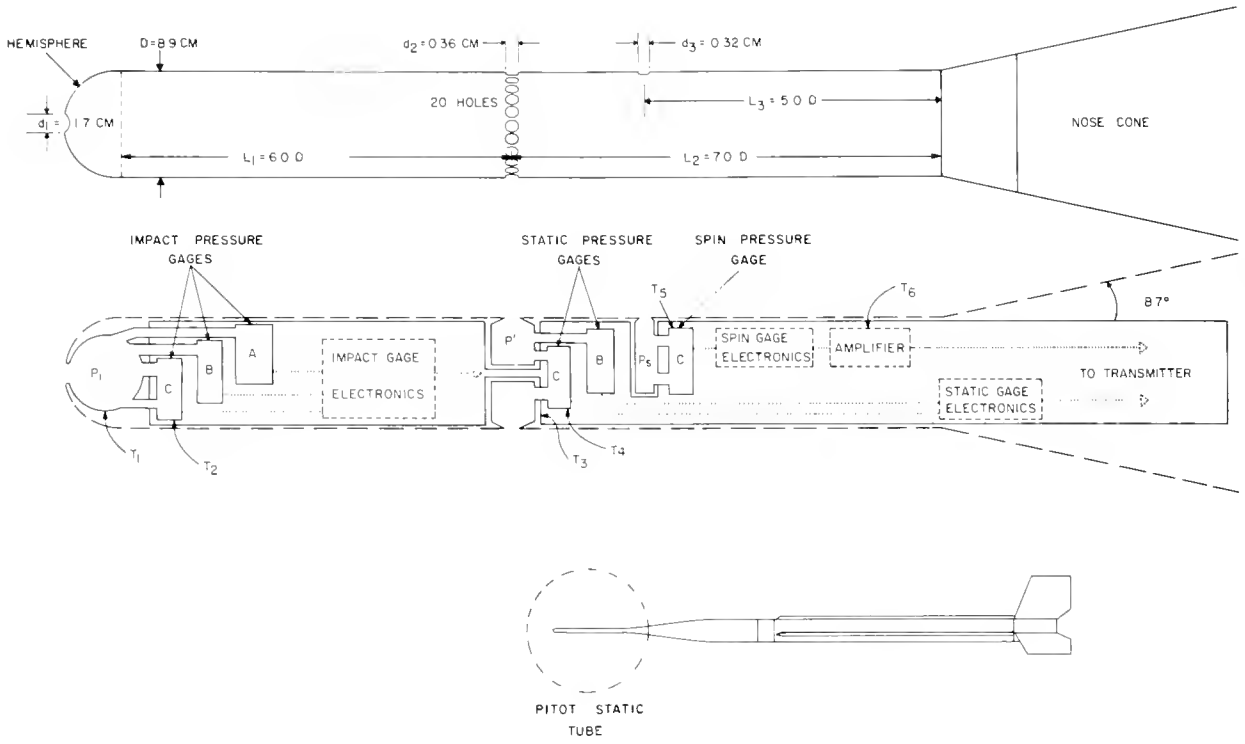

Figure 6. Schematic of pitot-static instrument (Ainsworth).

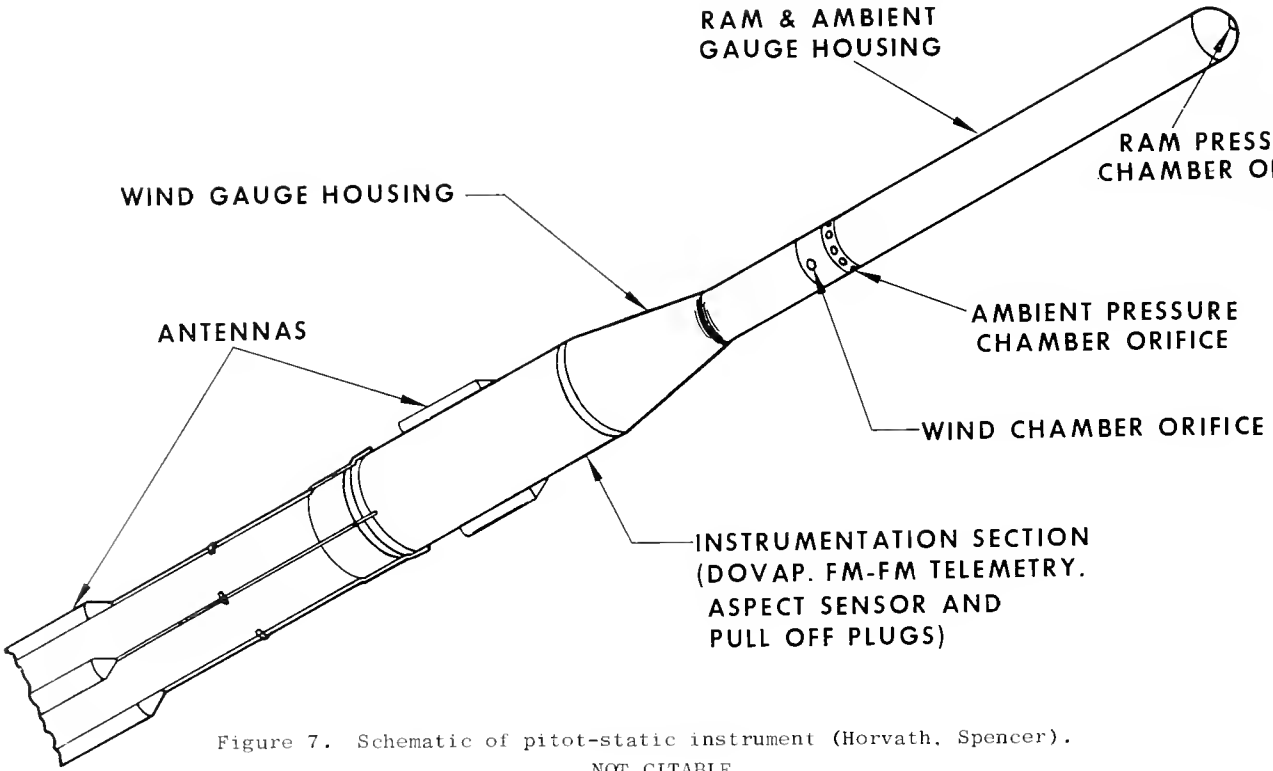

Figure 7. Schematic of pitot-static instrument (Horvath, Spencer).

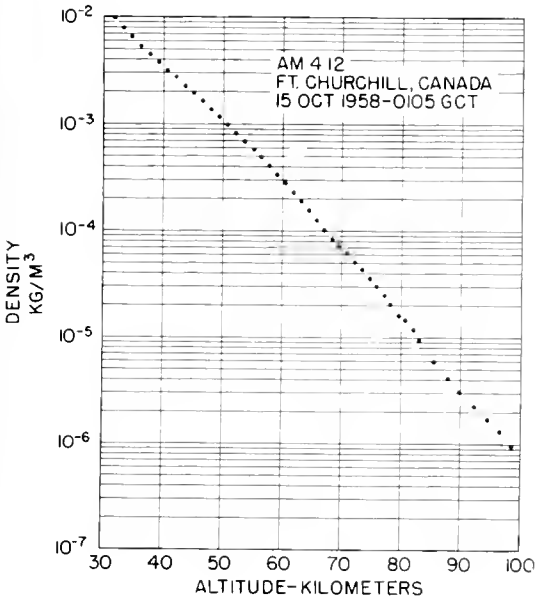

Figure 8. Density data obtained from right-circular cone technique (Spencer).

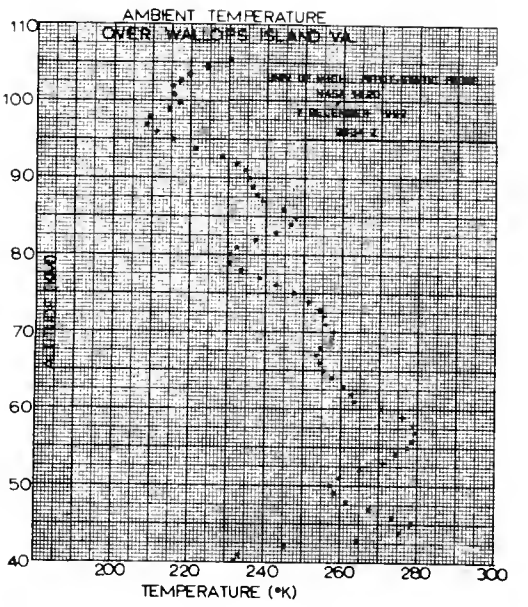

Figure 10. Temperature obtained from pitot-static instrument (Horvath).

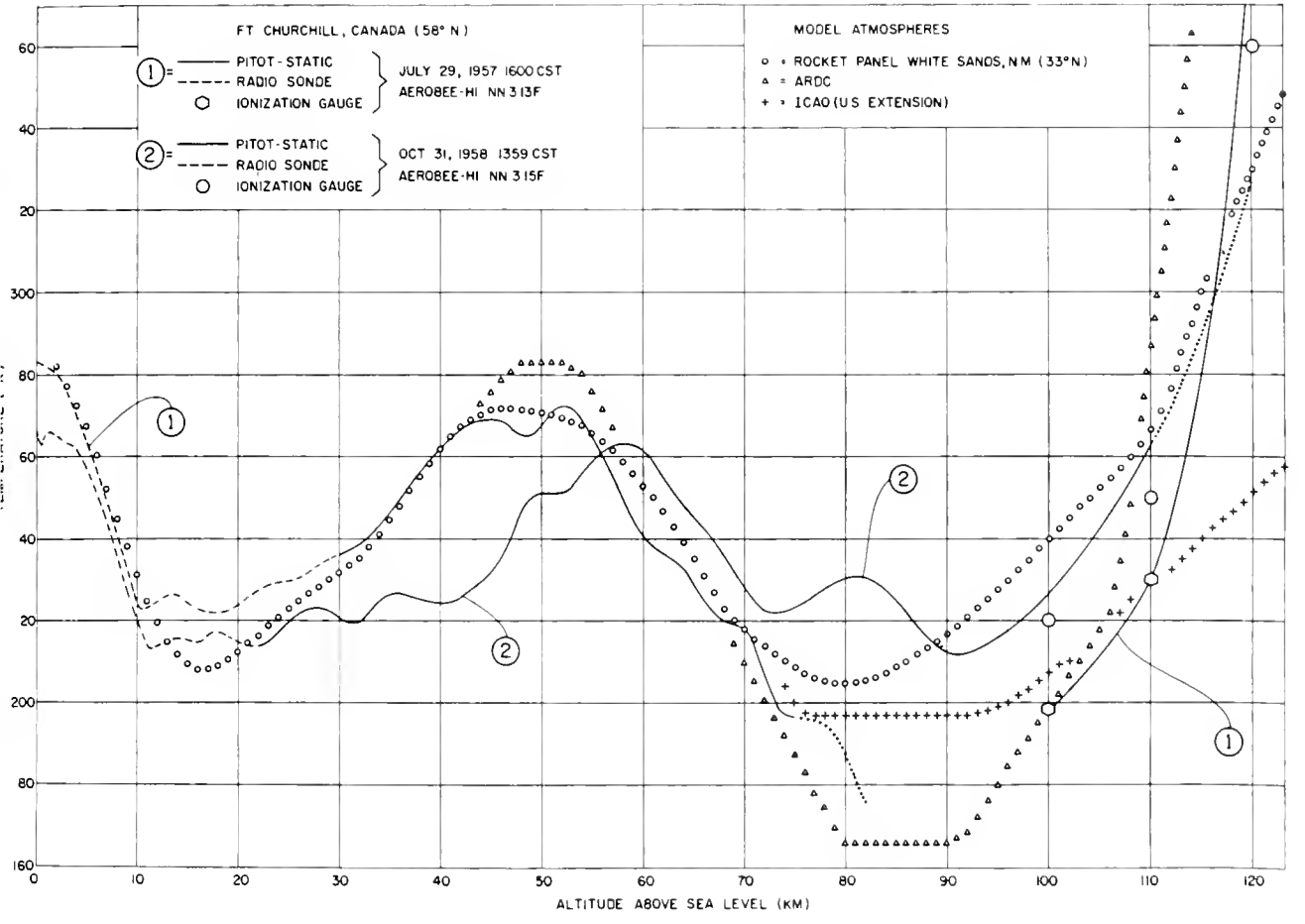

Figure 9. Temperature data obtained from pitot-static instrument (Ainsworth).

applications by Jones and Faucher have employed inflatable spheres which are either tracked by radar or which contain accelerometers, for acceleration measurements. Figure 5 is a photograph of the small sphere used extensively by Jones.

The fourth technique takes various forms, but in each case derives pressure, temperature, densities and wind data from surface (nosecone) pressure measurements. Measurements made using a right circular rocket nosecone permit free stream Mach number and hence ambient temperature determination (Spencer). Use of a variation of the familiar pitot-static form (Ainsworth, LaGow) likewise permits computation of the same values. In either application, because of the continuous profiles of pressure that are measured, a very detailed profile of the structural parameters can be obtained.

The present form of the experiment which has evolved from Ainsworth's approach (Horvath, Spencer), Figure 6, is illustrated in Figure 7. This version employs radioactive ionization gages for pressure measurement.

Figure 8 illustrates a density measurement using the right circular cone approach, and, Figures 9 and 10, data from the pitot-static version.

Figures 11 and 12 permit comparison of data from the various techniques. Figure 12 enables the most critical examination, as the temperatures plotted were obtained from a grenade, a sphere, and a pitot-static experiment combination carried out nearly simultaneously. The data are considered to be in quite good agreement, by the experimenters, providing a satisfying demonstration of the general validity of the quite different approaches.

The techniques described are being employed independently by several different experimenters, and are providing new information regarding the atmosphere on a global basis in the meteorological sense, and new, detailed structure data useful in studying the physics of the atmosphere.

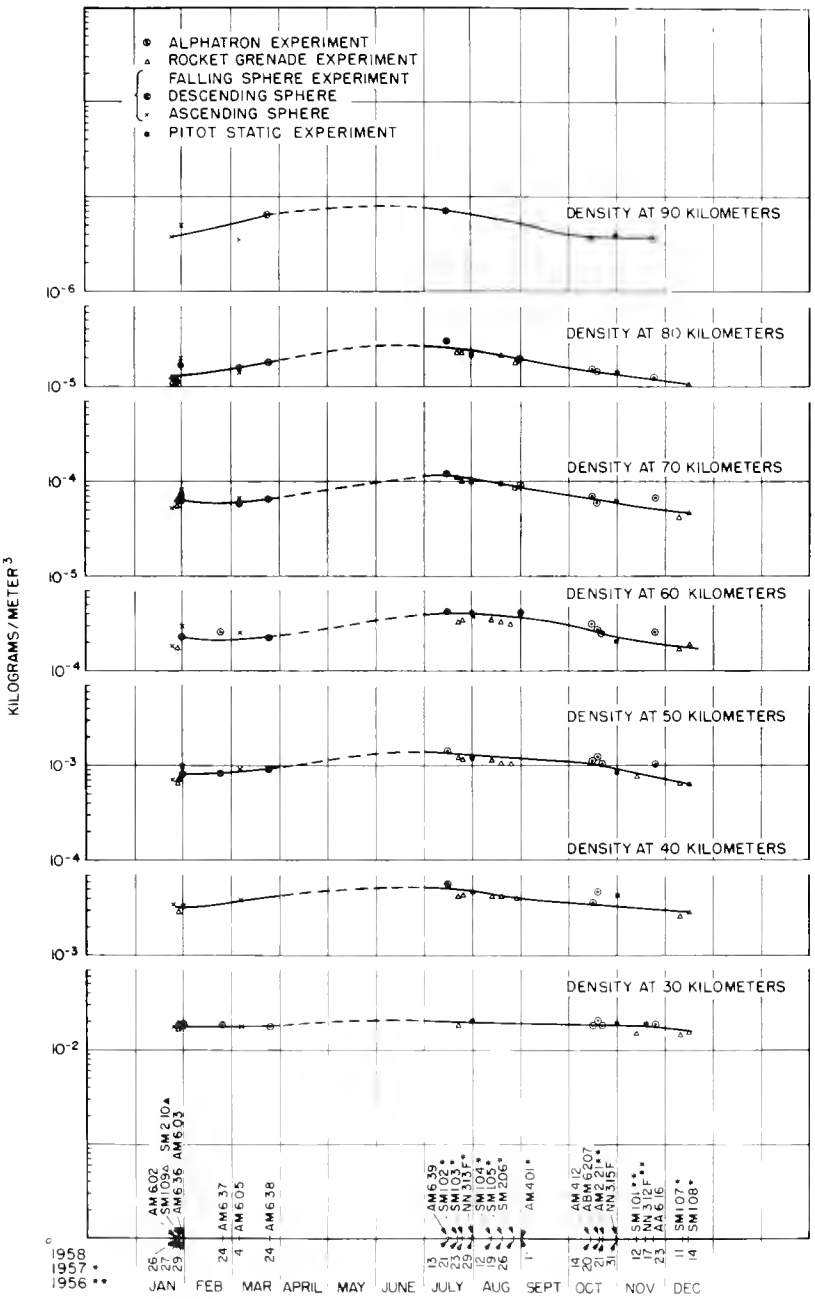

Figure 11. Seasonal variation of density obtained from various techniques (Spencer).

DISCUSSION

T.A. Chubb: One method which was not mentioned is the colorimetric method. This method is based upon how deeply various types of radiation penetrate into the earth's atmosphere, and has been used extensively by Dr. Hinteregger and also by NRL. Depending upon the portion of the spectrum used, different parameters are determined. If, for example, one is concerned about radiation between 1450 and 1500 A, then one measures essentially the partial pressure of O_2. What is really measured is the air mass between the vehicle and the sun, which is the light source. This is related to the pressure at a given altitude. If one works with a radiation band in the X-ray region where absorption is more or less independent of molecular com-

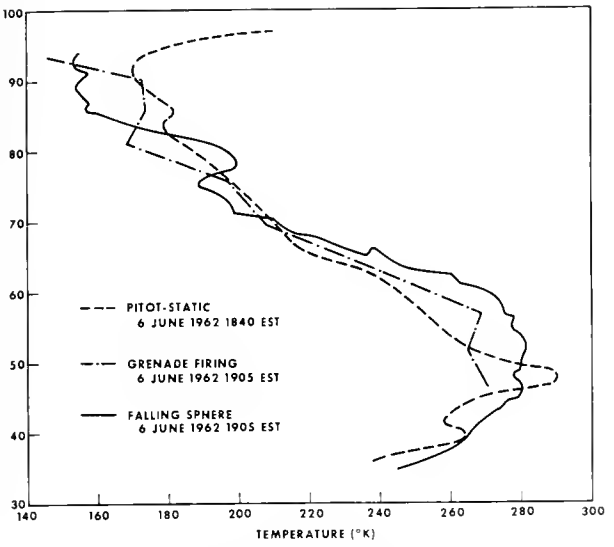

Figure 12. Temperature profiles from grenade, falling sphere and pitot-static experiment (Nordberg).

position, that is O and O_2 have the same absorption, one measures total density. Though this method does not lend itself with a single band to wide dynamic range, it seems to have considerable accuracy over a limited range, and for global studies it has a great deal to be said for it.

N.W. Spencer: There are a large number of available techniques; for example, back-scatter in which one uses some source in the rocket and the scatter is observed to measure the density, as in the searchlight experiment conducted many years ago. However, I have concentrated only on widely used techniques.

W. Nordberg: We have tried this method looking down from the Tiros satellite at a 300° black body, trying to measure the structure from above. The solar colorimetric technique gives information on the atmosphere from 100 km up, and we get it from 30 km down. The region from 30-100 km cannot be studied with this method.

S.A. Bowhill: A number of workers are planning to use the colorimetric method of density measurement. We are proposing to use a combination of Lyman α and 1450 A ionization chambers to follow molecular oxygen density from 70 to 130 km. The comment was made earlier that this method is inaccurate because of inaccurate knowledge of absorption cross sections for the various constituents. This aspect will not particularly concern us because we are interested essentially in a relative measurement of density between one occasion and another. However, it is important in resolving the composition of the atmosphere. I wonder if Dr. Chubb has any comment on the cross section question.

T.A. Chubb: This depends on the region of the spectrum. Between 1425 and 1500 A is the continuum absorption of oxygen; the absorption in this region is fairly well known from measurements of Watanabe and others at AFCRL. It is not too difficult to take a light source and a very narrow band detector calibrated in terms of the air mass between the light source and the detector. The Lyman alpha situation is more complicated; although the absorption coefficient for oxygen has been studied in considerable detail, especially by Weisler, there are problems of absorption by water vapor and maybe minor constituents (O_3 for example). When one measured in the atmosphere, one may not know adequately the make-up of the atmosphere in the region where Lyman alpha penetrates, about 85 km, to be sure there is no absorption due to ozone, water vapor, or nitric ozide.

For wavelengths in the further ultraviolet, particularly where absorption in the atmosphere is due to nitrogen bands such as the Lyman gamma line, the question is more complicated. The absorption of this line is dependent upon the temperature of the absorbing nitrogen and the line width of the sun, because absorption coefficients, in this region of band absorption, vary in the order of 1 A, which is also the probable half width of the Lyman gamma line. So if Lyman gamma absorption is measured there is probably a need for a further check.

In the X-ray region the absorption coefficients are empirically extrapolated from measured values for the lines, carbon, oxygen, and other wavelengths below about 16 A. There may be an uncertainty of 20-30% in the absorption coefficient, but no more; so this situation is better in the X-ray region.

K.W. Champion: I agree with Dr. Chubb that the region with greatest uncertainty is the Lyman gamma region, where Hinteregger has been working. Hoffman has recently reported some absorption measurements with fine structure and other details which are quite different from earlier measurements. A check of the cross section Hinteregger has used has shown a considerable range in some values.

On the falling sphere, AFCRL has continued development using the 7 inch sphere as a starting point. We have developed an accelerometer at the University of Utah that is 30 times more sensitive than before. We have been able to measure density with this sphere to 100 km; as Dr. Spencer mentioned, the upper limit is 150 km.

6.1 A TECHNIQUE FOR WIND MEASUREMENTS IN THE LOWER IONOSPHERE BY COLLECTION AND PROCESSING OF DOPPLER INFORMATION CONTAINED IN VHF RADAR RETURNS FROM METEOR TRAILS*

M. D. GROSSI
Smithsonian Astrophysical Observatory
Cambridge, Massachusetts

1. Introduction

The study for the development of a technique for wind measurements in the lower ionosphere, carried on by the Smithsonian Astrophysical Observatory is a research activity closely tied with the Harvard-Smithsonian Radio Meteor Project.

In fact the aeronomic measurements in the lower ionosphere will be performed by recording and processing doppler information contained in the meteor echoes obtained from the Havana, Illinois, 40.92 Mc/s radar facility.

The Havana multistatic radar is used by the Harvard-Smithsonian Radio Meteor Project to study meteors entering the upper atmosphere at heights between 70 and 110 km.

We now have one transmitter and 6 receivers, as shown in Figure 1 (two more receiving sites in remote locations will be added). One receiver is at the transmitter site, which is at the National Bureau of Standards station in Long Branch, near Havana, Illinois. The IF output (at 3 Mc/s) of the other 5 receivers, which are at outlying sites is brought to the transmitter site by wide-band two-wave microwave links (max. usable baseband BW 3.5 Mc/s).

The transmitting and receiving antenna at the main site is a double trough 60 m long, 21 m wide and 10.5 m high. The main beam is directed at azimuth 113° east of north and has an elevation of 43°. The remote sites have Yagi antennas, as a temporary substitute for troughs.

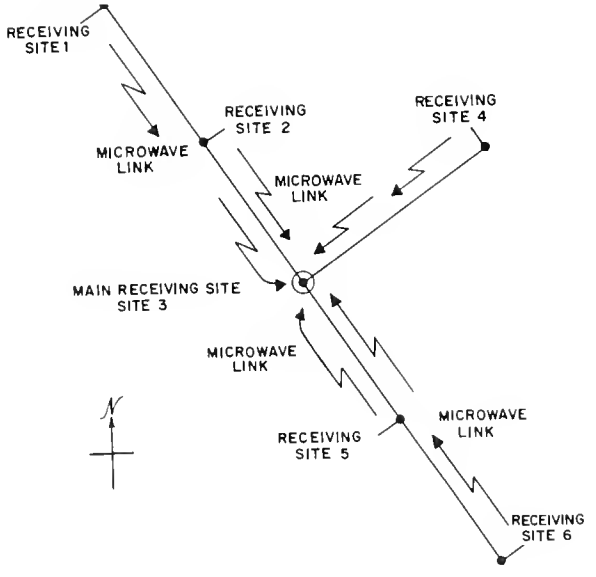

Figure 1. Map of receiver locations

The transmitter emits 740.74 quasi-gaussian pulses per sec, 6 microsec wide (and an extra pulse after every fifth pulse in order to remove range ambiguities for meteors distant more than 220 km) at a frequency of 40.92 Mc/s. At the transmitter site, the output of all stations is displayed on cathode ray tubes, which are arranged vertically; these tubes are photographed on 70 mm perforated film moving horizontally in front of them. The film does not move continuously at uniform speed. Figure 2 shows the record of one meteor on one of these films, enlarged about 3.5 times. This is a negative print; the original film has dark marks on an unexposed ground. The cathode ray tubes are turned on and the film started when an echo is detected at any station; when there is no longer an echo at any station, or after a predetermined interval of about 0.5 sec, if the echo persists, the film is stopped and the tubes turned off. The output of the receiver at each station appears as a series of vertical lines, each proportional in length to the amplitude of the received pulse. The doubled (fifth) pulses appear brighter than the others because the trace in the cathode ray tube is repeated. Station 3 is the transmitter site. The range (distance) of the meteor path from the transmitter site is indicated by a row of dots (appearing at the same time as the Fresnel pattern from station 3) between two rows of dots, which run all across the film. The lower continuous row of dots corresponds to 0 km range, and the upper to 200 km; the range of the meteor is found by linear interpolation from the position of the line of dots between them. In Figure 2 the range is 133 km. Disregard the extra row of dots below the 0 km line. This print also shows the saturation pips where the film started and stopped, but does not show the filmed clock presentation.

The films are now read with a Benson Lehner "Oscar" type N-2 and punched on IBM cards. The Fresnel patterns yield the speed of the meteor at different points along its path. The time intervals between the beginnings of the different Fresnel patterns yield the direction of motion. When the azimuth is measured, we will be able to deduce the heights.

*- The reported activity is sponsored by AF Cambridge Research Laboratories, under Contract AF 19(628)3248

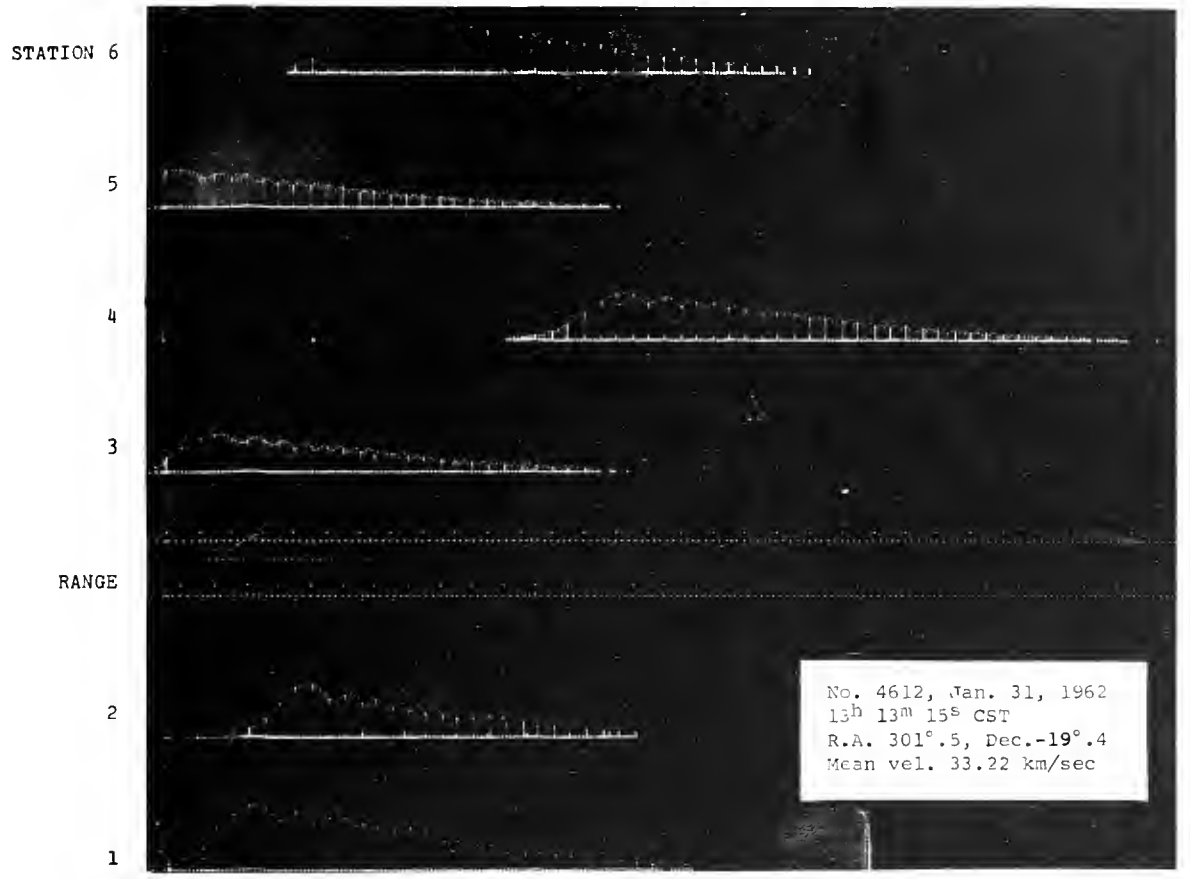

Figure 2. Typical photographic record of a meteor echo

An additional cathode ray tube (or possible 2) will be added to the display. The information appearing on this tube will be used to measure the azimuth of the meteor from the transmitter site. The form of display on this tube is not yet settled, but it is probable that, like the tubes showing the Fresnel patterns, it will show a line of varying length at each pulse.

Figure 1 shows a sketch map of the presently existing system. Each station is approximately 7 miles from the next.

Among the main scientific objectives of the Harvard-Smithsonian Radio Meteor Project are

1. Determination of trajectories, velocities and decelerations of meteors.

2. Measurement of the distribution of ions along a meteor trail.

3. An investigation of the physics of meteor processes, including related atmospheric, ionospheric and solar influences, impact phenomena and other relevant factors.

4. The groundwork for determining the volume and orbital characteristics of dust particles in the solar system.

Although the Radio Meteor Project will continue to record data on film, as briefly outined above, an 18-channel digital recording system will soon be installed at the main site in Havana. This system will accept video data obtained by detection of the IF from the receivers, remove (by gating) the transmitter main "band", digitize the video, and record it in an IBM- compatible format on half-inch magnetic tape that will be read by a IBM-7090 computer in Cambridge, Massachusetts. The project will use the films to select records on the tape for analysis and for other purposes. The tapes will also contain the information of interest to the Air Force, about winds at altitude of 70 to 100 km.

Winds do not directly affect the meteoroid, but carry the electron column away from the meteor track; expected doppler frequencies vary between 0.3 c/s and 300 c/s for RF carrier at 40.92 Mc/s.

We have various reasons for being interested in these doppler effects. The main one is that the evaluation of these frequencies allow wind measurements in the lower ionosphere. Another is that the wind, especially the wind shear, affects the Fresnel pattern, and its influence must be

accurately evaluated and corrected in order fully to utilize the Fresnel pattern itself in advanced meteor research. The need of measuring directly or indirectly such a low doppler frequency as 0.3 c/s at 40.92 Mc/s requires a modification of our present receiving system, as well as of the master oscillator of the transmitter. The system must become phase coherent and phase-scintillation free.

In addition, two new receiving sites, at a distance of about 50 km from the main site, must be added to the 6-station network illustrated in Figure 1, in order to obtain sufficient accuracy in the determination of the 3 components of the wind vector (see Figure 3).

In Havana the observed volume in the lower ionosphere when we are transmitting with both troughs of the present antenna system is

- 50 km characteristic dimension perpendicular to the beam
- 30 km characteristic dimension parallel to the beam
- 70 to 100 km (mostly 80 to 96 km) height of the volume above sea-level
- 140 km characteristic distance of the volume from the transmitter.

The frequency of reducible meteors is expected to be

$$N_{obs} \tilde{=} 500/hr \text{ (1000/hr at apex peak)}$$

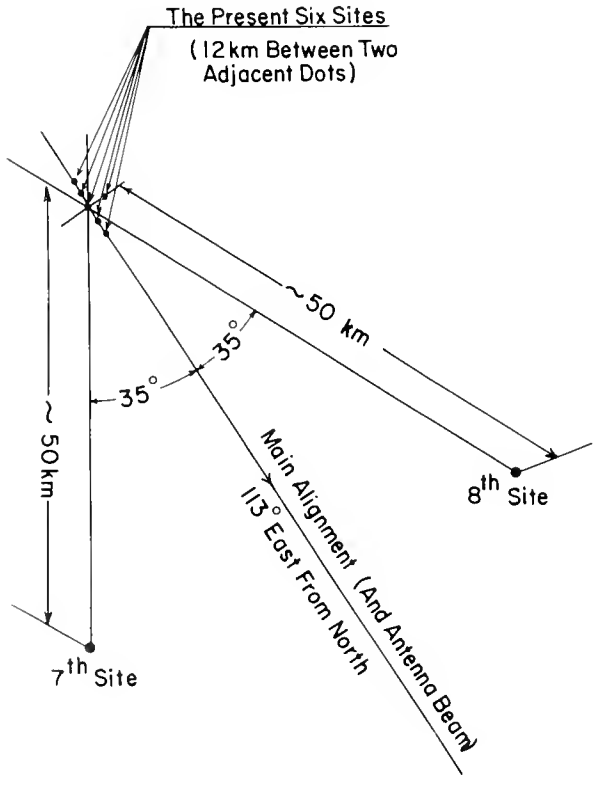

Figure 3. Best locations of the two new proposed receiving sites (7th and 8th)

Concerning the expected profile of the winds there are uncertainties, since observation and theory are inadequate to date.

We expect to find:

Wind max. amplitude : ~ 200 m/sec
Direction : horizontal within ~ 10%
Mean wind : vertical scale : ~50 km (circular period)
horizontal scale : ~500 km (circular period)
time scale : 1 day

Wave pattern:

Vertical scale ~ 5 km (circular period)
Horizontal " $\geq$ 50 km " "
Time scale $\tilde{\geq}$ 20 min

Wave patterns may also be observable in air density (equivalent amplitude in height 4 km). These patterns should be readily observable in the diffusion rates, if the heights are known within 1 km (ranges within 1.5 km), as will be possible with the Havana radar within a few months, when the azimuth and digital-recording equipment are in use.

2. Analysis of the Expected Accuracy Limits

In order to establish an upper bound in the expected measurement accuracy of doppler frequencies from the Havana radar, let us consider what the waveform presently radiated by the radar can ideally give in terms of range accuracy and (what is even more important to us) in terms of doppler frequency accuracy, for typical values of the signal-to-noise ratio offered by the station.

In this analysis assume for a moment that the receivers available there are optimum (for instance, designed on the basis of matched filters, cross-correlators, etc.). This assumption may appear quite restrictive, inasmuch as the Havana receivers have not been built along

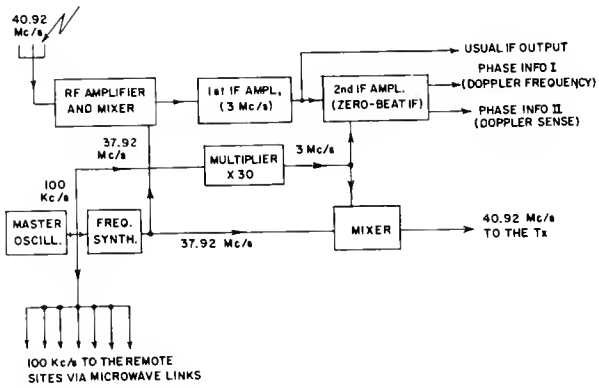

Figure 4. Block diagram of the equipment at the main site

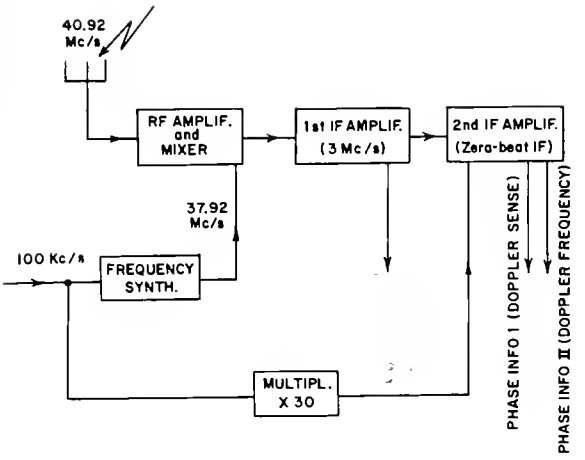

Figure 5. Block diagram of the equipment at each of the remote sites

these design criteria; we will see later, however, that this assumption is reasonable when the "gain" of the data processing is brought into the picture.

The ideal capabilities of the waveform are described by the ambiguity function.

Interesting parameters of the ambiguity function are the widths of the black dot at the origin of the Δf and τ axes, along said axes, on the "base" of the three-dimensional plot.

We have

$$\Delta = \frac{1}{T_B} = \frac{1}{0.05} \quad \text{c/s along the } \Delta f \text{ axis}$$

$\tau = 6\mu\text{sec}$ along the τ axis.

The calculation of the doppler frequency and range-measurement accuracies expected from the Havana radar can be performed by using the mentioned parameters (Δ, τ_o) of the ambiguity function and assuming for the signal-to-noise ratio a value typically available in the Havana system.

Suppose that the train of pulses we receive from a typical meteor trail contains n = 37 pulses (burst duration $T_B = 0.05$ sec) and that for every pulse the signal-to-noise ratio $\frac{S}{N} = 100$ (power ratio).

We have:

σ = standard dev. in range

$$= \frac{c}{2}\sigma_\tau = \frac{c}{2} \cdot \frac{1}{\frac{1}{\tau_o}\sqrt{2 \times n \times \frac{S}{N}}}$$

$$= \frac{3 \times 10^8}{} \cdot \frac{1}{\frac{1}{6.10^{-6}}\sqrt{2 \times 37 \times 100}} \tilde{=} 10 \text{ m}$$

where

$C = 3 \times 10^8$ m/sec is the velocity of light in vacuo;

σ_τ = standard deviation in time measurement;

τ_o = width of the central black dot, along the τ axis, of the ambiguity function.

The actual ranging capability of the Havana radar is right now below this ideal limit (of a factor of about 100), but a range servo unit, which should boost the range accuracy toward its ideal limit, is being considered and designed.

Even if this situation remains unchanged, however, it will hardly affect the accuracy of our aeronomic measurements.

Let us now consider the accuracy of the doppler frequency measurement, which is of primary direct importance for us.

We have here

$$\sigma_{\Delta f} = \frac{1}{\frac{1}{\Delta}\sqrt{2 \times n \times \frac{S}{N}}}$$

$$= \frac{1}{0.05\sqrt{2 \times 37 \times 100}} \tilde{=} 0.25 \text{ c/s},$$

where

$\sigma\Delta f$ = standard deviation in doppler frequency measurements

Δ = width along the Δf axis of the central black dot of the ambiguity function

The standard deviation in radial speed measurements is, consequently:

$$\sigma_{vel} = \frac{\lambda}{2} \sigma_{\Delta f} \tilde{=} 0.92 \text{ m/sec}$$

where $\lambda = 7.35$ m is the wavelength of the Havana radar.

Let us now see how far the present Havana radar is from this theoretical limit, with respect to the doppler frequency accuracy.

Suppose we measure doppler frequencies from differential phase variations of the return wave, from pulse to pulse (two adjacent pulses are 1.33 m/sec apart).

In this situation, the theoretical expectation for the standard deviation in phase measurement at each pulse (for the Havana facility) is

$$\sigma_\varphi = \frac{1}{2\frac{S}{N}} = \frac{1}{2.100} = 0.07 \text{ rad} = 4^\circ.$$

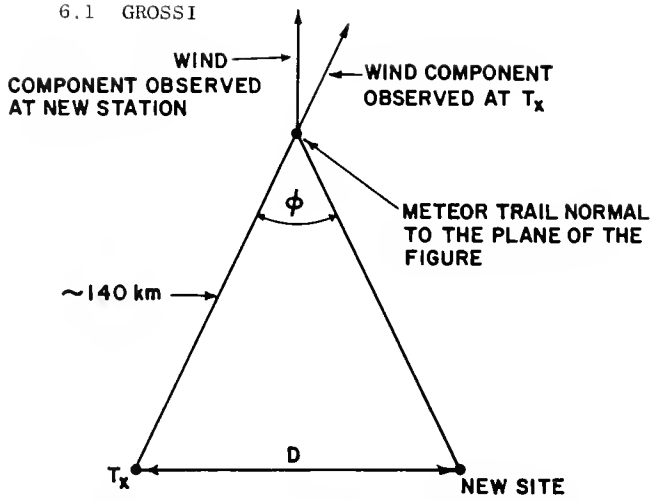

Figure 6. Geometry of the wind observations

And consequently,

$$\sigma_{\Delta f} = \frac{\frac{4}{360}}{1.33 \cdot 10^{-3}} \cong 8.5 \text{ c/s},$$

$$\sigma_{vel} = \frac{\lambda}{2} \times 8.5 \cong 31.5 \text{ m/sec.}$$

Preliminary measurements carried out in Havana confirm that the expected standard deviation $\sigma_{\varphi} \cong 4^{o}$ can be permanently achieved there when some modifications will be introduced into the equipment.

Therefore we could conclude that, after the planned modifications, the Havana system would present standard deviations in doppler frequency measurement about 33 times worse than ideal, which would not be an acceptable situation.

Here, however, the data processing of the HCO-SAO Radio Meteor Project introduces a significant improvement in the situation. A least-squares curve-fitting process applied to the phase information gains back this factor of 33 and goes straight to the ideal accuracy with σ_{vel} better than 1 m/sec.

Therefore, when the data processing is completed, the Havana facility becomes equivalent to a radar network with optimized detection processes, with the additional advantage of avoiding equipment complexity.

3. The Measuring System

A single high-stability master oscillator will be installed at the main site and utilized by the entire network. With reference to Figure 4, the master oscillator will work at 100 kc/s. By microwave links this frequency will be relayed to all the 7 remote stations as well as to the transmitter and receiver at the main site.

At the main site a frequency synthesizer generates the 40.92 Mc/s (Figure 4) utilized by the transmitter and the LO frequency for the main site receiver.

At each one of the remote sites a frequency synthesizer obtains an identical LO frequency (Figure 5).

Phase information to be utilized in the evaluation of the doppler frequency and of its sense (meteor trail radially approaching or receding, because of the wind) will be obtained as follows: The output of the IF (supposed at 3 Mc/s) beats with a second LO-sinusoid, phase coherent with the first LO, so that in absence of doppler, one has constant output (coherent detection). In the presence of doppler, unipolar video pulses (0 to +10 v) of variable amplitude, from pulse to pulse, are made to appear at the output of the unit. In such a system, where only one master oscillator provides the frequency generation of the entire network, one has to worry about coherence on a short-term basis, and not about the long-term behavior of the master oscillator.

4. The Data Processing

The following information channels will be made available to the project data processing. The information will be processed in a magnetic tape written in IBM-compatible format. The processing will be done in a IBM-7090 machine.

1. From each one of the 7 remote receiving sites we will have available:
   a) the amplitude of every echo burst (prf ~ 750 pps) vs. time. This is the type of information that the HCO/SAO Radio Meteor Project now uses. The Fresnel pattern appears in this information channel.
   b) two channels of phase information vs. time, recorded in one channel by a time-sharing arrangement, as a train of pulses of varying amplitude. These represent unambigously the phase of the wave at every pulse, from 0^{o} to 360^{o}. Phase information will be extracted and utilized during and after the generation of the Fresnel pattern.

2. From the main site:
   Information a) and b) as from the remote sites, and furthermore,
   c) range information vs. time
   d) direction of echo's angle of arrival vs. time (obtained with two phase information channels expressing Δ_{φ} of arrival at the two troughs of the antenna of the echo wave)

From information of types a) and c) we obtain:

1. the velocity of the meteor (11 to 72 km/sec), directly from the range and the oscillations in the Fresnel pattern;

2. the direction cosines (and the radiant) of the trail, obtained from the velocity of the meteor and the differences between the times of arrival of the leading edge of the Fresnel pattern at different receivers.

Adding information d), we locate the trail unambigously in three-dimensional space.

By then processing the phase information b), we obtain in amplitude and direction the motion of the ionized trail caused by the winds. A least-squares fitting is applied to the phase data to reduce significantly the inaccuracies of the equipment (by a factor of 33). This process directly yields the wind components along lines joining the meteor to the observing stations. When two observing stations are sufficiently separated, one wind component normal to these lines can be found. Three wind components can be found if two meteors are observed moving in different directions but passing through the same point; this requires 3 widely spaced non-collinear receiving stations. The wind vector is positioned in three-dimensional space by means of the data already deduced from a), c), d).

At the end of the process, wind information will be made available with the following estimated accuracies.

For the radial component of the wind the expected accuracy is as follows:

Assuming: Phase measurement in one pulse: $\sigma = 5^{\circ}$ (Greenhow's published records can be read to 3°)
usable echo duration ~ .05 sec
uncertainty in disentangling Fresnel oscillations from the phase: $\sigma \sim 15^{\circ}$ in phase over the usable length of the echo when the decay constant $> \sim .07^{\circ}$, which is mostly above 95 km: unimportant below ~ 95 km, (depending also somewhat on velocity, etc),

we will have for radial wind measures below 95 km:

$$\sigma = \left(\frac{\text{wavelength}/2}{.05 \text{ sec}}\right) \times \left(\frac{\sigma \text{ of mean of several phases}}{360^{\circ}}\right)$$

< 1 meter/sec

And, for radial wind measures above 95 km

$$\sigma \sim \left(\frac{\text{wavelength}/2}{.05 \text{ sec}}\right)\left(\frac{15^{\circ}}{360^{\circ}}\right) \sim 3 \text{ meter/sec.}$$

We will then have, for wind components normal to the line of sight,

$$\sigma = \frac{\sqrt{2}}{2 \sin \frac{\varphi}{4}} \times (\sigma \text{ of radial wind})$$

$$= \sim \frac{200}{D(\text{km})} \text{ m/sec (except above 95 km)}$$

where D is the distance between observing stations.

It is useful to recall that owing to the specular nature of the echo mechanism from the underdense meteors (the ones we work with), usually only one receiving site gets an echo at a given instant from a given meteor.

The determination of all 3 components of the wind at one point requires 2 distinct meteors through the same point (or nearly so), at the same time (or nearly so). Both meteors must be seen at the transmitter, and one at each of 2 remote sites.

The fraction F of the meteors seen at the transmitter that will also be seen at one of the new remote sites is a function of the meteor length and of the distance between new sites and transmitter.

With reference to Figure 6 we have

$$D \geq 140 \sin \varphi \text{ (km)},$$

where φ is the angle between the transmitter and receiver as seen at the meteor, and consequently, for F, we have

$$F \simeq \frac{2 \text{ meteor length}}{\pi \ 140 \sin \varphi} \simeq \frac{5}{D(\text{km})}.$$

The number N_3 of coincidences per hour necessary for the determination of all three components of the wind at one point, within L km (horizontally) and T minutes is:

$$N_3 \simeq 1.6 \times 10^{-5} F^2 L^2 T N_{obs}^2 \simeq \frac{10^2 L^2 T}{D^2}.$$

The present 6 stations can find:
characteristic scales of the variation of the wind
1 - 30 km vertically
5 - 50 km horizontally

$\geq$ 1 minute in time

Statistical distribution of vertical wind components (using stations 1 and 6):
Resolution: ~ 6 m/sec.

One new site will add a fairly complete knowledge of the horizontal winds (accuracy ~ 10 m/sec, except above 95 km), on the assumption that the vertical winds are small.

6.1 GROSSI

This site should be ~ 50 km away, whence $\sigma_{\perp}$ ~ 4 m/sec, F ~ 10%.

Another new site will add:

a slightly better knowledge of the horizontal winds (twice as much data);
a few determinations of all 3 components of the wind, but very important nonetheless.

These sites should be ~ 50 km away. Then (L = 5, T = 2)
N_3 ~ 2 determinations of all 3 components, per hour; accuracy ~ 4 m/sec.

ACKNOWLEDGEMENTS

The guidance of Dr. Gerald S. Hawkins and of Dr. Richard B. Southworth is gratefully acknowledged. Dr. R. B. Southworth furthermore contributed the section of this paper dealing with the data processions.

References

[1] D.W.R. McKinley. Ed. Meteor Science and Engineering, McGraw Hill, 1961.

[2] G.S. Hawkins. The Harvard Radio Meteor Project. Smithsonian Contributions to Astrophysics, Proceedings of the Symposium on the Astronomy and Physics of meteors. August 28 - September 1, 1961, vol. 7 pp. 53-62.

[3] A.C.B. Lovell. Ed. Meteor Astronomy, Oxford at the Clarendon Press, 1954.

[4] T.R. Kaiser., Ed. Meteors. Special supplement (vol 11) to the J. Atm. Terr. Physics, Pèrgamom Press Ltd., 1955.

[5] L.A. Manning. The Theory of the radio detection of meteors, J. Appl. Phys. vol 19, No. 8, pp. 689-699, 1948.

[6] D.W.R. McKinley and P.M. Millman. Determination of the elements of meteor paths from radar observations. Canadian J. of Res., A 27 53-67, 1949.

[7] J.S. Greenhow. A radio echo method for the investigation of atmospheric winds at altitudes of 80 - 100 km, using radio echoes from meteor trails. Philosophical Magazine, (7), 45, pp. 471-490, 1954.

[9] D.S. Robertson, D.T. Liddy, W.G. Elford. Measurements of winds in the upper atmosphere by means of drifting meteor trails, II, J. Atm. Terr. Physics, Vol. 4, pp. 271-284, 1953.

[10] W.G. Elford and D.S. Robertson. Measurements of winds in the upper atmosphere by means of drifting meteor trails, II, J. Atm. Terr. Physics, Vol. 4, pp. 271-284, 1953.

[11] M.I. Sholnik. Ed. Introduction to radar systems. McGraw Hill, 1962.

[12] R. Manasse. Summary of Maximum Theoretical Accuracy of radar measurements, Mitre Corp. Rep. SR 11, contract AF-33-(600)-39852, 1 April 1960.

[13] R. Manasse. Parameter Estimation Theory and some applications of theory to radar measurements. Mitre Corp. Rep. SR 12, contract AF-33-(600)-39852,1 April 1960.

DISCUSSION

G.V. Groves: Why would it not be preferable to use the method developed by the Adelaide Group in Australia? They do not need remote stations for their meteor radar system and the 3-component information is obtained with a monostatic radar arrangement, by processing radial velocity information more thoroughly.

M.D. Grossi: The experimental system we are setting up has the aim of studying various techniques able to maximize the number of wind determinations per hour. Our system includes the monostatic arrangement and at the end of our program we will have elements to make comparison between hourly determination of the wind obtainable monostatically versus the ones performed with the multistatic arrangement. The latter appears more promising from this standpoint.

N.W. Rosenberg: Are the 5 outlying sites needed to determine the origin of the wind vector and the 2 remote sites for accurate 3-component determination?

M.D. Grossi: Yes. Main site and 5 outlying site, through measurements of range, Fresnel pattern, determine the three-dimensional location of the meteor the velocity of the meteoroid, and its radiant. The distance of the remote sites from the main site has been chosen to obtain the required accuracy in wind velocity vector determination.

6.2 IONOSPHERIC WIND PATTERNS THROUGH THE NIGHT

N. W. ROSENBERG
Ionospheric Perturbations Branch, Upper Atmosphere Physics Laboratory
Air Force Cambridge Research Laboratories, L. C. Hanscom Field
Bedford, Massachusetts

Techniques for producing chemiluminous trails in the 90 - 150 km altitude region have been recently reported by this laboratory [1]. The use of such trails to measure winds and shears in the ionosphere is similar to that extensively used for twilight sodium trails, and Wind Measurements throughout the night are therefore possible for the first time. Four measurements between 1720 and 2245 CST 3 Dec 62 and four measurements between 1906 and 0406 CST 17 - 18 May 63 from Eglin AFB Florida are reported here and correlations of wind motions with altitude time and season are examined. (No vertical motions are available from these trail studies, but previous point releases suggest vertical velocities below 6 m/s at all altitudes of interest.)

Figures 1 and 2 present hodographs for the two nights. It will be seen that almost all wind vectors rotate clockwise (as viewed from above) with increasing altitude (i.e. veer as opposed to back, which describes a counter clockwise rotation.)

In Figures 3 and 4 NS and EW components are presented for the two nights. In Figure 3 (Dec 3) it is seen that the altitude interval between wind nulls at a given time (i.e. the half-wave length) increases from about 5 km at 100 km to about 20 km at 125 km. It is also seen that the maximum NS amplitudes increase from sunset to 2245 while the heights at which these maxima exist fall by about one-half wavelength over this five hour period. The EW amplitudes show similar wavelengths, and the only significant difference between the NS and EW components is that in the 100 km zone, the EW components decrease in amplitude with time, although two higher zones increase in amplitude with time.

In Figure 4 (May 17 - 18) excluding some complex patterns below 105 km, similar wavelengths and similar downward phase velocities to those of Figure 3 (Dec 3) are encountered, continuing through the night from sunset to sunrise. In this case, however, NS amplitudes decrease although EW amplitudes increase throughout the night.

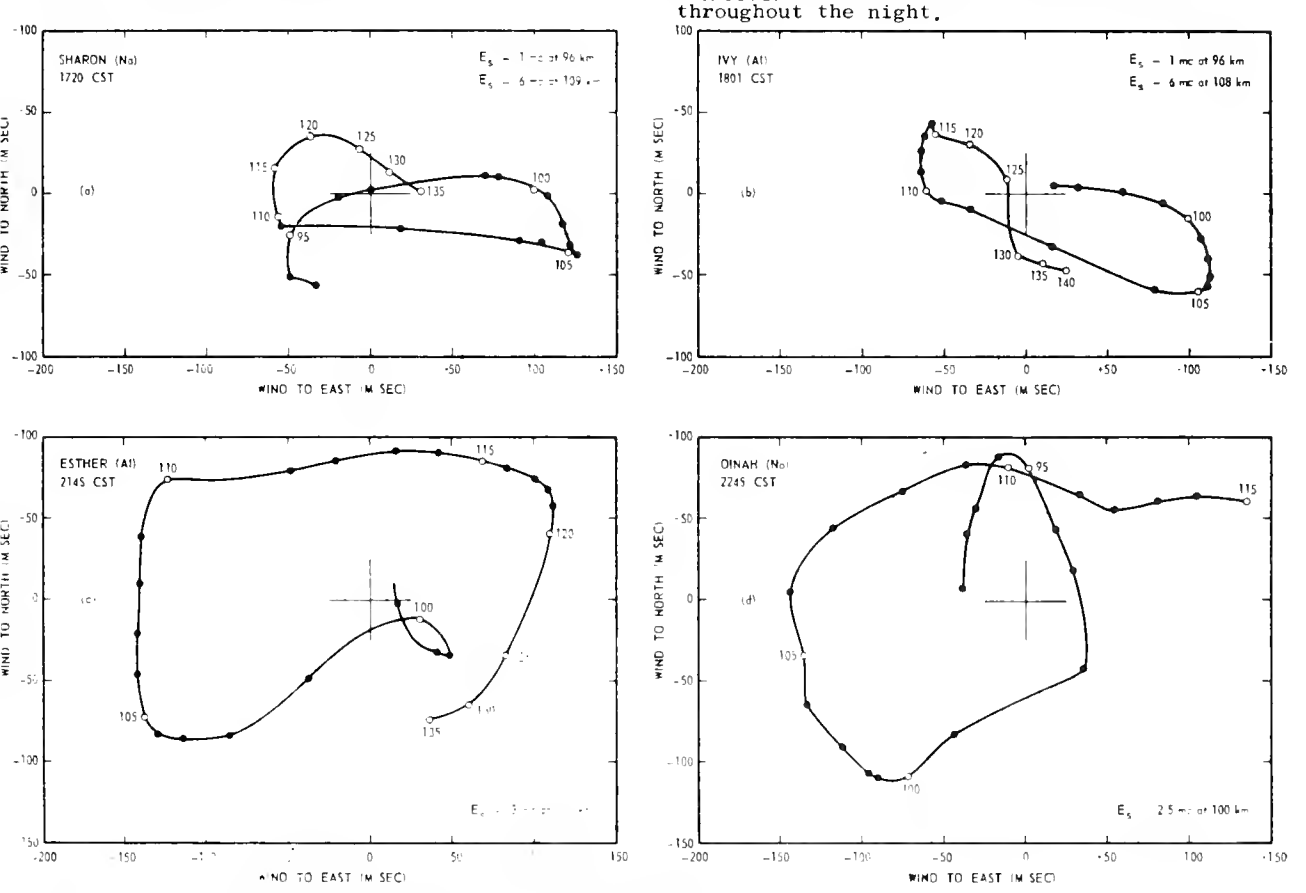

Figure 1. Wind hodographs - Eglin AFB, Fla. 3 Dec 1962

In Figures 5 and 6 an alternate presentation of the time variation of wind patterns is made. The wind vectors at a given altitude are connected to show variation with time. Figure 5 shows a general trend of winds veering into night, at all altitudes except for the highest (130 km). Figure 6 (May 17 - 18) shows even more strikingly the wind veering with time at all altitudes from 100 to 130 km. Note that the 100 km pattern is offset from the zero axis by an (apparently) non-diurnal component. Note further that veer is greatest (1 1/2 turns sunset - sunrise) at the lowest altitude and least (1/2 turn sunset - sunrise) at the highest altitude.

The veering with height at a given time coupled with a downward phase velocity leads to the veering with time at a given height.

The cooperation of Dr. H. D. Edwards and his associates at Georgia Tech who provided

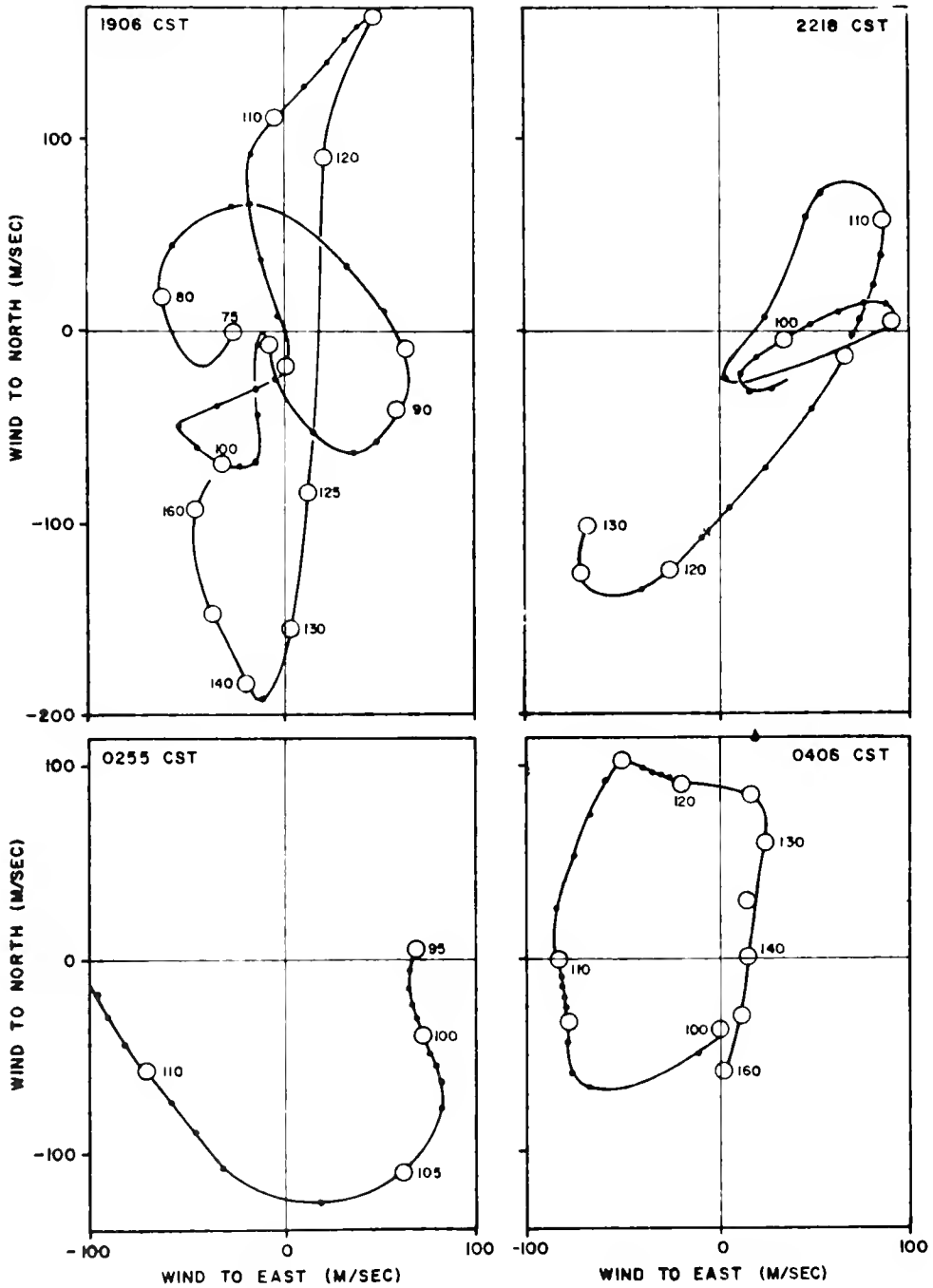

Figure 2. Wind Hodographs - Eglin AFB, Fla. 17 - 18 May 1963

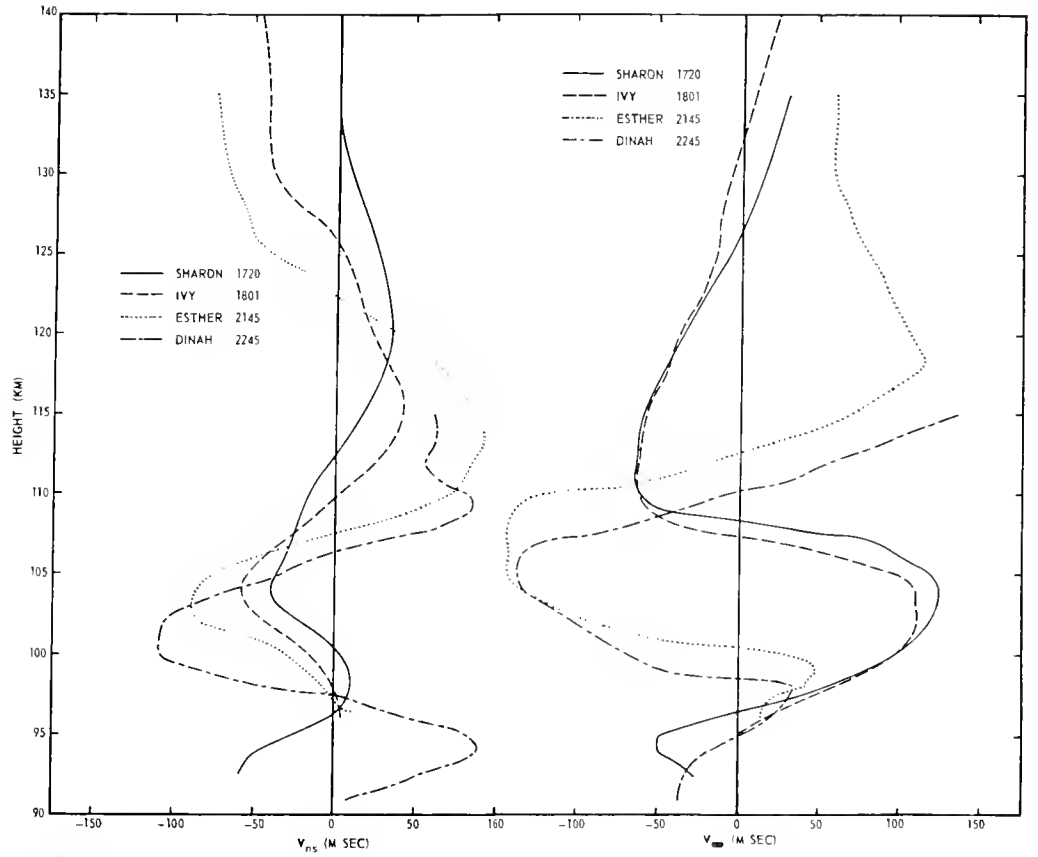

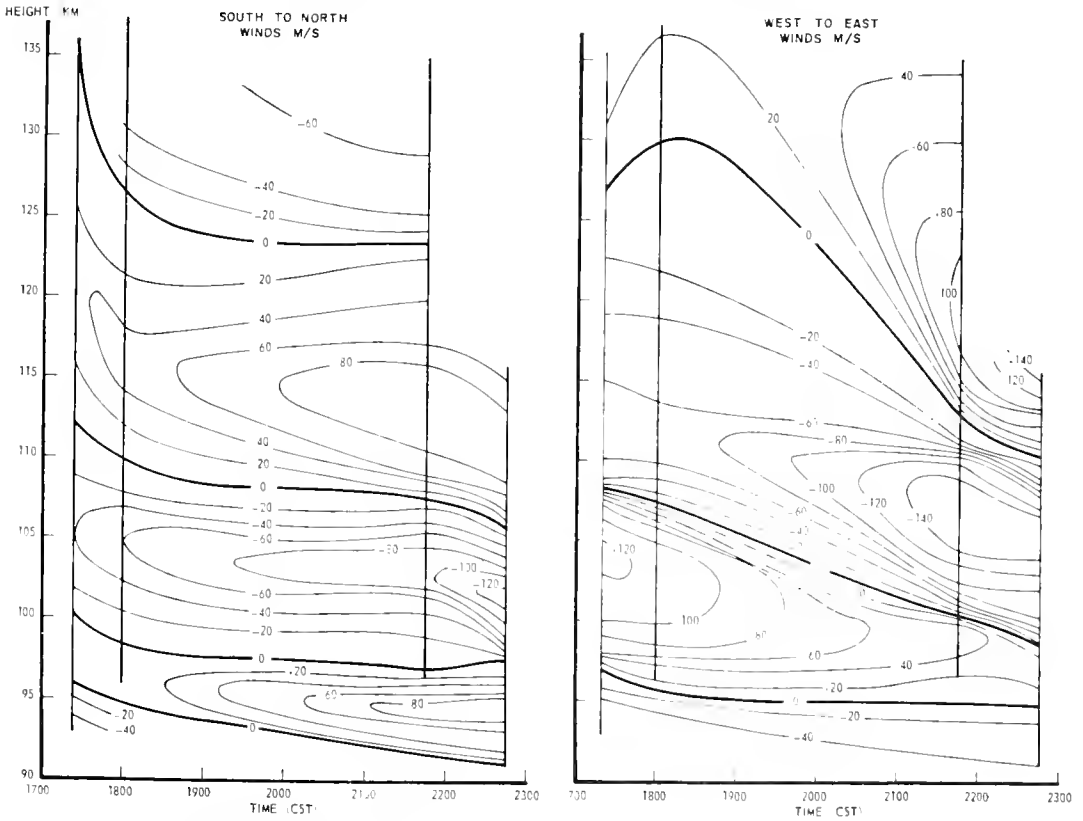

Figure 3a and 3b. Wind patterns - Eglin AFB, Fla. 3 Dec. 1962

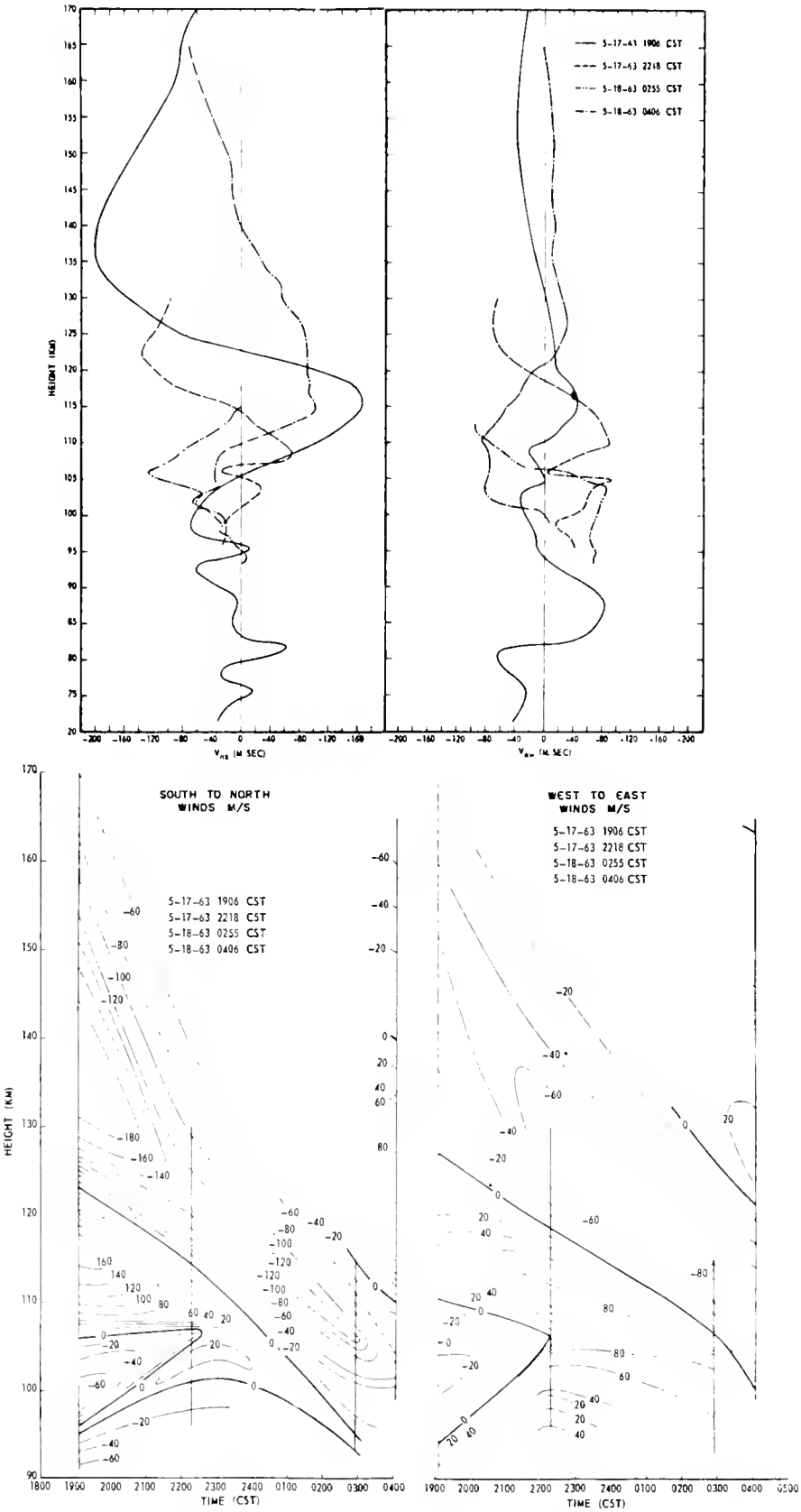

Figure 4a and 4b. Wind patterns - Eglin AFB, Fla. 17 - 18 May 1963

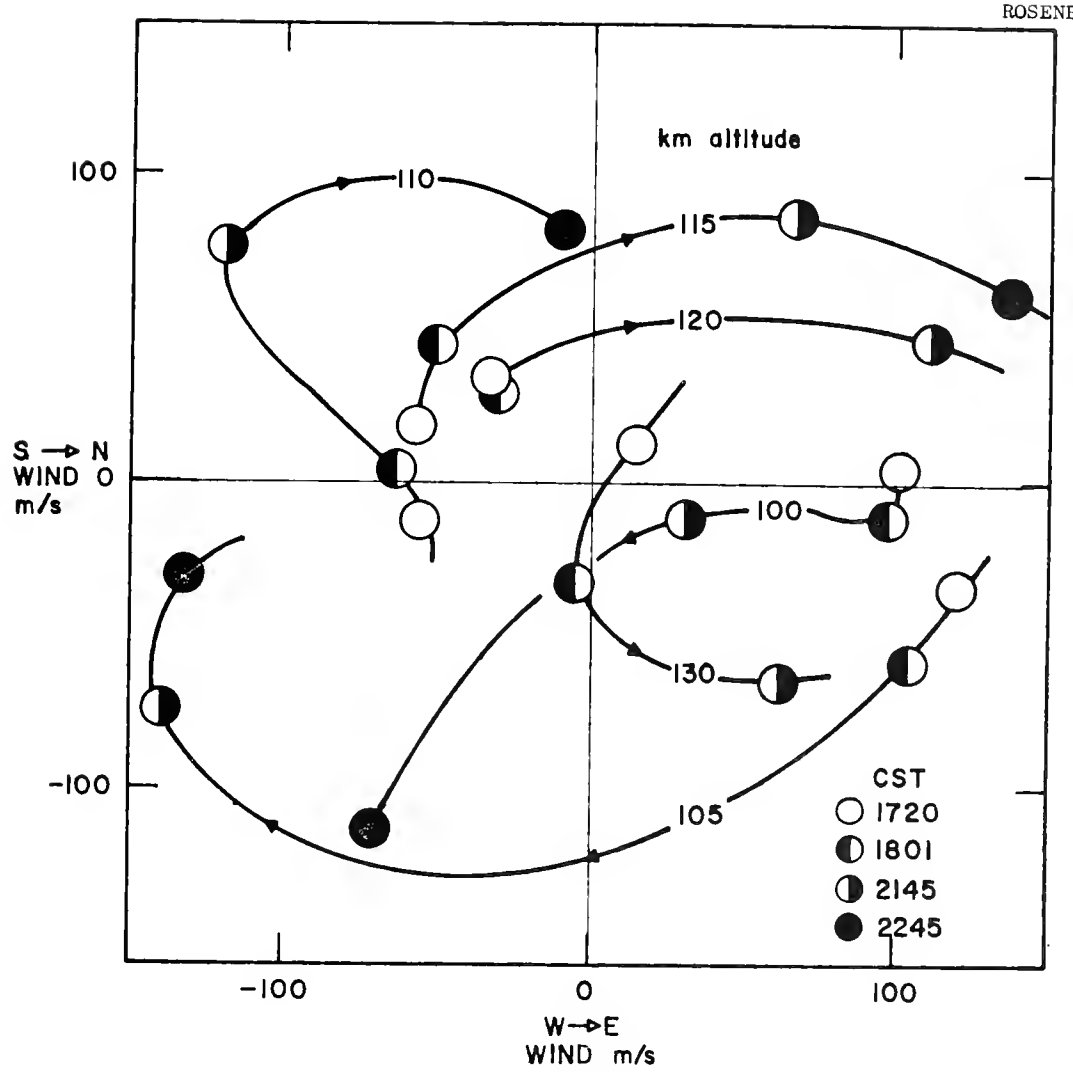

Figure 5. Wind vs. time at fixed altitudes 100 - 130 km Eglin AFB, Fla. (30^{o}N 80^{o}W) 3 Dec 1962

photography and photogrammetry is gratefully acknowledged.

References

[1] Rosenberg, Golomb and Allen, JGR 68 3328 (1963)
Rosenberg, Golomb and Allen, JGR 68 (Oct. 15, 1963)

[2] Manring, Bedinger, Knaflich, JGR 67 3923 (1962)

[3] Hines Q. J. Roy Met Soc 89 No. 379 (Jan., 1963)

DISCUSSION

S. A. Bowhill: Does the vertical velocity of the wave which you described as a vertically moving eddy along the trail of your shock wave picture correspond to the velocity of a gravity wave?

N. W. Rosenberg: This was a series of eddies that formed along the trail. There was no particular vertical motion to them. In fact the eddy motion is small compared to the horizontal wind motions and the trail literally breaks itself up into a series of clumps spaced regularly. The motion you are seeing could be towards you or away--it is a change in elevation angle rather than a change in altitude.

W. Nordberg: With your measurements and the conventional sodium experiments we are beginning to get some wind patterns. Previously we have only gotten wind data at these heights through meteor trails. There have now been enough chemiluminescence experiments for patterns to show up. Up to 80 km meteorological patterns, seasonal and other, are seen. Above 80 km things look utterly confused. You mentioned a spiral motion seen in either time or altitude. Sodium trails can of course be observed only in altitude. It seems to me

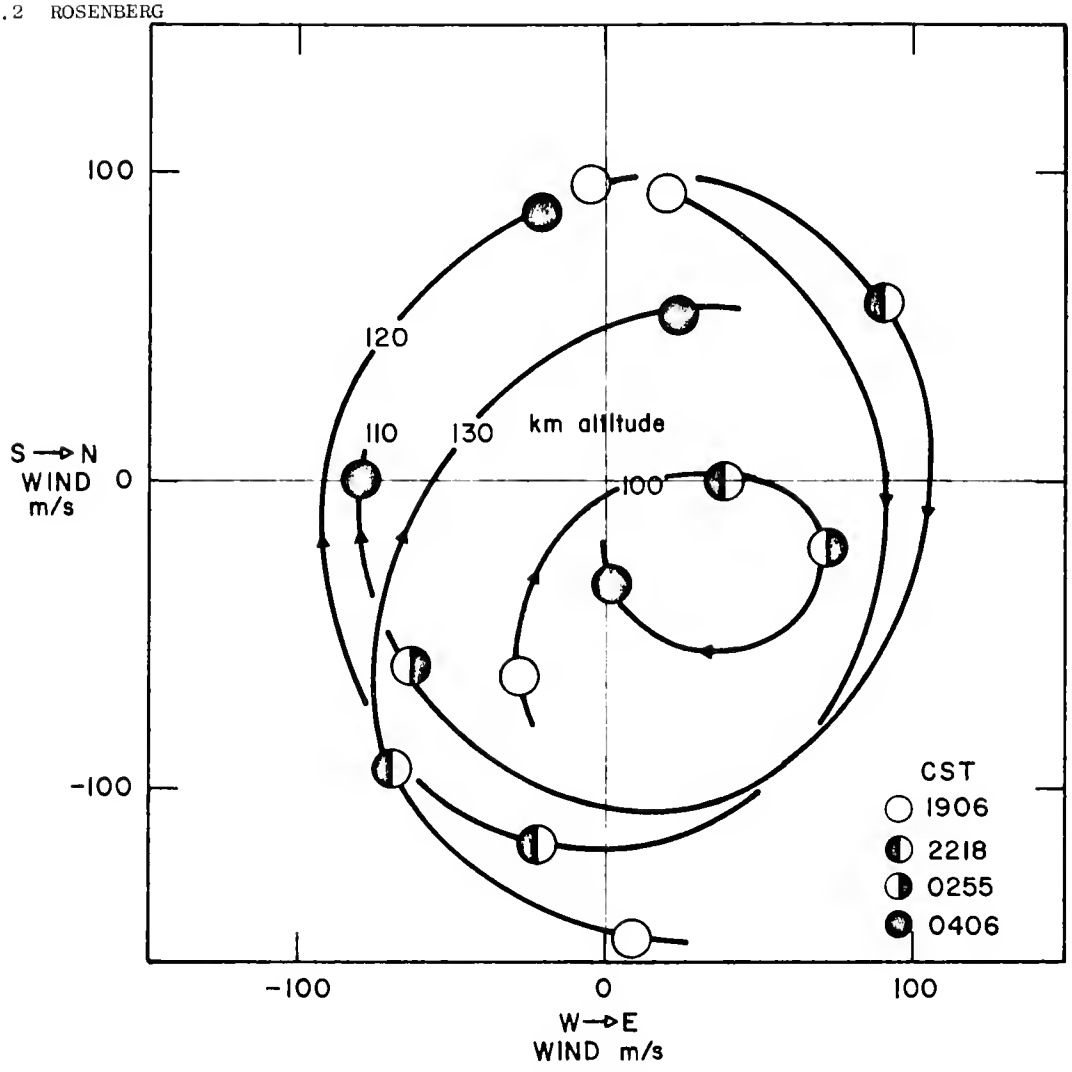

Figure 6. Wind vs. time at fixed altitudes 100 - 130 km Eglin AFB, Fla. (30^{o}N 80^{o}W) 17 - 18 May 1963

from data on sodium trails that around 130 or 140 km the rotation stops. Above that height the velocities show a regular pattern.

N. W. Rosenberg: Another way of looking at it is that in this altitude regime, the wave length of the vertical disturbance is a few km at 100 km, and becomes about 40 or 50 km at 140 km altitude. So any variations are over 50 or 100 km, which is why we do not find any further right spirals.

M. DUBIN
Headquarters
National Aeronautics and Space
Administration
Washington 25, D. C.

We will first discuss some important parameters that describe the physics of the lower ionosphere. One approach is to ask the origin of the energy of the various reactions. One can compute the ion energy rather easily; taking an ion concentration of about $10^5 cm^{-3}$, and about 10 ev per recombination, one obtains about 10^{-5} erg/cm^3.

A second source of energy is that of solar absorption. Below 3000 A wavelength, all the solar radiation is absorbed in the atmosphere above the surface of the earth. The Schumann-Runge region, from 1000 - 2000 A approximately, dissociates oxygen, and represents an energy of about 100 erg/cm^2sec; if this is to be absorbed in, say, a 100 km column, one finds an absorption energy (in daylight) of 10^{-5} erg/cm^3 sec. The absorption energy is therefore much greater than the total ion energy available in the atmosphere.

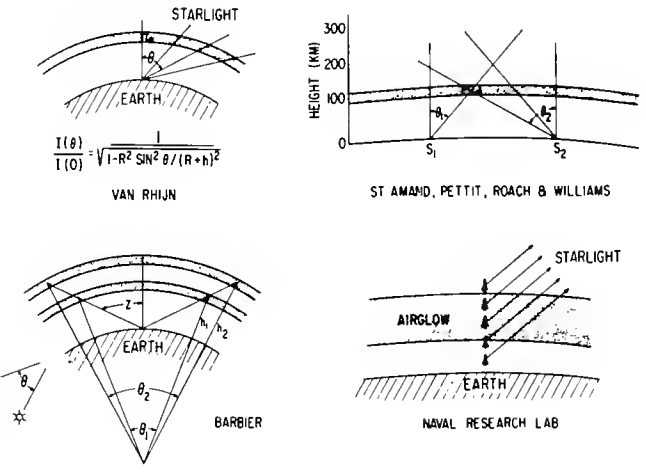

Figure 1. Four methods to determine the altitude of airglow emissions (after Packer).

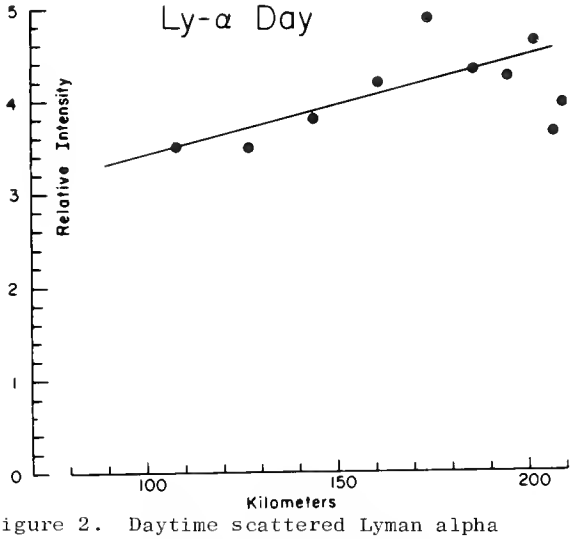

Figure 2. Daytime scattered Lyman alpha intensity (after Fastie).

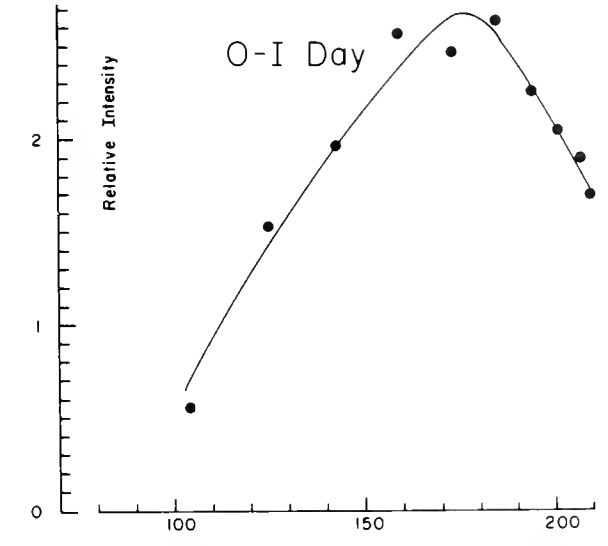

Figure 3. Daytime scattered O-I intensity.

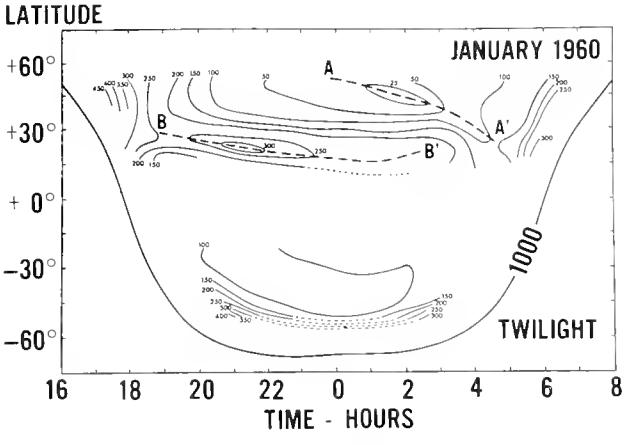

Figure 4. 6300 A emission observed from France, Africa and Antarctic.

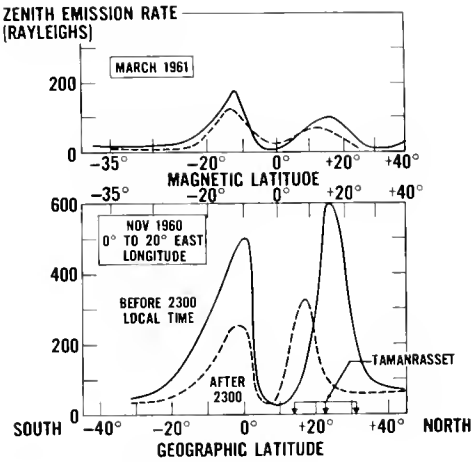

Figure 5. Latitude variation of 6300 A tropical arcs (after Barbiet et al., Elliott and Clark, and Blamont).

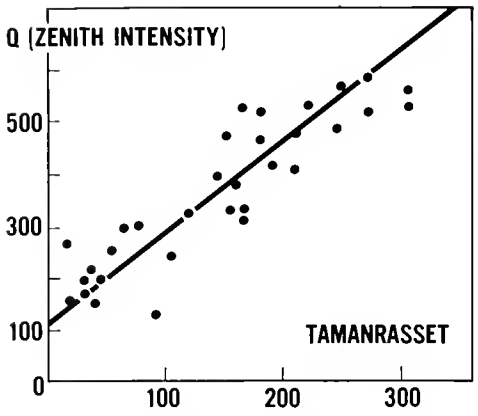

Figure 6. Correlation of 6300 A emission with F2-layer critical frequency (after Barbier and Glaume).

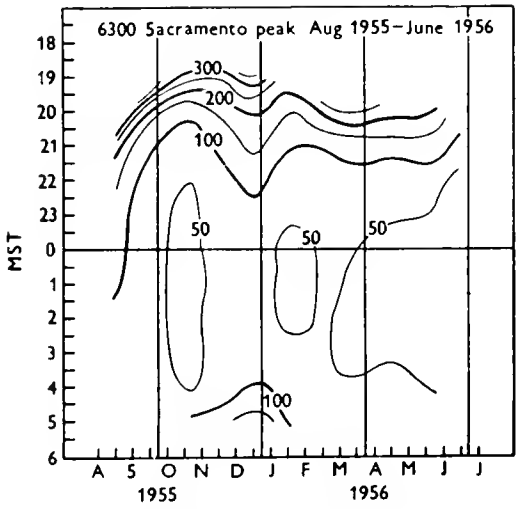

Figure 7. Diurnal and seasonal variation of 6300 A emission

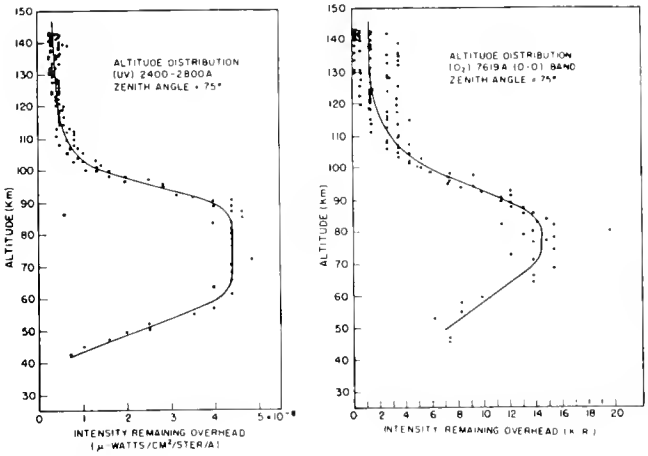

Figure 8. Altitude distribution of emission flux in Heryberg continuum and at 7619 A.

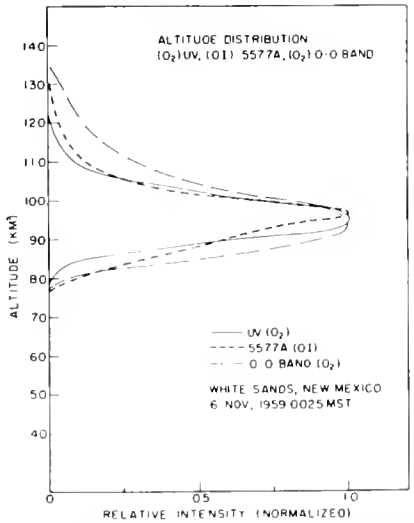

Figure 9. Altitude distributions of the oxygen green line and two O_2 emissions.

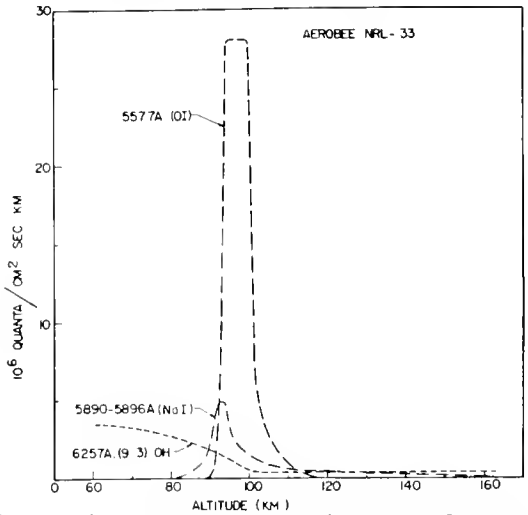

Figure 10. Altitude distributions of oxygen green line, hydroxyl band and sodium band.

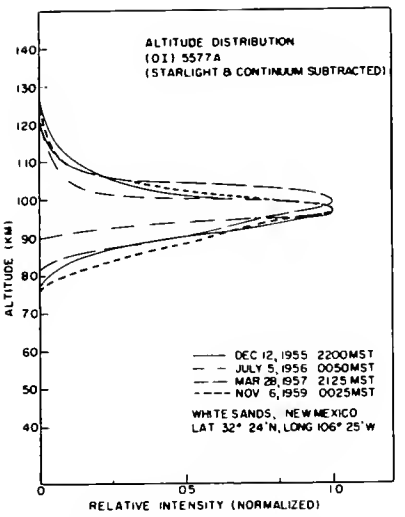

Figure 11. Comparison of green line altitude distributions over a 5 year period.

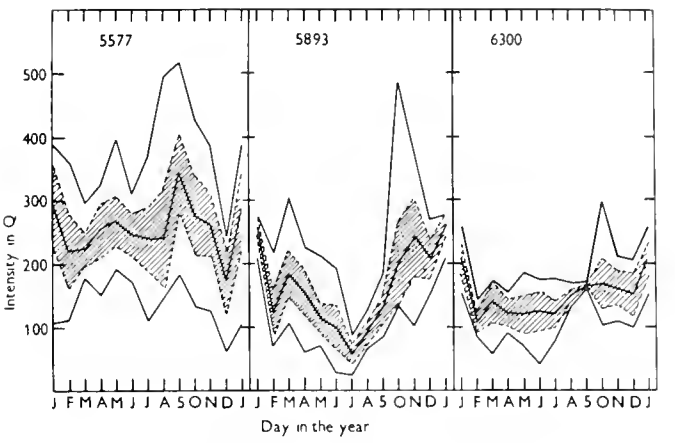

Figure 12. Annual variations of airglow emissions.

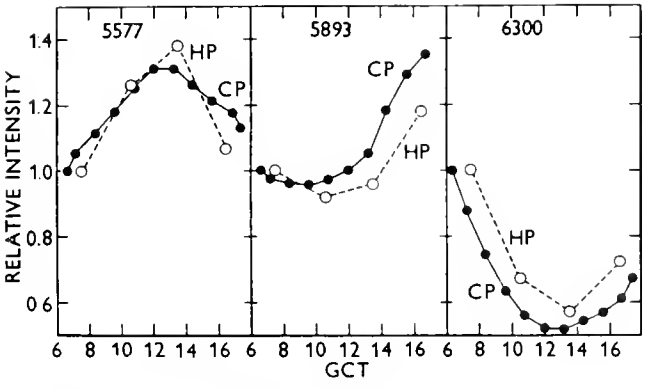

Figure 13. Diurnal variations of airglow emissions.

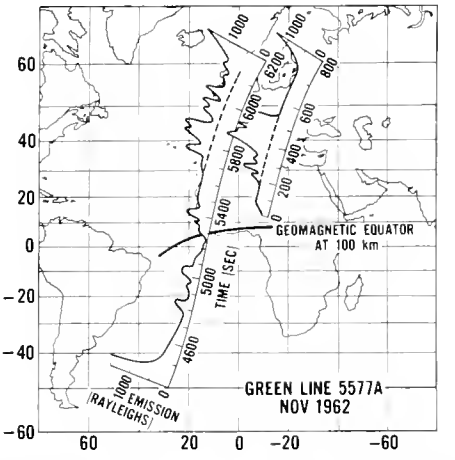

Figure 14. Satellite observations of oxygen green line (after Clark and Elliott and Blamont).

Thirdly, one may consider the energy of mass motion at, say, 100 km; with 10^{13} molecules/cm^3, and a velocity about 100 m/sec, this is found at 10^{-1} erg/cm^3.

Fourthly is the chemical energy of the atmosphere. The amount of molecular oxygen dissociated at the 100 km level, is about 10^{11} atom/cm^3; taking about 5 ev per recombination, the chemical energy available is about 1 erg/cm^3. Accordingly the airglow, which is produced by a release of chemical energy, ties into the source of motions, especially if the energy absorption is differentiated with the geographical distribution along the earth, and is therefore an extremely significant tool for aeronomic investigation.

For a number of years, the temperature of the atmosphere from 50 - 2000 km altitude has been measured by airglow methods. In the lower altitudes the OH bands have shown the extent of temperature variations, which are now consistent

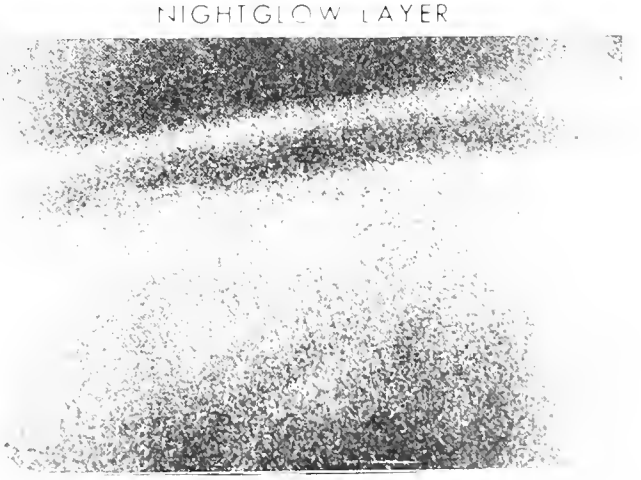

Figure 15. Photograph of 5577 airglow (after Cooper).

with measurements obtained by rockets. At the 100 km level, the 5577 A radiation has been dispersed using interferometers and other methods, giving temperatures again consistent with sounding rockets, but the temperature excursions are known somewhat better. At higher altitudes, the 6300 A radiation has been observed, as well as the N_2^+ first negative system rotation bands; the excursions of temperature for the latter in the aurora are from 700 - 3500 deg K. Similar results have been obtained from sounding rockets and from satellites.

Recently helium has been observed in the infrared, and the temperature and heat content of the atmosphere out to 1000 km have been determined. Similarly, much of our original knowledge of atmosphere composition was first obtained by airglow observations. The existence of N_2^+, atomic oxygen, and rare constituents, for example, sodium, were first demonstrated in the atmosphere by airglow measurements. The OH radical, in addition, has never been measured except by the airglow; helium and hydrogen in the atmosphere have also been measured in this way. The rare constituent calcium observed by the Soviet mass spectrometers was also observed by airglow.

The airglow observations have also given information about the effects of energetic particles on the atmosphere, for example the aurora; in addition, the circulation at altitudes above 100 km has been determined by Roach and others from movements of patches of airglow.

The advantage of the airglow observations for measurements in the atmosphere is that they are essentially passive direct measurements, in that one can look from a distance at a point in the atmosphere. They lend themselves, therefore, to ground observations, which have been going on for many years; and also to satellite measurements. One could look at the 80 - 120 km region from both satellites and rockets; the difficulty is in attaining sufficient angular resolution in the optical system.

Most of the techniques have been developed; they involve optical systems and extremely sensitive photomultipliers. Interference filters can be used to observe bands with very narrow resolutions, say, 10 A. Fast spectrophotometers are available now for the visible, the infrared, and the ultraviolet. The problem in airglow is not the instrumentation techniques, but their application to the atmosphere.

This can be illustrated with reference to the 5577 A radiation, the green line of atomic oxygen; Chapman has proposed a three-body reaction:

$$O + O + O \rightarrow O_2^* + O_{15}$$

Sinclair has considered excitation by collision with another atom. A problem is that the rate coefficient has to be very high for this reaction to occur. Recently Barth and Hildebrand, based on laboratory measurements, have proposed the pair of reactions:

$$O + O + M \rightarrow O_2^* + M$$

$$O_2^* + O \rightarrow O_2^* + O_{15}$$

Recombination of atomic oxygen gives an oxygen molecule which could give rise to the Herzberg bands in the near ultraviolet. The reaction, itself, is known to occur; one must note that either reaction gives the 5577 A band proportional to the concentration of atomic oxygen, and the green line is therefore a very sensitive measure of atomic oxygen concentration. In fact, the altitude of the 5577 A emission must be the altitude of the maximum of atomic oxygen in the atmosphere.

Table 1 illustrates the brightness of the airglow relative to other light sources in space.

Phenomenon	Relative Brightness
Milky way (mean)	7
Visible night glow (zenith)	1.0
1300A Orian Nebulosity (bright portion)	1.3
Middle UV night glow, 100A wide (edge-on)	1.3
Aurora IBC I	3.0
Lyman-α glow	10.0
Visible night glow (edge-on)	30.0
1300-1800Å Aurora over Wallops Island	30.0 to 300.0
Aurora IBC IV	3000.0

Figure 1, after Packer, shows various methods for determining the altitudes of airglow emissions. The Van Rhijn formula uses the effect of earth curvature; it has been applied to the sodium and to the oxygen green line airglow, sometimes with poor accuracy. Roach and his co-workers have found good altitudes by triangulating on perturbations in the distribution. Barbier identified altitudes from their known time dependence; these check well with rocket measurements.

Figure 2 shows a rocket measurement in the ultraviolet by Fastie, of the intensity of the sc scattered Lyman alpha radiation. This in turn is a measure of the temperature of the exosphere and the hydrogen content of the atmosphere. It is consistent with satellite data, and has been reviewed by Donahue and Fastie.

Figure 3 shows a feature of the daylight scattering at 1500 A: the distribution falls off, whereas multiple scattering would keep it constant. This condition has been examined by Donahue and Fastie, and they believe that Lyman beta and resonance excitation is not sufficient to give the 5 kR observed. Barth and Fastie have reviewed the problem and conclude that the energy of the electrons, as observed by Spencer and Hinteregger in this region could excite the atomic oxygen at 1500 A.

Next we will discuss some features of the 6300 A radiation. One mechanism for this is recombination of O_2^+ in the atmosphere. Another possible mechanism, suggested by the red arcs, is excitation by energetic electrons which may be present in the atmosphere. Figure 4 is a map showing the time in hours versus the latitude dependence of the phenomenon; Figure 5 shows the geographical distribution as a function of magnetic latitude, suggesting again the excitation by electrons which are magnetically controlled. Figure 6, after Barbier, from Tamanrasset, shows that the critical frequency and the intensity of the red oxygen glow have a significant correlation. Figure 7, taken at Sacramento Peak, shows that as a function of time of day the red airglow decreases in intensity; so if electrons are the cause of it, their quantity and energy must decrease over the day. Likewise there is a characteristic annual variation.

Figure 8 illustrates measurements from rockets, obtained by the NRL group, in the Herzberg radiation region. By differentiation, the altitude of the airglow may be found. Figure 9 demonstrates that the 5577 A vibration-excited band of O_2 and the Herzberg region fall at the same altitude; the peak of this reaction, which may be caused by a cube dependence on atomic oxygen concentration, is very sharp.

Figure 10 compares the intensity of the radiation which is involved in the oxygen green line, the hydroxyl band and the sodium band. Figure 11 shows various measurements indicating that the altitude of the peak is nearly constant at about 90 - 97 km for the 5577 A radiation.

Figure 12 shows the annual variation of the 5577, 5893 and 6300 A radiation. Since the 5577 line is a measure of the cube of the atomic oxygen density and its collision frequency, one can argue, that the atomic density has an annual variation. Hinteregger recently reported privately a measurement of atomic oxygen density in the daytime in October which was twice that in the early morning in June; this could be due either to a diurnal variation, which is not too likely, or a seasonal change of the kind mentioned above.

Figure 13 illustrates the diurnal variation of the same three radiations. The 6300 A decreases in intensity through the night, then increases early in the morning. If electron excitation is important, this would correspond to a variation of the electrons.

Figure 14 is a satellite measurement of the 5577 A radiation by Clark and Elliott and Blamont. It is possible that the intensity variation is a latitude measurement of the distribution of atomic oxygen on two sweeps. However, depending on the variation of albedo, it is possible to have an effect from the variation of cloud cover, and the measurement may be open to doubt. For this reason, use of the ultraviolet is preferred.

Table 2 gives a measurement of the altitude of the green airglow by Carpenter. He found the altitude by the time that the star effect went below the horizon, and he obtained 92 km for the middle layer.

Feature	Time 16^h+)	Angular zenith distances of Phecda (deg)	Capsule height (km) Above feature	Above ground	Height of feature (km)
Outside layer	48^{m}49^s	100.86	118	237	119
Middle of layer	50^{m}08^s	101.88	141	232	91
Lower boundary of layer	50^{m}41^s	102.22	149	230	81

Table 2. Angular zenith distances of Phecda and corresponding times, capsule heights, and heights of features of the airglow band (after Carpenter).

On the last Mercury flight, photographs of the 5577 A and green continuum were made by Cooper. Figure 15 is one such picture of the airglow, which shows as a thin layer here, with the earth visible in partial moonlight. The airglow was measured on a number of photographs, and the results of the measurements are shown in Table 3.

Picture No.	Time, G.m.t.	Angle between earth's limb and nightglow line, deg	Height of spacecraft above earth, km	Height of center of nightglow band, km	Latitude at which nightglow is observed	Angular width at half intensity of nightglow band, deg	Normal exposure time, sec
22	1342 50	3 82	241	111	27° S	0 66	30
23	1343 10	3. 26	240	105	26 5° S	89	10
25	1346 20	3 00	232	97	23° S	88	30
27	1349 30	2 26	220	75	18° S	71	120
28	1350 20	2 40	218	78	17° S	89	30
29	1350 40	2 41	217	77	16 5° S	87	10
31	1355 00	2 66	202	81	8° S	78	30
32	1355 10	2 85	202	81	8° S	78	10
35	1401 40	3. 20	181	87	8° N	92	10
Average	.....	2 86	.....	88	.....	0 80	.....

Table 3. Results of measurement of oxygen green line intensity from satellite photographs (after Cooper).

7.A DUBIN

The height of the center band of the airglow is given as a function of latitude. These altitude changes are more than 20 km, with a mean of about 88 km; this could be the diurnal variation shown earlier, since the intensity changed. It also could be an effect of the distribution of constituents in the atmosphere.

There are other airglow observations connected with certain phenomena in the atmosphere. For example, Roach has observed the motion of the 5577 A as a function of time. He observed cells that are about 2500 km in extent with a period of rotation of 5 hr. Rosenberg reported at this conference a period of rotation one and a half times at the 100 km level in a period of a little more than 5 hr.

8.A SOLAR RADIATION MEASUREMENTS

T. A. CHUBB
U. S. Naval Research Laboratory
Washington 25, D. C.

Solar radiation is generally thought of as coming from three regions of the sun; namely, the photosphere or visible disc of the sun, the corona or tenuous million degree outermost atmosphere of the sun, and the chromosphere, the transition region between photosphere and corona. The photosphere (Figure 1) consists of the outer layers of insulating gas which separate the sun's nuclear furnace from the frigid cold of outer space. Heat flows upward through these layers until it bursts through the absorbing solar gas. In the photosphere the gas temperature decreases with altitude as dictated by the direction of heat flow. The relative coolness of the outer photospheric layers shows up in the phenomenon of limb brightening, the existence of Fraunhofer absorption lines in the visible spectrum, and in the decrease in measured solar black body radiation temperature as one looks at the solar spectrum at increasingly short wavelengths in the middle ultraviolet. The ultraviolet temperature effect is a result of increasingly high optical absorption coefficients for solar gas in the spectral region below 3000 A.

When one makes photographs of the sun using radiation which is most highly absorbed by solar gas, one obtains disk images very different in character from the image seen in visible light. The solar image seen in Lyman alpha radiation, for example, (Figure 2) is a very polotchy disk showing many bright localized regions called plages. An examination of the spectrum between 1100 and 1600 A (Figure 3) shows the transition of solar emission from continuum radiation arising in the photosphere to emission line radiation arising in the chromosphere and corona. All the emission lines show the splotchy plage emission; in addition photospheric continuum radiation

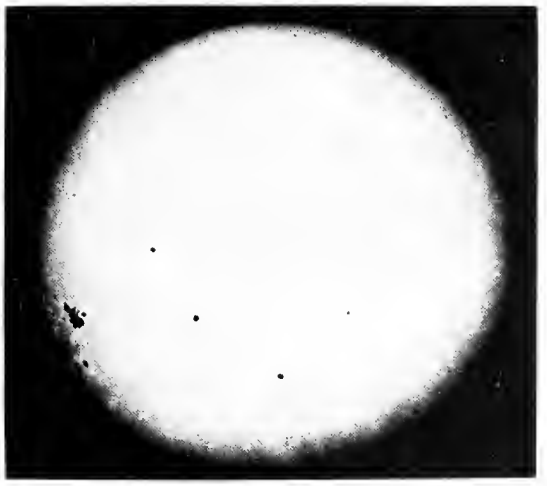

Figure 1. Photograph of the solar photosphere in white light

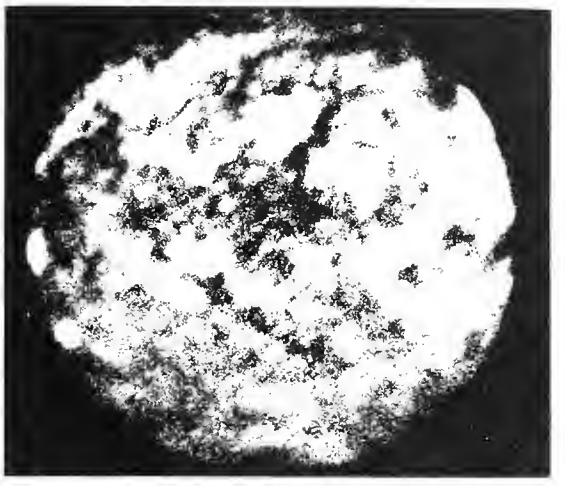

Figure 2. Photograph of the solar chromosphere in Lyman alpha radiation showing plage structure

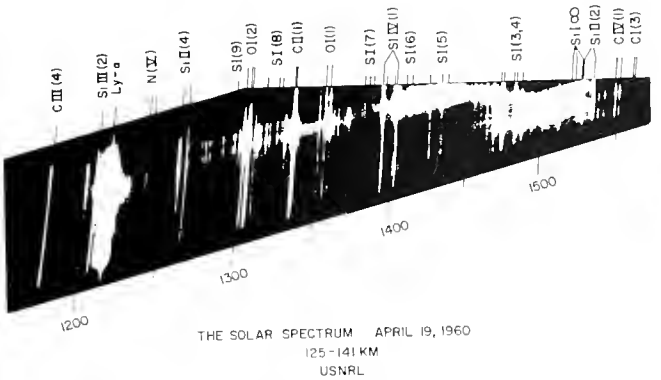

Figure 3. Solar spectrum 1170 - 1550 A showing plage structure in chromospheric lines

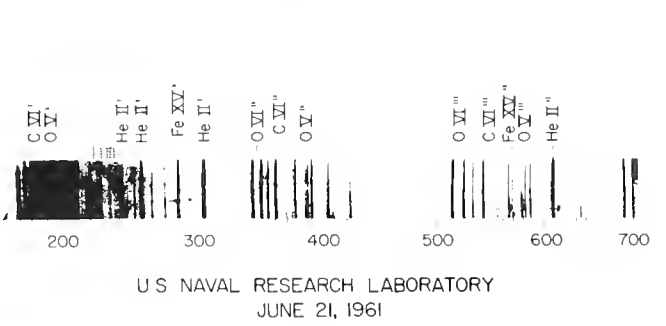

Figure 4. Far ultraviolet solar spectrum

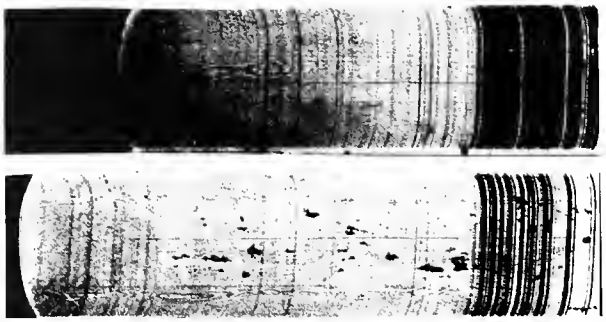

Figure 5. Solar spectrum 44-200 A, with intense unidentified lines near 170 A (right) and showing line structure in the x-ray region (left)

Figure 6. Solar spectrum in the 1025-1035 A region, showing (left) intense Lyman beta line with little limb brightening, and (center) O^{VI} lines with intense brightening

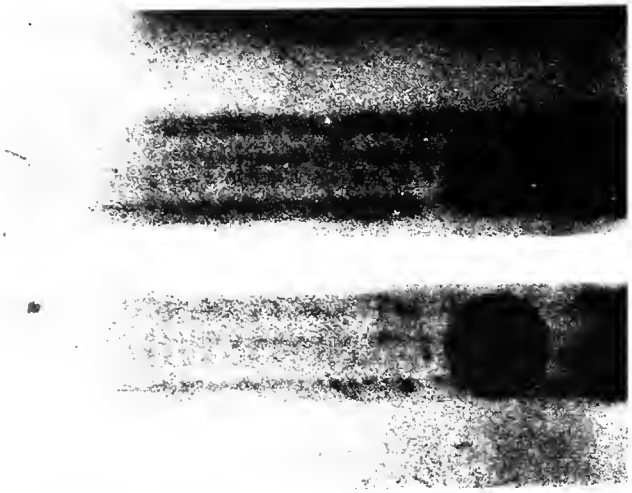

Figure 7. Solar x-ray disk images near 304 A showing (right) He^{II} with both disk and plage emission, and (center) Fe^{XV} with almost entirely plage emission

when observed below 1600 A shows plages indicating that plage regions extend downward to the photosphere. The emission line spectrum is characteristic of a region in which temperature increases with altitude, despite the upward flow of solar radiant heat. The dominance of line emission in the solar spectrum below 1400 A is present at shorter wavelengths at least down to 12 A. Of great importance are the Lyman alpha and beta lines at 1216 and 1025 A, helium radiations at 584 and 304 A, Fe XV and Fe XVI radiations near 304 A (Figure 4), a major group of unidentified lines near 170 A and emissions in the x-ray region below 60 A (Figure 5).

Solar emission lines do not all have the same characteristics. Some lines, for example, show strong limb brightening, others have a brightness at the limb almost equal to their brightness at the center of the disk. The O^{VI} lines at about 1030 A^{O} are examples of lines showing strong limb brightening (Figure 6).

Another manner in which the solar emission lines differ is in their relative brightness in plage regions as compared to their brightness in non-plage regions. Examples of lines showing considerable disk emission are the Lyman alpha and beta lines and the 584 and 304 A helium lines. In contrast the Fe^{XV} and Fe^{XVI} lines come exclusively or almost exclusively from plage regions. The presence of lines with considerable disk emission existing in the spectral neighborhood of lines coming almost entirely from plages is encountered even in the x-ray region of the spectrum below 25 A. However, the tendency for spectral lines to come predominantly from plages increases as one looks to shorter wavelengths (Figure 7).

The ratio of plage emission is probably a good measure of the time variability of emission lines. Lines with strong disk emission, such as Lyman alpha, are only slightly affected by solar activity. The variability of Lyman alpha is too small to be of geophysical significance. At shorter wavelengths Newpert and Behring find most of the lines between 170 and 400 A^{O} show intensity variability within the range of a factor 1.25 to 1.50, as observed during the flight of OSO A. In contrast the Fe^{XV} and Fe^{XVI} lines show variability of a factor of over 3 during the same time interval. The high variability of solar x-ray emission has been known for some years. Intensity fluctuations of a factor of 5 have been encountered at 50 A^{O}. At shorter wavelengths very much larger fluctuations, both as regards solar cycle changes and during solar activity events are encountered (Figures 8 and 9).

The most intensely variable portion of the solar spectrum (other than radio waves) is the high energy portion of the spectrum below 6 A. There is some evidence that iron line radiation in the neighborhood of 1.5 A shows rapid fluctuations, being present only during localized

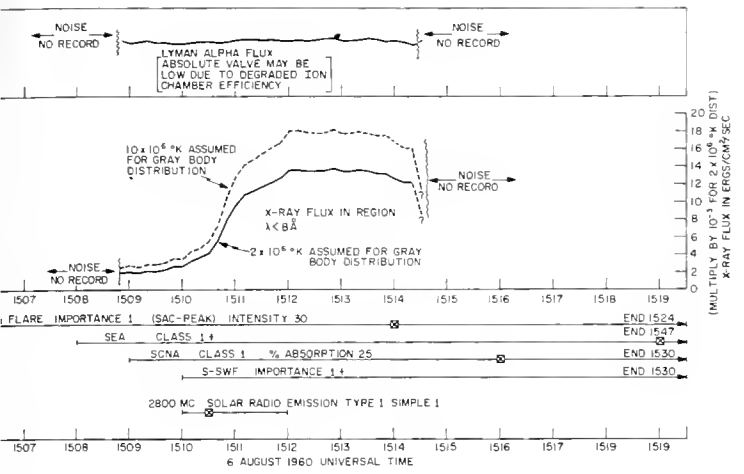

Figure 8. Lyman of alpha and x-ray flux during a limb flare

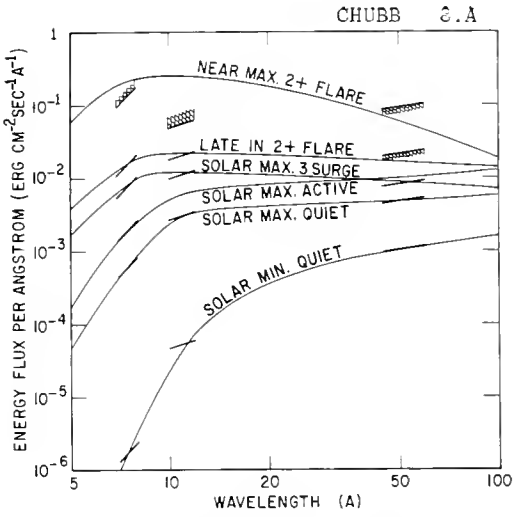

Figure 9. Solar cycle and solar flare variations in the soft x-ray region

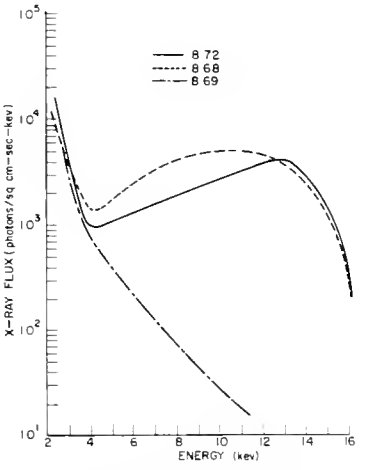

Figure 10. Comparison of spectra obtained from proportional counters in three flights in 1959

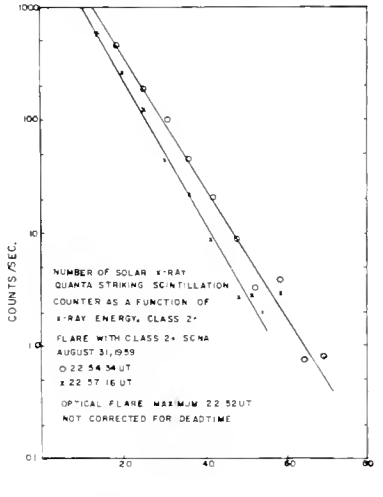

Figure 11. Solar spectrum in class 2^+ flare below 0.5 A, showing bremmstrahlung emission with about 120 x 10^6 deg K temperature

activity events on the sun (Figure 10). Such radiation probably plays the dominant role in SKD events, in which increased low D-region ionization is made evident by absorption of radio wave energy. In the most intense solar events, such as class 2+ flares in 1959 indicated that during the flare there existed plasmas on the sun at temperatures of 1 to 2 x 10^8 deg K (Figure 11). The total energy emitted in the spectral band below 0.5 A, however, was quite small, being several orders of magnitude less that emission in the 1-8 A region.

It is clear that a total picture of solar emission can only be obtained by continuous spectrophotometric monitoring of the sun. However, since it appears to be possible to classify all the varying solar lines in terms of their plage to disk brightnesses and their time variability, an alternate simpler system at solar monitoring seems worth while. It is possible to establish a set of solar activity indices by monitoring the radiation output of the sun over several x-ray bands where solar emission can be easily measured and where the emission shows greatest variability. Emission in such x-ray bands can serve not only to classify solar activity indices, but also to directly measure the ionizing fluxes which penetrate into the lower ionosphere. From continuous knowledge of such x-ray activity indices and from occasional spectrophotometric measurements over the whole spectrum the relationship between the intensity of individual emission lines and x-ray activity indices can be determined. With this knowledge, measurement of x-ray activity indices alone should give adequate spectral information to permit interpretation of Aeronomic measurements.

It is the hope that solar x-ray activity index information will be eventually available from satellite monitors on a continuous time basis. Once such a monitoring system is established, the main usefulness of radiation

Figure 12. Lyman alpha ion chamber

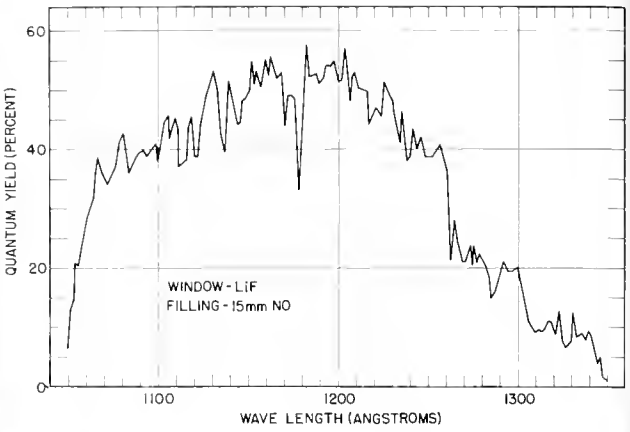

Figure 13. Spectral sensitivity of Lyman alpha ion chamber

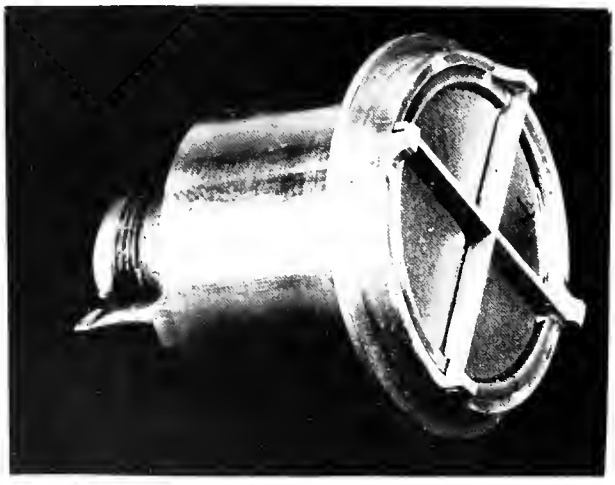

Figure 14. Typical x-ray ion chamber

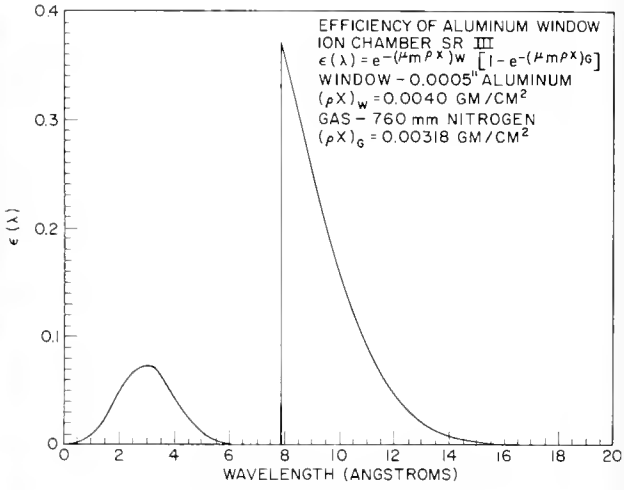

Figure 15. Efficiency curve for aluminum window ion chamber

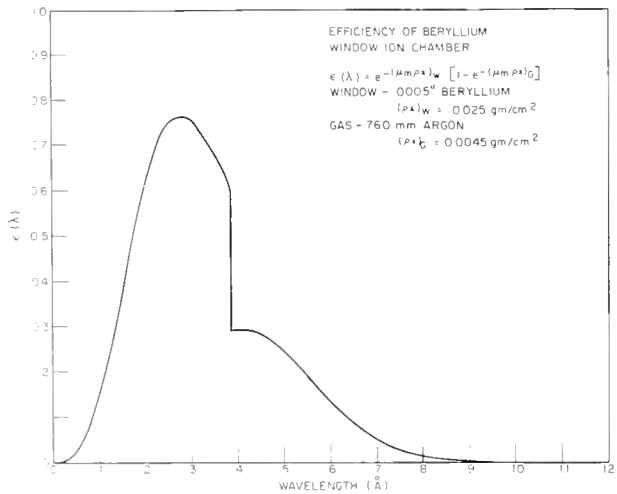

Figure 16. Efficiency curve for beryllium window ion chamber

monitors in aeronomy probes will be that of locating the rocket vehicle as regards the absorbing air mass between the rocket and the sun. The importance of this function should not be underestimated, however.

Some x-ray and ultraviolet detectors that have been used in monitoring solar radiation from small vehicles are illustrated in Figures 12 through 16. Also important, especially for studies directed toward SID events and solar events are the use of proportional and scintillation counters and counter spectrometers.

DISCUSSION

R.L.F. Boyd: The combined groups of the University College of London and the University of Leicester have been using two techniques which have not been widely used elsewhere in solar radiation measurements. One uses emulsion

detectors, with several different foils recovered afterwards and analysed to get spectral intensities and spectral slopes for the x-ray retion of solar radiation. The second technique uses proportional counters with kick-sorters in the softer range. I will show some results obtained by these techniques describing x-ray intensites through the solar cycle.

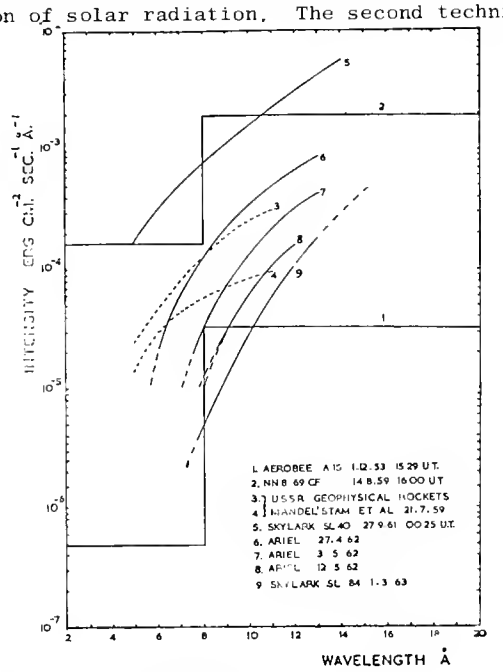

Figure A. A comparison of quiet-sun x-ray measurements

The curves in Figure A were obtained over a period of 3 years, the top one was made in 1961 while the bottom one was made in March, 1963. These curves show a progressive lowering in x-ray intensity. The block points represent results from NRL obtained by using the solar detector technique instead of proportional counters. The dotted lines are results from USSR rocket measurements, and I think the difference in slope may probably be accounted for by the fact that they used atmospheric absorption technique to get the spectral distribution. These results show the very definite fall in the intensity of x-ray radiation through the solar cycle.

We have also analysed about 20 solar flare spectra. These show a sudden rise of x-ray radiation about 20 minutes after the onset of the flare. Comparing with ionospheric effects, the 18 kc/s phase shift which indicates the effect of the flare at about 70 km, and a Doppler shift measurement which shows the effect of the flare at about 100 km, one notices detailed correlation with the way in which the flare spectrum itself has changed.

S. M. YEN
Aeronautical and Astronautical
Engineering Department,
University of Illinois
Urbana, Illinois

1. Introduction

It is essential to know the nature of instrument environment-interaction in measuring the structural parameters of the atmosphere by means of a rocket. In the first place, the relationship between the ambient parameters and the measured quantities have to be established by solving the transient interaction problem during the flight of a rocket. Secondly, a criterion should be established in locating the instrument so that the interference with reliable measurement by the flow conditions is as small as possible. Because of the high altitudes and high velocities reached by the rocket, the flow field resulting from the interaction covers the entire range of flow regimes as classified by aerodynamicists; therefore the above mentioned problems may be as complicated as the reentry problem of a space vehicle.

2. Flow Regimes

The flow field around a rocket moving at a supersonic speed can be divided into five parts: (1) free stream, (2) shock wave, (3) inviscid flow behind the shock wave, (4) viscous layer next to the surface, and (5) wake. In each part of the flow, theoretical and experimental techniques and correlation formulas used to evaluate the flow characteristics are different and these techniques have also been found to be applicable only over a certain range of flight conditions. Aerodynamicists have thus found it necessary to classify the flow regimes according to dimensionless parameters like Mach number, Reynolds number, and Knudsen number in attacking a flow problem around a body of a given size and configuration.

It has been proposed that the flow regimes be divided according to degree of departure from local thermodynamic equilibrium measured by Knudsen number (Kn) which is defined as the ratio of mean free path to a characteristic flow length. The following two limiting regimes can be established: (1) Continuum regime ($Kn \ll 1$), where the density is so high that intermolecular collisions dominate over collisions with the boundaries, and (2) Free molecule regime ($Kn \gg 1$), where the collisions with the boundaries dominate. There is a wide class of flow classifications between these two limiting regimes. The flow is considered to be rarefied with K_n of order one or greater. The concept of Knudsen number must be applied in context in connection with the particular characterisitic scale used and the phenomena of interest. For example, if a structure of shock wave is investigated, a local Knudsen number should be defined as a measure of steepness of local gradient and the flow in the shock wave should be considered rarefied. Since the departure from thermodynamic equilibrium in each part of the flow field is different, different flow regimes may exist around a given body configuration for a given set of free stream conditions. As discussed in detail by Grad [1], even in the case

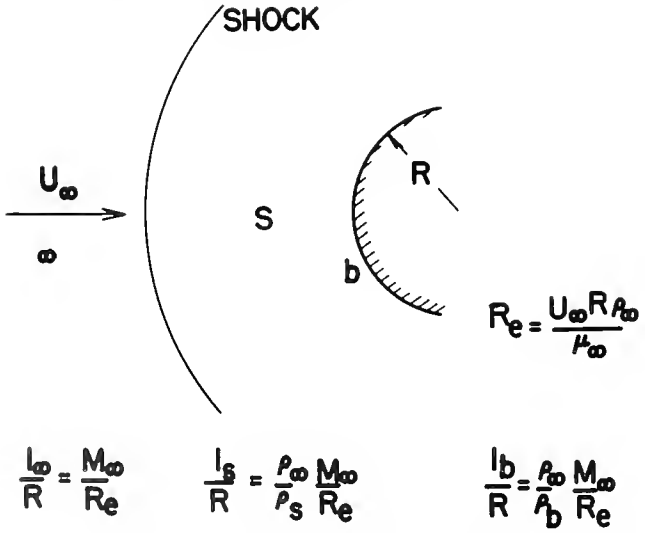

Figure 1. Mean free path in a flow field near the stagnation region of a blunt body.

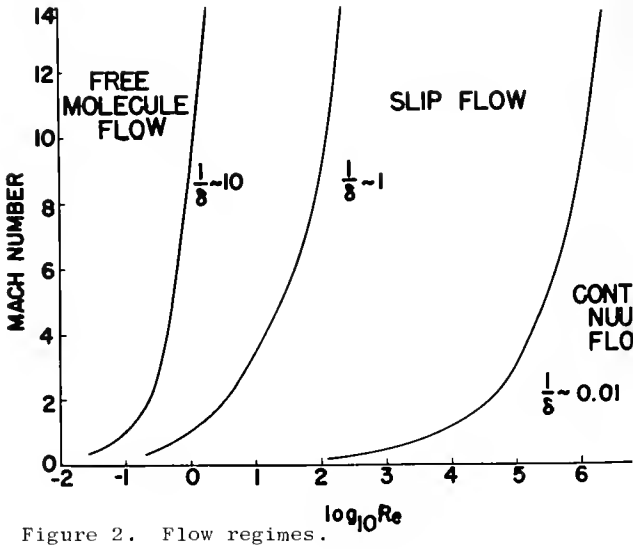

Figure 2. Flow regimes.

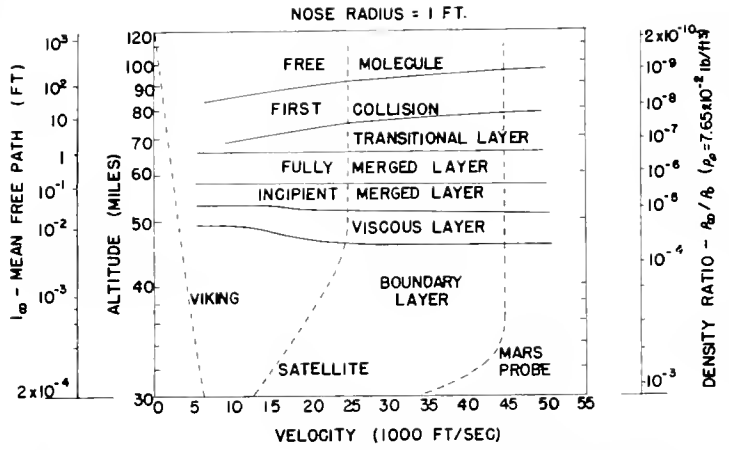

Figure 3. Flow regimes - Stagnation region of a highly cooled blunt body flying at hypersonic speed.

when free molecule flow is expected to exist next to the surface of a body, continuum flow prevails at a large distance and a complex transitional region is present in between. That is to say, the detached shock even exists in the free molecule flow provided that we look for it far from the body. At a distance comparable to mean free path, the emerging stream from the surface of the body will begin to encounter an incident flow and both will be altered. The emerging stream will be deflected back and eventually join the main stream while shielding the body from the incident stream which is deflected from the body.

It has been common to compare the characteristic length with the mean free path of the free stream in evaluating Knudsen number. This is not satisfactory as the mean free path can change appreciably in the flow field. The compression of the gas across a shock wave increases the local density appreciably and the mean free path behind the shock and at the body is appreciably smaller than its free stream value. Figure 1 shows schematically such variation of mean free path in the flow field near the stagnation of a blunt body.

The rarefied flow regime may be divided into the following regions: (1) free molecule flow: Kn = 10, (2) transition flow: kn = 0.1-10, (3) slip flow: Kn = 0.01 - 0.1. Slip flow is the region in which velocity and temperature jump occur at the surface. Tsien [2] defined the Knudsen number as the ratio of mean free path and boundary layer thickness and expressed the Knudsen number as a function of Mach number and Reynolds number so as to define the above mentioned flow regimes. The results are shown in Figure 2; however, the use of boundary layer thickness as the characteristic length is not satisfactory, since it is a high Reynolds number quantity [3, 4]. The necessity of a more refined study in defining flow regimes for a particular portion of flow field around a given body for given flight conditions was illustrated by Probstein [5] in his investigation of stagnation region for a highly cooled body at hypersonic speed. His results are shown in Figure 3 which indicates the boundaries of delimiting the important flow regimes for nose radius of 1 ft. The trajectory of satellite and that of a sounding rocket are also plotted in that figure.

The flow regimes classified in Figure 3 are briefly described as follows:

(1) Free Molecule

The mean free path of incident-emitted molecules is used to define the characteristic Knudsen number.

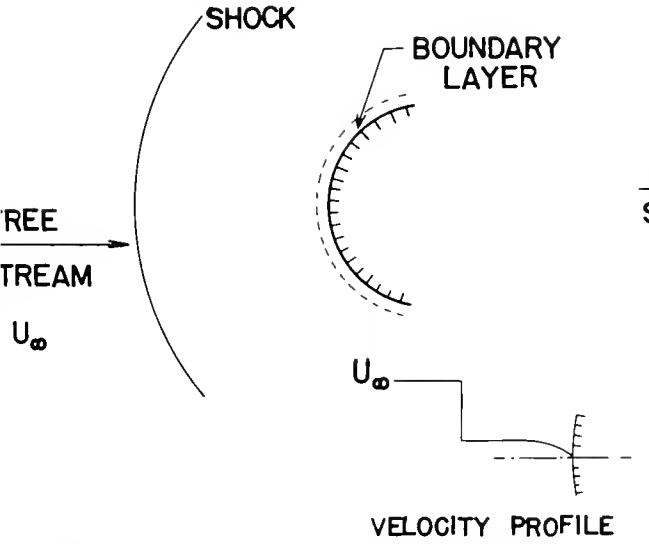

Figure 4. Flow regime - Boundary layer.

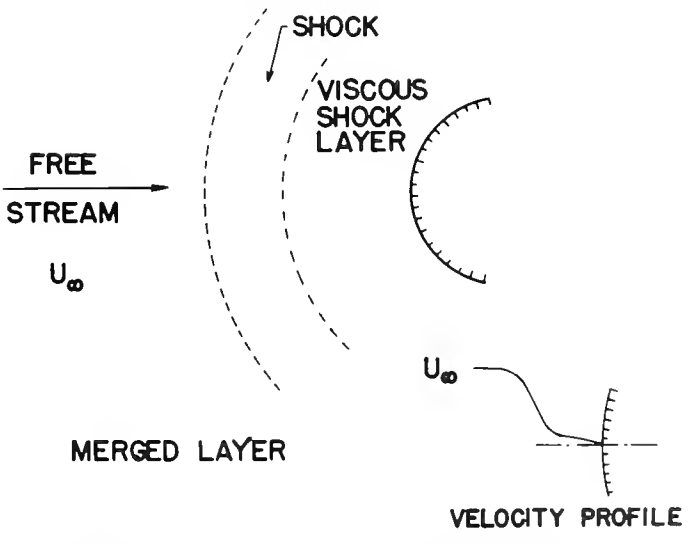

Figure 5. Flow regime - Viscous layer.

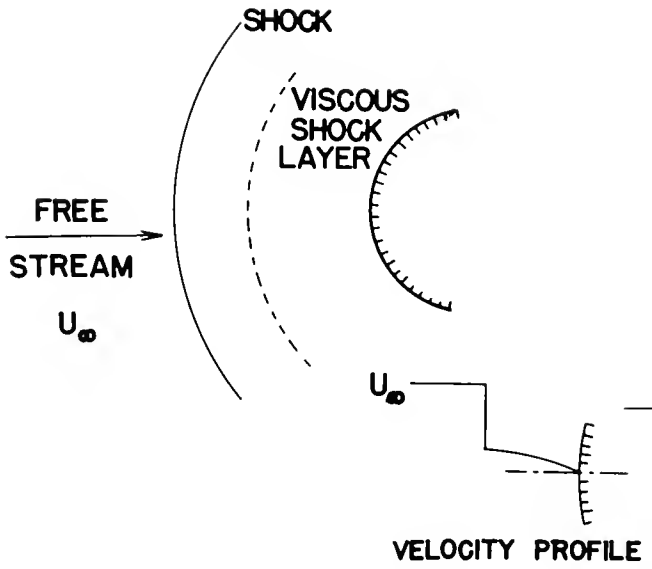

Figure 6. Flow regime - Merged layer.

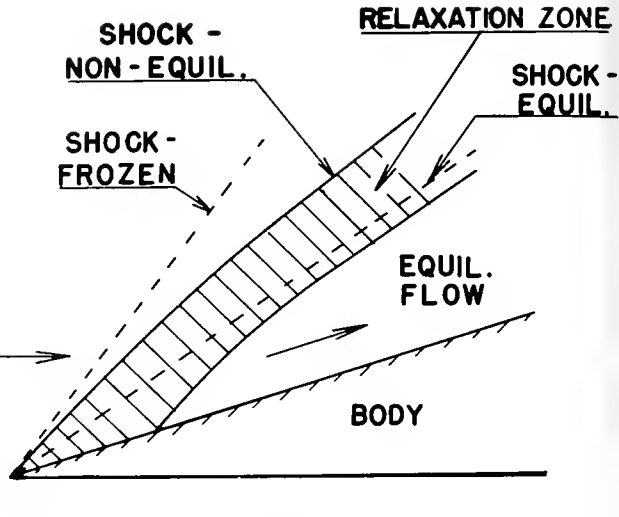

Figure 8. Non-equilibrium effects through an oblique shock wave.

The limiting Knudsen number is taken to be 10.

(2) Near Free Molecule

Free molecule solutions are to be modified by using a first-collision scheme. The analysis based on the consideration of only the collisions between reflected molecules (from the body surface) and incident molecules has been made.

(3) Transitional Region

Departure from thermodynamic equilibrium is so considerable that a full microscopic treatment of the flow problem by using Boltzmann's equation is necessary.

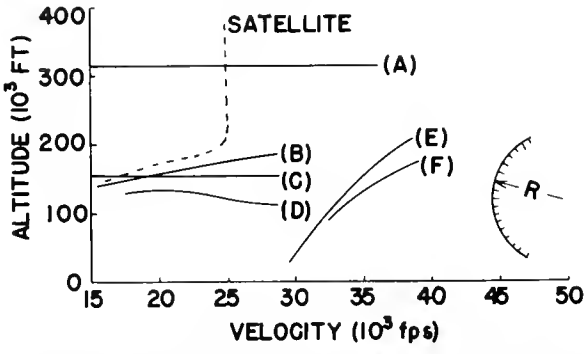

(A) MAX. ALTITUDE FOR CONTINUUM FLOW (R = 1FT)
(B) MAX. ALTITUDE FOR EQUIL. SHOCK LAYER (R = 1FT)
(C) DEPARTURE FROM THIN BOUNDARY LAYER (R = 1FT)
(D) MAXIMUM ALTITUDE FOR EQUIL. BOUNDARY LAYER (R=1ft)
(E) IONIZATION AFFECTING TRANSPORT PROPERTIES
(F) RADIATION LOSS AFFECTING FLOW FIELD

Figure 7. Boundaries delimiting some of the important domains in the continuum regime - stagnation region of a blunt body.

(4) Continuum Flow Regimes

(a) Boundary Layer

Reynolds numbers are high enough so that thin boundary layer concept holds for the viscous layer. For flow of lower Reynolds number some second-order effects have to be included in the analysis (Figure 4).

(b) Viscous Layer

Thin boundary layer concept is no longer applicable and the boundary layer thickens. The treatment with the complete Navier-Stokes equation is necessary. Shock wave is still thin (Figure 5).

(c) Incipient Merged Layer

The shock wave is thin but cannot be considered as discontinuous.

(d) Fully Merged Layer

Shock layer is almost in a continuum state. Shock wave is beginning to have a thickness approaching that of the body radius but is still smaller than it (Figure 6).

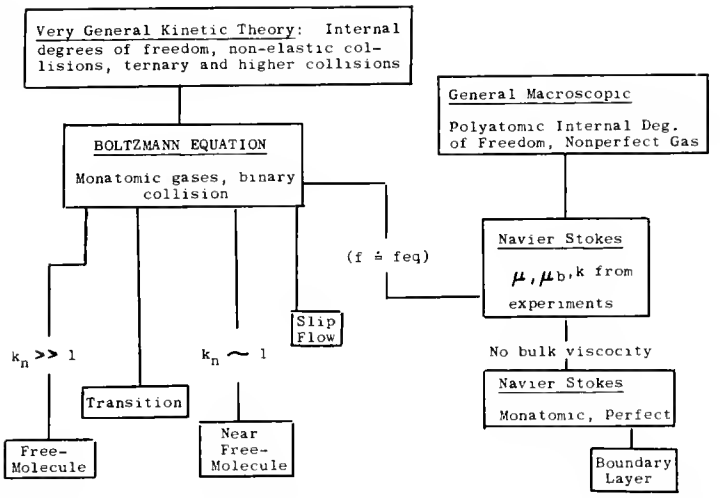

Figure 9. Block diagram of the fundamental equations and their assumptions for some flow regimes.

The criterion of determining those regimes are also discussed in detail by Probstein in other references [4, 6].

As seen from Figure 3, the transitional region is quite narrow, the lack of knowledge in that region is perhaps not serious for that problem. The plot of boundaries of flow regimes will be different for other flow conditions and body configuration. For nose radius greater than 1 ft., the boundaries in Figure 3 would move up.

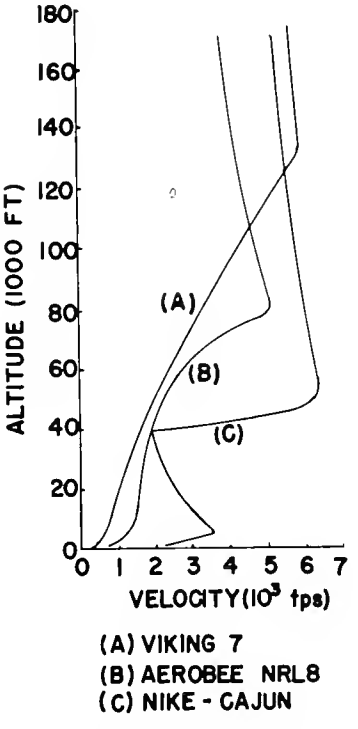

Figure 10. Typical flight trajectories of sounding rockets.

3. Theoretical Methods and Experimental Research

Kinetic theory provides a general formulation in which systems that depart considerably from states of local thermodynamic equilibrium can be studied; it has therefore been proposed to use the Boltzmann equation as the basic equation of gas-dynamics in the rarefied region. Some progress has been made in finding approximate solutions of the Boltzmann equation for certain simple problems.

Figure 9 is a block diagram showing some important flow regimes and the microscopic and macroscopic basic equations and the assumptions that are commonly used in analyzing flow problems in these regimes. In the continuum regime, even though Navier-Stokes equations are applicable and theoretical research has been carried out for many years solutions have been obtained only for a small number of problems, and some of them are strictly speaking applicable only to monatomic and perfect gases.

Thin boundary layer concept is valid only for flow of high Reynolds number. The boundary layer equations derived from the Navier-Stokes equations on the basis of that flow condition are still non-linear and it has not been found possible to obtain solutions that are valid for boundary layer over an arbitrary surface.

In the rarefied regime, there is a need of the development of approximate methods of finding solutions of the Boltzmann equations for flow in the transitional region, even for the case of monatomic gas. It is to be emphasized that only some simple functions of the low-order moments of the velocity distribution function are needed in flow field studies, since these functions are sufficient to determine the macroscopic flow variables of physical interest; therefore we need to find only an approximate distribution function accurate enough to determine those simple functions. Krook [7] has proposed the translation of a microscopic form of rarefied flow problem to an approximately equivalent continuum form by using the moment equations and the attack of the mathematically simpler continuum problem. The applicability of the Navier-Stokes solutions to part of the transitional regime has been investigated for certain problems (e.g. the strong shock wave) by comparing them with the approximate solutions of the Boltzmann equation. Recent advances in rarefied gas dynamics are given in references 8 and 9.

The present knowledge of flow problems is by no means complete in all flow regimes so that characteristics in the flow field in the vicinity of a body can be evaluated for all the conditions encountered during its flight. Even in the continuum regime many important effects due to flight at high speed and high altitude such as

those of non-equilibrium flow and those of ionization are yet to be completely evaluated for many important problems. Recent advances in such research have been reviewed by Cheng [10]. Figure 7 illustrates the important domains where the chemical or physical processes may arise in the stagnation region of a blunt body. For other configurations and sizes of the body, a similar plot may be made. The boundaries in Figure 7 define the limits in which some mathematical techniques can be used in certain regions (e.g. boundary layer technique) and non-equilibrium effects do not have to be taken into consideration (for both boundary layer and shock layer). Radiation and ionization effects are also shown. The following brief review on some significant theoretical methods and experimental research are divided into two parts: Equilibrium flow and non-equilibrium effects.

(1) Equilibrium Flow: Theoretical and experimental investigations of a flow field have been made on different parts of the flow field. The important subjects of research are: (1) inviscid flow, (2) boundary layer and viscous layer, (3) separated flows, (4) low density flow.

Techniques have been developed to calculate the supersonic portion of the inviscid flow field for an arbitrary body, the problem is to evaluate the subsonic and transonic region of blunt bodies and the supersonic conical flow field near the apex of pointed bodies.

Both experimental and theoretical studies have been made on the following problems of boundary layer for flow of high free stream Mach numbers: (1) displacement effect, (2) effect of yaw and nose bluntness, (3) transition of laminar to turbulent flow. Theories have been developed for viscous layers (merged layer) in the stagnation region of a blunt body. Some experimental data are obtained in the viscous layer for the case of low Mach number.

In the case of free molecule flow the accurate calculations of flow variables depends on the knowledge of the interaction between the gas particles and the surface. There is a lack of knowledge of basic information on the interaction for gas particles of suitable speed and for ionized particles. For example, the atmospheric density derived from satellite deceleration data is not considered to be precise because of the uncertainty in the values of surface accommodation coefficients.

The study of shock wave structure as a means of studying flow characteristics in the transitional regime has been mentioned earlier. The experimental results obtained have been limited to temperature profiles and shock wave thickness and those results are not adequate to assess the accuracy of the theoretical methods developed.

The methods are used to study the low density effects on viscous flow region: (1) modification of boundary layer to accout for high order effects, (2) use of full Navier-Stokes equations. Experimental data on heat transfer have been obtained in the stagnation region of a blunt body.

(2) Non-Equilibrium Effects: The non-equilibrium effects are schematically represented in Figure 9 [11] for a flow field with an oblique shock wave. The relative shock position corresponding to equilibrium, frozen, and non-equilibrium situation and the existence of a relaxation zone are shown. Even though that figure is based on a simplified picture of chemical kinetics, it nevertheless shows the importance of studying non-equilibrium effects.

Numerical solutions for the relaxation behind a normal shock have been obtained. Since the times required for vibrational and chemical equations are much longer than for translational and rotational relaxation that the shock has been considered to take place in two steps: translation-rotation shock and vibration and chemical adjustment zone. The extension of studying non-equilibrium flow field to the case with completed chemical reactions have been made. The relaxation during expansion around blunt bodies is of importance in the study of flow chemistry over after-bodies and in wakes.

One major difficulty in studying non-equilibrium flow chemistry is the uncertainty that arises from the extrapolation of experimental data on constants of reaction rates to high temperatures and low densities. Data on dissociation are obtained under conditions where considerable vibrational excitation has occurred.

Because of the importance of heat transfer in the stagnation region, non-equilibrium flow in the boundary layer has been investigated to a great extent for the case of stagnation region; however, work has also been done on flat plate.

As the gas rarefaction increases, the effect of non-equilibrium dissociation in the outer flow (outside of boundary layer) on the flow in the boundary layer is to be considered. In the stagnation region behind a shock wave, the degree of internal-mode or chemical change is to be ascertained.

4. Concluding Remarks

(1) The flow field in the vicinity of a sounding probe resulting from the interaction with the atmosphere varies with the position on its trajectory and includes all flow regimes - from continuum to free molecule.

(2) In each part of the flow field and each flow regime, the theoretical and experimental technique used to investigate the flow

field are different. Theoretical solutions and experimental results on important flow characteristics have been obtained for a certain part of the flow field in some flow regimes, and knowledge of flow characteristics in other flow regions are not completely known for all flow conditions encountered.

(3) A plot of boundaries delimiting pertinent flow regimes, similar to Figure 3, should be made for a sounding probe during its trajectory. (Some typical trajectories for sounding rockets are shown in Figure 10). To prepare such plot, study should be made of the part of the flow field of interest resulting from the interaction with the ambient atmosphere taking into the flow conditions encountered during the entire trajectory. The difficulty seems to be that it is necessary to know also some environment conditions of the atmosphere to be measured.

(4) The plot prepared can be used as a guide to select the proper method of interpreting the in-flight test data to determine the optimum location of installing instruments for reliable measurement during a flight, and to design the configuration of the sounding rocket.

References

[1] Grad, H., "Equations of Flow in a Rarefied Atmosphere", AEC Research and Development Report, AEC Computing and Applied Mathematics Center, New York University, NYO-2543, June 1959.

[2] Tsien, H. S., "Superaerodynamics, Mechanics of Rarefied Gases", J. Aero. Sci., Vol. 13, 1946, pp. 653-664.

[3] Liepmann, H.W. and Roshko, A., "Elements of Gasdynamics", John Wiley and Sons, 1956.

[4] Probstein, R.F., "Aerodynamics of Rarefied Gases", Rarefied Gas Dynamics, Pergamon Press, 1960, p. 258.

[5] Probstein, R.F., "Shock Wave and Flow Field Development in Hypersonic Re-entry", ARS J. Vol. 31, 185-194, 1961.

[6] Hayes, W.D. and Probstein, R.F., "Hypersonic Flow Theory", Academic Press, 1959.

[7] Krook, Max, "Continuum Equations in the Dynamics of Rarefied Gases", J. Fluid Mech., Vol. 6, part 4, pp. 523-541, 1959.

[8] Devienne, F.M. (ed), "Rarefied Gas Dynamics", Pergamon Press, 1960.

[9] Talbot, L. (ed), "Rarefied Gas Dynamics", Academic Press, 1961.

[10] Cheng, H.K., "Recent Advances in Hypersonic Flow Research", AIAA Journal, Vol. 1, No. 2, February 1963, pp. 295-310.

[11] Campbell, W.F. and Meyer, R.F., "Hypersonics, Part II", DME/NAE Quarterly Bulletin No. 1961 (4), National Research Council of Canada.

SYMBOLS

f	distribution function
Kn	Knudsen number
l	mean free path
M	Mach number
R	Radius
Re	Reynolds number
U	Velocity
ρ	density
μ	coefficient of viscosity
μ_b	coefficient of bulk viscosity

Subscripts

b	body surface
eq.	equilibrium
s	shock layer
∞	free stream

DISCUSSION

R.L.F. Boyd: Dr. Yen has pointed out that the important parameter in many of these problems in the Knudsen number which is the mean free path (λ) divided by some characterisitc dimension (L); but there is another parameter which is important when one is concerned with making observations in the ionosphere and studying the ionization; that is what I might call the Debye number, the Debye length (λ_D) divided by some characteristic dimension (L) because it is the Debye length which determins the characteristic of the plasma flow.

I have a diagram which shows the effect of the Debye length in making some measurements on

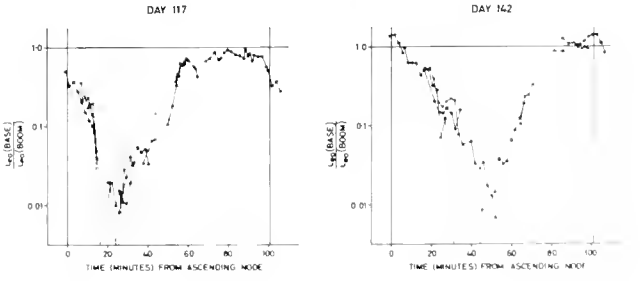

the satellite Ariel. As I mentioned earlier we had two probes which measured electron density and temperature, one of them on the end of a boom, the other on the base of the satellite itself, while the one on the end of the boom was mounted on a small body for which γ is roughly unity and the one on the base of the satellite for which γ was of the order of 10 or so. By studying the behavior of these two probes when either going forward or backward, one gets some idea whether there is any ram effect, or whether there is any depletion caused in the ionization by the body moving at hypersonic velocities.

The figure shows the ratio of the current to the probe in the base at space potential, to the current at space potential to the probe on the boom, versus time throughout a number of orbits. At one point the current at the base probe has fallen to less than 1% of the current to the probe on the boom; at this time the base of the satellite is in the rear of the motion, and there is a very strong depletion in the ionization. On the other hand, when the probe on the base of the satellite is moving forward and the probe on the end of the boom is facing backwards, both probes give effectively the same current within the limits of experimental error.

This shows that for a body comparable in size to the Debye length moving through ionization at hypersonic velocity, it gives neither a ram effect nor a depletion behind. However, for a body for which the Debye number is of the order of 0.1 there is still no ram effect, but a very significant depletion in the ionization due to the inability of the ions to get around rapidly enough behind the body.

S.M.Yen: We do not have too much knowledge in this area, but I can refer to the paper by Grad, "Equations of flow in a rarefied atmosphere" (reference 1), which takes into account the Debye length in its discussions.

R. Horowitz: In trying to calibrate a particular geometry in a wind tunnel for measurements in this region, is there any question about the scaling properties of a particular rocket configuration? Is this well enough known so one can essentially take a particular rocket geometry and adequately scale it to study the flow conditions in a wind tunnel?

S.M. Yen: The problem lies in producing the right environmental free-stream conditions because we do not have a means of producing the correct ionization density.

N.W. Spencer: This is a very important subject, particularly for those of you that are concerned with instrumentation for the D-region which falls in the transition region. Having been exposed to some of these problems through making structure measurements of right circular cones under these conditions, I am aware of the seriousness of the situation.

Dr. Yen's diagrams were for a condition where the velocity vector is fully aligned with the body. In the spherical case this is insignificant, but the other case was for an aligned wedge. Unfortunately, rockets do not behave entirely that way and it is only under the most unusual conditions that the angle of attack is zero for any length of time. Although the situation is complicated when the angle is zero, it is considerably more complicated, I am sure, than he can discuss when it departs from zero, and the case of a wedge when the angle exceeds the angle of the wedge it is almost hopeless to study theoretically.

This has some very important consequences in the D-region. The boundary layer imposes problems, because the properties of the ambient medium are not transmitted entirely through it. At least for neutrals, pressure is transmitted through the boundary layer under small angles of attack relatively undisturbed, but there is a temperature gradient and thus a density gradient. This means that for a Gerdien condenser where the measuring surfaces are behind the shock wave, the interpretation in terms of the ambient conditions becomes exceedingly complex.

There has been much work done with openings in the front ends of the cone, to further the pitostatic tube concept to lower densities, and this might be a fruitful source of information for those concerned with this problem.

S.M. Yen: The cone has received attention because it is geometrically rather simple, and the flow is constant along the geodesics. We need to know what happens to the flow when the cone is at a given angle of attack. Now for small angles I think the analysis can be carried out. Large angles pose two problems; one is the cross flow on top of a longitudinal flow, which creates a problem just like a cylinder. At a certain angle of attack at the wake, the boundary there will separate.

I personally am interested in this problem, particularly in the heat transfer characteristic. This involves what happens when the boundary layer of the flow has a cross-flow superposed on it. We will do more work in this direction especially in the hypersonic region, to try to handle the flow in between the shock wave and the cone as a one-layer problem. Another remark I would like to make, I think there was a problem yesterday concerned about a shock wave and a location of a local shock wave. If you have two bodies, and if you have a shock wave, and you have another body, regardless of how small this is, you have a shock wave and this will intersect. I think, as far as I can see, it will always be enclosed in the shock wave.

S.A. Bowhill: Concerning the possibility of measuring ion temperatures, what would be the effect on the energy distribution of the ions passing through the shock wave or the boundary layer? It is certainly true that for the neutral molecules the energy distribution is quite different as you go through the shock. Therefore it seems to me quite possible that the ionic energy distribution would also be quite different

S.M. Yen: Our boundary layer analysis could provide the velocity profile needed for such an analysis.

N.W. Spencer: Concerning the validity of drag measurements of satellites in the free molecule region; we made direct measurements of density and temperature with Explorer XVII. At the same time the satellite was tracked and therefore we have with us the same body for measurement of drag. These results are not ready yet, but they look favorable.

R. Prenalt: I have a question for Prof. Boyd. Was the little ball on the satellite so designed that it was altitude insensitive, and there should be no ram effect? And the fact that the ball and the satellite-mounted sensor gave the same results indicates that there is no ram effect on the satellite-mounted sensor.

R.L.F.Boyd: There are two points here. First, it was not a ball, it was roughly in the shape of a cylinder with about equal length and diameter; and the probe was on the plane end of it. If there had been a ram effect on the base probe, one would have expected to see the ratios invert, not just go to unity. One would expect to see the ratio become still greater than unity, and it never did so there is clearly no ram effect.

C.Y. Johnson: When the probe on the boom gets in the wake do you see a depletion?

R.L.F. Boyd: This I could not say because one needs to get things lined up rather exactly for this relatively large boom actually to pass through the wake. Even if it did, I am sure the depletion would be very much less than the depletion near the body, because it would be many Debye lengths away from the body.

10.1 POSITIVE ION COMPOSITION ABOVE WHITE SANDS, NEW MEXICO

J. C. HOLMES and J. M. YOUNG
E. O. Hulburt Center for Space Research
U. S. Naval Research Laboratory
Washington 25, D. C.

Two radio frequency positive ion mass spectrometers were flown on each of two Aerobee-150 rockets from White Sands Missile Range. The flights occurred at 0934 MST 15 February 1963 and 0106 MST 1 August 1963 and reached peak altitudes of 240 and 230 km respectively. The instruments were recovered after the first flight and were flown again on the second rocket. Thus, day and night measurements were made with the same identical instruments. The mass range covered on each flight by each spectrometer was from 12 to 35 AMU. Positive ions of masses 14, 16, 18, 24, 30 and 32 AMU were detected.

The mass spectrometers were mounted on opposite sides of the rocket so that ions entered perpendicular to the rocket axis. Two instruments were used so that the effect of the angle between the rocket trajectory and the mass spectrometer entrance direction could be more fully evaluated.

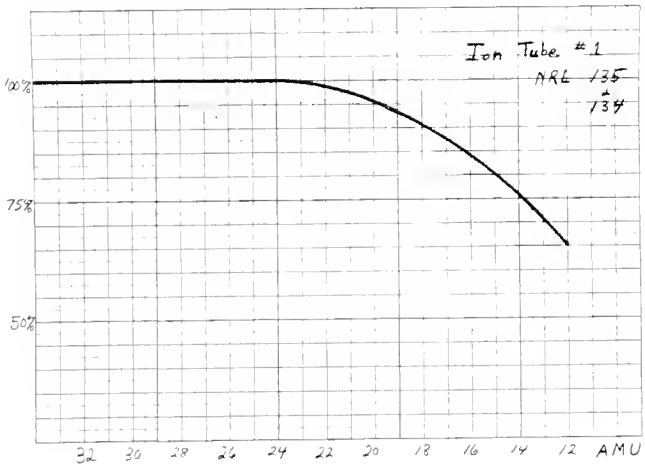

Figure 1. Sample mass calibration curve.

Bennet RF mass spectrometers, as is true with any mass spectrometer, must be laboratory calibrated so that the relative efficiency of the instrument versus mass number is known. Mass discrimination was found to occur in two general categories:

1. Change in effective stopping potential versus sweep voltage.

2. Overall focussing efficiency changes with sweep voltage.

These effects were evaluated with the resultant relative efficiency curve as shown in Figure 1. It cannot be overemphasized that such calibrations must be made if any meaning at all is to be attached to mass spectrometer measurements. The calibration curve, Figure 1, is not necessarily typical. Instruments used over wide ratios of mass number will probably show more discrimination. For this reason recent altitude results concerning the distribution of light ions should be re-evaluated in the light of a proper calibration.

With both instruments mounted on the side of our rocket, the vehicle was purposely de-spun after powered flight so that the ratio of tumble angular momentum to spin angular momentum would be favorable to a large free fall precession

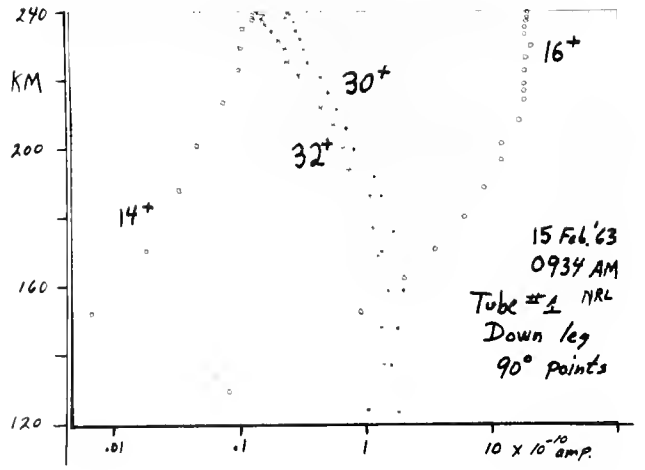

Figure 2. Currents for various masses at 90 deg angle of attack.

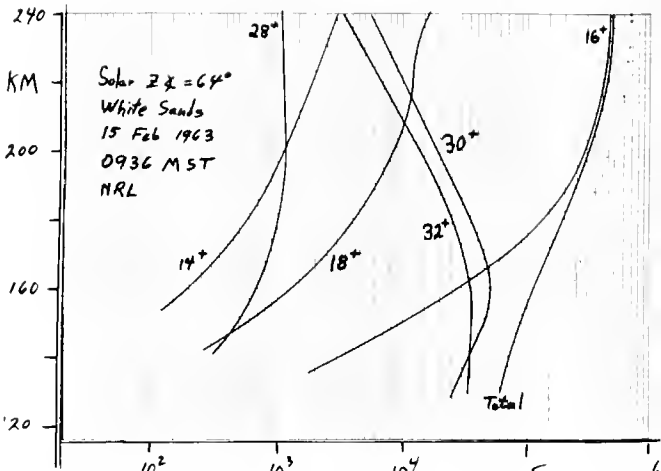

Figure 3. Daytime ion density profiles 0936 MST 15 February 1963.

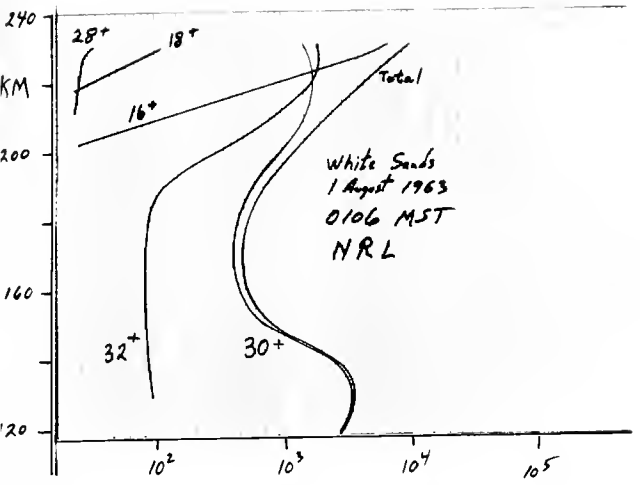

Figure 4. Nighttime ion density profiles 0106 MST 1 August 1963.

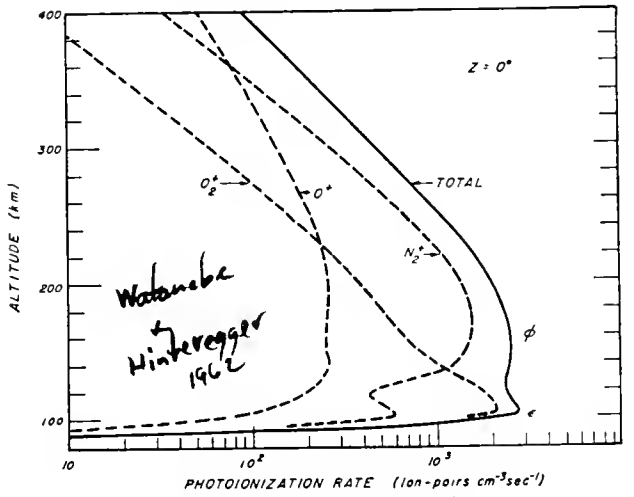

Figure 5. Photoionization rates (after Watanabe and Hinteregger).

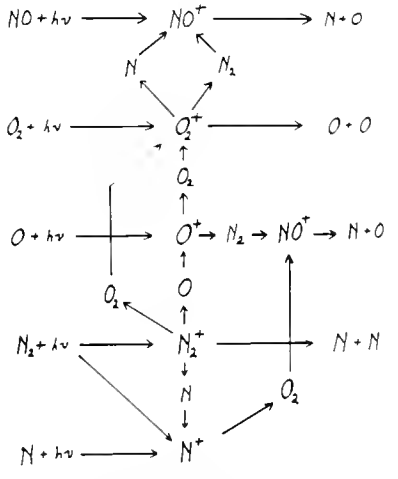

Figure 6. Ion chemistry in the E and F regions (after Nicolet and Swider).

cone with the resulting wide range of "trajectory-instrument" angles. The rocket spin "modulates" the collected ion currents, and this modulation must be evaluated in order to produce figures for ambient ion density. Smooth curves were drawn through the instantaneous values of collected ion current and a second set of curves were drawn through the 90° angle of attack points on the "modulated" curves. The resultant curves for each instrument were nearly identical. Figure 2 shows a set of 90° points through which the smooth curves in Figures 3 and 4 are drawn.

Figure 3 represents the daytime distribution of ionospheric ions. The abscissa, ion density, was converted from collected ion current to density by equating the total ion current measured at peak of flight to the total electron density value derived from ionosonde data taken during flight. This, of course, does not take into account the different diffusion rates for ions of different masses, and such corrections may be made at a later time. The total positive ion current, i.e., the sum of all measured ion currents is shown in Figure 3 and it compares favorably with the distribution of the ionosonde derived electron density which is shown displaced to the right of the "total" ion density curve. (The displacement shows the full electron density curve which would be obscured by the total ion curve had we drawn them coincident at peak altitude as is the actual case.)

Certain features of this daytime positive ion distribution should be noted.

1. 16^+ is by far the predominant ion above 180 kilometers.

2. 28^+ is present in small quantity at all altitudes.

3. 14^+ has a positive scale height (concentration gradient) throughout the altitude range covered.

4. 30^+ and 32^+ have constant (negative) scale heights above 180 km.

5. 30^+ concentrations are greater than 32^+ concentrations above 140 km and are less below 140 km.

6. 18^+ follows generally the shape of 16^+.

The night time distributions, Figure 4, plotted on the same abscissa, show:

1. 16^+ having decayed sharply at all altitudes.

2. 28^+ existing at a density of about 25 ions/cm^3 and having a positive scale height (concentration gradient $dn/dz>0$).

3. 30^+ and 32^+ having decayed below 180 km and having steep positive scale heights above 180 km.

4. A broad dip in the total ion concentration centered about 170 km.

5. A negative gradient for 30^+ below 150 km.

6. An 18^+ distribution again following 16^+.

These features suggest the following general descriptions of the atmosphere in the altitude range covered. We must first agree on certain phenomena which produce our ionosphere.

1. We shall use the Nier neutral atmosphere (Paper 10.2 at this conference).

2. The photoionization rates published by Hinteregger, Figure 5, as modified by the new neutral atmosphere are used.

3. We use the chemistry allowed by Nicolet and Swider, Figure 6.

It should be noted that $N^+ + O_2 \rightarrow NO^+$ is the only loss mechanism for N^+, which with the positive gradient for the N^+ daytime distribution suggests that the principal source of N^+ is direct photoionization of neutral N. The concentration of O_2 at high altitudes is very low (Nier atmosphere).

At 130 km in the daytime O_2^+ increases with decreasing altitude and NO^+ decreases. Because neutral N_2 has a large negative gradient in this region, the mechanism $O_2^+ + N_2 \rightarrow NO^+$ seems not to be very effective. The possibility of Lyman beta and other ultraviolet solar radiation being absorbed in this region (Figure 5) is attractive. O_2 is the only gas ionized by Lyman beta.

Because the only permitted loss mechanism for NO^+ is dissociative recombination, and because above 180 km $n(O^+) \approx n(e)$, and because in this region diffusion processes are much slower than the chemical production and low rages, the equating of NO^+ loss and production rates should be valid. The production of NO^+ seems to be predominantly

$$O^+ + N_2 \rightarrow NO^+ + N$$

$$\gamma_1 n(O^+) \cdot n(N_2) = \alpha_1 n(NO^+) \cdot n(e)$$

$$n(NO^+) = n(N_2) \frac{n(O^+)}{n(e)} \frac{\gamma_1}{\alpha_1}$$

$$n(NO^+) = \frac{\gamma_1}{\alpha_1} n(N_2)$$

where γ_1 and α_1 are the respective chemical reaction rate coefficients. Thus the density of NO^+ is anchored tightly to the neutral N_2 distribution, and the temperature of neutral N_2 thereby derived from this daytime ion data is 1609° K.

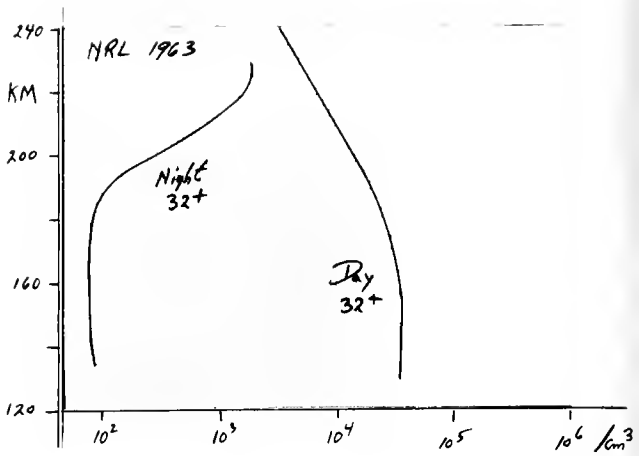

Figure 7. Day and night O_2^+ density profiles.

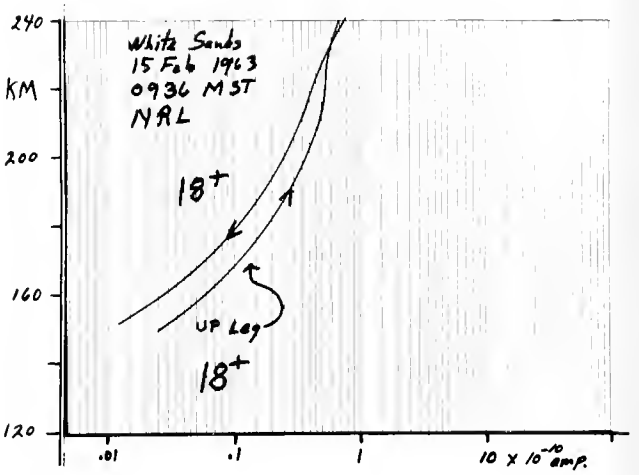

Figure 8. Up- and down-leg data for 18^+ ion.

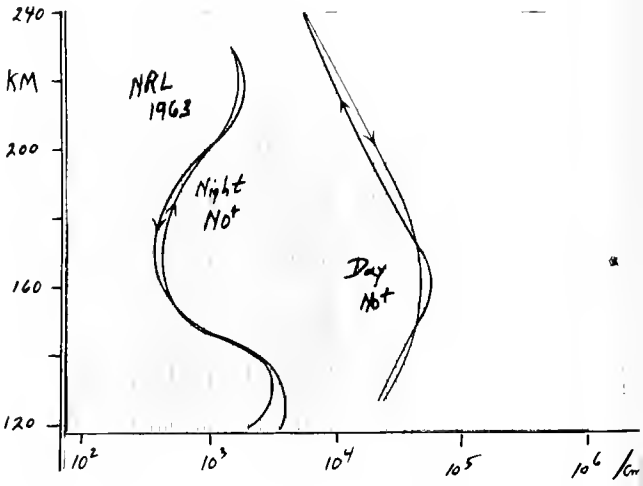

Figure 9. Up- and down-leg data for NO^+ ion.

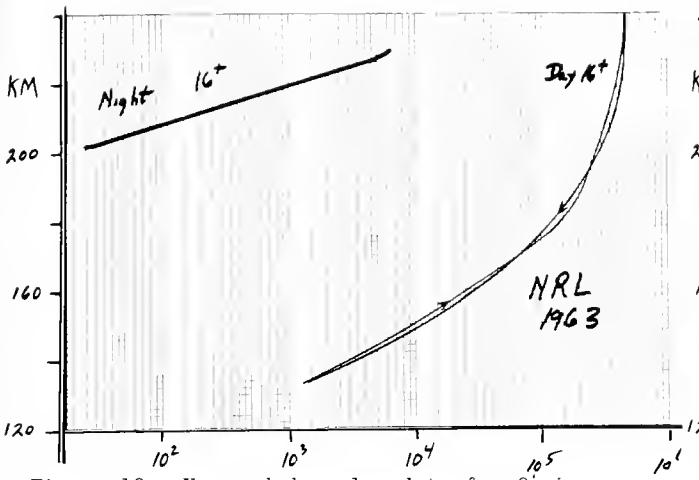

Figure 10. Up- and down-leg data for O^+ ion.

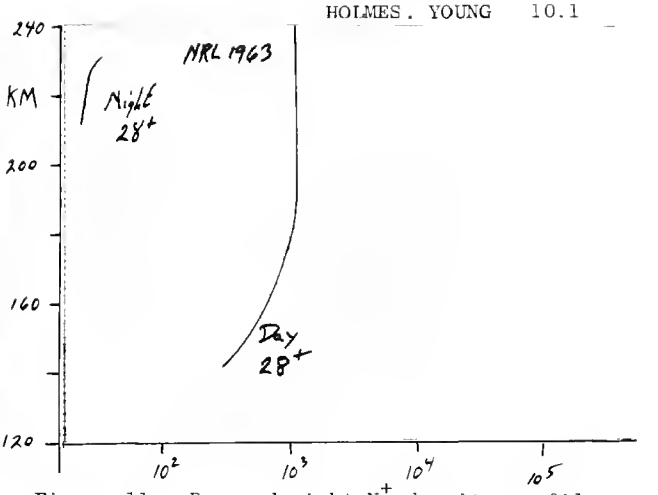

Figure 11. Day and night N_2^+ density profiles.

A similar argument is made for O_2^+ in the same altitude region, if we assume the photoionization is low:

$$\therefore \quad O^+ + O_2 \rightarrow O_2^+ + O \text{ (production)}$$

$$O_2^+ + e \rightarrow O + O$$

$$\gamma_2 n(O^+) n(O_2) = \alpha_2 n(O_2^+) n(e)$$

$n(O_2^+) = \frac{\gamma_2}{\alpha_2} n(O_2)$ and the distribution of O_2^+ is locked to the neutral O_2 scale height giving a derived temperature of O_2 of $1012^\circ K$.

The nighttime distribution of 16^+, 30^+ and 32^+ is evidence for the reations

$$O^+ + N_2 \rightarrow NO^+ + N$$

and

$$O^+ + O_2 \rightarrow O_2^+ + O$$

being very effective. The O^+ is supporting O_2^+ and NO^+ at night. The experimental data is the best experimental evidence to date for the existence of these ion-atom interchange reactions.

The positive slope of 16^+ at night suggests that diffusion is not very effective for 16^+ in this altitude region. Above 200 km O^+ is moving in its parent gas and the diffusion should be slow.

The nighttime distribution of 16^+ is very straight and suggests that the O_2 and N_2 scale height at night is constant in this altitude region.

The behavior of 30^+ at night is possibly explained by a NO^+ dissociative recombination coefficient which increases with temperature in the region 160 to 130 km.

The reduction in the densities of O_2^+ and NO^+ from day to night in the region of 150 km, assuming chemical processes only, result in values for α_{NO^+} and $\alpha_{O_2^+}$ of about $9 \times 10^{-8} cm^3/sec$. Figure 7 shows the day and night profiles for O_2^+.

The up- and down-leg daytime data on mass 18^+ is shown in Figure 8. The increasing difference between the values up and down intuitively suggests that 18^+ is a contaminant coming from neutral H_2O rocket outgassing.

$$H_2O + O^+ \rightarrow H_2O^+ + O$$

The nighttime up- and down-leg data show the same effect.

Up and down by curves for other masses are shown in Figures 8 and 9.

This good fit up and down is true for the other ions, with the exception of mass 18^+. We suggest that the other ions are truly ambient.

The daytime production rate of N_2^+ according to Watanabe and Hinteregger (using our modified neutral atmosphere) gives a very high value for the production rate figure of the order of 10^3 ions/cm^3sec, with most of the loss going to O^+ by $N_2^+ + O \rightarrow O^+$ if the dissociative recombination coefficient for N_2^+ is 10^{-7} cm^3/sec. At night N_2^+ should disappear almost instantly; in fact, there is some 28^+ at night (Figure 11). If there is some incoming nighttime radiation of 304 or 384 A, there would have to be about 10^6 photons/sec to maintain N_2^+ at the measured nighttime level.

Before discussing possible models, we should point out that in using this data we are assuming that the February morning flight occurred in an ionosphere that was the same as that which

was present in the late afternoon preceding the August night time flight. We assume a certain permissive chemistry and a certain incoming photoionizing radiation. With this in mind, we have made some primitive calculations which are to be considered only preliminary to more intensive analysis of the total distribution of ions over the entire altitude range covered. We find that if one simply takes daytime values of individual ion density at certain fixed altitudes and assumes dissociative recombination rates of 10^{-7} for N_2, O_2, and NO that it is impossible to pin down values for the ion-atom interchange reaction rates except for two, $N_2^+ + O \rightarrow O^+ + N_2$ and $O^+ + N_2 \rightarrow NO^+ + N$. The others may vary over wide ranges so that an immediate consequence of this initial look is the conclusion that a much more comprehensive examination of the complete altitude range covered is necessary. It does seem that some rates will turn out to be temperature dependent, but good figures are yet to come.

Mass 24^+ was seen as a minor constituent on both up and down legs of the daytime flight. It was seen over a very narrow altitude range in each case. Our analysis of the shape of this distribution is not yet complete.

DISCUSSION

A. Kavadas: You have shown a slide of NO^+ plotted against height, do you have any measurements of the electron density on the same flight? If so, was the curve the same shape?

J.C. Holmes: Yes, we do. In the daytime flight 16 AMU is the predominant ion in the upper region, so the electron density follows the 16 distribution. At lower heights the electron distribution fairly closely followed the sum of the ion densities down to 150 km or so. They were measured with the White Sands ionosonde. The ionosonde curve is plotted to the left side of the figure along with my total ion curve.

M. Dubin: Neutral water vapor surely can be a contaminant, but there is a suggestion that the ionized water vapor may not be. You have shown that the daytime density of mass 18 ions was about $10^9/cm^3$. How could you get an ionization rate sufficient to give this density?

In one rocket flight 20 kg of water vapor was released in the ionosphere in daylight; in another case 85,000 kg, the heights being 105 and 170 km. This water vapor was tracked by an ionosonde and nothing was observed.

As a possible explanation of your result there is an isotope of oxygen at mass 18 which on ground level is 0.2%. It appears also if you look at the way they trace the water vapor, the mass 18 and the 16 line have the same profile; they are down in number density by a factor of almost 100.

J.C. Holmes: I feel from the data, from the closeness with which the up- and down-leg curves follow each other, as strictly evidenced from the mass spectrometer, I would not be able to honestly classify the mass 18 as an atmospheric constituent at this time.

We are not suggesting that the sun ionized this 18; if it is a contaminant it comes from our rocket body, maybe from the back end of the motor, and if it ion-atom interchanges, say with 16 which is the major ion at these altitudes, it could account, I believe, for the amount of 18 that we see in the vicinity of the rocket. I do not see that the solar radiation would necessarily produce as much as we see in the vicinity of the rocket. If the 18 ion-atom interchanges with the 16^+, the release at 107 km might not show very much ionization instantly. The release at 170 km, may be it could perhaps have used up all the 16.

N.W. Spencer: It seems to me that the difference between the up-leg and down-leg in the mass 18 ion, supports the water hypothesis rather than the isotope of oxygen mentioned by Dr. Dubin.

L.G. Smith: How was the ion spectrometer calibrated?

J.C. Holmes: Our particular ion spectrometer covered a measured mass range of 35 AMU down to 14, a ratio of a little over 2 to 1, heavy to light ion mass ratio. There are several effects which have to be separated.

The stopping potential grids in the back of the spectrometer, which serve to discriminate against those ions which have not received the maximum energy, are not perfect stoppers. For instance there is a sweep in front of these which sweep the mass range. Now if you combine the sweep voltage with the stopping voltage you strengthen and lessen the effect of the stopping voltage with sweep; this effect has to be taken into account - one must run calibration curves of the effectiveness of the stopping potential versus sweep voltage for various lines.

One must also run curves on the general mass discrimination versus voltage due to focussing and so on. The tube is long compared to its diameter; things happen to the ions as they go down the tube, and these vary with accelerating voltage.

One must therefore calibrate the tube by putting the masses of a given constituent at different places on the sweep, to see if they appear with the same intensity. This has to be done with light masses and heavy masses over the entire range one will use in the experiment; otherwise some masses will not show.

The calibration was done in a bell jar, maintaining constant pressure and constant emisson.

W. Brubaker: Did you allow for the relative velocity of the ions? In the laboratory it was zero, while in the rocket it was not.

J. C. Holmes: The curves I showed are currents as measured without taking into account the effect of the velocity. There are also other effects which might tend to balance out the velocity effects and we did not take any of these into account at all.

10.2 THE NEUTRAL COMPOSITION OF THE ATMOSPHERE IN THE 100 TO 200 KM RANGE

A. O. NIER
School of Physics
University of Minnesota,
Minneapolis, Minnesota

and

J. H. HOFFMAN, C. Y. JOHNSON and
J. C. HOLMES
Naval Research Laboratory
Washington 25, D. C.

This is a preliminary report on an Aerobee flight, NC 3.115F, fired at the White Sands Missile Range at 0730 MST on June 6, 1963, for the purpose of measuring the neutral composition of the upper atmosphere. The rocket contained two magnetic mass spectrometers: a double-focusing instrument similar to one described earlier [14], and a simpler, single-focusing instrument. The two spectrometers were mounted 180° apart in the cylindrical section of the rocket as shown in Figure 1. The ion source regions were separated from the analyzer regions by narrow slits, making possible continuous pumping of the analyzer regions with one-liter-per-second sputter pumps. The ion sources, although recessed in the side of the rocket, were exposed directly to the ambient atmosphere after the caps over the ion sources were removed by a cutter mechanism, described earlier [14].

Data were obtained in the altitude range 95 to 209 km. Horizontal and vertical magnetometers, together with sun and earth cells, gave the orientation of the rocket at all times. The instruments covered the mass range 10 to 50 AMU, the spectra being swept with a period of approximately 2 sec. The filament of the double-focusing instrument failed in flight, but the single-focusing instrument functioned perfectly.

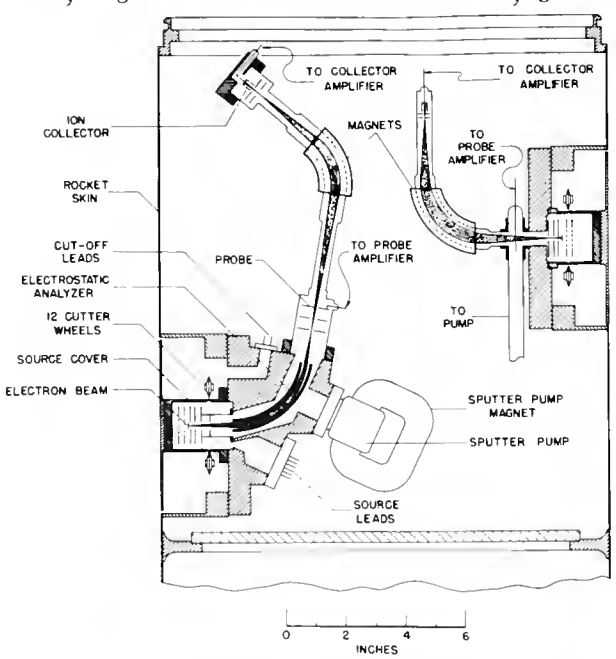

Figure 1. Schematic view of cross section of rocket showing mounting of mass spectrometers in rocket section

Figure 2 is a photograph of the ion source showing the open construction. It is estimated that approximately 1/3 of the particles intercepting the ionizing electron beam could do so without making any collisions with source parts or the side of the rocket. In addition to reading the analyzed ion current, each instrument had a probe which measured the total ion current leaving the ion source. The analyzer pressure was monitored, as were the total electron emission, the electron trap current and the ion accelerating voltage. Information was telemetered to earth by means of the DKT-7 telemeter system. The spectrometers were turned on before flight and left on throughout the flight.

Figure 3 is a photograph of a model showing the orientation of the rocket throughout the flight. Briefly it can be said that the axis of the rocket moved on the surface of a cone having a half-angle of approximately 50°. The rocket axis was nearly perpendicular to the trajectory for all but the beginning of the flight.

Figure 4 shows spectra 108 and 109 taken at approximately 300 sec after firing, corresponding

Figure 2. Photograph showing ion source of single-focusing mass spectrometer on mounting flange as seen in Fig. 1

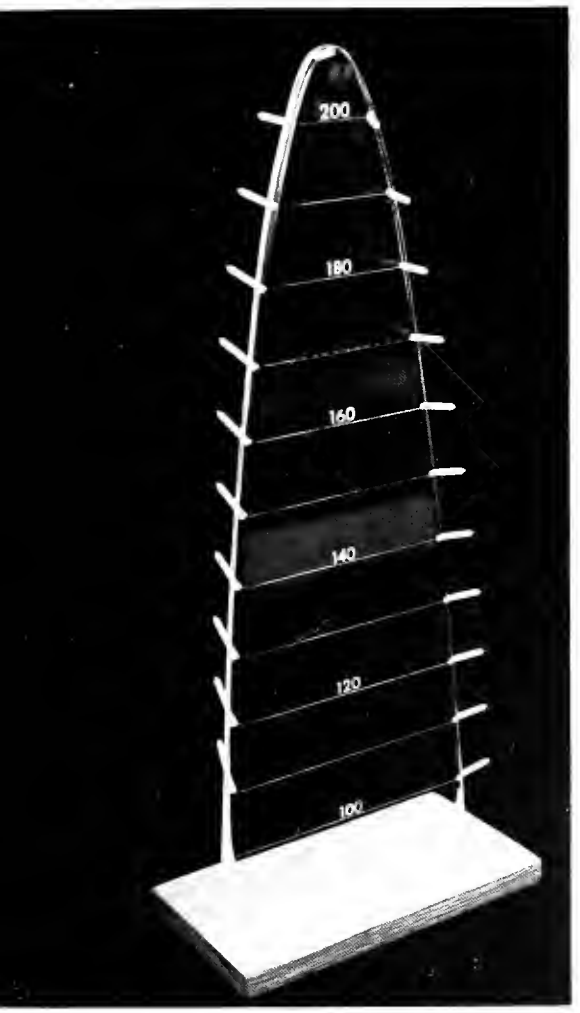

Figure 3. Photograph of model showing trajectory of rocket. Numbers refer to altitude. The pins represent the rocket at the various altitudes and clearly show the way in which the rocket axis rolls on the surface of a cone having a half-angle of approximately 50°.

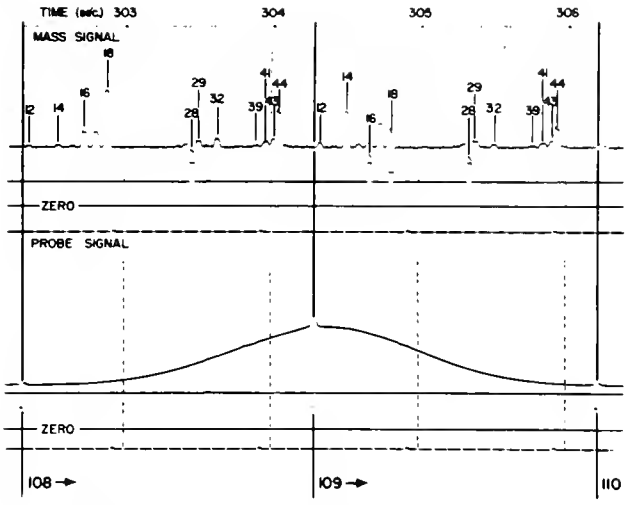

Figure 4. Mass spectra and probe currents during spectra Nos. 108 and 109. In spectrum 109 the marks below the 16, 18 and 28 peaks are from the telemeter channel recording the sensitivity of the amplifier. The marks indicate the sensitivity of the amplifier. The marks indicate that the 18 peak should be multiplied by 2 to give the true amplitude, the 16 and 28 peaks by 4. Likewise the 28 peak in specturm 108 should be multiplied by a factor of 4. Ten such shifts of sensitivity were possible, giving a total range change of $2^{10} = 1024$. The probe signal had a similar range changer, but since the signal did not exceed the telemeter scale, i.e., 5 volts, in these particular spectra, no change in sensitivity took place.

to an altitude of 191 km. The lower part of the figure gives the probe signal (i.e., the total ion current leaving the ion source) and clearly illustrates the effect of rocket roll on signal intensity. In these spectra, taken near peak of flight, the residual gases associated with the spectrometer or rocket constitute a larger proportion of the total gas than is the case at lower altitudes. The 18, 17 and a small part of the 16 peaks arise from the residual water vapor. The 44 peak and a small fraction of 28, 16 and 12 are due to CO_2. The odd mass peaks, 43, 41, 39, 29, 15 and the remainder of the 12 are attributed to unidentified hydrocarbon impurities associated with the rocket. The impurities, readily recognizable, were not so high as to have any appreciable effect on the components of interest to us in the flight.

When a pressure or composition-measuring gauge is mounted on the side or nose of a fast moving rocket, the reading will be affected by the motion of the vehicle relative to the atmosphere. This problem has been discussed by a number of authors [2, 4, 5, 6, 7]. Figure 5 illustrates the problem. Here we see a pressure-measuring device of some sort mounted just inside the skin of a rocket. In the figure it is assumed that the rocket is moving toward the left and downward so there is a mass motion of gas relative to the gauge represented by the vector V, having a component perpendicular to the opening of the pressure-measuring device $V_\perp$ as shown. The number density of a particular species of particle inside the gauge represented by n_1 is related to the ambient number density represented as n_o by the formula given. The function F(S) in the equation provides the modification needed to allow for the motion of the vehicle through the air. Thus we see that for S = 0, i.e., no component of motion of air toward or away from the gauge, F(S) = 1 and n_o and n_1 are related, as one would expect, by the

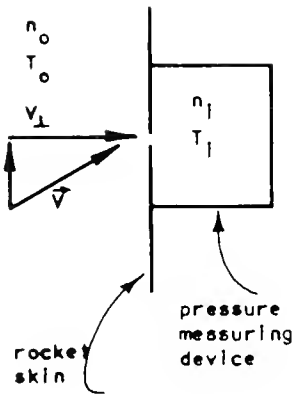

$$n_o = n_i \, (T_i/T_o)^{1/2} \Big/ F(S)$$

where $S = V_\perp / v_{p_o}$

and $F(S) = \left[(\pi)^{1/2} \, S(1 + \text{erf } S) + e^{-S^2} \right]$

Some typical values of F(S)

S	F(S)
0	1
1	3.6
2	5.3
-1	0.09
-2	0.0017

Figure 5. Schematic view of pressure-measuring device mounted on side of rocket. Ambient gas enters through hole as shown, and number density for a particular species inside is related to corresponding ambient density by equation given

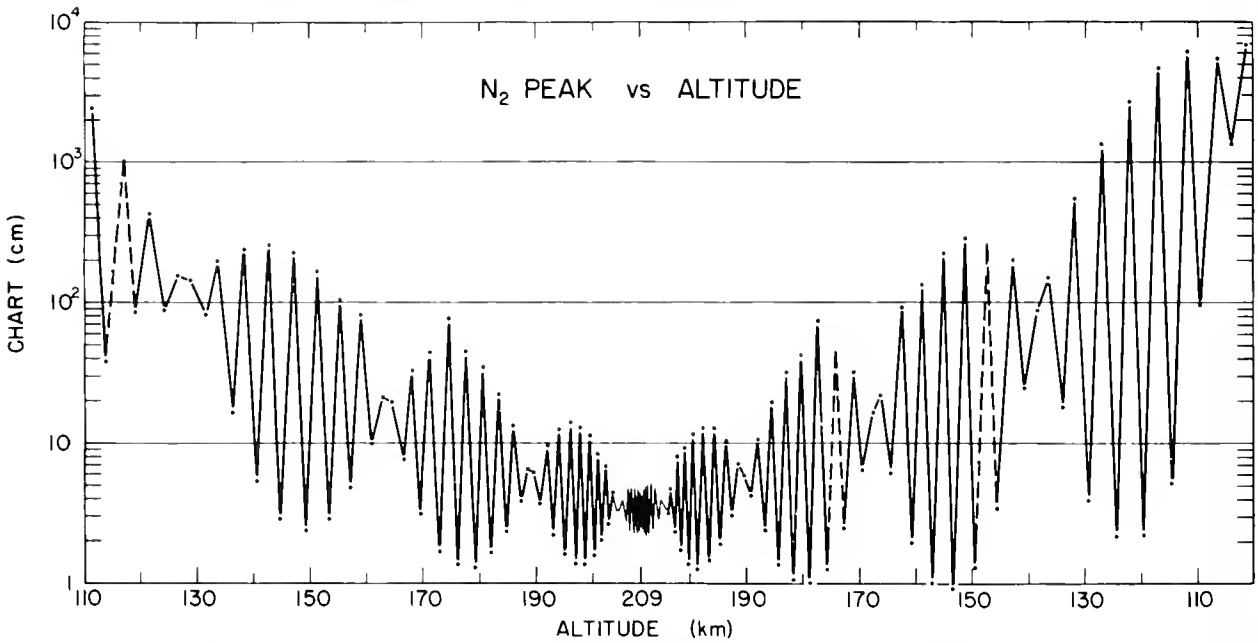

Figure 6. Variation of N_2 peak intensity versus altitude. Points for successive spectra are connected by lines. At positions of greatest modulation, for example 175 km on ascent, spectrometer points either "forward" or "backward" at time 28 peak is recorded. Note that at 120 km during descent, intensity of peak changes by a factor of over 1000 between successive spectra. Ordinate scale gives peak height in terms of equivalent cm deflection on telemeter chart for most sensitive step of amplifier. One cm deflection corresponds to a particle density of 5.66×10^8 N_2 molecules/cc as found by calibration in the laboratory. The overall sensitivity of the instrument was such that 1 cm deflection on telemeter chart corresponded to an N_2 ion current of approximately 10^{-12} amperes.

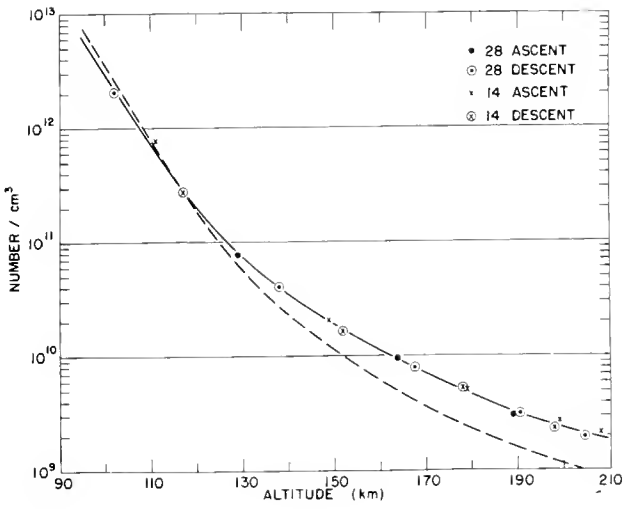

Figure 7. Variation of N_2 particle density determined from nodal points of Fig. 6 and companion plot for N (not reproduced in this paper). Solid curve assumes $n_o = n_1$ in equation of Fig. 5. Dashed curve assumes all particles ionized by electron beam have adjusted to temperature of ion source parts

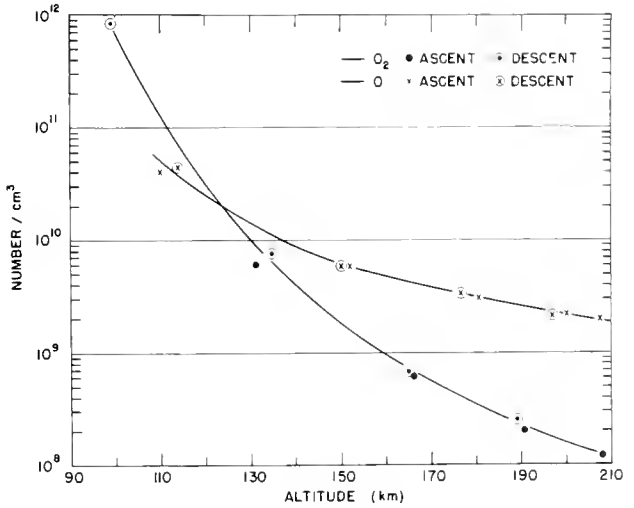

Figure 8. Variation of O_2 and O particle densities with altitude determined from nodal points of plots similar to Fig. 6. In plotting these, n_o is assumed equal to n_1

normal transpiration equation. When the motion of the vehicle is toward the air, extra molecules are collected; when it is away from the air, the slower molecules in the Maxwellian velocity distributions will not reach the gauge and there may be a sharp attenuation in the number of molecules actually collected. Fig. 5 also gives values of F(S) corresponding to several values of S. In the lower part of our flight (near 100 km), where the rocket has a speed several times the most probable molecular speed, one can obtain a variation of mass spectrometer readings of a factor of several thousand as the rocket rotates if the rocket axis is nearly normal to the velocity vector of the rocket.

Figure 6 gives the intensity of the mass peak (N_2) as a function of altitude. Points for successive spectra are connected by lines illustrating the appreciable change in peak height as the rocket rotates and precesses throughout flight. The rotation period of the rocket was approximately 4 seconds, almost exactly twice that of the sweep rate; thus the orientation of the spectrometer opening relative to the direction in which the rocket was moving at the time a particular peak such as 28 was read, changed but slowly throughout the flight. The beat appearance of the envelope of points illustrates this phenomenon. We note that because of the nearly integral multiple relationship between the periods, only four nodal points were obtained on either ascent or descent. These nodal points correspond to rocket positions were S = 0 and thus F(S) = 1. In principle, one should be able to correct all of the readings by applying the proper F(S) correction, thus obtaining a uniform, smooth curve relating particle density with altitude. Our analysis has not proceeded this far, and in this paper we will restrict ouselves to a discussion of the nodal points. Graphs showing the variation of the 14 peak (N) and the 32 peak (O_2) have the same general appearance as Figure 6. The O peak owes its presence primarily to atomic oxygen, which has a substantially lower mass and hence a higher speed in the Maxwellian velocity distribution. Thus F(S) does not vary so drastically throughout the flight, and hence the curve showing O variation throughout the flight does not exhibit as large roll modulations as is true for the other constituents discussed.

The mass spectrometer had been calibrated in the laboratory with air. Thus a relationship between number density of the various constituents and ion current was found. Figure 7 shows the N_2 number densities corresponding to the nodal points shown in Figure 6

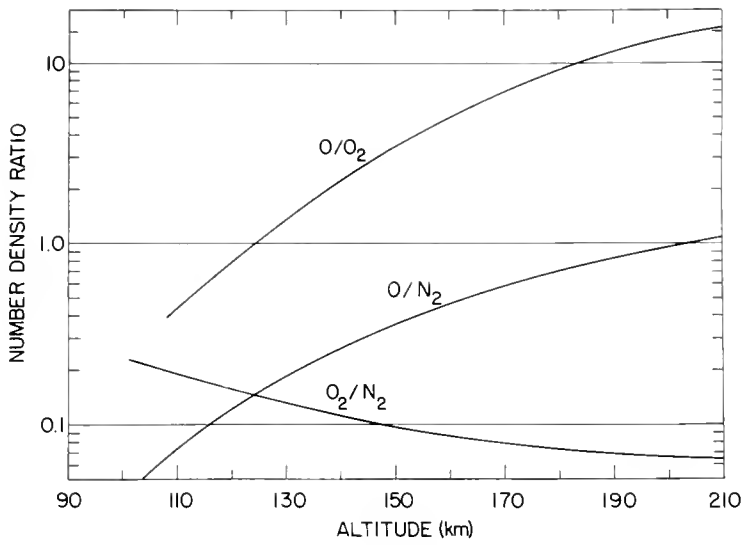

Figure 9. Variations of O/O_2, O_2/N_2 and O/N_2 ratios with altitude taken from ordinates of Figures 7 and 8

and in the companion N plot. The fact that the N_2 densities computed from the N peak intensities fall on the same curve as the points computed from the N_2 peak intensities indicated that the N/N_2 ratio in the atmosphere in the altitude range studied was low--probably less than 0.02. While the good agreement might conceivably be due to a change in calibration, coupled with the presence of some N, it seems highly improbable that if N were present in the atmosphere, its amount would be large enough and would vary with altitude in just the right way to compensate for possible change in calibration of the instrument. The figure actually shows two curves. The solid one assumes that $T_1 = T_o$, i.e., N_2 molecules are reflected from the ion source parts without a change in energy. On the other hand, if it is assumed that all molecules assume the temperature of the source before being ionized and measured, the dashed curve is obtained. For this, it is assumed that $T_1 = 293^{\circ}K$ and that T_o varies with altitude according to the 1962 U. S. Standard Atmosphere [13].

Curves analogous to Figure 7 were obtained for the molecular and atomic oxygen peaks, and these are shown in Figure 8. In computing the atomic oxygen densities, the relative cross section for ionization for O and O_2 are those given by Fite and Brackman [1] for 90 volt ionizing electrons. As in Figure 7, lower curves would be obtained if one assumed all of the particles came to temperature equilibrium with the ion source parts prior to passing through the ionizing electron beam. Since an estimated 1/3 of the particles measured had not made any collisions and the remainder very few, it seems that curves such as the solid one are to be preferred. The final result will have to await further experiments in which this point may be checked.

Figure 9 gives a summary of the results obtained. We see that the O/O_2 ratio increases with altitude, reaching a value of at least 15 at 209 km, the peak of the flight. The general form of the curve is consistent with the results of Schaefer which are presented in another part of the present conference. The O_2/N_2 ratio decreases with altitude in a manner which is consistent with diffusive separation of the O_2 and N_2 species. The present results contradict those of Meadows and Townsend [8] who found an increase in this ratio at the higher altitudes. Pokhunkov [12] reported a decrease in the ratio but not as great a one as that which we have found. The O/N_2 ratio increases with altitude, reaching a value of unity around 200 km.

An analysis of our results on argon is not yet complete. However, preliminary examination of the data indicates that the argon concentration is below normal, in qualitative agreement with the results of Meadows and Townsend [8] and Meadows-Reed and Smith [9]. From our data on the concentrations of O, O_2, and N_2 one can compute percentage composition as well as mean molecular weight as a function of altitude. The present results agree much better with the values assumed by Nicolet [10] than with those given by Hinteregger [3].

References

[1] Fite, W. L. and R. T. Brackmann, Ionization of atomic oxygen on electron impact, Phys. Rev. 113, 815-816, 1959.

[2] Havens, R. J., R. T. Koll and H. E. LaGow, The pressure, density, and temperature of the earth's atmosphere to 160 km, J. Geophys. Res. 57, 59-72, 1952.

[3] Hinteregger, H. E., Absorption spectrometric analysis of the upper atmosphere in the EUV region, J. Atmos. Sci. 19, 351-368, 1962.

[4] Horowitz, R. and D. Kleitman, A method for determining density in the upper atmosphere during rocket flight, U.S. Naval Research Laboratory Report No. 4246, 1953.

[5] Horowitz, R. and H. E. LaGow, Upper air pressure and density measurements from 90 to 220 kilometers with the Viking 7 rocket, J. Geophys. Res. 62, 57-78, 1957.

[6] Horowitz, R. and H. E. LaGow, Summer-day auroral-zone atmospheric structure measurements from 100 to 210 kilometers, J. Geophys. Res. 63, 757-773, 1958.

[7] LaGow, H. E., R. Horowitz and J. Ainsorth, Rocket measurements of the arctic upper atmosphere, Ann. Geophys. 14, 131-139, 1958.

[8] Meadows, E. B. and J. W. Townsend, Jr., IGY Rocket Measurements of Arctic Atmospheric Composition above 100 km, Space Research, pgs. 175-198, H. Kallman Bijl, ed., Interscience Publishers, New York, 1960.

[9] Meadows-Reed, E. B. and C. R. Smith, Mass spectrometric investigations of the atmosphere between 100 and 227 kilometers above Wallops Island, Virginia, NASA Technical Note D-1851, 1963.

[10] Nicolet, M., The composition and structure of the terrestrial atmosphere, Scientific Report No. 185, Ionospheric Research, The Pennsylvania State University, 1963.

[11] Nier, A. O., Small general purpose double focusing mass spectrometer, Rev. Sci. Instr. 31, 1127-1132, 1960.

[12] Pokhunkov, A., On the variation in the mean molecular weight of air in the night atmosphere at altitudes of 100 to 200 km from mass spectrometer measurements, Planet. Space Science 11, 297-304, 1963.

[13] Sissenwine, N., M. Dubin and H. Wexler, The U.S. Standard Atmosphere, 1962, J. Geophys. Res. 67, 3627-3630, 1962. For more extensive tabulation, see U.S. Standard Atmosphere, 1962, U.S. Government Printing Office Washington, D.C.

[14] Thorness, R. B. and A. O. Nier, Device for remote opening of a vacuum system, Rev. Sci. Instr. 33, 1005-1007, 1962.

10.3 RECENT RESULTS OBTAINED FROM A ROCKET-BORNE MASS SPECTROMETER

E. J. SCHAEFER and M. H. NICHOLS
University of Michigan
Ann Arbor, Michigan

1. Introduction

Until recently, mass spectrometer measurements of upper atmosphere neutral composition between 100 and 200 km altitude [1, 2] have yielded data which have consistently indicated the concentration of atomic oxygen to be an order of magnitude lower than the theoretical predictions of Nicolet [3] and the results of ultraviolet absorption measurements [4, 5]. Recent attempts by Pokhunkov [6]to apply corrections to his Bennett-tube data are based on assumptions of questionable validity and still yield a relative O_1/O_2 concentration ratio of approximately 1/3 the value obtained by the present authors. The reason for the low concentration of atomic oxygen which has thus far been observed has been postulated to be the loss of atomic oxygen within the instrument due to surface recombination at the walls.

This paper describes the development of an instrument designed to overcome this limitation. The results of the first successful daytime flight test are presented in detail and preliminary results of the first successful flight test are included. Both flights have yielded O_1/O_2 current ratios approximately an order of magnitude greater than obtained by former mass spectrometer measurements.

A secondary design objective which has been achieved was the design of an experiment within the size and weight capabilities of a small rocket such as the Nike-Cajun (or more recently, the Nike-Apache).

2. Instrumentation

The instrument selected for in-flight neutral composition analysis was the "massenfilter" first described by Paul, Reinhardt and von Zahn [7, 8] spaced 90° apart. Ions are injected along the axis of the rod structure where they are subjected to transverse DC and RF electric fields due to the potentials impressed on the rods. The ions of proper m/e ratio are stable in the transverse field and reach a collector at the far end of the rods. The current they deliver is an indication of their abundance. All other ions are unstable and are removed when their transverse amplitude of motion reaches a magnitude sufficient to cause collision with a rod. A mass spectrogram is obtained by sweeping the rod voltages so that the ions are collected sequentially

Figure 1. Flight massenfilter

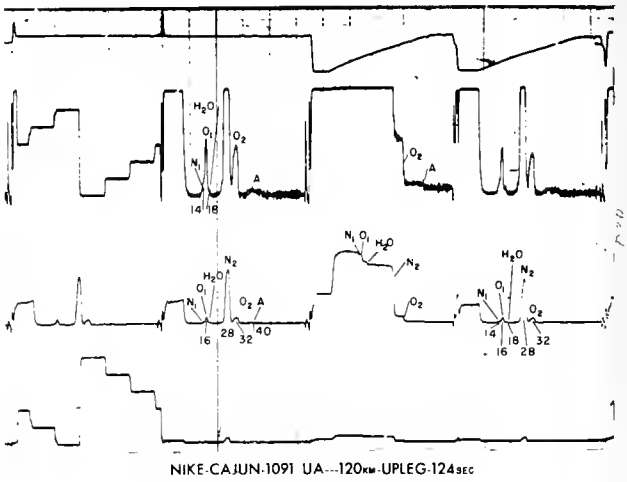

Figure 2. Flight spectra

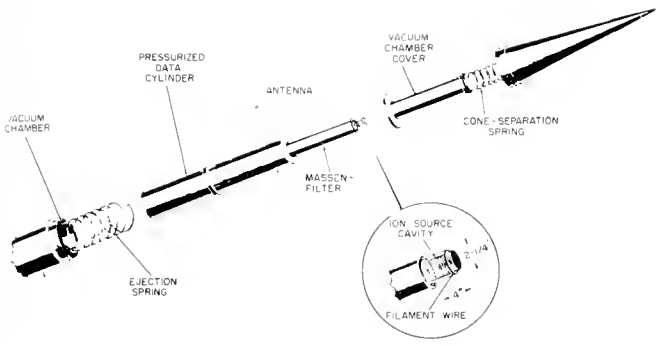

Figure 3. Diagram of ejection mechanism

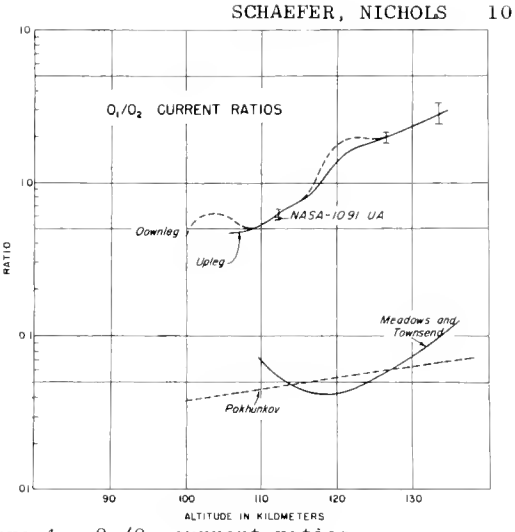

Figure 4. O_1/O_2 current ratios

in time according to their m/e ratios.

Because the analysis takes place by transverse action on the ions, the massenfilter possesses a unique property by which the indicated ion mass is independent of the axial ion velocity. This permits the use of an "open" ion source directly immersed in the ambient atmosphere. Each ambient particle experiences, on the average, the order of only one surface collision prior to ionization. Experimental data [9, 10] indicate recombination of atomic oxygen upon collision with a surface has a probability of the order of 1%. Thus the loss of atomic oxygen is negligible. The open ion source is illustrated in Figure 1 which is a photograph of a flight instrument. Ions are injected into the analyzing section through an inlet port 5×10^{-3} cm^2 in area. The total area of the analyzer breather holes seen near the base of the instrument (Figure 1) is 1.3 cm^2. Thus only a negligible fraction of the gas in the analyzer is returned to the ion source.

Two distinct types of spectra are obtained. When DC and RF voltages are applied, the "normal" spectra consisting of a series of peaks identifying each component individually is obtained. Application of a swept RF voltage alone removes ions one at a time in order of increasing m/e ratio. The resultant spectrum is a series of steps from which it derives the name "staircase". This latter mode of operation is useful in calibrating the heights of the major peaks of the normal spectrum where transmission is, in general, less than 100%. The residual current at the bottom of the staircase indicates the total of those ions having masses beyond the range of the instrument. Figure 2 is a reproduction of the spectra obtained at 120 km on the upleg of Nike-Cajun NASA 10.91 UA. The three channels correspond to three decades of sensitivity. Both the normal and staircase spectra are evident in Figure 2.

Finally, in order to eliminate contamination from gases trappea in the rocket and absorbed on its surfaces, the entire instrumentation is enclosed in a capsule (Figure 3) which is ejected from an evacuated container when altitude is reached. An attendant feature of ejection is the removal of aerodynamically heated surfaces from the vicinity of the instrument.

3. Daytime Flight Data

Nike-Cajun NASA 10.91 UA was fired from Wallops Island at 1302 EST, 18 May 1962. Apogee was 134.5 km. The spin period was 1.2 sec: and the precession period was 31 sec. Figure 4 illustrates the O_1/O_2 current ratio which was obtained and compares the results with those of other investigators.

The ion source accelerating grid (Fig. 1) was operated between 45 and 50 volts. However, because of space charge effects around the fine wires of the grid, the ionizing electrons had an energy less than the grid voltage. Comparison of laboratory calibration data with the data of Fite and Brackmann [11] indicate the effective

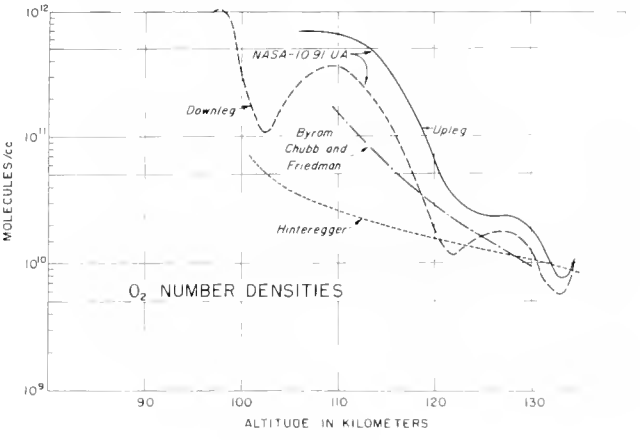

Figure 5. O_2 number densities

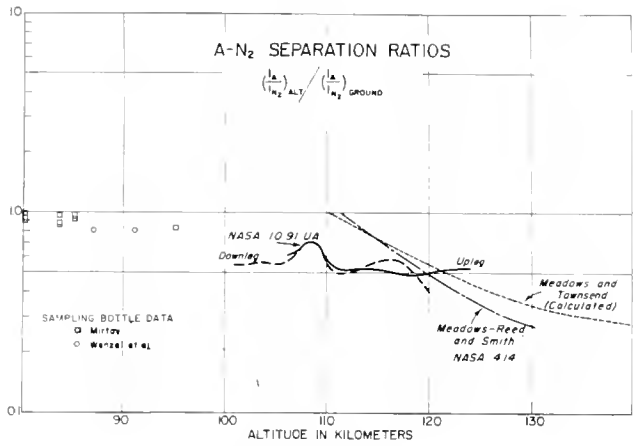

Figure 6. Argon-nitrogen separation ratio

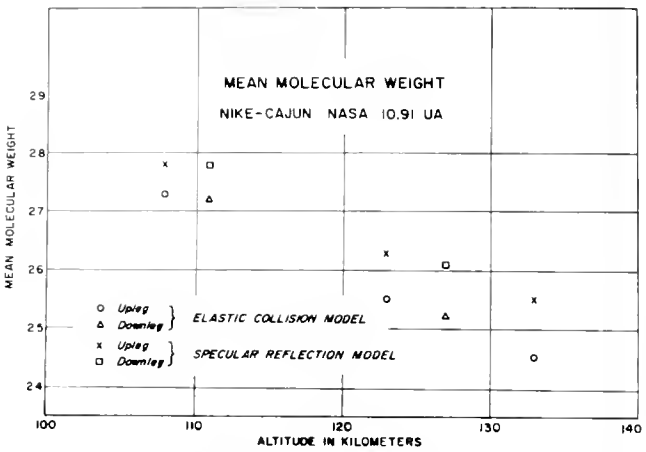

Figure 7. Mean molecular weights

electron energy was around 25-30 volts. At this energy, the experimental data of Fite and Brackmann indicate the ratio of the cross-sections of O_1 and O_2 is nearly unity. Thus the current ratios of Figure 4 are assumed to indicate the ratio of the number densities in the ion source.

In interpreting the data, the motion of the instrumentation must be taken into account. Precise quantitative analysis is prohibitively complicated due to the involved geometry of the ion source and the uncertainty in the nature of the interactions between the impinging particles and the metallic surfaces with an adsorbed gas layer. Defects in the existing data are discussed in a recent review of thermal accomodation coefficients by Hartnett [12]. Limits can be placed on the aerodynamic effects, however, by constructing idealized models. In this manner, lower limit to the correction necessary to relate the results of Figure 4 to the ambient can be obtained by assuming perfect reflection. Under this assumption, the ratio of the constituents is unchanged. An upper limit can be derived from a model in which the incident particles are assumed to undergo elastic collisions with the individual atoms of the base metal (M = 56) and that the impacts are "head-on". Then, neglecting thermal velocities of the metallic atoms, an enrichment factor of 1.7 for O_2 over O_1 can be obtained. A model which assumes complete thermalization of the incident particles yields an enrichment factor of 1.2 at apogee (V = 2.4 x 10^4 cm/sec at a surface temperature of 300 deg K. Since the upleg and downleg data of Figure 4 are in good agreement over most of the altitude range, it appears that the specular reflection model (no enrichment of O_2) is a better approximation than the elastic collision model. Hence the data of Figure 4 are assumed to reflect the ambient concentration ratios within, perhaps, 20%.

Figure 5 shows O_2 number densities deduced from the same flight.

The argon-nitrogen separation ratio obtained from this flight is presented in Figure 6 and compared with the results obtained by Meadows - Reed and Smith [13]. Sampling bottle data are also included. At this time we have no theory to account for the difference in the character of the results. (We note that the time constant of our ion source in reaching equilibrium with the ambient atmosphere is essentially zero.)

Mean molecular weight has been calculated for those points of the trajectory where the angle of attach most closely approached 90°. At these portions of the flight, it is felt the atmosphere in the ion source is most closely representative of the ambient. The mean molecular weight has been calculated for both the specular and elastic collision models, and the results are given in Figure 7. The solid curve is arbitrarily drawn closer to the points obtained from the specular reflection model to indicate the best judgment of the authors.

4. Nightime Flight Data

Nike-Apache NASA 14.08 UA was fired from

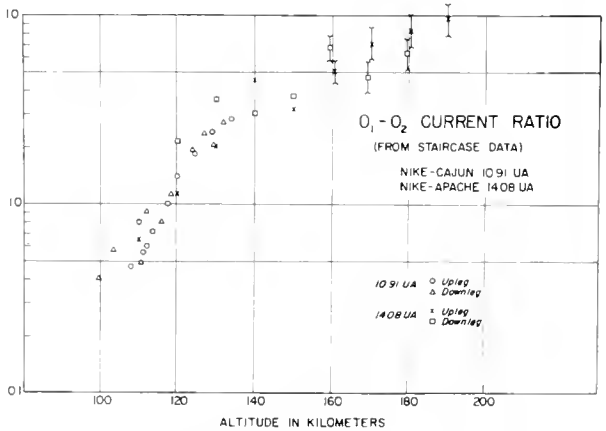

Figure 8. Comparison of O_1/O_2 current ratios by day and by night

Wallops Island at 0255 EST, 28 March 1963. Apogee was 190 km. O_1/O_2 current ratios have been calculated and are shown in Figure 8, compared with the daytime data.

A quick look at the N_1/N_2 ratio indicates that, if nitrogen were dissociated at all, N_1 exists in an amount which is less than 5% of N_2 in the altitude range covered by either flight.

References

[1] E. B. Meadows and J. W. Townsend, Jr. 1GY Rocket Measurements of Arctic Atmospheric Composition Above 100 km. Proc. First Int. Space Sci. Symp., Nice (1960). Ed. H. K. Kallmann Bijl (North-Holland, Amsterdam), 175-198.

[2] A. A. Pokhunkov. Mass Spectrometer Investigation of the Structural Parameters of the Earth's Atmosphere at Altitudes from 100 to 210 km. Planet Space Sci. 9 (1962), 269-279. Trans. from Iskusstvennye Sputniki Zemli 7 (1961), 89-100.

[3] M. Nicolet. Physics of the Upper Atmosphere. Academic Press, New York and London (1960). Ed. J. A. Ratcliffe, 29-35.

[4] E. T. Byram, T. A. Chubb, and H. Friedman. Dissociation of Oxygen in the Upper Atmosphere. Phys. Rev. 98 (1955), 1594-1597 (Fig. 4 abscissa are 1 km low as later corrected by authors).

[5] H. E. Hinteregger. Absorption Spectrometric Analysis of the Upper Atmosphere in the EUV Region. J. Atmos. Sci. 19 (1962), 351-368.

[6] A. A. Pokhunkov. On the Variation in the Mean Molecular Weight of Air in the Night Atmosphere at Altitudes of 100 to 210 km From Mass Spectrometer Measurements. Planet Space Sci. 11 (1963), 297-304. Trans. from Iskusstvennye Sputniki Zemli 12 (1962), 133.

[7] W. Paul, H. P. Reinhard, and V. von Zahn. Das Elektrische Massenfilter als Massenspektrometer und Isotopentrenner. Zeitschrift fur Physik, 152 (1958), 143-182.

[8] E. J. Schaefer and M. H. Nichols. Mass Spectrometer for Upper Air Measurements. Am. Rocket Soc. J. 31 (1961), 1773-1776.

[9] D. S. Hacker, S. A. Marshall, and M. Steinberg. Recombination of Atomic Oxygen on Surfaces. J. Chem. Phys. 35 (1961), 1788-1792.

[10] J. Wood and H. Wise. The Interaction of Atoms with Solid Surfaces, Rarefield Gas Dynamics. Academic Press, New York (1961), 51-59.

[11] W. L. Fite and R. T. Brackmann. Ionization of Atomic Oxygen on Electron Impact. Phys. Rev. 113 (1959), 815-816.

[12] J. P. Hartnett. A Survey of Thermal Accommodation Coefficients. Rarefied Gas Dynamics. Proc. of the 2nd Int. Symp. on Rarefied Gas Dynamics U. of Calif., Berkeley, Calif. 1960. Academic Press, New York and London, (1961). Ed. L. Talbot.

[13] E. Meadows-Reed and C. R. Smith. Mass Spectrometric Investigations of the Atmosphere Between 100 and 227 km Over Wallops Island, Va. NASA Tech. Note TND 1851.

DISCUSSION

C. Reber: What is the maximum relative velocity of the spectrometer before mass discrimination sets in?

E. J. Schaefer: The velocity at the lowest altitude at which we made a daytime measurement was approximately 1 km/sec; and the angle at which ions can be accepted in ejection is between 5 and 7 deg. The accelerating voltage is 45 volts, giving a transverse energy of about 0.8 ev which would be accepted by the massenfilter, and the equivalent energy of the stream of molecular oxygen traveling by would be about 0.1%; so, at least on the daytime flight, I think there is no problem.

C. Reber: Have you evaluated the recombination effect of the ion source of the instrument being able to see the hot filament?

E. J. Schaefer: The hot filament intercepts such a small angle from the ion source, that the relative number of atoms that would hit it and do any recombining on its surface would be negligible.

C. Reber: Was the recombination figure of 1% you mentioned, for gold?

E. J. Schaefer: I do not know the data for recombination on gold. The data were given for aluminum and platinum. For aluminum, as I recall, it was about 10%, at a fairly high temperature; but on platinum it was about 1%.

10.4 SOME RESULTS OF POSITIVE ION COMPOSITION MEASUREMENTS ABOVE WALLOPS ISLAND

H. A. TAYLOR
Goddard Space Flight Center
NASA
Greenbelt, Maryland

Since 1959, the Goddard Space Flight Center has maintained a program in ion composition as a part of a comprehensive program in aeronomy.

The ion composition program began with 2 flights of the Bennett RF spectrometer aboard Aerobee rockets, above Wallops Island, Va. These experiments were simply an extension of the experiment conducted by Johnson of NRL during the IGY. Figure 1 shows the results of these two flights, in terms of relative composition of positive ions in the sampled range of roughly 100 to 240 km. In each flight the relative composition of the principal ions NO^+, O_2^+ and O^+ was found to be in reasonable agreement with other probes of the same altitude region flown at other times and locations by NRL and in the USSR, also using the Bennett spectrometer.

Subsequent to these high mass studies, effort was directed to a measurement of low mass ions, in the range 1 - 5 AMU. Figure 2 shows a segment of flight data obtained from a flight of a Bennett tube aboard a Javelin rocket, to an altitude of 940 km above Wallops Island. The sweep period for mass analysis was approximately 1 sec. Masses 1 AMU (H^+) and 4 AMU (He^+) were the only positive ions detected in the 1 - 5 AMU range on this flight. Figure 3 shows the altitude distribution of H^+ and He^+ derived from this flight. Also shown is the total ion density distribution which was provided by a companion experiment, the electrostatic probe, which was flown aboard the same payload (by L. Brace of GSFC). Consideration of the relationships between these two sets of data has served to emphasize the importance in direct measurement probes of flying such closely related experiments together, under identical environmental conditions. (This data appears in the October 1963 JGR and reprints are available for distribution.)

Subsequent to the Javelin 8.23 probe, [illegible] effort has been directed toward preparation of positive ion experiments for the OGO satellite series (EGO and POGO).

To meet the increased requirements in weight and mechanical ruggedness required by the OGO constraints, the Bennett tube has been repackaged into a ceramic envelope, maintaining the same physics in the operation of the tube. Figure 4 is a photograph of the EGO ion spectrometer package, which shows two ceramic spectrometer tubes mounted side by side, above the electronics package.

The flight of most importance to this discussion was our latest, NASA 5.04. This used a solid propellant vehicle (Iris) capable of carrying the spectrometer to approximately 240 km.

There were two primary objectives for this flight. First, the instrumental objective was to flight check the new ceramic spectrometer tube. Second, the geophysical objective was

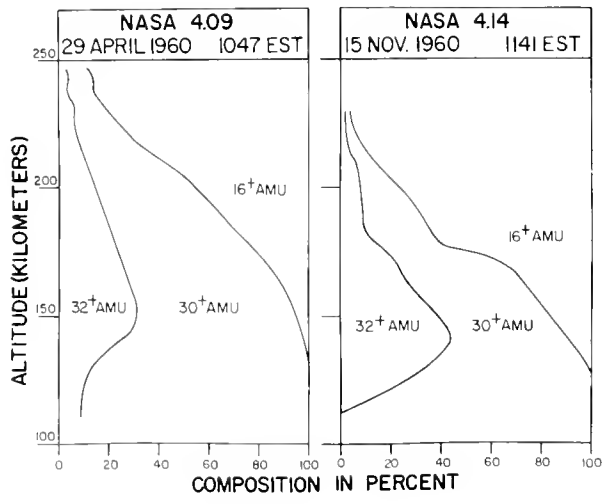

Figure 1. Distribution of the major positive ions above Wallops Island, Va.

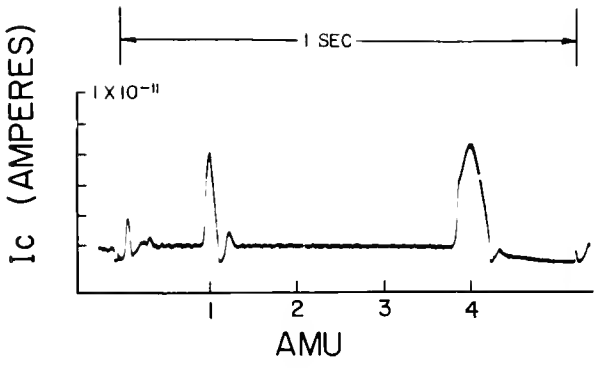

Figure 2. Typical ion spectrum from light ion Bennett spectrometer

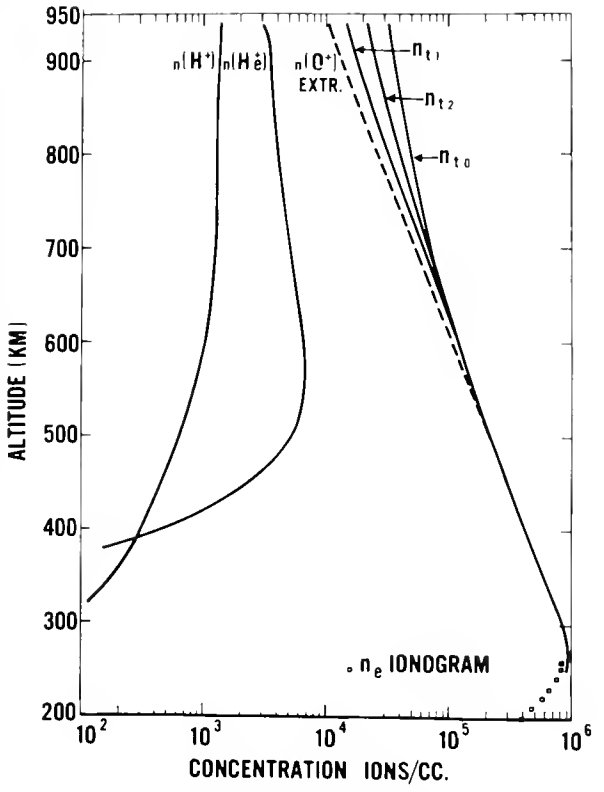

Figure 3. Altitude distribution of hydrogen and helium ions derived from spectrometer flight

to obtain for the first time ion composition data with a clean payload, separated from the rocket motor. Both of these objectives were realized, with satisfying results. Figure 5 shows the ejected payload package, and Figure 6 shows the spectrometer orifice, which was exposed along the long (spin) axis of the payload.

This particular flight serves as a very interesting study of the lower ionosphere with which we are concerned here, due to the low performance of the 5.04 rocket engine. As a result of premature burnout, the peak altitude achieved was 113 km rather than the predicted 240 km. For this reason, considerable time (~140 sec) was spent in the altitude range of ~ 90 to 113 km, over which data was recorded.

The first spectra were recorded at ~ 93 km, approximately 20 sec after payload separation. The separation velocity was ~ 6 feet per sec. Since the sweep rate was ~1 per sec, over 100 spectra were obtained, concentrated in the 20 km regime between 93 and 113 km. The important feature of this situation is that a much more intensive (spacewise) sampling of the lower altitudes was afforded, for the first time.

Figures 7 and 8 are photographs of the 5.04 telemetry record, showing typical spectra recorded in the mass range ~ 7 to 43 AMU. As shown the principal positive ions were at 30 AMU (NO^+) and 32 AMU (O_2^+), with trace constituents at 28 and 24 AMU.

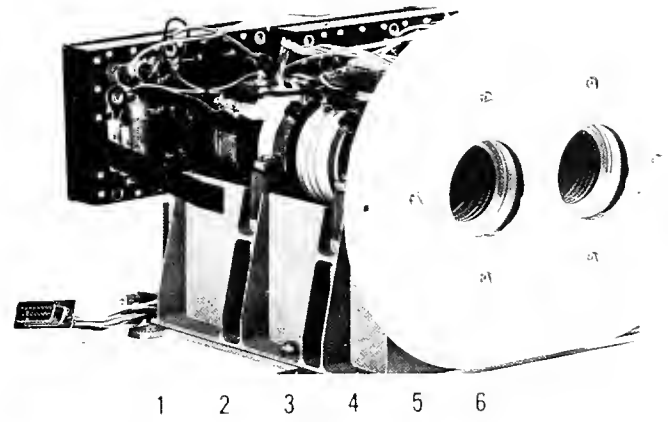

Figure 4. The EGO spectrometer package

Figure 5. Spectrometer package ejected from Iris vehicle

Figure 6. NASA 5.04 Iris spectrometer orifice

The relative concentrations of NO^+ and O_2^+ are shown vs. altitude in Figure 9. This figure does not show, unfortunately, the relative concentration of 24 and 28 AMU, whose distributions are quite interesting.

Although mass 28 was observed over most of the flight (104 km to 113 km) its concentration relative to NO^+ and O_2^+ was predominant in the level of 111 to 113 km.

Mass 24 was observed in only two distinct regions, near 93 km, and (like mass 28) in the level 111 to 113 km, approximately. It is believed that these stratifications are real, due to the high degree of altitude resolutions which was available in this flight. This flight may be compared with that of an ejected payload RF spectrometer flown by the USSR experimenters. Although the USSR experiment did not provide quite the same degree of altitude resolution, their reports indicate distributions of 28 AMU and 24 AMU which are similar to those reported here; the primary difference being that the 28 AMU and 24 AMU intensity layers were reported at somewhat higher altitudes. The Russians have attributed the 28 AMU peak to Si^+, on the argument that ionization processes are lacking for N_2 in this altitude region. The 24 AMU peak has been attributed to Mg^+, on the assumption that Si^+ and Mg^+ are of meteoric origin.

Finally, the importance of simultaneous related direct measurements should be encouraged. At GSFC, this is being pursued in the form of a Geoprobe rocket program. This is a planned series of geophysical probes which will combine measurements of electron and ion temperature and density, ion composition, neutral composition, and pressure. Figure 10 is a sketch of the first Geoprobe payload, scheduled for flight on a Javelin (up to 700 km) in the near future.

DISCUSSION

J. C. Holmes: How does the companion experiment (electrostatic probe) flown with the RF spectrometer on NASA 8.23 provide supporting data pertinent to the interpretation of the ion composition data?

H. A. Taylor: The electrostatic probe was flown to provide a direct measurement of ion density and temperature. The relationship between the measurement of total ion density provided by this device and the partial densities derived from the spectrometer measurements of H^+ and He^+ is best illustrated in Figure 3.

In this figure, the curve n_{to} is an "upper limit" total ion concentration, derived from the electrostatic probe ion current, assuming that only O^+ was present. The curve n_{tl} is the sum of the $n(H^+)$, $n(He^+)$ and $n(O^+)$ distributions. The $n(O^+)$ curve was obtained by simply extrapolating that portion of the n_{to} curve where O^+ clearly predominated and hydrostatic distribution was effective. The values

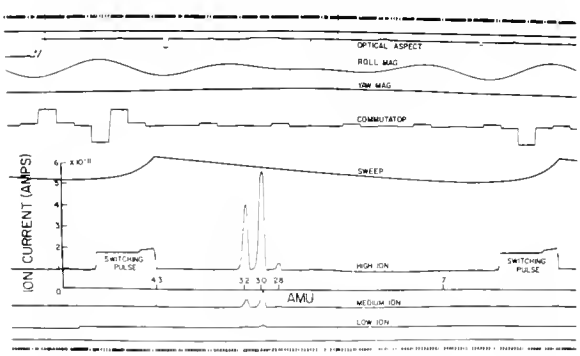

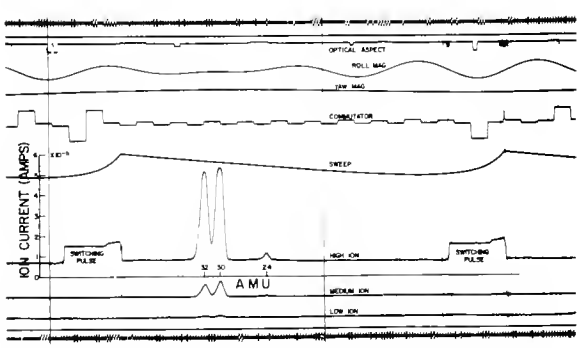

Figures 7 and 8. Typical ion spectra obtained from 5.04 Iris spectrometer 1803 UT 3 May 1962 Wallops Island

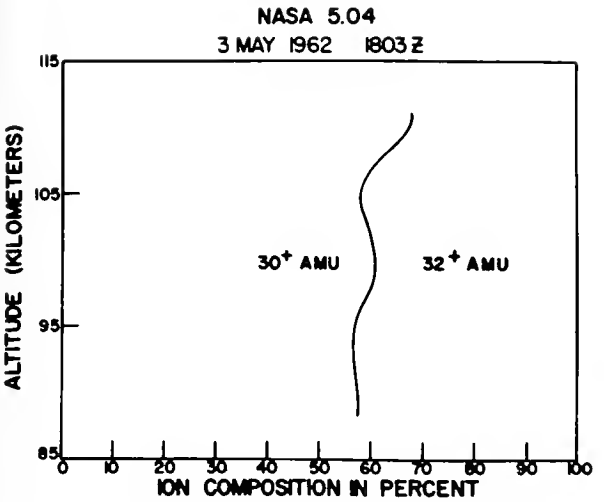

Figure 9. Relative concentration of O_2^+ and NO^+.

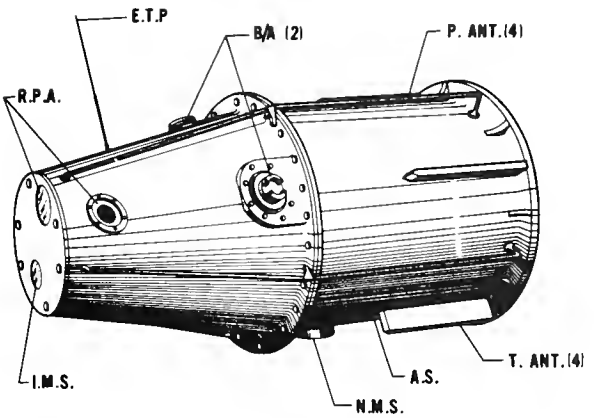

Figure 10. Geoprobe payload.

from the n_{t1} curve were in turn used to adjust the upper limit total concentration n_{to} for the presence of the lighter ions, H^+ and He^+, obtaining the final density distribution, n_{t2}. It is the illustrated degree of consistency in these data which lends signigicant support to the interpretation of the results from the individual measurements.

11.1 SIMULTANEOUS MEASUREMENT OF PLASMA DENSITY BY THREE DIFFERENT METHODS

J. BUCHAU, K.G. JACOBS, P. KAISER,
and K. RAWER
Ionospharen Institut Breisach,
Germany

During a Veronique firing on 1 May 1963 at Hammaguir (Sahara) the following three measurements have been made simultaneously*.

1. Impedance probe with variable frequency
2. Dispersive Doppler measurements on 5 and 20 MHz
3. Fieldstrength records of several LF and MF transmissions by an RF spectrometer.

1. With the impedance probe** the capacity of an antenna in front of the rocket was determined by recording as a function of frequency an RF voltage obtained in a serial combination of a resistor, a fixed capacitor C_2 and the plasma capacitor C_o (a parallel capacity C_1 to the latter is due to the connections inside the rocket). The applied RF voltage is stabilized and thus independent on the frequency; the voltage after the resistor is recorded, it is proportional to the absolute value of the current. The frequency variation was from 0.45 to 2.9 MHz in one second; frequency markers were derived from a fixed frequency oscillator.

With the expression of Kane, Jackson, and Whale [1] the plasma capacity

$$C = C_o\left(1 - \frac{X}{U}\,\frac{U^2 - G\,Y^2}{U^2 - Y^2}\right)$$

where

$$G = \int d\tau\, E^2 \cos^2\psi \Big/ \int d\tau\, E^2$$

(ψ angle between electric and terrestrial magnetic field, $d\tau$ volume element, X relative electron density, Y relative gyrogrequency, XU = 1-jz, Z relative collision frequency). In the general case the variation with frequency is characterized by two serial resonance maxima at pulsation (ω_s) and two parallel resonance minima (at ω_p).

If the variation of G with the frequency is neglected we find:

$$\omega_s^2 = \frac{1}{2}\,\omega_H^2\left(1 + p\frac{\omega_N^2}{\omega_H^2} \pm \sqrt{\left(1 + p\frac{\omega_N^2}{\omega_H^2}\right)^2 - 4Gp\frac{\omega_N^2}{\omega_H^2}}\right)$$

$$p = \frac{C_o}{C_o + C_1 + C_2}$$

$$\omega_p^2 = \frac{1}{2}\,\omega_H^2\left(1 + q\frac{\omega_N^2}{\omega_H^2} \pm \sqrt{\left(1 + q\frac{\omega_N^2}{\omega_H^2}\right)^2 - 4Gq\frac{\omega_N^2}{\omega_H^2}}\right)$$

$$q = \frac{C_o}{C_o + C_1}$$

If all four resonance frequencies were observed, one could determine the gyropulsation ω_H, the ratio G, the capacity of the ionic sheath which forms at the electrodes and, last not least, the plasma frequency. In our tentative experiment with a rather small frequency range only one serial resonance was measured. Substituting standard data for ω_H and G and neglecting the ionic sheath in evaluating of the plasma pulsation ω_N was possible. With G = 1/2, p = 1/9

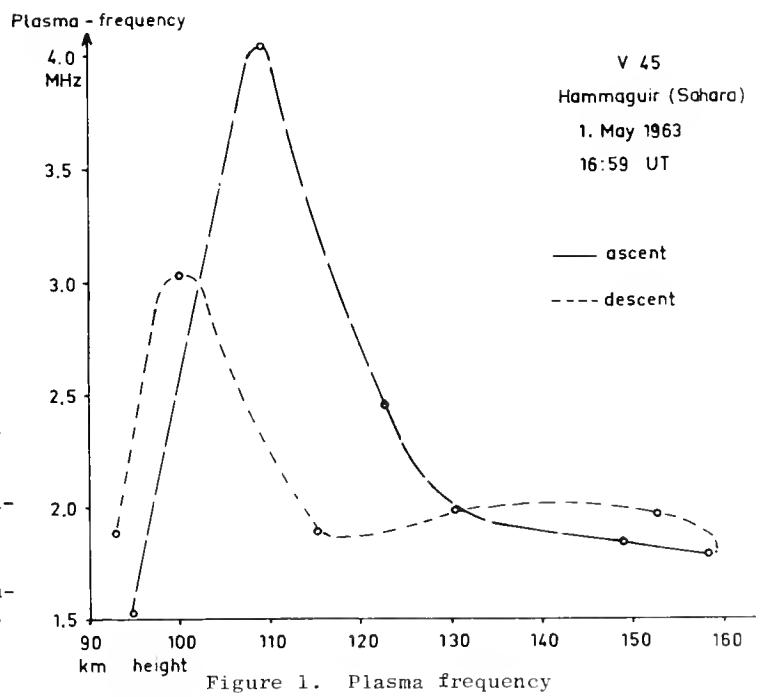

Figure 1. Plasma frequency

* Thanks to Deutsche Forschungsgemeinschaft and to the French Centre National des Etudes Spatiales.

** This part of our work has been sponsored by the Aerospace Laboratories of the USAF through the European Office, Aerospace Research, United States Air Force, Contract No. AF 61(052)-290.

and $f_H = 1.05$ MHz:

$$\omega_N^2 = \frac{\omega_s^2}{p}\,\frac{\omega_s^2 - \omega_H^2}{\omega_s^2 + G\omega_H^2} = 9\omega_s^2\,\frac{\omega_s^2 - (43.5)\times 10^{12}}{\omega_s^2 + (21.75)\times 10^{12}}$$

Figure 1 shows the plasma frequency so determined at ascent and descent. The data are tentative as the precession of the rocket has been neglected and the orbit at descent was estimated from simple formulae. (It is thought that the corresponding corrections would tend to shift the descent curve towards greater heights. The tentative curve is only based on a few measuring points; it shows clearly a maximum ionization in the E-region and a rather important decrease in the "valley region" above. Simultaneous ionosonde observations from the ground at a distance of roughly 20 km show the presence of sporadic E with a critical frequency of about 4 MHz [2]). The different maximum values found at ascent and descent are explained by the horizontal gradient of Es-ionization. Knowing the rocket attitude a final evaluation shall be possible giving details of the profile.

The accuracy of the present observations was limited by a jamming effect due to a telemetry transmitter. The uhf circuits introduced for protection decreased the sensitivity of the measuring device. It should be noted that the Figure gives only a few observation points so that the fine structure of Es for example is not resolved. This will later be done at the final evaluation.

2. The dispersive Doppler experiment* had first been intended mainly for noon observations. It is an inverse Seddon experiment with the transmitters on the ground, the receivers in the rocket. As the time firing was delayed to 17 h the ionospheric absorption of the ordinary component was rather small so that on 5 MHz a second wave reflected from the ionosphere was present. For this wave the geometrical Doppler-effect is not compensated when it is mixed with the 20 MHz wave. The corresponding Doppler beat is high at the beginning and decreases against the summit of the orbit. It is superposed to a slow beat. The high beat frequency can be determined quite accurately so that it can be used for reduction. As the final orbital and attitude data are not yet at hand a provisional reduction has only been made. It clearly shows an Es-layer 400 m in width at 106 km altitude, well below the E-layer maximum which appears at about 117 km.

3. The RF spectrometer covers the frequency ranges 160-240, 880-1250 and 3200-3400 kHz. Our experiment suffered from many local emissions in the different apparatus on board. These give additional spikes which are easily identified. A few broadcasting stations on the ground could be observed in intensity. We may cite one example only. Algiers I on 890 kHz was observed at rather low altitudes up to 85 km where the corresponding spike became very small and then disappeared. The absorbing zone covered the last few km only below that level. This result compares well with results from 1954, where at a noon firing the disappearance occurred at 83 km but the absorption influence began at somewhat lower height.

References

[1] Journ. of Res. (NBS), Vol. 66D No. 6, 641-648 (1962).

[2] Our thanks is due to Mr. Pron of the French Centre National des Etudes de Telecommunications who has made these observations with his recently developed ionosonde.

* These experiments have been developed with the financial help of Deutsche Forschungsgemeinschaft and of Bundesministerium fur Wirtschaft (contract No. J 458).

11.2 RADIO FREQUENCY PROBE MEASUREMENTS OF D-REGION ELECTRON DENSITY

W. J. HEIKKILA
Southwest Center for Advanced Studies, Post Office Box 8478
Dallas 5, Texas

The RF probe discussed in the earlier paper (Paper 2.3) was flown on two Black Brant rockets, fired at the Churchill Research Range, Canada, during the spring of 1963. The first firing, at 1431 hours CST, 7 May, was conducted during quiet daytime ionospheric conditions. The lower frequency mode, using an oscillator of about 4.5 Mc/s frequency, provided good results in the D-region above 75 km. Above this height the oscillator frequency showed a marked dependence on the bias voltage applied to the tip capacitor. This dependence provided positive identification of the plasma effect; it also served as an indicator of the importance of ion sheath effects.

The operation in the high frequency mode was similar to that in the low frequency mode in many respects, but was somewhat erratic and therefore the results are questionable. On the way down the operation on 4.5 Mc/s was apparently successful aga in below 100 km, and during the descent absorption of about 1.5 db occurred, having been over 2.5 db momentarily.

The results presented are still tentative and should be treated with caution. The electron density profiles obtained from the RF probe data are shown in Figure 1. The dashed curve shows the profile obtained on the first flight on a quiet afternoon including corrections of about 20% for sheath effects and other factors to agree with the ionosonde value for foE. The curve appears quite reasonable in comparison with the base of the normal E-region.

The other two curves are the profiles from the RF probe data on the ascent and descent during the auroral absorption event of June 10-11. Both show low values of electron density except above 87 km. The most notable feature is an enhanced layer of 3 km thickness from 87 to 90 km, with a density of about 1.5 x $10^5/cm^3$. This layer appears to be the only feature capable of significant absorption, as can be seen by the comparison with the straight line showing the density required to produce absorption of 0.1 db per km at 30 km, assuming the collision frequency profile adopted by Belrose, curve 1 of his Figure 3 at this conference; even this layer is incapable of more than 0.3 db of absorption, or about 1/5 of the observed total of 1.5 db on the riometer. Other evidence supports the identification of this layer as the main absorbing region. A positive ion probe instrumented by Dr. Willmore of University College, London, consisting of a small sphere held at a fixed negative potential, also showed the presence of this layer and no other. Furthermore, the ionosonde showed the sudden appearance of a sporadic E-layer at 90 km at about the time of the enhanced absorption, shown in Figure 2. The Es trace extends to over 8 Mc/s, and is intense enough to show multiple echoes. This rules out any significant absorption at lower altitudes.

The apparent inadequacy of the lower to produce the total of 1.5 db of absorption may possibly be due to one or more of several causes.

1. The probe results may be wrong in magnitude; the proper behavior of the probe on a quiet day at this altitude, however, lends weight to the probe data.

2. The rocket may have descended through a hole in the absorbing layer.

3. The riometer record may have been affected by reflection from the top-side of the layer.

4. The collision frequency may have been increased, possibly due to an increase in electron temperature. This appears to be not at all unlikely.

The height of this absorbing layer is much greater than that reported from our 1960 firing. However, that previous data was not supported by other lines of evidence as strongly as the present results, and experimental error cannot be completely ruled out. However, the difference may well be a real difference between particular events. In the present case the conclusions on height are reasonably certain, and only the magnitude remains in doubt.

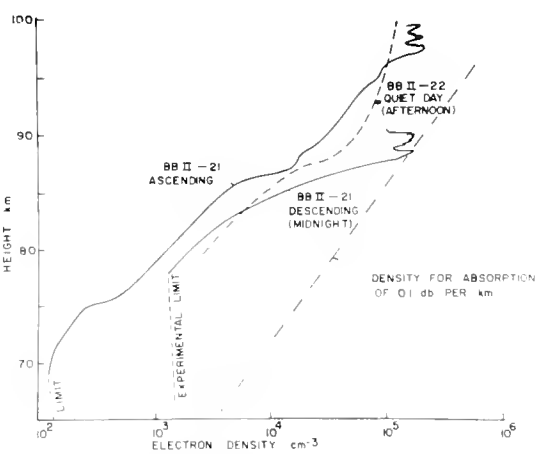

Figure 1. Preliminary results of firing Black Brant II-21 during auroral absorption event: 2305 CST 10 June 1963 (10.6 db ascending, 2.0 db descending).

Figure 2. Ionogram taken simultaneously with the rocket flight.

References

[1] Reid, G. C., and C. Collins, "Observations of Abnormal Absorption at Medium and High Latitudes", J. Atm. Terr. Phys., 15, 1 and 2, 63-81 (1959).

[2] Leinbach, H., and G. C. Reid, "Ionization of the Upper Atmosphere by Cosmic Rays of Solar Origin", Phys. Rev. Letters, 2, 2, 61-63 (January 15, 1959). See also, G. C. Reid and H. Leinbach, "Low Energy Cosmic Ray Events Associated with Solar Flares", J. Geophys. Res., 64, 1801-1805 (1959).

[3] Sen, H. K. and A. A. Wyller, "On the Generalization of the Appleton-Hartree Magnetoionic Formulas", J. Geophys. Res. 65, 12, 3931-3950 (1960).

DISCUSSION

A. Kavadas: Did you go through the aurora?

W. J. Heikkila: It was a cloudy night, so we could not tell.

C. G. Little: I would like to support the speaker's comments that the auroral absorption is tremendously variable from aurora to aurora. We have analyzed about 270 auroral events recently by the multi-frequency riometer technique. Many of these suggest that the absorption is occurring above 80 m. Others show quite convincingly that the absorption is occurring more or less uniformly at heights between 50 and 65 m. So I would like to stress that rocket measurements of auroral absorption must be expected to be extremely variable.

11.3 ELECTRON TEMPERATURE PROFILE DEPENDING UPON THE GEOMAGNETIC LATITUDE

K. HIRAO
Radio Research Laboratories
Kokubunji, Tokyo, Japan

1. Introduction

The electron temperature profiles have been measured by rocket at many locations. Though the electron temperature is not independent from the neutral gas temperature, it has still important geophysical meaning about the energy source which excites the upper atmosphere of the earth. In the present paper, the electron temperature profiles at Fort Churchill, Wallops Island, and Akita are examined with reference to the geomagnetic latitude of every station.

The electron temperature was pointed out to be affected considerably by the disturbance of the ionosphere by the group of the University of Michigan. The groups of the University of Michigan as well as of Japanese rocket team sent temperature-sensitive probes into space at Fort Churchill, Wallops Island, and Akita. These observations were carried out in both quiet and disturbed days.

At Wallops Island, both Michigan's Dumbbell probe and Japanese resonance probe were fired by NASA's rockets in quiet days. Both results are shown in Figure 1. The results of both probes are considered to agree well mutually from this figure. Therefore, the latitudinal distribution of electron temperature will be discussed in the following section by using these results.

The used data are tabulated in Table 1.

2. Experimental Results

The geomagnetic latitudes of Fort Churchill, Wallops, and Akita are 69 N, 49 N, and 29 N, respectively. Therefore, Fort Churchill is in the auroral region, and Wallops and Akita are in the intermediate latitude region.

Date	Time	Location	Ionospheric Condition	Rocket
3/16/60	1526CST	Ft. Churchill	Aur.Zone, Spread F.	Aerobee 300
6/15/60	1656CST	Ft. Churchill	Aur.Zone, Near quiet	Aerobee 300
8/3/60	1126EST	Wallops Is.	Magnetic storm end	Aerobee 300
3/26/61	115EST	Wallops Is.	Quiet	Aerobee 300
3/27/61	1308JST	Akita	Quiet	Kappa-8
10/24/61	1259JST	Akita	Rather disturbed	Kappa-8

Table 1. Tabulation of rocket experiments used in this paper.

The used data in quiet days at these stations were obtained during almost from 12 o'clock to 17 o'clock. After R. E. Bourdeau, the electron temperature at the altitude of 450 km is almost constant during this time interval. He analyzed the data obtained by the Ariel Satellite and derived the diurnal variation of electron temperature in three logitudinal zones of 0 to 20, 20 to 40, and 40 to 60.

Therefore, it is considered to be not necessary to make a local time correction on the quiet-day's data. As for the season of these data, Fort Churchill data were obtained on June 1960, while the other two data were on March 1961 with only one day's interval. The seasonal change of electron temperature, however, is not yet determined. So, the seasonal correction of these data is rather difficult.

Assuming that the electron temperature is not different between every station of the same latitude at the same local time, latitude distribution of electron temperature with its isothermal line can be shown in Figure 2. Considering from Figure 2, it is noticeable that the electron temperature is higher in high latitude than in low latitude. The temperature increase at a constant level seems to be also greater in high latitude than in low latitude. Bourdeau's analysis also shows that the electron temperature is higher in high latitude region than in low latitude through a day, while the rate of increase of temperature by latitude is rather small in high latitude region. In any case, the electron temperature is higher in high latitude region than in low latitude at the same altitude. This fact shows that the other heat source than the solar one should exist in high latitude region.

In disturbed days, data were also obtained at these three stations. The local time of these data were also in afternoon. And the seasons of observation were March, August, and October. It is considered to be necessary to make a correction by season as well as by some index representing ionospheric disturbance. However, the former is difficult as previously mentioned and the latter is also difficult due to

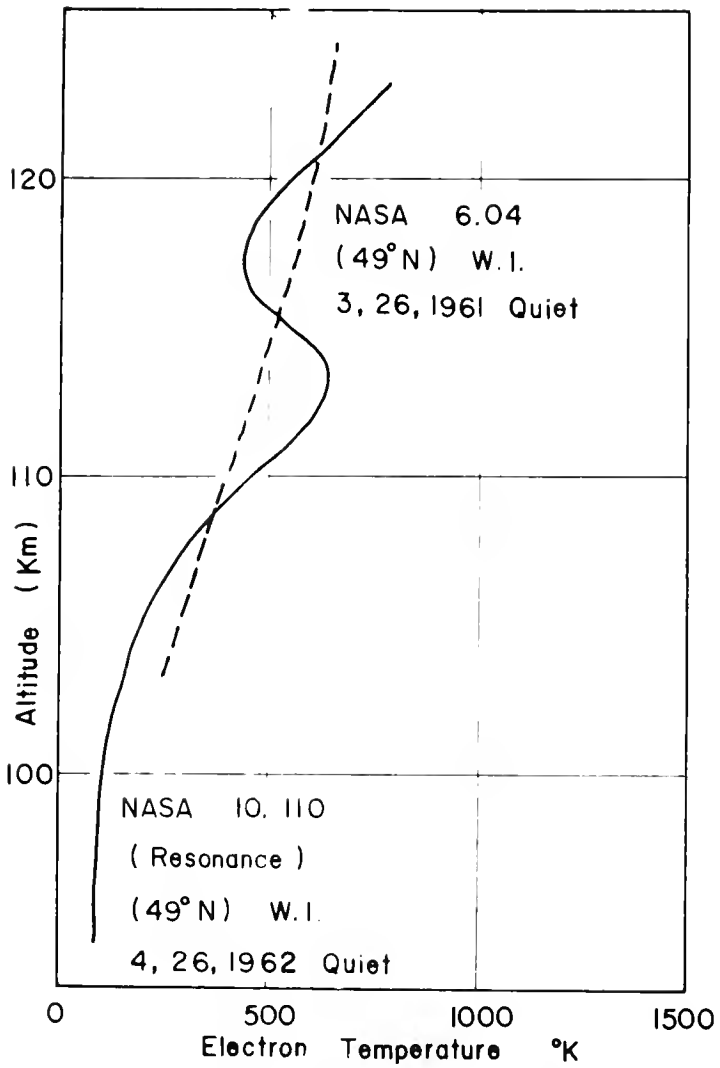

Figure 1. Comparison between Japanese and U S. probes.

the lack of data for statistics.

As these data were not obtained at the time of one event, it may be rather speculative to plot these data in one figure. In spite of this difficulty, the electron temperature distribution with isothermal lines is shown in Figure 3 by using these data. This figure seems very interesting. Generally speaking, the isothermal line runs from low altitude at high latitude region to high altitude at low latitude region. Therefore, the main heat source of electron gas exists at high latitude region. However, the pattern is not so simple as in the case of quiet day. In this figure, it is seen that the temperature raise at Wallops Island is more remarkable than at the other two stations. In quiet day, Wallops Island seems not to belong to the high latitude region but to the low latitude. However in disturbed day, the increase of electron temperature at Wallops Island is so large that Wallops Island seems to belong to the high latitude region in this case. Figure 4 illustrates the quiet-day latitude dependence of the temperature compared with the results of the Ariel satellite.

Now the difference between disturbed and quiet temperature at every point are plotted with also isothermal lines in Figure 5. From this figure, it is seen that the temperature change is fairly big at Wallops Island and not so big at the other two stations. The change at Wallops Island has a maximum at the height of about 130 km. These peculiar changes also cannot be considered to be caused by the solar radiation.

3. Concluding Remarks

The electron temperature is affected not only by the solar radiation but by the north origin energy. This fact is notified by the electron temperature distributions in both quiet and disturbed days. The north origin energy may be presumed to be corpuscular.

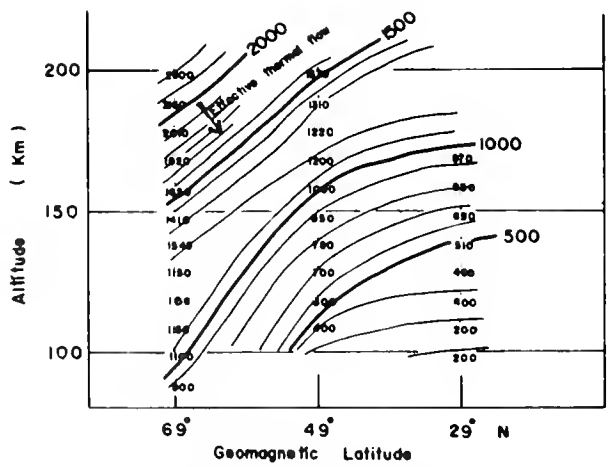

Figure 2. Isothermal line of electron temperature in ionosphere (quiet day).

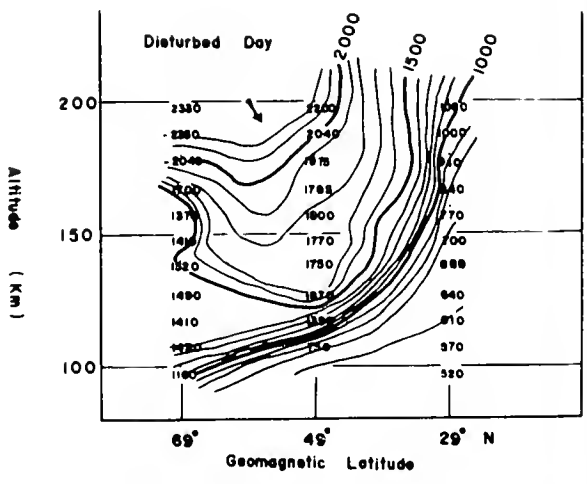

Figure 3. Isothermal line of electron temperature in the ionosphere (disturbed day).

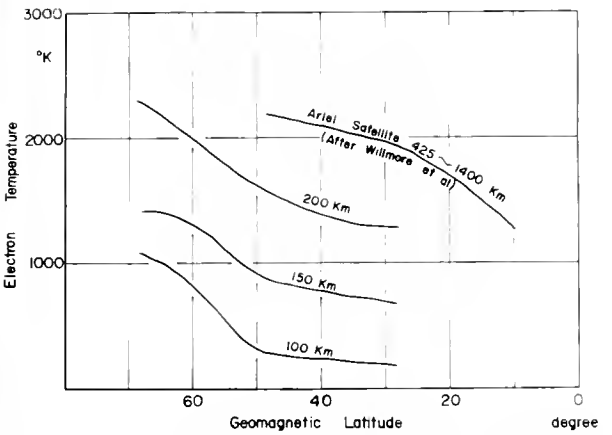

Figure 4. Comparison of rocket and satellite electron temperature measurements.

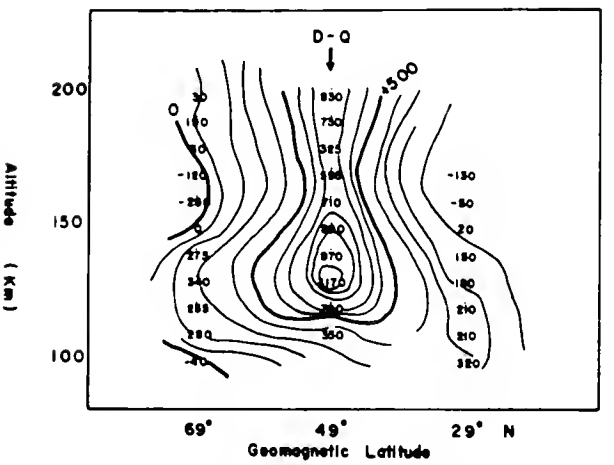

Figure 5. Disturbance field of electron temperature in the ionosphere.

Now, the author wishes very much to obtain the simultaneously observed rocket data of electron temperatures at widely distributed locations. The IQSY may be the best interval to get such data by international cooperative programs.

[1] R.E. Bourdeau: "Ionospheric Research from Space Vehicles", Report Goddard Space Flight Center X-615-62-234, Dec. 1962.

[2] N.W. Spencer, L.H. Brace and G.R. Carignan, "Electron Temperature Evidence for Non-thermal Equilibrium in the Ionosphere", Jour. Geophys. Res. 67 (1962) No. 1.

DISCUSSION

R.L.F. Boyd: I would like to say something about the Ariel data because I think it is being used to prove something we disagree with. I have with me a figure showing the variation of temperature with latitude obtained from the Ariel satellite using very much more data than was available to Dr. Hirao. There is a rise in temperature with latitude, but we believe from our fairly detailed calculations that this can be entirely accounted for in the daytime by solar heating and by taking into account the rate of exchange of energy between the photoelectrons and the plasma. So we do not think that in the daytime the rise in temperature with latitude is to be attributed significantly to corpuscular radiation. There certainly is a corpuscular heating at night, but it is quite small compared to the daytime.

11.4 ROCKET BORNE GYRO-INTERACTION EXPERIMENTS IN THE LOWER IONOSPHERE*

R. R. HODGES, JR.
Antenna Laboratory
University of Illinois
Urbana, Illinois

1. Introduction

Cross modulation of electromagnetic waves in the ionosphere, commonly known as the Luxembourg effect, was first reported by Tellegen[1] in 1933. Subsequently in 1934 Bailey and Martyn [2] explained this phenomena as a process in which electron temperature is modulated by the amplitude variations of a strong RF signal. Temporal changes are thus produced in the collision frequency and hence in the refractive index of the medium, which in turn modulates weaker signals of other frequencies propagating through the disturbed region.

In a magneto-plasma such as the ionosphere, the propagation of electromagnetic energy near the electron gyrofrequency is characterized by a large absorption index for the extraordinary wave in all directions of travel. Since this absorption exhibits a resonance behavior (of width roughly twice the collision frequency), and since electron temperature is affected by the absorption rate of RF energy, Bailey [3] in 1938 predicted that cross modulation would also have a resonance behavior when the strong disturbing signal is swept through the gyrofrequency. This has been verified [4,5]; however, instead of increasing the cross modulation, the resonance causes a decrease because the thickness of the heated layer is limited by the high absorption.

While the gyrofrequency offers no advantage in ground based cross experiments it was recognized that if radiated from a rocket in the lower ionosphere a pulse of gyrofrequency energy could produce a localized but intense increase in electron temperature. If the increased energy were great enough additional electrons could be produced by collisional detachment of ionization. The magnitudes of such disturbances and their decay rates could be detected by cross modulation or other techniques and the measurements related to ionospheric parameters.

Two such experiments have been instrumented and launched. Interpretation of the data has not been complted; however, some preliminary results have been obtained and are presented in this paper.

*This research has been sponsored by Geophysical Research Directorate of the Air Force Cambridge Research Center under contracts AF19(604) 5565 and AF19(628)2484.

2. Basic Experimental Technique

In the current rocket borne gyro-interaction studies a basic experiment has evolved. It consists of a pulsed gyrofrequency heating transmitter and a sensing wave receiver carried by a rocket. The sensing wave is transmitted from the ground and is detected at the rocket. Any disturbance produced by the heating transmitter produces cross modulation on the sensing wave.

Based on absorption considerations a sensing wave frequency near 2 Mc/s is optimum. A loop antenna within a fiberglass nose cone has been used to minimize the effects of the environment on antenna impedance.

Since the gyrofrequency is proportional to the terrestial magnetic field, it likewise has an inverse cube variation with distance from the center of the earth. However, the gyrofrequency at 100 km is within the gyroresonance for all lower altitudes. Therefore, the 100 km value is used. For launchings from Eglin Air Force Base, Florida, this frequency used is 1.41 Mc/s.

In this program two payloads have been launched, both from Eglin Air Force Base. These have been given the designations GIRE-I and GIRE-II (for "gyro-interaction rocket experiment") by which they will be referred in this paper.

3. GIRE-I

The GIRE-I payload was launched at 1318 hours CST on 1 May 1962. It was carried by an Aerobee AJ10-25 vehicle and reached a zenith altitude of 93 km.

The experiment included a 2.02 Mc/s sensing wave receiver and a pulsed 400 watt 1.41 Mc/s heating transmitter. The receiver used a loop antenna within a fiberglass nose cone. A dipole antenna consisting of two whips, each 3 m long, was used for the heating signal. During launch the whips were secured downward along the rocket body. At 62 km they were deployed forming a dipole oriented transverse to the vehicle roll axis.

At burnout of the sustainer motor (about 18 km) a mechanical failure occurred in a motor driven switch. One pole of this switch had served as a data commutator, the other as a clock to synchronize various measurements. Its stoppage eliminated the following measurements: 1.41 Mc/s radiated field intensity, radiated power,

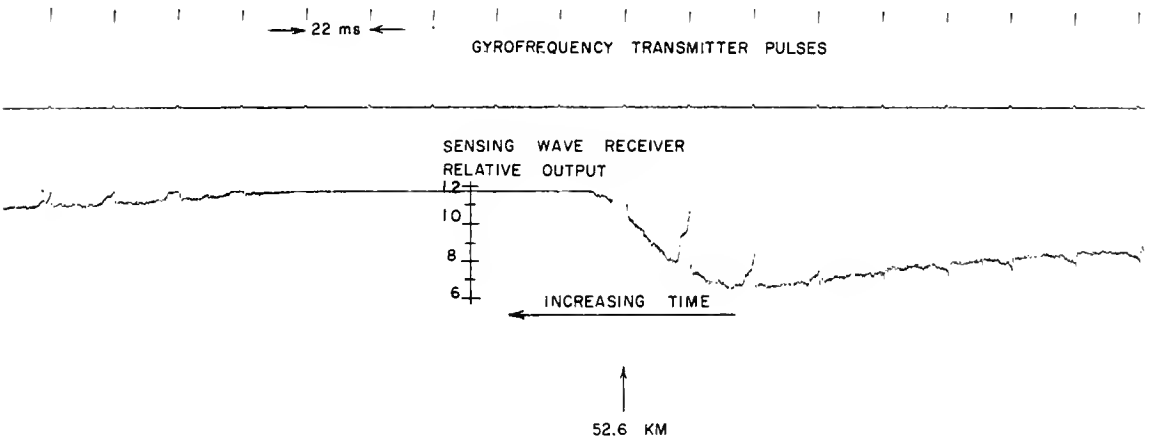

Figure 1. Characteristic modulation of sensing wave near polarization null at 52.6 km (GIRE-I). Rocket velocity 900 m/sec; rotation rate 42.2 deg/sec.

and antenna impedance; excitation light; nonlinear mixing of the 1.41 Mc/s and 2.02 Mc/s signals; and magnetic aspect. Also eliminated was the sequencing of the heating transmitter available power through steps of 4 and 40 watts as well as the 400 watt level.

The data obtained from this flight was limited to the 2.02 Mc/s sensing wave receiver output and the receiver AGC level.

The heating pulse duration was 500 microsec, the period between pulses 22 msec. The combined factors of the gyro-interaction and the high electric fields near the short dipole produced disturbances which involved increased electron densities above 40 km. The slow decay rate of electron density and the fast pulse repetition rate have complicated data interpretation above 70 km.

From 40 to 65 km a form of cross modulation characteristic of variation of polarization was recorded. Figure 1 shows a portion of the 2.02 Mc/s receiver output near 52.6 km during ascent. At this time the rotation of the rocket caused the linear polarization of the sensing wave and the receiving antenna to pass through a nearly orthogonal condition, or a null. (The general shape of the curve is due to slow AGC action). Each heating pulse is accompanied by a cross modulation wave shape which persists for several msec. The modulation prior to the polarization null is negative-going but changes to positive just as the null is past. A similar effect occurred at each null in this region, the negative going modulation becoming apparent about 25 deg of rotation prior to a null, changing to positive near the null and fading away by 25 deg past the null.

From the durations of these modulation wave shapes and rocket velocity the disturbances are estimated to have had longitudinal dimensions os 8 to 10 m. The abrupt termination of each wave shape suggests that the disturbances were fairly uniform and sharply bounded.

By assuming negligible electron density in the vicinity of the rocket just before a heating pulse and making the Born approximation for the perturbation of the fields in the disturbed region, the receiver output can be approximated as

$$V \tilde{=} g \left| a \cos\phi - Nb \sin\phi \right| \qquad (1)$$

where: g = receiver gain

ϕ = angle from the direction of polarization of the sensing wave to that of the receiving antenna measured counter clockwise when viewed upward in the northern hemisphere.

$ga \cos\phi$ = antenna voltage in the absence of electrons

$gNb \sin\phi$ = perturbation of antenna voltage due to electron density N in the disturbed region.

Since rocket rotation was in the direction of increasing ϕ an increase in N for $\phi < \pi/2$ would decrease V; for $\phi > \pi/2$ it would increase V. This is identical to the effect shown in Figure 1.

The rate of electron density decay can be found from this data if the loss process is exponential, i.e.,

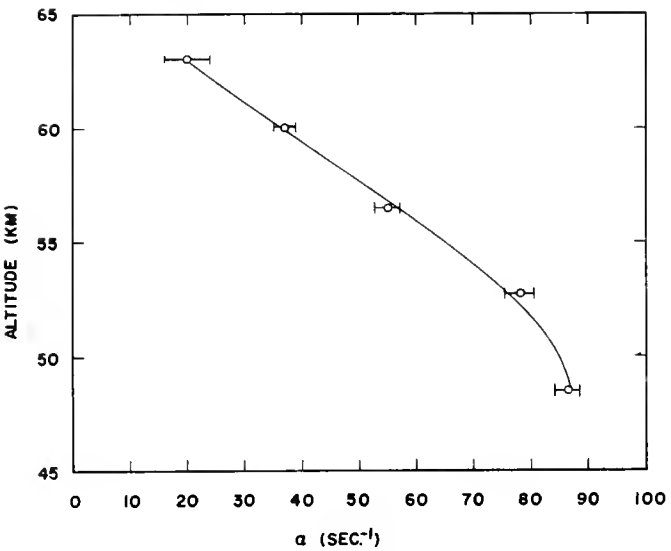

Figure 2. Electron density decay rate from GIRE-I flight of 1 May 1962.

$$N = N_1 e^{-\alpha t} \tag{2}$$

Assuming the electron density in the disturbed region to be initially uniform, from (1) and (2) it follows that

$$\alpha \simeq - \frac{\left.\frac{dV}{dt}\right|_{t=0_+} - \left.\frac{dV}{dt}\right|_{t=0_-}}{V(0_+) - V(0_-)} \tag{3}$$

where $t = 0 \pm$ refer respectively to conditions immediately after and before a heating pulse. The measured values of the electron loss rate are shown in Figure 2. The ratios of these values to the corresponding molecular densities, as given by Minzner et al. [6], are approximately the same. This indicates that the dominant electron removal process is two body radiative attachment. Molecular oxygen would be the logical second body. Assuming that 0_2 accounts for 20.9% of the molecular density the attachment coefficient would be $2 \pm .5 \times 10^{-14}$ cm^3/sec.

4. GIRE-II

The GIRE-II payload was launched at 1147 hours CST on 29 June 1963. Carried by an Aerobee AJ11-21, it reached a zenith altitude of 157 km. While this is far above the optimum zenith of 100 km, no rocket with the desired capability was available.

In contrast to the previous experiment the gyrofrequency disturbance of GIRE-II was intentionally made weak. The high electric fields of the dipole antenna were eliminated by use of a loop antenna. Since gyro-interaction involves dielectric properties of the medium this resulted in a more uniform but less efficient heating. A pulse width of 700 microsec and repetition rate of 10 per sec were used.

A loop antenna was also used for the 2.02 Mc/s sensing wave receiver. The two loops were oriented orthogonally in a fiberglass nose cone.

In addition to cross modulation other measurements included the RF voltage and real component of current of the heating antenna, and an impedance probe. A photo tube to detect excitation light did not function properly.

Vehicle attitude was sensed by three heliflux magnetometers, a solar eye, and a two axis free gyro. This portion of the payload was constructed by Spectral Physics Corporation for AFCRL.

Below 90 km cross modulation was negligible. This was in part due to the weak heating field, but more important the total absorption of the 2.02 Mc/s sensing wave was very small. Its reflection by the ionosphere produced a large standing wave ratio over most of the trajectory below the reflection level. In contrast there was no evidence of a reflected wave during the GIRE-I flight. Inasmuch as absorption requires the presence of electrons, the electron density below 90 km must have been much less during the second shot than during the first. The lack of cross modulation in the GIRE-II flight is partially the result of this difference in electron distribution.

At lower altitudes no evidence was found of the polarization rotation effects obtained in the

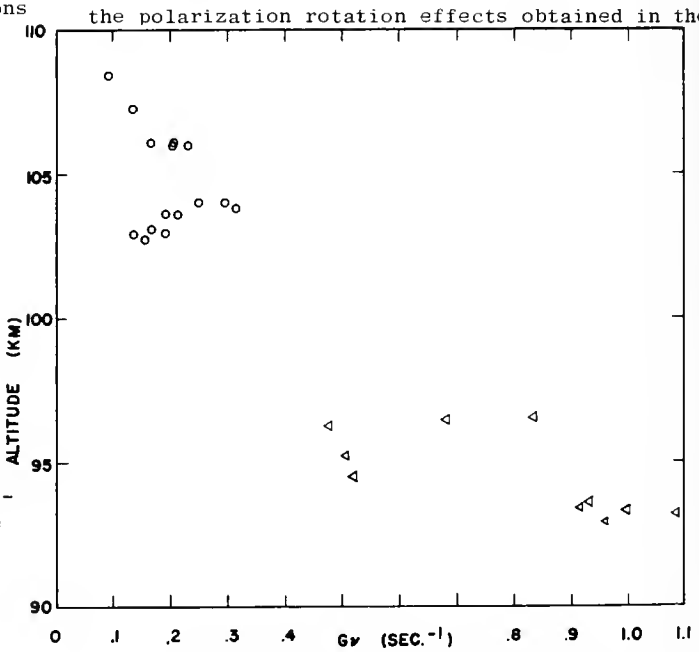

Figure 3. Experimental values of G from GIRE-II flight of 29 June 1963; △ indicates upper bound.

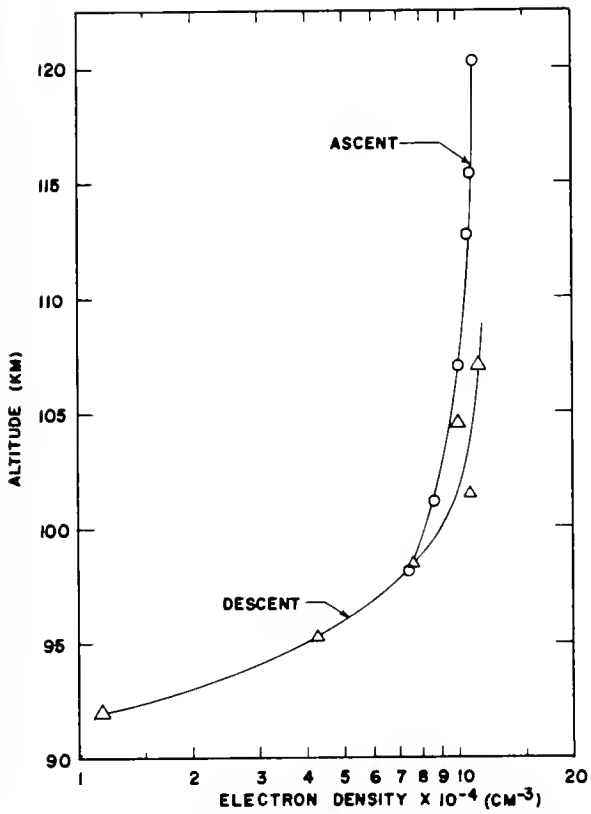

Figure 4. Probe measurements of electron density from GIRE-II flight of 29 June 1963.

first experiment. If this effect had been due to a spin population inversion of oxygen, which is paramagnetic, the effect would have been greater with the strong RF magnetic fields of the loop heating antenna of GIRE-II. Therefore, modulation of electron density is the most plausible explanation of the observed cross modulation below 65 km in the first experiment.

Near the sensing wave reflection level cross modulation due to electron heating was observed. Assuming collision frequency to be proportional to electron temperature, the rate of loss of electron temperature can be expressed

$$\frac{dT}{dt} = - G\nu \frac{T}{T(0_-)} [T - T(0_-)] \qquad (4)$$

or

$$T = \frac{T(0_-)}{1 - [1 - T(0_-)/T(0_+)]e^{-G\nu t}} \qquad (5)$$

where G = fraction of energy lost by an electron in a collision

ν = electron collision frequency at $T = T(0_-)$.

If the heated region extends several wavelengths the energy loss rate G can be found from the cross modulation data to be

$$G\nu < \frac{\left.\frac{dV}{dt}\right|_{t = 0_+}}{V(0_+)\ln[V(0_+)/V(0_-)]} \qquad (6)$$

Expression (6) would be exact if electron temperature decay were exponential (i.e., ν independent of T).

When the rocket is above the sensing wave reflection level the receiver input is due to plasma noise, or bremsstrahlung. Since the noise has a spectral density which is roughly proportional to the inverse square root of electron temperature (cf. Nawrocki and Papa [7]) the band limited receiver output is

$$V = C\, T^{-1/4} \qquad (7)$$

where C is a constant at a given altitude and antenna orientation. Assuming that electron temperature obeys (5), the energy loss rate $G\nu$ is

$$G\nu = \frac{4 \left.\frac{dV}{dt}\right|_{t = 0_+}}{V(0_+)\left[\left(\frac{V(0_-)}{V(0_+)}\right)^4 - 1\right]} \qquad (8)$$

Experimental value of G from (8) and the upper bound from (6) are shown in Figure 3.

The design of the impedance probe was based on the study of antenna impedance in a magnetoplasma by Balmain [8]. For a short dipole oriented parallel with the applied magnetic field the real part of the impedance has a resonance of width 2ν at approximately

$$\omega \simeq \sqrt{\omega_H^2 + \omega_N^2 - \nu^2} \qquad (9)$$

where ω_H = angular gyrofrequency

ω_N = angular plasma frequency

ν = collision frequency

The resonance is observed by applying a constant current swept frequency to a short probe and measuring the real component of antenna voltage. In this manner both plasma frequency and collision frequency can be telemetered as one waveshape. Since the minimum antenna voltage is determined by noise considerations, and the maximum by the range of impedance to be measured, the minimum detectable resonance width depends upon the electron heating produced by this maximum antenna voltage. In general the probe will not disturb the resonance width if the electric

field is much less than the characteristic "plasma field" [9] or

$$E \ll \sqrt{\frac{3}{2} KT \frac{m}{e^2} G \left[\nu^2 + (\omega - \omega_H)^2 \right]} \qquad (10)$$

where $\frac{3}{2} KT$ = mean electron energy

m = electron mass

e = electronic charge

This factor limited the collision frequency measuring capability of the probe used in the GIRE-II flight to the region below 90 km. However, the aforementioned lack of electrons at these altitudes resulted in no collision frequency data. Some electron densities were inadvertently measured at greater altitudes and are presented in Figure 4.

5. Conclusions

It has been demonstrated that localized perturbations of ionospheric properties can be produced by the radiation of pulses of gyrofrequency energy from a rocket borne transmitter. These disturbances are the results of increased electron temperature which can be made great enough to produce additional electrons by collisional detachment or ionization. The magnitude of the perturbations and their relaxation rates can be probed by means of cross modulation techniques. The results of such measurements can then be related to ionospheric properties.

In conjunction with these experiments an impedance probe has been developed to make rapid measurements of plasma and collision frequencies. This type of device will be useful in future experiments employing strong gyro-interaction effects.

References

[1] B.D.H. Tellegen, "Interactions between Radio Waves", Nature, Volume 131, p. 840 (1933).

[2] V.A. Bailey and D.F. Martyn, "The Influence of Electric Waves on the Ionosphere", Phil. Mag., Vol. 18, p. 369 (1934).

[3] V.A. Bailey, "On Some Effects Caused in the Ionosphere by Electric Waves", Part II, Phil. Mag., Vol. 26, p. 425 (1938).

[4] M. Cutolo, "Effects of Radio Gyrointeraction and their Interpretation", Nature, Vol. 166, p. 98, (1950).

[5] V.A. Bailey, R.A. Smith, K. Landecker, A.J. Higgs, and F.H. Hibbend, "Resonance in Gyro-Interaction of Radio Waves", Nature, Vol. 169, p. 911, (1952).

[6] R.A. Minzner, K.W. Champion, and H. Pond, "The 1959 ARDC Model Atmosphere", Air Force Surveys in Geophysics, No. 115, ARCRC (1959).

[7] P.J. Nawrocki and R. Papa, Atmospheric Processes, (Prentice-Hall, Inc., 1963) p. 9-36.

[8] K.G. Balmain, "The Impedance of a Short Dipole Antenna in a Magnetopolasma", Ph.D. Thesis, Dept. of Electrical Engineering, University of Illinois, Urbana, Illinois, May, 1963.

[9] V.L. Ginzburg and A.V. Gurevich, "Nonlinear Phenomena in a Plasma Located in an Alternating Electromagnetic Field", Soviet Physics Uspekhi, Vol. 3, p. 115, (1960).

11.5 DIRECT MEASUREMENT OF ATMOSPHERIC PRESSURE IN THE MESOSPHERE ABOVE HAMMAGUIR

G. ISRAEL
Laboratoire de Physique de l'Atmosphere
Universite de Paris
Paris, France

An aerodynamic method based on the measurement of air pressure at certain positions on the surface of a rocket has been used to compute atmospheric pressure above Hammaguir (Sahara).*

The pressure gages used were heat conductivity manometers with a good accuracy between 30 km and 90 km and specially developed for Veronique use. Figure 1 gives the position of

Table 1. VERONIQUE FLIGHTS, APRIL 1963 - HAMMAGUIR - (31 N)

	V 35	V 49	V 45
Data	20.4.1963	23.4.1963	1.5.1963
Time	$10^h24'$	$22^h04'$	$16^h59'$
Peak altitude (Km)	175	138	160
Spin rate (rpm)	12	15	12
Surface pressure	2 symmetrical gages	2 symmetrical gages	---
Impact pressure	1 gage	1 gage	---
Static pressure	----	----	1 gage

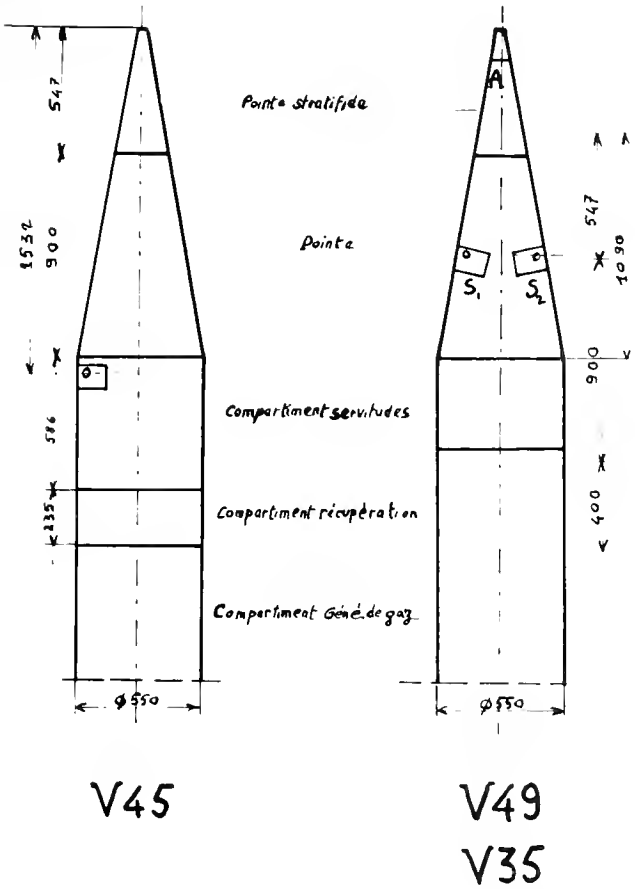

Figure 1. Position of gages in three rockets fired in April, 1963.

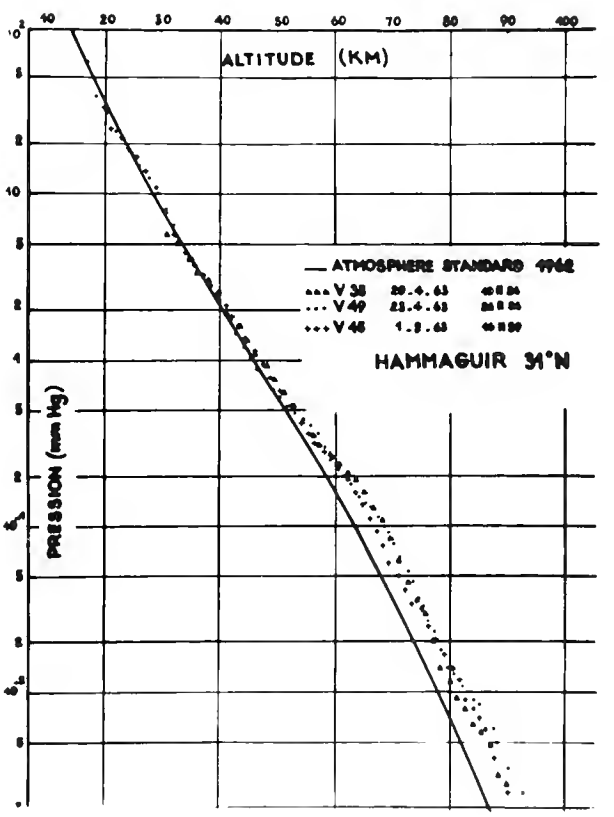

Figure 2. Pressure profiles as computed by the formula between 30 and 90 km.

* Thanks to the French Centre National d'Etudes Spatiales

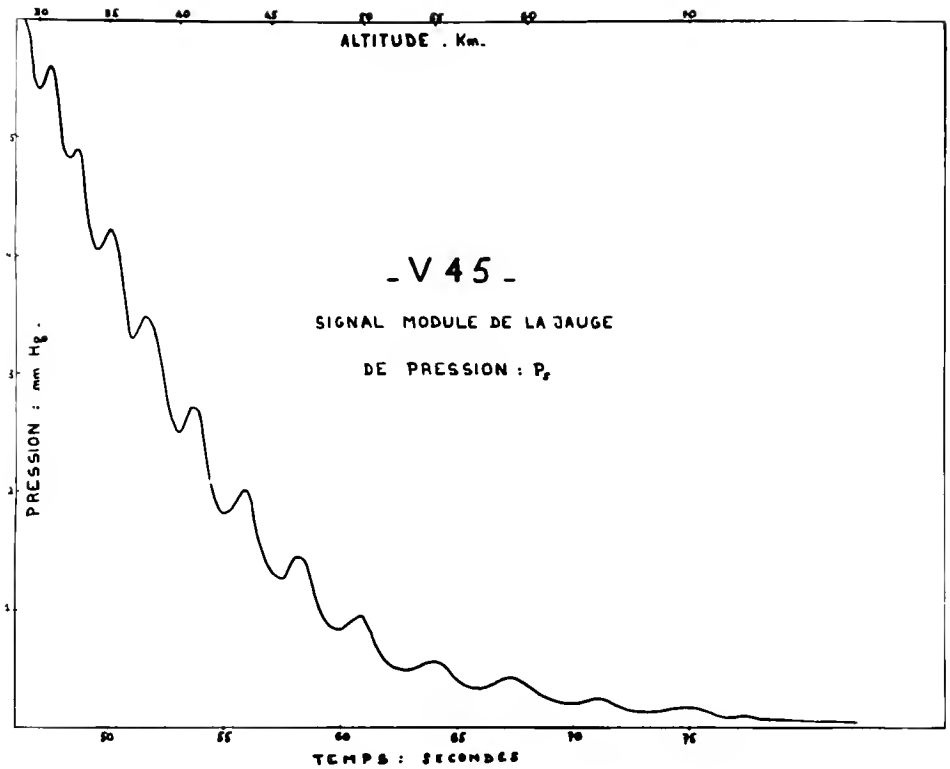

Figure 3. Altitude modulation of the apparent pressure.

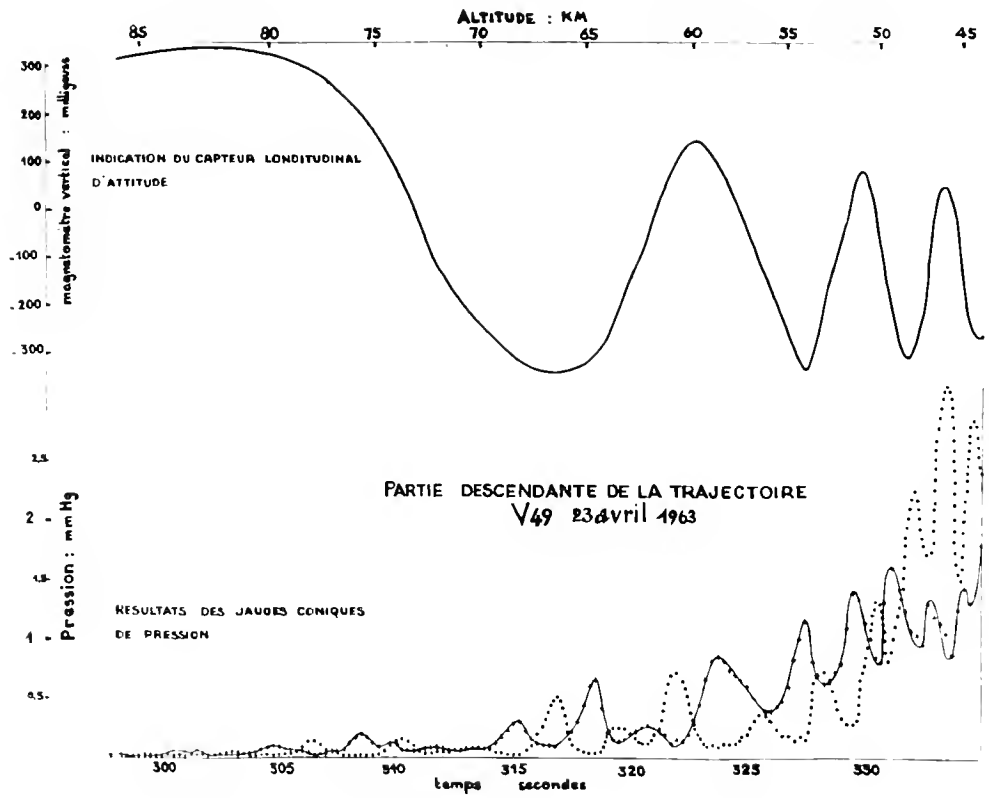

Figure 4. Altitude modulation of the apparent pressure on descending leg of trajectory.

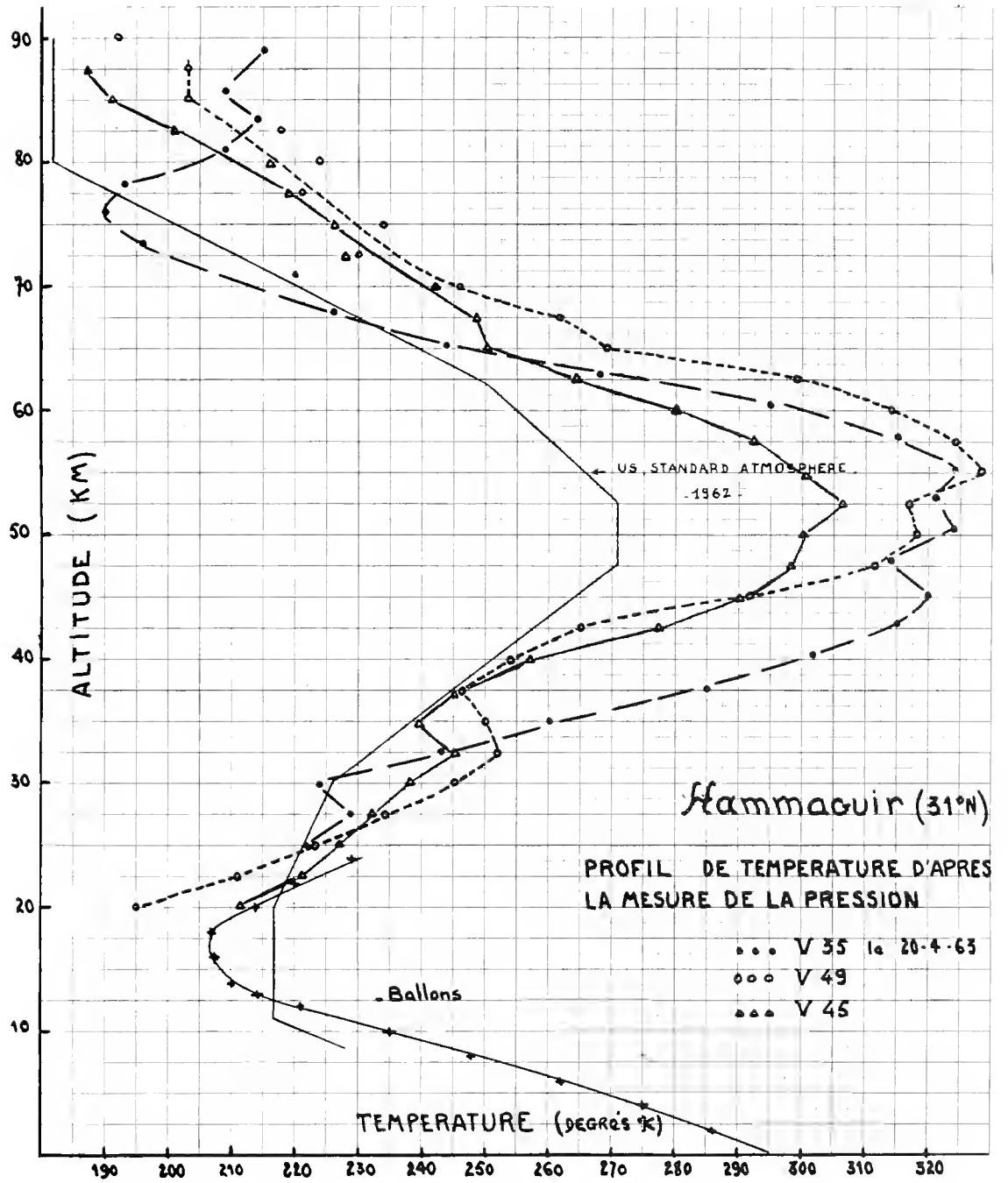

Figure 5. Temperature profile derived from the pressure measurement.

the gages in three rockets which were fired in April 1963 for exploration of the lower ionosphere (Table 1). In each gage thermistors were used in order to measure the temperature of the instrument. On surface pressure gages, no important variation of the wall temperature has been detected during the all flight. For the impact pressure gages the increasing of wall temperature occurs when the rocket has reached 150 km (50 deg C at the end of the flight).

Telemetry data reduction was made by computers and gave directly curves pressures vs time.

On the example of one firing V 35, we show how it is possible to compute the atmospheric ambient pressure by using the surface pressure data. Because of a strong sensitivity of the gages to over-pressure, the first ten seconds of the flight do not give useful results. On the contrary, between 30 km and 90 km (Mach = 5), it

is shown that a single formula gives the relation of the blunt nosed cone pressure with the ambient pressure. This formula which uses the hypersonic viscous interaction parameters

$$X = C \; M^3 \quad (R_e)_x$$

is

$$\frac{P_s}{P_\infty} = a + b \; X + c \; \frac{M^2}{(x/t)^{2/3}}$$

The term $c \; M^2/(x/t)^{2/3}$ where x is the abscisse of the position of the gage from the top nose and where t is the diameter of the blunt nose, correspond to the inviscid pressure field associated with the lunt nose of V 35 rocket.

For the surface pressure P_s we have chosen the mean value between the two symmetrical cone gages. The spin modulation is very apparent and can easily be taken into account. The rocket outgassing pressure becomes important at 70 Km(10 per cent of P_s). On the other hand, the slip flow effects are no more negligible after 80 Km, when the Knudsen number becomes equal to 0,1 ($X > 4$).

The Figure 2 gives the pressure profiles as computed by the formula between 30 Km and 90 Km. A certain modulation, probably due to the variation of rocket angles of attack, can be seen. Temperature profiles have been computed from the slope of the logarithmic pressure curves. The temperature maximums in the mesosphere seems to be too high (320° K), as referred to the atmospheric standard values; but they conform to the V 27 result in February 1961, also above Hammaguir.

11.6 MICROSTRUCTURE IN AURORAL DISPLAYS AND THE IONOSPHERE

A. KAVADAS
Institute of Upper Atmospheric Physics
Saskatoon, Saskatchewan, Canada

An appreciable number of experiments designed to measure ionospheric parameters deal in one way or another with an interaction between an incident electromagnetic wave and an ionized medium. The results of this interaction are in turn used to deduce the values and behaviour of the ionospheric parameters.

In order to facilitate mathematics or because we do not know enough about a medium we often introduce assumptions which are idealizations or just simplifications of a complex physical picture. Because the interpretation of the measurements dependes to a degree on these assumptions and because they are not always justified, more information about the medium and in particular its microstructure is highly desirable.

At present indirect experimental evidence suggests that such microstructure may exist but no direct measurements are available to substantiate this possibility.

Radio aurora, which like the ionosphere is a magneto-ionic medium, is thought to be turbulent and an increasing number of investigators attribute its ability to scatter radio waves to some kind of microstructure. Direct measurements may reveal the actual size or time variations of the small scale constituents of the aurora which are referred to as microstructure.

The detection and measurement of microstructure imposes some special conditions in the size, design, and building of the rocket instrumentation.

The measuring device must be small enough so that its presence at the point where the measurement is taking place does not disturb the microstructure. This condition can be easily satisfied if the measurement takes place away from the rocket by means of instrumented packages which are ejected.

These packages, besides being of small size, must also be capable of measuring, recording and transmitting the information to the ground.

Small ejected packages which can move freely through the medium without appreciably alterating its structure can be effectively used to study the size and time variations of auroral or ionospheric microstructure. A single Black Brant II rocket can carry as many as six large packages or about 10 small ones. These may be ejected in any desired sequence to provide samplings in various points in space as well as samplings at the same point in space but at various times.

Measurements with ejected packages reduce the possibility of errors which might arise if the medium in the vicinity of the rocket happens to become contaminated by exhaust gases. This is particularly true if the rocket uses a solid propelant.

A number of ejected package experiments have already been designed. Some of these have been tried while others are still in the development stage. The prototypes for two of these have already been flown, and although the results are still preliminary, a brief account of the experiments will be presented.

One of these, an electron density probe, has already been described by A. W. Adey in a previous paper (paper 1.1). Results of this experiment are not available because of malfunction in the instrumentation. The other experiment is a probe which can measure electric fields. This consists of a metallic container with a cover which is separated from the main body of the can

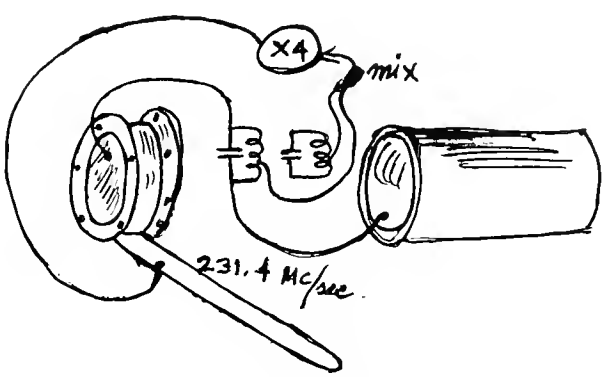

Figure 1. Circuit diagram of electric field probe

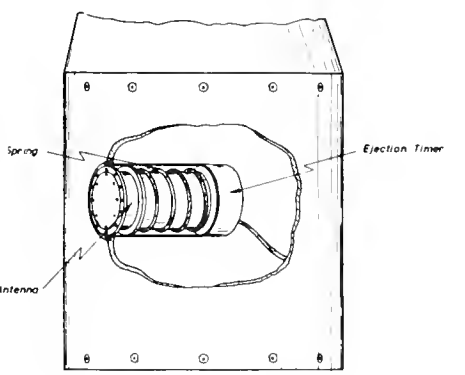

Figure 2. Probe ejection mechanism

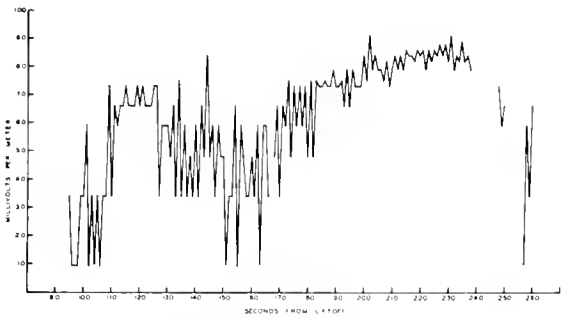

Figure 3. Electric field measured in auroral display

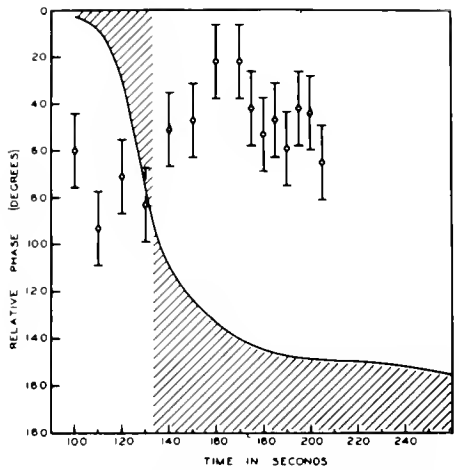

Figure 4. Comparison of observed and expected relative phases of electric field signal

by an insulator. The two parts of the probe, the cover and the can are connected to a voltage controlled capacitor (varicap), as shown in Figure 1. This condenser is part of a tank circuit. Every time a potential difference appears between the cover and the can the varicap changes its capacity. Another oscillator of fixed frequency is also incorporated in the package. If no potential difference is present between the can and the cover, the two oscillators are 1.25 kc/s apart. The moment a potential difference appears the frequency of the variable oscillator changes. The frequency difference between the two oscillators is recorded. This probe is capable of measuring without change of scale, field intensities from 1 to about 10,000 mV/m.

The probe is given an initial spin upon ejection so that if an external field is present the frequency deviates both ways, so that the recorder frequency deviation follows a sinusoidal variation in time. At the same time the intensity of the telemetered signal is recorded. This too will follow a sinusoidal curve. The geometry of the probe is such that if an electric field is present and it is parallel to the direction of the line joining the probe and the telemetry receiving antenna, the signal intensity and the frequency deviation will be in phase. This configuration provides some information on the instantaneous position of the package in a given plane of spin.

Figure 2 shows the ejection mechanism while Figure 3 shows the electric field measured during an auroral display. For the ascending leg of the trajectory, one may see a rapid fluctuation in the value of the electric field. During the descent of the probe conditions appear somewhat more quiet. Using the relative displacement between the maxima in the signal intensity and frequency deviation, it appears that the electric field has a direction not parallel to that of the magnetic field.

Two major sources of error are possible. The first is charge accumulation of different signs on the cover and can, because the velocity of the probe is higher than the positive ion velocity, while quite a bit lower than the electron velocity. This effect will manifest itself as an electric field in the direction of motion. This effect has not been observed, or least it was of minor importance, during the test flight fo the probe. Figure 4 indicates in the shaded area the the expected relative phases between the intensity of the signal and the frequency deviation during the flight. The measured relative phase falls outside this region suggesting that the maxima in frequency deviation are due to an electric field in a direction other than that of motion.

The second source of error becomes important when the probe spins in a plane which is not coplanar with the trajectory. In this case motion in the magnetic field will introduce an electric field perpendicular to both the velocity vector and the magnetic field. Consideration of the geometry of the trajectory and the direction of the magnetic field may indicate that this effect has not been seriously affected the measurements during the flight of the prototype.

A number of other packages are in various stages of construction with two of these scheduled to be fired in the near future. The purpse of one of these two experiments is to measure the density of neutral particles in the E- and F-regions. This is done by combining the information on collision frequency, electron density, and electron temperature. All these parameters can be obtained with one instrumented package. This particular experiment, however, utilizes the rocket from which the background temperature is measured spectroscopically.

A series of packages are also being prepared to be used for seeding experiments de-

signed to measure radar scattering cross sections of artificially induced ionization.

DISCUSSION

E. C. Whipple: I should like to make sure that I understand the principle of the measurement. The two portions of the probe which are insulated from each other, you assume come to equilibrium potential with the atmosphere, so that you measure a voltage difference and then divide by some effective length between the two parts.

A. Kavadas: No, this is a direct comparison. We calibrate the instrument with an electrometer. The values that I gave you in mV/m are values that we obtained in the laboratory. I do not have a slide of the calibration with me.

R. L. F. Boyd: How can you distinguish the effect of the magnetic field from the effect of such things as an anisotropic distribution of particle velocities? The magnetic field will affect the diffusion of ions to the probe, while an anisotropic distribution of particle velocities will affect the potentials to which the cylinder and the plate will be charged up.

A. Kavadas: We did not encounter any of these difficulties.

R. L. F. Boyd: The potentials that the probes adopt depend on the energy distribution of particles and the magnetic fields that are present. So how can one decide whether the difference of potential measured is due to the electric field or whether it is due to the anisotropy in the energy distribution of the particles?

A. Kavadas: What would be the difference; how do you define an electric field in the ionosphere?

R. L. F. Boyd: In the usual way.

J. E. Hall: You made no mention of the ($\underline{B}$ x $\underline{V}$) field, the induced field due to the motion across the magnetic lines of force. Did you observe this, and how do you take it into account?

A. Kavadas: I am not quite sure that you should observe it; but, assuming that you do, it is easy to take into account. You know at all times the relative positions of the maximum of the signal and the maximum of the field - if the field were there.

11.7 ION CONCENTRATION AND THERMAL ANALYSIS OF DATA OBTAINED FROM AN ION TRAP CARRIED IN A LOW-ALTITUDE ROCKET

W. C. KNUDSEN and G. W. SHARP
Research Laboratories
Lockheed Missiles and Space Company
Palo Alto, California

Under NASA Contract NASw-342 a Nike Apache rocket was flown containing a hemispherical grid ion trap. The rocket was launched on May 8, 1963, at 1223 EST from Wallops Island, Va. and rose to 167 km apogee. Usable data were obtained from approximately 100 to 150 km.

The hemispherical grid construction for the ion trap was chosen to simplify the effect of rocket precession on the data analysis and to satisfy as closely as possible the theoretically assumed behavior of the trap. The period of the retarding potential sawtooth cycle was approximately two seconds so that one ion current vs. retarding potential curve was obtained approximately every second. The limits of the retarding potential were -0.5 and 4.5 volts.

Analog retarding potential and ion current telemetry signals were digitized, correlated and corrected where necessary for rocket precession and a small periodic electronically produced noise signal. The result of this operation was a set of data consisting of 94 pairs of correlated ion current and retarding potential values for each sweep of the retarding potential between its limits. The temperature, ion number density, and rocket potential relative to the plasma were determined for each set of data by selecting the values of these parameters which minimized the sum of the squares of the deviations of the experimental ion current data from the theoretically computed value. A necessary parametric assumption was the gram molecular weight of the dominant ion. NO^+ was taken to be the dominant ion in the height range of concern consistant with ion mass spectrometer data.

Statistical estimates of the significance of the parameters were obtained from the analysis. The numerical techniques used to determine the values of the parameters and their significance is described by Moore and Zeigler [1] and McWilliams [2].

Results of the temperature analysis are illustrated in Figure 1. Each experimental temperature point located on the figure results from one set of data corresponding to one sweep of the retarding potential. All temperature determinations to 150 km are illustrated with one exception. Noise on the telemetry channel significantly altered the ion current curve for that particular temperature point. The data represented by dots only, are considered less relable than that indicated by circled dots. The judgment is based upon the amount of correction applied to the data and upon the appearance of the analog traces. The statistical standard deviation for the temperature is indicated by the error bars. All of the standard deviations were approximately 60 deg K with the exception of the three points in the lower right corner of the figure. Theoretical profiles for the temperature of the neutral constituents are

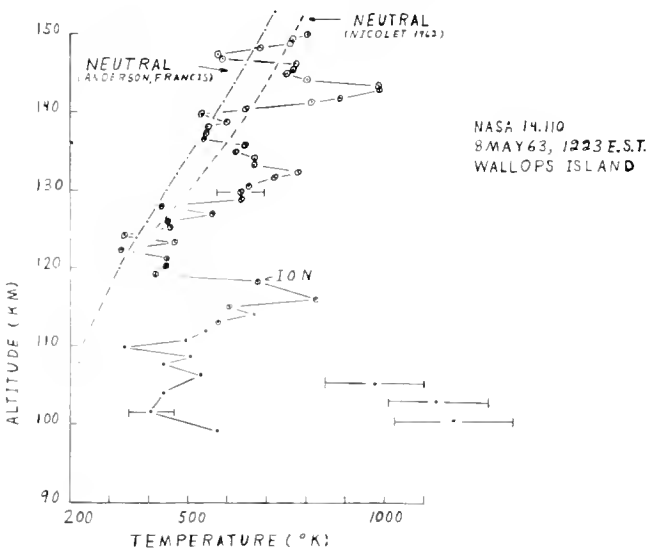

Figure 1. Ion temperature measurements on NASA rocket 14.110, 1223 EST, 8 May 1963, Wallops Island.

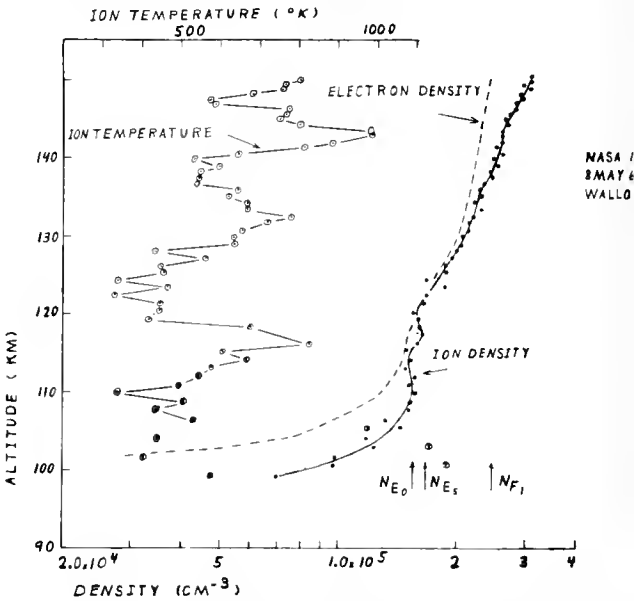

Figure 2. Ion density measurements on NASA rocket 14.110, 1223 EST, 8 May 1963, Wallops Island, compared with ionosonde electron density data.

illustrated by dashed lines. The profile labeled (Anderson, Francis) is based upon an unpublished atmospheric model formulated by A. D. Anderson and W. E. Francis of Lockheed Missiles and Space Company, which takes into account the sun spot number and time of day. The model isothermal temperature reached at higher altitude for the time of day and sun spot number appropriate for the rocket flight was 1180 deg K. The profile after Nicolet [3] was selected from a set of profiles contained in the cited reference. The profile selected was the one which most closely reached the same isothermal temperature at high altitude as the Anderson and Francis model.

The data indicate thermal layering of ions in the E region of the ionosphere with thickness of the layers approximately equal to the neutral scale height appropriate to the altitude and with the temperature at the layer peaks approximately 300 deg K above the corresponding troughs. Comparing the ion temperatures with the estimated neutral temperatures suggests that the ions may be at a temperature as large as 300 deg above that of the neutral temperature at the peaks. If both ions and neutral particles are assumed to have a common temperature then the thermal energy conducted into the troughs must be dissipated by radiation rather than conduction. It is assumed in the above speculation that the thermal layering is produced by the absorption of photons and has large horizontal dimensions when compared with the layering dimension.

The ion number density data, are illustrated in Figure 2. The temperature data and the electron density determined from an ionosonde taken at Wallops Island at the time of the flight are also shown for comparison purposes. The statistical standard deviation for the ion density is approximately the size of the dots and is not illustrated. This deviation is based on the statistical behavior of the data with each set of data and does not take into account any error in instrument parameters, such as the transmission factor of the ion trap grids. Each of the ion density data points has been multiplied by the factor of 1.59 to bring it to the position indicated. The laboratory calibration of the grid transmission factor was one source of systematic error.

Another source of systematic error in the ion density data is lack of knowledge of the angle of attack of the rocket. The rocket axis precessed about a total angular velocity vector L generating a cone with an unknown conic angle. Periodic variations in the attack angle which occurred when the axis of the precession cone, L, was not parallel to the velocity vector of the center of mass of the rocket were detectable in the data and removed in data preparation. Lack of knowledge of the conic angle and the angle between L and the velocity vector prevents removing possible systematic error which could not only displace the curve horizontally, but also stretch it. The systematic error under discussion does not affect the temperature analysis significantly.

The arrows labeled N_{E_O}, N_{E_S} and N_{F_1} indicate the electron density corresponding to critical frequencies read from the ionogram. With the first vertical slope of the ion density curve brought into horizontal coincidence with the arrow marked N_{E_O}, the second arrow comes into alignment with the peak of the second bulge. The correlation of the F_1 critical number density with a steep ion density is not obvious. As mentioned above, the ion density curve could be stretched as a result of systematic error.

Comparing the temperature profile with the ion density profile, there is no obvious correlation. The first significant temperature peak in the vicinity of 117 km is at the same altitude as the narrow bulge in the ion density. However, scatter in the data is, in places, as large as the inferred bulge and perhaps it is more plausible to consider the peak to occur at a broad inward inflection of the ion density curve. The temperature peak at approximately 143 km appears to correlate with a questionable steepening of the ion density curve at that altitude. The thermal peak at approximately 132 km may correlate with a questionable bulging of the ion density curve.

It is tempting to associate these apparent thermal layers with electron gradients responsible for sporadic E. Diffusive equilibrium is believed to exist above approximately 110 km, and if we consider the ions as behaving independently of the neutrals, as an ionic gas in a steady state condition, the ionic density would be reduced in hot regions. Assuming electrical neutrality and an insignificant number of negative ions, the thermal peaks would correspond to regions of low electron density. At least in the higher altitudes we might expect this mechanism to operate. Conversely, if the thermal regions are produced by photons of specific wavelength, as has been supposed, they are also the regions of the maximum rate of ion production. We might expect the thermal regions to be correlated with an enhanced ion concentration in the lower altitudes.

Whatever may be the correct correlation between the ion temperature and ion concentration profiles, it is clear that ionic thermal layering did exist in the E-region of the ionosphere on the day of this rocket flight. Further, the thermal layers have a depth that is approximately the same as the neutral scale height at the altitudes of the layer.

References

[1] McWilliams, P., 1963, "The Solution of the General Least Squares Problem with Special Reference to High-Speed Computers," Los Alamos Sci. Lab. Report, LA-2367 Addenda

[2] Moore, R. H., and Zeigler, R. K.,1960, "The Solution of the General Least Squares Problem with Special Reference to High-Speed Computers," Los Alamos Sci. Lab. Report LA-2367

[3] Nicolet, M., 1962, "A Representation of the Terrestrial Atmosphere from 100 KM to 3000 KM," The Penn. State Univ. Ionospheric Res. Sci. Report No. 155

DISCUSSION

M. A. Biondi: Is your analysis sufficiently sensitive to take into account the potential of the rocket body?

W. C. Knudsen: Yes, that was one of the parameters that was obtained from the flight of the rocket. It was -1.9 volts ±0.1 volts throughout the entire trajectory of the flight.

M. A. Biondi: A tenth of a volt is quite a few hundred degrees. Could not your shift between the ion and the gas temperature be easily accounted for by an error in the potential of the rocket body? Or is your analysis so sensitive to form that you can see this?

W. C. Knudsen: A change in rocket potential between one sweep of the retarding potential and the next would not affect the temperature computation. The shape of an ion current vs. retarding potential curve is not dependent upon the rocket potential provided the potential does not change significantly during the approximately 0.1 second period when the current is changing from zero to its maximum value.

The theoretical expression for the ion current vs. retarding potential was derived by assuming the ions had a Maxwellian velocity distribution in a coordinate system at rest relative to the center of Mass of the ions. Relative to the ion trap on a moving rocket, the ion velocity distribution would be skewed. It was the appropriate skewed velocity distribution function that was used in deriving the theoretical ion current vs. retarding potential expression.

The only experiment on the rocket was the ion trap experiment and the trap was located at the nose of the rocket with axis of symmetry on the symmetry axis of the rocket. A nose cone protected the ion trap during the early portion of the flight and was ejected at about 80 km altitude.

11.8 ROCKET-BORNE LANGMUIR PROBE MEASUREMENTS IN AURORA

A. G. McNAMARA
National Research Council
Ottawa, Canada

1. Experimental Objectives

The Langmuir probe experiments are designed for launching from Churchill, Canada, to make direct measurements during conditions of visual and radio aurora. Atmospheric parameters of particular interest are the electron and ion densities, electron temperatures, and the spatial structure of the ionization. The height region of greatest interest lies between 90 and 130 km. Simultaneous data is also obtained from a variety of ground-based experiments: auroral cameras, spectrographs, photometers, radars, riometers, ionosonde, and magnetometers. In addition to the atmospheric parameters, the multiple probe installation is designed to study the plasma collection processes as they are affected by sheath size, mean free path, and probe geometry.

2. Experimental Details of the Flights of April, 1963.

One rocket (AA26) carried a multiple probe installation consisting of a flush-mounted planar probe, a 1/4 inch sphere mounted 3 inches from the rocket skin, and two 3-inch spherical probes which were timed to extend on booms 18 inches long, 50 sec after launch. One 3-inch sphere had a constant potential applied while the current was measured continuously. The other three probes had sweeping potentials and were sampled sequentially by a common electrometer.

The second rocket (AD23) carried a simple (Langmuir) probe experiment, consisting of a single planar probe to which a constant positive DC bias was applied. This probe was capable of responding to very rapid variations of electron density. Since no V-I characteristic was swept out, calibration in terms of electron density were to be obtained from an ionosonde comparison or by comparison with a geometrically identical probe on rocket AA26.

The rockets were Black Brants, a solid fuel rocket of 17 inches diameter, capable of carrying a payload of 300 pounds. The cast magnesium alloy nose cone was scoured and cleaned prior to flight to achieve a large metallic area for the collection of charged particles. The rocket skin is used as the reference electrode of the Langmuir probe system.

3. Flight Performance.

Both rockets were fired on the night of April 5/6. 1963, on which there were strong

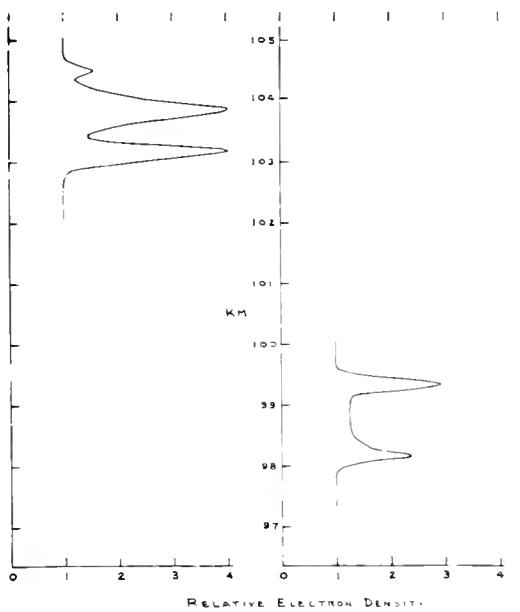

Figure 1. Sporadic E-layers observed at 0125 CST 6 April 1963 at Churchill.

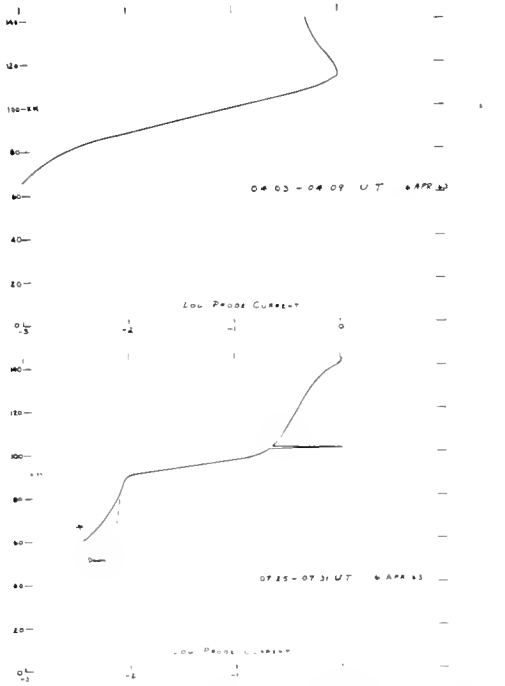

Figure 2. Preliminary electron-density-height profiles for two rocket flights.

auroral displays. The first rocket, carrying the multiple probe experiment, was fired at 2203 CST and achieved an altitude of 144 km. Complete telemetry and radar beacon tracking was obtained from launch to impact at 361 sec. All parts of the Langmuir probe experiment functioned well except for the loss of data from the swept 3-inch spherical probe due to a shorted coaxial cable.

The second rocket was fired at 0125 CST and reached 142 km. Telemetry was received for the 360 sec flight period, and radar beacon tracking was obtained from 113 sec to 360 sec.

4. Experimental Results.

The first rocket successfully passed through bright visual aurora of intensity III to IV. Probe currents were measurable from heights of 47 km to the apogee of 144 km. Ground-based observations indicated an average brightness of 900 kR in the 5577 A line, and 1.5 db auroral absorption at 30 Mc/s. Ionograms were very complex, with total absorption occurring on some scans. The most prominent feature of this flight profile derived from the Langmuir probe data is the absence of detailed structure within the ionization.

The second rocket, fired some 3 1/2 hr later, was also aimed at aurora, but due to the rapid variations of the aurora the region of the sky through which the trajectory passed was devoid of aurora. However, during this flight the 30 Mc/s absorption was absent and the ionosonde displayed very intense sporadic E activity. The Langmuir probe clearly showed two closely-spaced sporadic layers near 100 km altitude on both the up and down legs of the trajectory. The thickness of these imbedded layers was only 350 m at the half-density points. A magnified plot of the relative electron density distribution in these Es-layers is shown in Figure 1.

Figure 2 shows the preliminary height profiles of the two flights (not to the same scale). These curves have been drawn from smoother data, removing the vehicle wake effects. To a first approximation, theory shows that the probe current is proportional to the electron density above approximately 90 km altitude. Below 90 km, the simple Langmuir theory does not apply directly. However, L. G. Smith has shown that extension of the probe current curve to lower altitudes does give a profile similar to electron density derived from different experimental methods. At least, the current profile should be representative of any structural details and changes in the lower altitudes.

The top portion of Figure 2 shows the results for a flight through visual aurora. On the basis of a partial data analysis, the scale factor for the X-axis has been tentatively placed at a value of 2×10^5 electrons/cc.

The bottom portion of Figure 2 shows the case of a flight without visual aurora on the trajectory. This was obtained with a single planar probe with a fixed DC bias. Preliminary assessment of the ionosonde record and comparison with the geometrically identical probe on rocket AA26 results in an X-axis scale factor of 4×10^4 electrons/cc. The density and approximate altitude of the Es layers shown in detail in Figure 1, are represented in Figure 2 by the spike near 100 km. Although the peak density of the Es is not high, the extremely sharp density gradients produce Es-traces on the ionosonde extending much beyond the frequency corresponding to the critical density.

11.9: ROCKET MEASUREMENTS OF ELECTRON DENSITY IN THE D-REGION DURING AND AFTER A SOLAR ECLIPSE*

J.S. NISBET
Ionosphere Research Laboratory
Pennsylvania State University
University Park, Pennsylvania

ABSTRACT

Rocket measurements of electron density in the D-region of the ionosphere were made during the solar eclipse of July 20, 1963 at Fort Churchill and a control experiment was conducted several days later at the same time of day.

Two methods were used. The first was an ambient measurement of conductivity and capacitance at 100 kc/s and 512 kc/s between an insulated section of the nose-cone of the rocket and the main rocket body. The second was a propagation measurement of the signals received on two ferrite loop antennas, one along the rocket axis and the other at right angles to it. As the rocket was spinning this arrangement enabled the amplitude of three orthogonal components of the field to be measured.

1. Introduction

It was desired to measure electron densities in the D-region using small rockets.

Probe measurements in this region are complicated by the low electron densities with accompanying sensitivity problems, the presence of negative ions, high collision frequencies and the uncertainty in the boundary conditions at the probe caused by the ion sheath and possible effects of shock front perturbations.

Propagation measurements which can be made insensitive to perturbations due to boundary conditions at the rocket surface are complicated by reflection from higher ionospheric regions. If low frequencies are used, the necessary ray tracing or more complete wave analysis is almost impossible without at least a first order approximation to the electron density and collision frequency profiles. The approach used in this work has been to attempt to combine ambient and propagation measurements to obtain the advantage of both.

As it was intended to measure electron densities an AC probe method was adopted to mini-

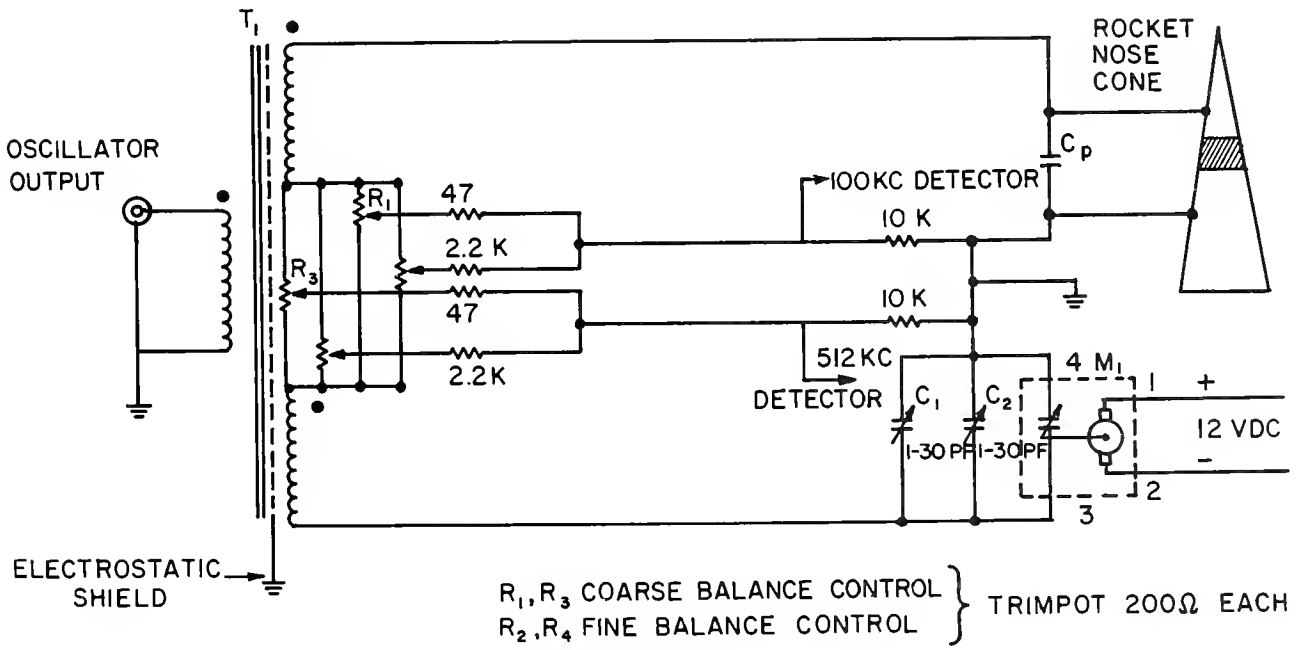

Figure 1. Capacitance conductance bridge circuit diagram.

* The research reported in this document has been sponsored by the Geophysics Research Directorate of the Air Force Cambridge Research Laboratory, Office of Aerospace Research, United States Air Force, under Contract AF19(604)-8012.

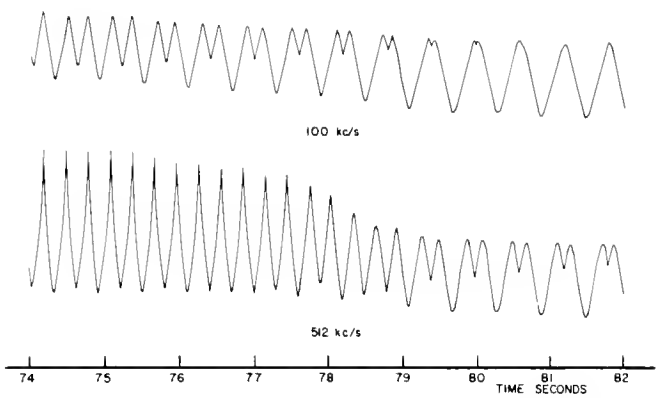

Figure 2. Output from capacitor probe.

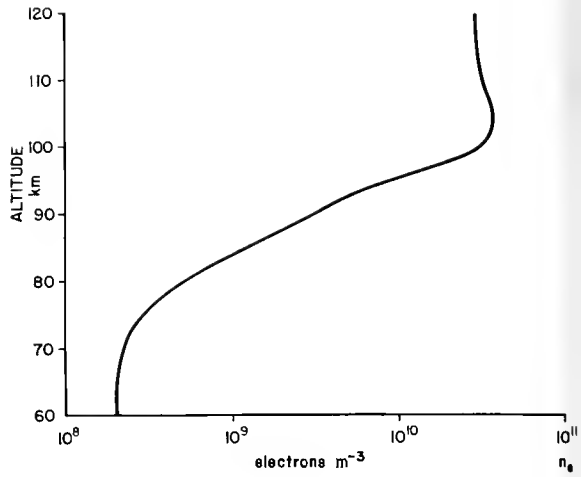

Figure 3. Electron density profile deduced from resistance and capacitance measurements at 100 and 512 kc/s.

mize the effect of negative ions and charged dust particles. An initial analysis indicated that by using frequencies of the order of a few hundred kilocycles per second a measurement of parallel conductance of a capacitance probe could be made quite sensitive at the low electron density levels in the lower D-region. In the upper D-region capacitance measurements on the same probe could be used for comparison purposes and to provide information on the collision frequency.

A block diagram of this is shown in Figure 1. The probes consist of the tip of the nosecone of a Black Brant II rocket insulated from the rest of the nosecone and the main rocket body by a Fluorosint insulator. This configuration was chosen to avoid interfering with the aerodynamical properties of the vehicles and the delay in starting measurements associated with erection mechanisms. The conductance and capacitance are measured using a transformer birdge circuit. In the bridge T_1 is a balanced shielded bifilar wound transformer arranged so that when the capacitance in the upper and lower arms are equal no voltage appears across the detector output providing Cp is purely reactive. By means of a small motor driven capacitor the lower arm is varied continuously and the value of Cp may be determined from the times at which the nulls are observed in the detector voltage. When Cp has a resistive component there is no longer a perfect null at the balance point and the minimum voltage is a function of the parallel resistance component. Figure 2 shows a typical voltage waveform obtained from the AGC circuit of a receiver arranged to have a logarithmic characteristic with input voltage. The birdge circuit is not frequency sensitive and in the experiments described 512 kc/s and 100 kc/s oscillators and detectors were paralleled.

In the propagation measurements signals wer received at the rocket on ferrite loop antennas. One of the antennas was aligned with the rocket axis and the other at right angles to it was rotated by the spinning motion used to stabilize the vehicle so that the magnetic field strength could be measured along three orthogonal azes. Signal strengths were measured using TRF receivers with crystal filters to limit the bandwidth.

2. Results

The equipment operated well and measurement were obtained continuously on all telemetry channels for both experiments.

Final trajectory and altitude information has not yet been received and much work remains to be done on the analysis. At this time only the most tentative results can be given which are subject to review as the analysis is completed. At present, in particular, the analysis has just proceeded to the point, at which tentative profiles from the probe measurement have been obtained for use in the analysis of the propagation experiment. The trajectories were very similar and it is interesting to compare the relative measurements of electron densities in the two flights, one during the period of the eclipse and the other several days later at the same local time.

It would appear from these results that the electron density was down by a factor of about 8 at around 70-80 km during the eclipse and that smaller changes were observed at 60 km and

100 km.

A first electron density profile obtained from these measurements is shown in Figure 3, for the flight during the eclipse. It was derived from capacitance and resistance measurements, and good consistency was found between the two frequencies at heights of 70-120 km on the up- and down-leg.

The results below 60 km should be treated with caution, since the resistance values found are perhaps two orders of magnitude lower than expected. Possibly collisional ionization or outgassing may be responsible. The theoretical sensitivity limit of 10 el/cm^3 was not attained due to this effect.

11.10: ELECTRON ENERGY SPECTRUM MEASUREMENTS DURING AURORAL ABSORPTION

J. ORTNER
European Preparatory Commission
for Space Research
36, rue LaPerouse, Paris 16

1. Introduction

A few rocket measurements of the energy spectrum of auroral electrons have been made during recent years. McIlwain [1] fired sounding rockets into visual aurora and a Canadian group [2] studied electrons and protons associated with auroral radio absorption. These investigations which were carried out from the Canadian range at Fort Churchill were limited to the energy range for electrons above 40 keV.

The purpose of the experiments which were performed from the Swedish rocket range at Kronogard (situated about 200 km south of Kiruna) was to study the electron energy spectrum below 50 keV during aurora. These were cooperative experiments between the Air Force Cambridge Research Laboratories and the Kiruna Geophysical Observatory under the auspices of NASA.

Nike-Cajun rockets have been used for these experiments, the payload of which included also sample cups to collect noctilucent cloud matter, and photographic emulsions for the detection of protons and heavier particles. Four rockets have been fired, two of which were flown during auroral absorption events. However, only one of the auroral shots was successful, since the equipment failed during the second flight.

2. Instrumentation for the Auroral Experiment

An electrostatic analyzer was developed by a group of American Science and Engineering, Inc., which was capable to measure the electron energy spectrum in the range 3 - 50 keV. Its block diagram is reproduced in Figure 1.

The analyzer consists of two concentric spherical plates to which a DC voltage is applied, modulated at 1200 cps. The voltage is exponentially swept between 7000 and 0 volts within 250 milliseconds. Electrons transversing the space between the plates are accelerated by a constant post-acceleration potential of 7000 volts applied to the surface of a scintillator. The output of the photomultiplier is then fed into the preamplifier circuit and passes through a band pass filter turned to 1200 cps. Thus, any noise which is not at 1200 cps is eliminated. The signal then enters the compression circuit the output of which is telemetered to the ground. By comparing this signal with the exponential voltage sweep the electron fluxes are obtained at any time as function of energy.

The main specifications of the electrostatic analyzer are the following: The radius of the inner analyzer plate is 4.8 cm and the distance between the plates 0.3 cm. The solid angle is determined by the spherical segment 90^{o} by 5^{o}, the area of entrance aperture 0.25 cm^{2}.

The electron energy range is 3 - 50 keV and the energy resolution was determined to be about 8%.

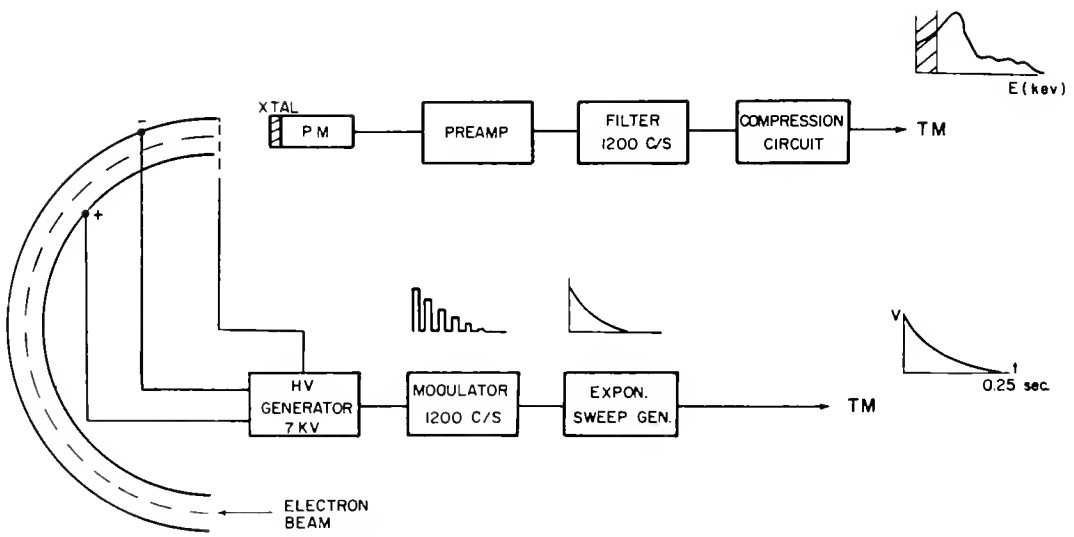

Figure 1. Electrostatic analyzer

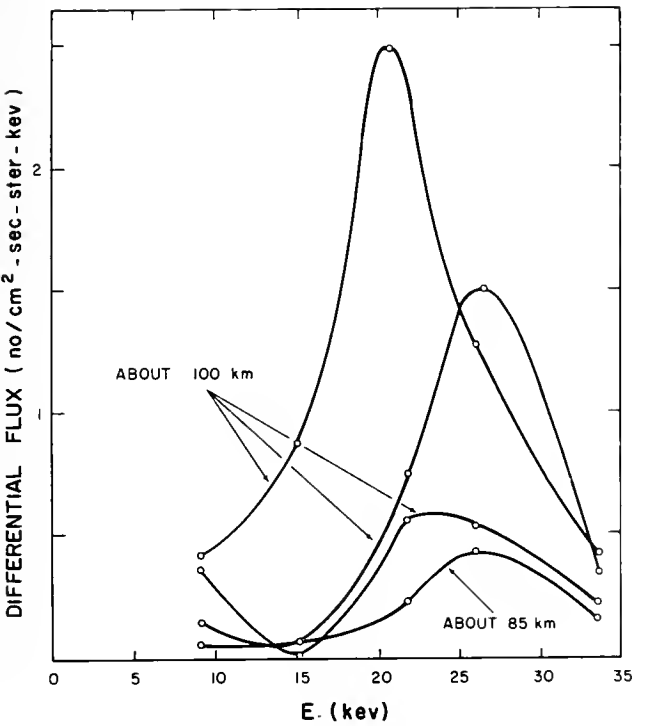

Figure 2. Energy spectra at various times.

3. Rocket Experiments and Results

The first rocket was launched on 7 August 1962 at 0047 UT when the 40 Mc/s riometer at Kronogard recorded about 1 db absorption of the auroral type. At the same time the 27 Mc/s riometer at Kiruna measured an attenuation in signal strength of 3 db and the magnetic X-component showed a deflection of about 300 gammas. These observations indicated an auroral event of medium intensity.

The rocket reached a peak altitude of 102.5 km which unfortunately was too low for obtaining complete information about the electron fluxes at low energies within the aurora. However, the analysis of the data shows a number of electron bursts in the region of the peak altitude attained by the rocket. Because of arcing between the analyzer plates at the maximum exponential sweep voltage, data on electron energies greater than 37 keV were lost. Electrons with energies up to 37 keV were recorded in the bursts, with a maximum intensity of about 10^9 electrons/cm^2.sec.ster. occurring at energies around 20 keV. These bursts did not seem to originate from any particular direction.

The duration of the observed electron bursts was rather short, since each burst lasted not longer than a few seconds. Thus, these bursts seemed to be caused by some sudden disturbances precipitating large numbers of electrons into the atmosphere in relatively short periods of time.

Figure 2 presents the observed differential electron fluxes at different times as function of energy. As can be seen, fluxes up to 2.5 x 10^8 electrons/cm^2.sec.ster.keV have been obtained at a height of 100 km. It is, however, rather doubtful if the peaks in electron fluxes between 18 and 28 keV were due to a smaller primary flux of electrons below these energies. The decreasing electron flux with energies less than 20 keV may possibly be explained by atmospheric absorption.

No electron bursts could be observed during the subsequent rocket flight of August 11 which was performed during quiet ionospheric conditions and was devoted to studies of the composition of noctilucent clouds. This fact proves the significance of the electron bursts obtained during disturbed ionospheric (auroral) conditions. Nevertheless, the results described above should still be considered as preliminary until further measurements studying other auroral events have been performed.

References

[1] McIlwain, C.E., Direct measurement of particles producing visible auroras. J. Geophys. Res. 65, 2727-2747, 1960.

[2] McDiarmid, I.B., Rose, D.C. and Budzinski, E., Direct measurement of charged particles associated with auroral zone radio absorption. Can. J. Phys. 39, 1888-1900, 1961.

DISCUSSION

W.J. Heikkila: I would like to comment on our DRTE rocket flights that are going on this year. The NRC are again making low electron energy measurements to about 10 keV. We at DRTE had a further experiment in which we used an electron multiplier to detect individual electrons down to about 30 ev. These packages all seem to be working, so, in due course, we hope to make a report on this.

G.C. Reid: I thought that I should point out that McIlwain's experiments several years ago in fact went down to energies below 5 keV. One of the most striking things about the results was that he found almost mono-energetic electrons at about 6 keV; they were not confined to energies above 40.

J. Ortner: Did he have a complete sweep?

G.C. Reid: No, I don't think so.

J. Ortner: The difference here is the complete spectrum between 3 and 50.

W.J. Heikkila: Concerning the difficulty of firing under these conditions: the results that I showed for during the disturbance - we had the rockets on the launcher 15 times before we were finally able to fire it on the 16th time.

11.11 SOME PRELIMINARY RESULTS OF A GERDIEN CONDENSER MEASUREMENT

A. PEDERSEN
Uppsala Ionospheric Observatory
Uppsala 10, Sweden

Preliminary results of a Gerdien condenser rocket probe experiment using a Gerdien condenser hanging under a parachute is given. Payload descent from about 85 km height is described and measurements of ion conductivities and concentrations are reported.

This experiment has been calibrated for a flight during polar black out conditions, when one can expect high ion and electron concentrations. Difficulties with the launch site in northern Sweden have lead to the solution that this rocket system has been undergoing a function test in the States.

Two experiments took place at White Sands on 8 October and 10 October 1963. During both flights the parachutes made of thin metalized mylar performed like ideal parachutes with a drag coefficient of 1.0 during the descent. The top of the two rocket trajectories were 88 km and 81 km and the parachutes and the instruments were separated from the rocket about 1 km before the top on both flights. The parachute used during the second flight was most probably partly torn during expulsion from the rocket and could not stand the strain from the drag forces deeper in the atmosphere. This parachute hit the ground like a streamer. The payload descent rates are shown in Figure 1.

On the first flight the antennas were broken during expulsion from the rocket and no data were obtained. The second flight was more successful and some information about positive and negative ion concentrations was obtained. The elongation mechanism which is supposed to increase the length of the line between the

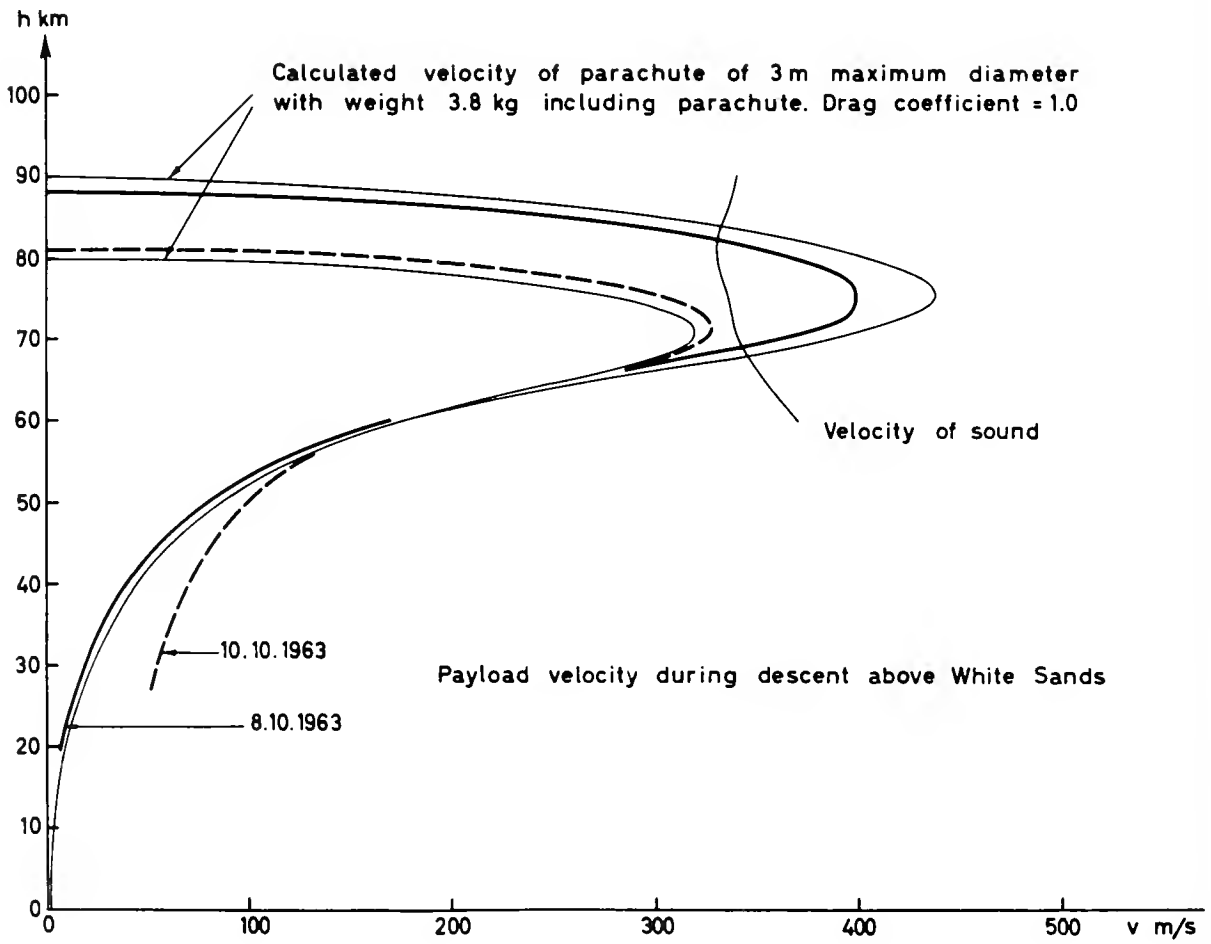

Figure 1. Payload descent rates

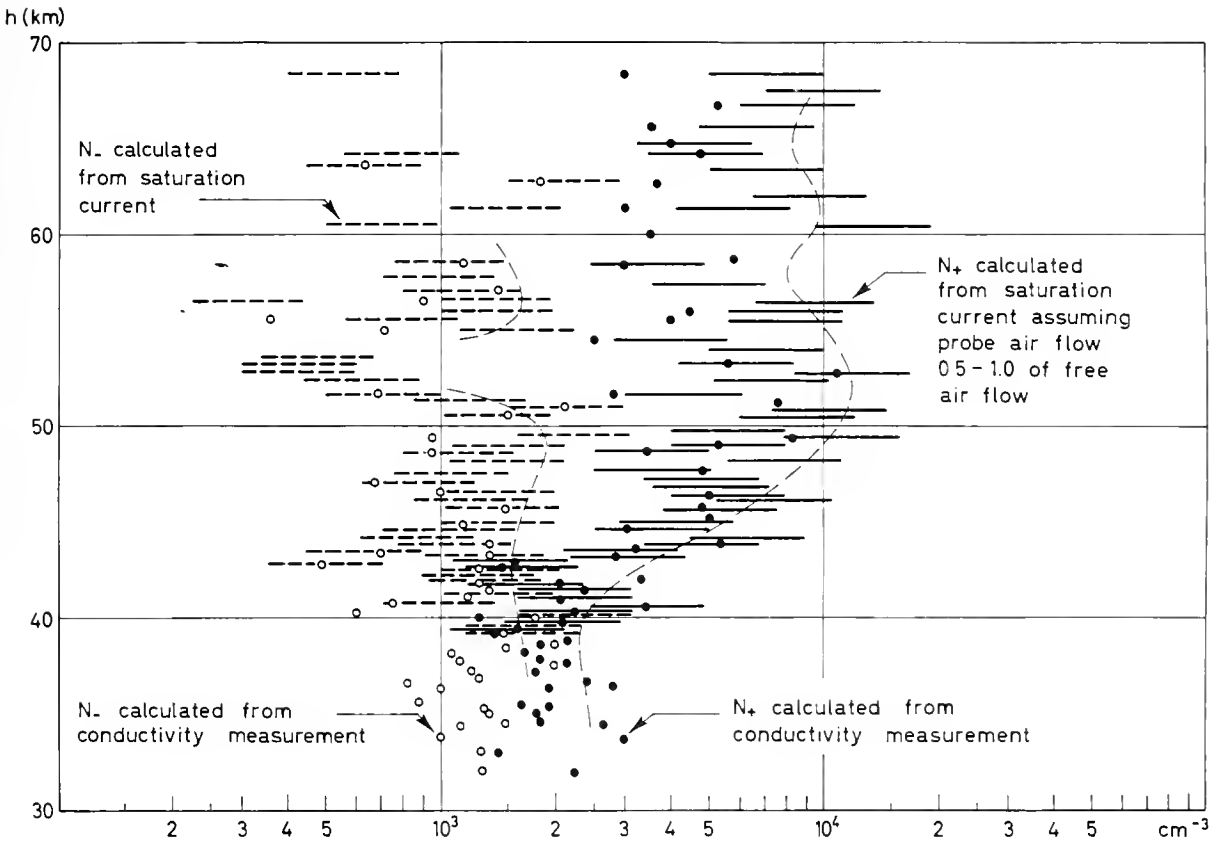

Figure 2. Positive and negative ion concentrations calculated from conductivity data

parachute and the probe with 23 m was destroyed during expulsion of the second payload and the distance between the parachute and the probe was only some 7 m, consequently the probe oscillated more than expected. The current-voltage characteristics which were telemetered to the ground showed some irregularities typical for a swinging motion of the measuring cylinder. Some current voltage characteristics could, however, be obtained from the large number of sweeps during the descent and parts of the characteristics could be obtained for the rest of the sweeps. The current voltage characteristic is shown in the description of the system (paper 3.2). No electrons were observed as these most probably were caught by the front field and did not pass the electrometer. Positive and negative ion concentrations have been derived from the current voltage characteristics in two ways.

First the ion concentrations have been derived from the slope of the i - V curve which is proportional with the conductivity. To obtain the concentrations it is necessary to know the mobility. It is assumed that the mobility follows the simple law,

$$k = k_o \frac{p_o}{p} \frac{T}{T_o}$$

The ground level mobilities of air ions

$$k_{o_-} = 2.4 \cdot 10^{-4} \frac{m^2}{V\ sec} \quad \text{and}$$

$$k_{o_+} = 1.9 \cdot 10^{-4} \frac{m^2}{V\ sec}$$

given by Siksna [1] have been used.

The second method is based upon knowledge about the effective cylinder opening for air flow and the air flow velocity through the probe. If these parameters are known the ion concentrations can be derived from the saturation current.

Figure 2 shows the positive and negative ion concentrations calculated from conductivity measurement and from saturation current. The spread of the points are caused by the oscillations of the probe, the smallest values being obtained when the cylinder is far off the vertical direction. The concentrations derived should consequently be equal to or smaller than the correct values.

There is a rather good agreement between the conductivity measurements and the saturation current measurements at altitudes between 40 and 50 km. This indicates that ions in this height range have mobilities similar to light air ions found at ground level. At present the method is not exact enough to give indication of type of ion or mixture of ions.

Above 50 km there is some difference between the positive ion concentrations derived from conductivity measurement and from saturation current. The explanation is probably that the drift velocity of the positive ions is smaller than assumed. Varney [2] has shown that the drift velocity of nitrogen ions changes from being proportional with E/p to being proportional with $\sqrt{E/p}$ at values of E/p 50 - 100 V/cm mm Hg. These values of E/p are obtained in parts of the probe in the upper height range.

If we assume $N_+ = N_- + N_e$ the ion profiles in Figure 2 indicates an incredible large number of electrons in the lower D-region. It is felt that such a large number of electrons is in disagreement with our present knowledge of the D-region electron concentrations. One possible explanation of the measurements is that negative ions in the D-region being of an unknown type have a poor mobility making a recording with the Gerdien condenser more difficult.

Another possibility is that electrons diffuse to dust particles forming negative ions with a mass several orders of magnitude larger than ordinary ions. These particles will pass through the cylinder without being collected.

This presentation must to some extent be considered as preliminary as the time available after the experiments has only allowed for the first quick data handling. More time and more detailed work is needed in order to sort out the various effects which may influence the measurements. It is believed, however, that the main character of the ion profiles in Figure 2 will be unchanged.

References

[1] Siksna, R., "Some Current Problems Concerning Air Ions," private communication, 1961.

[2] Varney, R. N., "Drift Velocity of Ions in Oxygen, Nitrogen and Carbon Monoxide," Phys. Rev. 89, 708 (1953).

DISCUSSION

R. L. F. Boyd: What negative ions were assumed and what mobility figures were used?

A. Pedersen: I assumed mobility of air in the laboratory for conductivity calculations. My data are not so good that I can distinguish between different types of ions at the moment.

R. L. F. Boyd: Is it not likely that, for example, some oxides of nitrogen might be there; this would make the mobilities a good deal smaller - thus explaining some of the discrepancy.

A. Pedersen: You mean that we have ions of so small a mobility that we can see them; yes, this could explain it.

L. C. Hale: How close to the ideal i - V curve you showed yesterday were your observed curves?

A. Pedersen: My observed curves were not very close. I have so much oscillation that it is difficult to say if I get a flat saturation.

11.12 POSITIVE AND NEGATIVE ION DENSITY MEASUREMENTS IN THE D- AND E-REGIONS

R. C. SAGALYN
Geophysics Research Directorate, Air Force Cambridge Research Laboratories
Bedford, Massachusetts

This paper describes measurements taken with two electrostatic analyzers, delivering negatively charged particles and positively charged particles, respectively; the negative ion current is distinguished from the electron current by assuming charge neutrality, as in the experiment described yesterday (paper 1.5).

Figure 1 shows results, obtained on two day and two night flights, for the rotation of negative ions to electrons and positive ions to electrons. They agree quite well with subsequent measurements obtained in the last eight months with low velocity Nike-Cajun rockets. In daytime we obtained negative ion to electron ratios at 40 to 50 km of about 100, decreasing very rapidly above 70 km, to about 0.1 at 80 km. The positive ion to electron ratios are approximately the same below 60 km decreasing very rapidly and approaching unity at around 80 km. This is very reasonable if one looks at the solution to the continuity equation, because in the daytime where equilibrium is very quickly reached, the rotation of positive ions to electrons is determined by the attachment frequency and the detachment processes such as photodetachment, collisional and associative detachment. If one assumes radiative attachment to 0, and two and three bodied attachment to 0_2, one finds that the attachment term certainly dominates the detachment process below about 60 km. In the vicinity of 70 to 75 km it begins to become negligible compared with the detachment and production terms, so the ratio approaches unity.

At night, on the other hand, in the vicinity of 100 km, the values of the ratios varied between about 0.8 and 3. Now the negative ion to electron ratio a few hours after sunset is equal to the ratio of the attachment frequency to the detachment frequency. We know the attachment frequency to 0 fairly well from Branscomb's work, so one can determine the associative detachment coefficient for the reactions

$$0^- + 0 \longrightarrow 0_2 + e$$

or

$$0^-_2 + 0 \longrightarrow 0_3 + e$$

as about 1.5×10^{-15} cm^3/sec.

Figure 2 shows a daytime measurement with a fairly high solar flux, of the positive ion, negative ion and electron densities. Here the

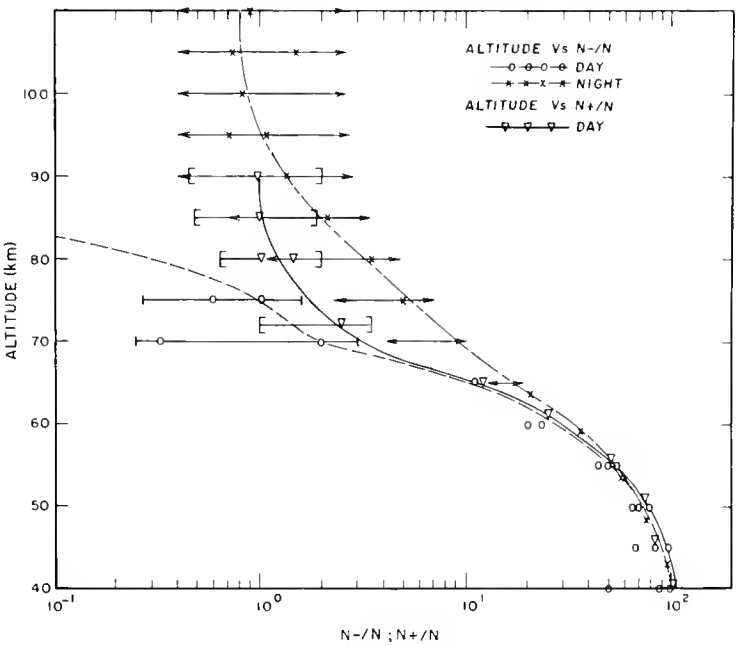

Figure 1. Ratios of negative ion and positive ion density to electron density

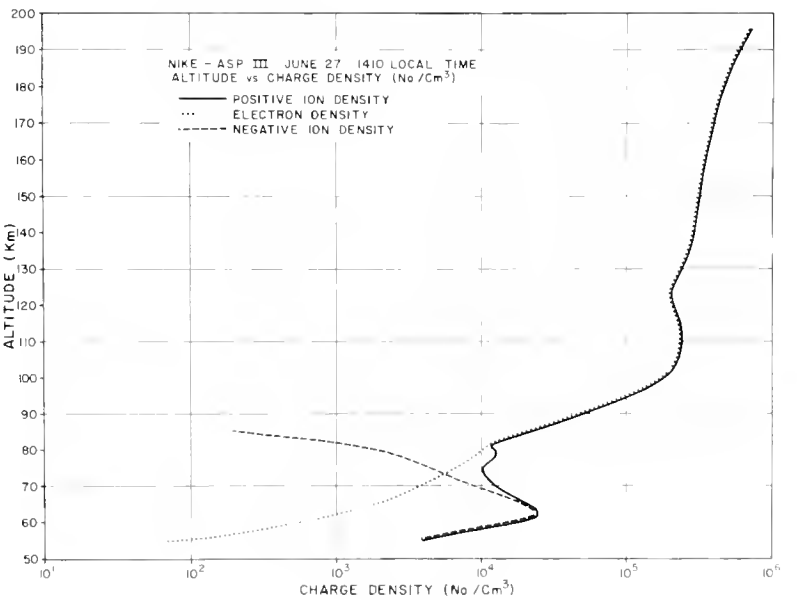

Figure 2. Positive and negative ion densities for daytime flight

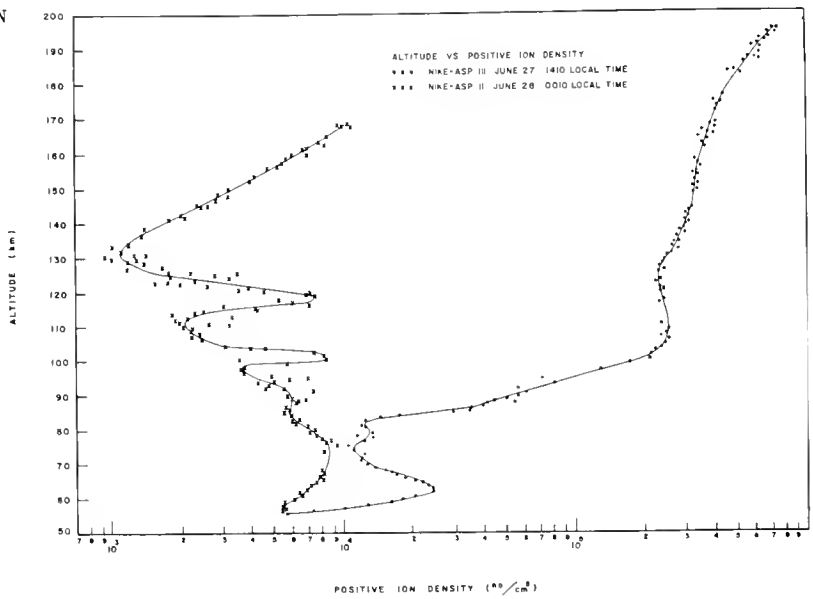

Figure 3. Comparison of day and night positive ion densities

negative ion and positive ion densities are closer than the experimental error up to about 65 km. The negative ions decrease very rapidly above this altitude, and are certainly not measurable above about 90 km. The electrons increase very rapidly in the vicinity of 60 to 90 km, and we find a peak in the D-region ion density, which varies in intensity, with no peak in the electron density.

Figure 3 shows the range of positive ion density, between day and night. The general distribution of positive ions in the E-region at night is in good agreement with the ionization expected, assuming a dissociative recombination coefficient of about 10^{-7} cm^3/sec, but the D-region density is definitely higher than expected. The electron density is on the order of 10^2 in the region below 70 km.

DISCUSSION

R. Horowitz: This morning we heard a very interesting paper about the various flow conditions. Many of us who instrument the rockets have seen this transition. I noticed that you have measurements from 40 or 50 up to 190 km. Have your measurements shown any transition region in the flow?

R. C. Sagalyn: We have not seen these effects in the detectors. We have carried out wind tunnel tests, still in progress, which show that with these mesh grids the shock front is behind the outer grid. There is a shock produced by the very small inner collector, with a very small Mach angle. In the integration over the sphere this is a very small contribution. However, we have done this only on low velocity vehicles. For example, on the Aerobee-Hi we begin to see re-entry ionization at about 55 km, so we cannot use that sort of vehicle.

G. C. Reid: You quoted a figure for the associative detachment coefficient. I had the impression this was almost completely unknown. Can you tell me how it was determined?

R. C. Sagalyn: We calculated it. We know that the primary attachment process is radiative attachment to oxygen, and that the primary detachment process is associative, because in the region of low temperature the collisional detachment is small.

11.13 LOWER IONOSPHERE PROFILES WITH A ROCKET-BORNE PROBE

L. G. SMITH
Geophysics Corporation of America
Bedford, Massachusetts

1. Simultaneous Measurement of Electron Density Profile and Wind Structure

The electron density profile shown in Figure 1 was obtained using the nose tip of the payload as the probing electrode; the current is proportional to electron density and the scaling factor is obtained from other (daytime) flights. The profile shows the characteristically irregular nighttime structure and in particular two well-defined layers: a lower (sporadic-E) layer between 98 and 102 km and an upper layer between 119 and 123 km.

The wind profile obtained 28 min layer by the sodium vapor technique is shown in Figure 2. (This data was supplied by E.R. Manring and J.R. Beddinger). The positions of the two layers are marked. It is seen that both occur near the mid-point of an East-West shear in which the motion is towards the East on the low side and toward the West on the high side. A shear in the opposite sense (near 111 km) does not correspond with any major feature of the electron density profile. These observations support the mechanism of formation of sporadic E-layers by wind shear as given by Whitehead and others.

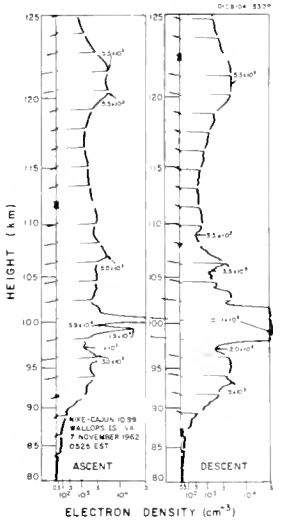

Figure 1. Electron density profile showing sporadic-E layer.

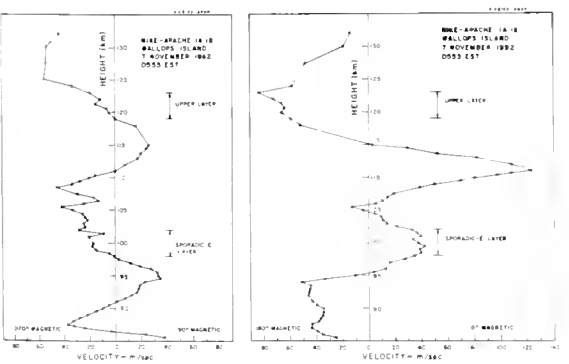

2. The DC Probe in the D-Region

The proportionality of probe current to electron density which is found in the E-region should break down in the D-region below about 85 km. However, when profiles of probe current as measured during the day, at sunset and at night are compared, as in Figure 3, it is found that these profiles are in general agreement with profiles of electron density measured by other, less direct, techniques. The relationship has not been established theoretically and the data obtained by the use of the probe in the D-region should be treated cautiously pending further investigation.

3. Observations During the Solar Eclipse of 20 July 1963

Six Nike-Apache rockets each instrumented to measure electron density and temperature and solar radiation by narrow band detectors, one an

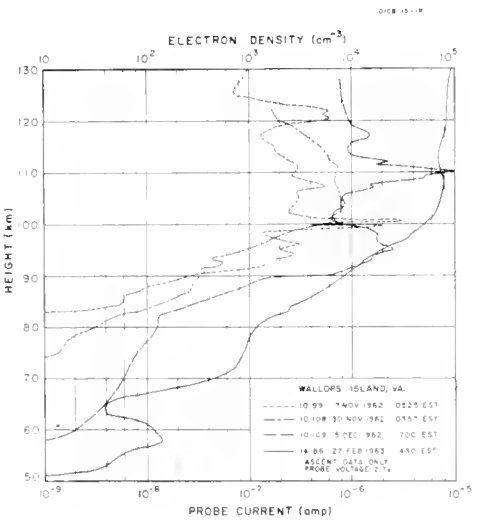

Figure 3. Profiles of probe current.

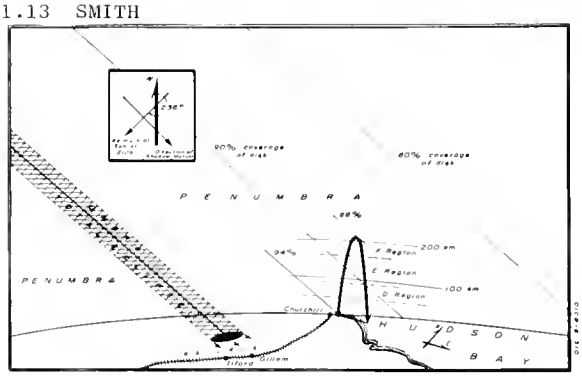

Figure 4. Relation of solar eclipse to rocket trajectories

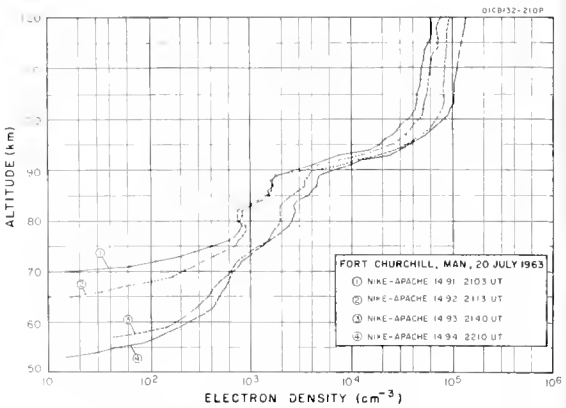

Figure 5. Profiles of electron density during the solar eclipse

ion chamber for Lyman alpha (1216A) and the other a Geiger counter for soft X-rays in the range 44-60 A, were launched at Fort Churchill during the solar eclipse of 20 July 1963. The position of the rocket trajectory in the penumbra at the time of maximum observation of the solar disc is shown in Figure 4. The first two vehicles failed but the other four, starting at mid-eclipse and ending with the end of the eclipse, were successful. The solar radiation data is not yet completely reduced and results of electron density and electron temperature only are given here.

The problem presented by eclipses is that even in a total eclipse, which may have a duration of totality of seven minutes, the electron density is never observed to fall below 30 per cent of the normal value. This has generally been ascribed to the "sluggishness" of the atmosphere, i.e., the finite recombination rate does not allow complete decay of electron density. The value of the recombination coefficient obtained in this way is about 2×10^{-8} $cm^3 sec^{-1}$ which is rather lower than values derived from the effect of solar flares and from laboratory measurements. Also the minimum of electron density would occur some five or ten minutes after the minimum of the illumination. The delay is, in fact, frequently not found.

The alternative explanation is that the ionosphere does, in fact, remain essentially in equilibrium but the rate of ionization does not decrease to zero at totality. This requires that the corona and other sources contribute about ten per cent of the flux of ionizing radiation in the E- and F1-regions. It has not yet been shown that this is the case. The series of flights was intended to provide data which would distinguish between these two explanations and would allow a better determination of the recombination coefficient in the E- and F1-regions.

The four profiles of electron density (assumed proportional to probe current) are shown in Figure 5. There is no significant time delay in the ionosphere above 90 km. From 75 km to 90 km the greater variability of the electron density shows up. Below 75 km a marked reduction in electron density is found. This shows up in Figure 6 in which the profiles have been normalized to unity at 105 km.

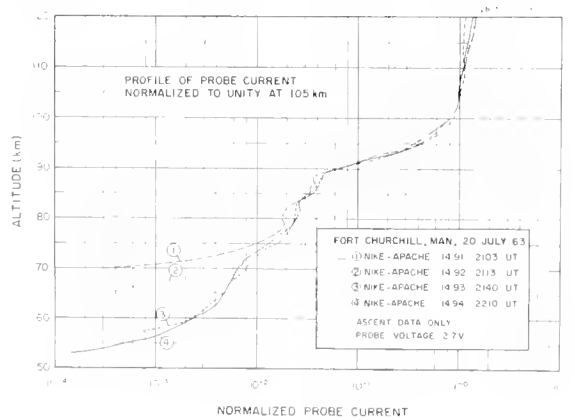

Figure 6. Normalized profiles of probe current.

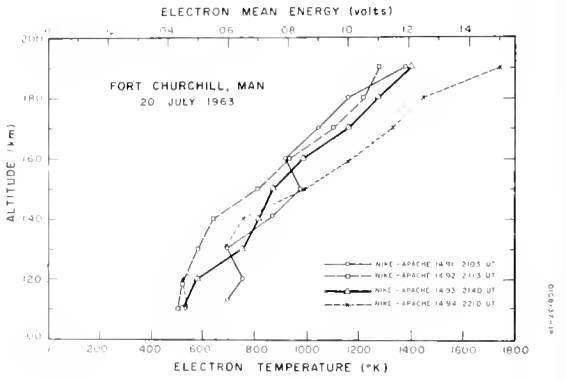

Figure 7. Electron temperature during the solar eclipse.

The greater effect in the lower D-region is believed to be due to the presence of negative ions. The ion equilibrium equation may be written

$$n = \left(\frac{q}{\alpha}\right)^{1/2} \left(\frac{1}{1+\lambda}\right)^{1/2}$$

where n = electron density

q = ionization rate

α = recombination coefficient

$\lambda = n_-/n$, negative ion/electron ratio

when $\lambda \ll 1$ this reduces to

$$n = \left(\frac{q}{\alpha}\right)^{1/2}$$

when $\lambda \gg 1$ the equation becomes

$$n = \left(\frac{q}{\alpha}\right)^{1/2} \frac{1}{\lambda 1/2} .$$

This, if the reduction in q is the same at all heights, the reduction in n will be greater in the lower D-region due to the λ term, which increases as the photo-detachment rate is reduced. The observations are assumed to indicate that λ=1 at about 75 km.

The final figure, Figure 7, shows some of the electron temperature data. The accuracy of each value is about $\pm$ 100 deg K and it is seen that up to 150 km there was no detectable change in temperature. Above 150 km the measurements of the final flight, at the end of the eclipse, shows a somewhat higher temperature than the preceding flights. The data appears to indicate a long thermal time constant for electron temperature and shows that temperature can have no more than a minor effect on the rate coefficients during the eclipse.

DISCUSSION

C.Y. Johnson: Do you attribute some of your troubles to the fact that you did not go into totality?

L.G. Smith: We went into a region where 10 per cent of the disc was visible. This is a pretty large reduction.

C.Y. Johnson: I think Chubb may help us out on this. Even though a large part of the disc is covered, that does not mean that some hot spot or source which is contributing the major amount of ionization is covered.

T.A. Chubb: One must distinguish between those lines which come from plages and those which come from the disc. For the Lyman β ionization, the rate should go pretty much as the area of the disc. We know that Lyman α does decrease, from the 1958 measurements, to well below 1 per cent. But there is always a Lyman α glow--the night airglow--which, even on the dark side of the earth, is down about a factor of 600, but is diffused all over the earth. I am not quite sure how bright this night Lyman α glow is in the day. The X-rays come primarily from the plages, and in the 1958 eclipse of the order of 5 per cent from the residual. That was a much larger eclipse than the Canadian eclipse even at totality.

L.G. Smith: In relation to this the relative reduction in electron density was about the same from 75 to 190 km. Considering the different ionizing constituents and, for example, the relative importance of X-rays, it is going to be quite a problem to explain why there is such a uniform reduction.

T.A. Chubb: As long as you still have 10 percent of the disc you do not run into the difficulty which occurs when you reach the last 2 percent.

L.G. Smith: I think there are cases where an explanation of the electron density requires that 10 percent of the ionizing flux remain during totality.

A. Nagy: The fact that you did not notice any significant change in electron temperature could perhaps be attributed to the possibility that, as Dr. Hirao and other workers mentioned, corpuscular radiation is significant at higher altitudes, and that this did not change significantly. I think that at Wallops Island during the eclipse Dr. Brace noticed a change in electron temperature.

L.H. Brace: The three temperature curves during the eclipse were lower; the last one was significantly higher and that was after the eclipse.

L.G. Smith: It was a small difference, probably more than the experimental error, but it does not have a significant effect on the rate coefficients.

N.W. Spencer: We had a flight at Wallops Island at much higher altitude--in the F-region--which showed the electron temperature considerably lower. Yesterday we showed an electron temperature profile for a normal afternoon which reached temperatures of 1800 deg K. We were down at least 50 percent from that during the eclipse.

G.C. Reid: Most people think that a large component of the ionization below 75 km is produced by galactic cosmic rays, and these should not change during the eclipse. This makes large changes even harder to understand. It has to go into λ effectively--a change in photodetachment.

L.G. Smith: As far as the D-region is con-

cerned, it probably changes the photodetachment --in other words, it's like a change from day to night. The rate of ion production is probably constant if it's cosmic ray ionization.

J.S. Belrose: Your results do not appear to agree with our observations on a normal day. We have made observations from sunrise to noon. The ionization between 50 to 60 km does not change at all over the day, but there is a large chage at about 75 km; whereas your results are exactly the opposite, with the largest change at the low heights.

R.L.F. Boyd: If we are to accept electron temperatures of the order of 600 degrees in the E-region, can this arise from the ionizing radiation? I have been thinking that it must surely be due to electric fields. Now am I quite wrong about it? It now appears that it could conceivably arise from ionizing radiation. Does it agree with the known fluxes?

M. Dubin: Hinteregger has measured by the retarded potential method the energy of electrons and gets energies to 25 ev.

K.W. Champion: Dalgarno has worked out the temperature differential of the electrons as a function of altitude, and it agrees quite well with the experimental data.

N.W. Spencer: I think we should believe the temperatures. We have numerous unpublished examples showing temperatures as high as 2000 deg K for thermal electrons. We do not yet fully understand these results, but I think they are a result of ionizing radiation of some form. There may be some electric field effects: these are much more likely to be stratified than general. Most of the data shows the temperatures to be considerably more general.

R.L.F. Boyd: If we are going to believe them then can we attribute it to fluxes? If I can quote Dalgarno, "the difference between electron temperature and gas temperature is a certain amount at about 200 km, but this difference vanishes below 120 km." He takes into account radiation down to 10 A.

E.C. Whipple: Hinteregger has recently pointed out privately the importance of photoelectrons as a heat source in the lower E-region.

C.G. Little: We have thermal noise measurements by the radio noise technique up in College. Our observations suggest thermal equilibrium for the electrons in the D-region. We see temperatures of the order of 220 to 280 deg K very consistently and temperatures of 2000 deg just do not fit. Our observations would refer to 50-100 km depending upon the degree of disturbance. The more the disturbance the lower would be the penetration.

J.O. Thomas: Dr. Smith's Figure 1 shows the result of a beautiful experiment which confirmed a suggestion first proposed by Dungey--and later worked out in detail by Whitehead and Storey and others--that some types of sporadic E would be associated with certain kinds of wind shears; he showed that the maximum of the sporadic E-layer occurred at the same height as the node of the wind shear--the idea being that the electrons are pushed down from above and up from below. Dr. Rosenberg yesterday showed a curve which appeared to give a contrary result to that found by Dr. Smith.

N.W. Rosenberg: My plot was of wind shear versus altitude; Smith's plot is of wind versus altitude. If you differented his curve, it would be wind shear versus altitude and essentially show the same thing as my figure.

E.K. Smith: Were the wind shear values available on the downward path as well as the upward?

N.W. Rosenberg: No.

L.G. Smith: The sodium trail is too faint by that time.

K. Hirao: It is very interesting that the electron temperature changed in the solar eclipse. If you can subtract the effect of the solar eclipse itself, then it is very important for the study of the electron temperature mechanism.

G.C. Reid: In measuring electron temperature, do you implicitly assume a Maxwellian distribution?

L.G. Smith: For convenience you do; but you would be aware if it was not Maxwellian, as you would not get the linear plot on semi-log coordinates. We go through the full analysis, plotting the current on semi-log paper versus the voltage, making sure it is exponential over a dynamic range of about 50 to 1 in current.

G.C. Reid: So if it were a Maxwellian distribution corresponding to perhaps 200 or 300 degrees with a long high-energy tail, this could not produce an effective temperature of 600 deg.

L.G. Smith: No. We measure energies from about zero to about 4 times the mean energy.

11.14 RF PROBE MEASUREMENTS FROM A RECENT CHURCHILL FIRING INTO AN AURORAL ABSORPTION

J. C. ULWICK and W. PFISTER
Geophysics Research Directorate,
Air Force Cambridge Research Laboratories
Bedford, Massachusetts

and

O. C. HAYCOCK
Department of Electrical Engineering
University of Utah
Salt Lake City, Utah

On 26 July 1963 a Black Brant rocket was launched at Churchill, Canada, carrying several experiments for the measurement of electron density in the ionosphere. From magnetic aspect sensors and solar sensors it was determined that the rocket had a spin rate of approximately 3 rps and a precession cone angle of approximately 0.5 deg. No flight trajectory information was available, so the trajectory of a Black Brant flown on 20 July 1963 having the same launch angle and flight time has been utilized.

Figure 1 shows the rocket nose cone and the location of each of the experiments flown. The results of the conductivity probe and propagation experiment conducted by Pennsylvania State University are the subject of another paper (paper 11.9). The results of the retarding potential probe, plasma frequency probe, resonance probe and standing wave impedance probe experiments conducted as a joint effort of the Air Force Cambridge Research Laboratories and the University of Utah are the subject of this paper. The whip antennas shown form a 16 foot dipole when erected which is time-shared between the standing wave impedance probe and the plasma probes.

Figure 2 shows a sample of the telemetry data for the standing wave impedance probe and the plasma probes at 95 sec after launch corresponding to a rocket altitude of approximately 110 km. The top trace is the frequency monitor output with the corresponding frequencies noted on one of the sweeps. The middle subcarrier output is the plasma frequency probe monitor which is alternating every 0.2 sec between a plasma frequency measurement and a calibration measurement. The lower subcarrier output is an alternating measurement every 0.2 sec of the standing wave impedance probe and the resonance probe. The resonance probe had DC voltages of 0, 1.3, 2.6, and 5.2 volts applied periodically.

The retarding potential probe experiment consisted of two detectors to cover the range of current collection from 10^{-8} to 10^{-12} amp and were operated as ion traps. These detectors were flown on the side of the vehicle as an exploratory experiment. The results of the current collected as a function of altitude for both the 20 July and 26 July rockets are shown in Figures 3 and 4. No attempt is made at present to interpret the data in terms of ion density. One can note, however, that the current collected near rocket peak altitude is approximately 1.5 times larger for the 26 July rocket compared with the rocket flown during the eclipse.

Figure 5 shows the electron density as a function of time with corresponding altitudes noted for the plasma frequency probe and the resonance probe. The results correspond fairly well, with the plasma frequency results consistently somewhat higher than those of the resonance probes. The plasma frequency probe shows the effect of rocket spin in more detail than the resonance probe because the rate of measurement of the plasma frequency probe was 4 times as great. Both probes show results that are not symmetrical about rocket zenith which

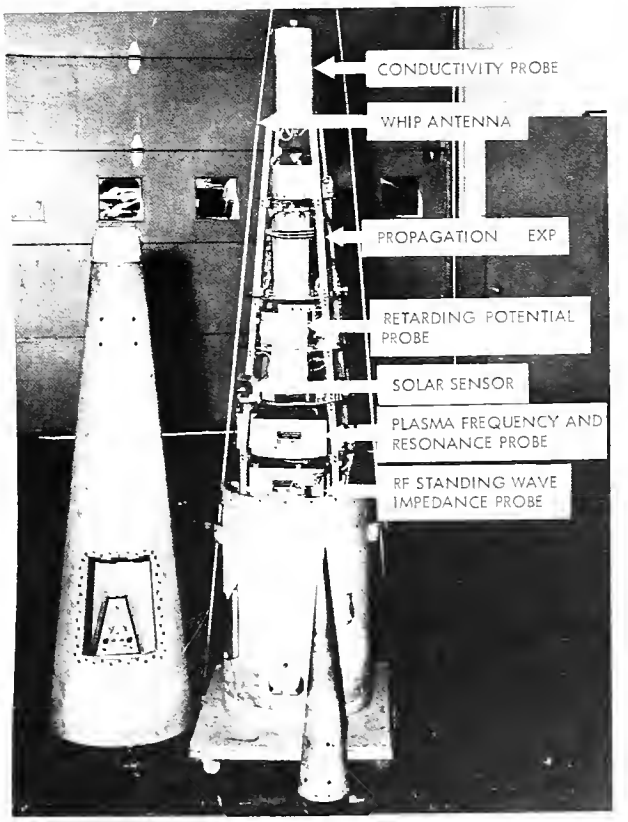

Figure 1. Locations of the various experiments in the payload

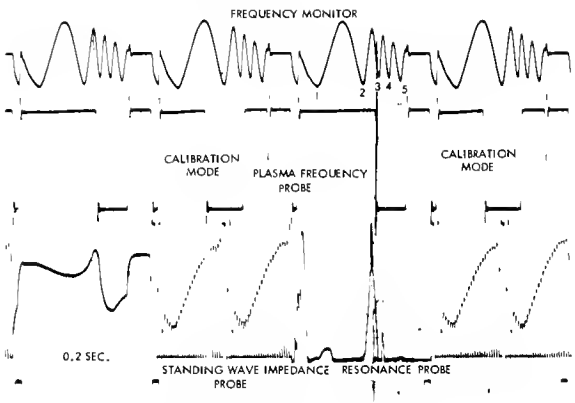

Figure 2. Standing wave impedance probe telemetry data

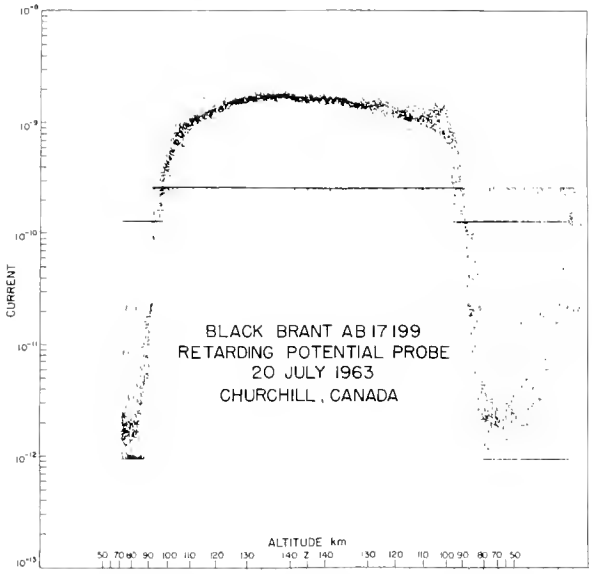

Figure 3. Retarding potential probe current, 20 July 1963 firing

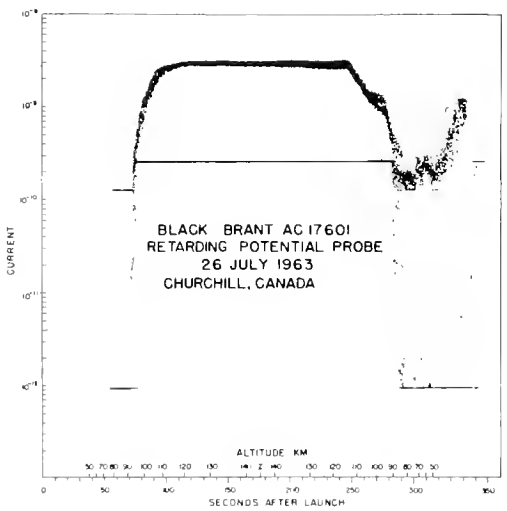

Figure 4. Retarding potential probe current, 26 July 1963 firing

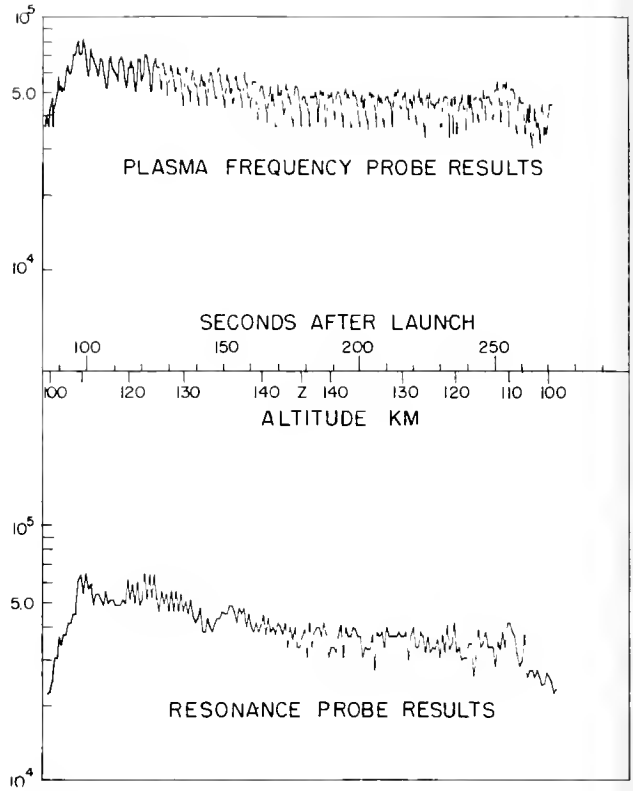

Figure 5. Electron density from plasma frequency probe and resonance probe, Black Brant 17.601, 26 July 1963 firing

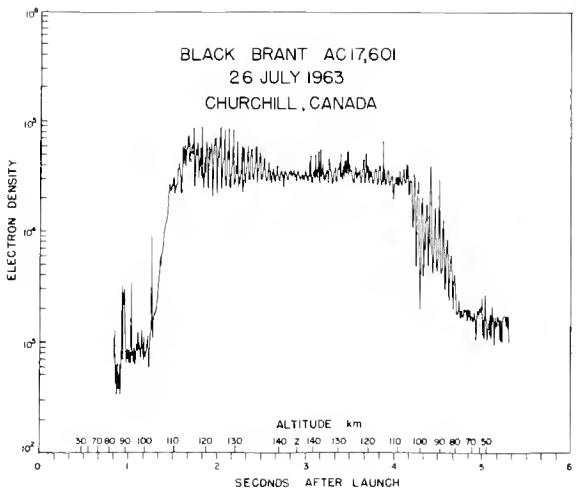

Figure 6. Electron density from standing wave impedance probe

we believe is due to an outgassing effect.

Figure 6 shows the standing wave impedance probe results. If one compares the average of these densities with those from the plasma probes a good correspondence is noted.

The standing wave impedance probe results with peaks going to approximately 10^5 electrons per cc at 120 km an ascent corresponds with the ionosonde critical frequency of 2.9 Mc/s. The plasma frequency probes results were somewhat lower. The spin modulation and the effects of outgassing are also evident in these data. However, it is difficult to explain the magnitude variations shown here not present in the plasma probe results.

DISCUSSION

C. Y. Johnson: Can the horizontal distance the rocket travels give a structure change?

J. C. Ulwick: The rocket traveled about 8 km; it impacted about 80 km distant.

R. Horowitz: At what altitude did the current start up?

J. C. Ulwick: The detector was exposed at about 85 km; we almost immediately started getting current, and it peaked at about 100 km.

12.1 ELECTRON CONTENT OF THE D-REGION BY THE METHOD OF PARTIAL REFLECTION

J. S. BELROSE
Defence Research Telecommunications Establishment
Defence Research Board
Ottawa, Ontario, Canada

1. Introduction

Numerous deductions about D-region electron densities have been made from ground-based techniques, but most of these must be treated with caution, since they have all been made somewhat indirectly, by studying its effects on waves which have traversed it to be reflected in layers above (MF and HF absorption measurements) or by studying waves returned from within it on a few isolated frequencies (LF and VLF propagation experiments). It is difficult to devise ground-based experiments which give reliable electron density distribution data in the D-region. One of the best at present is the partial reflection experiment.

This experiment records the amplitude of weak echoes partially reflected from ionization irregularities in the 50 - 100 km height range. The amplitude of these partly reflected waves is determined partly by the process of scattering responsible for their return, and partly by their travel through the region below the scatterer. A study of the different amplitudes of the Ordinary and Extra-ordinary component waves provides useful information about electron densities, and collision frequencies in the ionospheric D-region. Although the method is not without its limitations, it seems to give data which are not better obtained by other available ground-based techniques.

This method is being extensively used at DRTE Ottawa. Results so far obtained support the theory that two quite different ionization mechanisms are responsible for D-region electron densities. Since one of these is believed to be normal cosmic rays, there is particular value in studying the D-region at high latitudes, where such effects would be expected to be a maximum. DRTE has installed a partial reflection equipment at Resolute Bay in the summer of 1963, and plans to install equipment at Fort Churchill in the summer of 1964. The installation at Fort Churchill is of particular interest to the participants of this conference, since it will provide the opportunity of bringing together one of the best ground-based techniques for comparison with rocket techniques.

In the paper a brief account will be given of the experimental technique, the method of analysis, and some results for quiet days.

2. The Experimental Techniques

Since it required to receive very weak echoes, with reflection coefficients of 10^{-3} to 10^{-6}, these can be observed only if the transmitter power is very great, the background noise is small, or special techniques are used to improve the signal-to-noise ratio. The DRTE experiment uses high transmitter power (100 or 1000 kw) high antenna gain (10 - 12 db) equipments. Clear echoes are obtained from heights as low as 50 km during the day, but atmospheric noise and station interference have so far prevented the making of useful observation at night.

A-scan records of single pulse transmissions are recorded automatically every 2 seconds. Two exposures are taken in quick succession, separated by 1/25 sec. Between these two exposures the sense of the polarization on both transmission and reception are reversed, as well as the direction of the spot deflection of the cathode ray tube. Figure 1 shows a typical record, where O-mode is upwards deflection and X-mode is downwards deflection. Transmitter power was 100 kw. The echo marked A is due to incomplete suppression of the O-mode echo from the E-layer (the suppression of the unwanted magneto-ionic mode is 40 - 60 db).

3. Method of Analysis

The amplitude of radio waves partially reflected from D-region ionization irregularities is determined partly by the reflection coefficient of the scatterers, and partly by absorption in the region below the scatterers. Thus, if $A_{x,o}$ is amplitude of extra-ordinary or ordinary wave reflected from a scatterer at a height h, and $R_{x,o}$ is the effective reflection coefficient of the scatterer, then

$$\frac{A_x}{A_o} = \frac{R_x}{R_o} \exp\left[-2\int_o^h (k_x - k_o)\, dh\right]$$

where K is the absorption coefficient integrated up to the scatterer and back. Now it can be shown that, whereas $R_{x,o}$ are dependent on parameters of the irregularity (the fraction change in refractive index), R_x/R_o is essentially not but depends only on the wave frequency ω, the gyrofrequency ω_H, and the electron collision frequency ν_m. Thus if $\nu_m(h)$ is known, N(h) can be determined. The generalized Appleton-Hartree equations are used in the analysis.

4. The Collision Frequency of Electrons

It is necessary to know the collision frequency height curve before the echo amplitude data can be interpreted in terms of electron density. The experiment gives a measure of collision frequency at low heights, since if

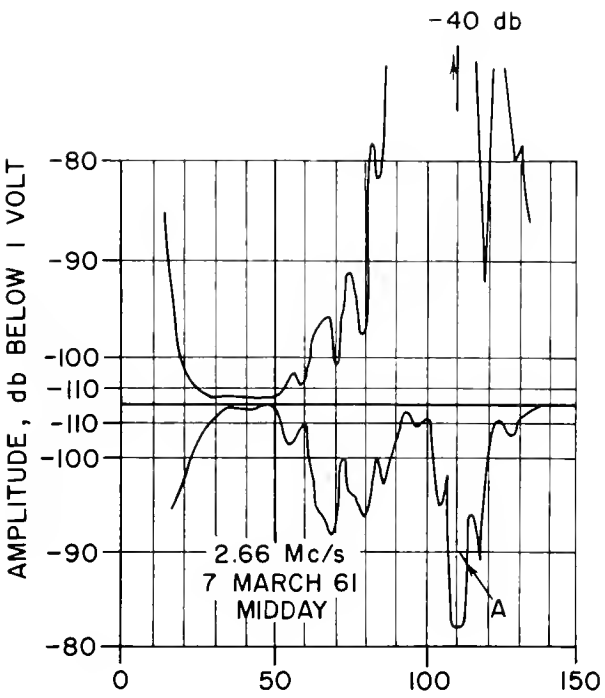

Figure 1. A-scan record of single pulse transmission

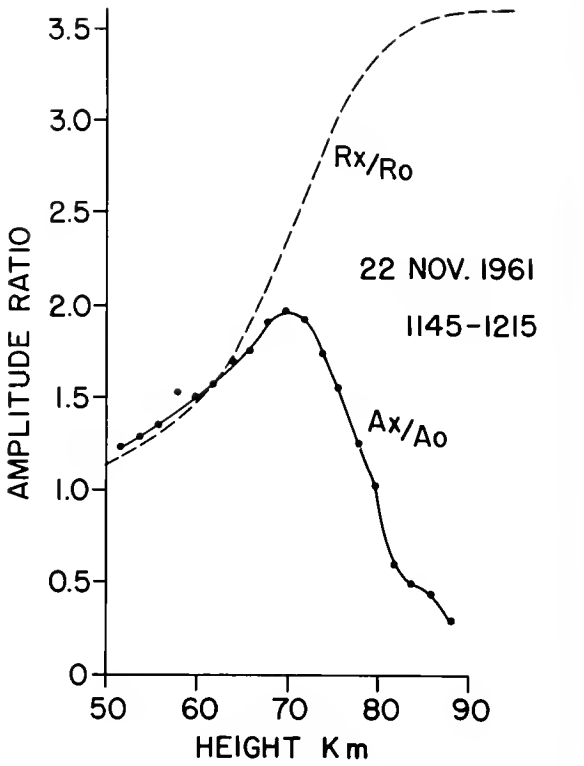

Figure 2. Experimental results for a quiet day in November

the differential absorption is small $A_x/A_o \approx R_x/R_o$, and hence the measured values of A_x/A_o can be interpreted to give values of ν_m. It is necessary to assume a scale height for the atmosphere, or to rely on other data to have values at higher heights.

Figure 2 shows data made on a quiet day in November. The R_x/R_o curve has been calculated from a collision frequency curve 1, to be discussed. It can be seen that the differential absorption is small below 60 km.

Collision frequency values deduced from this figure for the height range 50 - 60 km, as well as those available from other sources, are shown in Figure 3. The data attributed to Kane have been measured by rockets at Fort Churchill during Polar Cap Absorption events, and the data attributed to Schlapp have been measured at Cambridge by a group retardation method. These values have been corrected for use with generalized magneto-ionic formulas. The solid curve labelled Curve 1 has been calculated using a formula given by Phelps based on laboratory measurements by Phelps and Pack, and van Lint, et al., and the COSPAR International Reference Atmosphere (CIRA 1961). Since the November data of Belrose and Kane lie below Curve 1, Curve 2 has been drawn through these data, but with the same scale height as Curve 1. Curves 1 and 2 are not believed to represent a seasonal variation but do show a variability in

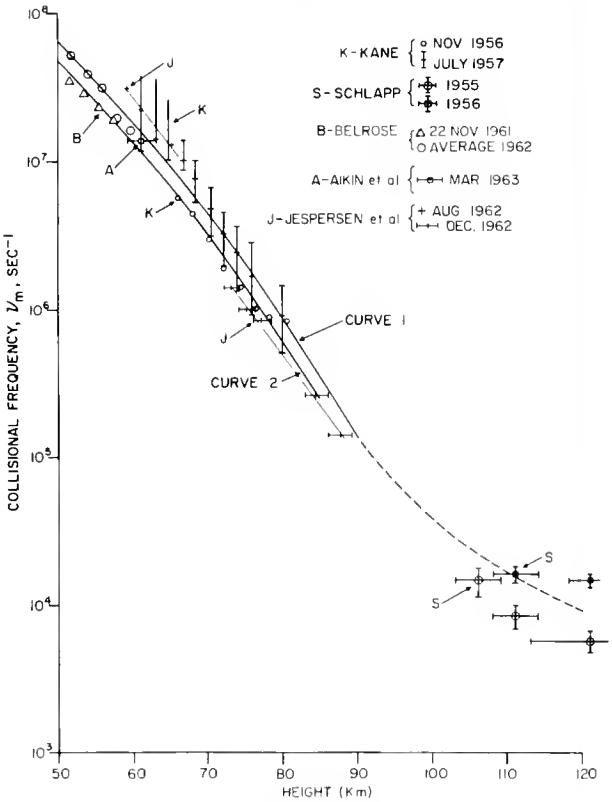

Figure 3. Collision frequencies as deduced from experiments

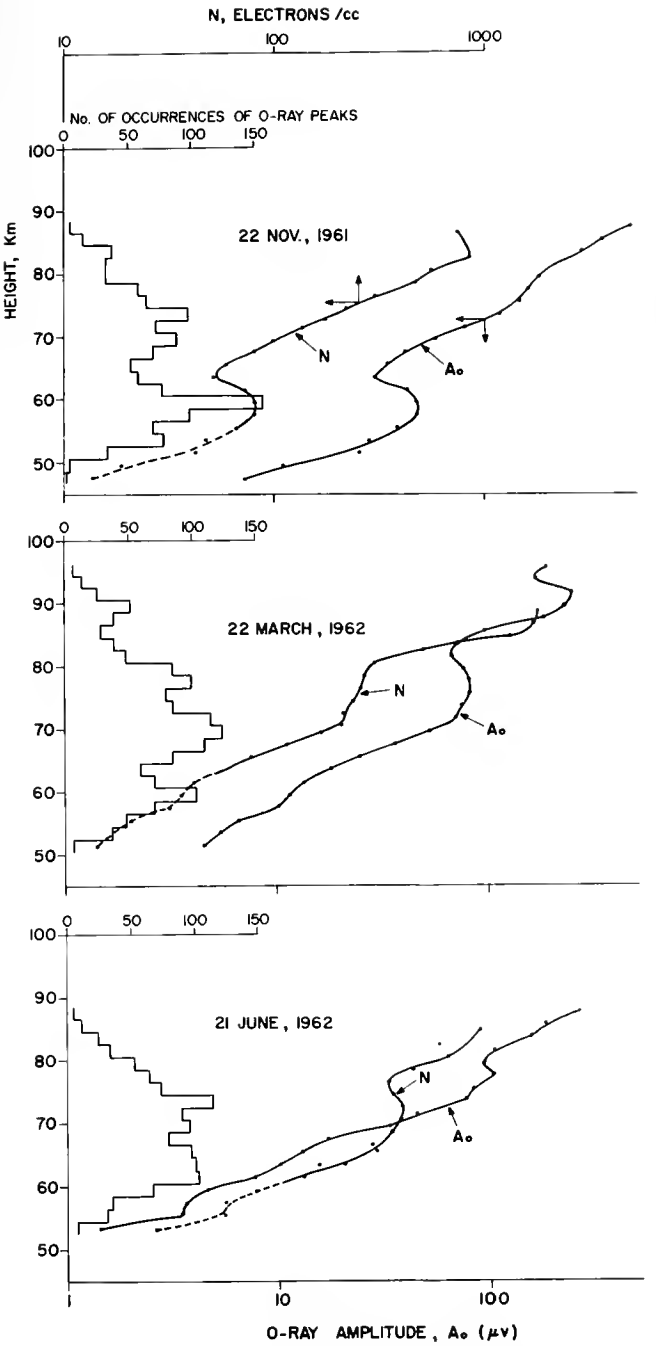

Figure 4. Data on a winter, an equinox and a summer day

the data. The data attributed to Jespersen, et al., has been measured by a multifrequency experiment which measured differential absorption, differential phase, and ionospheric attenuation during auroral absorption. It is not, however, necessarily representative of quasi-equilibrium conditions.

5. Interpretation in Terms of Electron Density

Once a collision frequency height curve has been decided upon, the $A_X/A_O(h)$ data can be

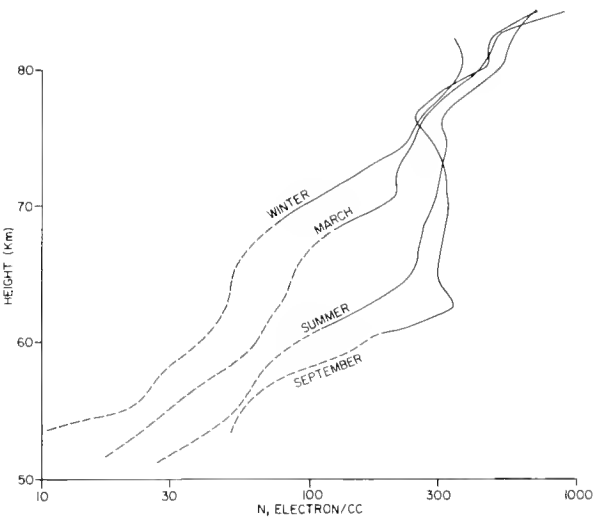

Figure 5. Electron density profiles for magnetically quiet days

analysed to give N(h) data. Since the electron density is determined from the slope of the A_X/A_O and R_X/R_O curves, it is not critically dependent on the actual values of collision frequency, but does depend on the slope or scale height of the collision frequency profile. The scale height for collision frequency seems to be fairly well established by the available data.

6. Some Results

Figure 4 gives some results on individual quiet days to illustrate the relation between some of the measured and derived parameters. Note that the amplitude of the O-mode $A_O(h)$ and the electron density N(h) are remarkably similar. In fact it has been assumed with reasonable theoretical justification that they are proportional at low heights, where the differential absorption is too small to reliably measure the electron density. These parts of the curve are shown by the dashed line.

Note that the electron density data shows three separate strata: (1) the E-layer above 80 - 85 km, (2) the D-layer between 65 - 80 km, and (3) a lower lying stratum designated the C-layer below 65 km. The quasi peak of the C-layer apparently can on occasion be very pronounced (e.g., on 22 Nov.), but in most instances it appears merely as a change in slope of the N(h) curve. The change in slope at the base of the E-layer is usually marked, and there is some evidence that there is a minimum in the electron density there on some occasion. The location where this change occurs is lower in summer than in winter.

Figure 5 shows electron density data deduced for 5 magnetically quiet days each month for winter (Nov., Dec., and Jan. 1961-62) and

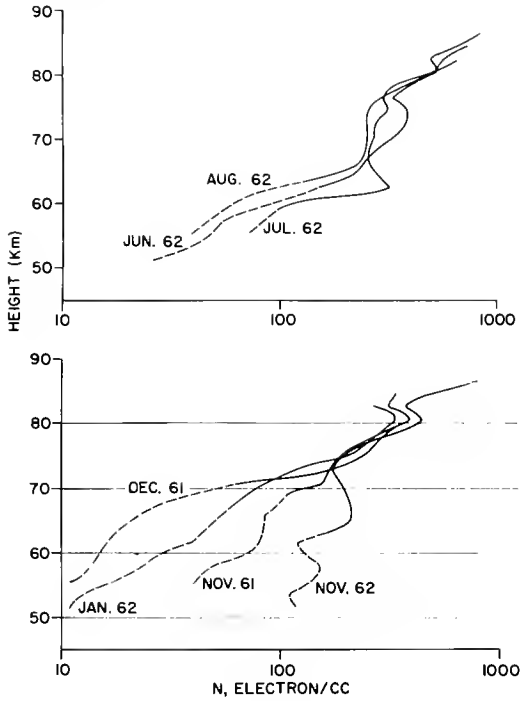

Figure 6. Electron density profile variability

summer (June, July, and Aug. 1962) together with March and September, 1962. These data show marked seasonal changes in the electron density (particularly near 65 km); and a seasonal asymmetry in that March looks like an in-between month whereas September is more like a summer month.

Figure 6 illustrates that there is little variability during the 3 summer months, but considerable variability during winter months. While the data does suggest that there is a minimum in the electron density below 70 km in December, since November 1961 and November 1962 seem to be quite different (although there was little difference in the mean sunspot number), it is not yet clear whether there is a systematic average variation during winter months, or merely that 5 days data in winter shows considerable variability.

7. Limitations of the Experimental Technique

Since the electron density changes in the lower ionosphere by five orders of magnitude, it is not possible to obtain measured data by the partial reflection experiment for the entire height interval 50 - 100 km unless more than one observing frequency is used. By utilizing two, viz., 2.66 and 6.275 Mc/s, we have obtained information about electron densities and collision frequencies under normal and abnormal conditions in this height range. The experiment does not, however, give useful result on most occasions above about 90 km. The partially reflected echoes for greater heights appear to come obliquely from preferred scatter heights within the E-region.

8. Conclusions

The paper has described the partial reflection technique which is being used by DRTE to study the electron density of the D-region. While a proper assessment of the electron density data, by comparison with other experiments made at the same place and time, has not yet been made, nevertheless the experiment does provide reliable self consistent data for studying electron density variations in the D-region, and the information provided does not seem to be better obtained by other available ground based techniques.

The results which we have shown for electron density show that there is great regularity from day-to-day during the three summer months on quiet days, whereas there is great irregularity from day-to-day in winter. Since the winter variability seems to occur predominately in the height range below 70 km, where the ionization source should be fairly constant since it is believed to be normal cosmic rays, the irregularity must be due to changes (on a time scale of days) of atmospheric constituents which affect electron loss processes. The cause of such changes must be related to some sort of atmospheric meteorology. It is well known for example that temperature measurements by balloons at heights of 25 - 30 km show great regularity in temperature from day-to-day in summer, but great irregularity in winter. Except for the one occasion, viz. February 1952, which was the occasion of the famous Berlin warming, no direct associations between stratospheric weather and mesospheric ionization changes have been established. On this occasion the lower ionosphere ionization was so markedly greater than normal that these days were termed winter days of anomalous absorption. This variability in winter make rocket studies of the lower ionosphere difficult, since rocket techniques constitute only random samples.

On some days in winter the measured values of A_x/A_o at low heights do not seem to be reasonably interpretable in terms of a collision frequency height curve, unless the collision frequency were almost constant over this ten kilometer height range (50 - 60 km), where on normal days it should change by almost a factor of four. It might be possible to explain the observations by postulating a marked temperature inversion in the 50 - 60 km height range, but if this is the explanation it must be a very pronounced effect, and it must be stable on time scale of days.

The winter irregularity, combined with the seasonal asymmetry, remain so far unexplained. While the ground based data provides the opportunity of studying the occurrence of the phenomena, if as postulated it is related to some change of atmospheric parameters, appeal for confirmation must be made to rocket experiments.

The data give support to the suggestion that two ionized strata are formed within the D-region, and these have been designated the D- and C-layers. Since the C-layer is believed to be ionized by normal cosmic rays, there is particular value in studying the lower ionosphere at high latitudes, where such effects would be expected to be a maximum. DRTE has installed a partial reflection equipment at Resolute Bay in the summer of 1963, and plans to install an equipment at Fort Churchill in the summer of 1964. The installation at Fort Churchill is of particular interest since it will provide the opportunity of bringing together the potentials of one of the best ground-based techniques, for comparison with rocket techniques.

DISCUSSION

S. A. Bowhill: I believe that the winter variability you discussed corresponds to days of abnormally high vertical incidence high frequency absorption, and the occurence of the so-called sporadic D-layer. Do you have any data on the timescale of this variation?

J. S. Belrose: The curves I have shown are not associated with the winter anomaly since the absorption was not excessive on these five quiet days. However, on other days, high absorption is found. The absorption is reasonably stable on a given day; in a 3-hour period centered on a local midday (all the observations I have shown here are local midday), the electron density profiles from observations made at 15-minute intervals will all be about the same. The variation is from day to day, not from minute to minute.

J. Ortner: Would the winter and summer curves appear the same in other years?

J. S. Belrose: A marked seasonal asymmetry has long been known in LF and VLF propagation. The winter effect appears in the months of October or November and disappears in the months of February to May. The turn-over point on our curve of A_X/A_O shows a systematic variation from month to month, occurring at 71.5 km in winter, and at 61.5 km in summer, with this regular seasonal asymmetry.

W. J. Heikkila: Dr. Belrose has used the generalized magneto-ionic theory; I have noticed that many people still seem to be using the Appleton-Hartree formulation in which γ is considered independent of energy. This does not seem to be appropriate to the lower D-region.

12.2 ROCKET MEASUREMENTS OF LOW FREQUENCY WAVEFIELDS FOR THE DETERMINATION OF D-REGION ELECTRON DENSITIES

J. E. HALL
DSIR, Radio Research Station
Slough, Bucks., England

This report presents the early results from a rocket experiment designed to determine the distribution of electrons in the D-region of the ionosphere. A continuous wave of frequency 202 kc/s was transmitted from the ground to a rocket. In the ionosphere the wave was reflected, absorbed and the polarization modified. The form of the resulting standing wave pattern depended on the height distribution of electron concentration and collision frequency. The aim of the experiment was to send a rocket through this wave pattern to measure the field distribution and to deduce the ionospheric parameters.

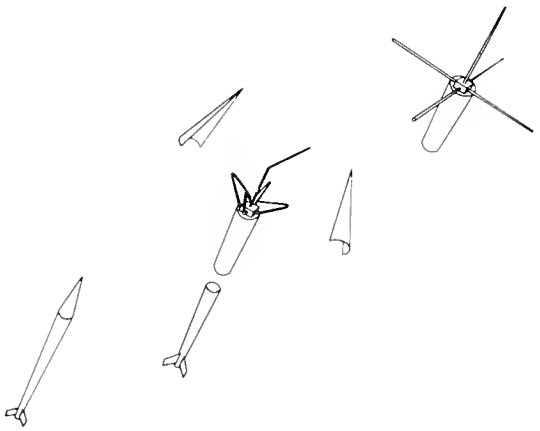

Figure 1. Erection of rocket aerials

This experiment was first performed, in collaboration with a group at Sheffield University, during the late summer of 1962 and repeated in a modified form during the spring of this year. Skylark rockets have been used for the experiment and were flown from the range at Woomera, Australia.

A 500 watt transmitter was connected to a horizontal half-wave dipole aerial, mounted 10 m above the ground, at a site near to the point beneath the predicted apex of the rocket trajectory. Because of the considerable ground losses, the effective radiated power was only about 10 watts but this was sufficient to give an adequate signal to noise ratio up to the height of reflection. The first two rockets were equipped with three mutually perpendicular receiving aerials which were folded inside a protective nose cone during the early part of the flight where the aerodynamic forces were great. At a pre-arranged height the nose cone was discarded, as shown in Figure 1, and the aerials unfolded to form two dipoles of length 4.3 m perpendicular to the rocket axis and a monopole which, together with the instrument section of the rocket body, formed a third dipole of similar length. In recent flights these aerials have been replaced by three ferrite rod aerials mounted beneath a glass fiber nose cone.

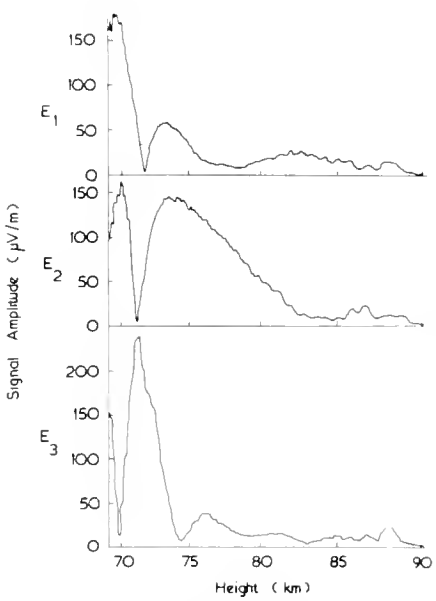

Figure 2. Field strength measured by SL 108 at 202 kc/s

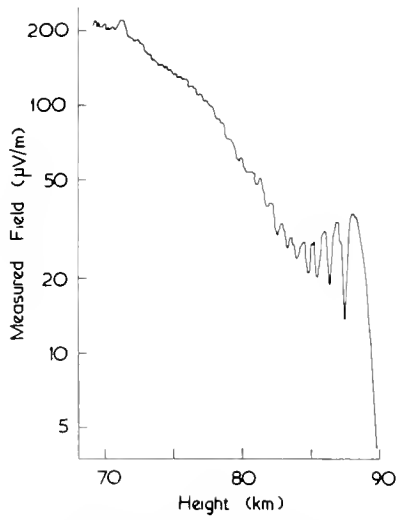

Figure 3. Combined measured fields $\sqrt{E_1^2 + E_2^2 + E_3^2}$

Three separate receiver were used and, by means of telemetry, a record was made on the ground of the three amplitudes received. The part of this record for the up-leg of the flight is shown in Figure 2. The orientation of the rocket was continuously changing during flight and this produced modulation of the signal which obscured the amplitude changes produced by the ionosphere. When the preliminary analysis was made the attitude of the rocket at each point of the trajectory was unknown and a scalar field quantity

$$F = \sqrt{E_1^2 + E_2^2 + E_3^2},$$

independent of the attitude, was therefore derived from the voltages E_1, E_2, and E_3 measured at the three aerial

This is given in Figure

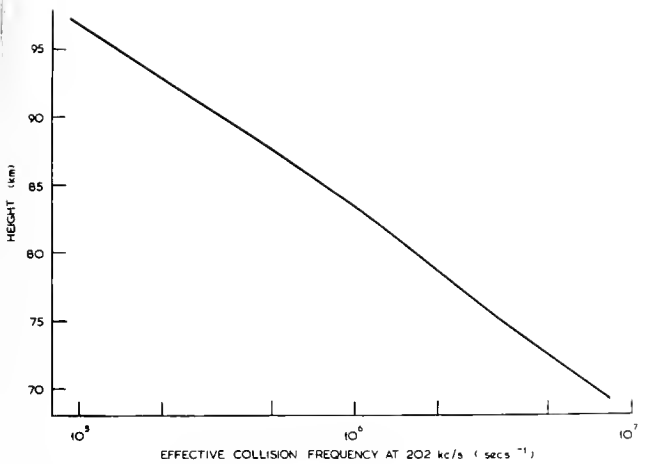

Figure 4. Effective collision frequency as a function of height

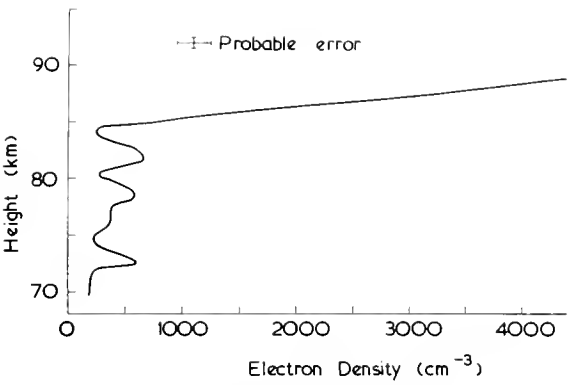

Figure 5. Daytime model ionosphere

where it can be seen that all modulation due to the motion of the rocket has been eliminated. From this curve it is noticeable that (a) ionospheric absorption causes the wave amplitude to decrease by a factor of ten between 70 and 80 km (b) above 80 km the reflected wave was strong enough to produce a well-defined standing wave (c) the wavelength of the standing wave increased with increasing height and (d) total reflection occurred at a height of about 89 km. The results were interpreted in the following way.

A horizontally stratified model ionosphere was postulated with a particular height variation of electron density and collision frequency. The wavefield that would be set up in this ionosphere by the signal from the transmitting aerial was calculated using a full-wave solution of the wave equation. The model ionosphere was repeatedly changed until it yielded results closely resembling those derived from the experiment. In practice the iteration could be speeded up considerably by using the simpler ideas of magneto-ionic theory to deduce the best way to modify the ionospheric model, but a full-wave solution was necessary to calculate the details of the wavefield. The collision frequency ν was assumed to be given by $\nu \propto \rho T$ where ρ and T are the density and temperature of the neutral atmosphere (taken from CIRA, 1961). The constant of proportionality was deduced from the present results by matching the depth of the standing wave pattern near the reflection level. Molmud has shown that the ratio between ν_{eff} and the simple kinetic theory ν depends on whether ν is greater or less than the angular wave frequency, where ν_{eff} is the collision frequency appropriate to the Appleton-Hartree equation. Allowance has been made for this effect and Figure 4 gives a plot of the effective collision frequency for 202 kc/s.

One rocket was launched on 20th September 1962 at 1351 LMT and on this occasion the LF wave

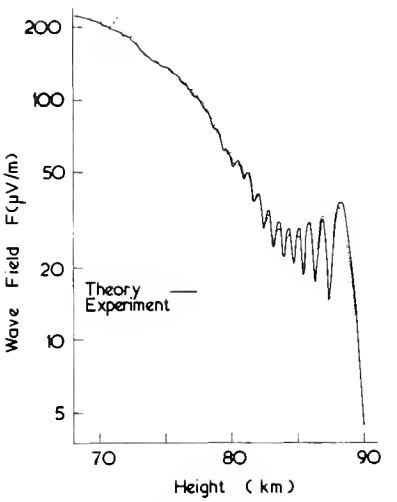

Figure 6. Theoretical field strength for daytime model ionosphere compared with field measured by SL 108

was reflected at about 89 km. The electron density model yielding the best fit to the experiment (Figure 5) had a steeply decreasing electron density from about 4000 cm^{-3} at 85 km. Between 70 and 85 km the electron density varied much less, fluctuating between 250 and 500 cm^{-3}. One cannot attach too great a significance to the small fluctuation in electron density below 84 km since the estimated error in density ($\pm$ 150 cm^{-3}) is of similar magnitude. However, the experimental results correspond more closely to the wavefield calculated using the curve of Figure 5 rather than a smooth curve which ignores the fluctuations. A comparison between the theoretical and measured wavefields is given in Figure 6.

A second rocket was flown shortly after midnight but unfortunately the peak of the

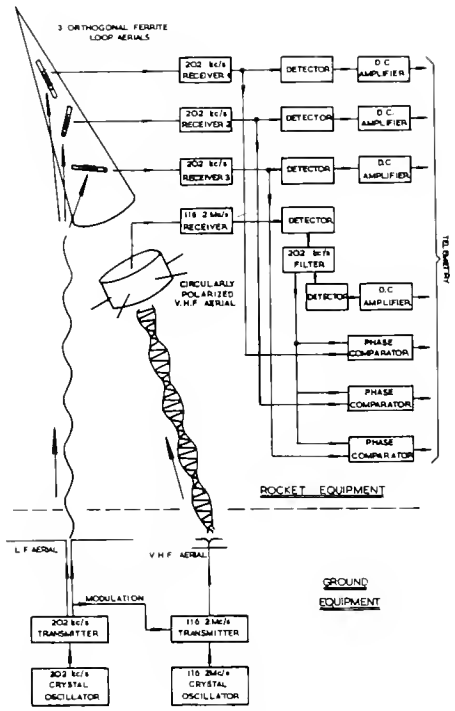

Figure 7. R. R. S. Rocket experiment R2

rocket trajectory, 111 km, was below the reflection height of the LF wave. However, the signal was received throughout the flight and a tentative night time electron density profile has been deduced. In this, the electron density increases from 150 cm^{-3} at about 87 km to a peak of about 2200 cm^{-3} at 95 km. Above this there is evidence that the density decreases to 800 cm^{-3} and then increases to 1000 cm^{-3} at 104 km with, perhaps, smaller peak at about 102 km. There was no sporadic E at 95 km at the time of the flight, but sporadic E developed at this height during the next hour, giving partial reflection up to about 3 Mc/s. It may also be worth noting that this is exactly the height at which long-persistence meteor echoes are observed on meteorwave radar systems.

Electron density models have not yet been deduced from the measurements made during the two recent rocket flights in which ferrite loop aerials were used but, as in the first daytime experiment, the reflection height was about 90 km corresponding to an electron density at this height of about 4000 cm^{-3}.

In future experiments it is intended to measure the phase as well as the amplitude of the signals received at the rocket. A block diagram for this experiment is given in Figure 7. To facilitate this, a VHF signal, amplitude modulated by the 202 kc/s signal, will be transmitted to the rocket and the modulation will be used as a phase reference for the directly transmitted 202 kc/s wave. This will enable the polarization and phase velocity of the wave to be determined and hence a more accurate ionospheric model.

DISCUSSION

J. S. Belrose: In your experimental data there is hardly any standing wave pattern at heights below 80 km. How do you get so much detail from the curve?

J. E. Hall: The lower part of the profile depends on the absorption of the signal, even in the full wave solution. The details in the rate of absorption of the signal with height give the fluctuations in the profile. The error which I showed is of the order of the fluctuations, but I think they are significant.

S. A. Bowhill: Could you say something about the calibration procedures for obtaining the field strength from the measurements of the voltages at the antenna?

J. E. Hall: We calculate the effective length of the aerial from its dimensions, as very nearly half the tip-to-tip length. We know its impedance and how it is likely to vary in the ionosphere. Our circuitry was arranged so that there was no change in the output of the receiver as we changed the aerial impedance by a factor of ten in a simulating network.

S. A. Bowhill: Is it conceivable that some of the very small fluctuations in electron density might be due to incompletely removed attitude effects?

J. E. Hall: We looked into this very carefully, and they do not correlate.

G. C. Reid: The scale size of your fluctuations looks very similar to the scale size of the wind shears we have heard about. This may give some evidence that the Whitehead mechanism is working down at these levels and producing concentrations of electron density. It would be interesting to have simultaneous wind measurements during some of these flights.

J. E. Hall: Yes, and more accurate measurements of the fluctuations would be desirable.

S. A. Bowhill: Did you at any time see the extraordinary component beyond the level of reflection of the ordinary component?

J. E. Hall: We observed the penetrating mode on the second pair of flights using the ferrite loop aerials. This was partly because of higher sensitivity, and partly because the magnetic component is larger than the electric component, the refractive index being large. It also depends very much on the direction of propagation of the wave with respect to the magnetic field, and therefore on the exact trajectory.

12.3 ELECTRON DENSITY OBSERVATIONS IN THE D-REGION DURING AURORAL ABSORPTION

B. LANDMARK
Norwegian Defence Research Establishment
Kjeller, Norway

and

O. PETERSEN
Technical University of Denmark
Copenhagen, Denmark

Abstract

This paper describes results from measurements of electron density and collision frequency distributions in the D-region from three rocket flights from northern Norway. A multifrequency propagation experiment making use of ground based transmissions and reception in the rocket, was used. All three rockets were fired under conditions of auroral type absorption.

1. Introduction

A joint research program has been undertaken between research groups in Denmark, Norway and the USA (National Aeronautics and Space Administration). In this program up to the present five rockets have been launched, and the purpose of the paper is to describe some of the most important results obtained from the first three of these.

TABLE I.

	Ferdinand I	Ferdinand II	Ferdinand III
Time of launch	Aug. 18, 1962 0809 EMT	Dec. 14, 1962 2152 EMT	Dec. 11, 1962 0427 EMT
Total flight time	308.5 sec	338.0 sec	334.0 sec
Time of peak	156.0 sec	172.8 sec	171.0 sec
Peak altitude	101.5 km	122.9 km	120.8 km
Horizontal range		135.5 km	164.5 km

In all three rockets, a multifrequency propagation experiment was flown in order to measure the distribution of free electrons and their collision frequency in the D-region, during conditions of auroral type absorption. The principles of the experimental method will be dealt with briefly in Section 2, and the results discussed in Section 3.

2. Experimental Method

In this section is described the experimental method employed in order to measure electron density and collision frequency distribution in the D-region.

2.1 Principle of Propagation experiment

Two types of measurements were made:

(a) The relative amplitude of signals transmitted from the ground and received in the rocket.

(b) The phase relationship between signals of different frequencies, transmitted from the ground and received in the rocket.

Amplitude recordings were made at the following frequencies: 2,5, 4.9, 15.0 and 22.5 MHz. From such observations the absorption indices, and thus a function of the electron density N and the collision frequency ν, can be measured as a function of height. The transmissions at the three lowest frequencies were made alternately in the ordinary and extraordinary modes of polarization, and the differential absorption (difference of absorption in the two modes) could therefore be determined.

The second method is that developed by Seddon and Jackson [1]. In our experiment the phase relationship between signals transmitted from the ground and received in the rocket was studied. In principle this method measures a relationship between the refractive indices of waves in the ionosphere, by comparing the doppler frequencies of signals of different wavelengths. The phase relationship was observed between signals at the following frequencies: 2.5, 15.0, 22.5 and 35 MHz. Since only the lowest

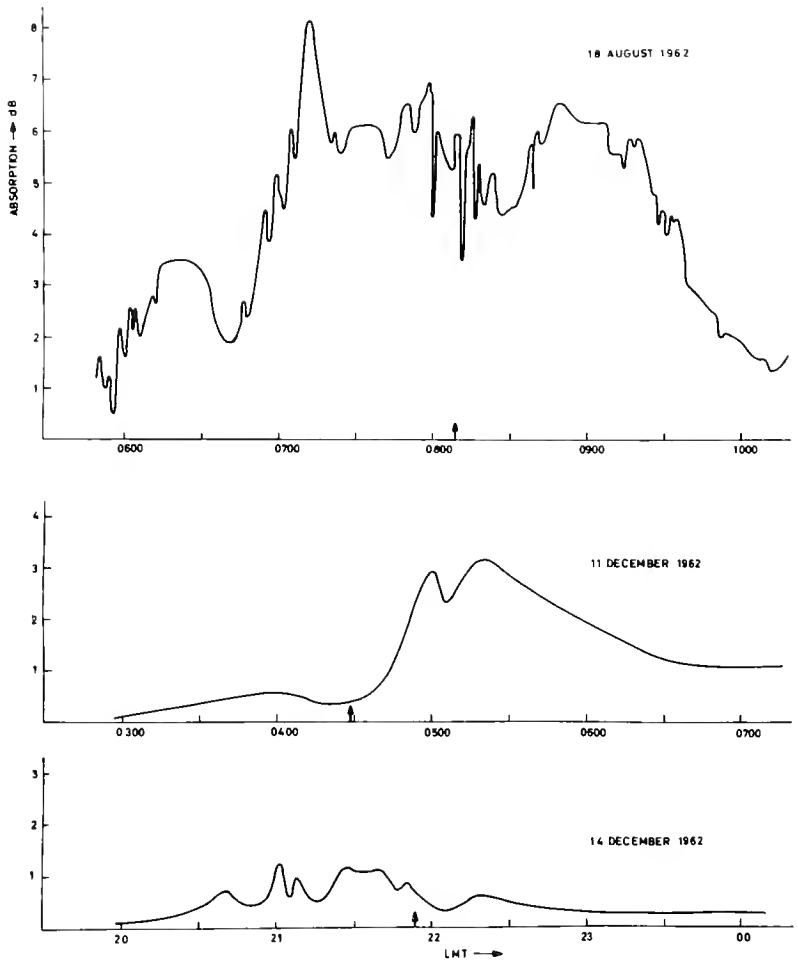

Figure 1. Results from riometer observations

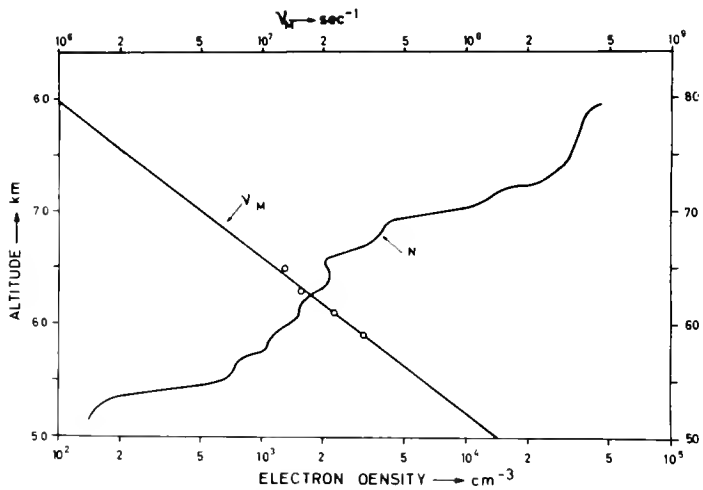

Figure 2. Profiles of electron density N and collision frequency ν_M obtained from Ferdinand I

frequency, 2.5 MHz, is markedly influenced by the ionosphere, the measurements give the refractive index at this frequency with good approximation. Furthermore, due to the fact that we transmitted alternately in the ordinary and extraordinary modes, the refractive index in both modes could be studied.

By using four frequencies in the phase experiment, it was possible to eliminate the effects of rocket spin. A more detailed description of the experimental method and equipment is given elsewhere [2].

2.2 Trajectory Observations

A simple slant range system was used in order to determine the trajectory of the rocket. Such a system measures the slant range to the rocket as a function of time.

It has been shown by Jackson and Radicella [3] that on the assumption that the upper part of the trajectory is ballistic, quite a reliable height/time curve can be deduced from an observed slant range/time curve. The detailed analysis of our results will be given elsewhere [4] and in this paper therefore we shall limit ourselves to state that the accuracy with which the height time curve can be deduced is estimated to be better than 1 km.

3. Results

In the analysis of the observations we have used the generalized Appleton-Hartree theory, which accounts for the dependance of the collision cross section of the electrons on their energy [5]. The parameter used is then ν_M, the collision frequency of monoenergetic electrons of energy u = kT.

3.1 Results from some related observations

The most important trajectory characteristics are summarized in Table I.

During the periods of the firings, h' f observations were made at the Auroral Observatory in Tromso. Ferdinand I was fired in a period with quite high auroral type absorption, and no echoes could be observed on the h' f recording.

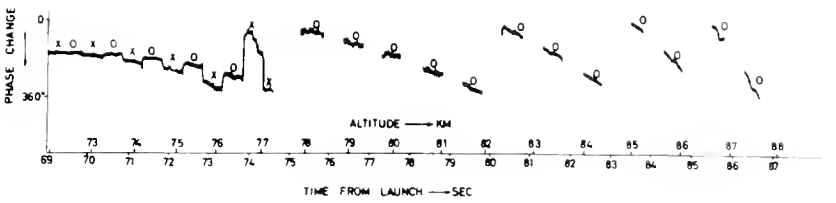

Figure 3. Phase recording obtained from Ferdinand II
Alternate transmissions in the ordinary and extraordinary mode

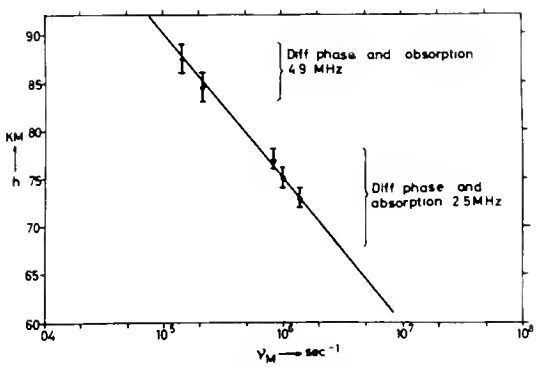

Figure 4. Collision frequency results from Ferdinand II

Ferdinands II and III were fired in periods when only faint traces of sporadic E could be observed.

Riometer observations were made at the range (at 27.6 MHz), in Tromso (at 27.6 MHz) and at a field laboratory in Lavangsdalen (at 20 MHz). The distance from the range both to Tromso and Lavangsdalen is about 140 km.

At Lavangsdalen observations of D-region back scatter or partial reflections (Gardner and Pawsey method) were also made in a period around the time of the launching. The results from these observations were in good agreement with those obtained from the rockets.

In Figure 1 are shown the results obtained from the riometer at the range. It is seen that Ferdinand I was fired in a period with quite high auroral type absorption, while Ferdinand II and III were fired during rather weak events.

3.2 Analysis of results

The electron density and collision frequency distributions derived from results from Ferdinand I are shown in Figure 2.

For the height range between 52 and 67 km, a reliable curve for the difference in absorption between the ordinary and extraordinary waves at 2.5 MHz could be established. By comparing this differential absorption with the difference in absorption between the ordinary component of the 2.5 and the 22.5 MHz signal, both N and ν_M could be determined in this height range. This method is based on the assumption that the variations of the unabsorbed signals at the two frequencies are similar; an assumption that seems reasonable as the signal levels at the two frequencies vary similarly below the levels where the ionospheric effects are important. The results are also consistent with the observed phase changes at 2.5 MHz.

For heights above 67 km, we have not sufficient results to enable us to deduce both the N and ν_M values. For this region we have then extrapolated the ν_M-curve and used the measurements (or results) to derive the continuation of the N-curve.

For the height range between 67 km and 71 km the results have been derived by comparing the amplitude variations at 2.5 and 22.5 MHz. For the height range between 71 km and 76 km no reliable measurements were obtained, but above 76 km quite good readings of the difference of the amplitudes of the ordinary waves at 15 MHz and 22.5 MHz could be made, and by comparing these with similar readings below 71 km, the integrated differential absorption between these heights could be determined, and tentative electron densities were obtained (deduced) up to 80 km.

In Figure 3 phase recordings at 2.5 MHz in Ferdinand II are shown. The illustration shows how first rapid changes are observed in the extraordinary mode as compared with those in the ordinary mode. In this interval, where both modes could be observed, quite good results were also obtained for the differential amplitude, so that both electron density and collision frequency values could be deduced.

For the height range between 76 km and 84 km the phase changes in the ordinary mode could still be observed, and from these an electron density curve could be deduced.

From the observed amplitude variation at 4.9 MHz it was possible to deduce both the differential absorption and the Faraday rotation of the plane of polarization, and thus to derive both electron density and collision frequency values in the height range from 81 to 89 km.

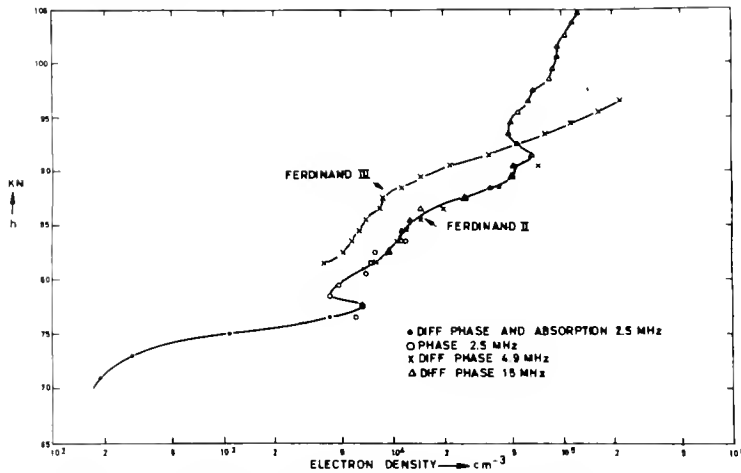

Figure 5. Profiles of electron density N derived from results from Ferdinand II and III

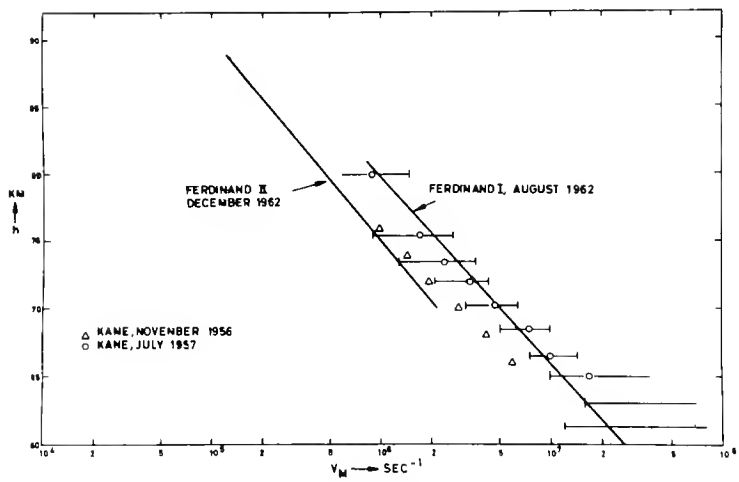

Figure 6. Comparison of our results (continuous curve) with results obtained previously by Kane

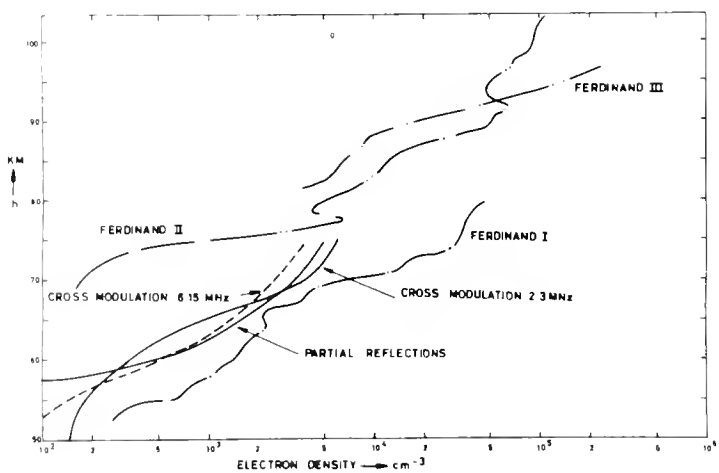

Figure 7. Comparison of electron density profiles with previous results from cross modulation and partial reflection observations

The Faraday rotation effect could also be deduced from the 15 MHz recordings and from these an electron density profile could be derived up to heights of more than 100 km.

In Figure 4 the collision frequency values derived from Ferdinand II results are shown. In Figure 5 we have shown the electron density curve that was obtained. The results from Ferdinand III are shown in the same illustration. In this rocket a fault occurred in the 15 MHz receiver. This fault also destroyed the amplitude and phase recordings at 2.5 MHz. It was possible, however, from the results at 4.9 MHz to observe a Faraday rotation effect similar to that described above from the observations of Ferdinand II, and therefore to construct an electron density profile for the height range between 81 km and 97 km. Unfortunately, the amplitude data were not accurate enough to permit us to derive the collision frequency values.

3.3 Discussion of results

It has been experienced by others that a propagation technique may not be too useful as a tool for measuring electron density profiles in the disturbed arctic ionosphere. This is mainly due to rapid time changes experienced in the ionizing radiation. Our results have shown that in the D-region it is possible to perform such measurements. The qualitative nature of the results should, however, be stressed, and the detailed structure in the observed profiles should not be regarded as significant.

In Figure 6 the results obtained for collision frequency values are compared with results previously obtained by Kane [5]. Our results are shown as continuous lines, while the results obtained by Kane are shown as circles and triangles.

A marked difference is noted between the curves obtained on the two flights for which collision frequencies values were available. A similar difference was also observed by Kane, and the highest values were observed during summer in both his and our case. Whether this difference is due to a seasonal effect, or only indicates a great variability in the values of the collision frequency is difficult to say before more data becomes available.

In Figure 7 we have shown on the same graph the electron density profiles obtained from our three experiments. In the illustration is also shown an average

electron density profile as deduced from observations of cross modulation and partial reflections by Holt el al [6]. These profiles are average over results with an average riometer absorption of 1 db, and one should therefore expect the profiles to be somewhere in between the results from Ferdinand I and II.

4. Conclusion

A rather complicated experiment involving transmissions at 5 frequencies, was used in order to perform measurements of electron density and collision frequencies in the lower D-region during auroral type absorption. The main reasons for choosing such a system were that:

a) the effects introduced on the phase recording by spinning of the rocket could be eliminated.

b) the system provided a fair amount of overlapping information, and covered greater height range.

Our results have shown that it is possible to obtain quite good information about the rocket spin by rather simple methods, and we are at present planning to simplify our experiments to include transmissions at three frequencies only.

References

[1] J. C. Seddon, J. Geophys. Res. 58, 323 (1953)

[2] M. Jespersen et al,, Norwegian Space Research Committee, Report no. 3 (1963).

[3] J. E. Jackson and S. M. Radicella, Report X-615-62-139, NASA (1962).

[4] B. Bjelland, Norwegian Space Research Committee - Report no. 4 (1963).

[5] J. A. Kane, Radio Wave Absorption in the Ionosphere (ed. N. C. Gerson) 338, (1962), Pergamon Press.

[6] O. Holt, B. Landmark and F. Lied, NDRE-report 35.

DISCUSSION

W. J. Heikkila: Have you found any difficulty with the propagation experiment because of time variations during the disturbancee?

B. Landmark: We know that the detailed structure we see is not significant but we feel that the propagation experiment works in the D-region, and also in the quiet E-region. We regard these results as qualitative rather than quantitative.

S. A. Bowhill: What was the reason for the roll modulation of your signal in the region where the extraordinary wave had already been absorbed and you were left with a circularly polarized wave?

B. Landmark: If the plane of polarization is not perpendicular to the axis of the rocket you will have such a modulation, and the rocket has a considerable horizontal range when this effect occurs.

J. S. Belrose: Your collision frequency values which go up to 85 km do not look very different from normal. Therefore something must be terribly different at greater heights. In all other types of absorption events, most of the absorption one measures on riometers occur in the 50-60 km height range. How much absorption would you have to attribute to heights above 80 km?

B. Landmark: We cannot directly observe riometer absorption with our technique, but we had to have some absorption occurring at fairly high levels, say around 80 km, especially for the two weak events.

12.4 AN EXAMINATION OF D-REGION AERONOMY WITH A VLF IONOSPHERIC SOUNDING SYSTEM

W. F. MOLER
U. S. Navy Electronics Laboratory
San Diego, California 92152

The U. S. Navy Electronics Laboratory has developed and operated periodically for two years a phase-stable continuous-wave VLF D-region sounding system. The system, located in S. W. Arizona, consists of five phase and amplitude sensitive receivers placed in three mobile vans, two orthogonal horizontal half-wave dipole transmitting antennas aligned in and normal to the geomagnetic meridian, and a 30 kw phase stable transmitter capable of operation from 8.2 kc/s to 50 kc/s. During the experiments, to be described, the sounder was operated at 8.2, 13, 17 and 23 kc/s.

A horizontal half-wave transmitting antenna next to a conducting plane has a radiation pattern with a maximum of the horizontally polarized component radiated upward and normal to the antenna axis and a deep null in the vertically polarized component along the normal to the antenna axis. Figure 1 shows a plan view of the theoretical ground wave pattern of the vertically polarized component of the transmitted waves compared with the measured pattern at 14 kc/s. The measurements were carried out in a helicopter flying with an extended vertical whip at 200 feet in a 10 mile radius about the transmitter. The field in the null was more than 20 db down from that off the end of the antenna.

In the experiments performed by NEL the transmitting antenna in the magnetic meridian was excited and receivers were placed in the ground wave null approximately 100 km magnetically east and west of the transmitter (see Figure 2). At these distances it is possible to measure the phase and amplitude of waves, once-reflected from the ionosphere and polarized in and normal to the plane of propagation, with little ground wave contamination. Figure 3 illustrates a phase-amplitude diagram through the day, and Figure 4 shows the phase variation in a sudden ionosphere disturbance (SID).

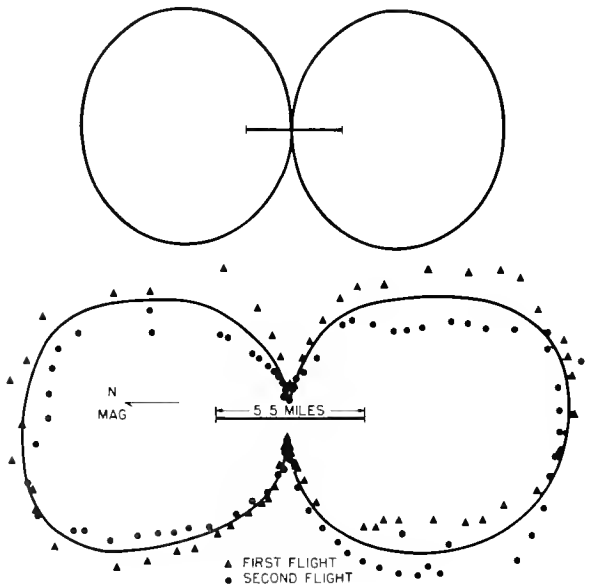

Figure 1. Ground wave radiation pattern for a horizontal half wave dipole at 14 kc/s

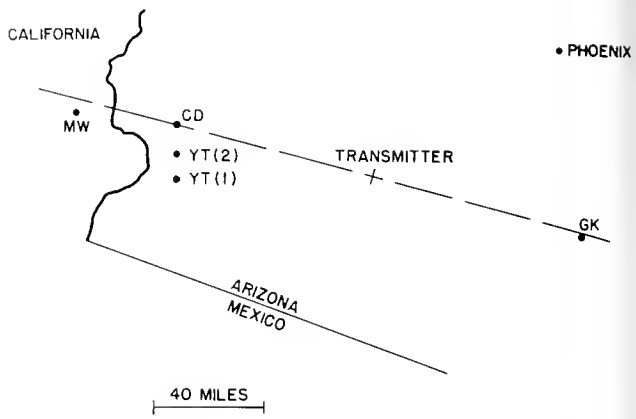

Figure 2. Location of receiving sites

Although the general distribution of field strength about the antenna is known to be that of a toroid bisected by the ground plane the actual field intensities as a function of elevation and azimuth are so uncertain as to preclude the calculation of ionospheric reflection coefficients (and consequently electron distributions) directly from received fields. How-

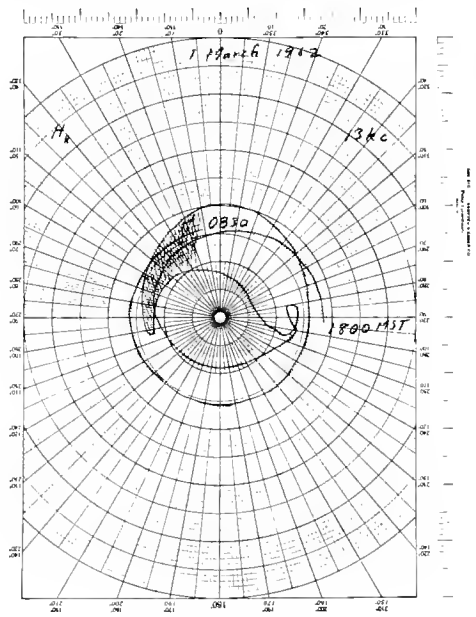

Figure 3. Phase-amplitude diagram at 13 kc/s, 0830-1730 MST, March 1, 1962

ever, by measuring the relative phase and amplitude of waves polarized in and normal to the plane of propagation one may ascertain the phase differences between and the ratio of the amplitudes of the two wave components. By so doing at several radio frequencies a reasonably large range of heights within the ionosphere may be examined. The experimental results are then compared with those given by a full-wave solution for propagation transverse to the geomagnetic field through an ionosphere with arbitrary height distributions of electron density and electron collision frequency. By making this comparison for a variety of ionospheric models it is possible to find a best fit to experimental results.

The approach used for numerical solution of the propagation equations is that described by Budden and Barron [1]. The method is discussed and reduced to computer form in NEL Technical Memorandum No. 439 by L. Fedor and E. Gossard [2], and programmed in NELIAC for the CDC 1604 by Mrs. Joy Fedor.

The experimental observations were made over a period of about one hour centered about local noon. Ten minute observations on each polarization were carried out alternately on each of two receivers at each receiving site. The records were taken during February, March, May, June, July and October, 1962, and during February and May 1963. The noontime solar zenith angles (χ) ranged from 9^{o} to about 45^{o} but for the purposes of comparison with theoretical electron density profiles the observations have been grouped into classes of $\chi = 10^{o}$, $\chi = 15^{o}$, and $\chi = 40^{o}$. A considerable day to day and seasonal variation appeared in the records with the larger variations occurring during the winter months.

The ionospheric models tested were constructed from the following considerations:

1. The collision frequency profile was kept constant. A comparison was made between the collision frequencies calculated from the collision cross sections found by Huxley [3] and those arrived at by Fejer [4] and they were found to be nearly identical. Fejer's exponential profile was selected for use in the computer solution.

2. Steady state solutions were assumed for calculating the electron density profiles.

3. The ionizing radiations considered for the calculated profiles were L_{α}, L_{β}, 1-10A X-rays, and cosmic rays for solar quiet conditions. The X-ray continuum was considered to be represented by average values for 2A, 4A, and 6A. The appropriate zero optical depth pair production rates are listed as follows:

Radiation	Production Rate
L_{α}	3.68×10^{-7} pairs/mol/sec
L_{β}	5.52×10^{-9} pairs/mol/sec
2A	1.64×10^{-18} paris/mol/sec
4A	9.9×15^{-17} pairs/mol/sec
6A	2.74×15^{-15} pairs/mol/sec
Cosmic rays	1.7×10^{2} pairs/cm^3/sec/atmosphere

4. The electron production and other reaction rates were calculated using the atmospheric densities, temperatures and percentage compositions from the ARDC model atmosphere.

5. Two sets of attachment, detachment and recombination rates were used and are listed as follows:

	Rate 1	Rate 2	
Dissociative Recombination	3×10^{-8}	10^{-7}	cm^3 sec^{-1}
Radiation Recombination	---	10^{-12}	cm^3 sec^{-1}
Dielectronic Recombination	---	10^{-12}	cm^3 sec^{-1}
Three body Recombination	---	10^{-11}	cm^3 sec^{-1}
Electron attachment frequency	$5 \times 10^{3} \rho/\rho$	P(mm Hg) $+ 10^{8} (\rho/\rho_{.})^{2}$	sec^{-1}
Photo detachment	0.44	0.44 detachments	ion^{-1} sec^{-1}
Collisional detachment	2×10^{-17}	2.4×10^{-20}	cm^3 sec^{-1}
Two body mutual neutralization	10^{8}	10^{8}	cm^3 sec^{-1}
Three body mutual neutralization	8×10^{-3} $PT^{-5/2}$ P = mm Hg	8×10^{-3} $PT^{-5/2}$	cm^3 sec^{-1}
Associative detachment	---	5×10^{-14}	cm^3 sec^{-1}

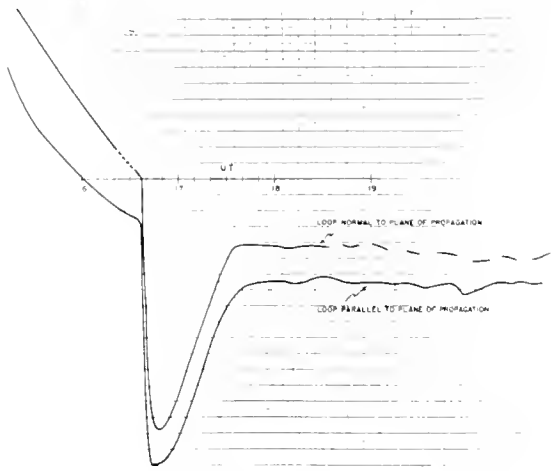

Figure 4. Phase variation through a SID

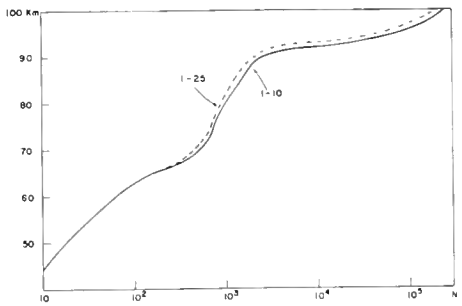

Figure 5. Electron profiles consistent with data taken when χ = 10°.

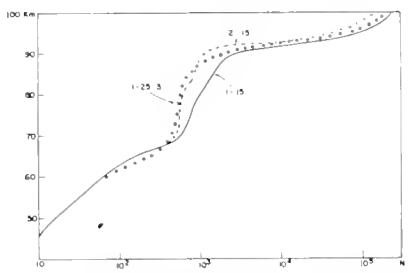

Figure 6. Electron profiles consistent with data taken when χ = 15°.

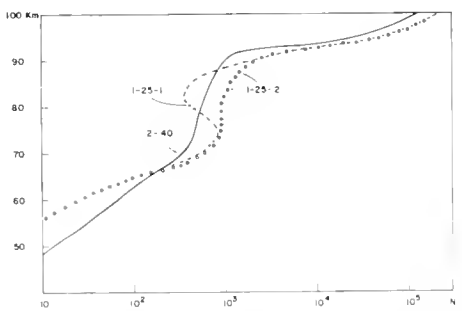

Figure 7. Electron profiles consistent with data taken when χ = 40°.

The calculated electron density profiles shown in Figures 5, 6 and 7 are identified by the prefix number 1 or 2 depending on the reaction rates used and the number which follows identified the solar angle. Profiles with a third number were arbitrarily drawn as departures from profile 1-25.

Figure 5 shows the electron density profiles calculated for solar angles of 10° and 25°. All observations of amplitude ratios and phase differences made when χ was near 10° agreed with those calculated from one or the other of the profiles depending on radio frequency and direction of propagation. Similarly the profiles shown for χ of 15° and χ of 45° showed similar agreement although the range is materially greater for the larger angles.

The most significant correlation between the process curves and experimental results comes about when averages are considered. Insomuch as the atmospheric densities and temperatures are best interpreted as average values it is not surprising that correlations between radio data calculated from theoretical process curves for the average solar position during all the observations and the average observational radio data is quite high. The average solar angle of the sun was 23.6° for all observing periods. Figure 8 shows the average phase angle difference and amplitude ratios for all measurements compared with theoretical values for process profile 1-25.

Probably the greatest virtue of the VLF sounder used in conjunction with the proper theoretical program is the ability to reject certain ionospheric models as being incompatible with experiment. The reverse procedure of ascertaining the correct model from experiment requires a great deal of model testing and consequently much computer time.

The electron density profiles obtained from nighttime data exhibit a rather interesting behavior. Quite large phase changes are noted at night, and these have a tendency to approximate 180° or 360°. Simultaneously the rapid phase changes are accompanied by a sharp drop in signal level. They occur over large areas at receiver site separations of typically 40 miles within a few minutes of each other. Figure 9 shows an example of phase changes noted at three receivers. It can be seen that the same phase perturbation appeared at different times through the three stations. We have noticed this time and again; one of them was so coherent that we were able to clock the direction and speed at roghly a 100 m/sec coming from the southeast on this particular occasion.

Probably the more significant effect is a preference for the direction of propagation where these appear. During last June and July one of the stations observed a large number of these cycles. They showed a preference for in-

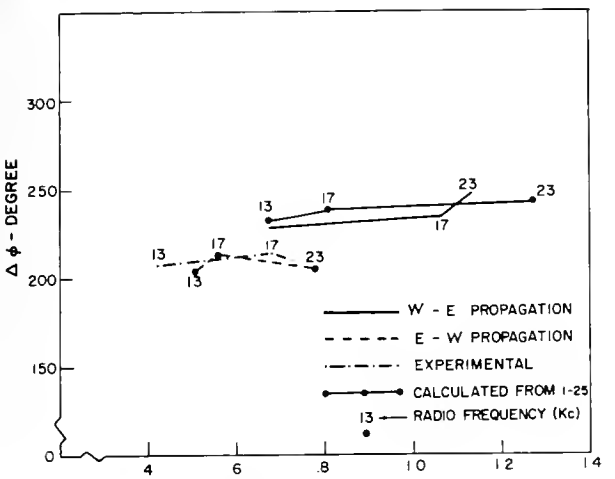

Figure 8. Phase difference as a function of conversion coefficient for frequencies of 13-23 kc/s.

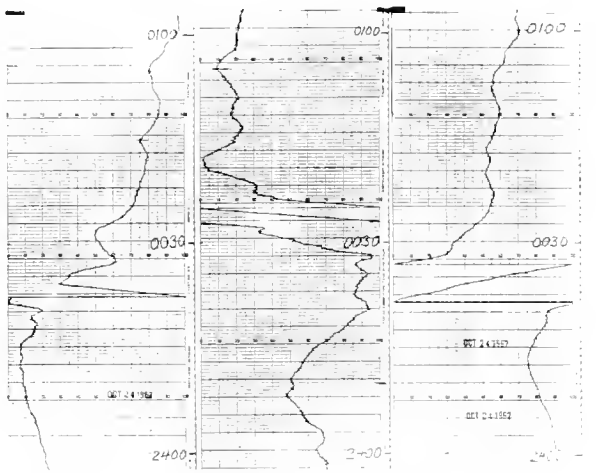

Figure 9. Nighttime phase changes observed at three spaced receivers

crease in phase, a preference for 360° rotation, and they were indicative of an ionosphere that was gradually going right down to the ground, if one were to interpret this as height changes. At the same time, a station to the west showed reasonably quiet phase records with very little change. It should be noted that phase noise is much greater for W - E propagation than for E - W, and the waves polarized normal to the plane of propagation exhibit a much greater incidence of large phase excursions than waves polarized in the plane of propagation.

The model of the ionosphere best able to explain these data appears to be a step model where there is a steep gradient in the E Region with densities of the order of 10^3 electrons/cc. If this base is placed at 100 km, then there should be a ledge of about 180-200 electrons/cc.

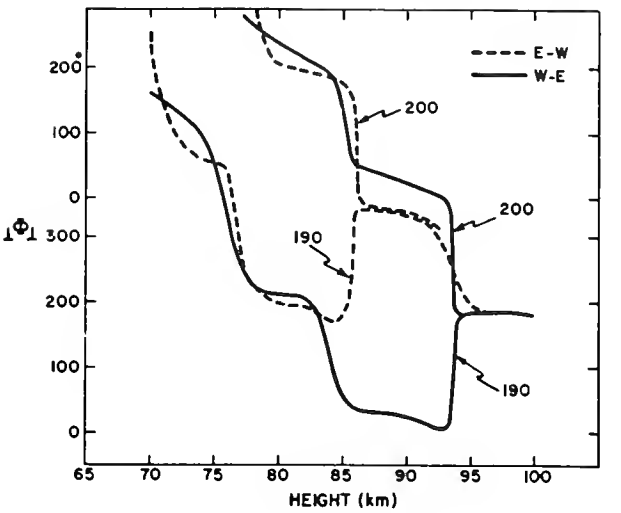

Figure 10. Theoretical phase changes with a step model ionosphere

extending downward to about 90-95 km and then dropping sharply to around 10-20 at 85 km. Then with very slight undulations of the lower layer (slight increases of electron density or slight changes of the E-region with this dimension) one indeed would get a very rapid phase shift on one polarization, and it may be an advance or a retardation.

Figure 10 represents a phase plot if one were to take a solid E-region at 100 km and reflect waves off of this as a solid bank. If we put a 200 electrons/cc ledge below here, and gradually lowered this ledge to around 95-93 km (10^2 electrons), we would experience at the ground a very rapid phase shift which would be a phase advance. Similarly, if there were around 190 electrons/cc, we would get a phase retardation. This is for W-E propagation. For E-W propagation, we find we have to take this ledge considerably lower (to about 85 km), and then we get roughly the same response. So between the experimental and this evidence, it appears that during June and July, at least, we did have some sort of a two-step arrangement where the electron density was oscillating around 180 to 200 electrons/cc, because we had both phase advances and phase retardations.

One cannot call on moving horizontal facets or turbulence of any sort to explain this, because it would be rather unusual to have things roughly 50 miles apart with the reflection point in the ionosphere, and have a completely different ionosphere at the two points. That is, extremely rough for propagation one way, and smooth for propagation the other. So rather than a mechanical oscillation of phase, one would think it would have to be something to do with the non-reciprocal propagation.

References

[1] Barron, D.W. and Budden, K.G., Proc. Royal Society, Vol. 249, pp 387-401, 1959.

[2] Fedor, L. and E.E. Gossard, NEL TM-439, Nov. 1960.

[3] Huxley, et al., Proc. Royal Society 218, P 511, 1953.

[4] Fejer, J.A. and R.W. Vice, J. Atmos. and Terrest. Physics, 16, 291-306, 1959.

DISCUSSION

J.S. Belrose: At higher latitudes we do not see these wave interference effects. Observations were made in England using a loop aerial to balance out the ground wave at about the same distance (100 km to the E of the transmitter), and on quiet days these interference effects were never seen. Observations made on the east coast of Canada to the north of the transmitter did not show them and observations made on the west coast of Canada about 100 km to the west of the transmitter did not show them on quiet nights.

W.F. Moler: The picture I showed was for a wave propagated into the ionosphere horizontally polarized and received horizontally polarized. From the loop in the plane of propagation the vertically polarized component was relatively quiet and if one plots out the reflection coefficients for the same profile one does not see this rapid phase change. In other words the converted wave is relatively smooth whereas the other is not.

S.A. Bowhill: Some observations at Cambridge did in fact show the effects that Dr. Belrose has described. They were CW signals at 30 kc/s frequency; the range of the transmitter was about 30 km, very close to vertical incidence. Superimposed on the usual phase-amplitude pattern of the abnormal component, almost before the phase revolution had started in the early morning, a series of loops were described. On some occasions these phase loops encircled the origin, in which case they would give a progressive decrease in the effective height of the layer; at other times they did not. Clearly these do not correspond to an effective decrease in the layer height as on one occasion the layer would have ended up 10 km below ground level! Nevertheless it is obviously a phase interference effect of exactly the kind you've described. The other piece of evidence was on a frequency of 70 kc/s, where Weekes made a long series of observations of the diurnal variation of phase of the horizontally polarized wave relative to the ground wave. These showed apparent net decrease in the height of reflection with time.

J.H. Cahn: Have any effects on the measured collision frequency been seen when the power of the transmitter is varied?

W.F. Moler: We keep at a continuous 30 kw or at least as close to that as we can.

J.S. Belrose: We have measured the amplitude ratio between the three magneto-ionic components at 100 kw and at 1000 kw and not observed any change in the amplitude ratio.

12.5 D-REGION ELECTRON DENSITY PROFILES DURING AURORA USING THE COSMIC NOISE TECHNIQUE

C. G. LITTLE and G. M. LESFALD
Central Radio Propagation Laboratory
National Bureau of Standards
Boulder, Colorado

and

R. PARTHASARATHY
University of Alaska
College, Alaska

The purpose of this contribution is to describe briefly the preliminary results of an analysis of multifrequency cosmic noise absorption data taken at College, Alaska during aurora.

Single-frequency riometer data give no information as to the height at which the absorption is occurring. However, the authors have shown [1] that cosmic noise absorption data taken on widely spaced frequencies can be used to derive "best-fit" electron density profiles over the height range approximately 30 to 75 km. Basically, the method depends on the fact that the ratio of absorption observed on two frequencies is a function of ν/ω in the absorbing region and therefore of height; for $\nu \ll \omega$ (great heights) the standard f^{-2} dependence of the absorption will be observed. The exponent decreases to zero as ν/ω is increased to large values (i.e. to low height).

TABLE I

Value of n	No. of times observed
Less than 1.0	None
1.0 - 1.1	2
1.1 - 1.2	-
1.2 - 1.3	1
1.3 - 1.4	6
1.4 - 1.5	2
1.5 - 1.6	8
1.6 - 1.7	8
1.7 - 1.8	16
1.8 - 1.9	24
1.9 - 2.0	26
2.0 - 2.1	11
2.1 - 2.2	5
2.2 - 2.3	3
2.3 and greater	None

Table I gives the frequency of occurrence of different values of the exponent n, in the relationship

$$A(f_e) = Cf_e^{-n}$$

Here C is a constant, $A(f_e)$ is the absorption in decibels on a given effective frequency f_e (after correction to pencil beam and for leakage between polarization modes), and $f_e = f \pm f_2$, where f is the observing frequency and f_2 is the electron gyrofrequency corresponding to the longitudinal component of the magnetic field. A relationship of this form is found to be satisfied (within experimental error) by essentially all the multi-frequency auroral data we have examined. The value of n varies from event to event, and is determined with an uncertainty of approximately $\pm$ 0.1. The data refer to 112 sets of absorption data taken during some 70 different events during the period January 1, 1961, through March, 1961.

The above table is based on unfiltered data; it is thought that the small number of values in which n is greater than 2.1 may be due to screening by ionospheric reflection of the lowest frequencies, resulting in excessive attenuation of the lowest frequencies. (It is

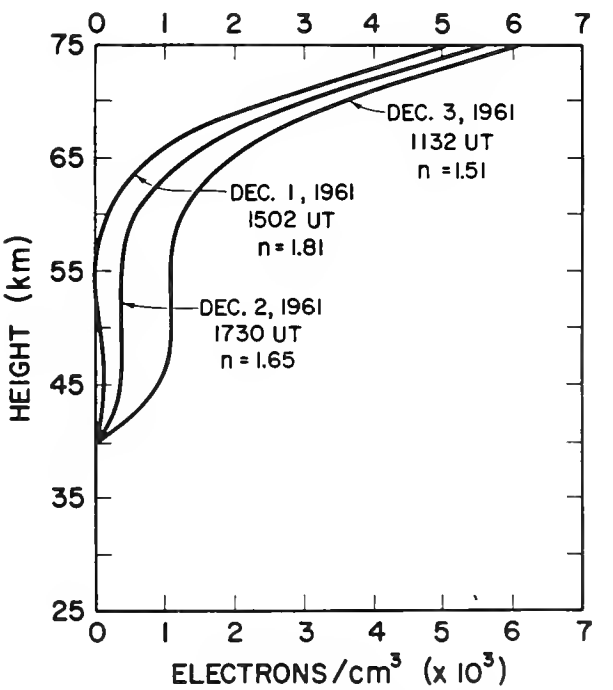

Figure 1. Three auroral electron density profiles (best-fit cubic profiles for the observed values of n)

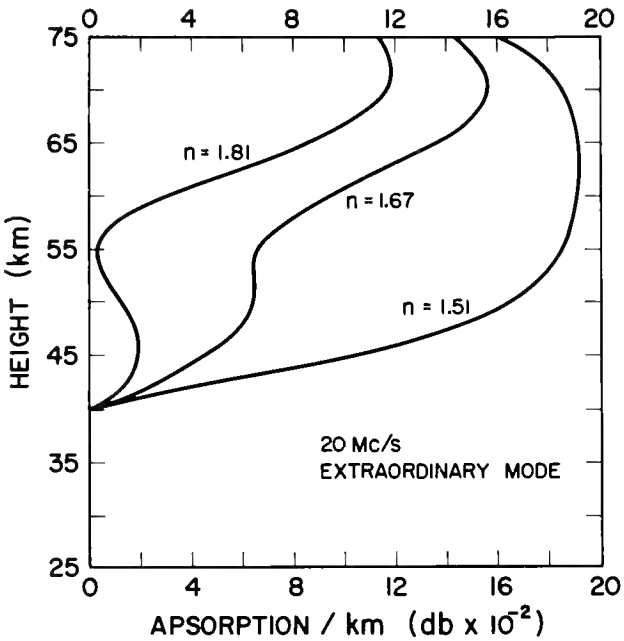

Figure 2. Absorption profiles for three values of n used in Figure 1.

hoped that it will be possible to use the ionosonde data to filter the data for this effect).

Figure 1 gives three D-region cubic profiles giving essentially exact fit for values of n = 1.51, 1.65 and 1.81. Note that the abcissa is electron density on a linear scale. Figure 2 gives the variation of absorption with height for each of these profiles. Note that for exponents of 1.51, the absorption occurs approximately uniformly over the height range 50-70 km, and that for n = 1.81 the absorption peaks slightly above 70 km. Table 1 suggests that approximately 60% of the observations give profiles of ionization and absorption as occuring at heights greater than indicated by the curves in the upper left of Figures 1 and 2; and approximately 10% of the absorption or ionization profiles occurring at heights lower than the lowest curves on Figures 1 and 2.

The variability of the exponent n is therefore taken as a clear indication of the extreme variability of the shape as well as in the intensity of auroral density profiles, between different events, and also at different times within a single event. This variability we of course attribute to changes in the energy spectrum of the incident particles. The "tail" in the ionization profile reaching down to heights of the order 40 km at low values of n we attribute to bremsstrahlung from X-rays produced by the more energetic incident electrons. Present evidence suggests that there is no marked systematic dependence of n (and hence of the shape of the profile) with the intensity of the absorption.

Reference

[1] Parthasarathy, R., G.M. Lesfald and C.G. Little, "Derivation of Electron-Density Profiles in the Lower Ionosphere using Radio Absorption Measurements at Multiple Frequencies", J. Geophys. Res. 68, No. 12, 3581-3588, June 15, 1963.

DISCUSSION

A. Kavadas: In calculating your heights from the ratio ν/ω, do you assume that you have non-deviative absorption?

C.G. Little: Yes. Actually the program does not require that, but in practice at the frequencies we are using, it is non-deviative.

A. Kavadas: When you have aurora you may have fine structure which could presumably scatter cosmic radiation.

C.G. Little: This could happen. One would pick it up on the ionosonde from below unless the absorption was such as to cut it down.

J.S. Belrose: In your explanation for exponents greater than two, you mentioned ionospheric screening. What does this mean?

C.G. Little: If at the lower cosmic noise frequencies the ionosphere is over-dense, then one would see an increased attenuation on the lower frequencies, so the exponent would be greater than 2.2.

G.C. Reid: Two groups of workers have recently reported that auroral absorption seems to show essentially no day-to-night variation in intensity; which in turn would seem to indicate that most of the absorption must be considerably higher than the level where $\nu = \omega$ on a statistical basis.

C.G. Little: Certainly our statistical distribution would suggest that the vast majority of the auroral absorption profiles that one will observe will show the absorption occurring at heights like 70 km and above. It's only the exceptional events where the absorption is predominantly at the lower heights.

M.A. Biondi: Is this analysis based on the assumption that the collision frequency is independent of energy?

C.G. Little: No. It would shift the heights by a few kilometers if we had failed to make that correction.

13.1 IONIZATION BY AURORAL ELECTRONS

I.G.POPPOFF and R.C. WHITTEN
Stanford Research Institute
Menlo Park, California

1. Introduction

For many years, observations have been made of "soft" electromagnetic radiation at low altitudes in the auroral zone. Van Allen [10] suggested that the observed radiation was bremsstrahlung generated by low energy electrons. Following this suggestion, Chapman and Little [4] and Chapman [5] prepared models of the lower ionosphere which showed that this interpretation was consistent with observations of radio absorption in the auroral zone. Meanwhile, observations were made by Anderson and Enemark [1] of the bremsstrahlung spectrum which furnished the basis for estimates of the spectrum of the generating electrons. Although the source of the electrons is still somewhat controversial, it has been shown that qualitative correlations exist with geomagnetic activity and with solar activity.

Recently, Brown and Campbell [2] reported simultaneous observations of radio noise absorption and radiation flux during a magnetic disturbance at College, Alaska, on June 25, 1961. The existence of these observed data provided the opportunity to attempt the construction of a model of the ionization produced by auroral electrons and the resulting electron and ion profiles. Although the model is not yet complete, a considerable portion of the work has been done and will be described in this paper.

2. Ionization by Electrons

The procedure followed was generally that suggested by Chamberlain [3], which is essentially to consider the incident electrons as a plane source normally incident to the atmosphere. By making such an assumption, the extensive work of Spencer [9] at the National Bureau of Standards could be utilized. The weakness of this assumption would seem to lie in the obvious fact that the electrons are not normally incident but arrive with an angle of incidence controlled by the geomagnetic field in the bombardment area. Quite obviously, a calculation that considered these factors would be beyond the resources of this study. However, calculations reported by Pedersen [8] show that the penetration altitude would not change appreciably with angle of incidence. For example, he notes that 100 keV electrons at vertical incidence would penetrate to 80 km, whereas at angles of incidence 30 and 60 off the vertical, they would penetrate to 81 and 85 km, respectively.

Brown and Campbell [2] reported an electron flux of 10^8 per cm^2 sec in the energy range greater than 50 keV at the peak of the ionization event. In making their estimate an electron spectrum of $N_e = k\,E^{-5}$ was assumed and the computing procedure reported by Anderson and Enemark [1] was utilized to obtain electron flux estimated from measured X-ray fluxes. An area of bombardment of 15,000 to 40,000 km^2 was estimated.

Using the above data, an extension of the National Bureau of Standards work, and the ARDC 1959 model atmosphere, an altitude profile of the peak ionization rate was computed. The energy range was extended to 10 keV* in the low energy and to 200 keV in the high energy end of the reported spectrum. The results are illustrated in Figure 1.

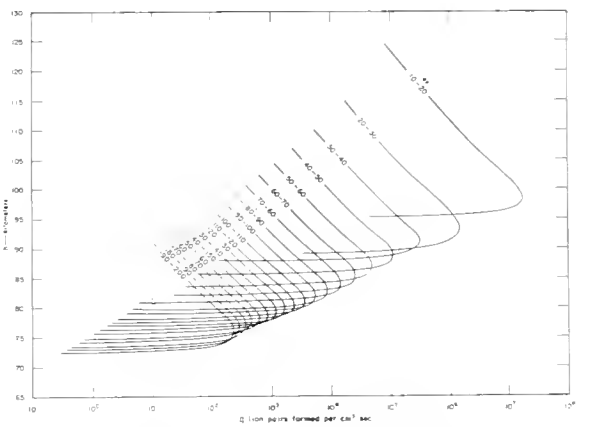

Figure 1. Ionization rate vs. altitude (per energy interval)

3. Ionization by Bremsstrahlung

Obviously (see Figure 1) the altitudes at which incident primary electrons are absorbed and bremsstrahlung is produced vary greatly with energy from about 75 to 100 km for the energy range considered. Inasmuch as the penetration altitude of the bremsstrahlung is a function of the source altitude, this should be considered in the calculation of bremsstrahlung ionization rate profiles. In these calculations, it was assumed that bremsstrahlung is produced at the altitude of peak absorption of the incident primary electrons in the energy ranges used in preparing the curves of Figure 1.

*Presentations by both Dr. Ortner and Dr. Heikkela indicate that the electron spectrum should be extended to lower energies.

Table I

INITIAL CONDITIONS AND RECOMBINATION PARAMETERS

Altitude (km)	Recombination Parameters					Initial Conditions	
	α_D [a] cm^6/sec	α_i [b] cm^6/sec	βm [c] sec^{-1}	ρ [d] sec^{-1}	γn [e] sec^{-1}	Ne cm^{-3}	λ [f]
45	2.0×10^{-6}	1.0×10^{-8}	9.7×10^{1}	0.1	4.0×10^{-3}	20	9.7×10^{2}
50		1.0×10^{-8}	2.5×10^{1}	0.1	6.0×10^{-3}	30	250
55			9.5×10^{0}		4.0×10^{-3}	50	95
60	2.0×10^{-6}		2.4×10^{0}		9.0×10^{-4}	2×10^{2}	24
65	1.5×10^{-6}		6.9×10^{-1}		4.0×10^{-4}	2.5×10^{2}	6.9
70	1.0×10^{-6}		2.0×10^{-1}		2.0×10^{-3}	4×10^{2}	2.0
75	8.0×10^{-7}		4.5×10^{-2}		4.0×10^{-3}	6×10^{2}	0.3
80	6.0×10^{-7}		9.0×10^{-3}	0.1	1.0×10^{-2}	6×10^{2}	4.5×10^{-2}
85	5.1×10^{-7}		2.0×10^{-3}	1.0	1.5×10^{-2}	1.5×10^{3}	2×10^{-3}
90	5.0×10^{-7}		4.0×10^{-3}		3.0×10^{-2}	2×10^{3}	4×10^{-3}
95	4.7×10^{-7}		6.7×10^{-3}		5.0×10^{-2}	6×10^{3}	7×10^{-3}
100	4.2×10^{-7}		2.7×10^{-3}		2.0×10^{-2}	3×10^{4}	2.7×10^{-3}
105	3.8×10^{-7}		2.2×10^{-3}		1.6×10^{-2}	10^{5}	2.2×10^{-3}
110	3.4×10^{-7}		1.3×10^{-3}		1.0×10^{-2}	2×10^{5}	1.2×10^{-3}
115	3.0×10^{-7}		5.4×10^{-4}		4.0×10^{-3}	2×10^{5}	5.4×10^{-4}
120	2.6×10^{-7}	1.0×10^{-8}	2.7×10^{-4}	1.0	2.0×10^{-3}	2×10^{5}	2.7×10^{-4}

[a] Values of α_D below 75 km assume a clustering of molecules, values of α_D above 80 km from curves of temperature dependence in Whitten and Poppoff (1963).

[b] Three-body Thompson coefficient below 45 km.

[c] Above 85 km radiative attachment to O considered dominant, below 80 km three-body attachment to O_2 considered dominant.

[d] Above 85 km detachment from O^- considered dominant, below 80 km detachment from O_2^- considered dominant.

[e] Above 65 km associative detachment considered dominant, below 60 km collisional detachment considered dominant.

[f] Above 85 km initial λ considered equal to $\beta r[O]/\rho(O^-)$
Below 80 km initial λ considered equal to $\beta[O_2]/\rho(O_2^-)$

where

βr = radiative attachment coefficient for O
$[O]$ = concentration of atomic oxygen
β = three-body attachment for $O_2 = K[O_2]$ (see Sec. III A3)
$[O_2]$ = concentration of molecular oxygen
$\rho(O^-)$ = photo detachment rate for O^-
$\rho(O_2^-)$ = photo detachment rate for O_2^-

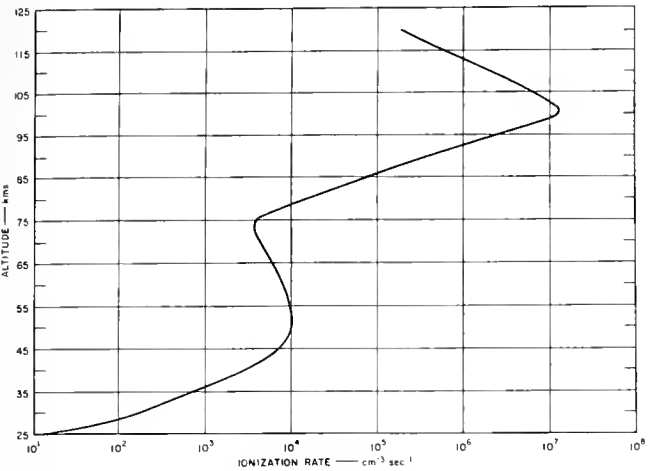

Figure 2. Peak ionization rate profile - electron plus bremsstrahlung.

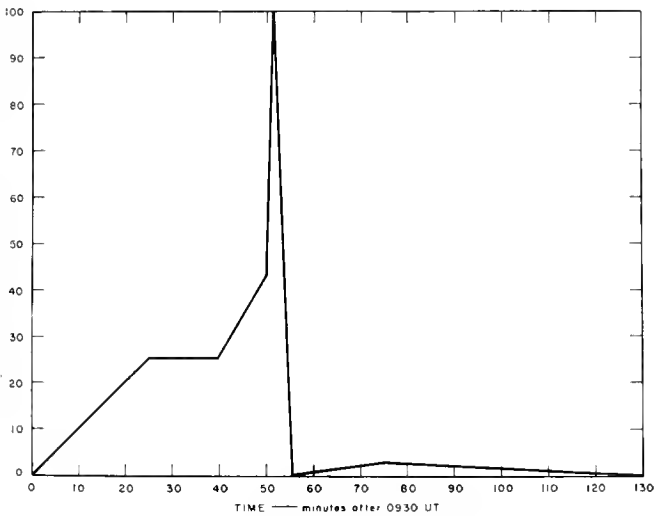

Figure 3. Temporal variation of ionizing pulse.

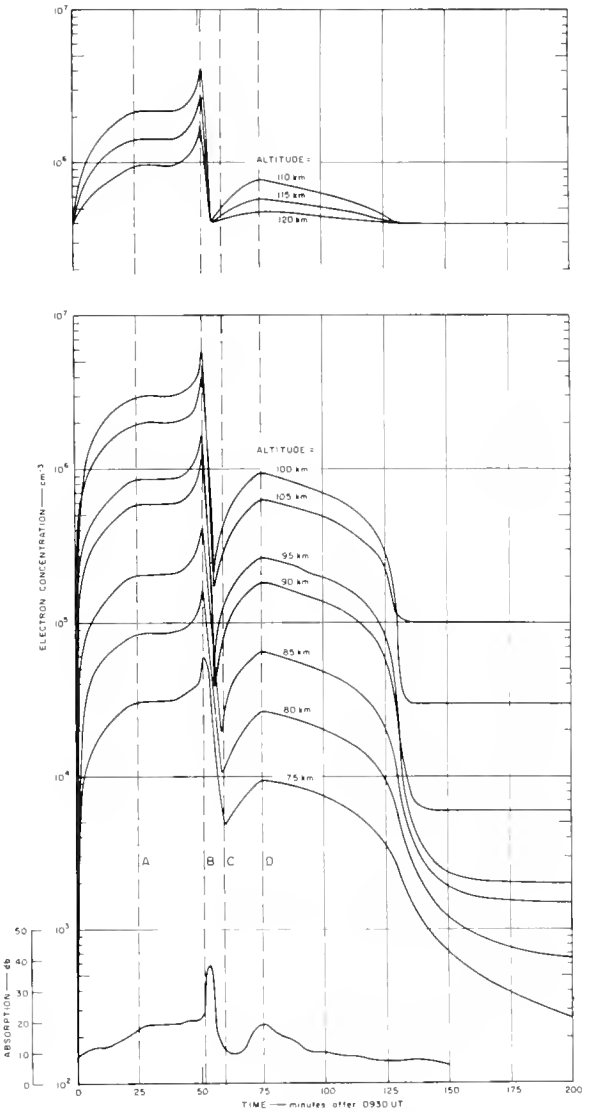

Figure 4. Calculated temporal variations of electron densities and observed cosmic noise absorption.

Profiles of ionization produced by bremsstrahlung generated by electrons in each of the several electron energy ranges were computed. The calculated ionization rates were then summed for each altitude and a profile was prepared of ionization rates produced by bremsstrahlung generated by the entire spectrum of electrons.

Bremsstrahlung spectra were computed by following the treatment described by Anderson and Enemark [1]. The number of photons in the energy interval E_a to E_{a+1}, produced by N electrons of energy E, in a material having a radiation length l_R, is found to be

$$n(E_a;E_{a+1}) = \frac{N(E)}{2000\ l_R}\left[E \ln \frac{E_{a+1}}{E_a} - (E_{a+1} - E_a)\right]$$

The number of photons produced in each of a series of energy intervals from 1-2 keV up to the energy interval of the primary electrons was then computed for each electron energy interval used in Figure 1.

The bremsstrahlung flux at the distance R from a large isotropic radiation can be computed as follows: The contribution from each unit increment is

$$dI = \frac{2\Pi i_0 r dr}{B^2} A\ B$$

where i_0 is the number of photons emitted per unit source area and r is the distance from the center of the source to the unit source. A and B are attenuation and scattering terms respectively.

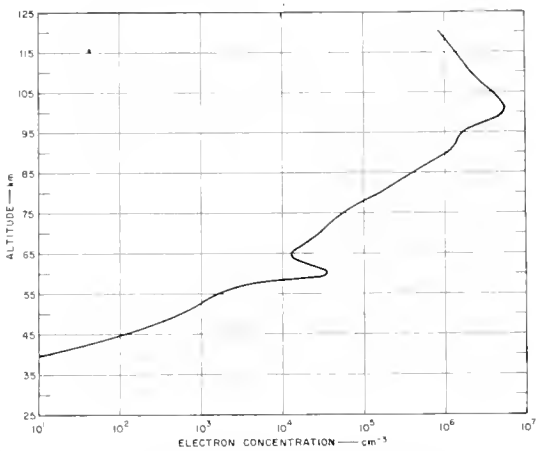

Figure 5. Electron concentration profile at peak ionization (51.6 min).

The total flux at altitude h produced by bremsstrahlung photons of energy E_p emitted from a source at altitude h + d is

$$I(h,E_p) = \int_o^{r>>R} dI$$

The ionization produced at h by the absorption of photons with energy E_p is

$$q(h,E_p) = I\ E_p\ \mu_a \frac{\rho}{\rho_o} \left(\frac{1000}{35}\right) \text{ ion pair/cm}^3\text{sec}$$

where μ_a is the linear absorption coefficient, ρ is the atmospheric density at h, and ρ_o is the density at NTP conditions.

The total ionization rate at an altitude h is

$$q_h = \Sigma\, q(H,\ E_p)$$

where q is summed over the photon energy spectrum for the bremsstrahlung produced by primary electrons, in a particular energy interval E_e, absorbed at an altitude h + d; and then summed over the entire spectrum of primary electrons, absorbed over the entire altitude range of interest. Analysis of the calculated profiles indicates that the lowest energy electron group (10-20 keV) dominates the bremmstrahlung ionization effect.

The combined electron-bremsstrahlung ionization rate profile for peak primary electron flux is presented in Figure 2. The temporal variation of the ionization rate q presented in Figure 3 is a smoothed version of the bremsstrahlung curve recorded by Brown and Campbell [2].

4. Electron and Ion Densities

Knowing the ionization rate, q, as a function of time and altitude, the free electron concentration, N_e, and the ratio of negative ions to electrons, λ, can be computed by utilizing the following well-known continuity equations Mitra, [7]; Whitten and Poppoff, [11])

$$\frac{dN_e}{dt} = \frac{q(t)}{1+\lambda} - (a_D + \lambda a_i)N_e^2 - \frac{N_e}{1+\lambda}\frac{d\lambda}{dt}$$

$$\frac{1}{1+\lambda}\frac{d\lambda}{dt} = \beta m - \lambda[\rho + \gamma n + N_e(a_i - a_D) - \frac{q(t)}{N_e(1+\lambda)}]$$

where a_D is the dissociative ion-electron recombination coefficient, a_i is the ion-ion mutual neutralization coefficient, β is the electron-oxygen attachment coefficient, ρ is the negative-ion photodetachment rate, γ is the negative-ion collisional detachment coefficient, m is the concentration of the attaching species (O_2 or O), and n is the concentration of the species causing collisional type detachment.

Calculations of temporal variations in electron concentration were made for the altitude range 75 to 120 km and are presented in Figure 4. Calculations of an electron density profile was made for the peak ionization rate (51.6 minutes) for the range 40 to 120 km (Figure 5). The coefficients for recombination, neutralization, attachment and detachment were taken from Whitten and Poppoff [12]. The initial conditions for λ were taken from Whitten and Poppoff, [12]. The coefficients used for altitudes below 80 km become increasingly more speculative as the altitude decreases. The assumptions made in selecting coefficients for the lower altitude regions are noted in Table I.

Although the observations by Brown and Campbell [2] were made in the vicinity of local midnight, calculations indicate that the atmosphere was illuminated throughout the observing period above at least 3 km. Therefore, there should be no question about the occurrence of photodetachment above the ozone layer.

Comparisons of the temporal-variation curves of electron densities (Figure 4) and the temporal-variation of cosmic noise absorption is dependent on free electron densities, the similarity between the shape of the electron concentration curves and the shape of the cosmic noise curve indicates that the auroral ionization model is at least partially valid. It is interesting to note that the decay of the electron density curves (after the two ionization maxima at 51.6 and 75 mins) resemble the decay of the cosmic noise absorption curve more closely as the altitude decreases. The results are not yet sufficiently complete to determine the altitude range that is most effective in producing this particular cosmic noise record. However, the data do seem to indicate that the lower altitude electron densities are important.

Inasmuch as the collision frequency increases rapidly with decreasing altitude and the electron density in the range 75 km to 60 km decreases slowly with altitude (and in fact increases to a maximum point at 60 km according to Figure 5) it seems reasonable to expect that the electrons in this region are very important in producing cosmic noise absorption.

Ionization in this region is caused by bremsstrahlung rather than primary electrons. (Compare Figures 1 and 2.) Therefore, if the apparently important influence of lower altitude electron concentrations is confirmed by future results, the importance of bremsstrahlung will also be demonstrated.

References

[1] Anderson, K.A. and D.C. Enemark. Balloon observations in the auroral zone II. J. Geophys. Res. 65, 3521 (1960).

[2] Brown, R.R. and W.H. Campbell. An auroral zone electron precipitation event and its relationship to a magnetic bay. J. Geophys. Res. 67, 1357 (1962).

[3] Chamberlain, Joseph W. Physics of the Aurora and Airglow. Academic Press. New York and London, 1961.

[4] Chapman, Sydney and C. Gordon Little. The non-deviative absorption of high frequency radio waves in auroral latitudes. J.Atmos. Terr. Phys. 10, 20 (1957).

[5] Chapman, S. Disturbances in the lower auroral ionosphere. J. Atmos. Terr. Phys. 15, 29 (1959).

[6] Davis, L.R., O.E. Berg and L.H. Meredith. Direct measurement of particle fluxes in and near auroras. Space Research. North-Holland Publishing Co. Amsterdam, 1960. p. 721.

[7] Mitra, S.K. The Upper Atmosphere. 2nd ed. The Asiatic Society. Calcutta, 1952.

[8] Pedersen, Arne. D-layers in the subauroral zone. J. Geophys. Res. 67, 2685 (1962).

[9] Spencer, L.V. Energy dissipation by fast electrons. National Bureau of Standards Monograph 1. Sept. 10, 1959.

[10] Van Allen, J.A. Interpretation of soft radiation observed at high altitudes in northern latitudes. Phys. Rev. 99, 608 (1955).

[11] Whitten, R.C. and I.G. Poppoff. A model of solar-flare-induced ionization in the D-region. J. Geophys. Res. 66, 2779 (1961); (Corrigendum) 67, 2986 (1962).

[12] Whitten, R.C. and I.G. Poppoff. Ion kinetics in the lower ionosphere, submitted for publication.

[13] Winckler, J.R., P.D. Bhavsar and K.A. Anderson. A study of the precipitation of energetic electrons from the geomagnetic field during magnetic storms. J. Geophys. Res. 67, 3717 (1962).

DISCUSSION

H. Dolezalek: A number of observations indicate an influence of the aurora on atmospheric-electric parameters close to ground. If we assume following Whipple that conductivity in the region above 35 km, in general, is reduced by dust, the enhanced ionization by auroral bremsstrahlung may change the columnar resistance and thus the air-earth current density to be measured at ground. This explanation of the observation is, at present, no more than a hypothesis. However, if proven, it establishes another tool for this research. The phenomenon is studied, at present, by Dr. Gassmann of AFCRL and ourselves.

J. Ortner: You assumed vertical incidence of the electrons when you calculated the ionization rates. Our data and Dr. Ore's group in Canada have shown that electrons come from all directions, and not only vertical incidence should be considered.

A. Pedersen: Is this true also for high energy electrons of some 200 keV?

W.J. Heikkila: The observations on our rockets by McDermott and Rose show them travelling more or less perpendicular to the magnetic field lines, like trapped particles near the mirror points, so that they were at a considerable angle to the vertical.

I.G. Poppoff: It is the low energy electrons which seem to be most important. They are very quickly scattered in all directions, and this has been taken into account in Spencer's work, so the error may not be great.

G.C. Reid: In assuming a power law spectrum you have to cut it off somewhere, or you get to infinite numbers at zero energy. Where was this cutoff?

I.G. Poppoff: Our calculations went down to 10 keV.

G.C. Reid: What is the physical explanation of the bump you found in the electron density profile about 60 km?

I.G. Poppoff: Only that there were two profiles in essence that connected in such a way that you get the bump.

13.2 ON THE NEGATIVE ION COMPOSITION OF THE D-REGION

G. C. REID
Central Radio Propagation Laboratory
National Bureau of Standards
Boulder, Colorado

It has been realized for many years that atmospheric processes involving negative ions must play an important role in the lower ionosphere, due to the high collision frequencies of free electrons, and the consequent high probability of attachment. Before one can arrive at any quantitative estimate of D-region parameters, however, it is necessary to know the nature of the negative ions involved, and to have some idea of their relative importance.

In making a first guess at the negative ion composition, it is natural to look first at the major neutral constituents. Of these, nitrogen does not form a stable negative ion, and can be immediately ruled out. Both molecular and atomic oxygen, however, do form negative ions, and as a consequence it has been common in the past to assume that the dominant negative ion species throughout most of the D-region is O_2^-, with a contribution from O^- in the upper regions where the dissociation of oxygen becomes appreciable. The tendency to make this assumption has been aggravated by the fact that quantitative calculations are impossible on any other basis, since so little is known about other negative ion species. The purpose of this paper is to point out that the assumption of the dominance of O_2^- is apparently at variance with certain observational features, and to make an urgent plea for direct in situ measurements of negative ion composition.

The role of negative ions is shown most dramatically in the phenomenon of polar-cap absorption (PCA) of radio waves, caused by the incidence of energetic solar protons. The electron density in the D-region during one of these events undergoes a change by a factor of about 5 to 1 in going from daytime to nighttime conditions, and it is now generally accepted that the cause of this change lies in the occurrence of photodetachment during daytime. In examining the details of the change, however, we find two important points which appear to be inconsistent with the assumption that the dominant negative ion species is O_2^-. The first of these concerns the nighttime electron density. If photodetachment were the only mechanism capable of removing electrons from negative ions, we should expect the ionization to disappear almost completely at night, since free electrons would become attached very rapidly, and would then remain attached until sunrise. As mentioned above, however, the steady-state nighttime electron density is of the order of one-fifth of the daytime value. This large nighttime electron density is usually explained by invoking collisional detachment, whereby an atom or molecule with sufficient thermal kinetic energy can remove the extra electron from a negative ion by collision. From PCA data, Bailey and Branscomb [1] have estimated that a collisional detachment coefficient of about 2×10^{-17} cm^3 sec^{-1} is required to explain the observed day-to-night ratio of absorption, a value which is fairly consistent with the value of 0.15 ev for the electron affinity of O_2^- found from the laboratory photodetachment measurements of Smith, Burch and Branscomb [7]. More recently, however, the collisional detachment coefficient of O_2^- has been measured in the laboratory by Phelps and Pack [5], and found to be about 4×10^{-20} cm^3 sec^{-1} at D-region temperatures. If the collisional detachment rate were as low as this in the D-region, the nighttime electron density would be virtually nonexistent. The electron affinity corresponding to this collisional detachment rate is about 0.46 ev, or three times that found by Smith, Burch and Branscomb [7]. There is no reason to doubt the validity of Phelps' and Peck's result, and if we wish to retain O_2^- as the dominant negative ion, we must look to some process other than collisional detachment to maintain the high nighttime electron densities.

The second piece of evidence comes from the detailed behavior of PCA during sunrise and sunset. This point has been discussed in some detail by Reid [6], and will merely be briefly summarized here. The essential point is that all PCA events seem to indicate that the shadow marking the transition from daytime to nighttime conditions in the absorbing region is that of the top of the ozone layer rather than that of the solid earth. The implication is that the photodetaching radiation is not in the visible region of the spectrum, but is largely ultraviolet, with wavelengths less than about 3000 A. While there is considerable uncertainty concerning the electron affinity of O_2^-, it is certainly less than 1 ev, corresponding to a wavelength of 12400 A, and it is extremely unlikely that the visible spectrum would be incapable of producing photodetachment. A wavelength of 3000 A corresponds to a quantum energy of about 4 ev, but the affinity of the ion could be somewhat less than this in view of the rather slow rise of the photodetachment cross-section from the threshold which is expected for most molecular ions.

Two possible candidates for the role of dominant negative ion have appeared, but unfortunately our knowledge of their properties is meager in the extreme. The first is NO_2^-, whose possible importance in the atmosphere was first pointed out by Branscomb [2]. This

ion appears to form very readily in laboratory experiments, and Johnson, Heppner, Holmes and Meadows [4] found it to be the dominant negative ion during rocket-borne mass-spectrometer measurements in the E-region. There seems to be little doubt that NO_2^- has an affinity of the required order of magnitude. As a result of experiments in which NO_2^- was formed by charge transfer, Curran [3] has reported an affinity greater than about 3.8 ev. A somewhat lower value is indicated in recent measurements made by Smith (private communication), who found an appreciable amount of photodetachment occurring at the blue end of the visible spectrum.

The second candidate is the negative ion of ozone, O_3^-, and here our knowledge is even more scanty. Thermochemical evidence quoted by Branscomb [2] indicate that the affinity may be in the neighborhood of 3 ev, which may well be sufficient to account for the twilight PCA measurements, but no direct laboratory measurements have as yet been carried out.

We are thus confronted with a paradoxical situation in the interpretation of PCA observations. The twilight observations indicate that we should look to a negative ion whose affinity is considerably higher than that of O_2^- for an explanation. The high nighttime electron densities, on the other hand, suggest that the affinity of the ion must be lower than that of O_2^- if we are to explain the presence of the electrons by collisional detachment, as has frequently been done in the past. There are in fact other ways of explaining the nighttime absorption, and these must be given serious consideration. For instance, the effect of freshly-released 'hot' electrons has not yet been considered quantitatively. Such electrons will have a very high collision frequency, but a low probability of attachment, and may produce considerably more absorption than their number might indicate. Also, Whitten and Poppoff [8] have pointed out the possible importance of associative detachment reactions of the type

$$O_2^- + O \rightarrow O_3 + e.$$

The rates of these reactions are not known, but may well be high enough to explain the nighttime electron densities. Since they depend on the presence of atomic oxygen, however, their importance is likely to be confined to the upper part of the absorbing region.

In conclusion, it is obvious that our knowledge of the negative ion composition of the D-region is in a very primitive state, and it appears that the best approach to a solution of this problem lies in the use of carefully designed rocket mass-spectrometer techniques. It is important that experiments of this type be carried out at a variety of latitudes and times of day, since the existence of latitudinal and diurnal variations in the negative ion composition might not be altogether unexpected. Until such measurements have been carried out, there would appear to be little further point in attempting to calculate such parameters as electron density in the D-region, since the results would be in serious doubt.

References

[1] Bailey, D.K. and L.M. Branscomb: Bull. Am. Phys. Soc. (II) 5, 123 (1960).

[2] Branscomb, L.M.: Adv. in Electronics and Electron Physics 9, 43 (1957).

[3] Curran, R.K.: Phys. Rev. 125, 910 (1962).

[4] Johnson, C.Y., J.P. Heppner, J.C. Holmes and E.B. Meadows: IGY Rocket Series 1, 123 (1958).

[5] Phelps, A.V. and J.L. Pack: Phys. Rev. Letters 6, 111 (1961).

[6] Reid, G.C.: J. Geophys. Res. 66, 4071 (1961).

[7] Smith, S.J., D.S. Burch and L.M. Branscomb: Ann. de Geophys. 14, 225 (1958).

[8] Whitten, R.C. and I.G. Poppoff: J. Geophys. Res. 67, 1183 (1962).

DISCUSSION

A.V.Phelps: To add to the confusion regarding the possible identity of the negative ion, I would suggest the candidate, CO_4^-. We have measured the lifetime of O_2^- in mixtures of O_2 and CO_2, and find that at densities corresponding to, say, 20 km, the lifetime is less than something like 100μsec. It is risky to extrapolate this to lower densities and higher altitudes, but if one were to go to 60 km and assume a simple two-body effective stabilization process, then you would end up with lifetimes of O_2^- of about 1 sec.

There is also another candidate. When we say we have measured the detachment rate, we are talking about what we firmly believe are thermal populations of excited states of O_2. Now there have been considerable evidences in various parts of the ionosphere of excited electronic states of oxygen. These could enhance detachment rates considerably.

G.C. Reid: I was not aware of much evidence for the existence of these states, but if they did exist in large numbers they could change the picture completely.

M.A. Biondi: Other negative ions will not help in explaining the anomalies of the PCA event in the sense that the two ions you cited as candidates (O_3^- and O_2^-) would make the detachment rates smaller.

G.C. Reid: Yes, these two effects go against each other.

K.W.Champion: Firstly, I do not think much CO_2 or carbon molecules are likely in the D-region, although perhaps with the material put up by missiles, there may be in time. Secondly, the daytime atomic oxygen profile below 90 km falls off by a factor of two fairly sharply, then seems to remain relatively constant down to about 60-70 km. Of course at nighttime, the lower edge will decay, but you may possibly have enough left to explain the associative detachment process.

J. Ortner: Dr. Hultquist and myself studied a large number of polar cap events, and found a height of 48.3 km instead of 60 km as the boundary when the effect starts to be recognized. We thought about the ozone layer, and we thought that it couldn't help since the affinity of the electrons to O_2^- is so small (0.5 ev). Hultquist tried to find some explanation by calculating values of λ which were quite different from those given by Nicolet and others. Rocket measurements are needed to measure λ very low down.

13.3 ION KINETICS IN THE LOWER IONOSPHERE

R. C. WHITTEN and I. G. POPPOFF
Stanford Research Institute
Menlo Park, California

1. Introduction

In view of Dr. Reid's excellent discussion of negative ions, my intended one would be redundant and so I shall confine my talk to recombination and to charge rearrangement (charge transfer and ion-atom inter-change) reactions. In these areas numerous laboratory experiments have been carried out within the last few years; several ionospheric measurements have also been employed to obtain useful information on rate constants.

Unfortunately, interpretation of these experimental results is extremely difficult; values of the rate constants reported for various reactions sometimes differ by as much as an order of magnitude, depending upon the experimental approach and method of analysis. Further ambiguity arises from lack of knowledge of the importance of metastable excited states of ions and neutral particles, both in the laboratory experiment and in the ionosphere. If the state of the laboratory system is markedly different in so far as metastable states are concerned, one is not justified in blindly applying to the ionosphere the experimentally determined rate constants.

Although this paper does not report any new aeronomic measurements, it does employ the published results of previous measurements to obtain more information on the rates of some important ionic processes in the lower ionosphere. This information in turn can be applied to interpret the results of ionospheric measurements.

1. Dissociative Recombination

Numerous laboratory measurements of the dissociative recombination coefficients of N_2^+ and O_2^+ have been carried out (see Table I) and from these it is possible to derive an approximate power law for the temperature variation of these parameters:

$$\alpha_D(N_2^+) \approx 5 \times 10^{-5}\ T^{-3/4}\ cm^3\ sec^{-1}$$

$$\alpha_D(O_2^+) \approx 9 \times 10^{-5}\ T^{-1}\ cm^3\ sec^{-1}$$

The available information on the dissociative recombination coefficient of NO^+ is very meager. It includes several laboratory measurements (see Table I) and a value obtained by Bowhill [5] ($\alpha_D = 6 \times 10^{-9}$ cm^3 sec^{-1}) from analysis of the diurnal variation and variation during a solar eclipse of E-layer electron density by means of a two-ion model. Although these data yield the temperature law

$$\alpha_D(NO^+) \approx 3 \times 10^{-4} T^{-3/2}\ cm^3\ sec^{-1},$$

they should be viewed with caution. In fact, the very use of a power law is open to question (see, e.g. Bates and Dalgarno [1]).

Several other values of dissociative recombination coeffiecients have been obtained from riometer data. The authors (Whitten and Poppoff [26]) computed an effective recombination coefficient ($\alpha_D \approx 1 \times 10^{-7}$ cm^{3}sec^{-1}) using both riometer data and solar flare X-ray data supplied by Chubb and Kreplin of NRL and which is roughly equal to that suggested by L.G. Smith yesterday. LeLevier [16] recently computed some limits on α_D from riometer data obtained during the 1962 nuclear tests (3×10^{-7} cm^{3}sec^{-1}) which are larger than our value. We do not know the reason for the difference; it may be due to experimental error or it may be the result of an ion-atom interchange process (sec (5) in section II).

From these results we can construct a model of the daytime recombination coefficient for the altitude interval 80 to 140 km, assuming that ion ion recombination is not important above 80 km. The model, shown in Figure 1, is based on middle latitude temperature profiles taken from the U.S. Standard Atmosphere [24] and on the relative concentrations of ionic species as reported by Taylor and Brinton [23]. The profiles A_1 and A_2, which merge at about 110 km altitude, correspond to the normal and disturbed D-regions, * respectively. Mitra's [18] noontime quiescent model for middle latitudes is also presented.

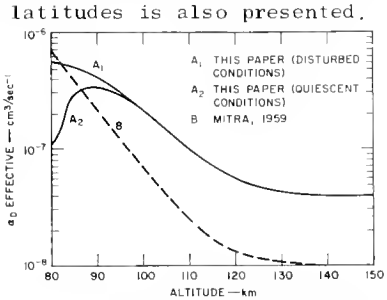

Figure 1. Models of the Daytime Ionospheric Electron Recombination Coefficient above 80 km Altitude.

*It is assumed that the dominant quiescent D-region ion above 80 km is NO^+ and that the disturbed D-region ions are in general a mixture of NO^+ and O_2^+; the first assumption may not always be justified [19].

TABLE I

LABORATORY MEASUREMENTS OF DISSOCIATIVE RECOMBINATION COEFFICIENTS $\alpha_D(cm^3\ sec^{-1})$

Investigators	$\alpha_D(N_2^+)$	$\alpha_D(O_2^+)$	$\alpha_D(NO^+)$
Kasner, Rogers, and Biondi [14]	[a] $(5.9 \pm 1) \times 10^{-7}$	[a] $(3.8 \pm 1) \times 10^{-7}$	
	[b] 2×10^{-6}		
Biondi [3]	$(2.8 \pm 0.5) \times 10^{-7}$	$(1.7 \pm 1) \times 10^{-7}$	
Holt [13]		3×10^{-7}	
Faire and Champion [9]	4.0×10^{-7}		
Biondi and Brown [4]	11.4×10^{-6}		
Faire, Fundingsland, Aden, and Champion [8]	1.4×10^{-6}		
Bialecke and Dougal [2]	[c] 6.7×10^{-6}		
	[d] 8.7×10^{-7}		
Sayers [20]	[e] 1.1×10^{-7}	[f] 4×10^{-8}	
Lin [17]			[g] 10^{-9}
Gunton and Inn [12]			[h] 1.3×10^{-6}
Doering and Mahan			$(3^{+17}_{-2}) \times 10^{-7}$

a for pressures $\lesssim$ 0.01 mm Hg; temp ~ 300°K

b for pressures $\gtrsim$ 0.1 mm Hg; temp ~ 300°K

c at 92°K

d at 300°K

e at 3200°K

f at 2500°K

g at 5000°K

h for pressures > 0.1 mm Hg; temp ~ 300°K

2. Charge Transfer and Ion-Atom Interchange

Charge transfer and ion-atom interchange reactions are very important in controlling ionospheric relaxation rates by "shuffling" the identities of the ions as rapidly as they can be created. The nature of the ionic species in turn has an important bearing on the rate of electron recombination and hence on the electron density profile. The following reactions are probably the dominant ones in the shuffling process

$$O^+ + O_2 \longrightarrow O + O_2^+ \quad (1)$$

$$N_2^+ + O \longrightarrow N_2^+ + O^+ \quad (2)$$

$$N_2^+ + O_2 \longrightarrow N_2 + O_2^+ \quad (3)$$

$$O^+ + N_2 \longrightarrow N + NO^+ \quad (4)$$

$$O_2^+ + N_2 \longrightarrow NO + NO^+ \quad (5)$$

Reaction (5) involves the breaking and reforming of double and triple bonds and hence is

expected to have a large activation energy. In fact, some Russian investigators (see Talrose et al. [22] have found an activation energy of 7 kcal/mole for the somewhat similar process

$$N_2^+ + O_2 \longrightarrow NO + NO^+ \qquad (6)$$

If we further assume that the transmission coefficient is unity for collisions in which the potential barrier is surmounted and that the reaction collision frequency per O_2 molecule is $\sim 10^{-9}$ (Gioumousis and Stevenson, 1958), we obtain an upper limit for the reaction rate constant of about 10^{-16} cm^3 sec^{-1} at a temperature of 200°K. If $k_5 > 10^{-19}$ cm^3 sec^{-1}, reaction (5) cannot be neglected in the D-layer.

It is possible to make estimates of the rate constants characteristic of reactions (1) to (4) if one knows reasonably well the neutral particle densities, the ion production rates (e.g. as determined by Watanabe and Hinteregger [25]), the dissociative recombination rates, electron densities, and the relative ion concentration (e.g. see Taylor and Brinton [23]). These may be obtained by inserting in the equilibrium kinetic equations the values of the known parameters at some given altitude (we selected 150 km) and solving for the rate constants. We obtained

$$k_1 \sim 2 \times 10^{-11} \text{ cm}^3 \text{ sec}^{-1}$$
$$k_2 \sim 2 \times 10^{-11} \text{ cm}^3 \text{ sec}^{-1}$$
$$k_3 \sim 2 \times 10^{-10} \text{ cm}^3 \text{ sec}^{-1}$$
$$k_4 \sim 6 \times 10^{-13} \text{ cm}^3 \text{ sec}^{-1}$$

Of these, k_1, k_3, and k_4 have recently been measured in the laboratory; the results are

k_1	Dickinson and Sayers [21]	2.5×10^{-11} cm^3 sec^{-1}
	Sayers [21]	1.6×10^{-11} cm^3 sec^{-1}
	Langstroth and Hasted [15]	1.8×10^{-12} cm^3 sec^{-1}
	Fite, Rutherford, Snow, and Van Lint [10]	(1 to 15) $\times 10^{-11}$ cm^3 sec^{-1}
k_3	Fite, Rutherford, Snow, and Van Lint [10]	2×10^{-10} cm^3 sec^{-1}
k_4	Talrose, Markin, and Larin [22]	$\leq 6.7 \times 10^{-12}$ cm^3 sec^{-1}
	Sayers [21]	2.5×10^{-11} cm^3 sec^{-1}
	Langstroth and Hasted	4.7×10^{-12} cm^3 sec^{-1}

The agreement between our estimates of k_1 and k_3 is quite good--in fact the agreement is perhaps misleading. The lack of agreement between our estimate of k_4 and the laboratory measurements is unresolved.

The concentrations of N_2^+, O_2^+, O^+, and NO^+ at various altitudes have been computed using our estimated rate constants and by means of the laboratory measurements listed above. They are shown in Figures 2 and 3, respectively.

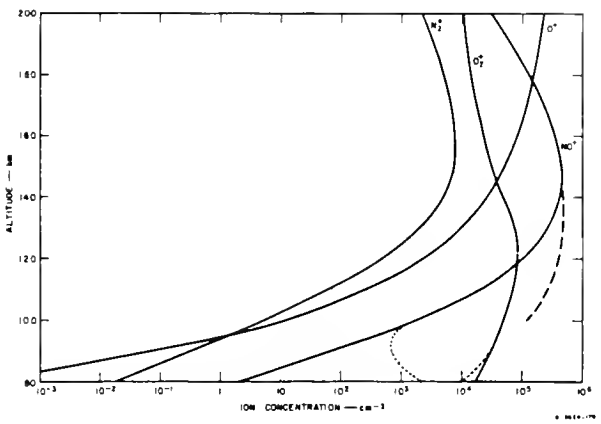

Figure 2. Equilibrium ion concentration above 80 km. These concentrations were computed using the values of the rate constants k_1, k_2, k_3, and k_7 obtained from the mass spectrometric observations. The dashed line represents the observed concentration of NO^+. The dotted lines represent the equilibrium concentrations of NO^+ and O_2^+ if $k_\Phi = 10^{-19}$ cm^3 sec^{-1}.

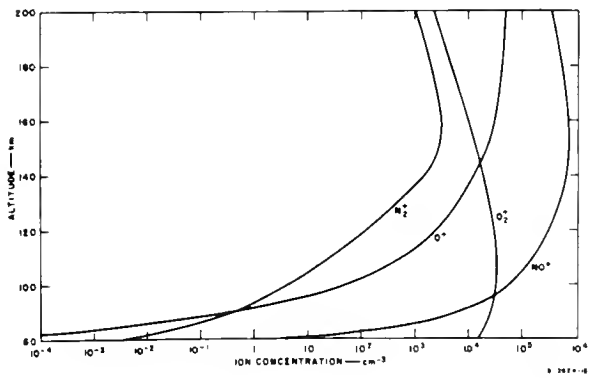

Figure 3. Equilibrium ion concentration above 80 km. These concentrations were computed using the mean values of recent laboratory measurements of k_1, k_3, and k_7. Our values of k_2 and $k_\Phi = 0$ were used in the computations.

13.3 WHITTEN, POPPOFF

The broken line in Figure 2 was obtained from the observed relative ion concentration of NO^+; the dotted lines show the equilibrium concentrations of NO^+ and O_2^+ if $k_5 = 10^{-19}$ cm^3 sec^{-1}. Agreement between measured relative ion densities and the profiles shown in Figures 2 and 3 are only qualitative, I think that Dr. Holmes implied yesterday that he encountered the same difficulty and that the discrepancies may be due to temperature dependence of the rate constants; we agree. We do not have sufficient information at the present time to resolve the difficulty, however.

References

[1] Bates, D. R. and A. Dalgarno, Electronic recombination, in Atomic and Molecular Processes, Ed. by D. R. Bates, Academic Press, New York, 1962.

[2] Bialecke, E. P. and A. A. Dougal, Pressure and temperature variation of the electron-ion recombination in nitrogen, J. Geophys. Res. 63, 539 (1958).

[3] Biondi, M. A., Advances in Electronics 18, Academic Press, New York, 1963.

[4] Biondi, M. A. and S. C. Brown, Measurement of electron-ion recombination, Phys. Rev. 76, 1697 (1949).

[5] Bowhill, S. A., The effective recombination coefficient of an ionosphere containing a mixture of ions, J. Atmos. Terr. Phys. 20, 19 (1961).

[6] Dickinson, P. H. G. and J. Sayers, Ion charge exchange reactions in oxygen afterglows, Proc. Phys. Soc. 76, 137 (1960).

[7] Doering, J. P. and B. H. Mahan, Photoionization of nitric oxide, J. Chem. Phys. 36, 669 (1962).

[8] Faire, A. C., O. T. Fundingsland, A. L. Aden, and K. S. W. Champion, Electron recombination coefficient measurement in nitrogen at low pressure, J. Appl. Phys. 29, 928 (1958).

[9] Faire, A. C. and K. S. W. Champion, Measurement of dissociative recombination and diffusion in nitrogen at low pressures, Phys. Rev. 113, 1 (1959).

[10] Fite, W. L., J. A. Rutherford, W. R. Snow, and V. A. J. Van Lint, Ion-neutral collisions in afterglow, Discussions Faraday Soc. 33, 264 (1962).

[11] Gioumousis, G. and D. P. Stevenson, Reactions of gaseous molecule ions with gaseous molecules. V. Theory, J. Chem. Phys. 29, 294 (1958).

[12] Gunton, R. C. and E. C. Y. Inn, Rates of electron removal by recombination, attachment and ambipolar diffusion in nitric oxide plasmas, J. Chem. Phys. 35, 1896 (L) (1961).

[13] Holt, E. H., Electron loss processes in the oxygen afterglow, Bull. Amer. Phys. Soc. 4, 112 (1959).

[14] Kasner, W. H., W. A. Rogers, and M. A. Biondi, Electron-ion recombination coefficients in nitrogen and in oxygen, Phys. Rev. Lett. 7, 321 (1961).

[15] Langstroth, G. F. O. and J. B. Hasted, General discussion, Discussions Faraday Soc. 33, 298 (1962).

[16] Le Levier, R. E., J. Geophys. Res. 68 (1963).

[17] Lin, S. C., Avco Research Note No. 210 (1960) (Unpublished).

[18] Mitra, A. P., Time and height variations in the daytime processes in the ionosphere. I. A noontime model of the ionosphere loss coefficient from 60 to 600 km over middle latitudes, J. Geophys. Res. 64, 733 (1959).

[19] Poppoff, I. G. and R. C. Whitten, D-region ionization by solar x-rays, J. Geophys, Res. 67, 2986 (1962).

[20] Sayers, J., Recent laboratory studies of recombination cross sections, in Solar Eclipses and the Ionosphere, Ed. by W. J. G. Beynon and G. M. Brown, Pergamon Press, London, New York, 1956.

[21] Sayers, J., Ionic recombination, in Atomic and Molecular Processes, Ed. by D. R. Bates, Academic Press, New York, 1962.

[22] Talrose, V. L., M. I. Markin and I. K. Larin, The reaction $O^+ + N_2 \rightarrow NO^+ + N$, Discussions Faraday Soc. 33, 257 (1962).

[23] Taylor, H. A. and H. C. Brinton, Atmospheric ion composition measured above Wallops Island, Virginia, J. Geophys. Res. 66, 2587 (1961).

[24] U. S. Standard Atmosphere, Government Printing Office, Washington, 1962.

[25] Watanabe, K. and H. E. Hinteregger, Photoionization rates in the E and F regions, J. Geophys. Res. 67, 999 (1962).

[26] Whitten, R. C. and I. G. Poppoff, A model of Solar flare-induced ionization in the D-region, J. Geophys. Res. 66, 2776 (1961), Corrigendum 67 (1962).

DISCUSSION

M. A. Biondi: In the table from which you deduced a temperature dependence from the mass spectrometer studies of the afterglow, the values from the various workers refer to different ions. One really ought not to get temperature dependencies from work by Sayers which refers to a different ion than our work. For example, some of the work refers to N_4^+ ions, in all probability, rather than N_2^+ ions, and other of the work refers to O_3^+ ions rather than O_2^+.

R. C. Whitten: I tried to take these out by taking the high values for the rate constants. In any event, the temperature law should certainly not be taken too seriously.

J. C. Holmes: I tried to make some similar calculations using our new data; I was able to put limits on k_2 and k_4 at certain altitudes, but found that reactions k_1 and k_3 swap off, and I could not put values on them.

R. C. Whitten: I do not recall any lack of information. I picked 150 km because O^+ was just beginning to come in, and there was a measurement on it: the ion production rates were fairly well known, and the electron densities. Below 150 km there was nothing on O^+. I found that I certainly could not trust these values to better than an order of magnitude (except for k_4, which looked like it should be about half an order of magnitude).

14.1 CONCLUDING STATEMENT ON ELECTRON AND ION DENSITY

L. G. SMITH
Geophysics Corporation of America
Bedford, Massachusetts

Although this conference is aimed primarily at instrumentation and techniques, the final test is the results obtained, and we have seen in this conference an impressive number of workers actually measuring or claiming to measure electron and ion density in the D-region. My impression of the propagation techniques is that there is even more complexity in the theory than I had earlier appreciated; however, this is not a fundamental limitation. We saw impressive examples of the use of the partial reflection technique given by Dr. Belrose. It should be possible to observe D-region electron density profiles on an almost continuous basis by this method.

Probes, both DC and RF have been described in many variations. The RF probes will be covered by Dr. Pfister, and I shall confine my remarks to the DC probes. The term is taken to include linear probes, with or without grids. The use of the probes in the region above about 85 km is on a relatively sound theoretical basis. Free molecular flow is assumed, and the presence of negative ions neglected. The shape of the electrode is not critical and is determined in some cases by mere convenience, as in the case of the nose-tip electrode or the flush mounted disc electrode, or in others by good scientific reasons, as in the wire grid probe of Dr. Hirao. Both Dr. Hirao and Dr. McNamara have used an assembly of electrode shapes on the same rocket, and as I understand it, they find no fundamental difference in the data from the different probes.

Still in the E-region and at higher altitudes, the use of probes with grids was described by Mrs. Sagalyn and by Dr. Knudsen. The addition of a grid to suppress photoemission current from the collector is an important, practical advantage over the first ion trap used by Gringauz on Sputnik III. Otherwise the additional complexity of the ion trap is difficult to justify; though this is a debatable point. In the lower ionosphere the number density of negative ions can be determined, at present, only as the difference between the concentration of positive ions and of electrons. Mrs. Sagalyn described the use of the ion trap for such measurements.

As has been pointed out earlier, linear probe theory is based in a very simple way on the kinetic theory of gases, and this breaks down in the D-region. The most important factor here is the short mean free path; the motion of the particles is affected considerably by the collisions of electrons and ions with the neutral gas particles, and a conductivity treatment becomes appropriate. As I indicated in the opening paper, the difference between these two treatments is not as great as might at first seem to be the case, and it should be possible to treat the transition region without great difficulty.

The current to an electrode at a small positive potential shows a height variation in the D-region which indicates that the probe current is proportional to electron density. Dr. Landmark showed profiles of probe current obtained in this way on the same rocket flight in which electron density was measured by propagation experiments, both differential absorption and Faraday rotation, and he found good agreement between the two profiles. There is an obvious need for further inter-comparison of the techniques, particularly under daytime conditions of low electron density.

The main conclusion in the area of electron density measurements for the D-region is that there are now sufficient techniques to choose from that the study of the region can proceed confidently. The situation with respect to negative ions is not satisfactory, and no very convincing measurements--direct or indirect--are yet available. The ion trap and the conductivity probe are expected to be most valuable in this area.

The aerodynamic problem for rockets in the D-region is formidable. Mrs. Sagalyn mentioned wind tunnel tests of a spherical ion trap which indicate a less profound effect than would have been anticipated. Further wind tunnel tests are indicated, but my personal feeling is that difficulties of simulation make inter-comparison of techniques in the actual ionosphere preferable. This again is a debatable point, and of course there is a place both for wind tunnel tests and actual rocket flights.

DISCUSSION

R. L. F. Boyd: There is a very strong case for more studies in which we have, for example, impedance probes of the Sayers type, resonance rectification probes, and one of the more conventional Langmuir probes, put together on the same vehicle and used under circumstances where we have a good idea of what it is we are studying, so that we are trying to explore not the ionosphere but the instrumentation. I would like to see a great deal more of this sort of comparison done toward the measurement of electron density. I personally would expect the resonance rectification probe to give the best results.

L. G. Smith: I believe Dr. Hirao and the NASA group have made such joint measurements.

K. Hirao: Measurements in the lower ionosphere should be made by the meshed probe or the ion probe, and conductivity measurements are also possible. The resonance probe can be used down to 93 or 95 km; below this it is very difficult to use the resonance probe for electron density or temperature.

J. Ortner: Supporting Prof. Boyd's viewpoint, I would suggest the combination of a probe experiment with a propagation experiment on the rocket. We always use this combination, together with, if possible, a partial reflection experiment on the ground.

L. G. Smith: My point was that it is practical now actually to plan an experiment to measure electron density profiles, and diurnal variations in the D-region, but one could not think of doing that for negative ions at this time.

W. J. Heikkila: The plasma sheath is usually regarded as unwanted and attempts are made either to remove it or to correct for it before deducing electron density, etc. However, the plasma sheath has many properties which may be exploited. In a simple plasma, the sheath thickness depends on the Debye length, which is related to the electron temperature as well as density, so this is a possible attack on the temperature as well. When we go down lower in the D-region where there are negative ions present, the sheath thickness will be modified; because what is needed is to collect a certain amount of positive charge within the sheath to neutralize the effect of a potential, and this depends on the positive ion density rather than the electron density, so if you can make measurements of both the sheath thickness and the electron density, this gives the negative ion concentration as well. And finally, if a very large potential is applied to a sphere in a plasma, the distribution of the positive ions within the sheath will depend upon the number of collisions that the ions make within the sheath, and therefore the positive ion mean free path is also involved. One would have to know the potentials of the probe accurately, with respect to the plasma.

14.2 CONCLUDING STATEMENT ON ELECTRON TEMPERATURE

R. L. F. BOYD
Department of Physics, University College of London
Gower Street, London WC1, England

All of the methods of measuring electron temperature presented at the conference have made some use of retardation analysis of probe curves. That is to say they have all employed the Boltzmann relation. In particular, it is to be noticed that none of the measurements of collision frequency were interpreted by their authors in terms of temperature. This is unfortunate in that there is a great need for a completely different method of measuring electron temperature from the probe techniques. Four methods of analyzing probe curves seem to be in common use, and generally, an accuracy of about $\pm$100 degrees is claimed.

First of all there is analysis by conventional semi-logarithmic plot of the current against voltage. The essential feature here is to employ a probe sufficiently small to permit it to be driven up to space potential without introducing problems associated with electron depletion or "current dumping." Brace favors thin wire cylindrical probes as giving a small diameter and yet adequate collecting area. Voltage sweeps are fast--less than one second if possible, in order to minimize errors due to changing aspect. Smith employs this method of analysis on intermittently obtained characteristics from the conical tip of a nose cone. The advantages are simplicity, both of the theory and of the instrumentation.

Secondly, there is the symmetrical double probe analysis. Here the current dumping problem is overcome by simply taking it into the analysis and making the system symmetrical, and it has the great advantage of an ejectable package that can be got well away from contamination and disturbance by the vehicle. This is Spencer's system--only a small part of the retardation characteristic near to floating potential is actually made use of when analyzing for the temperature and this may seem at the present stage of the art to be somewhat of a disadvantage. On the other hand, as confidence in the measurements grow, and as our experience grows, this will probably cease to be a drawback for situations where we can be quite sure that the distribution is Maxwellian.

Then thirdly, there is the analysis of resonance rectification characteristics. The resonance probe may be used to obtain temperature by comparing the current drawn at frequencies above critical with that drawn at lower frequencies. This current difference is a function of the second and higher derivatives of the curve. The use of a single radio frequency amplitude, however, is insufficient unless the probe is biased to a porential only a little below that of space, because otherwise the unknown value of the positive ion and photo currents make it impossible to establish the point on the characteristic to which the value of the second derivative applies. The Japanese work has overcome this problem by applying successively two different radio frequency amplitudes which differ by a factor of two. If you do this, you make use of the fact that the high derivatives of the curve also influence the rectification characteristics and you can obtain the ratio of two derivatives and hence the value of T_e. The main advantage of this method is that it is ancillary to the very effective resonance rectification approach for finding the plasma density. Like the symmetrical probe, however, it suffers from the disadvantage, that as normally employed, it only makes use of the part of the I-V curve near to floating potential. And, of course, this is the part that is most likely to be disturbed by other influences such as the photoelectric current or the positive ion current. There is, however, no reason in principle why the probe should not be scanned in voltage so as to measure the characteristics at some point rather further away from floating potential.

Then fourthly, there is the Druyvesteyn analysis. The system employed in the Ariel satellite makes an in-flight determination of the first and the second derivatives from the I-V characteristic by employing the curve to mix two small audio voltages of different frequency. The self-consistency of two probes used on the same satellite vehicle and the statistical analysisof some tens of thousands of characteristics lead to an expected accuracy of the order of $\pm$4%. The principal advantages of the method are the very efficient use of telemetry bandwidth and the insensitivity to most of the forms of characteristic "noise," i.e., voltage variations of the vehicle, which might occur. These effects are largely eliminated by the use of very narrow band amplifiers, and only noise coming within the band width of the amplifiers is relevant. The principal disadvantage of the method is its relative complexity and, for that reason, relatively high cost.

Two basic methods of measuring ion temperature are in use, namely orbital motion analysis and retardation analysis. Most workers strongly favor the use of spherically symmetrical systems, but one paper presented the use of a plane orifice with a hemispherical grid system behind it. It was not clear what special advantages were claimed for this geometry, but it is possible that it was concerned with some practical problems related to the permitted payload configuration.

The orbital motion type of ion trap uses a small inner sphere and a relatively large and coarse spherical grid. Ions entering the space between the spheres perform orbits determined by the potentials on the spheres and the ion energy; so an analysis of the current-voltage characteristic leads to a value for the mean ion energy or the temperature.

The retardation type of ion trap uses a very fine outer grid of almost the same diameter as the sphere, and proceeds by making a complete Druyvesteyn analysis of the energy distribution. The probe curve is extracted electronically in just the same way as for the determination of the second derivative in the electron studies, and this analysis then leads to an ion energy distribution. This again may be interpreted in terms of the ion energy and the ion mass spectrum.

One important paper pointed out the problem of testing ion and electron probes in the laboratory. The intrinsic problem is that of obtaining a very low temperature plasma. The Japanese workers described an ingenious discharge tube in which a low temperature plasma is produced by mixing the canal rays from two subsidiary hot cathode discharges with the thermal electrons from another pair of cathodes. In this way a controllable temperature, low density plasma was obtained. I think we shall soon find a number of these systems in use throughout the world.

Turning to the results of measurements, the rather scanty data on temperature in the lower ionosphere almost all point to values around 500 deg K for quiet conditions near 100 km. One notable exception is a curve obtained with the resonance rectification probe which gave a value falling to about 100 deg K at 100 km; however, it is necessary to note that most workers claim an accuracy of only a hundred degrees.

The only data presented on ion temperatures in this region were obtained with the orifice probe, and gave similar values, near 500 deg K. The theoretical difficulties of these values should not be underestimated; they may well present an insuperable objection to accepting 500 deg K for the ions. Such objections are not at present insuperable for the electrons.

For the electron temperatures, it seems to me a three-pronged attack on the problem is called for.

First of all, we need more theoretical work to examine the energy inputs necessary to maintain a temperature difference of some 300 deg K between the electrons and the neutral gases in the neighborhood of 100 km. Radiation sources of such energy would not seem promising when the sun is not disturbed. Electric fields in the ionosphere, either steady or oscillatory, and corpuscular radiation should be examined.

Secondly, there should be further study of the limitations of the techniques. It may be that the differentiating techniques, such as those thay my own group have used with Ariel, and the Japanese group have used with resonance rectification probes, tend to read low. On the other hand, I suspect that if there are errors in the conventional analysis, they make the system tend to read high. These matters need investigating. Is there, for example, a work function change of a few millivolts that arises under the differing bombardment conditions the probe is subjected to as its potential is changed, and if so, might this perhaps set a lower limit to the temperature that one can expect to measure instrumentally? Much more laboratory work is needed and, incidentally, it should be conducted not only in mercury vapor.

The third attack on the problem seems to me a series of flights aimed primarily to establish complete confidence in the techniques. We need several approaches, including radio methods, to try to measure the temperatures. This means increasing the sensitivity of our equipment to measure temperatures at lower electron concentrations. Low latitude night-time flights should be made where the radiation and corpuscular heating might be minimized so that there is a chance of examining thermal equilibrium situations.

One study of the latitude variation and the effects of geomagnetic disturbance was presented. While the data is at present inadequate, the results are most suggestive, and it is hoped that they will provide a stimulus for a concerted attack, with more than one group involved, on this important problem of the lower ionosphere. In seeking to interpret temperature measurements, however, it is worth noting that temperature is a measure of a condition depending both on heat input and on heat loss, and it seems to me that it would be a grave mistake automatically to interpret every change in temperature as due to a change in heating. A change in cooling can be just as important.

DISCUSSION

G. C. Reid: You mentioned the difficulty of obtaining cold plasma in the laboratory. I wondered if anyone has investigated the use of strong radioactive sources such as cobalt 40.

R. L. F. Boyd: To produce a dense plasma at, say, a micron pressure by means of radioactive source is to produce too much interference by radioactivity. It may be possible at 10-100 mm pressure, but to do it at the sort of pressures where Langmuir probes are useful, is out of the question.

E. C. Whipple: Pedersen used a radioactive source when testing his Gerdien condenser in the laboratory, though his pressures were not too low.

K. W. Champion: A radioactive source is satisfactory at high pressures, but at very low pressures the plasma will not be cold, because the electrons and ions produced will have high energy, and can only come down to thermal energy as a results of collisions.

H. Dolezalek: I have calculated that up to about 70 km, one may simulate by radioactive sources the natural ionization; but it would be difficult to create a very dense plasma since the ionization is mostly made by alpha rays only.

N. W. Rosenberg: We have some laboratory tests in cesium plasmas where the heating is provided by mercury vapor lamps centrally located, and with this uv, which is all above quartz cutoff, we are getting currently 10^7 to 10^9 electrons per c.c. in a 100 micron plasma; and presumably you could get even lower than this. Using a uv source, of course, the very high energies in a so-called hot plasma are absent.

E. K. Smith: The startling thing to me at this conference has been the high electron temperatures which were shown; 1500 deg for Wallops Island on a disturbed day and 600 deg lower down in the atmosphere. Is there any way of finding out if these are real--some confirming experiment that can go along with the present equipment.

N. W. Spencer: We have measured temperatures considerably higher than that in the higher part of the trajectory. One of the highest we have observed, and we have full confidence in it, is on the order of 3500 degrees, at about 230-40 km.

M. A. Biondi: Were your temperatures from the long exponential tail on the probe curve?

N. W. Spencer: Yes. These values were measured under spead F conditions over Fort Churchill. However, we have conducted simultaneous measurements using the long cylindrical probe in which we get well into the distribution and can, in fact, go all the way to plasma potential, and we find that they are in agreement; by and large we have equilibrium under all conditions we have seen.

14.3 CONCLUDING STATEMENT ON IMPEDANCE

W. PFISTER
Geophysics Research Directorate
Air Force Cambridge Research Laboratories
Bedford, Massachusetts

We have heard about a variety of methods which use the principle of the impedance probe to measure ionosphere quantities, basically electron densities and collision frequencies. Sometimes the approaches are quite similar and only the technique in the impedance measuring device is different. In other cases the approach is radically different.

On the one side there is the philosophy to design an experiment in wuch a way that the analysis is made simple. This leads to the choice of a high operating frequency, high compared with the plasma frequency and the collision frequency, and it leads to a small capacitor of parallel geometry and to provisions to remove the ion sheath and also to drive out the electrons altogether out of the capacitor. Left is the instrumental problem to measure extremely small changes in capacitance. Prof. Sayers showed an ingenious way to overcome this problem.

The opposite approach is to operate an experiment in wuch a way that small changes in the ionospheric parameters produce large changes in impedance. One would use, in this case, big capacitors like sections of the rocket body. One would use lower operating frequencies like the plasma frequency, or another sensitive frequency below the plasma frequency, or the gyrofrequency. The complications in this approach are that we might have to compute the driving point impedance in terms of a generalized dielectric tensor of the magnetoionic medium, and together with an awkward shape of the condenser; this could be a job for a big computer. A further complication is introduced by the ion sheath, especially when it starts to oscillate with the operating frequency.

The problems connected with this approach have only been touched at this conference, but not treated in any detail. Nevertheless we consider this approach not only very challenging but also very promising. What looks at first only as a disturbing effect might be utilized in a more sophisticated experiment as a means to obtain more basic parameters of the medium.

So far the impedance probe has been used to measure electron densities. In this conference we have heard about successful measurements of collision frequencies. We have seen that it is possible to study characteristics of the ion sheath with an impedance probe technique. And to go a step further, it seems entirely possible to use the impedance probe technique in the study of electron temperatures; and, with the help of the earth's magnetic field, to look even into the mass distribution of the ions.

Now, like almost all of the probes, the impedance probe is not free from disturbing effects of the vehicle itself. Wake effects and boundary layer effects are of concern, especially in the lower D-region. Certain types of disturbing effects have been reported which appear to occur only with specific rocket vehicles, in this case, the Black Brant rocket. No satisfactory explanation has been suggested; however, an unusual outgassing phenomenon is most likely the cause. We should not be unduly concerned with these disturbing effects as they can be overcome. A solution can always be found in nose cone separation or ejection of packages, an example of which we have seen at this conference.

14.4 CONCLUDING STATEMENT ON CONDUCTIVITY

E. C. WHIPPLE, JR.
NASA
Goddard Space Flight Center
Greenbelt, Maryland

Some of us have discussed with Dr. Yen the shock wave problem in front of our Gerdien condenser, and I would like to report on some of the results. Apparently the problem is not as bad as we had been anticipating. The problem is to know the volume rate of air flow through the condenser so that one can calculate the ion density from the saturation current. It turns out that this problem is very similar to that of the intake to a jet engine, which has been worked on considerably. There is a nozzle, and a condenser is a nozzle of sorts. For a given Mach number, depending on the geometry, there will be some minimum area in the condenser. As long as this minimum area is greater than a certain critical minimum area, which is determined by the intake area and by the Mach number, then the airflow will be divergent, and the shock will be swallowed. All the shock waves will be internal to the condenser, with the result that the intake aperture is the effective aperture that should be used in calculating the air flow. Also the free-stream Mach number is that which should be used in calculating the airflow. This makes the calculation very straightforward, with no problems about effects wuch as spillage. With the geometry so that the flow diverges, the critical minimum area can be computed from tables, and one should be careful that the minimum area is larger than this critical number.

The second comment has to do with some concepts in atmospheric electricity that are familiar to people who have been working nearer to sea level; some of these apply to higher altitudes, and might be useful in our analysis of D-region problems. At sea level, there is an electric field, even in fair weather, on the order of about 100 volts/m. The cause of this is fairly well understood. One may consider a spherical condenser, the earth being the negative electrode and the atmosphere the positive electrode. The spherical condenser is charged by thunderstorms throughout the earth. The thunderstorm acts like a generator with the resulting current flow up into the high atmosphere, then horizontally and down to the fair-weather part of the earth. There is space charge in the atmosphere, and the ion current flows from a thunderstorm area horizontally at some altitude that has not yet been determined. Kasimir and others have shown that this critical altitude where the current flow goes horizontal, is probably around 100 km. This means that the electric field which is present at the earth's surface in fair weather, and which decreases roughly exponentially with altitude, should be present all the way up to about 100 km. In fact, the product of the electric field and the conductivity should be constant and equal to the current density, about 10^{-12} amp/m^2.

We heard yesterday about one measurement of electric field. I believe that any technique for measuring field should be examined very carefully, especially to see the effects of interactions with the plasma. If a valid technique can be developed, however, this is another way of getting at the conductivity, and the current density, and of measuring the pattern of the current flow. It might also be promising to try and measure the field or the conductivity near thunderstorms, where the field is much larger and easier to measure.

The final comment concerns the presence of dust in the atmosphere and its importance. I am rather surprised that we have heard no descriptions of techniques of determining dust densities. Dust is important in providing a recombination circuit for ions and electrons; dust particles provide a surface to which ions or electrons are attracted. If they hit the surface they become neutralized.

As an illustration one may assume a dust density of one cm^{-3}, with a radius of 0.1 micron. The rate at which ions will be lost by diffusion to a dust particle will be given by the surface area of the dust $4\pi r^2$ times the thermal velocity of the ion, which one may take as 3×10^4 cm/sec. Dividing by 4 for the diffusion term, and taking a typical recombination coefficient of 10^{-7} cm^3/sec, the ratio of the loss rates by diffusion to dust and volume recombination comes out to be about 100/N, where N is the ion density. In other words, the two rates are equal for an ion density of about 100 cm^{-3}, and the loss rate to the dust becomes more important as the ion density decreases. Even if there are 1000 ions/cm^3, the loss rate to dust is still 10%, large enough to be significant.

In each of four flights at Wallops Island over the last two years we have seen a minimum in the electron density between 80 and 84 km, which is also the altitude of the temperature minimum, where noctilucent clouds are seen, whenever they occur. There was recently a report by an MIT group, who used a laser radar, and detected dust particles at 80 km and at higher altitudes. I therefore suggest that dust measurements be taken seriously and that they be correlated with the charged particle measurements.

DISCUSSION

H. Dolezalek: I want to comment on measuring electric field strengths in space; the USA and USSR attempted to do this with field mills, but were unsuccessful because the ion sheath on the field mill is too thick, and the very minute electric field cannot be detected. A new method to determine electric fields in space, however, could be proposed, consisting essentially of two or more inflatable spheres, kept at environmental potential by using special techniques. The potential difference between these spheres could be measured electrometrically; if four spheres are applied, all three spatial components of the electric field can be measured. The method is only applicable where the environmental gradients, except the potential gradient, are sufficiently small, that the effects of ion sheath, photo-electric currents and convection currents would be equal and thus cancel out. The magnetic field must be measured simultaneously, in order to take account of the potential differences induced by the magnetic field in the connecting wires. Furthermore, the spheres must be large enough to overcome the leakage current which would go along the ion sheaths along the insulating hoses which connect the spheres. I think this principle is probably good for interplanetary space. How far down, closer to earth, it might be used must still be investigated.

A. Kavadas: Do you think this method would eliminate the errors that other methods introduce?

H. Dolezalek: It would certainly eliminate the error introduced by the ion sheath for the field mill method.

R. L. F. Boyd: Were the spheres to be kept at plasma potential; and if so, how do you get rid of the very strong electron current, which would charge up the whole system in about 10^{-6} sec?

H. Dolezalek: As soon as the spheres deviate from the environmental potential, one applies the technique I briefly mentioned, which is nothing but the old water-dropper principle of Lord Kelvin.

I refer to ejecting very many small bodies, which carry away the surplus charge. One could use a metallic powder, which would imply some difficulties--there would be some frictional electrification, for instance--but this can be investigated in the laboratory.

N. W. Rosenberg: I believe the dust concentration proposed by Dr. Whipple, at that level, would make a significant difference to sunset airglow measurements. It would amount to about 10^{-5} of moonlight, and would certainly be noticeable even in layers 1 km thick, so either the concentrations are substantially smaller than this or one could invoke them only on very rare occasions.

E. C. Whipple: 1 cm^{-3} was estimated as the right order of magnitude for noctilucent clouds. Of course, noctilucent clouds are not common. There have been some recent measurements involving collection of dust. Do you have any figures?

M. Dubin: Giovnelli made a determination of concentration about ten years ago and he found somewhere about 100 cm^{-3} of particles a little larger than 0.1 micron. The collections reported by Witt, Hemenway, and Silverman at the COSPAR meeting, in noctilucent clouds, gave a few particles per cm^3 at 0.2 cm. The measurements without noctilucent clouds give about a hundred times less. There are only two measurements plus a measurement from White Sands.

I heard today from Ruttenberg that a recent explosion of a volcano, as observed by Meinel, shows dust at the 70 km level for over a month, so the hold-up time for dust can be quite long.

H. Dolezalek: If dust is a persistent characteristic of the high atmosphere, this would have an atmospheric electric consequence which could be measured. The conductivity would no longer increase exponentially from the ground to the ionosphere, and since there is a current from the ionosphere to the ground, the potential between the ionosphere and ground must be much higher than assumed so far. This would imply that the potential of the generator, namely the thunderstorm, must be much higher than has so far been observed. We cannot tell what is the average thundercloud or the average potential, between its top and bottom. If more measurements on this were available, it would be possible to calculate the conductivity above the thundercloud through the ionosphere and down to ground, and derive some information on the dust problem.

J. S. Belrose: Dr. Whipple quoted some NASA results of electron densities showing a minimum near the temperature minimum in support of his dust arguments. The only results which I have seen so far were presented by Aikin, Kane and Troim in Europe last summer; they show a "D" region electron density profile more or less constant with height, except for just one point at a much lower electron density. My profiles do not usually show such a deep minimum.

J. Kane: That one point represents the average electron density over the kilometer segment, and is based on something like ten observations of the Faraday path. It was a daytime measurement.

14.5 CONCLUDING STATEMENT ON NEUTRAL AND ION COMPOSITION

C. Y. JOHNSON
Naval Research Laboratory
Washington 25, D. C.

In the field of ion and neutral composition, I think we have got a different outlook on the situation at this meeting. There were four main speakers in the section: Dr. Holmes, Dr. Taylor, Dr. Nier, and Dr. Schaefer.

Dr. Holmes described the two recent results from two ion spectrometer flights at White Sands. The marked reduction in the ion distribution from day to night shows us for the first time really what the ionosphere is doing. I think our previous measurements for Churchill show us what is happening in a region that is aurorally active, and it was very difficult to do anything with that type of data. However, we now have, I believe, a better knowledge of the six main ionized constituents of the upper atmosphere--mass 14, 16, 18, 28, 30, and 32. Of these, we feel we can eliminate mass 18 as being a water vapor contaminant. The predominant ions are 30, 32, and 16; 14 and 28 come in as minor ions. Occasionally there is a mass 24 ion observed; this was well demonstrated by Dr. Taylor's results on a flight which was aimed at high altitude, but failed to reach the altitude intended. He obtained, instead, a very good distribution of the mass 32, and 30 ion in the lower region between about 85 and 115 km. He also detected masses 28 and 24 in that same region.

To pass over to the neutral composition now, I will take them in reverse order of the firings. Dr. Nier's instrument was a 90 deg single-focusing mass spectrometer which was pumped internally by a vac-ion pump, and covered the altitude range from about 100 km to 209. The roll rate of the rocket was 4 sec and the sweep rate of the mass spectrometer was 2 sec. The combination of these two produced a beat note characteristic, and by looking at the 90 deg or ambient points in this beat note distribution, the density of the various constituents could be determined rather easily. On the basis of that quick analysis, Dr. Nier was able to show the density of N_2, O and O_2. A contaminant, again water vapor, shows up in the spectra. Dr. Nier's results showed that there was no nitrogen dissociation, but that there was oxygen dissociation. He also showed that from the scale heights he could derive temperatures from the three constituents O, O_2, and N_2, which were reasonably consistent within themselves and varied from about 250 deg K at 110 km to about 1000 deg K at 200 km.

Dr. Schaefer's results, which were obtained earlier, are backed up by Dr. Nier's. He used a massenfilter, and a very open ion source, which is relatively insensitive to the attitude of the rocket; as opposed to the Nier instrument, which is mounted on the side of the rocket and is extremely sensitive to the roll modulation. Schaefer's results also showed the oxygen dissociation. He also measured the A/N_2 ratio for diffusive separation and found it consistent with the previous sample bottle measurements which were taken prior to the IGY. He also noted that there was not the abrupt discontinuity at a separation ratio of unity in the diffusive separation results. I think that these new developments in the neutral composition field are more consistent with the theories of diffusive separation and the dissociation of oxygen by solar radiation.

There is a disagreement, however, between the mass spectrometer results and the results obtained by Hinteregger by the optical absorption method; I hope that this can be resolved. When it is, I believe that we will have tied down the composition of the high atmosphere and we will then be able to work on its variations. Hinteregger already reports a variation with his technique, although he does not have the same distribution.

The neutral and ion composition below 100 km was not discussed in the meeting. That, I think, will come when we get the better instruments for that region, in due time.

DISCUSSION

M. A. Biondi: Are there any concrete plans for negative ion determinations at these levels, other than by Gerdian condenser method?

C. Y. Johnson: Plans to fly the negative ion spectrometers again have been discussed in our group, but we have not at this moment decided whether to or not. Two problems are whether the ambient can be distinguished from contamination produced by the rocket; and whether the ambient negative ions can be pulled into the instrument in the presence of a negative rocket potential.

R. L. F. Boyd: We have studied this problem, and are working on a little mass spectrometer for negative ions; a time of flight instrument, in which the path length is expected to be about 0.5 cm. The problem is just that mentioned by Dr. Johnson, of getting the negative ions into the system. We have studied this in the laboratory, and found that they frequently fail to enter an ordinary mass spectrometer. It may be necessary to use an extremely small tube which is put into the plasma, a tube small compared to the Debye length. However, we believe that with a hypersonic vehicle it is possible to get the negative ions to a probe

while keeping the electrons back, because the energy of the ions is much larger in the plane of reference of the vehicle; we are working on these principles.

M. Dubin: Since positive ion species can now be identified, a measurement as a function of time during the night, or through the evening, would give the rate coefficients for the processes and a better understanding of the mechanism.

K. W. Champion: I would like to stress the need for further calibration work with mass spectrometers. In particular, they need to be calibrated for the relative sensitivity of ionization of atomic and molecular oxygen. This can be done in the laboratory without too much difficulty on a static system.

C. Y. Johnson: We have planned to fly three rockets essentially at sunset, after sunset, and before sunrise; this is a major undertaking. After hearing the discussion in the conference, I don't know whether everyone would agree that the same ionosphere would be measured because of winds; however, the measurement still has to be made.

Concerning the calibration of the neutral mass spectrometers: for Dr. Nier's unit which I am more familiar with, the calibration was done for air and hence included O_2. The best that we have on O is the cross section of Fite and Brackman, approximately the same cross section for O and O_2. It was not calibrated for an O source; however, I think the data tends to substantiate the validity of the calibration.

D. Alpert: There is a possibility of a very large production of O by electron impact at surfaces on which O_2 is absorbed. This effect can be very large; even where one knows that one has O_2 in volume, one can get a very large peak for the O^+ ions from the surface. If the mass spectrometer does not specifically eliminate the possibility of such ions arriving at the collector, sizeable errors may occur. Of course the fact that the two experiments of Schaefer and Nier, using non-identical mass spectrometers, give the same results, are evidence in the other direction, but one should look carefully at both instruments to see that they did not make the same error.

N. W. Spencer: The calibration of the mass spectrometer is quite complex; for one thing the sensor is direction sensitive in most cases. One therefore needs to build a source for the mass spectrometer so that the calibration factors are known for the different entrance angles at which the neutral particles enter the source. Another problem is to generate the gas in an adequate form so that the calibration can be made; a further difficulty is that in use one encounters significant velocities that are not encountered because of only thermal energies being present in the laboratory.

C. Y. Johnson: Dr. Nier's spectrometer is mounted on the side of the vehicle, and is highly roll modulated. The theory should tell us that the roll modulation for the O peak is a certain amplitude: we took the 90 deg point to show the data here. When we get into the analysis of each data point, we will find that there is an error in the density at those points; if so, we may say that we have a contribution, possibly, from the O_2. If there is no error, according to the theory, I would say that it is probably entirely O that we are measuring. This is still not an absolute calibration, however. We can tell whether or not it is clean, but we do not yet know the absolute density. I would like to emphasize that the roll modulation effect is a very powerful tool in rocketry. It has been used by all the groups with the exception of Dr. Schaefer, who went to the opposite extreme to get away from it.

14.6 CONCLUDING STATEMENT ON PRESSURE, DENSITY AND WIND

N. W. SPENCER
NASA
Goddard Space Flight Center
Greenbelt, Maryland

In the measurement of structural properties of the mesosphere and lower thermosphere, the techniques are varied and I will just summarize them briefly. The grenade technique leads directly to temperature measurement and winds up to the order of 90 kilometers. This method is characterized primarily by what we believe to be its very high accuracy in temperature determination. The points measured, although they represent averages over altitude regions, probably have an accuracy of a very few degrees.

The second technique that has been very useful is that of seeding the atmosphere; for example, with sodium. It leads directly to winds and to temperatures at higher altitudes. One of its primary features is that the winds are directly observed through the trail movement, and it permits the study of a changing situation, because in effect the sensor is there for as much as three-quarters of an hour. As far as the sodium is concerned, its use is confined to dawn and twilight; however, the technique has been extended through the use of other seeding elements by Dr. Rosenberg, and measurements have been made throughout the night. This is a very great advance.

The falling sphere technique leads directly to density, from which temperature can be computed. It is characterized primarily by great simplicity, which makes it very mobile. It has great use in making latitude surveys.

The final technique which has emerged uses various forms of pressure gauge configuration on a rocket nose cone; it perhaps poses some of the more difficult instrumentation problems, but has an advantage in that it will permit an extremely detailed measurement of the structural parameters. Most of these are characterized by a short mean-free path situation. We did not get into extensive discussion of these parameters and their variations, except incidentally. The scale height is the prime means today for deducing the temperature by this measurement technique. There is , however, another possibility which has not as yet been exploited, namely, measuring the energy distribution of the neutral particles. This is considerably more difficult, in that the neutrals are not as easy to move as the charged particles, posing some additional problems.

All these techniques, however, are in use today, and we can look forward to extensive measurements as well from the meteorological standpoint as from the point of view of the physics atmosphere. Efforts are being made to extend the altitude region so that one may get considerably greater information about the interesting region around the thermopause.

Dr. Grossi spoke about a very interesting new method to observe the meteor trails in which he spoke of using synchronized VHF radar observations, and a Doppler technique. In his system all the data is piped to a central location by microwave links, and permits computation of winds in the lower thermosphere by observing the movement of the trails. The accuracy appears to be very good. He claims 4 m/sec on a statistical basis--1 m/sec I believe is the figure for the radial component only.

Probably the most exciting discussion arose from the wind results presented by Dr. Rosenberg. The wind structure of the atmosphere has been discussed for some time, and I think we are finally beginning to see the overall pattern. Very strong seasonal effects have been seen in the lower regions from sodium and grenade work; westerly winds in the winter, changing over in the equinox period to easterlies in the summer, with real breakdowns in the circulation patterns at the equinox times where there is flow along the meridional direction. Present measurements are providing new data in this regard, and researchers the world over are now trying to get together to make simultaneous measurements.

Progressing to higher altitudes, however, we see strong wind shears in the lower thermosphere which are beginning to be associated with sporadic E although the results do not yet appear entirely consistent. In particular, a great circulation of direction of the winds appears as the altitude increases. The seeding methods provide our only significant means at this time for studying winds in the region up to 200 km, where the atmosphere is very tenuous.

Rosenberg also spoke of observing acoustic waves and probable effects of gravity waves at the higher levels. This fits in with some other work, not reported here, on wave effects in the atmosphere. It has been observed, for example, in grenade temperature measurements, that there is a variation with a scale of about 5 or 6 km.

14.7 CONCLUDING STATEMENT ON AIRGLOW

M. DUBIN
Headquarters
NASA
Washington 25, D. C.

The dayglow and nightglow and the twilight observations from remote sites including satellites, and from instruments on sounding rockets can be used for measuring the variations of the concentrations of certain constituents, especially when the reactions, by which the lines or bands are excited, are known. Temperatures may also be determined. The excitation of the green line of oxygen, which probably depends on the third power of the oxygen concentration, in a three body reaction, appears to be a possible method for obtaining this concentration. There is some other evidence, and there are experiments going on which weren't mentioned. Maier at GSFC recently flew a sodium light source and measured the back scattering from resonantly excited sodium in the atmosphere. In this way, the distribution of sodium, a rare constituent, can be obtained. Potter at Ames Research Center has attempted to check his theory, for excitation of sodium by metastable states of molecular oxygen, by releasing ozone in the region near 80 km, and the same reaction should give some information on the distribution of concentration of hydrogen. His work so far has been unsuccessful.

The profile of optical spectra in the daytime may be used to determine the distribution of bands and lines in the lower atmosphere to determine composition in this region. Barth has in two flights attempted to do this in the near uv for the molecular oxygen concentration from 70 to 100 kilometers. In the light of recent measurements of composition and motion described by Rosenberg at this conference, much of the airglow data in the green line of oxygen may well be worth further study. Roach has observed large clouds, all of the 5577 A radiation, about 2500 km across, with a period of rotation of about 5 hr, similar to the period described by Rosenberg for the same altitude. Tohmatsu and Nagata have developed a model of ionospheric motions to explain the world-wide variation of the green line based upon a small component of vertical motion. Such small vertical motions have been observed from measurements involving chemical releases, and also from radar measurements of meteors. The auroral and polar regions may also be studied by airglow analysis. The discovery by Crosswhite, Fastie, and Markham in 1959, that most of the airglow energy is in the ultraviolet and that several species could be identified in this manner, speaks for further study using rocket soundings. Probably the outstanding advantage of the airglow technique for measurement in the lower ionosphere is the fact that observations may soon be made from satellites. For POGO, for example, measurements may be obtained of the global distribution of the atomic oxygen lines at 5577, 6300, and 1300 A and the N_2^+ recombination distribution at 3914 A, using photometers. The distribution of ozone and molecular oxygen in this region could be obtained possibly from the back-scatter in the near uv in the daytime albedo, using a spectrometer in the ultraviolet.

14.8 CONCLUDING STATEMENT ON SOLAR RADIATION

T. A. CHUBB
Naval Research Laboratory
Washington 25, D. C.

The solar spectrum has been measured in various ways by using grating and crystal spectographs and spectrophotometers, by pulse amplitude spectometers such as mentioned by Prof. Boyd, and by narrow band photometers, sensitive to bands of ultraviolet and X-ray radiation. Now, it seems clear that ultimately the main solar monitoring can be expected to be done from satellites since they can stay up in orbit for long times and can get continuous data on the sun. But nonetheless, there is good reason for monitoring the solar radiation by aeronomy probes at times when the satellite monitoring is not effective. In addition, the radiation monitors aboard aeronomy probes serve to get a reading of the position of the aeronomy probe relative to the ionizing source, the sun. In other words, if one carries such photometers, one knows, at the critical times, the amount of material between the sun and the probe.

At night time one must not always assume that all sources of ionizing radiation have disappeared and that the only thing left is corpuscular radiation. We know that there exists a 0.01 erg/cm^2 sec Lyman alpha radiation. We do not know what the situation is in the helium line emissions that may come into the earth. There is an upper limit of .001 erg/cm^2 sec, but numbers up to this are at present possible. In addition, we know that there is something like 10^{-7} or maybe quite a bit more, of soft X-ray radiation from at least one celestial source; and that there is some far ultraviolet radiation, probably again something of this order of magnitude, or maybe higher, coming from the stars. This has been observed only down to the band 1050 to 1180 Angstroms, but since it's continuum radiation, presumably, rather than line radiation, it can be expected to extend down to close to the Lyman limit.

ATTENDEES

CONFERENCE ON DIRECT AERONOMIC MEASUREMENTS

IN THE LOWER IONOSPHERE

1. Alpert, D.
Coordinated Science Laboratory
University of Illinois
Urbana, Illinois

2. Baker, K.
Upper Air Research Laboratory
University of Utah
Salt Lake City, Utah

3. Balmain, K. G.
Department of Electrical Engineering
University of Illinois
Urbana, Illinois

4. Belrose, J. S.
Defence Research Telecommunications
Establishment
Defence Research Board
Ottawa, Ontario, Canada

5. Berning, W. W.
Ballistics Research Laboratories
Aberdeen Proving Grounds
Aberdeen, Maryland

6. Bhattacharya, A. (Reporter)
Department of Electrical Engineering
University of Illinois
Urbana, Illinois

7. Biondi, M. A.
Department of Physics
University of Pittsburgh
Pittsburgh, Pennsylvania

8. Bowhill, S. A.
Department of Electrical Engineering
University of Illinois
Urbana, Illinois

9. Boyd, R. L. F.
Department of Physics
University College of London
Gower Street, London W.C. 1, England

10. Brace, L. H.
Goddard Space Flight Center
NASA
Greenbelt, Maryland

11. Brinton, H. C.
Goddard Space Flight Center
NASA
Greenbelt, Maryland

12. Brubaker, W.
Bell and Howell Research Center
360 Sierra Madre Villa
Pasadena, California

13. Cahill, L.
University of New Hampshire
Department of Physics
Durham, New Hampshire

14. Cahn, J. H. (Observer)
Department of Electrical Engineering
University of Illinois
Urbana, Illinois

15. Champion, K. W.
Geophysics Research Directorate
Air Force Cambridge Research Laboratories
Bedford, Massachusetts

16. Cherrington, B. (Reporter)
Department of Electrical Engineering
University of Illinois
Urbana, Illinois

17. Chivers, H. J. C. (Observer)
Central Radio Propagation Laboratory
National Bureau of Standards
Boulder, Colorado

18. Chubb, T. A.
Naval Research Laboratory
Washington 25, D. C.

19. Deschamps, G. (Observer)
Department of Electrical Engineering
University of Illinois
Urbana, Illinois

20. Detert, D. (Reporter)
Department of Electrical Engineering
University of Illinois
Urbana, Illinois

21. Dolezalek, H.
Research & Advanced Development Division
AVCO Corporation
201 Lowell Street
Wilmington, Massachusetts

22. Dubin, M.
Headquarters
NASA
Washington 25, D. C.

23. Duff, G. (Reporter)
Department of Electrical Engineering
University of Illinois
Urbana, Illinois

24. Everitt, W. L. (Observer)
Dean, College of Engineering
University of Illinois
Urbana, Illinois

25. Faruqi, A. Z. (Observer)
(Pakistan Space Committee)
Space Physics Research Laboratory
University of Michigan
Ann Arbor, Michigan

26. Ferraro, V. C. A. (Observer)
Department of Astronomy
University of Illinois
Urbana, Illinois

27. Gautier, T. N. (Observer)
Central Radio Propagation Laboratory
National Bureau of Standards
Boulder, Colorado

28. Geisler, J. (Reporter)
Department of Electrical Engineering
University of Illinois
Urbana, Illinois

29. Gerrish, S. D. (Observer)
Headquarters
Pacific Missile Range
Point Mugu, California

30. Goldstein, L.
Department of Electrical Engineering
University of Illinois
Urbana, Illinois

31. Grard, R.
Radioscience Laboratory
Stanford University
Stanford, California

32. Groves, G. V. (Observer)
Physics Department
University College of London
London, England

33. Grossi, M. D.
Smithsonian Astrophysical Observatory
Cambridge, Massachusetts

34. Gschwendtner, A. B. (Observer)
Department of Electrical Engineering
University of Illinois
Urbana, Illinois

35. Haaland, C. M. (Observer)
IIT Research Foundation
10 West 35th Street
Chicago, Illinois

36. Hale, L. C. (Observer)
Ionosphere Research Laboratory
Pennsylvania State University
University Park, Pennsylvania

37. Hall, J.
Radio Research Station
Department of Scientific and Industrial Research
Ditton Park, Slough, Bucks, England

38. Heikkila, W. J.
Southwest Center for Advanced Studies
P. O. Box 8478
Dallas 5, Texas

39. Herzog, R. F. K.
Geophysics Corporation of America
Bedford, Massachusetts

40. Hirao, K.
Radio Research Laboratories
Ministry of posts and Telecommunications
Kokubunji P. O., Koganei-shi
Tokyo, Japan

41. Hodges, R. R.
Department of Electrical Engineering
University of Illinois
Urbana, Illinois

42. Hofer, J. C. (Local Arrangements)
Electrical Engineering Department
University of Illinois
Urbana, Illinois

43. Holmes, J. C.
Naval Research Laboratory
Washington 25, D. C.

44. Horowitz, R. (Observer)
Headquarters
NASA
Washington 25, D. C.

45. Israel, G.
Universite de Paris
Faculte des Sciences
Physique de L'Atmosphere
Paris, France

46. Johnson, C. Y.
Naval Research Laboratory
Washington 25, D. C.

47. Jones, L. M.
Department of Aeronautical Engineering
University of Michigan
Ann Arbor, Michigan

48. Jordan, E. C. (Observer)
Head, Department of Electrical Engineering
University of Illinois
Urbana, Illinois

49. Kane, J.
Goddard Space Flight Center
NASA
Greenbelt, Maryland

50. Kavadas, A.
University of Saskatchewan
Saskatoon, Canada

51. Kesler, O. (Reporter)
Department of Electrical Engineering
University of Illinois
Urbana, Illinois

52. Kirkwood, B. D. (Observer)
Coordinated Science Laboratory
University of Illinois
Urbana, Illinois

53. Kleiman, G. (Reporter)
Department of Electrical Engineering
University of Illinois
Urbana, Illinois

54. Knudsen, W. C.
Lockheed Missiles and Space Division
3251 Hanover Street
Palo Alto, California

55. Landmark, B.
Norwegian Defence Research Establishment
Kjeller
Lillestrom, Norway

56. Little, C. G.
Central Radio Propagation Laboratory
National Bureau of Standards
Boulder, Colorado

57. Mathur, N. (Reporter)
Department of Electrical Engineering
University of Illinois
Urbana, Illinois

58. Maynard, N. (Observer)
Department of Physics
University of New Hampshire
Durham, New Hampshire

59. McCoy, J. G. (Observer)
White Sands Missile Range
White Sands, New Mexico

60. McNamara, A. G.
National Research Council
Sussex Drive, Ottawa
Ontario, Canada

61. Miyazaki, S.
Radio Research Laboratories
Kokubunji P. O., Koganei-shi
Tokyo, Japan

62. Moler, W. F.
U. S. Navy Electronics Laboratory
San Diego, California

63. Nagy, Andrew
Space Physics Research Laboratory
University of Michigan
Ann Arbor, Michigan

64. Newton, G. (Observer)
Goddard Space Flight Center
NASA
Greenbelt, Maryland

65. Nier, A. O. C.
Department of Physics
University of Minnesota
Minneapolis 14, Minnesota

66. Nisbet, J. S.
Ionosphere Research Laboratory
Pennsylvania State University
University Park, Pennsylvania

67. Nordberg, W.
Goddard Space Flight Center
NASA
Greenbelt, Maryland

68. J. Ortner
European Preparatory Commission for
Space Research
36 Rue La Perouse, Paris, 16^{e}, France

69. Oster, A. L.
AVCO Corporation
201 Lowell Street
Wilmington, Massachusetts

70. Paramasivaiah, P. (Reporter)
Department of Electrical Engineering
University of Illinois
Urbana, Illinois

71. Pearse, C. A.
Bellcomin, Inc.
1100 17th St.,N. W.
Washington 6, D. C.

72. Pedersen, A.
Uppsala Ionospheric Observatory
Uppsala 10, Sweden

73. Petersen, O. E. (Observer)
Ionospheric Research Laboratory
Copenhagen, Denmark

74. Pfister, W.
Geophysics Research Directorate
Air Force Cambridge Research Labs
Bedford, Massachusetts

75. Phelps, A. V. (Observer)
Westinghouse Research & Development Center
1310 Beulah Road, Churchill Boro
Pittsburgh 35, Pennsylvania

76. Poppoff, I. G.
Stanford Research Institute
Menlo Park, California

77. Pound, R. (Reporter)
Department of Electrical Engineering
University of Illinois
Urbana, Illinois

78. Prenatt, R.
Ballistics Research Laboratory
Aberdeen Proving Ground
Aberdeen, Maryland

79. Procunier, R. W. (Observer)
Department of Physics
University College of London
London, England

80. Raether, M.
Coordinated Science Laboratory
University of Illinois
Urbana, Illinois

81. Reber, C.
Goddard Space Flight Center
NASA
Greenbelt, Maryland

82. Reid, G. C.
Central Radio Propagation Laboratory
National Bureau of Standards
Boulder, Colorado

83. Richards, E. N. (Observer)
Department of Mathematics
Boston College
Boston, Massachusetts

84. Richter, H. L.
Electro-Optical Systems, Inc.
125 Vinedo Avenue
Pasadena, California

85. Rishbeth, H. (Observer)
Central Radio Propagation Laboratory
National Bureau of Standards
Boulder, Colorado

86. Rosenberg. N. W.
Air Force Cambridge Research Laboratories
Hanscom Field
Bedford, Massachusetts

87. Ruttenberg, S.
National Academy of Sciences
Washington 25, D. C.

88. Sagalyn, R. (Mrs.)
Geophysics Research Directorate
Air Force Cambridge Research Laboratories
Bedford, Massachusetts

89. Schaefer, E. J.
High Altitude Eng. Lab., North Campus
University of Michigan
Ann Arbor, Michigan

90. Smith, E. K. (Observer)
Central Radio Propagation Laboratory
National Bureau of Standards
Boulder, Colorado

91. Smith, L. G.
Geophysics Corporation of America
Bedford, Massachusetts

92. Spencer, N. W.
Goddard Space Flight Center
NASA
Greenbelt, Maryland

93. Sticha, P. (Reporter)
Department of Electrical Engineering
University of Illinois
Urbana, Illinois

94. Stone, C. A. (Observer)
IIT Research Institute
Chicago, Illinois

95. Takayama, K.
Institute of Plasma Physics
Nagoya University
Tokyo, Japan

96. Taylor, H. A.
Goddard Space Flight Center
NASA
Greenbelt, Maryland

97. Thomas, J. O. (Observer)
Space Sciences Division
Ames Research Center, NASA
Moffitt Field, California

98. Ulwick, J. C.
Geophysics Research Directorate
Air Force Cambridge Research Laboratories
Bedford, Massachusetts

99. Van Zandt, T. E.
Central Radio Propagation Laboratory
National Bureau of Standards
Boulder, Colorado

100. Whipple, E. C.,Jr.
Goddard Space Flight Center
NASA
Greenbelt, Maryland

101. Whitten, R. C.
Stanford Research Institute
Stanford, California

102. Yeh, K. C. (Observer)
Department of Electrical Engineering
University of Illinois
Urbana, Illinois

103. Yen, S. M.
Department of Aeronautical and
Astronautical Engineering
University of Illinois
Urbana, Illinois

104. Young, J. (Observer)
U. S. Naval Research Laboratory
Washington 25, D. C.

INDEX OF AUTHORS CITED

ADEN, A. L. 208
AINSWORTH, J. 125
ALLEN, E. F., Jr. 93
ANDERSON, K. A. 201
AONO, Y. 16, 28, 40
APPLETON, E. V. 40, 56
ARGENCE, E. 5
ARNDT, D. 50
BAILEY, D. K. 203
BAILEY, V. A. 146
BAKER, K. D. 40
BALMAIN, K. G. 146
BARRON, D. W. 194
BATES, D. R. 208
BEDINGER, J. 93
BELROSE, J. S. 51
BERG, O. E. 201
BHAVSAR, P. D. 201
BIALECKE, E. P. 208
BIONDI, M. A. 208
BJELLAND, B. 189
BOURDEAU, R. E. 5, 141
BOWHILL, S. A. 5, 208
BOYD, R. L. F. 28
BRACE, L. H. 141
BRACKMANN, R. T. 124, 129
BRANSCOMB, L. M. 203
BRINTON, H. C. 208
BROWN, S. C. 208
BUDDEN, K. G. 194
BUDZINSKI, E. 163
BURCH, D. S. 203
BURKE, M. J. 50, 51
BYRAM, E. T. 129
CAMPBELL, W. F. 111
CAMPBELL, W. H. 201
CARIGNAN, G. R. 141
CHAMBERLAIN, J. W. 201
CHAMPION, K. W. 146, 208
CHAPMAN, S. 201
CHENG, H. K. 111
CHILDS, E. C. 40
CHUBB, T. A. 129
COLLINS, C. 138
CURRAN, R. K. 203
CUTOLO, M. 146
DALGARNO, A. 208
CAVIS, L. R. 201
DEVIENNE, F. M. (ed.) 111
DICKINSON, P. H. G. 208
DINGLE, R. B. 50
DOERING, J. P. 208
DOLEZALEK, H. 60
DONLEY, J. L. 5
DOTE, T. 16, 28
DOUGAL, A. A. 208
DUBIN, M. 125
ELFORD, W. G. 88
ENEMARK, D. C. 201
FAIRE, A. C. 208
FEDOR, L. 194
FEJER, J. A. 194
FITE, W. L. 124, 129, 208
FORSYTH, P. A. 40
FRIEDMAN, H. 129
FUNDINGSLAND, O. T. 208
GARRIOTT, O. K. 44
GINZBURG, V. L. 146
GIOUMOUSIS, G. 208
GOLD, E. 40
GOLOMB, D. 93
GOSSARD, E. E. 194
GRAD, H. 111
GREENHOW, J. S. 88
GUNN, R. 58
GUNTON, R. C. 208
GUREVICH, A. V. 146
HACKER, D. S. 129
HARA, E. H. 50
HARTNETT, J. P. 129
HASTED, J. B. 208
HAVENS, R. J. 125

HAWKINS, G. S. 88
HAYCOCK, O. C. 40
HAYES, W. D. 111
HEIKKILA, W. J. 40
HERMAN, J. R. 40
HIBBEND, F. H. 146
HIGGS, A. J. 146
HINES, Q. J. 93
HINTEREGGER, H. E. 5, 125, 129, 208
HIRAO, K. 16, 19, 40
HOFFMAN, W. C. 40
HOLT, E. H 208
HOLT, O. 189
HOROWITZ, R. 125
ICHIKAWA, Y. 19
ICHIMIYA, T. 16, 28
IKEGAMI, H. 19, 28
INN, E. C. Y. 208
JACKSON, J. E. 40, 189
JESPERSEN, M. 189
JOHNSON, C. Y. 203
KAISER, T. R. 88
KANE, J. A. 5, 40, 189
KASNER, W. H. 208
KAVADAS, A. 40
KLEITMAN, D. 125
KNAFLICH, H. 93
KOLL, R. T. 125
KROOK, M. 111
LA GOW, H. E. 125
LANDECKER, K. 146
LANDMARK, B. 189
LANGILLE, R. C. 40
LANGSTROTH, G. F. O. 208
LARIN, I. K. 208
LEINBACH, H. 138
LE LEVIER, R E. 208
LESFALD, G. M. 196
LIDDY, D. T. 88
LIED, F. 189
LIEPMAN, H. W. 111
LIN, S. C. 208
LITTLE, C. G 196, 201
LOVELL, A C. B 88
MAEDA, K. 19
MAHAN, B. H. 208
MANASSE, R. 88
MANNING, L. A. 88
MANRING, E. 93
MARKIN, M. I. 208
MARSHALL, S. A. 129
MARTYN, D. F. 146
MASSEY, H. S. W. 40
MC DIARMID, I. B. 163
MC DONALD, N. A. 40
MC ILWAIN, C. E. 163
MC KIBBIN, D. D. 5
MC KINLEY, D. W. R. 88
MC WILLIAMS, P. 156
MEADOWS, E. B. 125, 129
MECHTLY, E. A. 5
MEREDITH, L. H. 201
MEYER, R. F. 111
MILLMAN, P. M. 88
MINZNER, R. A. 146
MITRA, A. P. 208
MITRA, S. K. 201
MIYAZAKI, S. 16, 19, 28, 40
MLODNOSKY, R. F. 44
MOORE, R. H. 156
MURAOKA, T. 19
NAWROCKI, P. J. 146
NICHOLS, M. H. 129
NICOLET, M. 125, 129, 156
NIER, A. O. 125
PACK, J. L. 203
PAPA, R. 146
PARTHASARATHY, R. 196
PAUL, W. 67, 129
PEDERSEN, A. 201
PFISTER, W. 40
PHELPS, A. V. 203
PICKAR, A. D. 40
POKHUNKOV, A. 125, 129
POND, H. 146
POPPOFF, I. G. 201, 203, 208
PROBSTEIN, R. F. 111
RADICELLA, S. M. 189

RATCLIFFE, J. A. 56
RAWER, K. 5
REID, G. C. 138, 203
REINHARD, H. P. 129
ROBERTSON, D. S. 88
ROGERS, W. A. 208
ROSE, D. C. 163
ROSENBERG, N. W. 93
ROSHKO, A. 111
ROTHWELL, P. 40
ROY, S. K. 50
RUTHERFORD, J. A. 208
SAGALYN, R. C. 5
SAYERS, J. 40, 208
SCHAEFER, E. J. 129
SCOTT, J. C. W. 40
SEDDON, J. C. 5, 189
SEN, H. K. 50, 138
SHOLNIK, M. I. 88
SIKSNA, R. 166
SISSENWINE, N. 125
SMIDDY, M. 5
SMITH, C. R. 125, 129
SMITH, L. G. 58
SMITH, R. A. 146
SMITH, S. J. 203
SNOW, W. R. 208
SPENCER, L. V. 201
SPENCER, N. W. 141
STEINBERG, M. 129
STEVENSON, D. P. 208
STOREY, L. R. O. 40
SWANU, W. F. G. 58
TAKAYAMA, K. 16, 19, 28
TALBOT, L. (ed) 111
TALROSE, V. L. 208
TAMAKI, F. 16, 28
TAYLOR, H. A. 208
TELLEGEN, B. D. H. 146
THOMPSON, J. B. 28
THORNESS, R. B. 125
TOWNSEND, J. W. Jr. 125, 129
TRIEAL, H. 40
TSIEN, H. S. 111
ULWICK, J. C. 40
VARNEY, R. N. 166
VAN ALLEN, J. A. 201
VAN LINT, V. A. J. 208
VICE, R. W. 194
VON ZAHN, V. 67, 129
WAGER, J. H. 40
WATANABE, K. 208
WEXLER, H. 125
WHALE, H. A. 40
WHIPPLE, E. C. Jr. 58
WHITTEN, R. C. 201, 203, 208
WILSON, H. A. 40
WINCKLER, J. R. 201
WISE, H. 129
WISNIA, J. 5
WOOD, J. 129
WYLLER, A. A. 50, 138
YEN, J. L. 40
ZEIGLER, R. K. 156